

LOW DENSITY LIPOPROTEIN
TRANSPORT AND METABOLISM
IN THE ARTERIAL WALL

by

George Alexander Truskey

B.S.E., University of Pennsylvania
(1979)

SUBMITTED TO THE CHEMICAL ENGINEERING
IN PARTIAL FULFILLMENT OF THE
REQUIREMENTS FOR THE DEGREE OF

DOCTOR OF PHILOSOPHY

at the

MASSACHUSETTS INSTITUTE OF TECHNOLOGY

September 1985

Copyright (c) 1985 Massachusetts Institute of Technology

Signature redacted

Signature of Author

Chemical Engineering
September 6, 1985

Signature redacted

Certified by

Clark K. Colton
Thesis Supervisor

Signature redacted

Certified by

Kenneth A. Smith
Thesis Supervisor

Signature redacted

Accepted by

MASSACHUSETTS INSTITUTE OF TECHNOLOGY
Chairman, Departmental Graduate Committee

OCT 22 1985

Archives LIBRARIES



77 Massachusetts Avenue
Cambridge, MA 02139
<http://libraries.mit.edu/ask>

DISCLAIMER NOTICE

Due to the condition of the original material, there are unavoidable flaws in this reproduction. We have made every effort possible to provide you with the best copy available.

Thank you.

The images contained in this document are of the best quality available.

LOW DENSITY LIPOPROTEIN TRANSPORT AND METABOLISM IN THE ARTERIAL WALL

by

George Alexander Truskey

Submitted to the Chemical Engineering on September 6,
1985 in partial fulfillment of the requirements for the degree
of Doctor of Philosophy.

Abstract

Low density lipoprotein (LDL) transport and metabolism in the arterial was studied as a function of time following intravenous injection of radiolabeled LDL and methylated LDL (mLDL). mLDL was used because it does not bind to the LDL receptor. LDL and mLDL transmural profiles, mean relative concentrations, and cumulative degradation were similar at all times studied. Degradation became significant at 4 hr and reached a maximum between 24 and 48 hr. In order to account for differences in the plasma decay of LDL and mLDL, the steady state tissue concentration and rate of degradation in response to a step change in plasma concentration were calculated from data for a biexponentially decaying plasma concentration. The LDL tissue concentration and rate of degradation at steady state were, respectively, two and three times larger than the values obtained with mLDL, suggesting that the receptor-mediated pathway is active in the arterial wall in vivo. The calculated mass transfer coefficients for LDL and mLDL were found to decrease with increasing circulation time.

A mathematical model of LDL transport and metabolism in the arterial wall was developed. Rate constants for cellular internalization and degradation were obtained by fitting kinetic data for LDL metabolism by cultured aortic smooth muscle cells. Transport parameters were obtained by fitting 0.5 hr data. For constant mass transfer coefficients, no parameter set yielding agreement between model predictions and data for mean relative concentrations and cumulative degradation could be obtained. When time varying mass transfer coefficients were used in the model, data could be fit to obtain parameters for binding to the extracellular matrix. Model results indicate that degradation is the major mechanism for the removal of LDL from the tissue, the receptor-mediated pathway accounts for about 60% of all LDL degraded by the tissue, and matrix-bound LDL represents the major tissue concentration at long circulation times.

Thesis Supervisor: Clark K. Colton
Title: Thesis Supervisor
Thesis Supervisor: Kenneth A. Smith
Title: Thesis Supervisor

Acknowledgements

First, I would like to thank my advisors, Ken Smith and Clark Colton for their advice and encouragement throughout the course of the thesis. A special debt of gratitude is owed to Peter Davies who made available his laboratory for the cell culture experiments and who provided a stimulating intellectual atmosphere. I'd also like to thank the Whitaker Health Sciences Foundation for their financial support.

While working on this thesis, I have made a number of friends who have contributed in many ways. Eric Morrel and Maria Navarro gave their time freely to help out on experiments and to listen to the myriad of problems encountered while analyzing the data and developing the mathematical models. Thanks also to other members of the "Athero Group" at MIT, including Jocelyn Scott, Jay Schnitzer, and Ron Tompkins. Howard Bernstein deserves special thanks, not only for putting up with my complaining, but for also being a good friend. David Yarmush and Regina Murphy were extremely helpful towards the end of the thesis, performing HPLC and QLS analysis for me. Thanks also to the people in Peter Davies lab, including Henry Warren, Susan O'Connor, Barbara Eisenhaure, Clay Thomason, and Pip Diehl. The encouragement and support of my family throughout my education has been most appreciated. Finally, my largest debt of gratitude goes to my wife, Linda. She has persevered throughout the course of this thesis, and her understanding, compassion, and love have helped to make all of this worthwhile.

To Linda

Table of Contents

Abstract	2
Acknowledgements	4
List of Figures	10
List of Tables	20
1. Introduction	24
1.1 Structure of Low Density Lipoprotein	26
1.2 Structure and Function of the Arterial Wall	26
1.2.1 Endothelium	28
1.2.2 Media	30
1.3 LDL Metabolism by Cultured Cells and In Vivo	35
1.3.1 Receptor-Mediated Metabolism by Cultured Cells	35
1.3.2 Receptor-Independent Metabolism by Cultured Cells	42
1.3.3 Receptor-Mediated and Receptor-Independent LDL Metabolism in Vivo	49
1.4 LDL Interactions with the Extracellular Matrix	54
1.4.1 In Vitro Studies of Lipoprotein-Glycosaminoglycans Interactions	56
1.4.2 In Vitro Studies of Lipoprotein-Elastin Interactions	59
1.4.3 Partitioning of Macromolecules between Plasma and Tissue	60
1.5 Experimental Studies of Macromolecular Transport and Metabolism in the Arterial Wall	62
1.5.1 Effects of Position, Pressure, and Local Hemodynamics	62
1.5.2 Transmural Concentration Profiles	65
1.5.3 LDL Metabolism in the Arterial Wall	69
1.6 Thesis Objectives	71
2. Kinetic Analysis of LDL Metabolism by Cultured Aortic Smooth Muscle Cells	75
2.1 Introduction	75
2.2 Qualitative Presentation of Experimental Observations	77

2.3	Model Development	81
2.3.1	Kinetic Model for Receptor-Mediated Metabolism	81
2.3.2	Kinetic Model for Receptor-Independent Metabolism	95
2.3.3	Parameter Estimation	99
2.4	Materials and Methods	104
2.5	Results	110
2.5.1	Validation of Experimental Techniques	110
2.5.2	Determination of Rate Constants for Receptor-Mediated LDL Metabolism	113
2.5.3	Comparison of Receptor-Mediated Metabolism in Rabbit and Bovine Smooth Muscle Cells	141
2.5.4	Pulse-Chase Experiments	143
2.5.5	Regulation of the LDL Receptor by LDL	149
2.5.6	Effect of NH_4Cl on LDL Metabolism	153
2.5.7	Determination of Rate Constants for Receptor-Independent LDL Metabolism	157
2.5.8	Metabolism of Methylated LDL	166
2.5.9	Comparison with Other Models	177
2.6	Discussion	185
3.	The Effects of Endothelial Cell-Smooth Muscle Cell Interactions on Smooth Muscle Cell LDL Metabolism	196
3.1	Introduction	196
3.2	Previous Results with Platelet-Derived Growth Factor, Conditioned Media, and Coculture	197
3.2.1	Platelet-Derived Growth Factor	197
3.2.2	Endothelial Cell Conditioned Media	198
3.2.3	Coculture of Endothelial Cells and Smooth Muscle Cells	202
3.3	Materials and Methods	208
3.4	Results	215
3.4.1	^3H -Thymidine Autoradiography of Smooth Muscle Cells Cocultured with Endothelial Cells	215
3.4.2	Endothelial Cell Specific Stimulation of LDL Metabolism	217
3.4.3	Effect of Endothelial Cell Number	223
3.4.4	Kinetic Analysis of LDL Metabolism in Smooth Muscle Cells Cocultured with Endothelial Cells	226

3.4.5 Production of Ammonium Ion by Bovine Endothelial Cells and its Effect upon LDL Degradation	233
3.4.6 Growth Factor Independent Stimulation of LDL Metabolism	239
3.5 Discussion	243
4. An Experimental Investigation of Receptor-Mediated and Receptor-Independent Accumulation and Degradation of LDL in the Rabbit Arterial Wall In Vivo	249
4.1 Introduction	249
4.2 Materials and Methods	251
4.3 Results	259
4.3.1 Plasma Decay of Radiolabeled LDL and mLDL	259
4.3.2 Transmural and Average Tissue Concentrations	267
4.3.3 LDL and mLDL Accumulation and Degradation in the Aorta	288
4.3.4 Steady State Tissue Concentration and Rate of Degradation in Response to a Step Input	295
4.3.5 Estimated Transendothelial Transport Mass Transfer Coefficients	308
4.3.6 Characterization of LDL	320
4.4 Discussion.	323
5. Mathematical Models of LDL Transport and Metabolism in the Rabbit Arterial Wall In Vivo	332
5.1 Introduction	332
5.2 Mechanisms of LDL Transport and Metabolism in the Arterial Wall	333
5.3 Model Development	335
5.3.1 Interstitial Concentration	335
5.3.2 Constitutive Relations	341
5.3.3 Species Conservation Relations	346
5.3.4 Boundary Conditions	358
5.3.5 Nondimensionalization	363
5.3.6 Solution	368
5.4 Results	370

5.4.1 Determination of Transport Parameters	370
5.4.2 Estimation of Transmural Profiles and Cumulative Degradation at Long Circulation Times	380
5.5 Discussion	428
6. Conclusions and Recommendations	453
A. Estimation of Rate Constants for Receptor-Mediated LDL Metabolism from Published Data	455
A.1 LDL Binding at 4°C	455
A.2 Receptor-Mediated LDL Metabolism at 37 °C	458
B. Minimization Criterion for Multiple Response Data	476
B.1 Derivation of Minimization Criterion	476
B.2 Numerical Determination of the Parameter Estimates	479
B.3 Example	481
C. Estimation of Steady-State Concentration and Rate of Degradation	485
D. Pharmacokinetic Models of ¹²⁵ I-LDL Plasma Decay Curves	492
E. Solution of Transport Equations	498
F. Data from Cell Culture Experiments	521
G. Data from In Vivo Experiments	543
H. Computer Codes	582
References	631

List of Figures

1-1	Chemical composition of repeating disaccharide units of glycosaminoglycans of the arterial wall	33
1-2	Receptor-mediated and receptor-independent mechanisms of LDL metabolism	36
1-3	Transmural Profiles of LDL and Albumin in the Rabbit Thoracic Aorta (From Bratzler et al. [1977b])	66
1-4	Schematic Diagram of Experimental and Theoretical Studies	73
2-1	Description of Typical Experiment at 37 °C.	78
2-2	Results from a Typical Pulse-Chase Experiment	82
2-3	Schematic of LDL Methylation	108
2-4	Removal of unbound ¹²⁵ I-LDL.	111
2-5	Fits of combined data for receptor-mediated metabolism of LDL from six experiments.	115
2-6	Comparison of model fits obtained from individual responses, two responses, and all responses with data for internalized and degraded LDL.	123
2-7	Expt. BSMC6: LDL metabolism as a function of time and concentration.	128
2-8	Expt. BSMC10: LDL metabolism as a function of time and concentration.	130
2-9	Expt. BSMC29: LDL metabolism as a function of time and concentration.	132
2-10	Expt. BSMC33: LDL metabolism as a function of time and concentration.	134
2-11	Expt. BSMC35: LDL metabolism as a function of time and concentration.	136
2-12	Expt. BSMC40: LDL metabolism as a function of time and concentration.	138
2-13	LDL binding, internalization, and degradation by rabbit and bovine aortic smooth muscle cells.	142
2-14	Semilogarithmic Plot of the Disappearance of Intracellular LDL	145

from Bovine Smooth Muscle Cells.

2-15	Semilogarithmic Plot of the Disappearance of Intracellular LDL from Human Skin Fibroblasts.	146
2-16	Fitting Pulse-Chase Experiments: Bovine Smooth Muscle Cells.	148
2-17	Fitting Pulse-Chase Experiments: Human Skin Fibroblasts.	148
2-18	Regulation of the LDL Receptor on Bovine Smooth Muscle Cells (Expt. BSMC37).	151
2-19	Regulation of the LDL Receptor by Rabbit and Human LDL (Expt. BSCM42).	152
2-20	Effect of NH_4Cl on the kinetics of LDL metabolism.	155
2-21	Fits of combined data for receptor-independent metabolism of LDL from six experiments.	161
2-22	Combined data for receptor-independent binding of LDL from six experiments.	165
2-23	Expt. BSMC6: Receptor-Independent LDL internalization and degradation as a function of time and concentration.	167
2-24	Expt. BSMC10: Receptor-Independent LDL internalization and degradation as a function of time and concentration.	168
2-25	Expt. BSMC29: Receptor-Independent LDL internalization and degradation as a function of time and concentration.	169
2-26	Expt. BSMC33: Receptor-Independent LDL internalization and degradation as a function of time and concentration.	170
2-27	Expt. BSMC35: Receptor-Independent LDL internalization and degradation as a function of time and concentration.	171
2-28	Expt. BSMC40: Receptor-Independent LDL internalization and degradation as a function of time and concentration.	172
2-29	Expt. BSMC38. LDL and mLDL Competition Experiment.	175

2-30	Expt. BSMC41. LDL and mLDL Competition Experiment.	176
2-31	LDL and mLDL binding, internalization, and degradation following four hr incubation.	178
2-32	Pulse-chase experiment with ^{125}I -transferrin, data from Ciechanover et al. [1983a].	184
3-1	LDL metabolism by fibroblasts following incubation with conditioned media (from Witte et al. [1982]).	199
3-2	Total and Cell-Associated Ammonia Production in Endothelial Cell Conditioned Media (Data from Table 3-I).	203
3-3	Relationship between ammonium ion concentration and inhibitory index.	204
3-4	Confluent Bovine Aortic Endothelial Cells Cultured on Solid Plastic Microcarriers. x 480	205
3-5	Growth Curves of Bovine Aortic Smooth Muscle Cells. (From Davies et al. [1985])	206
3-6	Effect of Endothelial Cell Number on Smooth Muscle Cell Growth (From Davies et al. [1985]).	207
3-7	LDL metabolism by smooth muscle cells alone or cocultured with microcarrier-bound endothelial cells or smooth muscle cells (from Davies et al. [1983]).	209
3-8	Microcarrier Coculture Apparatus	213
3-9	Experimental Protocol for Coculture	215
3-10	Expt.BSMC30: Receptor-mediated LDL metabolism by smooth muscle cells incubated with endothelial cell conditioned-media or cocultured with endothelial cells.	221
3-11	Expt. BSMC30: Receptor-Independent LDL metabolism by smooth muscle cells incubated with endothelial cell conditioned media or cocultured with endothelial cells.	222
3-12	Smooth muscle cell LDL metabolism as a function of endothelial cell mass.	225

3-13	Expt. BSMC17: Receptor-mediated metabolism in smooth muscle cells following coculture with endothelial cells.	228
3-14	Expt. BSMC17: Receptor-independent metabolism in smooth muscle cells following coculture with endothelial cells.	229
3-15	Expt. BSMC29: Receptor-mediated LDL metabolism by smooth muscle cells following 48 hr of coculture with endothelial cells.	234
3-16	Expt. BSMC29: Receptor-independent LDL metabolism by smooth muscle cells following 48 hr of coculture with endothelial cells.	236
3-17	Dialysis membrane prevents growth factors from reaching smooth muscle cells	240
3-18	Absence of mitogen-independent stimulation of LDL metabolism in smooth muscle cells incubated with endothelial cell conditioned media (from Davies et al. [1985]).	243
4-1	^{125}I and ^{14}C -Sucrose Labels as Markers of LDL Uptake and Degradation.	252
4-2	Covalent Attachment of ^{14}C -Sucrose to LDL	254
4-3	Representative plasma decay curves of ^{125}I -LDL (Expt. 24C2) and ^{125}I -mLDL (Expt. 24M2)	259
4-4	Plasma decay curves for all experiments 4 hr or longer.	363
4-5	Combined Plasma Decay Curves of Navarro [1984] and This Study.	264
4-6	Comparison of the best fit values for plasma decay curves.	266
4-7	Plasma decay curves of ^{125}I - and ^{14}C -sucrose labeled LDL and mLDL	268
4-8	Individual Section Profiles and Animal Average for Expt. 30C1.	269
4-9	Individual Section Profiles and Animal Average for Expt. 4C3.	270
4-10	Animal Average Profiles for 0.5 hr LDL Experiments.	271
4-11	Animal Average Profiles for 4 hr LDL Experiments.	272

4-12	Average Profiles for 24 hr LDL Experiments.	273
4-13	Animal Average Profiles for 72 hr LDL Experiments.	274
4-14	Animal Average Profiles for 0.5 hr mLDL Experiments.	275
4-15	Animal Average Profiles for 4 hr mLDL Experiments.	276
4-16	Animal Average Profiles for 24 hr mLDL Experiments.	277
4-17	Animal Average Profiles for 72 hr mLDL Experiments.	278
4-18	Grand Average Profiles for LDL and mLDL.	279
4-19	Comparison of 4 hr and 24 hr Grand Average LDL and mLDL Transmural Profiles without Aberrant Profiles (4C6 and 24C1).	281
4-20	Mean Relative Average Concentrations of LDL and mLDL. Experiments 4C6 and 24C1 were excluded from the average values for LDL.	287
4-21	^{125}I and ^{14}C -Sucrose Labeled LDL and mLDL Mean Relative Concentrations in the Rabbit Aorta	289
4-22	LDL and mLDL Tissue Concentrations and Cumulative Degradation in the Rabbit Aorta.	294
4-23	Comparison of Fits of Empirical Functions to Data for LDL Degradation.	301
4-24	Best Fits of Equation (4-13) to Mean Relative Tissue Concentrations Obtained by Frozen Serial Section Microtomy.	302
4-25	Comparison of fits of mean relative concentrations: A. all transmural profiles (Figure 4-24); B. transmural profiles without 4C6 and 24C1; C. pooled data from this study and Navarro [1984]; D. pooled data without experiments 4C6 and 24C1; E. Navarro [1984].	305
4-26	Transmural Profiles of LDL and mLDL at Steady State Following a Step Change in Plasma Concentration.	306
4-27	Transmural Profiles of LDL at Steady State Following a Step Change in Plasma Concentration. Profiles were calculated with and	307

without experiments 4C6 and 24C1.

4-28	Weighted Mass Transfer Coefficient as a Function of Time.	315
4-29	Determination of k_E as a Function of time by Fitting equation (4-26) to ^{14}C -Sucrose Data.	217
4-30	Normalized Mass Transfer Coefficient for LDL and mLDL	318
4-31	Comparison of Calculated and Predicted Values of k_E' .	319
4-32	Comparison of Calculated and Predicted Values of k_E' based upon fits of C_T/C_{p_o} and C_d/C_{p_o} and equation (4-28).	321
4-33	Elution Profile of LDL on a Superose 6 HPLC column.	322
4-34	Comparison of 0.5 hr ^{125}I -LDL Transmural Profiles with the Results of Bratlzer et al. [1977b].	327
4-35	Comparison of 4 hr ^{125}I -LDL Transmural Profiles with the Results of Bratlzer et al. [1977b].	328
4-36	Comparison of 24 hr ^{125}I -LDL Transmural Profiles with the Results of Bratlzer et al. [1977b].	329
4-37	Comparison of ^{125}I -LDL Mean Relative Tissue Concentrations with the Results of Bratlzer et al. [1977b].	330
5-1	Schematic illustration of arterial wall showing modes of LDL transport and reaction thought to occur in the rabbit thoracic aorta.	334
5-2	Model fits of all 0.5 hr LDL and mLDL transmural profiles for three (A), four (B), and five (C) parameter models.	373
5-3	Model fits of combined 0.5 hr LDL and mLDL transmural profiles for the three parameter model.	374
5-4	Model fits of individual animal 0.5 hr LDL transmural profiles to the three parameter model.	375
5-5	Model fits of individual animal 0.5 hr mLDL transmural profiles to	377

the three parameter model.

5-6	Comparison between model predictions and LDL transmural profiles for constant mass transfer coefficients and no binding to the extracellular matrix ($\phi_b^2 = 0.0$).	386
5-7	Comparison between model predictions and LDL mean relative concentrations and cumulative degradation for constant mass transfer coefficients and no binding to the extracellular matrix ($\phi_b^2 = 0.0$).	387
5-8	Comparison between model predictions and mLDL transmural profiles for constant mass transfer coefficients and no binding to the extracellular matrix ($\phi_b^2 = 0.0$).	388
5-9	Comparison between model predictions and mLDL mean relative concentrations and cumulative degradation for constant mass transfer coefficients and no binding to the extracellular matrix.	389
5-10	Best fit of LDL transmural profiles for constant mass transfer coefficients and no binding to the extracellular matrix.	391
5-11	Comparison between model predictions and LDL mean relative concentrations and cumulative degradation for constant mass transfer coefficients and no binding to the extracellular matrix.	392
5-12	Best fit of mLDL transmural profiles for constant mass transfer coefficients and no binding to the extracellular matrix.	393
5-13	Comparison between model predictions and mLDL mean relative concentrations and cumulative degradation for constant mass transfer coefficients and no binding to the extracellular matrix	394
5-14	Effect of ϵ_f on model predictions for LDL (A) mean relative tissue concentrations and (B) cumulative degradation for constant mass transfer coefficients.	396
5-15	Effect of ϵ_f on model predictions for mLDL (A) mean relative tissue concentrations and (B) cumulative degradation for constant mass transfer coefficients.	397
5-16	Comparison of fits of LDL and mLDL for (A) constant and (B) time-varying permeabilities.	399

5-17	Comparison of model fits with time-varying permeabilities to grand average transmural profiles using all LDL profiles.	401
5-18	Predicted values of mean relative tissue concentrations and cumulative degradation.	402
5-19	Comparison of model fits with time-varying permeabilities to grand average transmural profiles without experiments 4C6 and 24C1.	405
5-20	Predicted values of mean relative tissue concentrations and cumulative degradation using parameter estimates obtained by fitting grand average transmural profiles without experiments 4C6 and 24C1.	406
5-21	Comparison of model fits with time-varying permeabilities to grand average mLDL transmural profiles.	407
5-22	Predicted values of mLDL mean relative tissue concentrations and cumulative degradation.	409
5-23	Comparison of model predictions with estimated steady state profile in response to a step change in plasma concentration.	413
5-24	Comparison of model predictions with estimated steady state concentration of mLDL in response to step change in plasma concentration.	414
5-25	Effect of endothelial cell degradation upon cumulative LDL (A) and mLDL (B) degradation.	419
5-26	Effect of endothelial cell degradation upon cumulative LDL (A) and mLDL (B) degradation for constant ϕ_{ie}^2 .	420
5-27	Effect of ϕ_b^2 on mean relative LDL tissue concentration and cumulative degradation.	422
5-28	Effect of m on mean relative LDL tissue concentrations and cumulative degradation.	423
5-29	Effect of binding to the receptors (ϕ_r^2) on mean relative LDL tissue concentrations and cumulative degradation.	425
5-30	Effect of receptor binding (ϕ_r^2) on LDL transmural profiles at 4 and 24 hr.	426

5-31	Effect of receptor-mediated internalization (β) on LDL transmural profiles at 4 and 24 hr.	427
5-32	Effect of receptor-mediated degradation, $\phi_{d_1}^2$, on LDL mean relative tissue concentrations and cumulative degradation.	429
5-33	Effect of $\phi_{e_1}^2$ on LDL mean relative tissue concentrations and cumulative degradation.	430
5-34	Effect of ϕ_i^2 on mLDL mean relative tissue concentrations and cumulative degradation.	431
5-35	Effect of $\phi_{d_2}^2$ on mLDL mean relative tissue concentrations and cumulative degradation.	432
5-36	Effect of $\phi_{e_2}^2$ on mLDL mean relative concentrations and cumulative degradation.	433
5-37	Predicted mean relative concentrations of (A) $\bar{\theta}_T$, $\bar{\theta}_f$, $\bar{\theta}_b$, and total cellular concentration ($\bar{\theta}_{LR} + \bar{\theta}_{LRi} + \bar{\theta}_{Li}$), and (B) $\bar{\theta}_f$, $\bar{\theta}_{LR}$, $\bar{\theta}_{LRi}$, and $\bar{\theta}_{Li}$.	444
5-38	Predicted mean relative LDL concentrations of (A) $\bar{\theta}_T$, $\bar{\theta}_f$, $\bar{\theta}_b$, and total cellular concentration ($\bar{\theta}_{LR} + \bar{\theta}_{LRi} + \bar{\theta}_{Li}$), and (B) $\bar{\theta}_f$, $\bar{\theta}_{LR}$, $\bar{\theta}_{LRi}$, and $\bar{\theta}_{Li}$.	445
5-39	Predicted mean relative mLDL concentrations of $\bar{\theta}_T$, $\bar{\theta}_f$, $\bar{\theta}_b$, and $\bar{\theta}_{Li}$.	446
5-40	Transmural profile of the fraction of receptors bound to LDL at 1 hr calculated using parameter values from best fit of (A) LDL transmural profiles (case D, Figure 5-17); and (B) LDL transmural profiles without experiments 4C6 and 24C1 (case D, Figure 5-19).	449
5-41	Transmural profile of cumulative degradation products of LDL at 24 hr calculated using parameter values from best fit of LDL transmural profiles without experiments 4C6 and 24C1 (Figure 5-19)	451

without (A) and with (B) endothelial cell metabolism.

A-1	Fitting data of Goldstein et al. [1976]	457
A-2	Fitting data of Basu et al. [1978]	457
A-3	Fitting Pulse-Chase Results of Brown and Goldstein [1976]	462
A-4	LDL internalization in normal human fibroblasts and fibroblasts from patients heterozygous for familial hypercholesterolemia.	463
A-5	Semilogarithmic plot of the decrease in the fraction of LDL bound to the cell surface of fibroblasts from patient JD, homozygous for familial hypercholesterolemia.	464
A-6	Pulse-chase experiments of Aulinkas et al. [1981].	466
A-7	Short-Time Kinetics of Binding and Internalization (from Goldstein et al. [1976]).	468
A-8	Fitting Data of Vlodaysky et al. [1978].	470
A-9	Fitting Data of Reckless et al. [1978].	472
A-10	Fitting Data of Eisele et al. [1980].	473
B-1	Approximate 99.75% confidence contours (from Box and Draper [1965]).	484
F-1	Correlation between smooth muscle cell mass and cell number.	542

List of Tables

1-I	Molecular Weight and Radius of LDL	27
1-II	Chemical modifications of lysine and arginine residues of LDL	48
2-I	Rate Constants for Receptor-Mediated Internalization	89
2-II	Smooth Muscle Cell Metabolism of LDL Prepared by Two Different Methods	113
2-III	Estimated Rate Constants for Combined Data of Receptor-Mediated Metabolism	119
2-IV	Correlation Matrices of Parameters	121
2-V	Rate Constants for Receptor-Mediated LDL Metabolism from Individual Responses or Two Responses	126
2-VI	Rate Constants for Receptor-Mediated LDL Metabolism from Fits of Individual Experiments	140
2-VII	Comparison of Parameter Groups for Bovine and Rabbit Smooth Muscle Cells	143
2-VIII	Rate Constants Estimated from Pulse-Chase Experiments	147
2-IX	Effect of 10 mM NH_4Cl on Rate Constants for Receptor-Mediated LDL Metabolism	154
2-X	Rate Constants for Combined Data of Receptor-Independent Metabolism	159
2-XI	Matrix of Correlation Coefficients for Receptor-Independent Metabolism	164
2-XII	Rate Constants for Receptor-Independent Metabolism in Individual Experiments	173
2-XIII	^{125}I -LDL Metabolism in the Presence of 500 $\mu\text{g}/\text{ml}$ LDL or mLDL	174
2-XIV	Rate Constants for mLDL Metabolism	177

2-XV	Rate Constants for Receptor-Mediated Metabolism of Transferrin	182
2-XVI	Parameter Correlation Matrix for Fit of Data of Ciechanover et al. [1983a]	183
2-XVII	Effect of Cell Density Upon Rate Constants and Receptor Number	191
2-XVIII	Average Value of Rate Constants for Receptor-Mediated LDL Metabolism and Comparison with Estimates from Published Data	192
2-XIX	Average Value of Rate Constants for Receptor-Independent Metabolism and Comparison with Estimates from Published Data	194
3-I	Production of Ammonia by Endothelial Cells and Inhibition of Degradation (From Cornicelli et al. [1983]).	201
3-II	³ H-Thymidine Labeling of Smooth Muscle Cells	216
3-III	Effect of Coculture and Conditioned Media on LDL Metabolism by Smooth Muscle Cells	218
3-IV	LDL Metabolism by Smooth Muscle Cells Following a 45 hr Coculture Incubation	219
3-V	Best Fit Parameters of Equation (3-6) to Data in Figure 3-12	226
3-VI	Expt BSMC17: Parameters for Receptor-Mediated Metabolism of LDL by Smooth Muscle Cells Cocultured with Endothelial Cells	231
3-VII	Expt BSMC17: Parameters for Receptor-Independent Metabolism of LDL by Smooth Muscle Cells Cocultured with Endothelial Cells	232
3-VIII	Expt. BSMC29: Rate Constants for LDL Metabolism Following Coculture	233
3-IX	Ammonium Ion Production	239
3-X	Growth Factor Independent Stimulation of LDL Metabolism	241
3-XI	Growth Factor Independent Stimulation Requires Coculture	242
4-I	Fractional Catabolic Rates	261

4-II	Best Fit Parameters of Plasma Decay Curves for ^{125}I -Labeled LDL and mLDL	263
4-III	Comparison of Plasma Decay Curves	265
4-IV	Comparison of LDL and mLDL Grand Average Profiles	283
4-V	Comparison of LDL and mLDL Grand Average Profiles at 4 and 24 hr without Experiments 4C6 and 24C1	286
4-VI	Comparison of LDL and mLDL Mean Relative Concentrations	286
4-VII	Comparison of Mean Relative ^{125}I Tissue Concentrations	290
4-VIII	Steady State Tissue Concentration and Rate of Degradation in Response to a Step Change in Plasma Concentration	298
4-IX	Comparison of Estimated Values of $\theta_d(\infty)$ and R_d for Various Functions	300
4-X	Steady State Tissue Concentration in Response to a Step Change in Plasma Concentration	303
4-XI	Mass Transfer Coefficients for LDL and mLDL at 0.5 hr	311
4-XII	Comparison of Mass Transfer Coefficients in the Rabbit Arterial Wall Estimated for Short Circulation Times	313
4-XIII	Fitting Equation 4-29 to ^{14}C -Sucrose Uptake Data	320
4-XIV	Fractional Catabolic Rates of Normal and Modified LDL in Rabbits	325
4-XV	Fractional Catabolic Rates of LDL in Normal and WHHL Rabbits	326
4-XVI	Comparison of Mean Relative Tissue Concentration of Radioiodinated LDL from Various Studies with Normal Animals. (Modified from Bratzler et al. [1977b])	332
4-XVII	Mean Relative Tissue Concentrations of ^{125}I - and ^{14}C -sucrose-labeled Lipoproteins in Rabbits	335
4-XVIII	Weighted Mass Transfer Coefficient Estimated from Mean Relative Tissue Concentrations of ^{14}C -Sucrose	337

5-I	Dimensionless Groups Used in Transport Model	366
5-II	Transport Parameters Determined from Nonlinear Regression of 0.5 hr LDL and mLDL Transmural Profiles	379
5-III	Parameter Correlation Matrix for Pooled LDL and mLDL Data	381
5-IV	Values of Dimensional Constants Used in Model Calculations for Constant Mass Transfer Coefficients	382
5-V	Dimensionless Groups Used in Model Calculations	384
5-VI	Best Fit Parameters Obtained by Nonlinear Regression of Mode for Constant Mass Transfer Coefficients to Transmural Profiles	390
5-VII	Best Fit Values of Bi_o and Bi_c from Fitting 0.5 hr Data	398
5-VIII	Metabolic Parameters Obtained by Nonlinear Regression of Model to Transmural Profiles for Time-Varying Mass Transfer Coefficients	403
5-IX	Comparison of Model Estimates of ψ_T and R_d with Estimates from Linear Systems Theory	439
5-X	Distribution of Tissue Concentrations at Steady State Following a Step Change in Plasma Concentration	440
5-XI	Importance of Receptor-Mediated and Receptor-Independent Degradation	442
A-I	Rate Constants for LDL Binding to its Receptor at 4 °C	459
A-II	Equilibrium Constants for LDL Binding at 4 °C	460
A-III	Rate Constants Estimated from Published Data	467
A-IV	K_{int} at 37 °C	475
B-I	Data for Example	482
B-II	Parameter Estimates for Example	483

Chapter 1

Introduction

The transport and metabolism of lipoproteins in the arterial wall is important in atherogenesis. The hallmark of the atheromatous lesion is the intracellular and extracellular accumulation of cholesteryl esters which are derived from low density lipoprotein (LDL) in the plasma (Zilversmit [1968], Smith and Slater [1970]). Immunohistochemical techniques have identified LDL in atheromatous plaques (Hoff et al. [1975], Hoff and Gaubatz [1977]) and in the normal aorta (Hoff et al. [1977], Smith and Staples [1980]). ^{125}I -LDL and other radiolabeled proteins (e.g. albumin and fibrinogen) can enter and accumulate within the vessel wall (Okishio [1961], Duncan et al. [1963], Calvert et al. [1975], Ghosh et al. [1976], Bell et al. [1974a,b], Bratzler et al. [1977a,b]). Transmural concentration profiles of ^{125}I -LDL and ^{125}I -albumin indicate that entry is from the vessel lumen as well as the vasa vasorum (Bratzler et al. [1977a,b], Ramirez et al. [1984]) and the intimal endothelium accounts for a significant amount of the total mass transfer resistance in the arterial wall (Bratzler et al. [1977a,b,c], Ramirez et al. [1984], Truskey et al. [1981]). Although the mechanisms governing LDL transport in the arterial wall have been, in part, elucidated, the extent of lipoprotein metabolism and the effect of diffusion and transendothelial transport on the rates of cellular uptake and degradation are poorly understood.

Low density lipoprotein is the major cholesterol carrying lipoprotein in the plasma and is the final product in the transport of cholesterol from the liver to sites of metabolism. Cholesterol is required for cell membrane synthesis and as a precursor for steroid hormone production. Like many other cell types, cultured

arterial endothelial and smooth muscle cells internalize and degrade LDL by receptor-mediated and receptor-independent mechanisms (Coetzee et al. [1979], Eisele et al. [1980], Fielding et al. [1979], Goldstein and Brown [1977], Reckless et al. [1978], Stein and Stein [1975], van Hinsbergh et al. [1983], Weinstein et al. [1976]).

The contribution of the receptor-mediated pathway to LDL metabolism in the arterial wall in vivo is of interest because this pathway may be altered or bypassed during atherogenesis. Growth factors from platelets and endothelial cells stimulate fluid phase endocytosis and LDL binding, internalization, and degradation by smooth muscle cells and fibroblasts (Chait et al. [1980], Cornicelli et al. [1983], Davies and Ross [1978, 1980], Davies et al. [1980, 1985], Davies and Kerr [1982a], Witte and Cornicelli [1980], Witte et al. [1982]). In addition, the content of hydrolytic enzymes increases in the cells present in the atherosclerotic plaque (Wolinsky et al. [1979]) which may further alter LDL metabolism. Thus, an understanding of the relative importance of receptor-mediated LDL metabolism in the normal vessel wall is crucial to understanding the pathological state.

In this chapter literature relevant to LDL transport and metabolism in the arterial wall is reviewed, followed by presentation of thesis objectives. The purpose of the review is to present sufficient detail in order to understand the thesis objectives and results presented in subsequent chapters. The structure of LDL is considered first. This is followed by a description of the structure and function of the arterial wall, and discussions of LDL metabolism in cultured cells, LDL interactions with the extracellular matrix, and experimental studies of LDL transport and metabolism in the arterial wall.

1.1 Structure of Low Density Lipoprotein

LDL consists of a hydrophobic core of triglyceride and esterified cholesterol surrounded by phospholipid, protein, and free cholesterol (Hatch and Lees [1968]), and its composition by weight is: 21% protein, 22% phospholipid, 11% triglyceride, 37% cholesteryl esters, and 8% free cholesterol (Kezdy [1977]). The protein consists of two monomeric units (known as apoprotein B) of molecular weight 250,000 (Steile and Reynolds [1979]). The protein portion confers specificity upon LDL, allowing it to be recognized by receptors on the cell surface.

The molecular weight and radius of LDL have been determined by a variety of techniques and results are summarized in Table 1-I. Similar values have been obtained by quasielastic light scattering, analytical ultracentrifugation, and X-ray small angle scattering, while gel chromatography yields a higher value. LDL is roughly spherical (Gotto et al. [1968]) with a Stokes-Einstein radius between 9.5 nm and 12.9 nm; analytical techniques yield values similar to those obtained by negative staining electron microscopy. Agarose gel chromatography of LDL yields a single, sharp, symmetrical peak (Margolis [1967], Rubenstein and Steiner [1976]), although the charge and cholesterol to protein ratios are heterogeneous as determined by ion exchange chromatography (Rubenstein and Steiner [1976]). For all calculations, molecular weights of 2.5×10^6 and 5×10^5 for LDL and apoprotein B, respectively, were used.

1.2 Structure and Function of the Arterial Wall

The large elastic arteries, such as the aorta, consist of three structurally distinct regions: intima, media, and adventitia. The intima, the region closest to the lumen, consists of endothelium, subendothelial space, and internal elastic lamina.

Table 1-I: Molecular Weight and Radius of LDL

MW, g/mole x-10 ⁶	r, nm	Method	Reference
3.5	12.9	Gel chromatography	Margolis [1967]
	10.8-11.0	Negative staining	Gotto et al. [1968]
2.2	9.5	Analytical ultracentrifugation	Hatch and Lees [1968]
2.7	10.1	Analytical ultracentrifugation	Fisher et al. [1971]
2.9 ± 0.3		Analytical ultracentrifugation	Fisher et al. [1972]
2.7 ± 0.5		Analytical ultracentrifugation	Schumaker et al. [1973]
2.4	12	X-ray small angle scattering	Muller et al. [1978]
2.31 ± 0.09		Quasielastic light scattering	Crossley et al. [1981]
	11.9 ± 0.7	Quasielastic light scattering	Mitterer et al. [1982]

The endothelium forms a continuous monolayer in contact with the blood. Endothelial cells are attached to the underlying tissue by a basement membrane of collagen and glycoprotein. The media consists of concentric bands of fenestrated elastic lamellae separated by smooth muscle cells and an extracellular matrix of collagen, elastic fibers, and proteoglycans (Ross and Glomset [1976]). In those animals with arteries containing more than 30 lamellae, the outer media contains a network of capillaries and lymphatic terminals - the vasa vasorum (Wolinsky and Glagov [1967]). The outermost layer is the adventitia which consists of fibroblasts

and smooth muscle cells interspersed with collagen and proteoglycans. There are no organized elastic lamellae in the adventitia.

1.2.1 Endothelium

Endothelial cells are separated by interdigitating clefts, 10 nm to 20 nm in width, containing gap and tight junctions (Huttner et al. [1973a], Alberts et al. [1983]). Gap junctions, also known as communicating junctions, allow small molecules to pass directly from the cytoplasm of one cell to the cytoplasm of another. Tight junctions are punctate regions of close apposition of endothelial cell membranes and are believed to act as permeability barriers. Schwartz and Benditt [1972] have observed numerous regions of complete occlusion in the intercellular clefts of aortic endothelium and have been unable to discern continuous paths from the luminal side to the abluminal side.

Ultrastructural evidence suggests that molecules as large as 4 nm in diameter can pass through the intercellular junctions. Huttner et al. [1973b] have observed horseradish peroxidase (HRP) (molecular weight 40,000; Stokes-Einstein radius 5 nm) on both sides of incomplete tight junctions and around large gap junctions. Florey and Sheppard [1970] and Stein and Stein [1973] report that HRP passes through intercellular junctions. Schwartz and Benditt [1972], however, have been unable to determine whether HRP passes through the junctions, although it is observed in vesicles and subendothelium. Colloidal gold (Stokes-Einstein radius of 15 nm) and ferritin (Stokes-Einstein radius of 5.5 nm) are not observed in endothelial junctions (Huttner et al. [1973b], Stein and Stein [1973]).

Proteins too large to pass through the intercellular clefts are transported across the endothelium in endocytotic vesicles (Buck [1958], Florey and Sheppard [1970], Huttner et al. [1973b], Simionescu et al. [1976], Stein and Stein [1973]).

Vesicles have an average diameter of 65 nm (Chien [1978]) and can be as large as 120 nm in diameter (Schwartz and Benditt [1972]). Vesicles are most frequently observed attached to the luminal and abluminal membranes by means of stalks 20 nm to 30 nm in diameter (Chien [1978]).

There are two populations of vesicles, coated and uncoated. Coated vesicles, which derive their name from their fuzzy appearance in electron micrographs, contain a transmembrane protein, clathrin, involved in receptor-mediated endocytosis of proteins. The clathrin coat is shed shortly after vesicle formation (Pearse and Bretscher [1981]). Uncoated vesicles include coated vesicles which have lost their coat as well as uncoated vesicles which form following membrane invagination and budding (Chien [1978]). The role of coated and uncoated vesicles in transendothelial transport is unknown, although the results of Vasile et al. [1983] suggest that uncoated vesicles formed by membrane invagination are involved in transendothelial transport.

Many coated and uncoated vesicles that appear unattached in one section may be attached when viewed from another plane of section. Applying ruthenium red (which stains only attached vesicles) to glutaraldehyde-fixed canine carotid artery, Chien et al. [1982] have observed that only 25% of all nominally free vesicles are actually unattached and 8.2% of all vesicles are unattached. Using the same technique, Davies and Kuczera [1981] have observed that, in cultured bovine endothelial cells, 47% of all nominally free vesicles are unattached and coated vesicles represent 15% of the free vesicles. Differences between the two studies may reflect actual variability in the number of attached vesicles or an artifact of cells in culture.

The ultrastructure of vesicles suggests that they transport molecules up to 30 nm in diameter. HRP (Buck [1958], Florey and Sheppard [1970], Huttner et al.

[1973b]), lactoperoxidase (molecular weight 80,000) (Simionescu et al. [1976]), ferritin (Florey and Sheppard [1970]), and LDL (Stein et al. [1973], Vasile et al. [1983]) have been observed in endocytotic vesicles.

Much like capillary endothelium, arterial endothelium is comprised of four major regions: 1) a nuclear region; 2) an organelle region adjacent to the nuclear region; 3) the peripheral zone; and 4) a parajunctional zone (Chien [1978]). The nuclear zone contains only the nucleus and a small amount of cytoplasm and is devoid of other organelles. Within the organelle region are mitochondria, endoplasmic reticulum, polysomes, microtubules, the Golgi apparatus, centrioles, and lysosomes. The peripheral zone contains the largest amount of cytoplasm and most of the organelles, with the exception of the Golgi and centrioles. The parajunctional zone is the thinnest region and rarely contains organelles.

Endocytotic vesicles are not distributed uniformly throughout the endothelial cell. Their density is highest in the peripheral zone, followed by the nuclear zone, organelle region, and parajunctional zone. Using freeze fracture techniques, Jan [1984] has determined that the parajunctional zone in canine carotid endothelium comprises 25% of the endothelial surface and is free of surface attached vesicles.

1.2.2 Media

Extracellular Matrix The media consists of smooth muscle cells surrounded by an extracellular matrix of elastin, collagen, and proteoglycans.

Elastin is confined largely to the elastic lamellae which are 2.5 μm thick bands with occasional fenestrations. Elastin probably exists as a random network with limited amounts of short range structure due to hydrophobic interactions among nonpolar amino acids (Gosline [1976]). It is covalently linked to microfibrils (Cliff [1971]). Elastin undergoes reversible extension; hence it can withstand the high

pressures generated by the heart. Consequently, its concentration is highest near the aortic arch (Gosline [1976]). Elastin content in the human aorta varies with age and medial position; it is highest near the intima and is higher in the thoracic aorta (46% of total dry weight) than abdominal aorta (36% of total dry weight) (Rucker and Tinker [1977]). This medial-adventitial gradient reverses with age (Feldman and Glagov [1971]).

Collagen consists of three α helix polypeptide chains. Due to differences in the α chains, collagen exists in several different forms, two of which (types I and III) are found in blood vessels. Type I collagen forms striated fibrils 100 nm to 320 nm in diameter which may aggregate to form larger collagen fibers (Linsenmayer [1981]). Type III collagen is similar to type I collagen, forming smaller fibrils 25 nm to 40 nm in diameter. Immunofluorescent techniques have been used to identify type I collagen in the media and adventitia, and type III collagen in the subendothelial space and the media (Burke and Ross [1979]). Types I and III collagen have also been extracted from aortic tissue. Collagen and elastin are apparently synthesized by smooth muscle cells (Burke and Ross [1979]).

Proteoglycans are large (molecular weights $1 - 4 \times 10^6$) protein polysaccharides composed of a protein core covalently linked to glycosaminoglycans (Comper and Laurent [1978]). Structural knowledge of proteoglycans is derived largely from studies of cartilage proteoglycans, which are believed to be similar to aortic proteoglycans (Hascall and Hascall [1981]). The most commonly accepted structure of proteoglycans is the so-called bottle brush configuration (Wight [1980]) in which the many attached glycosaminoglycans protrude from the protein backbone. In cartilage and aorta, it is believed that proteoglycans form larger structures by binding to hyaluronic acid. Such a structure may result in steric exclusion and restricted diffusion of macromolecules.

Glycosaminoglycans are linear polysaccharides consisting of repeating units of hexosamine and hexuronic acid (Comper and Laurent [1978]). The major glycosaminoglycans are presented in Figure 1-1. The disaccharides contain carboxylate, sulfate esters, and sulfamino groups which are completely ionized under physiological conditions. The polyanionic groups, which range from one per disaccharide in hyaluronic acid to four per disaccharide in heparin, influence the interaction of glycosaminoglycans with other molecules (Hascall and Hascall [1981], Wight [1980]). Hyaluronic acid is not covalently linked to protein to form proteoglycans, although it may form noncovalent interactions with proteoglycans (Comper and Laurent [1978]).

The most common glycosaminoglycans in the arterial wall are hyaluronic acid, chondroitin-4-sulfate, chondroitin-6-sulfate, dermatan sulfate, and heparan sulfate (Figure 1-1). Glycosaminoglycans comprise one to two percent of dry tissue weight (Mathews [1975]). The glycosaminoglycan content varies among species and with position in the vasculature (Wight [1980]). In man, glycosaminoglycan content is 40% higher in the abdominal aorta than in the thoracic aorta. Glycosaminoglycan concentrations are higher in the inner media in porcine, bovine, and human thoracic aorta. In rabbit thoracic aorta, however, glycosaminoglycan concentrations are uniform throughout the vessel wall (Massaro et al. [1979], Wight [1980]).

Proteoglycans extracted from bovine and human aorta are polydisperse and can bind with hyaluronic acid to a limited extent to form larger aggregates (McMurtery et al. [1979], Oegema et al. [1979], Gardell et al. [1980], Salisbury and Wagner [1981]). Ruthenium red, which stains proteoglycans, stains the luminal surface of the endothelium. Particulate granules of ruthenium red are associated with the basement membrane surrounding smooth muscle cells and 20-50 nm polygonal granules of ruthenium red are present in the extracellular matrix (Wight

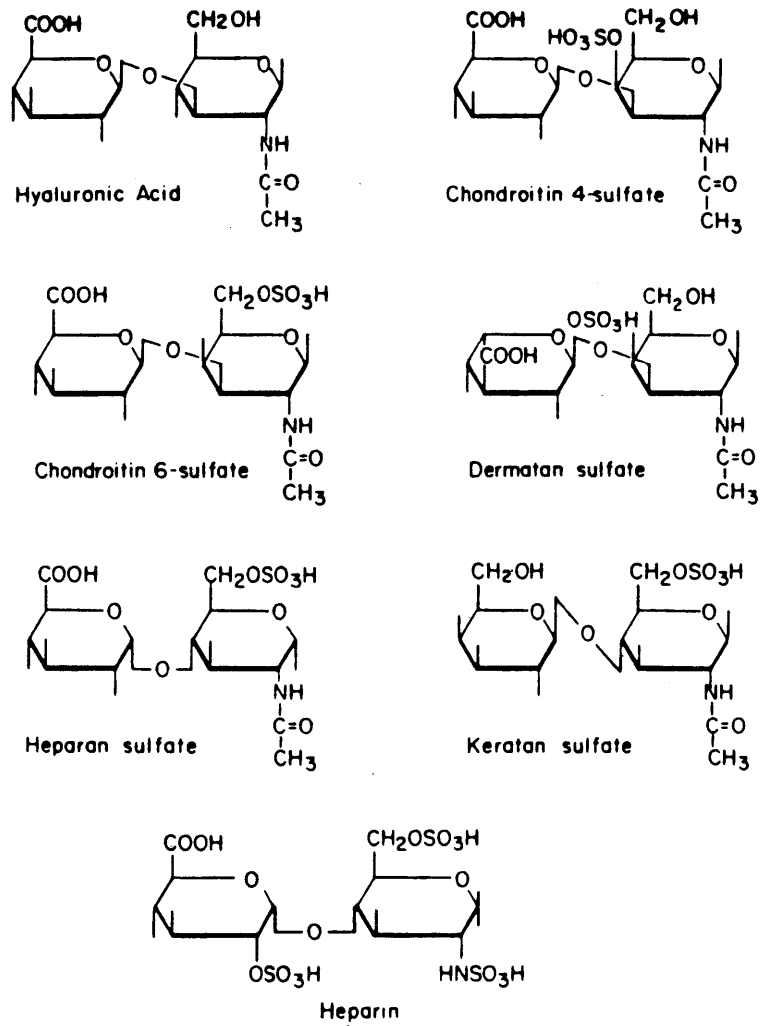


Figure 1-1: Chemical composition of repeating disaccharide units of glycosaminoglycans of the arterial wall (from Wight [1980]).

and Ross [1975]). The polygonal granules are located at the juncture of several elastic fibers and at regular distances along collagen fibrils. These granules are susceptible to chondroitinase which indicates that they are proteoglycans. Wight [1980] suggests that proteoglycans may be necessary in forming a meshwork with collagen and elastin.

Smooth Muscle Cells Arterial smooth muscle cells contain significant amounts of myofilaments and are surrounded by a basement membrane about 100 nm thick containing collagen and glycoprotein (Pearse and Paule [1960], Gerrity and Cliff [1975]). The cells are arranged circumferentially and tend to be elongate, although in the adult their shape is irregular (Gerrity and Cliff [1975], Todd et al. [1983]). In the adult rat thoracic aorta (12 weeks or older), the smooth muscle cell volume is about $1000 \mu\text{m}^3$ and the smooth muscle cells occupy between 25% and 30% of the total wall volume (Gerrity and Cliff [1975], Bucher et al. [1982]); cell volumes vary from $790 \mu\text{m}^3$ in the mesenteric artery to $2500 \mu\text{m}^3$ in the tail artery (Todd et al. [1983]). The average smooth muscle width in the rat tail, mesenteric, and femoral arteries is about $20 \mu\text{m}$ (Todd et al. [1983]). Generally, a single cell spans the space between two elastic lamellae (Pearse and Paule [1960]), although there are occasional regions of overlap of smooth muscle cells near the elastic lamellae (Gardell et al. [1980]). Rhodin [1977] has suggested that smooth muscle cells are bound to elastin by collagen fibrils.

Numerous surface invaginations and endocytotic vesicles are present in electron micrographs (Coltoff-Schiller et al. [1975]). These vesicles are similar to those in endothelial cells and range in diameter from 65 nm to 100 nm (Coltoff-Schiller et al. [1975]). Few lysosomes are present, and, in the rabbit aorta, lysosomal hydrolase activity is about 40% of that in the liver (Peters et al. [1972]).

1.3 LDL Metabolism by Cultured Cells and In Vivo

LDL is too large to permeate across cell membranes. Instead, it is internalized by receptor-mediated and receptor-independent mechanisms in order to meet the cellular demand for cholesterol (Figure 1-2). The receptor-mediated pathway is a specific and regulated mechanism for the metabolism of LDL, whereas nonspecific mechanisms, which include fluid phase and adsorptive endocytosis, are unregulated. The importance of each pathway depends upon LDL concentration, the duration of exposure to LDL, and the metabolic state of the cell. Fibroblasts, endothelial cells, and smooth muscle cells exhibit qualitatively similar behavior. Since the majority of studies have been performed with cultured human fibroblasts, these results are reviewed in some detail. Specific features of LDL metabolism by endothelial cells and smooth muscle cells are also presented.

1.3.1 Receptor-Mediated Metabolism by Cultured Cells

In receptor-mediated metabolism (Figure 1-2), LDL binds to a cell surface receptor which is specific for apoprotein B. The LDL receptor is not stationary, but rather it diffuses along the cell surface.¹ The receptor-ligand complex is internalized during the formation of a coated vesicle. Once internalized, LDL dissociates from its receptor. The receptor is then recycled for another round of binding and internalization (Brown et al. [1983]). The vesicle containing LDL ultimately fuses with either lysosomes, wherein LDL is hydrolyzed, or the cell membrane, releasing LDL to the extracellular medium (exocytosis).

¹The diffusion coefficient of the LDL receptor on human fibroblasts is 4.5×10^{-11} cm²/s at 28 °C (Barak and Webb [1982]). This value falls within the range reported for a variety of other membrane proteins (10^{-11} to 8×10^{-10} cm²/s) (Hillman and Schlesinger [1982], Webb et al. [1982]), but is significantly less than the value predicted from hydrodynamic theory using membrane viscosity (Saffman and Delbruck [1975]). This discrepancy is probably due to interactions between membrane proteins and the cytoskeleton (Barak and Webb [1982], Alberts et al. [1983]).

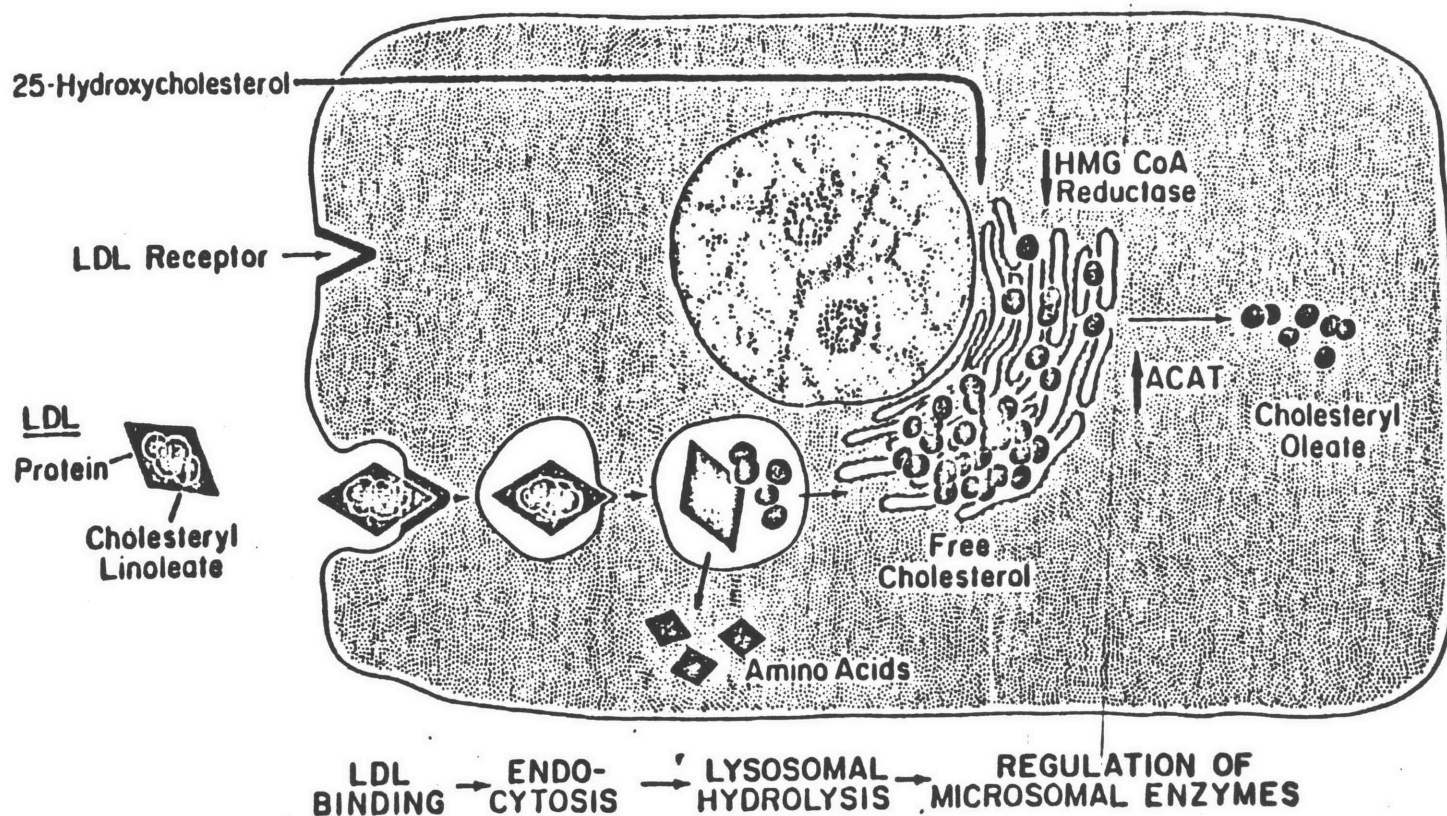


Figure 1-2: Receptor-Mediated and receptor-independent mechanisms of LDL metabolism

Electron microscopy studies demonstrate that LDL (in the form of LDL-ferritin complexes) binds to receptors which are concentrated in coated pits on the surface of the cell membrane (Anderson et al. [1976, 1977a,b]). Approximately 70% of surface-associated LDL is found in these regions, which account for about 2% of the surface area; the other 30% of surface-bound LDL is spread over the remaining 98% of the membrane surface. The coated regions vary in length from 0.1 to 0.2 μm (Anderson et al. [1976, 1977a], Vermeer et al. [1980]). Many of these regions appear as indentations in the plasma membrane, some of which are forming endocytotic vesicles. In these indentations LDL is either attached to the surface or apparently free. These coated regions contain a transmembrane protein (clathrin) which is responsible for their fuzzy appearance in electron micrographs (Heuser

[1980], Pearse and Bretscher [1981]). In fibroblasts from patients with homozygous familial hypercholesterolemia, a disease in which the LDL receptors are absent or defective, coated pits and vesicles are present but LDL is not bound to the membrane in these regions (Anderson et al. [1976]).

The number of receptors on the cell membrane depends upon the extracellular concentration of LDL and the growth state of the cells. Receptor number is regulated by the lysosomal metabolism of LDL. Within the lysosomes, cholesteryl esters are hydrolyzed to free cholesterol and diffuse into the cytoplasm. The increase in cytoplasmic cholesterol elicits three important cellular responses (Figure 1-2): 1) suppression of 3-hydroxy-3-methylglutaryl coenzyme A reductase (HMG CoA), the rate limiting enzyme for endogenous cholesterol synthesis (Brown et al. [1974]); 2) stimulation of acyl coenzyme A:cholesteryl acyltransferase (ACAT) activity, an enzyme involved in the esterification of cholesterol (Goldstein et al. [1974]); and 3) suppression of LDL receptor synthesis (Brown and Goldstein [1975]). The number of LDL receptors present on the cell membrane of growing human fibroblasts incubated in lipoprotein deficient serum is between 15,000 and 70,000 at 37 °C (Goldstein and Brown [1977]). Regulation of the receptors occurs with a half time of 20 hr (Brown and Goldstein [1975]).

At 37 °C, LDL receptors on human fibroblasts are saturated at human LDL concentrations above 50 µg LDL protein/ml (Brown et al. [1976]). LDL receptors on rabbit, swine, and bovine aortic smooth muscle cells and arterial and venous bovine and human endothelial cells saturate at LDL concentrations above 100 µg/ml (Stein and Stein [1975], Weinstein et al. [1976], Reckless et al. [1978], Coetzee et al. [1979], Fielding et al. [1979], Eisele et al. [1980], van Hinsbergh et al. [1983]).

The Effect of Growth Factors on LDL Metabolism The expression of LDL receptors is also dependent upon the growth state of the cell. Quiescent cells have

low cholesterol requirements and a reduced number of LDL receptors whereas growing cells are actively synthesizing cell membrane, require cholesterol, and have increased numbers of LDL receptors. Addition of growth factors (e.g. platelet derived growth factor (PDGF), and fibroblast growth factor (FGF)) to quiescent fibroblasts and smooth muscle cells stimulates LDL binding, internalization, and degradation after 8 hr (Chait et al. [1980], Davies et al. [1980], Witte and Cornicelli [1980], Witte et al. [1982]). (Endothelial cell growth is not dependent upon growth factors (Davies et al. [1980]) and confluent monolayers are not stimulated by growth factors.) The increase in LDL metabolism and the nuclear incorporation of ³H-thymidine reach a maximum 24 hr after the addition of growth factor and decline thereafter (Chait et al. [1980], Witte and Cornicelli [1980], Witte et al. [1982]). Increased LDL metabolism depends upon growth factor concentration and saturates at a PDGF concentration of 50 ng/ml (Witte and Cornicelli [1980]). The primary effect of growth factors on LDL metabolism appears to be an increase in receptor number (Chait et al. [1980], Witte et al. [1982]).

Cultured endothelial cells secrete a number of growth factors, some of which bind to the PDGF receptor on smooth muscle cells (Gadjusek et al. [1980], DiCorleto et al. [1983], DiCorleto and Bowen-Pope [1983], Fox and DiCorleto [1984]). Incubation of quiescent human skin fibroblasts with conditioned media from porcine aortic endothelial cells (Witte et al. [1982]) or coculture of bovine aortic endothelial and smooth muscle cells (Davies et al. [1983, 1985]) results in the stimulation of LDL binding and internalization by fibroblasts or smooth muscle cells. LDL degradation is also increased in coculture, but with conditioned medium LDL degradation does not increase. Like kidney epithelial cells (Glacken and Sinsky [1985]), porcine aortic endothelial cells secrete millimolar amounts of ammonium ion, a lysosomotropic agent which raises lysosomal pH, inactivating

lysosomal enzymes (Cornicelli et al. [1983]). Incubation of fibroblasts with equivalent concentrations of ammonium chloride inhibits LDL degradation, suggesting that ammonium ion secreted by porcine endothelial cells is responsible for LDL degradation in fibroblasts (Cornicelli et al. [1983]). Bovine smooth muscle and endothelial cells secrete much lower amounts of ammonium ion and LDL degradation is not inhibited (Chapter 3, Truskey and Davies [1985]).

Exocytosis of Internalized LDL Smooth muscle cells and fibroblasts are capable of returning internalized LDL to the cell surface by exocytosis (Aulinskas et al. [1981, 1985], Greenspan and St. Clair [1984]). Exocytosis accounts for as much as 20% of the ligand lost from the cell during a pulse-chase experiment. The amount of ligand undergoing exocytosis is increased after fibroblasts are incubated with lysosomotropic agents. LDL is modified during exocytosis (Greenspan and St. Clair [1984], Aulinskas et al. [1985]); only 70% is precipitated by an anti-LDL antibody, and the modified LDL exhibits a higher buoyant density than native LDL, suggesting a loss of cholesterol or an increase in protein. This modification may occur in the Golgi (Greenspan and St. Clair [1984]).

LDL Metabolism by Endothelial Cells Confluent monolayers of endothelial cells exhibit contact-inhibited regulation of LDL metabolism. Confluent bovine aortic endothelial cells bind 50% less LDL and internalize and degrade 90% less LDL than subconfluent cells (Vlodavsky et al. [1978], Fielding et al. [1979]) suggesting that cell-cell contact inhibits receptor expression as well internalization or degradation. Incubation of contact-inhibited endothelial cells in lipoprotein-deficient serum does not result in subsequent increases in receptor number or stimulation of cholesterol esterification. With confluent human and rabbit arterial and venous endothelial cells, LDL internalization and degradation are one-third their values in subconfluent cells (Henriksen et al. [1982], van Hinsbergh et al.

[1983]).

LDL receptor expression can also be influenced by the cell density of subconfluent fibroblasts, smooth muscle cells, and endothelial cells (Chait et al. [1979], Kenagy et al. [1983, 1984]). Fewer receptors are expressed at higher cell densities than at lower cell densities. As a result, LDL binding, internalization, and degradation are less at higher cell densities than at lower densities. Although cells at lower densities are more likely to divide, density dependent stimulation of LDL metabolism is independent of growth state (Kenagy et al. [1984]).

Vascular endothelial cells possess a distinct receptor for acetylated LDL (Stein and Stein [1980], van Hinsbergh [1983]), a modified form of LDL with increased negative charge, which does not bind to the LDL receptor. (Macrophages also express the receptor for acetylated LDL (Brown and Goldstein [1983]). Bovine aortic endothelial cells degrade three to nine times as much acetylated LDL as native LDL (Stein and Stein [1980]); human umbilical venous and arterial endothelial cells bind about 50% more acetylated LDL than LDL but internalization and degradation are not increased proportionately. The acetylated LDL receptor on bovine aortic endothelial cells is saturated at 10 to 20 $\mu\text{g/ml}$ (Stein and Stein [1980]). Although acetylated LDL is not formed in vivo, it serves as an analog for possible modified forms of LDL.

Incubation of rabbit aortic or human umbilical vein endothelial cells with human LDL produces a modified form of LDL which does not bind to the LDL receptor, but does bind to the acetylated LDL receptor (Henriksen et al. [1981, 1982, 1983]). Smooth muscle cells are able to modify LDL but to a reduced extent. Bovine aortic endothelial cells, however, cannot modify LDL (Henriksen et al. [1982]). Macrophages possess receptors for acetylated LDL and degrade more endothelial cell modified LDL than normal LDL. Guinea Pig smooth muscle cells,

which have fewer receptors for acetylated LDL, degrade 50% less endothelial cell modified LDL than normal LDL (Henriksen et al. [1982]).

Endothelial cell modified LDL exhibits an increased buoyant density and electrophoretic mobility. The mass fraction of cholesteryl esters decreases by 67%, with smaller decreases in cholesterol, phospholipid, and triglyceride content (Henriksen et al. [1982]). Very low density lipoprotein (VLDL) and high density lipoprotein (HDL) are not modified by endothelial cells (Henriksen et al. [1982]).

Approximately 10^7 endothelial cells can modify as much as 200 μ g of LDL in 24 hr. The modification probably occurs on the cell surface, since this amount of LDL could not be internalized in 24 hr by 10^7 cells (Henriksen et al. [1983]). Endothelial cell modification of LDL is blocked when LDL is incubated with endothelial cells in the presence of anti-oxidants, suggesting that free radical peroxidation of LDL is responsible for the modification (Steinbrecher et al. [1984]).

Endothelial cells can be grown on polycarbonate and polytetrafluoroethylene filters (Taylor et al. [1981], Baetscher and Brune [1983], Territo et al. [1984]) as well as on amnion (Furie et al. [1984]). Confluent monolayers of cells contain gap and tight junctions and exhibit an increased electrical resistance when compared to subconfluent endothelial cells (Baetscher and Brune [1983], Furie et al. [1984]). (The electrical resistance of confluent monolayers of endothelial cells *in vivo* is not known.) Confluent endothelial cells are less permeable to water, albumin, and LDL than are subconfluent cells. Permeability to LDL and albumin increases following treatment of monolayers with EDTA or as a result of monocyte migration. Permeabilities of confluent monolayers are greater than those measured *in vivo*. These systems can be of great value in studying transendothelial transport, but require further characterization and development.

1.3.2 Receptor-Independent Metabolism by Cultured Cells

In addition to receptor-mediated metabolism, macromolecules are internalized and degraded by two nonspecific mechanisms: fluid phase and adsorptive endocytosis. Although quantitative comparisons of the rate of formation of coated and uncoated vesicles are lacking, both types of vesicles may participate in receptor-independent metabolism.

Fluid Phase Endocytosis In fluid phase endocytosis solute molecules are internalized with the fluid during vesicle formation. Fluid phase endocytosis is measured using a tracer molecule which neither permeates across the cell membrane nor adsorbs on the plasma membrane (e.g. sucrose, HRP, or polyvinylpyrrolidone (PVP)) (Davies [1984]). The rate of internalization is first order in ligand concentration. Both sucrose and PVP are not hydrolyzed in lysosomes and the amount internalized increases linearly for many hours. HRP is degraded in lysosomes with a half life between 6 and 7 hr in fibroblasts and macrophages (Steinman and Cohn [1972], Steinman et al. [1976]) and 18 hr in endothelial cells (Davies and Ross [1978], Davies et al. [1981]). Initially, the cellular concentration of HRP increases and, after about an hour, reaches a plateau which represents a steady state between internalization and degradation (Davies and Ross [1978]). This quantitative discrepancy between kinetic observations and the known rate constant for HRP degradation is most likely due to the rapid exocytosis of internalized HRP (Besterman et al. [1981], Adams et al. [1982]). Fluid phase endocytosis does not occur at or below 4 °C and the process occurs with an activation energy of about 18 kcal/mole over the temperature range 4-37 °C (Steinman et al. [1974], Mahoney et al. [1977], Pratten et al. [1980]).

The rate of fluid endocytosis is usually reported in terms of the endocytotic index (EI) which is defined as the initial rate of fluid endocytosis divided by the

medium concentration and has units of $\text{nl}/(10^6 \text{ cells} \cdot \text{hr})$ or $\text{nl}/(\text{mg cell protein} \cdot \text{hr})$ (Pratten et al. [1980]). EI is analogous to a first order rate constant for a heterogeneous reaction. Using ^{14}C -sucrose as the tracer, the endocytotic index is about $50 \text{ nl}/(10^6 \text{ cells} \cdot \text{hr})$ for quiescent monkey aortic smooth muscle cells and bovine aortic endothelial cells (Davies et al. [1980], Davies [1984]). For a typical cell volume of $10^3 \mu\text{m}^3$, this corresponds to internalization of 5% of the cell volume per hr. When HRP is used as the tracer, the endocytotic index is about one-third lower. Using PVP as the tracer Leake and Bowyer [1981] have obtained endocytotic indices of $90 \text{ nl}/(\text{mg cell protein} \cdot \text{hr})$ and $56 \text{ nl}/(\text{mg cell protein} \cdot \text{hr})$ for porcine aortic smooth muscle cells and endothelial cells, respectively. Since about 0.3 to 0.7 mg cell protein is equivalent to 10^6 cells, either the endocytotic indices for porcine cells are less than the values for monkey and bovine cells or the EI measured with PVP is less than that measured with sucrose. To date, this discrepancy has not been clarified.

The rate of fluid endocytosis is greater in growing cells than in quiescent cells. As early as 6 hr after addition of PDGF to quiescent, subconfluent monkey arterial smooth muscle cells, the rate of ^{14}C -sucrose internalization increases two-fold (Davies and Ross [1980]). The rate of fluid endocytosis reaches a maximum 10 hr after addition of PDGF and remains constant for another 20 hr before declining. Fluid endocytosis in confluent cells is not altered following addition of PDGF to the medium. In growing smooth muscle (Davies and Ross [1980]) and endothelial (Davies et al. [1980]) cells, the rate of fluid endocytosis declines from $150 \text{ nl}/(10^6 \text{ cells} \cdot \text{hr})$ to $50 \text{ nl}/(10^6 \text{ cells} \cdot \text{hr})$ as the cells approach confluence. Removal of some endothelial cells from a post-confluent monolayer by scraping results in a 50% increase in the rate of fluid endocytosis by the remaining cells as measured for the entire dish; presumably the rate of endocytosis increases to a greater extent in those

cells adjacent to the scraped area than in cells farther from the scrape site.

The rate of fluid endocytosis of PVP by porcine aortic smooth muscle cells decreases 50% to 60% after incubation with colchicine (a microtubular disrupting agent) (Leake et al. [1982]), 80 mM sucrose, or chloroquine (Muir et al. [1984]). Incubation of smooth muscle cells with 80 mM sucrose or chloroquine results in the exocytosis of lysosomal enzymes (Leake et al. [1981]).

Using a cone and plate viscometer, Davies et al. [1984] have measured changes in the rate of fluid endocytosis by bovine aortic endothelial cells in response to the applied fluid shear stress. Exposure of endothelial cells to shear stresses of 1 to 15 dyne/cm² (shear rates of 150 to 2300 s⁻¹) for times ranging from 15 min to 2 hr results in up to a seven-fold increase in the rate of fluid endocytosis of HRP compared to cells incubated in the absence of shear stress. Exposure of endothelial cells to shear stress for periods longer than 2 hr does not produce any change in the rate of endocytosis relative to control cells exposed to no shear stress. Removal of cells from shear stresses after a 48 hr exposure results in an increased rate of endocytosis relative to cells not exposed to shear stress. Cells appear to respond to the magnitude of the shear stress as well as to changes in the shear stress. The rate of fluid endocytosis is unaffected by application of a rapidly oscillating shear stress (time averaged shear stress: 8 dyne/cm²) of 1 Hz in laminar flow. (This frequency is close to that of the normal human heartbeat and represents physiological oscillations in shear stress to which the endothelial cells are continuously exposed in vivo.) In contrast, the rate of endocytosis increases when cells are subjected to square wave pulses in shear stress (3 to 13 dyne/cm²; time averaged shear stress: 8 dyne/cm²) with a frequency of 1 cycle per 15 min.

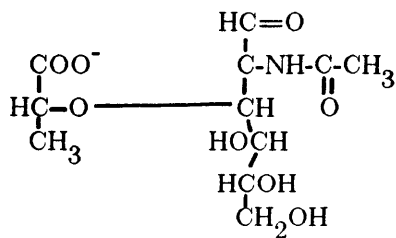
A number of cell types release internalized tracers by exocytosis (Besterman et al. [1981], Adams et al. [1982]). When cells are loaded with tracer and the loss of

tracer from the cell is measured as a function of time, exocytosis is rapid, resulting in the release of 30% to 50% of internalized tracer in about 15 min at 37 °C. After the period of rapid exocytosis most remaining pinocytotic vesicles containing tracer have fused with lysosomes, halting further exocytosis (Besterman et al. [1981]).

Nonspecific Adsorptive Endocytosis Nonspecific adsorptive endocytosis involves adsorption to the cell membrane followed by vesicle formation. Examples of molecules internalized by adsorptive endocytosis include albumin, colloidal gold, cationic ferritin, cationic HRP, HDL, and LDL (Danon and Skutelsky [1976], Skutelsky and Danon [1976], Miller et al. [1977], Williams et al. [1981], van Hinsbergh et al. [1983]). The plasma membrane on endothelial cells and smooth muscle cells contain anionic sites associated with the glycocalyx (Shiraham and Cohen [1972], Skultelsky and Danon [1976], Pelikan et al. [1979]). These sites are uniformly distributed and bind cationic ferritin and cationic HRP. At least 50% of these sites are sialic acid groups² (Skultelsky and Damon [1976]). Adsorptive endocytosis can result in the internalization of 3 to 20 times more solute than by fluid endocytosis (Miller et al. [1977], van Hinsbergh et al. [1983]). Although there are a finite number of adsorption sites, saturation has generally not been observed experimentally.

Molecular charge may also influence rates of degradation and cellular

²Sialic acids are N-acyl derivatives of neuraminic acid, such as N-acetylmuramic acid (Lehninger [1975], pp. 260,262):



Sialic acids are terminal residues on oligosaccharides of gangliosides and glycoproteins protruding from the cell membrane surface.

processing. Anionic HRP is degraded by bovine aortic endothelial cells with a half time of 96 hr, neutral HRP with a half time of 18 hr, and cationic HRP with a half time of 8.2 hr (Davies et al. [1981]). Nilsson et al. (1983) report that in rat aortic smooth muscle cells cationic ferritin appears in the Golgi apparatus before it appears in the lysosomes. Anionic ferritin, however, is not observed in the Golgi.

Receptor-Independent Metabolism of LDL Receptor-independent metabolism has been examined in culture using mutant cells lacking LDL receptors, incubation of normal cells with ^{125}I -LDL and an excess of unlabeled LDL, and chemical modification of LDL to block LDL binding. In culture, all three methods yield qualitatively similar results. Nonspecific internalization and degradation of LDL are linear functions of LDL concentration for LDL concentrations as high as 200 $\mu\text{g/ml}$ (Goldstein and Brown [1977b]). LDL internalized by nonspecific mechanisms is not able to regulate cholesterol esterification and endogenous cholesterol synthesis (Goldstein and Brown [1974], Goldstein et al. [1974]). The lack of regulation by the receptor-independent pathway may be important in the formation of atherosclerotic plaques.

Patients suffering from the homozygous form of familial hypercholesterolemia have elevated levels of cholesterol and triglycerides in their serum and die from atherosclerosis in their teens and early twenties (Goldstein and Brown [1983]). Skin fibroblasts cultured from these patients lack functional LDL receptors, and these cells are unable to regulate endogenous cholesterol production (Brown and Goldstein [1974], Stein et al. [1976], Miller et al. [1978]). Three specific defects have been identified: 1) the receptor is unable to bind to LDL; 2) the receptor binds LDL, but to a reduced extent; and 3) the receptor binds LDL in a normal fashion, but the receptor-LDL complex is not internalized (Goldstein et al. [1977]).

Biochemical studies of LDL receptor synthesis indicate that the receptor is a

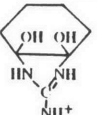
glycoprotein with a molecular weight of 160,000 g/mole. It is synthesized as a 120,000 g/mole precursor which is then enlarged in the endoplasmic reticulum (Tolleshaug et al. [1983]). A study of 77 patients homozygous for familial hypercholesterolemia showed that: 1) in 12 patients no detectable 120,000 molecular weight precursor was formed; 2) in 11 patients the 120,000 molecular weight precursor was synthesized, but was either not processed or processed incorrectly; and 3) in 54 patients at least some of the complete 160,000 molecular weight receptor was synthesized (Tolleshaug et al. [1983]).

A strain of rabbits, designated Watanabe heritable hyperlipidemic (WHHL) rabbits, has been developed. These rabbits spontaneously develop increased serum levels of cholesterol and triglycerides and exhibit aortic atherosclerosis (Watanabe [1980], Buja et al. [1983]). Like humans homozygous for familial hypercholesterolemia, fibroblasts and hepatocytes from WHHL rabbits lack functional receptors.

Chemical modification of lysine and arginine residues blocks binding to the LDL receptor, whereas modification of the cysteine residues by reductive alkylation does not inhibit binding (Weisgraber et al. [1978]). The effect of chemical modification of other amino acid residues has not been examined. Chemical modifications of lysine and arginine residues are summarized in Table 1-II. More arginine residues than lysine residues must be modified in order to block receptor binding, although the number of lysine residues required to completely inhibit binding depends upon the particular modification used. Except for reductive methylation and glycosylation, all methods of modification alter the net charge on LDL, making it more electronegative.

LDL modified by acetylation, acetoacetylation, and malondialdehyde is recognized by a receptor, known as the acetyl-LDL receptor, on macrophages,

Table 1-II: Chemical modifications of lysine and arginine residues of LDL

Treatment	Residue Modified	Structural Modification	Percent Modification to Block Binding	Electrical Charge	Reference
1,2-cyclohexanedione	arginine		55	increased negative charge	Mahley et al. [1977]
diketene (acetoacetylation)	lysine	$-\text{NH}-\overset{\text{O}}{\parallel}{\text{C}}-\text{CH}_2-\overset{\text{O}}{\parallel}{\text{C}}-\text{CH}_3$	18	increased negative charge	Weisgraber et al. [1978]
carbamylation (potassium cyanate)	lysine	$-\text{NH}-\overset{\text{O}}{\parallel}{\text{C}}-\text{NH}_2$	30	increased negative charge	Weisgraber et al. [1978]
reductive methylation	lysine	$-\text{NH}^+(\text{CH}_3)_2$	30	unchanged	Weisgraber et al. [1978]
acetylation	lysine	$-\text{NH}-\overset{\text{O}}{\parallel}{\text{C}}-\text{CH}_3$	not determined	increased negative charge	Basu et al. [1976]
glycosylation	primary amines	$-\text{NH}=\text{CH}-\overset{\text{O}}{\parallel}{\text{C}}-\text{CHOH}$	23 - 37	unchanged	Sasaki and Cottam [1982]
malondialdehyde	lysine	$-\text{N}=\text{CH}-\overset{\text{H}}{\underset{\text{HO}}{\text{C}}}-\overset{\text{OH}}{\underset{\text{HO}}{\text{C}}}-\overset{\text{H}}{\underset{\text{OH}}{\text{C}}}-\text{CH}_2\text{OH}$	not determined	increased negative charge	Fogelman et al. [1980]

Kupfer cells of the liver, and endothelial cells (Mahley et al. [1979a,c], Stein and Stein [1980], Schechter et al. [1981], van Hinsbergh et al. [1983]). The acetyl-LDL receptor is not regulated in the same fashion as the LDL receptor. When incubated with acetylated LDL macrophages, accumulate lipid and resemble foam cells found in atherosclerotic plaques, whereas when macrophages, fibroblasts, smooth muscle cells, and endothelial cells are incubated with LDL there is little lipid accumulation and cells maintain their normal appearance (Goldstein et al. [1979]).

Chemical modifications of LDL by acetylation and malondialdehyde treatment may have biological correlates. Endothelial cells and aggregated platelets modify LDL to a form which is recognized by the acetylated LDL receptor (Henriksen et al. [1982, 1982, 1983], Fogelman et al. [1980]). LDL isolated from normal and atherosclerotic human aortae by differential ultracentrifugation and anti-apoprotein B affinity chromatography is similar to plasma LDL in lipid composition, lipid/protein ratio, and size (Hoff and Gaubatz [1982]). Aortic-derived LDL does, however, show an increase in stearate content and electrophoretic mobility (Hoff and Gaubatz [1982]). Alterations in the surface charge of LDL are not related to sulfated glycosaminoglycans associated with isolated aortic LDL (Hoff and Gaubatz [1982]). LDL which accumulates within the arterial wall may represent LDL modified by endothelial cells or a subclass of LDL which is preferentially retained by the extracellular matrix and/or smooth muscle cells.

1.3.3 Receptor-Mediated and Receptor-Independent LDL Metabolism in Vivo

Receptor-mediated and receptor-independent metabolism can be examined in vivo by measuring: 1) LDL binding to freshly isolated blood cells and membranes from animal organs; 2) plasma decay and tissue uptake of normal and chemically

modified LDL; and 3) LDL metabolism in receptor-deficient animals.

Freshly isolated lymphocytes from normal humans express functional LDL receptors that regulate cholesterol metabolism, but lymphocytes from patients with homozygous familial hypercholesterolemia do not express functional receptors (Brown et al. [1980]). In cows, membrane homogenates show LDL receptor activity (Brown et al. [1980]). Tissues with the highest levels of LDL receptor activity, such as the adrenal gland and ovaries, are involved in the production of steroid hormones. Receptor activity is also present on membranes from adipose tissue, liver, heart, skeletal muscle, kidney, thymus, lung, ileum, testis, brain, jejunum, spleen, erythrocytes, and pancreas.

The contribution of receptor-mediated and receptor-independent metabolic pathways by all tissues to the plasma clearance of LDL is assessed by comparing, in the same individual or animal, the plasma decay of labeled LDL and chemically modified LDL. Since modified LDL does not bind to the LDL receptor, it would be expected that the plasma clearance of LDL modified by methods listed in Table I-II would be slower than the plasma clearance of unmodified LDL. Acetylated and acetoacetylated LDL, however, are removed more rapidly than normal LDL (Mahley et al. [1979c], Pitas et al. [1985]) which is due to uptake of acetylated acetoacetylated LDL by macrophages and Kupfer cells (Mahley et al. [1979c]).

In rat, rabbit, monkey, guinea pig, and man, LDL modified by either reductive methylation, 1,2-cyclohexanedione treatment, or glycosylation is removed more slowly from the plasma than unmodified LDL (Shepherd et al. [1979], Mahley et al. [1980], Slater et al. [1980], Sasaki and Cottam [1982], Steinbrecher et al. [1983]). Differences in the plasma decay curves of normal and chemically modified LDL are often compared in terms of the fractional catabolic rate (FCR), which represents the inverse of the mean time a molecule spends in the plasma before it is removed

irreversibly (see Chapter 4, Section 4.3, and Appendix D for additional details). The fractional catabolic rates of reductively methylated LDL, cyclohexanedione-treated LDL, and glycosylated LDL are 30% to 50% of the fractional catabolic rate of unmodified LDL. (The range in the values is due to variability among species and differences in the plasma decay of the various modified forms of LDL.) Since these modified forms of LDL can only be metabolized by nonspecific mechanisms, differences in the fractional catabolic rates suggest that 50% to 70% of all LDL degradation occurs via the receptor-mediated pathway.

In vivo studies have been conducted to examine the distribution of receptors among the various organs and tissues. Using ^{125}I -LDL and ^{125}I -labeled cyclohexanedione-modified LDL (^{125}I -CHD-LDL), Slater et al. [1980] have found that all tissues in the rabbit demonstrate some receptor activity, and the liver, spleen, and lymph nodes are the most active. Following 12 weeks of cholesterol feeding, tissue concentrations of ^{125}I -LDL and ^{125}I -CHD-LDL decreased suggesting alterations in receptor-mediated and receptor-independent metabolism.

Schnitzer [1983] has applied the method of absolute quantitative autoradiography to measure ^{125}I -LDL concentrations in selected tissues of the squirrel monkey 30 min after injection of tracer. Hepatocytes, cholesterol utilizing cells of the adrenal gland (cortical cells) and testes (Leydig cells), and renal mesangial cells exhibit the highest concentrations of ^{125}I -LDL, which probably results from receptor-mediated metabolism. Significantly lower levels are present in the adrenal medulla, zona glomerulosa, testicular germinal center, lymph nodes, and gastrointestinal tract. Focal areas of high ^{125}I -LDL concentration are observed in the arterial wall of arteries supplying the adrenal gland, lymph node, small intestine, and liver. Schnitzer [1983] suggests that measuring tracer concentrations in whole samples of fixed tissues is subject to artifacts from retained intravascular

blood and the presence of cell types with varying degrees of receptor expression.

The tissue concentration of ^{125}I -labeled proteins represents undegraded protein and does not reflect the rate of degradation or the steady state levels in each tissue. In order to measure protein degradation in vivo, Pittman and colleagues (Pittman and Steinberg [1978], Pittman et al. [1979a, 1983]) have covalently attached ^{14}C -sucrose and ^{125}I -tyramine cellobiose to proteins. Unlike ^{125}I , these labels accumulate intracellularly upon degradation of protein. Thus, tissue associated concentrations of ^{14}C -sucrose and ^{125}I -tyramine cellobiose represent total uptake, whereas protein bound ^{125}I represents nondegraded protein.

^{14}C -sucrose labeled lipoproteins have been used to study degradation sites of LDL in the rat (Pittman et al. [1982a, 1983] Carew et al. [1982], pig (Pittman et al. [1979b]), and rabbit (Pittman et al. [1982b], Navarro [1984]). Tissue concentrations have generally been measured 24 hr after injection of tracer at which time ^{14}C -sucrose radioactivity associated with the tissues is assumed to represent degraded LDL. (This assumption is only strictly true if all LDL which has accumulated has been degraded.) The liver accounts for 50% of all LDL degraded. Adipose tissue, skeletal muscle, intestine, spleen, and lung each contributed about 3% to 8% of total degradation. When tissue degradation is expressed per gram of tissue, the adrenal gland is the most active tissue, followed by liver, ovaries, spleen, and intestines. LDL degradation, as measured by the activity of ^{14}C per gram of tissue, is consistent with the results obtained with isolated membranes (Brown et al. [1980]).

Carew et al. [1982] have measured tissue activities of ^{14}C -sucrose-labeled LDL and methylated LDL in the rat 24 hr after injection. In all tissues examined activity of ^{14}C -sucrose mLDL per gram of tissue was less than or equal to the activity of ^{14}C -sucrose LDL per gram of tissue; significant differences are observed only in

those tissues with fenestrated capillaries, such as adrenal, liver, ovary, kidney, and large intestine. When rats are infused with rat LDL for 72 hr in order to raise the plasma cholesterol level, the plasma decay of ^{14}C -sucrose LDL is slowed relative to ^{14}C -sucrose-LDL plasma decay in control rats receiving a saline infusion and resembles the plasma decay of ^{14}C -sucrose mLDL. The plasma decay of ^{14}C -sucrose mLDL is the same in LDL infused and control rats. Tissue concentrations of ^{14}C -sucrose-labeled LDL and mLDL in liver, adrenal, ovary, and large intestine are similar. Thus, as a result of raising the plasma concentration of LDL, LDL receptor number declines, demonstrating that the LDL receptor is regulated *in vivo*.

Navarro [1984] has measured tissue concentrations of ^{125}I - and ^{14}C -sucrose-labeled human LDL and mLDL in rabbits for circulation times ranging from 30 min to 72 hr. In order to account for undegraded lipoprotein in the tissues, the concentration of degradation products is calculated as the difference between the mean relative tissue concentrations of ^{14}C and ^{125}I . In the liver, spleen, and kidneys, LDL degradation is significant as early as 30 min. Cumulative degradation of LDL reaches an asymptotic value between 16 and 24 hr in most tissues. For mLDL there is negligible degradation in all tissues at 30 min, and at all other times mLDL degradation is significantly less than LDL degradation. The results at longer circulation times are consistent with the results of Pittman and Carew.

Metabolic studies with ^{14}C -sucrose-labeled LDL have been extended to WHHL rabbits (Pittman et al. [1982b]). Plasma decay of LDL in WHHL rabbits is slower than in normal rabbits, and resembles plasma decay of methylated LDL. The relative contribution of individual tissues are similar in normal and WHHL rabbits, except for the adrenal gland which is more active in normal animals.

WHHL rabbits have proven to be extremely valuable models to study the role of the LDL receptor in cholesterol homeostasis (Goldstein et al. [1983b]). The

decrease in the rate of plasma clearance of LDL in these animals is due to the absence of the LDL receptor. Surprisingly, WHHL rabbits (as well as patients with familial hypercholesterolemia) show an increased rate of production of LDL which acts as a compensatory mechanism to permit sufficient cellular uptake by nonspecific mechanisms. LDL is the end product of the metabolism of very low density lipoprotein (VLDL). VLDL is converted to intermediate density lipoprotein (IDL) by lipoprotein lipase present on capillary endothelium of adipose and muscle tissue. IDL is then converted to LDL in the plasma by unknown mechanisms. Normally only 10% of the circulating IDL is converted to LDL; the remaining 90% is removed by the LDL receptor-mediated pathway in the liver. In WHHL rabbits the absence of functional LDL receptors results in the conversion of almost all IDL into LDL leading to LDL overproduction (Goldstein et al. [1983b]).

1.4 LDL Interactions with the Extracellular Matrix

Lipoproteins are found in two forms in atheromatous lesions, one which is extractable in 0.15 M saline and can be measured by immunoelectrophoresis, and another, which is not extracted in saline (Srinivasan et al. [1975a, 1978, 1980], Hollander [1976], Smith et al. [1976], Hoff et al. [1978], Bradby et al. [1979]). The tightly bound LDL is released by treatment with plasmin (Smith et al. [1976]) or a combination of collagenase and elastase (Srinivasan et al. [1978, 1980], Bradby et al. [1979]). About 13% of the total cholesterol is extracted with 0.15 M saline, 60% with collagenase, and 17% with elastase. In all three fractions lipoproteins are associated with chondroitin-6-sulfate and hyaluronic acid (Smith et al. [1976], Bradby et al. [1979]). Extracts from human fibrous plaques and fatty streaks contain about seven times more cholesterol and nine times more glycosaminoglycan than extracts from normal human intima (Srinivasan et al. [1975]). These results

are consistent with the network structure of the arterial wall in which collagen, elastin, and proteoglycan are intimately associated.

As noted previously, LDL isolated from normal and atherosclerotic aorta is similar to plasma LDL except that stearate content and electrical charge are increased in LDL isolated from the aorta. These differences between plasma and aortic LDL may reflect modification of LDL by endothelial cells (Henriksen et al. [1981, 1982, 1983]) or selective retention of a subclass of LDL (Hoff and Gaubatz [1982]).

Hoff et al. (1977, 1978, 1979) have used immunoperoxidase techniques to localize apoprotein B in human atherosclerotic lesions. Apoprotein B is localized to the surface of spherical structures with diameters ranging from 25 nm to 300 nm. These structures are associated with collagen and elastin. Morris et al. [1978] have observed that apoprotein B is associated with lipid-containing regions of collagen as well as with ruthenium red stained regions adjacent to an abnormal form of collagen (fibrous long spacing collagen).

Based upon the extractability of lipoproteins from atherosclerotic plaques with saline and specific enzymes, Hollander [1976] has suggested that LDL and VLDL are present in the arterial wall in three forms, each of which consists of a lipoprotein-glycosaminoglycan complex. The three forms include a saline extractable or unbound lipoprotein complex and lipoprotein complexes bound to collagen or elastin.

Collagen, elastin, and glycosaminoglycan content and structure in the atherosclerotic plaque are different than those of normal aorta. LDL binding to the extracellular matrix in the normal aorta is qualitatively and quantitatively different (Kramsch and Hollander [1973], Morris et al. [1978], Camejo [1982]).

1.4.1 In Vitro Studies of Lipoprotein-Glycosaminoglycans Interactions

In vitro, aortic glycosaminoglycans bind to LDL and VLDL, but not to HDL (Amenta and Waters [1960], Gero et al. [1961], Bihari-Varga and Vegh [1967]). At low ionic strengths of divalent cations, aortic extracts of glycosaminoglycans form a precipitate with apoprotein B. The precipitate can be dissolved by high concentrations of Na^+ , K^+ , NH_4^+ , and Ca^{++} . These early studies are of limited value because no distinction was made among various glycosaminoglycans and unphysiological salt concentrations were used.

Iverius [1972] has coupled aortic glycosaminoglycans to Sepharose beads and determined that glycosaminoglycan binding to LDL and VLDL is dependent upon ionic strength. LDL and VLDL behave in the same fashion. At low ionic strengths binding is negligible. As the ionic strength is increased, binding increases, reaching a maximum between ionic strengths of 0.05 and 0.15. At higher ionic strengths binding decreases until an ionic strength of 0.3 at which there is no binding. At physiological ionic strengths only heparin and dermatan sulfate bind to LDL and VLDL; chondroitin sulfate and heparan sulfate reach maximum binding at ionic strengths of 0.05, and by 0.1 binding is negligible. Modification of the charge of the lysine residues by acetylation (Iverius [1972], Mahley et al. [1979b]) or carbamylation (Mahley et al. [1979b]) blocks LDL and VLDL binding to dermatan sulfate and heparin. Reductive methylation of lysine residues, which does not alter the charge of the residue, results in only a 15% decrease in binding of LDL to heparin (Mahley et al. [1979b]).

Using the same approach as Iverius, Srinivasan et al. [1975b] and Ericson et al. [1977] have studied the effect of divalent cations on the binding of lipoproteins and heparin. At the same ionic strength, more LDL binds in the presence of divalent than monovalent cations. Binding reaches a maximum at an ionic strength of 0.1,

similar to the value observed by Iverius using NaCl. At ionic strengths above 0.1, the extent of binding depends upon the cation; binding is least for Ca^{++} and greatest for Mn^{++} . Acetylated LDL binds to heparin in the presence of Ca^{++} , although binding is qualitatively and quantitatively different than with LDL.

Glatz and Vislocky [1979] have studied the kinetics of LDL binding to heparin coupled to Sepharose 4B in a well-stirred batch reactor. Binding is rapid, reaching a steady state after 4 min. An equilibrium dissociation constant ($K_d = k_{-1}/k_1$) of $2.3 \pm 0.2 \times 10^{-6}$ M was obtained in a 0.144 NaCl and 2×10^{-3} M Ca^{++} solution buffered with 0.01 M Tris, pH 7.4. Glatz and Vislocky have analyzed their data in terms of a transport model which included a mass transfer resistance from the fluid to the bead and diffusion and binding to heparin within the bead. The mass transfer coefficient was estimated from correlations for mass transfer in agitated slurries, which yielded a value of 1.75×10^{-4} cm/s for a 35 μm bead. A diffusion coefficient of 5×10^{-8} cm^2/s was obtained by comparing model predictions with uptake in beads which did not contain heparin. Using these estimated values for the equilibrium constant, mass transfer coefficient, and diffusion coefficient, and assuming instantaneous equilibrium, Glatz and Vislocky have obtained good agreement between data and model predictions.

Taken together, these results suggest that the interaction between lipoproteins and glycosaminoglycans is rapid and ionic in nature, probably involving basic amino groups (lysine and arginine) and bridges between ionic groups by divalent cations (Srinivasan et al. [1975]). The utility of Sepharose coupled glycosaminoglycans is limited because the coupling of glycosaminoglycans to a solid support may influence glycosaminoglycan binding to LDL.

In order to avoid problems associated with immobilized glycosaminoglycans, Pan et al. [1978] have studied LDL binding to ^3H -heparin in solution. Binding of

heparin to LDL is saturable, depends upon pH, with a maximum at 8.5, and, in 0.1 M Tris, decreases with increasing concentrations of NaCl, $(\text{NH})_2\text{SO}_4$, and KH_2PO_4 ranging from 0.005 to 0.5 M. Binding was measured by separating LDL-heparin complexes from free heparin by gel chromatography on Sepahadex G-150, a method which may alter equilibrium between heparin and LDL. Fractionation of ^3H -heparin reveals that only heparin with molecular weight greater than 4000 binds to LDL. Binding of heparin to LDL is inhibited by the presence of cationic poly-DL-lysine or poly-DL-ornithine and alteration of the charge of lysine and arginine residues by acetylation and cyclohexanedione treatment, results consistent with the observations of Iverius [1972] and Mahley et al. [1979b] using immobilized heparin.

In vivo, glycosaminoglycans are attached to protein. Camejo et al. [1980] and Mourao and Bracamonte [1984] have isolated a proteoglycan from human thoracic aorta which binds LDL. The proteoglycan consists of chondroitin-6-sulfate, dermatan sulfate, and possibly heparin. The glycosaminoglycans are responsible for binding to LDL and binding depends upon pH and ionic strength.

Vijayagopul et al. [1981] have isolated a proteoglycan from bovine aorta which contains chondroitin sulfate and dermatan sulfate. LDL and VLDL form soluble and insoluble complexes with this proteoglycan, whereas HDL does not form any complexes. Insoluble complex formation depends upon calcium ion concentration, with an optimum at 30 mM. At a given concentration of proteoglycan and calcium ion, insoluble complexes contain greater amounts of LDL than VLDL, and insoluble complex formation is inhibited by albumin. Insoluble complex formation is a function of proteoglycan concentration, 150 $\mu\text{g}/\text{ml}$ LDL, insoluble complex formation reaches a maximum between 50 and 75 $\mu\text{g}/\text{ml}$ proteoglycan, and decreases at higher concentrations. The decrease in insoluble complex formation at higher proteoglycan concentrations may be due to interactions between

proteoglycan molecules. Insoluble complexes are inhibited by alteration of the charge of lysine or arginine residues by diketene modification and cyclohexanedione treatment. At low calcium concentrations (≈ 3 mM) soluble complexes between LDL and proteoglycan are formed. For an LDL concentration of 440 $\mu\text{g/ml}$, soluble complex formation saturates at a proteoglycan concentration of 150 $\mu\text{g/ml}$

1.4.2 In Vitro Studies of Lipoprotein-Elastin Interactions

Free cholesterol, phospholipids, and triglycerides from LDL and VLDL bind to delipidated aortic elastin extracts (Morris et al. [1978], Noma et al. [1981, 1983]) More lipids bind to elastin derived from atheromatous plaques than from normal intima, possibly due to an increase in the number of amino acids containing polar side groups in atheromatous plaque elastin (Morris et al. [1978], Tokita et al. [1977]). The ratio of free cholesterol and triglycerides bound to elastin is similar to the ratio in the native lipoproteins, but phospholipids bind to a decreased extent (Noma et al. [1981]). HDL inhibits LDL binding to elastin in a concentration dependent fashion which is not attributable to removal of free cholesterol from elastin by HDL (Tokita et al. [1977]).

Kramsch and Hollander [1973] report that very little LDL and VLDL protein binds to elastin after a four hour incubation at 37 °C, although by 24 hr "small amounts" of protein are bound to elastin. Noma et al. [1983] report that LDL binds to elastin after an 18 hr incubation at 37 °C. The protein to free cholesterol ratio is higher than in the native protein.

Modification of the arginine and lysine residues of LDL protein causes a decrease in protein binding to elastin (Noma et al. [1983]) This effect is not simply due to alterations of the charge on the protein, since reductively methylated LDL also binds to a lesser extent. As pH increases from 6.0 to 8.0, free cholesterol

binding decreases by 60%. Free cholesterol binding also depends upon ionic strength, reaching a maximum at an ionic strength of 0.56. Noma et al. [1983] suggest that elastin interacts separately with LDL protein, free cholesterol, phospholipid, and triglyceride and that the protein may be essential for the interactions to occur.

1.4.3 Partitioning of Macromolecules between Plasma and Tissue

The conceptual view of the extracellular matrix is that of a gel containing a network of crosslinked and entangled macromolecules and surrounding smooth muscle cells. This gel occupies a volume which is inaccessible to other molecules. The limited size of accessible or interstitial volume excludes larger molecules, resulting in partitioning between tissue and plasma. Partitioning is due to steric exclusion of macromolecules due to overlap of solute molecules with the matrix constituents (Giddings et al. [1968]), and binding of water to the extracellular matrix. Although theories have been developed to calculate the equilibrium partition coefficient for a sphere in a monodisperse network (Ogston et al. [1958], Giddings et al. [1968]), no theory is available for a polydisperse random network such as tissue, the molecular morphology of which is unknown.

Partitioning can be studied experimentally by equilibration of a solute between a fluid phase and tissue. The equilibrium partition coefficient (K_p) is defined as:

$$K_p = \frac{\langle C \rangle}{C_p} \quad (1-1)$$

where $\langle C \rangle$ is the average concentration in the interstitial fluid (mol/cm^3) and C_p is the concentration in the equilibrating fluid (mol/cm^3). $\langle C \rangle$ cannot be measured, but rather C_f , the mole/ cm^3 tissue, is determined. C_f and $\langle C \rangle$ are

related by ϵ_w , the volume of interstitial fluid per volume of tissue:

$$\frac{C_f}{C_p} = \frac{\epsilon_w \langle C \rangle}{C_p} = \epsilon_w K_p = \epsilon_f \quad (1-2)$$

Thus, by measuring ϵ_w and ϵ_f , K_p can be determined.

The interstitial volume fraction, ϵ_w , can be measured using a low molecular weight tracer which cannot permeate across the cell membrane, such as ^{14}C -sucrose, ^{14}C -inulin, or ^{14}C -mannitol. Reliable estimates for ϵ_w range from 0.33 to 0.62 with an average value of 0.43 for the thoracic and abdominal aorta and carotid artery in the dog, pig, rat, and rabbit (summarized in Harrison and Massaro [1976]).

Measurements of ϵ_f for proteins is difficult because many proteins bind to the extracellular matrix and because several hours are required for equilibration of the protein solution with the tissue which may result in swelling or other damage to the tissue. Albumin has been used by a number of investigators, although it has not been established whether it binds to the extracellular matrix. Estimates of ϵ_f for albumin range from 0.17 in the rabbit thoracic aorta (Bratzler and Schwarz [1977]) to 0.15-0.26 for canine thoracic aorta (Fry [1983]). In order to prevent osmotic gradients between tissue and medium, Bratzler and Schwarz [1977] added 4.5% (w/v) albumin to Krebs' Ringer phosphate buffer and Fry [1983] added 2% (w/v) to Dulbecco's buffered saline with glucose. When diluted serum is used, ϵ_f ranges from 0.10 to 0.13 in the canine thoracic aorta (Fry [1983]), and 0.064 to 0.11 in the rabbit thoracic aorta (Caro et al. [1980, 1981]). ϵ_f also depends upon the applied transmural pressure (Caro et al. [1981]). In the rabbit aorta, ϵ_f is 0.064 at 0 mm Hg, decreasing to 0.031 at 70 mm Hg and 0.024 at 180 mm Hg.

1.5 Experimental Studies of Macromolecular Transport and Metabolism in the Arterial Wall

Macromolecular transport in the walls of large arteries has been studied in a number of experimental animals. Radiolabeled cholesterol, fibrinogen, albumin, HDL, and LDL accumulate within the arterial wall. Uptake is subject to a number of factors, including position within the arterial tree and/or local hemodynamics, integrity of the endothelium, and blood pressure.

1.5.1 Effects of Position, Pressure, and Local Hemodynamics

The uptake of low (Evans blue dye) and high (HRP, albumin, fibrinogen, and LDL) molecular weight species is not uniform within the cardiovascular system. In laboratory animals, Evans blue permeability is greatest in the sinuses of Valsava, the ascending aorta, the coronary ostia, and the first trifurcation (Somer and Schwartz [1971], Fry [1973]). Albumin (Bell et al. [1974a]), fibrinogen (Bell et al. [1974b]), and cholesterol (Somer and Schwartz [1971]) uptake is greater in regions where Evans blue uptake is enhanced. These regions of high permeability appear to be similar to those areas where lipids accumulate in the early stages of atherosclerosis.

Focal regions of enhanced HRP uptake have been observed en face and by transmission electron microscopy (Huttner et al. [1973a,b], Stemerman [1981]). These HRP permeable regions, which range in size from 150 μm to 850 μm in diameter, are much smaller than Evans blue dye stained regions, and tend to be concentrated at the ostia of arterial branches. HRP typically stains 1% to 5% of the normal rabbit aorta (Morrel [1983]), although staining of as much as 12% of the normal rabbit thoracic aorta has been observed (Stemerman [1981]). About 45% of the thoracic aorta is stained in rabbits maintained on a hypercholesterolemic diet

for 6 weeks (Stemerman [1981]). HRP permeable regions are also permeable to LDL (Morrel et al. [1983], Tompkins [1983], Stemerman et al. [1984]). Evans blue stained regions have a 60% greater permeability to macromolecules (Bell et al. [1974a,b]) than nonstained regions, whereas LDL concentrations in HRP permeable regions are about 35 times above those in nonstained regions (Stemerman et al. [1984]) and concentrations 200 times greater than nonstained regions have been observed (Morrel [1983]). The existence of punctate regions of enhanced HRP and LDL permeability suggests the presence of focal regions where transendothelial transport has been altered, although the mechanisms involved are unknown (Stemerman et al. [1984]).

Fibrinogen (Bell et al. [1974b]), albumin (Duncan and Buck [1961], Fry [1973]) and LDL (Duncan et al. [1963]) uptake is higher in the canine aortic arch than in the canine thoracic or abdominal aorta. Bell et al. [1974a,b] suggest that uptake in the aortic arch is greater than in the abdominal aorta as a result of the greater distension of the arch during the cardiac cycle.

Focal areas of enhanced solute uptake have been associated with regions of high (Fry [1973]) and low (Caro et al. [1971], Colton et al. [1972]) shear rate (or shear stress) at the luminal surface of the arterial wall. Several in vitro studies have been carried out with fully-developed steady flow of serum to investigate the effects of shear rate, shear stress, and position on the uptake of cholesterol (Caro [1973, 1974], Caro and Nerem [1973]) and albumin (Nerem et al. [1976]). For shear stresses as high as several hundred dyne/cm², uptake increases nonlinearly with shear stress. The weak dependence on shear stress is greater for cholesterol than for albumin. Uptake is also dependent upon position. This is in contrast to the theoretical prediction for limitation of uptake rate by a developing concentration boundary layer. Moreover, the uptake rate is several orders of magnitude smaller

than predicted if the concentration boundary layer were the controlling resistance. Taken together, these results show that transport in blood is not a significant mass transfer resistance for the uptake of macromolecules and that the observed weak dependence upon shear stress represents a direct effect upon one or more transport mechanisms in the arterial wall, rather than an effect upon the concentration boundary layer thickness. Such effects might include damage to the endothelial cells resulting in increased endothelial permeability, increased transport through intercellular clefts, and increased vesicular transport (Fry [1973, 1976], Weinbaum et al. [1980]).

Substantially increased permeability in regions of much higher shear stress may be the result of alterations in the endothelial cell layer. Shear stresses greater than 400 dyne/cm^2 can tear endothelial cells from the underlying tissue (Fry [1973]). Under normal physiological conditions, the maximum shear stress in the human arterial tree has been estimated at about 200 dyne/cm^2 , less than the critical yield stress for endothelial cells.

In vivo (Duncan et al. [1962]) and in vitro (Duncan et al. [1965], Fry et al. [1981b], Fry [1983]) studies have demonstrated that albumin accumulation in the canine aorta depends on blood pressure and stretching of the arterial wall. Uptake is greatest in the ascending thoracic aorta and decreases with distance down the descending thoracic aorta. Increased pressure enhances uptake in the ascending aorta but not in the descending aorta (Duncan et al. [1965]). The regions of highest uptake are also the most distensible. Albumin uptake is also increased as a result of either steady or oscillatory stretching of tissue (Duncan et al. [1965], Fry [1983]), although others have observed no effect of stretching. This increased uptake may be due to the increase in luminal surface area upon stretching (Chien et al. [1981]). Increased blood pressure may alter the uptake process not only by increasing the

hydraulic flux, but also by increasing the normal stresses acting on the tissue. In vitro, the effect of increased pressure upon uptake is much less when the albumin solution contains serum (Fry [1983]).

In vitro, albumin permeability across canine carotid artery decreases with temperature from 37 °C to 15 °C with an activation energy of 12 kcal/mole (Siflinger et al. [1975]). Permeability of rabbit aortic endothelium to colloidal gold is unaffected by size from 14 nm to 40 nm which indicates that adsorptive endocytosis may be involved in the uptake process (Winlove et al. [1982]). As with albumin, uptake decreases when serum is added to the perfusate (Winlove et al. [1982]). Although no major loss of endothelium is observed in these in vitro studies, the integrity of the endothelium has not been assessed. Uncertainties about the metabolic state of the endothelium and underlying media are a major limitation of in vitro studies.

1.5.2 Transmural Concentration Profiles

Transmural concentration profiles have been measured for fibrinogen, albumin, and LDL in vivo. Albumin and fibrinogen profiles in the swine aorta 2 hr after injection of radiolabeled proteins show significant gradients near the lumen, suggesting entry from the blood plasma (Bell et al. [1974a,b]). Fibrinogen profiles are nearly flat except near the luminal side, whereas albumin profiles have a continuous gradient. Duncan et al. [1959] report greater albumin accumulation in the intima than in the media or adventitia. Adams et al. [1968, 1970, 1977] have observed higher levels of albumin near both the intimal and adventitial regions than in the middle of the media in rat and rabbit aortae, suggesting entry from both the lumen and the adventitia. Qualitatively similar results have been observed in vitro (Bratzler and Schwarz [1977], Fry et al. [1980, 1981a], Fry [1983], Tedgui and Lever

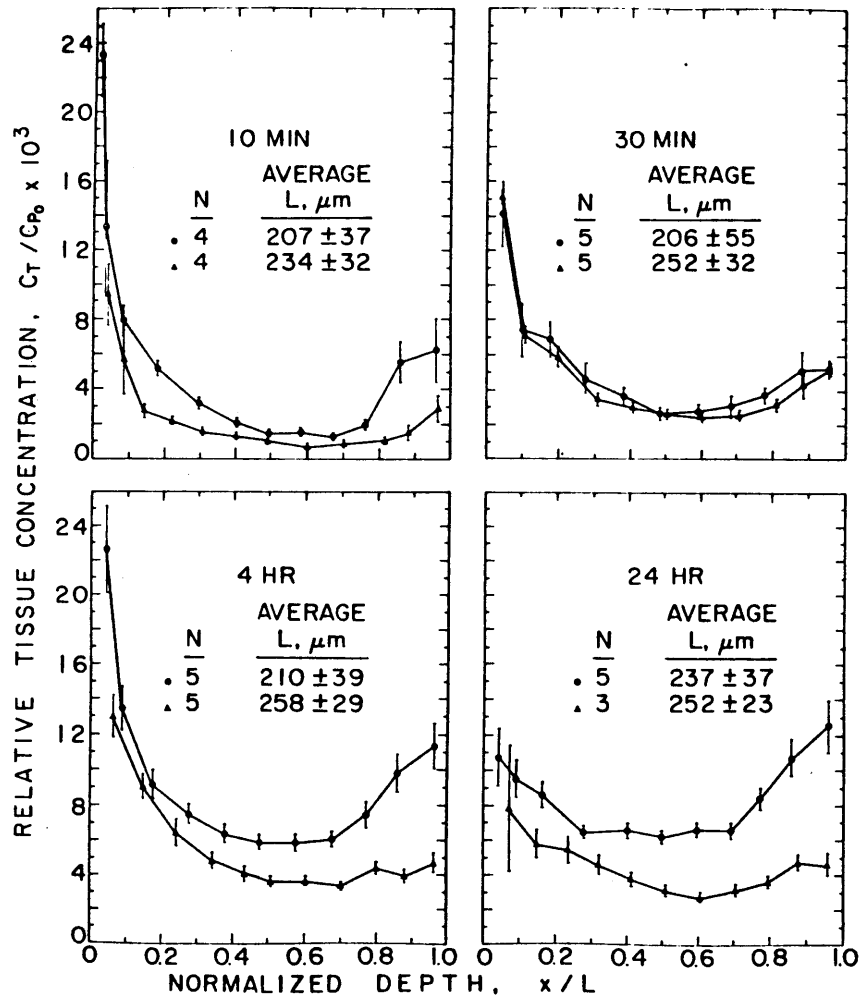


Figure 1-3: Transmurial Profiles of LDL (▲) and Albumin (●) in the Rabbit Thoracic Aorta (From Bratzler et al. [1977b])

[1985], Scott [1984]).

Bratzler et al. [1977a,b] have measured concentration profiles for ^{125}I -albumin and ^{125}I -LDL in the thoracic aorta of the rabbit using a frozen serial section microtomy technique. The results obtained with ^{125}I -LDL are qualitatively similar to those obtained with ^{125}I -albumin (Figure 1-3). Up to 4 hr after injection, transmural concentration profiles of trichloroacetic acid (TCA) precipitable radioactivity (i.e. protein bound) for both tracers have steep gradients near the intimal surface, have moderate gradients near the medial-adventitial border, and are relatively flat in the middle of the media. The results are consistent with the entry of radioiodinated protein into the media from both the luminal and adventitial sides. The steep intimal gradient have disappeared by 24 hr. Concentration levels are otherwise comparable to those at 4 hr. The relative concentration levels and the rate of influx is greater for labeled albumin than for labeled LDL, thereby suggesting that the transport mechanism(s) involved may be in part dependent on molecular size. The very low values for relative tissue concentration are noteworthy. The concentration of ^{125}I -LDL in tissue ranges from 10^{-3} to 10^{-2} times its initial concentration in plasma; the mean value reaches a maximum of about 5×10^{-3} at 4 hr following injection. The magnitudes of labeled albumin concentrations are only slightly higher than those for LDL.

Using frozen serial section microtomy, Ramirez et al. [1984] have obtained transmural profiles for ^{125}I -albumin transport across de-endothelialized rabbit thoracic aorta. In these experiments, the endothelium was removed from unconscious rabbits by means of a saline-filled Fogarty 4F arterial embolectomy balloon catheter. The profiles from anesthetized control animals are similar to those of Bratzler et al. [1977a] except that the concentration gradients are less steep at the luminal surface. Following removal of the endothelium the concentrations

increase by an order of magnitude and the shape of the profile changes indicating an increase in convective transport across the tissue (Ramirez [1979]).

Recently, the technique of quantitative autoradiography has been developed and applied to the study of LDL transport in the arterial wall (Morrel [1983], Schnitzer [1983], Tompkins [1983]). This technique allows examination of regions of tissue separated by as little as 1 μm , thus permitting detailed study of spatial variations in transport properties. Transmural profiles of ^{125}I -LDL in HRP impermeable regions of the aorta 30 min after injection are similar to those of Bratzler et al. [1977b] with two major exceptions: 1) mean relative tissue concentrations are an order of magnitude lower, and 2) concentration gradients at the medial-adventitial interface are generally not observed. Upon removal of the endothelium, ^{125}I -LDL tissue concentrations are about 50 times greater than in nonballooned control animals (Schnitzer [1983]). Moderate gradients are observed near the intimal surface.

An extensive examination of ^{125}I -LDL transmural profiles in four squirrel monkeys 30 min after tracer injection has shown that, regardless of location in the vasculature, endothelial permeability to LDL is generally low (Tompkins [1983]). Coronary and pulmonary arteries and the inferior vena cava tend to have higher permeabilities than other regions of the vasculature.

Morrel [1983] has used quantitative autoradiography to measure transmural profiles of ^{125}I -LDL in HRP-permeable regions in the rabbit aorta, which have described in Section 1.5.1. At 30 min, there are steep intimal gradients extending 20-40 μm into the media. LDL concentrations are substantially increased in a region extending 100-150 μm from the point of highest concentration. The average tissue concentration is as much as 200 times greater than in adjacent regions of lower HRP and LDL permeability.

1.5.3 LDL Metabolism in the Arterial Wall

Until recently, LDL metabolism in the arterial wall has been difficult to demonstrate. Bratzler et al. [1977a,b] have observed that trichloroacetic acid (TCA) soluble ^{125}I radioactivity in the arterial wall slowly increases with time, suggesting that some labeled protein may be catabolized to TCA-soluble fragments by aortic tissue. The use of TCA soluble ^{125}I radioactivity to assess cellular degradation in vivo is of limited value for two reasons. First, TCA soluble radioactivity represents free ^{125}I and ^{125}I -tyrosine which can be readily separated (Bierman et al. [1974]). ^{125}I -tyrosine is the byproduct of cellular degradation of ^{125}I -LDL (Goldstein and Brown [1977]). Free ^{125}I is derived from residual ^{125}I in the injectate and any ^{125}I cleaved from ^{125}I -LDL, and does not represent degraded LDL. Secondly, both ^{125}I and ^{125}I -LDL rapidly equilibrate between plasma and the arterial wall (Donovan [1980]), and tissue-associated ^{125}I -tyrosine does not necessarily represent degradation products generated by the tissue.

Mathematical models of LDL transport and metabolism in the arterial wall have been used to examine the relative importance of transendothelial transport, medial diffusion and convection, binding to the extracellular matrix and cellular uptake and degradation (Bratzler et al. [1977c], Truskey et al. [1981]). The media is represented as a continuum and species conservation equations are derived for LDL freely diffusible in the extracellular fluid, bound to the extracellular matrix, and within cells. Binding is assumed to be reversible, resulting in a non-diffusible complex. The rate of cellular permeation is assumed to be linearly proportional to the concentration difference between free and intracellular solute and the rate of degradation is represented by a reaction which is first order in the intracellular concentration.

The boundary condition at the intimal endothelium is derived from a balance

which equates convective, diffusive, and endocytotic transport across the endothelium to convection and diffusion in the media. A comparable relation is obtained at the medial-adventitial interface to describe transport between the media and capillary and lymphatic vessels.

A wide range of parameter estimates have been investigated in order to find one or more combinations which yield reasonable agreement between theoretical prediction and the experimental ^{125}I -LDL concentration profile data (Bratzler et al. [1977c], Truskey et al. [1981]). Good agreement between prediction and data for 10 and 30 min experiments is obtained with inclusion of only diffusion and convection in the media. The predicted profiles are unsatisfactory at 4 hr and longer, but agreement is improved when binding, cellular permeation, and intracellular degradation are included in the model.

The magnitudes of the parameters provide a basis for assessing the relative importance of different metabolic phenomena on ^{125}I -LDL transmural transport. Rates of intracellular permeation and degradation are rapid relative to diffusion and serve as an internal sink for the irreversible removal of LDL. This accounts for the rapid decrease in the rate of TCA-precipitable labeled LDL accumulation in the wall which is observed at times greater than 30 min (Bratzler et al. [1977a,b]). At the same time, but at a much slower rate, LDL binds to the extracellular matrix. At longer times, diffusion of free solute is in a quasi-steady state and the concentration of free solute is relatively low because it is rapidly internalized and degraded. Most of the ^{125}I -LDL is bound to the extracellular matrix. The reverse binding reaction occurs very slowly, and the small decrease in concentration after 67 hr suggests heterogeneity in binding constants, i.e, some of the ^{125}I -LDL is bound nearly irreversibly.

These theoretical analyses were performed without experimentally determined

values for metabolic terms or demonstration of degradation in the arterial wall. One of the objectives of this thesis was to determine the value of rate constants for receptor-mediated and receptor-independent LDL metabolism by smooth muscle cells and to use these constants in order to predict concentration profiles and cumulative degradation in the rabbit thoracic aorta in vivo.

Carew et al. [1984] have used ^{125}I -tyramine cellobiose labeled and ^{125}I labeled LDL and methylated LDL to assess the relative contributions of receptor-mediated and receptor-independent LDL degradation in the arterial wall for a circulation time of 24 hr. They report that the intima is responsible for 40% of all LDL and methylated LDL degraded in the aorta and receptor-mediated pathway is responsible for between 40% and 50% of the LDL degraded by the aorta. Autoradiographs of ^{125}I -tyramine cellobiose labeled LDL in the rabbit aorta 24 hr after injection depict steep intimal gradients, suggesting either severe diffusional limitations or a position dependent rate constants for LDL degradation.

1.6 Thesis Objectives

The objectives of this thesis are:

- To obtain a quantitative understanding of transport and metabolism of LDL in the arterial wall.
- To assess the relative contributions of transendothelial transport, medial diffusion, and cellular metabolism of LDL to accumulation and degradation of LDL.
- To determine the relative importance of receptor-mediated and receptor-independent metabolism.

Three approaches were taken. First, LDL metabolism by aortic smooth muscle cells was studied in cell culture. Secondly, in vivo tracer studies were performed to measure LDL tissue concentrations and cumulative degradation. Third, theoretical

models of LDL transport and metabolism in the arterial wall were developed and applied to *in vivo* data.

Figure 1-4 is an overview of the experimentation and theoretical model development. In culture, quiescent bovine aortic smooth muscle cells were incubated with radioiodinated LDL or methylated LDL and receptor-mediated and receptor-independent binding, internalization, and degradation were measured as a function of time and medium concentration. Kinetic models were used to obtain rate constants for binding, internalization, degradation, and exocytosis. These rate constants were compared with values derived from literature data. Separate experiments were performed to compare LDL metabolism by bovine and rabbit smooth muscle cells, study exocytosis directly, examine the effect of NH_4Cl on the kinetics, and estimate the number of receptors expressed *in vivo*. This is discussed in Chapter 2.

LDL metabolism by smooth muscle cells was studied after smooth muscle cells have been cocultured with endothelial cells. Kinetic models were again applied to determine rate constants. Differences between coculture and conditioned media as well as growth factor independent stimulation of LDL metabolism were studied. This is presented in Chapter 3.

LDL metabolism was studied in the rabbit *in vivo*. Radiolabeled LDL was injected, plasma concentrations were measured, and the animals were sacrificed after circulation times ranging from 0.5 to 72 hr. In one set of experiments with only ^{125}I as the label, frozen serial section microtomy was used to measure tissue concentration profiles in the aortic wall. In a second set of experiments both ^{125}I and ^{14}C -sucrose labels were used. Due to low specific activities of ^{14}C -sucrose labeled lipoproteins, tissue concentrations were measured by counting whole samples of glutaraldehyde-fixed tissue. These experiments provide data on the cumulative

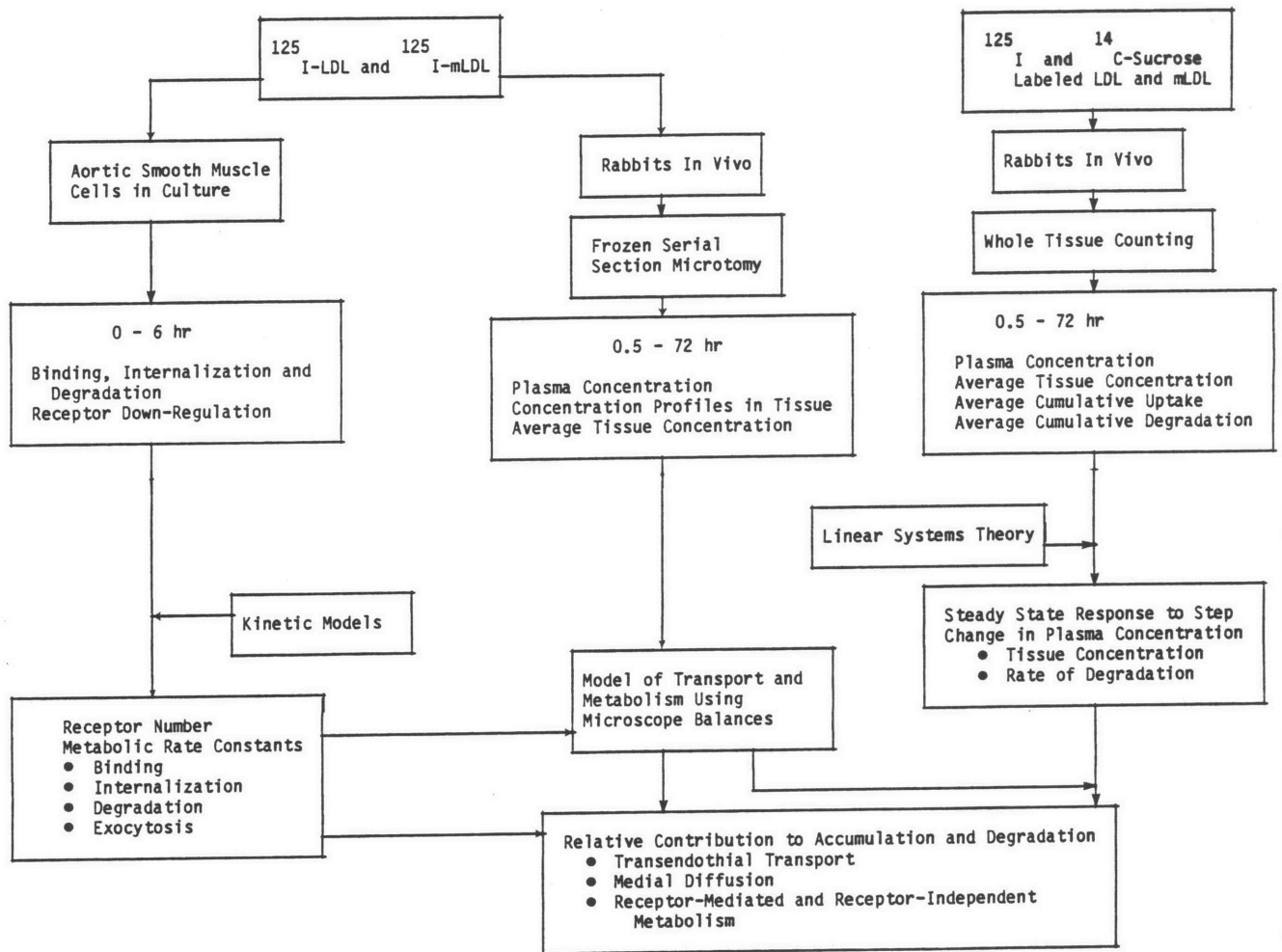


Figure 1-4: Schematic Diagram of Experimental and Theoretical Studies

uptake and degradation of LDL. Linear systems theory was used to estimate the steady state tissue concentration and rate of degradation in response to a step change in plasma concentration. These results are presented in Chapter 4.

Mathematical models were developed to describe LDL transport and metabolism in the arterial wall, incorporating kinetic models for receptor-mediated and receptor-independent LDL metabolism. Transport parameters were determined from 30 minute experiments during which metabolic phenomena are unimportant. Kinetic constants determined in culture were compared with values estimated in vivo. The results of the modeling were used to assess the relative importance of transport and metabolism. This material is discussed in Chapter 5.

Chapter 2

Kinetic Analysis of LDL Metabolism by Cultured Aortic Smooth Muscle Cells

2.1 INTRODUCTION

Cell culture is an idealized system for the study of LDL metabolism. Kinetics of receptor-mediated and receptor-independent binding, internalization, and degradation by arterial smooth muscle cells can be examined free of diffusional limitations which may occur in the vessel wall *in vivo*. In addition, LDL concentrations can be readily controlled and receptor-mediated and receptor-independent pathways can be easily distinguished (Goldstein and Brown [1977a,b]).

Cell culture is, however, not without problems. The isolation procedure may select particular subpopulations of arterial smooth muscle cells (Chamley-Campbell et al. [1979]). Primary and subcultured cells are morphologically and biochemically distinct from cells *in vivo* (Peters et al. [1972], Chamley et al. [1977], Fowler et al. [1977], Chamley-Campbell et al. [1979, 1981], Chamley-Campbell and Campbell [1981], Campbell et al. [1981], Yau-Young et al. [1981], Sprague et al. [1982], Campbell et al. [1983]). Furthermore, the constituents of the arterial wall (e.g. endothelial cells, smooth muscle cells, extracellular matrix) may further regulate LDL metabolism (Witte and Cornicelli [1980], Davies and Kerr [1982a], Witte et al. [1982]). Nevertheless, modeling LDL metabolism by cultured cells is a quantitative test of proposed mechanisms (Goldstein and Brown [1977a,b]) and will, at least, offer a first order approximation of LDL metabolism *in vivo*.

The objectives of this part of the thesis were: 1) to develop kinetic models of

receptor-mediated and receptor-independent LDL metabolism by cultured cells; and 2) to determine rate constants from data. These models formally resemble models for receptor-mediated and receptor-independent metabolism of a number of other proteins (Besterman et al. [1981], Wiley and Cunningham [1981, 1982], Bridges et al. [1982], Schwartz et al. [1982], Zigmond et al. [1982], Ciechanover et al. [1983a]).

Rate constants were determined from a single experiment by application of the minimization criterion of Box and Draper [1965] for multiple response data. The accuracy of the parameter estimates is greater than if parameters were determined by separately fitting each response (Box and Draper [1965], Hunter [1967]). Rate constants were determined by fitting experimental measurements for bovine aortic smooth muscle cells performed in this study as well as literature data for fibroblasts, smooth muscle cells, and endothelial cells from several species. In addition to studying the kinetics of LDL metabolism, experiments were conducted to: 1) examine methylated LDL metabolism; 2) directly measure exocytosis; 3) examine the effects of NH_4Cl , which inactivates lysosomal enzymes, on the kinetics; and 4) examine receptor down-regulation. The effect of interactions between endothelial cells and smooth muscle cells on LDL metabolism by smooth muscle cells is considered in the next chapter.

Kinetic models developed in this chapter along with estimated values of the rate constants were used in models of LDL transport and metabolism in the arterial wall in vivo (Chapter 5). Consequently, experimental conditions in culture were chosen to closely correspond to those in vivo. Experiments were conducted with human LDL and quiescent bovine and rabbit aortic smooth muscle cells. Human LDL was chosen because it was used in the in vivo experiments (Chapter 4). Although in vivo experiments were performed on rabbits, bovine smooth muscle cells were used in culture because of the availability of bovine aortae, ease of

isolation of bovine smooth muscle cells, and large numbers of isolated cells. Selected comparisons of the kinetics by bovine and rabbit cells were performed. Experiments were conducted with quiescent cells in order to mimic the *in vivo* growth state. Cells were incubated with lipoprotein-deficient serum in order to increase receptor expression. Additional experiments were performed to examine receptor regulation.

2.2 QUALITATIVE PRESENTATION OF EXPERIMENTAL OBSERVATIONS

In order to provide a framework for the theoretical models discussed below, experiments typical of those described in the literature are discussed. LDL is used as a model ligand throughout, not only because of its relevance to the subject of this thesis, but also because of the wealth of data available.

Qualitative results from a typical set of experiments at 37 °C are presented in Figure 2-1. These results are representative of data obtained with growing and quiescent fibroblasts, smooth muscle cells, and endothelial cells. Cells are grown on plastic petri dishes and form a flat, subconfluent monolayer. At the beginning of the experiment, radiolabeled LDL is added to the culture medium and, at various intervals, LDL bound to the cell surface, internalized, and degraded is measured by procedures discussed in Materials and Methods (Section 2.4). The concentration of radiolabeled LDL added to the medium ranges from 1 µg/ml to 150 µg/ml, and incubation periods range from 1 min to 360 min. Incubation times are sufficiently short that receptor regulation, which occurs with a half-time of 20 hr (Brown and Goldstein [1975]), is unimportant.

The results in Figure 2-1 represent the total amounts bound, internalized, and degraded by the cells and are usually expressed as (ng LDL protein)/(mg cell protein) or (ng LDL protein)/(10⁶ cells). Surface binding increases rapidly at first

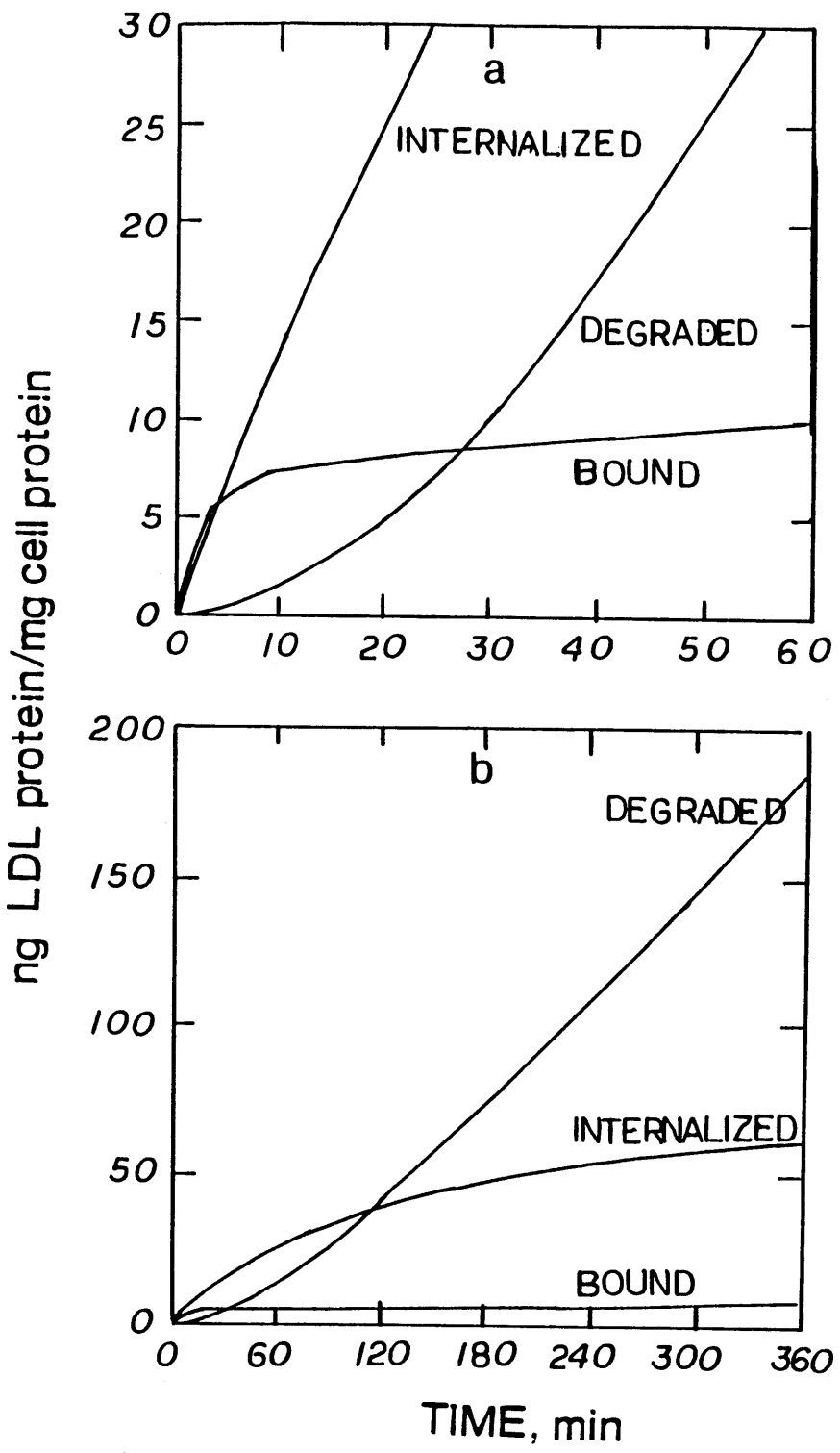


Figure 2-1: Qualitative Description of Typical Experiment at 37 °C. Binding, internalization, and degradation were measured as a function of time for 10 $\mu\text{g/ml}$ ^{125}I -LDL

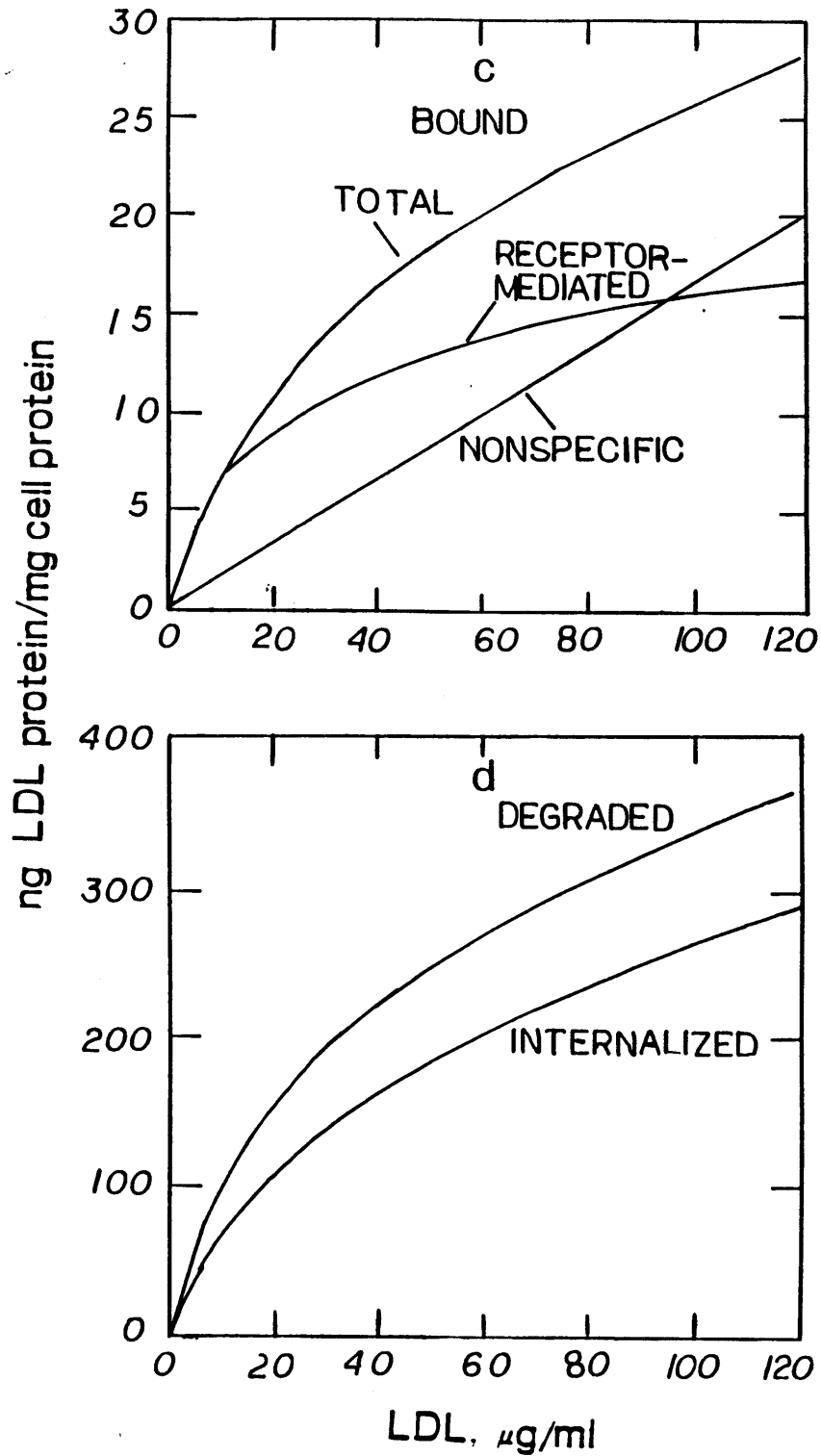


Figure 2-1 (continued) ^{125}I -LDL binding, internalization, and degradation were measured as a function of concentration at four hr.

(Figure 2-1a), due to formation of LDL-receptor complexes. At later times, receptor binding reaches a steady state, and the small increase in surface binding with time reflects nonspecific adsorption to the cell membrane and extracellular matrix. Internalization is rapid, with an initial rate slightly less than the initial rate of binding (Figure 2-1a). The steady state amount internalized per mg cell protein (Figure 2-1b), reached after two to four hours, reflects a balance between internalization and degradation by receptor-mediated and receptor-independent mechanisms. Amino acids, representing protein degradation products, appear in the extracellular medium after a lag time (Figure 2-1a) ranging from 5 to 30 min (Anderson et al. [1977a]). The lag time probably results from the transport of LDL, which is in endocytotic vesicles, to lysosomes. Protein degradation products are measured in terms of ^{125}I -tyrosine, the major radiolabeled product. Greater than 95% of all degradation products are present in the medium (Goldstein and Brown [1974]). After two to three hours the rate of degradation becomes constant. For typical experiments of six hr duration, the total amount of LDL bound, internalized, and degraded represents between 1% and 10% of the initial amount of LDL added to the medium.

The sketches in Figure 2-1c,d represent binding, internalization, and degradation as a function of LDL concentration after a four hr incubation. At low concentrations the receptor-mediated pathway dominates and the curves resemble Langmuir adsorption isotherms. At higher concentrations, receptors are saturated, nonspecific mechanisms dominate, and binding, internalization, and degradation increase linearly with concentration (shown for bound LDL in Figure 2-1c).

Another typical experiment which yields insight into the relationship between bound, internalized, and degraded LDL is the so-called pulse-chase experiment. Cells are incubated with radiolabeled LDL at 4 °C (pulse), after which the medium

is removed and cells are washed to remove unbound LDL, and fresh medium is added, without labeled LDL. The cells are warmed to 37 °C and binding, internalization and degradation are measured after various incubation times (chase). In order to assess receptor-mediated metabolism, a separate group of cells undergo the same procedure except that, during the pulse period, cells are incubated with radiolabeled LDL and an excess of unlabeled LDL. Radiolabeled LDL bound, internalized, and degraded in the presence of an excess of unlabeled LDL represents nonspecific metabolism. Receptor-mediated metabolism is determined by subtracting the nonspecific contribution from total levels of bound, internalized, and degraded LDL.

Results from a typical pulse-chase experiment are presented in Figure 2-2. Data are presented as fractions of the initial amount bound. The decrease in binding is exponential and represents internalization of receptor-ligand complex and dissociation of ligand from the receptor. Intracellular LDL increases at first, representing internalization, and eventually reaches a maximum as receptor-bound LDL on the surface approaches zero. As significant amounts of intracellular LDL are degraded, the concentration decreases and the amount degraded increases. The relationship between binding, internalization, and degradation in the pulse-chase experiment is similar to that observed for molecules involved in a sequential chemical reaction.

2.3 Model Development

2.3.1 Kinetic Model for Receptor-Mediated Metabolism

In general, the ligand binds reversibly to a receptor on the cell surface. the receptor-ligand complex is internalized by the formation of a coated vesicle. Once formed, vesicles rapidly lose their clathrin coat. Ligand dissociates from the receptor

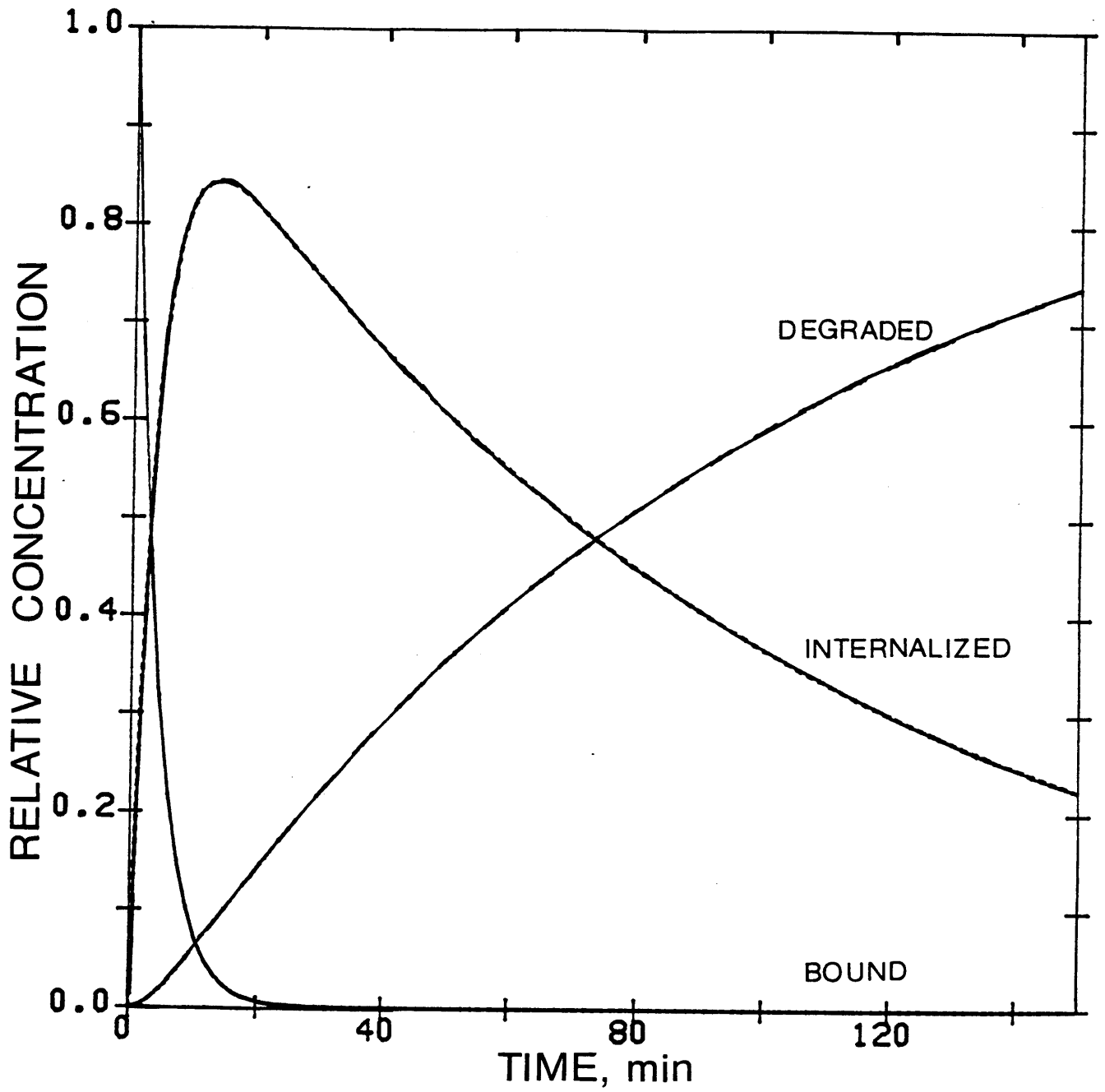


Figure 2-2: Results from a Typical Pulse-Chase Experiment

in the vesicle (or endosome), and ligand is either returned to the medium by exocytosis or is degraded in secondary lysosomes.

The first step in receptor-mediated metabolism involves the reversible binding of ligand to its receptor on the cell surface. Receptors can be divided into two classes (Kaplan [1981]). Class I receptors are activated by ligand binding which subsequently alters either membrane permeability to small ions or the concentration of intracellular mediators. Although ligand-receptor complex internalization occurs via coated vesicles, it is not necessary for ligand function. Examples of class I receptors are receptors for growth factors (Carpenter and Cohen [1975]), insulin (Marshall and Olefsky [1980]), and chemotactic peptides (Zigmond et al. [1982]). Class II receptors act primarily to internalize ligands; alterations in cell behavior result from the metabolism of internalized ligand. Examples of class II receptors include receptors for LDL (Goldstein and Brown [1977a,b]), asialoglycoproteins (Bridges et al. [1982], Schwartz et al. [1982]), and transferrin (Ciechanover et al. [1983a]). Although the models described below have been developed for ligands internalized by class II receptors, they apply equally well to ligands internalized by class I receptors. The models explicitly describe the metabolism of only the labeled portion of the ligand, which is generally the protein moiety.

The formation of the ligand-receptor complex is a reversible bimolecular reaction between ligand and receptor:



where L represents the free ligand, R the receptor, and LR the receptor-ligand complex. [L] has units of μg ligand protein/ml (or mol/l) and [R] and [LR] have units of ng ligand protein/(mg cell protein) (or mol/(mg cell protein)).

At 4 °C, vesicle formation and ligand internalization do not occur. Pitas et al. [1979] have determined that, for LDL binding to its receptor at 4 °C, $k_1 = 3.3 \times 10^6 \text{ M}^{-1}\text{min}^{-1}$, $k_{-1} = 3.8 \times 10^{-3} \text{ min}^{-1}$, and $K_d = k_{-1}/k_1 = 1.14 \times 10^{-9} \text{ M}$. From Scatchard analysis of equilibrium measurements, Pitas et al. found that K_d is equal to $2.8 \pm 0.4 \times 10^{-9} \text{ M}$, in close agreement with kinetic studies.

Class II receptors are randomly distributed over the plasma membrane surface (Bretscher [1984]). Internalization of receptor-ligand complex occurs in clathrin-coated pits which comprise about 2% of the membrane surface (Anderson et al. [1976, 1977]). Receptors diffuse on the cell surface until they contact coated pits which are believed to contain binding sites for receptors. Some receptors require ligand binding before binding to coated pits (Ciechanover et al. [1983b]), whereas other receptors (e.g. LDL) bind to membrane proteins in coated pits even in the absence of ligand (Anderson et al. [1976, 1977], Vermeer et al. [1980]). For those receptors which require ligand binding before binding to coated pits, ligand binding may induce a conformational change in the receptor, enabling it to bind to the coated pit.

Once within the coated pit, the ligand-receptor complex is internalized by the formation of coated vesicles 50 nm to 150 nm in diameter (Anderson et al. [1977a], Pearse and Bretscher [1981]). Vesicle formation occurs continuously, regardless of the presence of ligand. The mean lifetime of a coated pit is between 2 and 5 min (Anderson et al. [1976, 1977a], Vermeer et al. [1980], Pearse and Bretscher [1981], Brown et al. [1983]). Internalization of LDL (Brown et al. [1983]), transferrin, and insulin (Ciechanover et al. [1983b]) receptors is independent of the presence of ligand, since these receptors bind to coated pits even in the absence of ligand. Asialoglycoprotein receptors and epidermal growth factor receptors require ligand binding before binding to coated pits and are therefore internalized only after ligand

binding (Pastan and Willingham [1981]).

The rate of internalization of receptor-bound ligand depends upon the fraction of receptors in coated pits. This fraction depends upon the flux of receptors in and out of coated pits and the affinity of receptors for binding sites in the coated pits. For receptors which bind to coated pit proteins in the absence of ligand, the rate of receptor localization in coated pits is (Goldstein et al. [1981, 1984], Wolfsky and Goldstein [1984]):

$$\frac{d[R_p]}{dt} = k_+[P][R_n] - (k_- + \lambda)[R_p] \quad (2-2)$$

where $[R_p]$ is the surface concentration of receptors in coated pits, $[R_n]$ is the surface concentration of receptors not in coated pits, $[P]$ is the number density of coated pits per unit area of cell surface, k_+ (cm^2/min or cm^2/s) and k_- (min^{-1} or s^{-1}) are, respectively, associative and dissociative rate constants for receptor binding to the coated pits, and λ (min^{-1}) is the rate constant for vesicle formation. The first term on the right hand side of (2-2) represents receptor binding to the coated pit, the second term represents receptor dissociation, and the third term represents internalization. The rate of receptor internalization is first order in the receptor concentration in the coated pit.

At steady state, the fraction of receptors in coated pits is obtained by rearranging equation (2-2):

$$\frac{[R_p]}{[R_n] + [R_p]} = \frac{k_+[P]}{k_- + \lambda + k_+[P]} \quad (2-3)$$

Equation (2-3) has been used by Goldstein et al. [1981] to estimate k_+ at 37 °C. For human fibroblasts at 4 °C, the fraction of LDL receptors in coated pits ($[R_p]/([R_n]+[R_p])$) is 0.69 ± 0.11 (Anderson et al. [1976, 1977a]). The distribution at 37 °C is believed to be similar (Anderson et al. [1982]) and the surface density of

coated pits on the cell surface at 37 °C is $r[P_{4^{\circ}\text{C}}]$, where $[P_{4^{\circ}\text{C}}]$ is the surface density of coated pits at 4 °C and r is the ratio of the number of coated pits on the surface at 37 °C to the number of coated pits at 4°C. Goldstein et al. [1981] have calculated values of 0.53 ± 0.10 and $0.58 \pm 0.05 \mu\text{m}^{-2}$ for r and $[P_{4^{\circ}\text{C}}]$, respectively, from electron microscopy studies of Anderson et al. [1977a,b], Vermeer et al. [1980], and Orci et al. [1978]. This yields an estimate of $[P]$ equal to $0.31 \pm 0.09 \mu\text{m}^{-2}$. Goldstein et al. [1981] have estimated λ to be $0.25 \pm 0.05 \text{min}^{-1}$ from data of Brown and Goldstein [1976] and Goldstein et al. [1976]. For irreversible binding of receptor to the coated pit, $k_- = 0$, Goldstein et al. [1981] obtained $2.4 \times 10^{-10} \text{cm}^2/\text{s}$ for k_+ . If k_- is nonzero, then k_+ must be even larger.

An upper limit for k_+ has been estimated for diffusion limited binding of LDL receptors to coated pits on fibroblasts (Goldstein et al. [1981, 1984]). The membrane is modeled as a two dimensional surface with coated pits acting as absorbing disks. Each pit is characterized by a radius s and a mean lifetime of $1/\lambda$, which represents the time required to form a vesicle. Two models of coated pit recycling have been considered by Goldstein et al. [1984]. In one model, the coated pit returns to the same position it previously occupied (Pastan and Willingham [1981, 1983]). In the other model, the coated pit reforms at a new location (Anderson et al. [1977b]). k_+ is evaluated as the flux of receptors at the coated pit divided by the average concentration of receptors outside the pits. For $\lambda = 0.25 \text{min}^{-1}$ and receptors with diffusion coefficients greater than $10^{-11} \text{cm}^2/\text{s}$, Goldstein et al. [1984] have found that k_+ is independent of the particular model for coated pit recycling because the time required for the receptor to diffuse to a coated pit is shorter than the time required for the coated vesicle to recycle back to the membrane.

For the LDL receptor on human fibroblasts, the diffusion coefficient is $4.5 \times$

10^{-11} cm²/s at 28 °C (Barak and Webb [1982]) from which Goldstein et al. [1984] have estimated that k_+ is about 2×10^{-10} cm²/s and about 60% of the receptors are in coated pits for $\lambda = 0.25$ min⁻¹, which is close to the experimentally observed value of 0.69 ± 0.11 . A similar calculation for EGF ($D=8 \times 10^{-10}$ cm²/s; Hillman and Schlesinger [1982]) indicates that all of the receptors are located in coated pits for $\lambda < 0.5$ min⁻¹.

The rate of internalization (r_i) of receptor-bound ligand complex is first order in the concentration of receptor-ligand complex in the coated pit:

$$r_i = \lambda[LR_p] \quad (2-4)$$

LDL binds to all receptors on the cell surface (Anderson et al. [1976]). Receptor regulation occurs with a half-time of 20 hr (Brown and Goldstein [1975]) and the response to growth factors occurs with a half time of about 5 hr (Witte et al. [1980]). These events are slow relative to receptor diffusion and binding to coated pits, which takes only a few minutes. Thus, the receptor distribution is at steady state under most experimental conditions. If binding of the receptor to the coated pit does not alter the rate constants for ligand-receptor binding, the fraction of the ligand-receptor complex in coated pits is equal to the fraction of receptors in coated pits (equation (2-3)) and the rate of internalization is:

$$r_i = \frac{\lambda k_+[P][LR]}{k_- + \lambda + k_+[P]} \quad (2-5)$$

where [LR] is the total concentration of ligand-receptor complex on the cell surface. Equation (2-5) is strictly valid for receptors which bind to coated pits regardless of the presence of the ligand, and which are regulated slowly relative to receptor binding to coated pits and internalization. For simplicity, $\frac{\lambda k_+[P]}{k_- + \lambda + k_+[P]}$ is set equal to k_2 , the rate constant for ligand internalization by receptor-mediated endocytosis.

At 37 °C, the coated pit concentration is constant (Anderson et al. [1982]). For slow diffusion of receptors relative to internalization and slow dissociation of receptors from coated pits, (i.e. $k_+[P] \ll \lambda$) k_2 is equal to $k_+[P]$ and is limited by receptor diffusion into coated pits. If receptor diffusion is rapid relative to vesicle formation (i.e. $k_+[P] \gg k_- + \lambda$), k_2 is approximately equal to its maximum value, λ .

k_2 for a number of ligands is presented in Table 2-I. (Estimation of the rate constants from literature data is presented more fully in Appendix A.) The half-times range from 1.5 to 4.6 min, similar to estimates obtained for vesicle internalization. The variability among the estimates may reflect differences in the growth states of the cells, as well as differences among cell types and species.

Following internalization, vesicles rapidly lose their clathrin coat and become acidified (Tycko and Maxfield [1982]). In the acidic environment, ligand dissociates from its receptor (Dautry-Varsat et al. [1983]) and the receptor is removed from the vesicle (or endosome) and recycled to the cell membrane where it undergoes another round of binding and internalization. During this time endosome size increases as a result of fusion of endosomes with each other. The endosome, containing free ligand, eventually fuses with either a lysosome, wherein the ligand is degraded, or the cell membrane, releasing the ligand back into the extracellular medium (exocytosis). Exocytosis may occur after passage through the Golgi apparatus (Greenspan and St. Clair [1984]). Mechanisms involved in sorting vesicles for exocytosis or vesicle-lysosome fusion are not known.

For LDL, the overall process can be described schematically:

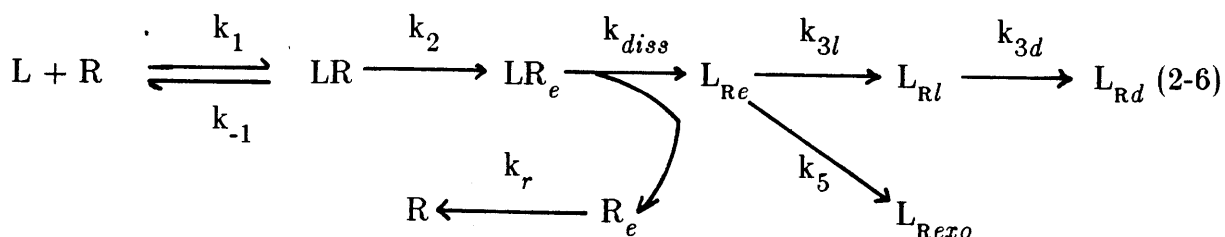
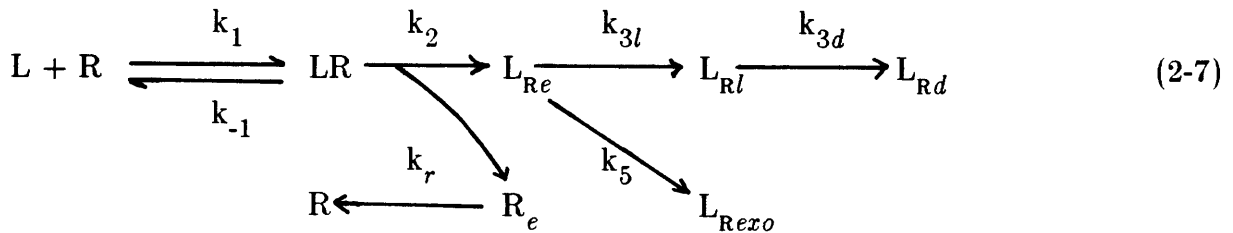


Table 2-I: Rate Constants for Receptor-Mediated Internalization

Ligand	Cell Type	k_2, min^{-1}	$t_{1/2}, \text{min}$	Growth State	Reference
Epidermal Growth Factor	human fibroblasts	0.17	4.1	growing, subconfluent	Wiley and Cunningham[1981]
Human asialoorosomuroid	rat hepatocytes	0.39	1.8	freshly isolated	Weigel and Oka [1982]
	human hepatoma	0.2	3.5	freshly isolated	Bridges et al. [1982]
	human hepatoma	0.47	1.5	growing, subconfluent	Schwartz et al. [1982]
Rabbit transferrin	rabbit reticulocytes	0.45	1.5	freshly isolated	Iacopetta and Morgan [1983a]
Human transferrin	human hepatoma	0.25	2.8	growing, subconfluent	Ciechanover et al. [1983]
Human LDL	human fibroblasts	0.20-0.23	3.0-3.5	growing, subconfluent	Brown and Goldstein [1976]
				growing, subconfluent	Goldstein et al. [1977]
Chemotatic peptides	rabbit leukocytes	0.15	4.6	freshly isolated	Zigmond et al. [1982]

where LR_e represents receptor-bound ligand in endosomes; L_{Re} , free ligand in endosomes, R_e , free receptor in endosomes; L_{Rl} , free ligand in lysosomes; L_{Rexo} , ligand returned to the medium by exocytosis; and L_{Rd} , degraded ligand. The notation L_R is used to denote ligand which is metabolized by the receptor-mediated pathway as opposed to ligand which is metabolized by the receptor-independent pathway. Concentrations of endosomal, lysosomal, degraded ligand, and ligand which has undergone exocytosis are in units of (ng ligand protein)/(mg cell protein). k_{diss} (min^{-1}) is the rate constant for receptor-ligand dissociation in the endosomes, k_r (min^{-1}) is the rate constant for receptor recycling, k_{3l} (min^{-1}) is the rate constant for delivery of ligand to lysosomes, k_{3d} (min^{-1}) is the rate constant for lysosomal degradation of ligand and k_5 (min^{-1}) is the rate constant for exocytosis. k_{-1} and k_{diss} represent values of the rate constant for receptor-ligand dissociation at two different values of pH.

Ligand-receptor dissociation in the acidified endosome occurs rapidly and is probably not limiting for subsequent metabolism (Brown et al. [1983]). Thus, internalized ligand is assumed to be dissociated from the receptor and equation (2-6) can be simplified:



Material balances on bound, endosomal, lysosomal, and degraded LDL are:

$$\frac{d[LR]}{dt} = k_1[L][R] - (k_{-1} + k_2)[LR] \quad (2-8)$$

$$\frac{d[L_{Re}]}{dt} = k_2[LR] - (k_{3l} + k_5)[L_{Re}] \quad (2-9)$$

$$\frac{d[L_{Rl}]}{dt} = k_{3l}[L_{Re}] - k_{3d}[L_{Rl}] \quad (2-10)$$

$$\frac{d[L_{Rd}]}{dt} = k_{3d}[L_{Rl}] \quad (2-11)$$

The rate of accumulation of receptor-bound ligand on the cell surface (equation (2-8)) is equal to the difference between the rate of ligand binding and the rates of ligand-receptor dissociation and internalization. Accumulation in vesicles (equation (2-9)) is a balance among vesicle formation and internalization, vesicle-lysosome fusion, and exocytosis. Accumulation in lysosomes (equation (2-10)) is a balance between vesicle-lysosome fusion and lysosomal hydrolysis.

Cell surface receptor number is a balance among receptor synthesis, receptor recycling, internalization of receptor and receptor-ligand complex, and degradation of receptor. For measurements of LDL metabolism which occur over time scales short relative to the time for down-regulation of the receptor (20 hr) the number of receptors on the cell surface is constant (Brown and Goldstein [1975]), implying that receptor recycling and synthesis are exactly balanced by receptor internalization and degradation. Thus:

$$[R_T] = [R] + [LR] \quad (2-12)$$

Inserting equation (2-12) into equation (2-8) and rearranging yields:

$$\frac{d[LR]}{dt} = k_1[L][R_T] - (k_1[L] + k_{-1} + k_2)[LR] \quad (2-13)$$

The amount of ligand bound, internalized, and degraded is, at most, a few

percent of the amount of ligand initially added to the medium, and the ligand concentration is approximately constant ($[L] = [L_o]$) (Goldstein and Brown [1976]). For constant ligand concentration, equations (2-9) to (2-11) and (2-13) are linear first order ordinary differential equations which were solved by standard methods (Hildebrand [1976]). At $t=0$, all cell associated concentrations are zero, and the solution to these equations is:

$$[LR] = \frac{[R_T][L_o]}{K_{int} + [L_o]} (1 - e^{-kt}) \quad (2-14)$$

$$[L_{Re}] = \frac{k_2[R_T][L_o]}{K_{int} + [L_o]} \left[\frac{1 - e^{-k_x t}}{k_x} - \frac{e^{-kt} - e^{-k_x t}}{k_x - k} \right] \quad (2-15)$$

$$[L_{Rl}] = \frac{k_2 k_{3l} [R_T][L_o]}{K_{int} + [L_o]} \left[\frac{1}{k_x} \left(\frac{1 - e^{-k_{3d} t}}{k_{3d}} - \frac{e^{-k_x t} - e^{-k_{3d} t}}{k_{3d} - k_x} \right) - \frac{1}{k_x - k} \left(\frac{e^{-kt} - e^{-k_{3d} t}}{k_{3d} - k} - \frac{e^{-k_x t} - e^{-k_{3d} t}}{k_{3d} - k_x} \right) \right] \quad (2-16)$$

$$[L_{Rd}] = \frac{k_2 k_{3l} k_{3d} [R_T][L_o]}{K_{int} + [L_o]} \left\{ \frac{1}{k_x} \left[\frac{tk_{3d} - (1 - e^{-k_{3d} t})}{k_{3d}^2} - \frac{1}{k_{3d} - k_x} \left(\frac{1 - e^{-k_x t}}{k_x} - \frac{1 - e^{-k_{3d} t}}{k_{3d}} \right) \right] - \frac{1}{k_x - k} \left[\frac{1}{k_{3d} - k} \left(\frac{1 - e^{-kt}}{k} - \frac{1 - e^{-k_{3d} t}}{k_{3d}} \right) - \frac{1}{k_{3d} - k_x} \left(\frac{1 - e^{-k_x t}}{k_x} - \frac{1 - e^{-k_{3d} t}}{k_{3d}} \right) \right] \right\} \quad (2-17)$$

where $K_{int} = \frac{k_{-1} + k_2}{k_1}$, $k = k_1[L_o] + k_{-1} + k_2$, and $k_x = k_{3l} + k_5$. The total intracellular concentration ($[L_{Ri}]$) is equal to the sum of $[L_{Re}]$ and $[L_{Rl}]$. K_{int} is analogous to the Michaelis constant in enzyme kinetics and $K_{int}/[L_o]$ represents the ratio of the time for ligand binding to the time for disappearance of receptor bound

ligand from the cell surface by dissociation and internalization. k and k_x (min^{-1}) represent, respectively, lumped first order rate constants for binding and loss of ligand from the cell by degradation and exocytosis.

Equations (2-8) to (2-11) can be simplified further by lumping the endosomal and lysosomal compartments into a single intracellular compartment. Lumping is strictly valid if degradation is rapid relative to endosome-lysosome fusion. There is limited data to support this simplifying assumption. Electron microscopy studies of receptor-mediated metabolism of LDL, epidermal growth factor, and asialoglycoprotein indicate that there is a delay ranging from 5 to 30 min before ligand is observed in lysosomes (Anderson et al. [1977a,b], Wall et al. [1980], Pastan and Willingham [1981], Willingham and Pastan [1981], Merion and Sly [1983]). Herman and Albertini [1984] used time-lapse video intensification microscopy to examine the fate of fluorescently labeled LDL by granulosa cells. Following LDL binding, endosomes and lysosomes undergo a spatial reorganization, moving to the nuclear region where they fuse. Lysosome-endosome fusion begins about 30 min after LDL is added. Fusion of endosomes and lysosomes is blocked by addition of microtubule disrupting agents. Furthermore, studies with isolated uncoated vesicles and lysosomes in vitro indicate that fusion of these two organelles is rapid, with a half-time of about 2 min, and coated vesicles are unable to fuse with lysosomes (Altstiel and Branton [1983]). These results suggest that endosome transport is the rate-limiting step for delivery of ligand to lysosomes.

For degradation limited by vesicle-lysosome fusion ($k_{3l} \ll k_{3d}$), the pseudo-steady state approximation can be applied to equation (2-10) to yield:

$$\frac{d[L_{Ri}]}{dt} \approx 0 \quad (2-18a)$$

and

$$[L_{Ri}] = \frac{k_{3l}[L_{Re}]}{k_{3d}} \quad (2-18b)$$

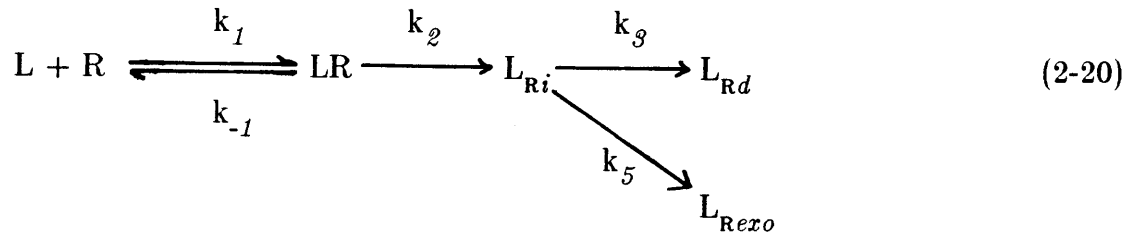
The total intracellular concentration, $[L_{Ri}]$, which is equal to the sum of endosomal and lysosomal concentrations, can then be expressed in terms of $[L_{Re}]$:

$$[L_{Ri}] = [L_{Re}] + [L_{Rl}] = \left([L_{Re}] \left(1 + \frac{k_{3l}}{k_{3d}} \right) \right) \quad (2-19a)$$

With the assumption that $k_{3l} \ll k_{3d}$, equation (2-19a) simplifies to:

$$[L_{Ri}] \approx [L_{Re}] \quad (2-19b)$$

Thus, the intracellular concentration is approximately equal to the endosomal concentration. With these simplification, the model represented by (2-7) becomes:



Material balances on these species are:

$$\frac{d[LR]}{dt} = k_1[L_o][R_T] - k[LR] \quad (2-21)$$

$$\frac{d[L_{Ri}]}{dt} = k_2[LR] - (k_3 + k_5)[L_{Ri}] \quad (2-22)$$

$$\frac{d[L_{Rd}]}{dt} = k_3[L_{Ri}] \quad (2-23)$$

where k_3 is equal to k_{3l} . In this simplified model (equations (2-21) to (2-23)) the

rates of ligand degradation and exocytosis are first order in the total intracellular concentration of ligand.

The solutions to equations (2-21) to (2-23) are:

$$[LR] = \frac{[R_T][L_o]}{K_{int} + [L_o]} \left(1 - e^{-kt}\right) \quad (2-24)$$

$$[L_{Ri}] = \frac{k_2[R_T][L_o]}{K_{int} + [L_o]} \left(\frac{1 - e^{-k_x t}}{k_x} - \frac{e^{-kt} - e^{-k_x t}}{k_x - k} \right) \quad (2-25)$$

$$[L_{Rd}] = \frac{k_2 k_3 [R_T][L_o]}{K_{int} + [L_o]} \left[\frac{tk_x - (1 - e^{-k_x t})}{k_x^2} - \frac{1}{k_x - k} \left(\frac{1 - e^{-kt}}{k} - \frac{1 - e^{-k_x t}}{k_x} \right) \right] \quad (2-26)$$

An additional simplification in the above models has also been considered, that exocytosis is negligible (i.e. $k_5 = 0$). Since only the total intracellular concentration is measured experimentally, the model represented by (2-7) is indistinguishable from the model represented by equation (2-20) for the case of no exocytosis.

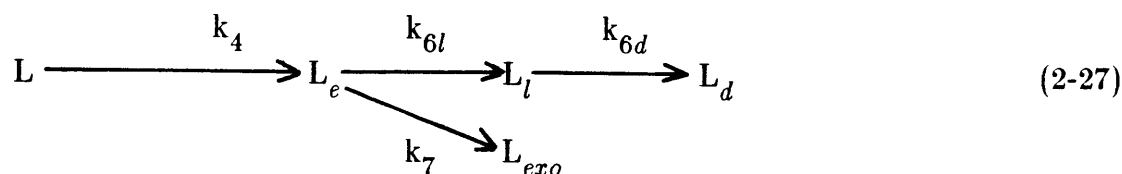
Examination of published data indicates that dissociation of the receptor is slow relative to internalization of receptor-ligand complex (i.e. $k_{-1} \ll k_2$) and k_{-1} can be neglected (see Appendix A). Use of this observation reduces the number of constants to be determined.

2.3.2 Kinetic Model for Receptor-Independent Metabolism

In addition to the receptor-mediated pathway, uptake can also be by nonspecific mechanisms - fluid endocytosis and adsorptive endocytosis. The role of uncoated and coated vesicles in nonspecific uptake mechanisms has not been established. Endocytosis of proteins by endothelial and smooth muscle cells is often

associated with newly formed or forming uncoated vesicles (Florey and Shepherd [1970], Casley-Smith and Chin [1971], Schwartz and Benditt [1972], Coltoff-Schiller et al. [1976], Nilsson et al. [1983]). In a study of ferritin-labeled LDL uptake by human fibroblasts, Anderson et al. [1977b] observed regions of the cell membrane in the process of forming uncoated vesicles, but LDL-ferritin complexes were not associated with these structures. Vasile et al. [1983], however, observed LDL particles associated with coated and uncoated regions of the rat aortic endothelium in situ.

Although the mechanisms involved in receptor-independent internalization have not been clearly established, this pathway can be represented schematically as:



where L_e and L_l represent endosomal and lysosomal solute internalized by receptor-independent mechanisms, respectively, L_d represents degraded solute, and L_{exo} represents solute which has been returned to the medium by exocytosis. Unlike receptor-mediated endocytosis, the rate of uptake is linearly proportional to the ligand concentration with rate constant k_4 (ml medium/(mg cell protein · min)). k_4 represents a first order rate constant for a heterogenous reaction and is analogous to the endocytotic index (Section 1.3.2). This model of receptor-independent internalization is strictly true if nonspecifically adsorbed ligand is in a quasi-steady state and the ligand concentration is significantly below saturation. These assumptions are examined further in Sections 2.5.7 and 2.6. Receptor-independent internalization and degradation of LDL by fibroblasts are linear in ligand concentration for concentrations as high as 150 $\mu\text{g/ml}$ (Brown and Goldstein [1976]).

Vesicle-lysosome fusion, degradation, and exocytosis are analogous to the same processes described for the receptor-mediated pathway. Since the mechanisms may differ, the rate constants are assumed to be different. For solute internalized by nonspecific mechanisms, k_{6l} (min^{-1}) is the rate constant for delivery of solute to the lysosomes, k_{6d} (min^{-1}) is the rate constant for degradation of solute, and k_7 (min^{-1}) is the rate constant for exocytosis.

For constant ligand concentration, material balances for internalized and degraded ligand are:

$$\frac{d[L_e]}{dt} = k_4[L_o] - (k_{6l} + k_7)[L_e] \quad (2-28)$$

$$\frac{d[L_l]}{dt} = k_{6l}[L_e] - k_{6d}[L_l] \quad (2-29)$$

$$\frac{d[L_d]}{dt} = k_6[L_l] \quad (2-30)$$

where $[L_o]$ is the medium concentration (ng/ml), $[L_e]$ and $[L_l]$ are the concentrations (ng/(mg cell protein)) of solute in the endosomes and lysosomes, $[L_d]$ is the concentration (ng/(mg cell protein)) of degradation products in the extracellular medium, and $[L_{exo}]$ is the concentration (ng/(mg cell protein)) of solute which has been returned to the medium by exocytosis.

At the beginning of an experiment, solute of concentration $[L_o]$ is added to the medium and intracellular and degraded concentrations are zero. For this set of initial conditions, the solutions to equations (2-28) to (2-30) are:

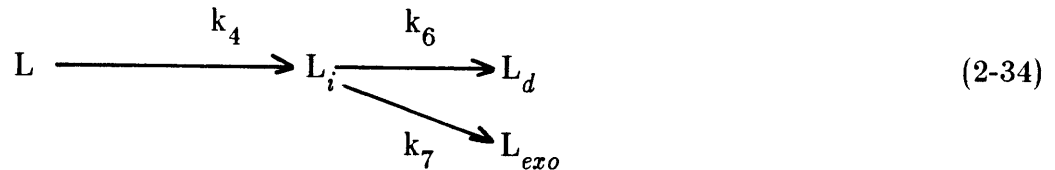
$$[L_e] = \frac{k_4[L_o]}{k_{6l} + k_7} \left(1 - e^{-(k_{6l} + k_7)t} \right) \quad (2-31)$$

$$[L_i] = \frac{k_4 k_{6l} [L_o]}{k_{6l} + k_7} \left(\frac{1 - e^{-k_{6d}t}}{k_{6d}} - \frac{e^{-(k_{6l} + k_7)t} - e^{-k_{6d}t}}{k_{6l} + k_7 - k_{6d}} \right) \quad (2-32)$$

$$[L_d] = \frac{k_4 k_{6l} k_{6d} [L_o]}{k_{6l} + k_7} \left[\frac{t}{k_{6d}} - \frac{1 - e^{-k_{6d}t}}{k_{6d}^2} - \frac{1}{k_{6l} + k_7 - k_{6d}} \left(\frac{1 - e^{-(k_{6l} + k_7)t}}{k_{6l} + k_7} - \frac{1 - e^{-k_{6d}t}}{k_{6d}} \right) \right] \quad (2-33)$$

The total intracellular concentration of ligand internalized nonspecifically is equal to the sum of equations (2-31) and (2-32).

Equations (2-28) to (2-30) can be simplified by lumping the endosomal and lysosomal concentrations. If degradation is rapid relative to vesicle-lysosome fusion (i.e. $k_{6l} \ll k_{6d}$), then $[L_i] \ll [L_o]$ and the total intracellular concentration ($[L_i]$) is approximately equal to $[L_e]$. For this limiting case, equation (2-27) becomes:



For constant ligand concentration, material balances for internalized and degraded ligand are:

$$\frac{d[L_i]}{dt} = k_4 [L_o] - (k_6 + k_7) [L_i] \quad (2-35)$$

$$\frac{d[L_d]}{dt} = k_6 [L_i] \quad (2-36)$$

The solutions to equations (2-35) and (2-36) are:

$$[L_i] = \frac{k_4[L_o]}{k_6 + k_7} \left(1 - e^{-(k_6 + k_7)t} \right) \quad (2-37)$$

$$[L_d] = \frac{k_4 k_6 [L_o]}{k_6 + k_7} \left(t - \frac{1 - e^{-(k_6 + k_7)t}}{k_6 + k_7} \right) \quad (2-38)$$

2.3.3 Parameter Estimation

Ligand binding, internalization, and degradation are multiple responses which depend upon two independent variables, time and concentration. If only a single response is measured, such as internalization, the rate constants are determined by minimization of the sums of squares of the deviations between experimental observations and the predicted value:

$$SS(\mathbf{b}) = \sum_{i=1}^m (y_i - f(\mathbf{b}, \mathbf{x}_i))^2 \quad (2-39)$$

where y_i is the value of the dependent variable or response at the i^{th} measurement, \mathbf{b} is the estimate of the parameter vector, \mathbf{x}_i is the value of the vector of independent variables at the i^{th} measurement, and $f(\mathbf{b}, \mathbf{x}_i)$ is the model-generated value. If more than one response is available, then parameter estimates are improved by using all of the measured responses (Box and Draper [1965]).

If the variance-covariance matrix of the responses is known, then the minimization is simply a generalization of least squares (Box and Draper [1965], Hunter [1967]):

$$SS(\mathbf{b}) = \sum_{s=1}^n \sum_{t=1}^n \sigma^{st} \sum_{i=1}^m (y_{is} - f_s(\mathbf{b}, \mathbf{x}_i))(y_{it} - f_t(\mathbf{b}, \mathbf{x}_i)) \quad (2-40)$$

where y_{is} and y_{st} represent, respectively, the values of the s^{th} and t^{th} responses, $f_s(\mathbf{b}, \mathbf{x}_i)$ and $f_t(\mathbf{b}, \mathbf{x}_i)$ are the corresponding model-generated values, and σ^{st} is an element of the inverse of the covariance matrix (with elements σ_{st}). Quite often this variance-covariance matrix is unknown, and Box and Draper [1965] have used

Bayes' theorem to derive a generalized minimization criterion for the regression of multiresponse data. The criterion requires the minimization of the following determinant \mathbf{F} :

$$\det(\mathbf{F}) = \begin{vmatrix} \sum_{i=1}^m e_{i1}^2 & \sum_{i=1}^m e_{i1}e_{i2} \cdots & \sum_{i=1}^m e_{i1}e_{in} \\ \sum_{i=1}^m e_{i2}e_{i1} & \sum_{i=1}^m e_{i2}^2 \cdots & \sum_{i=1}^m e_{i2}e_{in} \\ \vdots & \vdots & \vdots \\ \sum_{i=1}^m e_{in}e_{i1} & \sum_{i=1}^m e_{in}e_{i2} \cdots & \sum_{i=1}^m e_{in}^2 \end{vmatrix} \quad (2-41)$$

where e_{ir} is the error of the i^{th} observation of the r^{th} response

$$e_{ir} = (y_{ir} - f_r(\mathbf{b}, \mathbf{x}_i)) \quad (2-42)$$

The diagonal terms in equation (2-41) represent the sums of squares associated with each response and the off-diagonal terms represent the sums of cross-products of the responses. (Derivation of equation (2-41) is discussed in Appendix B.) The matrix \mathbf{F} is symmetric and represents the Bayesian estimate of the variance-covariance matrix. For a single response ($r=1$), equation (2-41) reduces to the familiar form for least squares, equation (2-39).

The simplest multiple response problem involves two responses, which corresponds to experimental data for receptor-independent internalization and degradation. For this case, equation (2-41) becomes:

$$\det(\mathbf{F}) = \begin{vmatrix} \sum_{i=1}^m e_{i1}^2 & \sum_{i=1}^m e_{i1}e_{i2} \\ \sum_{i=1}^m e_{i2}e_{i1} & \sum_{i=1}^m e_{i2}^2 \end{vmatrix} \quad (2-43a)$$

$$\det(\mathbf{F}) = \sum_{i=1}^m e_{i1}^2 \sum_{i=1}^m e_{i2}^2 - \left(\sum_{i=1}^m e_{i1} e_{i2} \right)^2 \quad (2-43b)$$

In each of the terms of the determinant of \mathbf{F} , the residuals from one response act as weights for the residuals of the other response (Box and Draper [1965]). As a result, even if one response is larger in magnitude than the other, the determinant of \mathbf{F} is not biased towards this response.

For three responses, corresponding to receptor-mediated metabolism in which bound, internalized, and degraded solute are measured, equation (2-41) becomes:

$$\begin{aligned} \det(\mathbf{F}) = & \sum_{i=1}^m e_{i1}^2 \sum_{i=1}^m e_{i2}^2 \sum_{i=1}^m e_{i3}^2 + 2 \sum_{i=1}^m e_{i1} e_{i2} \sum_{i=1}^m e_{i2} e_{i3} \sum_{i=1}^m e_{i1} e_{i3} \\ & - \left(\sum_{i=1}^m e_{i1} e_{i3} \right)^2 \sum_{i=1}^m e_{i2}^2 - \left(\sum_{i=1}^m e_{i2} e_{i3} \right)^2 \sum_{i=1}^m e_{i1}^2 \\ & - \left(\sum_{i=1}^m e_{i1} e_{i2} \right)^2 \sum_{i=1}^m e_{i3}^2 \end{aligned} \quad (2-44)$$

As with two responses, the residuals from one response are weighted by those from the other two responses.

Minimization of equation (2-41) has proven to be computationally inefficient (Jutan [1976]). As a result, the minimum of $\det(\mathbf{F})$ was determined by an iterative approach developed by Jutan [1976]. The advantage of this approach is that it reduces minimization of equation (2-41) to minimization of equation (2-40) which is a generalized form of least squares that can be solved using standard techniques for nonlinear regression.

The algorithm is as follows. An initial guess of the parameter vector, \mathbf{b}_0 , is supplied from which the matrix \mathbf{F} is calculated. $\mathbf{F}(\mathbf{b}_0, \mathbf{x}_i)$ serves as an estimate of

the variance-covariance matrix. Equation (2-40) is then solved and a new estimate of \mathbf{b} is obtained from which \mathbf{F} is recalculated. This process continues until both the parameter vector \mathbf{b} and $\det(\mathbf{F})$ change by less than some specified tolerance.

Marquardt's method was used in the iterative process to determine the best fit value of the parameters. This method is a compromise between steepest descent and linearization methods (Marquardt [1963]). Steepest descent is used initially to determine a region in the parameter space in which a Taylor series approximation of the model function is valid. The linearization method is then used to determine the minimum of $\det(\mathbf{F})$. Mathematically, the parameter estimation algorithm requires solution of the following system of equations (Marquardt [1963]):

$$(\mathbf{A} + \lambda\mathbf{I})\mathbf{d} = \mathbf{g} \quad (2-45)$$

where \mathbf{d} is the correction vector of the parameters:

$$\mathbf{d} = \mathbf{b} - \mathbf{b}_0 \quad (2-46a)$$

and

$$\mathbf{A} = \mathbf{X}^T\mathbf{F}^{-1}\mathbf{X} \quad (2-46b)$$

$$\mathbf{g} = \mathbf{X}\mathbf{F}^{-1}\mathbf{e} \quad (2-46c)$$

The matrix \mathbf{X} is the Jacobian matrix of the parameters with elements:

$$X_{ik} = \sum_{s=1}^n \frac{\partial e_{is}}{\partial \beta_k} \quad (2-46d)$$

\mathbf{e} is the error vector, $(e_{i1} \ e_{i2} \ \cdots \ e_{is})$, e_{ir} is defined by equation (2-42), β_k are elements of the parameter vector \mathbf{b} , and \mathbf{F}^{-1} is the inverse of the estimated variance-covariance matrix. Derivatives were calculated numerically:

$$\frac{\partial e_{is}}{\partial \beta_k} \approx \frac{e_{is}(\beta_k + \delta\beta_k) - e_{is}(\beta_k)}{\delta\beta_k} \quad (2-46e)$$

The covariance matrix of parameters was calculated in a manner analogous to that for a single response (Himmelblau [1970], p. 197):-

$$\text{cov}(\mathbf{b}) = \frac{\det(\mathbf{F})}{m-n} (\mathbf{X}^T \mathbf{X})^{-1} \quad (2-47)$$

where m is the number of data sets and n is the number of parameters. The variance of the fitted parameters is given by the diagonal elements of the covariance matrix (equation (2-47)). The standard deviation is simply the square root of the variance. Also of interest is the correlation coefficient matrix of the parameters. The correlation between parameters β_k and β_l is defined as:

$$\rho_{kl} = \frac{\text{cov}(\beta_k \beta_l)}{\text{var}(\beta_k) \text{var}(\beta_l)} \quad (2-48)$$

For $k = l$, $\text{cov}(\beta_k \beta_k) = \text{var}(\beta_k)^2$ and $\rho_{kk} = 1$. ρ_{kl} ranges in value from -1 to 1; a negative correlation coefficient indicates that the value of parameter k decreases as the value of parameter l increases, whereas a positive correlation coefficient indicates that the value of parameter k increases as the value of parameter l increases. A correlation coefficient with an absolute value greater than 0.95 suggests that parameters k and l are highly correlated and the model may contain too many parameters to adequately fit the data (Draper and Smith [1981]).

Computer codes for the minimization program are presented in Appendix H. The program output includes the initial guess, the value of $\det(\mathbf{F})/(m-n)$, the estimated covariance matrix \mathbf{F} , the number of iterations required to reach convergence, the best fit values of the rate constants and the linearized estimate of the standard deviation, the matrix of correlation coefficients, and the value of the

residuals.

2.4 MATERIALS AND METHODS

Smooth Muscle Cell Culture Bovine smooth muscle cells were cultured from explant outgrowths by the method of Ross [1971]. The adventitia and outer media were carefully removed from sterile bovine thoracic aortae (J.J. Trelegan and Sons, Cambridge, MA) in a laminar flow tissue culture hood. The ends of the aortae were cut off and discarded. The inner media and intima were washed several times with Dulbecco's modified Eagle's medium (DMEM) supplemented with 2 μ mol/ml glutamine and 100 unit/ml each of penicillin and streptomycin (M.A. Bioproducts, Walkersville, Md). Endothelial cells were removed by scraping the intimal surface with a scalpel blade. The media was cut into 2 mm squares and placed in 100 mm diameter petri dishes. A drop of 10% (v/v) calf serum (M.A. Bioproducts) in DMEM (10% CS-DMEM) was placed on each square and the dishes were maintained in a humidified incubator at 37 °C (95% air, 5% CO₂). After 24 hr, the medium was removed and enough 10% CS-DMEM was added to submerge the tissue slices. The medium was changed every other day. Typically three aortae were used to prepare explant cultures. Throughout the course of the experimental program, bovine smooth muscle cells were obtained from 30 different aortae. No attempt was made to compare LDL metabolism by cells from different explants.

After 7 to 10 days, the remaining bits of tissue were removed and the cells which grew out of the tissue were allowed to reach confluence (primary culture). At confluence, cells were passaged (2:1) by trypsinization (3 ml of 2.5% trypsin in modified Hanks' balanced salt solution without Ca⁺⁺ and Mg⁺⁺ (M.A. Bioproducts) for 3 to 4 min at 37 °C). Cells passaged after the first trypsinization were labeled the first subculture. All cells were in subcultures 2 or 3 at the time of

the experiment. For an experiment, cells were trypsinized and plated at 5×10^4 cells/35mm dish in 10% CS-DMEM. The cells were maintained in a humidified incubator at 37 °C and 95% air and 5% CO₂. After 48 hr, the cells were washed once with Hanks' balanced salt solution (HBSS) and the medium was replaced with 5% (v/v) plasma derived serum in Dulbecco's modified Eagle's medium to arrest cell growth.

Plasma-Derived and Lipoprotein-Deficient Serum Plasma-derived serum (PDS) was prepared by the method of Vogel et al. [1978]. Cationic growth factors were removed by passage over a carboxymethyl-Sephadex (CM-50, Pharmacia Fine Chemicals, Piscataway, NJ) chromatography column. The resulting PDS was dialyzed against phosphate buffered saline, pH 7.4, concentrated to 50 mg protein/ml by ultrafiltration, and stored frozen. Protein concentrations were measured by the method of Lowry et al. [1957].

Lipoprotein-deficient serum (LPDS) was prepared by a modification of the method of Weinstein et al. [1976]. Human plasma (American Red Cross, Boston, MA), was dialyzed against three changes of 6 l each of 0.15 M NaCl 0.001 M Na₂EDTA (solution A), pH 8.6, at 4 °C for 24 hr. The density of the plasma was adjusted to 1.25 g/cm³ by addition of NaBr (Hatch and Lees [1968]). The solution was centrifuged for 48 hr at 60,000 rpm in a Beckman Ti 60 rotor at 15 °C. The bottom fraction was isolated and dialyzed for 24 hr against 2 changes of 4 l each of 0.1 M Tris buffer, pH 7.4, at 4 °C. The solution was then passed over a CM-50 column to remove cationic growth factors, concentrated to 50 mg protein/ml by ultrafiltration, and dialyzed against phosphate buffered saline, pH 7.4.

Total, free, and esterified cholesterol in one preparation of LPDS were measured by Barbara Eisehaure at Brigham and Women's Hospital using the methods of Gamble et al. [1978] and Heider and Boyett [1978]. Total cholesterol

concentration was 39.8 $\mu\text{g/ml}$, free cholesterol concentration was 16.3 $\mu\text{g/ml}$, and esterified cholesterol concentration was 23.5 $\mu\text{g/ml}$. A discussion with Jerry Faust of the University of Texas Health Science Center at Dallas indicated that these concentrations fell within the range of values typically obtained with LPDS.

Isolation and Radiolabeling of LDL LDL was isolated from recovered human plasma (American Red Cross, Boston, MA) by a modification of conventional precipitation techniques (Cornwall and Kruger [1961], Burstein et al. [1970]). Two units of plasma were dialyzed for 24 hr against three changes of 6 l each of 0.15 M NaCl ($\rho = 1.006 \text{ g/cm}^3$) containing 1 mM Na_2EDTA , pH 8.6, at 4 °C. 35 ml aliquots of plasma were pipetted into centrifuge tubes to which were added 1.4 ml containing 5000 units/ml sodium heparin (Sigma Chemical Company, St. Louis, MO) and 1.75 ml 1 M MnCl_2 . The tubes were mixed, stored on ice for 30 min, and then centrifuged for 30 min at 4 °C at 2400 rpm (1100 g) in a 7 inch swinging bucket rotor (Model PR-6, Damon/IEC, Needham Heights, MA). The supernatant was aspirated from each tube, and the precipitate containing the β -lipoproteins was solubilized by the addition of 2.0 ml of 2 M NaCl containing 1 mM Na_2EDTA , pH 8.6 to each tube. Following prolonged mixing, any undissolved residue was physically removed. The contents of the tubes were pooled, and the volume brought up to 45 ml with 2 M NaCl containing 1 mM Na_2EDTA , pH 8.6. 7.0 ml of this protein solution was pipetted into each of six centrifuge tubes (nominal volume 13.2 ml) (Beckman Instruments Inc., Wakefield, MA) on top of which were layered 3.5 ml of 0.15 M NaCl. The tubes were centrifuged in an SW 41 rotor (Beckman) at 41,000 rpm at 15 °C for 20 hr. The LDL band was removed by puncture of the tube with a 25 gauge needle (1.5 - 2 ml per tube). The LDL was pooled and dialyzed at 4 °C for 24 hr against three changes of 2 l each of solution A, pH 8.6. Purity was assessed by double radial immunodiffusion, immunoelectrophoresis, and

cellulose acetate electrophoresis (Hatch and Lees [1968]). Protein content was measured by the method of Lowry et al. [1957].

LDL was iodinated with Na^{125}I (New England Nuclear, Boston, MA) by the method of McFarlane [1958] as modified by Bilheimer et al. [1972]. Non-protein-bound radioactivity was removed by passing over a PD-10 column (G-50, Pharmacia Fine Chemicals) which was followed by dialysis against solution A, pH 8.6, at 4°C. Greater than 97% of the total ^{125}I was precipitable in 10% trichloroacetic acid. By chloroform-methanol extraction (Folch et al. [1957]) only 2% of label was associated with lipid. Protein content of ^{125}I -LDL was determined and specific activities have ranged from 100 to 400 cpm/ng protein.

Methylation of LDL Lysine residues of ^{125}I -LDL were methylated by a modification of the methods of Means and Feeney [1968] and Weisgraber et al. [1978] (Figure 2-3). To a 1 ml solution containing 6 - 10 mg LDL in solution A, pH 8.6, were added 0.5 ml 0.3 M sodium borate buffer, pH 9.0, and 1 mg sodium borohydride (Sigma Chemical Co.), followed by six 1 μ l additions of 37% (w/v) aqueous formaldehyde (Fischer Scientific Co.) over the next 30 min. After the last addition the reaction mixture was dialyzed overnight at 4 °C against solution A, pH 8.6.

The extent of modification was assessed by the trinitrobenzene sulfonic acid (TNBS) test (Habeeb [1966]). To 1 ml of protein solution (0.6 - 1.0 mg/ml) was added 1 ml 4% (w/v) NaHCO_3 , pH 8.5, and 1 ml 0.1% (v/v) aqueous TNBS. The solution was incubated for 2 hr at 40 °C. 1 ml of 10% (w/v) sodium dodecyl sulfate was then added to solubilize the protein and prevent its precipitation upon addition of 0.5 ml 1 N HCl. The mixture was allowed to sit for 30 min, after which the absorbance at 280 nm was measured. Typically, methylation of LDL resulted in a 36% reduction in absorbance relative to unmodified LDL indicating that 36% of the

REDUCTIVE METHYLATION OF LDL

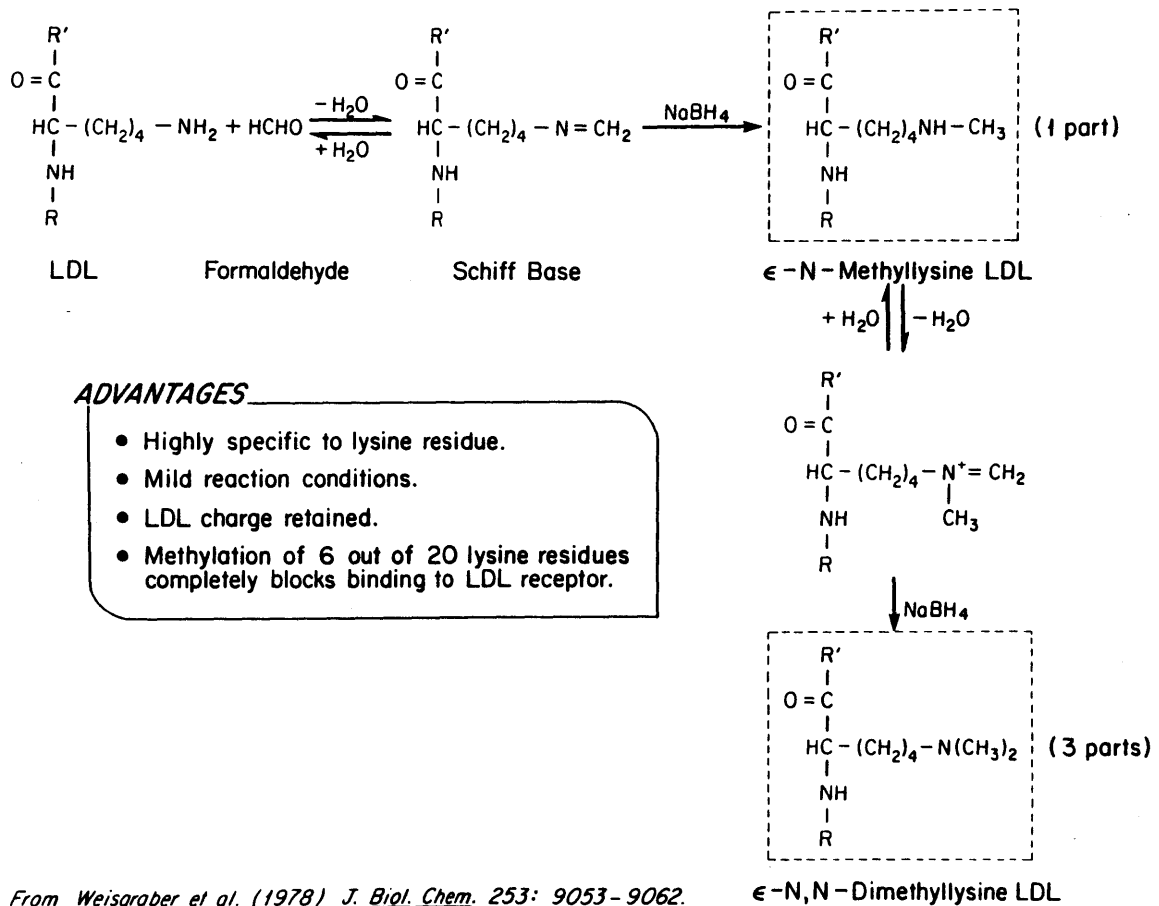


Figure 2-3: Schematic of LDL Methylation

lysine residues were modified. This modification was sufficient to inhibit more than 95% of the binding ability of LDL to its receptor. Results of the TNBS test are presented in Appendix F.

Lipoprotein Metabolism Binding, internalization, and degradation of ^{125}I -LDL were determined using standard procedures (Goldstein et al. [1983a]). Subconfluent cultures of quiescent smooth muscle cells were incubated with lipoprotein-deficient, growth factor-deficient serum for 48 hr. Cells were incubated with ^{125}I -LDL at 37 °C for periods appropriate to each experiment. At the end of the experiment, the dishes were rapidly chilled to 4 °C and the medium was removed for the determination of LDL degradation. The cells were washed eight times with HBSS containing 2 mg/ml bovine serum albumin, followed by one rinse with HBSS alone. The cells were incubated at 4°C with HBSS containing 10 mg/ml sodium heparin (Grade 1, Sigma Chemical Co., St. Louis, MO) for one hour to release LDL from its receptors on the cell surface (Goldstein et al. [1976]). The heparin-containing medium was removed and counted to determine the amount of binding. The cells were then rinsed once with HBSS and were dissolved in 0.1% (w/v) sodium dodecyl sulfate for determination of cell associated ^{125}I (internalized LDL) and total cellular protein. LDL degradation was determined as trichloroacetic acid-soluble ^{125}I -tyrosine activity in the culture medium. Free ^{125}I was removed by oxidation to iodine and partition into chloroform (Bierman et al. [1974]).

In all experiments, receptor-independent LDL binding, internalization, and degradation were determined by incubation of a second group of quiescent smooth muscle cells with ^{125}I -LDL containing 500 $\mu\text{g}/\text{ml}$ unlabeled LDL. Receptor-mediated metabolism was determined by subtracting receptor-independent binding, internalization, and degradation from total binding, internalization, and degradation. Cell free dishes were incubated with ^{125}I -LDL in parallel to the above

and the amount degraded was subtracted from the specific and nonspecific contributions. Examples of all calculations used to determine binding, internalization, and degradation are presented in Appendix F.

2.5 RESULTS

2.5.1 Validation of Experimental Techniques

Following incubation of smooth muscle cells with ^{125}I -LDL, unbound ligand was removed by successive washings at 4 °C. Since the amounts bound and internalized are about 1% of the amount of radiolabeled LDL in the medium, the washings must be thorough. The procedure involves eight washes prior to addition of heparin. After each of the first three washes with 2 ml 0.2% (w/v) BSA in HBSS per dish, the wash medium is rapidly removed. In the next four washes the medium is incubated with the cells for 3 to 4 min. In the eighth wash HBSS is used and the wash is rapidly removed.

The removal of unbound ^{125}I -LDL from dishes containing bovine smooth muscle cells and cell-free dishes is shown in Figure 2-4. The amounts of ^{125}I -LDL removed from smooth muscle cells and cell free dishes during the first two washes are similar. From the third to the seventh wash the amount of ^{125}I -LDL removed from smooth muscle cell containing dishes is greater than that removed from cell free dishes. This difference may represent ^{125}I -LDL loosely bound to the cell surface and extracellular matrix.

At the ninth wash 1 ml of 10 mg/ml heparin is added to each dish and the dishes are incubated for 1 hour at 4 °C. Incubation with heparin results in a significant increase in the amount of ^{125}I -LDL removed from smooth muscle cells. In contrast, there is only a slight increase in the amount of ^{125}I -LDL removed from

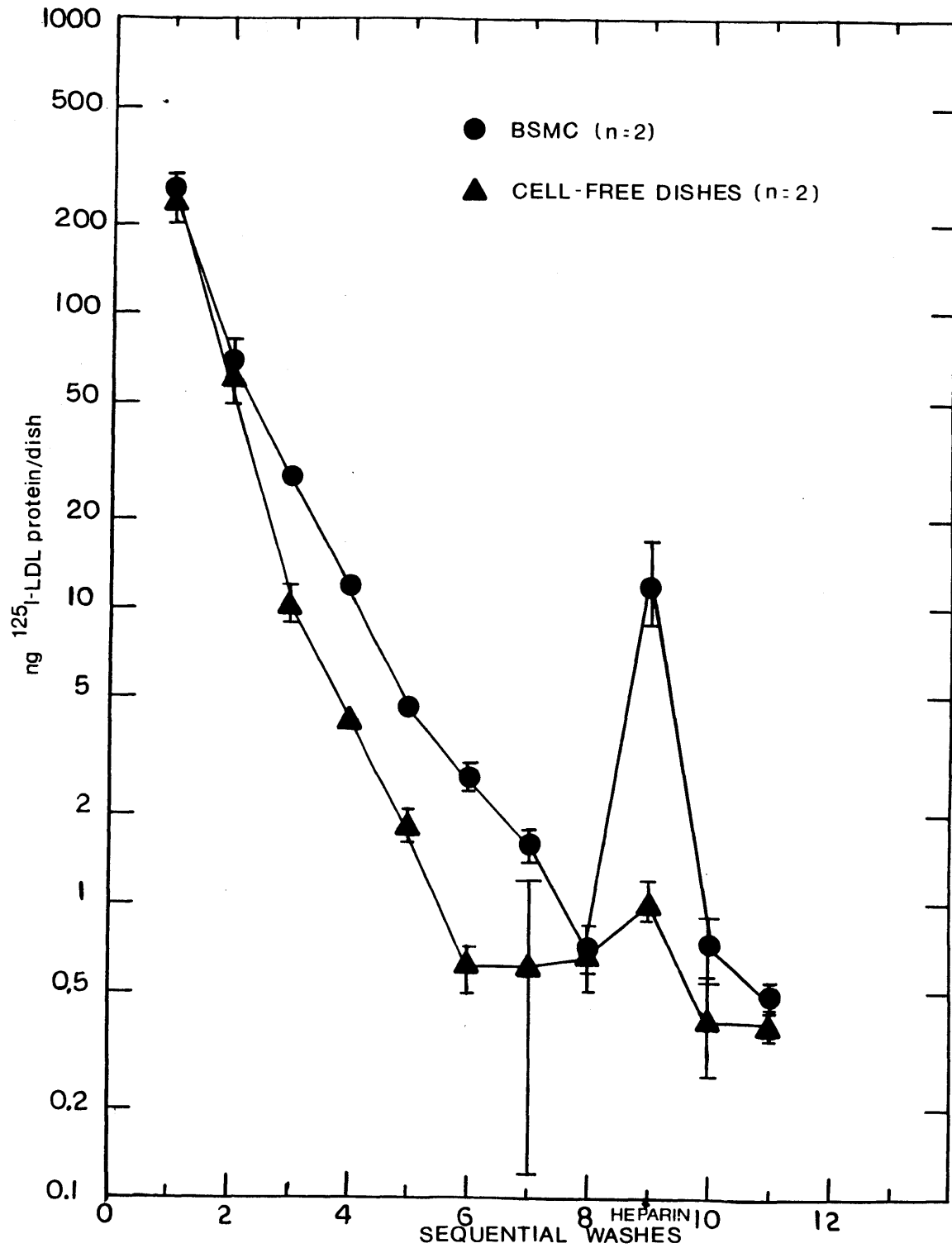


Figure 2-4: Removal of unbound ^{125}I -LDL. Following incubation at 37°C dishes were washed as described in text and total radioactivity in each wash was determined.

cell free dishes. Thus, the washing protocol efficiently removes unbound LDL, and heparin competitively removes LDL from the cell surface receptor.

For a typical experiment involving 30 to 60 dishes, 30 min are required to perform the eight washes. During this time LDL dissociates from its receptor at 4 °C and the amount of receptor-bound LDL thus measured from the heparin wash may underestimate the true amount bound to the receptors. The first order rate constant for receptor dissociation is $3.8 \times 10^{-3} \text{ min}^{-1}$ at 4 °C (Pitas et al. [1979]). After 30 min, 11% of the total amount bound to the receptors/dish (i.e. the amount of ^{125}I -LDL released by heparin) dissociates during the washes. For the results presented in Figure 2-4, this corresponds to 1.3 ng. Since this value is about equal to the normally observed experimental variability in amount of LDL bound, data were not corrected for the amount of LDL dissociated from the receptor during the washes. The amount of intracellular LDL/dish is typically 10 to 20 times greater than the amount bound. Presumably, this intracellular LDL remains within the cell during the washes at 4 °C, since fusion of vesicles with the cell membrane does not occur at this temperature.

LDL used in all experiments was isolated by heparin-manganese precipitation. This technique of isolation may alter the properties of LDL, or residual heparin associated with isolated LDL may interfere with receptor binding. These possibilities were examined by comparing the metabolism of LDL isolated by heparin-manganese precipitation and differential ultracentrifugation (Havel et al. [1955]). (100 μg of LDL, as ^{125}I -LDL, isolated by differential ultracentrifugation were kindly provided by Professor Monty Krieger of the Biology Department at MIT.)

Results of a two hour incubation with 10 $\mu\text{g}/\text{ml}$ ^{125}I -LDL at 37 °C are presented in Table 2-II. LDL, isolated by the two different methods is bound, internalized, and degraded to the same extent. Because of the small number of

samples (2 dishes for each type of LDL), differences in intracellular LDL concentrations are not significant at the 95% level of confidence. Thus, the method of LDL preparation does not alter the cellular metabolism of LDL. Addition of 10 units/ml heparin (60 $\mu\text{g}/\text{ml}$) at the beginning of the ^{125}I -LDL incubations results in a 40% decrease in binding, internalization, and degradation.

Table 2-II: Smooth Muscle Cell Metabolism of LDL Prepared by Two Different Methods

	LDL Preparation Method	
	Heparin/Manganese Precipitation	Differential Ultracentrifugation
<hr/>		
(n=2)		
Bound, ng/mg	15.4 \pm 2.7	15.9 \pm 2.1
Internalized, ng/mg	233 \pm 5	195 \pm 14
Degraded, ng/mg	150 \pm 6	152 \pm 11
<hr/>		
Addition of 10 U/ml Heparin to dishes (n=1)		
Bound, ng/mg	7.94	9.8
Internalized, ng/mg	139	108
Degraded, ng/mg	88	85

2.5.2 Determination of Rate Constants for Receptor-Mediated LDL

Metabolism

In order to determine the rate constants using the minimization criterion (equation (2-41)) for multiple response data, quiescent, subconfluent bovine smooth muscle cells were incubated with either 10 $\mu\text{g}/\text{ml}$ ^{125}I -LDL for times ranging from 2

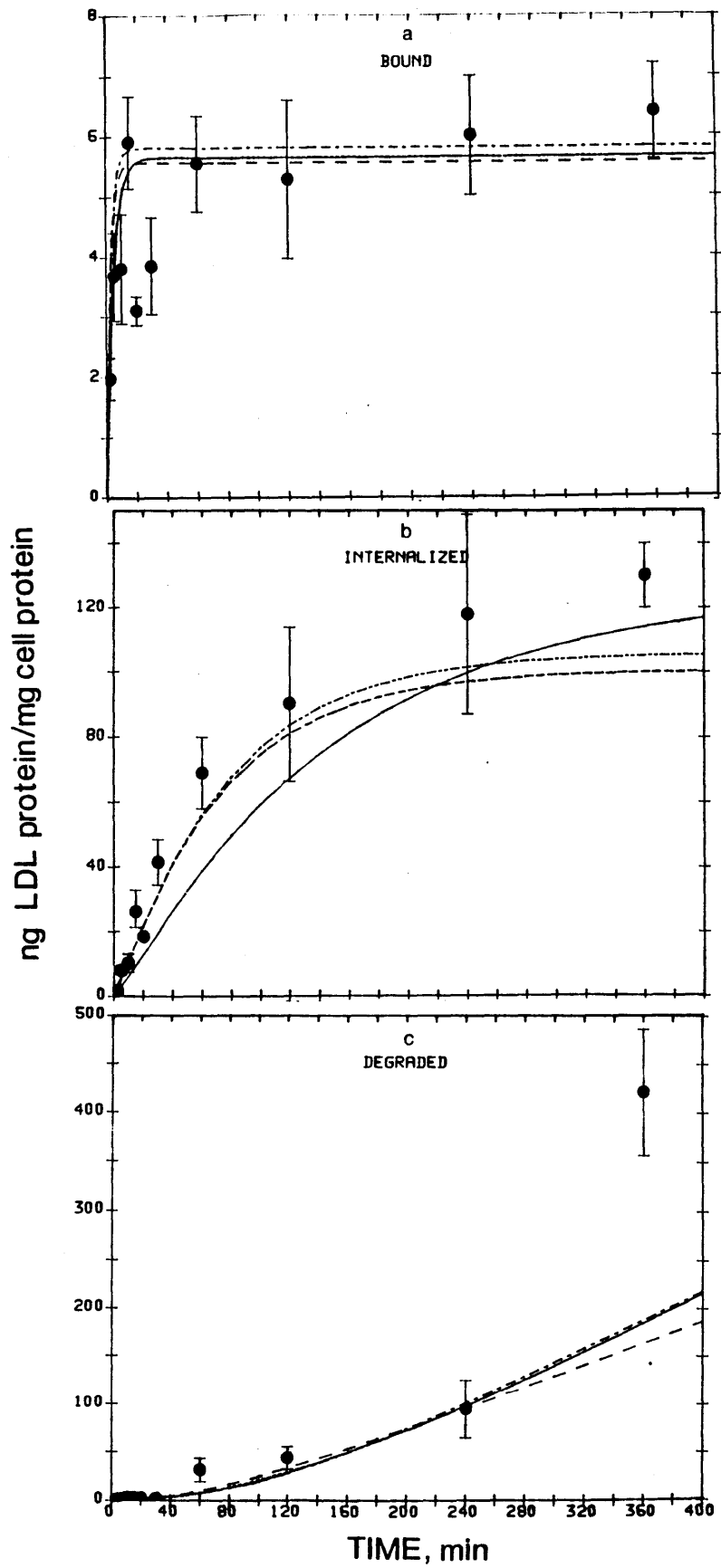
min to 6 hr or for 4 hr with ^{125}I -LDL concentrations ranging from 1 $\mu\text{g}/\text{ml}$ to 120 $\mu\text{g}/\text{ml}$. At the end of the incubation, bound, internalized, and degraded ^{125}I -LDL were measured as described in the Materials and Methods section. Nonspecifically bound, internalized, and degraded ^{125}I -LDL were determined in separate incubations and the results were subtracted from the total amounts bound, internalized, and degraded per mg cell protein to obtain the receptor-mediated contribution. Results are presented as $\text{ng } ^{125}\text{I}\text{-LDL protein}/(\text{mg cell protein})$.

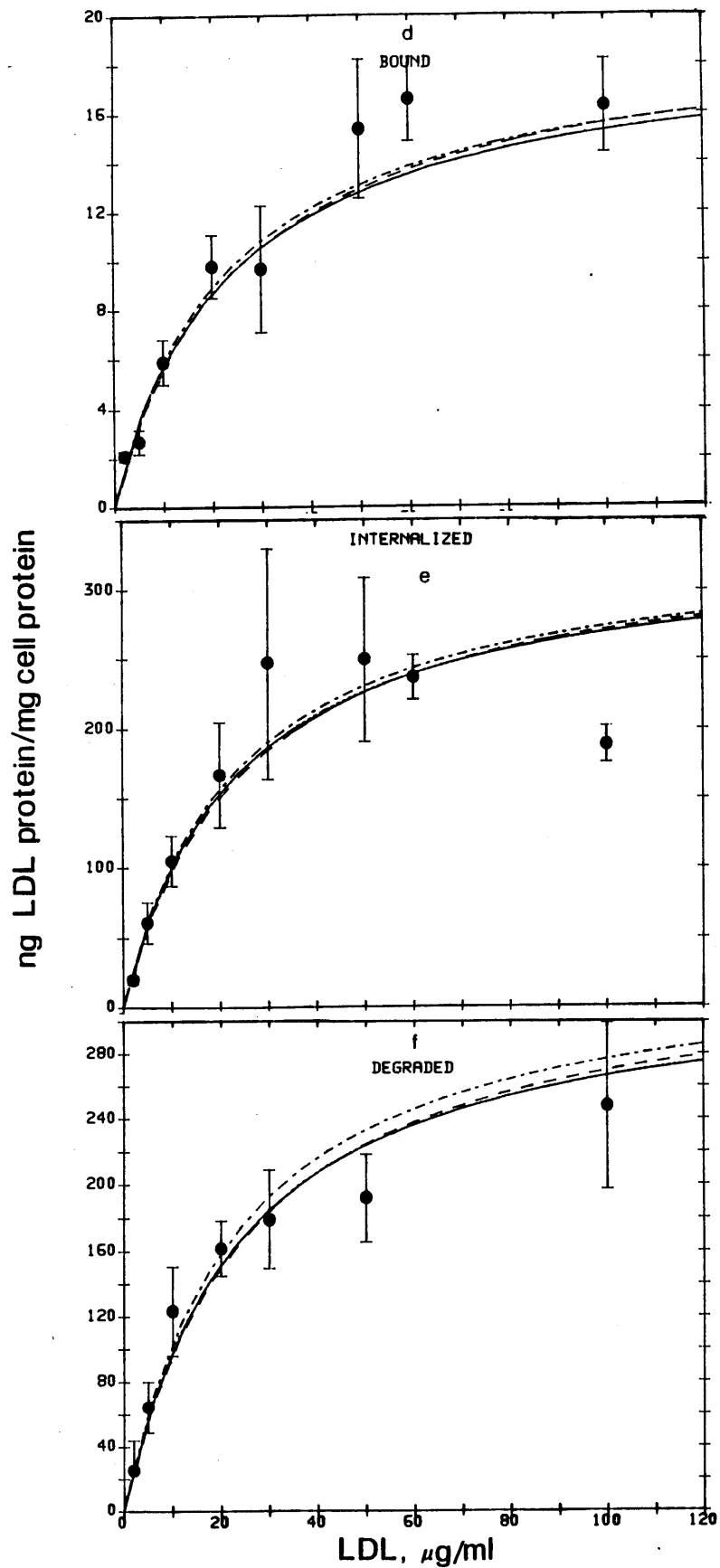
Results from six experiments were pooled together and the average values are presented in Figure 2-5. (Individual experiments are discussed below.) For the kinetic experiments, averages were calculated at each time, whereas, for binding, internalization, and degradation as a function of concentration at a single time, concentrations differing by less than 2 $\mu\text{g}/\text{ml}$ were pooled and averaged. The error bars are equal to the standard error of the mean for the pooled samples.

The behavior of binding, internalization, and degradation is similar to that described for results sketched in Figure 2-1. Binding is rapid, reaching a steady state after 15 min. Internalization of receptor-bound LDL is slower, and may be approaching a steady state by six hr. There is a 30 min lag before degradation products appear in the medium, after which degradation increases rapidly. A steady state does not appear to be reached by six hr.

The smooth curves in Figure 2-5 represent best fits of the individual data points to the models described in Section 2.3 as determined by minimization of the determinant of \mathbf{F} , equation (2-41). The models are: 1) the complete model (equation (2-7)) which includes exocytosis and separate endosomal and lysosomal compartments; 2) the lumped model (equation (2-20)) consisting of a single intracellular compartment and including exocytosis; and 3) the lumped model neglecting exocytosis (i.e., $k_5 = 0$).

Figure 2-5: Fits of combined data for receptor-mediated metabolism of LDL from six experiments. Binding, internalization, and degradation were measured as a function of time for an ^{125}I -LDL concentration of $10\ \mu\text{g}/\text{ml}$ (2-5a,b,c) and as a function of LDL concentration at 4 hr (2-5d,e,f). Smooth curves represent best fits of data by minimization of the determinant of the matrix \mathbf{F} : --- complete model with two intracellular compartments and exocytosis; -- lumped model with one intracellular compartment and including exocytosis; and — lumped model without exocytosis. A total of 188 data points were fit simultaneously.





Examination of published data (Appendix A) indicates that at 37 °C, dissociation of LDL from its receptor is much slower than internalization of the LDL-receptor complex (i.e., $k_{-1} \ll k_2$). Initial parameter estimates included k_{-1} , but it was found that the models were insensitive to its value as long as it was less than k_2 . For subsequent parameter estimates k_{-1} was set equal to zero.

Rate constants for the three models along with the values of the determinant of \mathbf{F} are presented in Table 2-III. Error estimates represent standard deviations based upon the linearized estimate of the covariance matrix, equation (2-47). Since the best fit value of $[R_T]$ was calculated as the ng LDL bound/mg cell protein, the number of receptors per cell was obtained using an experimentally determined relation between cell protein mass and number of receptors, 0.33 mg cell protein/(10^6 cells) and a molecular weight of LDL equal to 500,000 g/mole.

All three models give similar fits of data, except for fits of internalization as a function of time in which the lumped model without exocytosis underestimated internalization prior to the establishment of a steady state. The fit to this transient period is significantly improved by including exocytosis. All of the models underestimate the amount degraded at six hr (Figure 2-5c). This point represents the average of three dishes of cells from one experiment (BSMC6), whereas all other points represent the average of 15 to 20 dishes of cells for all six experiments. Since there are fewer data points at six hr, the model effectively gives less weight to this time than to other times.

The values of $\det(\mathbf{F})$ as well as estimates of the receptor number are similar for all three models (Table 2-III). The complete model (column 1) and the lumped model including exocytosis (column 2) yield similar values for k_1 and k_2 . Parameter standard deviations of k_{3b} , k_{3d} , and k_5 for the complete model are at least two times the value of the parameter estimate, suggesting that all of the parameters cannot be

uniquely determined. With the other two models parameter standard deviations are no more than 50% of the value of the individual rate constants. Lumping the intracellular compartments does not alter the value of k_1 and k_2 , whereas neglecting exocytosis results in changes in k_1 , k_2 , and k_3 . If exocytosis were unimportant, these parameters should not be affected.

Table 2-III: Estimated Rate Constants for Combined Data of Receptor-Mediated Metabolism

Parameter	Complete Model	Lumped Model with Exocytosis	Lumped Model without Exocytosis
$k_1, M^{-1}min^{-1} \times 10^{-7}$	0.52 ± 0.20	0.50 ± 0.17	0.32 ± 0.06
k_2, min^{-1}	0.24 ± 0.10	0.25 ± 0.07	0.15 ± 0.01
k_{3l} (or k_3), min^{-1}	0.0142 ± 0.0317	0.0057 ± 0.0006	0.0067 ± 0.0004
k_{3d}, min^{-1}	0.014 ± 0.029		
k_5, min^{-1}	0.012 ± 0.066	0.008 ± 0.005	
R_T , number/cell	7600 ± 700	7800 ± 800	7500 ± 700
$\det(\mathbf{F}) \times 10^{-11}$	1.35	1.42	1.44

The matrix of correlation coefficients and the parameter standard deviations can be used to assess whether a model is overdetermined (Draper and Smith [1981], p. 487). Highly correlated parameters have a correlation coefficient greater than 0.95 (Draper and Smith [1981], p. 487). The correlation matrix was computed from equations (2-47) and (2-48) and the elements of the matrices for each model are presented in Table 2-IV. For the complete model k_{3d} and k_{3l} , k_5 and k_{3l} , and k_5 and k_{3d} are highly correlated which indicates that changes in the value of either k_{3l} , k_{3d} , or k_5 results in changes in the value of the other two parameters. The large

standard deviations and the high correlations among k_{3l} , k_{3d} , and k_5 suggest that the complete model contains more parameters than can be accurately estimated from the available data. (Measurements of endosomal and lysosomal concentrations are needed to adequately judge the validity of this model. Although the two compartments can be distinguished using electron microscopy, there is no technique available to provide such measurements for the purposes of testing kinetic models.) Since the lumped model with exocytosis yields fits almost identical to those obtained with the complete model and k_1 and k_2 are unchanged, this simplified model provides an adequate representation of the data.

Parameter standard deviations for both lumped models are quite reasonable, although they are lower with for the model without exocytosis (Table 2-III). Including exocytosis in the model results in a high correlation between k_5 and k_2 . Nevertheless, inclusion of exocytosis results in an improved fit of internalization as a function of time (Figure 2-5b).

The value of using the determinant of the \mathbf{F} matrix (equation (2-41)) and the need to include exocytosis in the model were examined by fitting the individual responses to the lumped model without exocytosis. Fitting bound LDL alone yields estimates for k_1 , k_2 , and R_T , while fitting internalized and degraded LDL separately yields k_3 in addition to the other parameters.

Rate constants obtained from fitting either individual responses or two responses are presented in Table 2-V along with the value of $\det(\mathbf{F})$, and the fits are presented in Figure 2-6. Note that $\det(\mathbf{F})$ depends on the magnitude of the measured values and the order of the matrix. It is useful for comparing results when the same number of responses are fit. Fitting bound LDL alone (not shown in Figure 2-6) produces estimates with reasonably small standard deviations. k_2 is similar to the value obtained with the lumped model neglecting exocytosis, while k_1

Table 2-IV: Correlation Matrices of Parameters

Complete Model

	k_1	k_2	k_{3l}	k_{3d}	k_5	R_T
k_1	1.000	0.898	0.445	-0.481	0.578	-0.220
k_2	0.898	1.000	0.537	-0.579	0.680	0.184
k_{3l}	-0.445	0.537	1.000	-0.998	0.983	0.124
k_{3d}	-0.481	-0.579	-0.998	1.000	-0.991	-0.147
k_5	0.578	0.680	0.983	-0.991	1.000	0.155
R_T	-0.220	0.184	0.124	-0.147	0.155	1.000

Lumped Model Including Exocytosis

	k_1	k_2	k_3	k_5	R_T
k_1	1.000	0.124	-0.199	0.128	0.898
k_2	0.124	1.000	-0.753	0.984	0.093
k_3	-0.199	-0.753	1.000	-0.691	-0.304
k_5	0.128	0.984	-0.691	1.000	0.104
R_T	0.898	0.093	-0.304	0.104	1.000

Lumped Model Without Exocytosis

	k_1	k_2	k_3	R_T
k_1	1.000	-0.116	-0.129	0.886
k_2	-0.116	1.000	0.128	-0.325
k_3	-0.129	0.128	1.000	-0.306
R_T	0.886	-0.325	-0.306	1.000

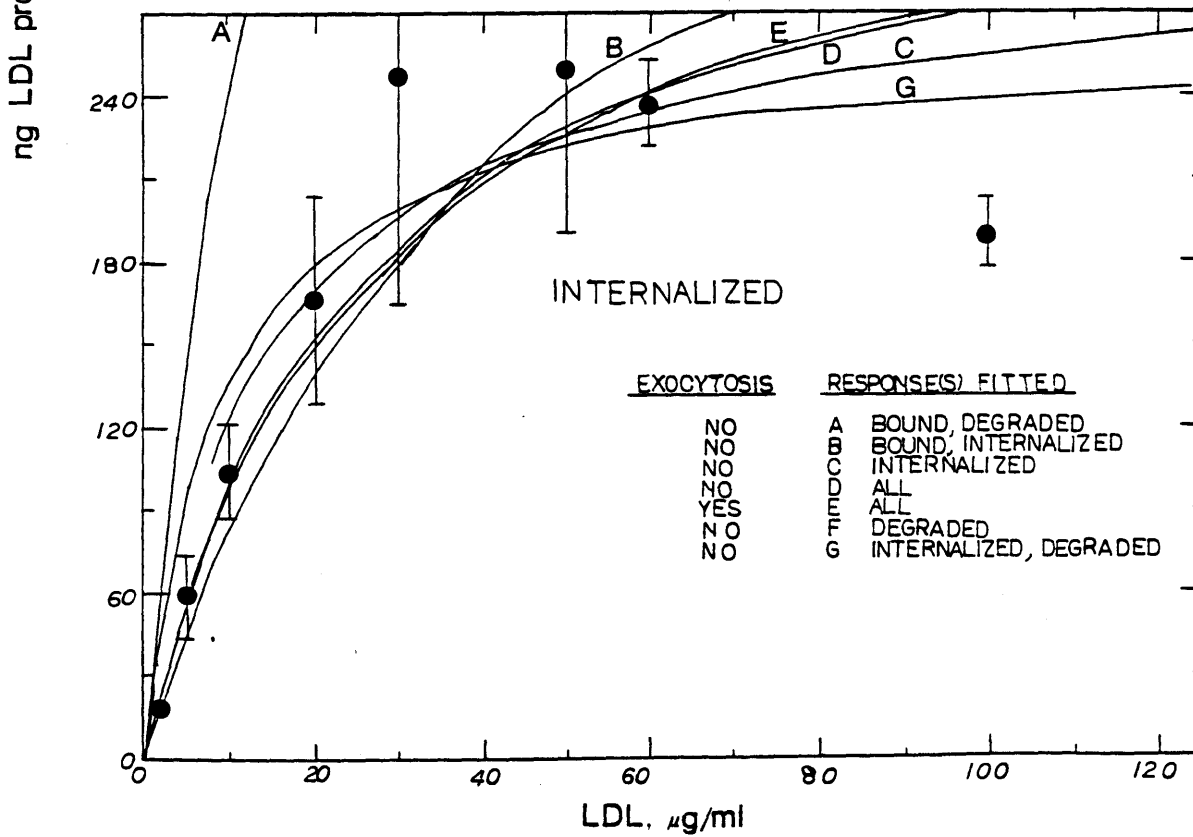
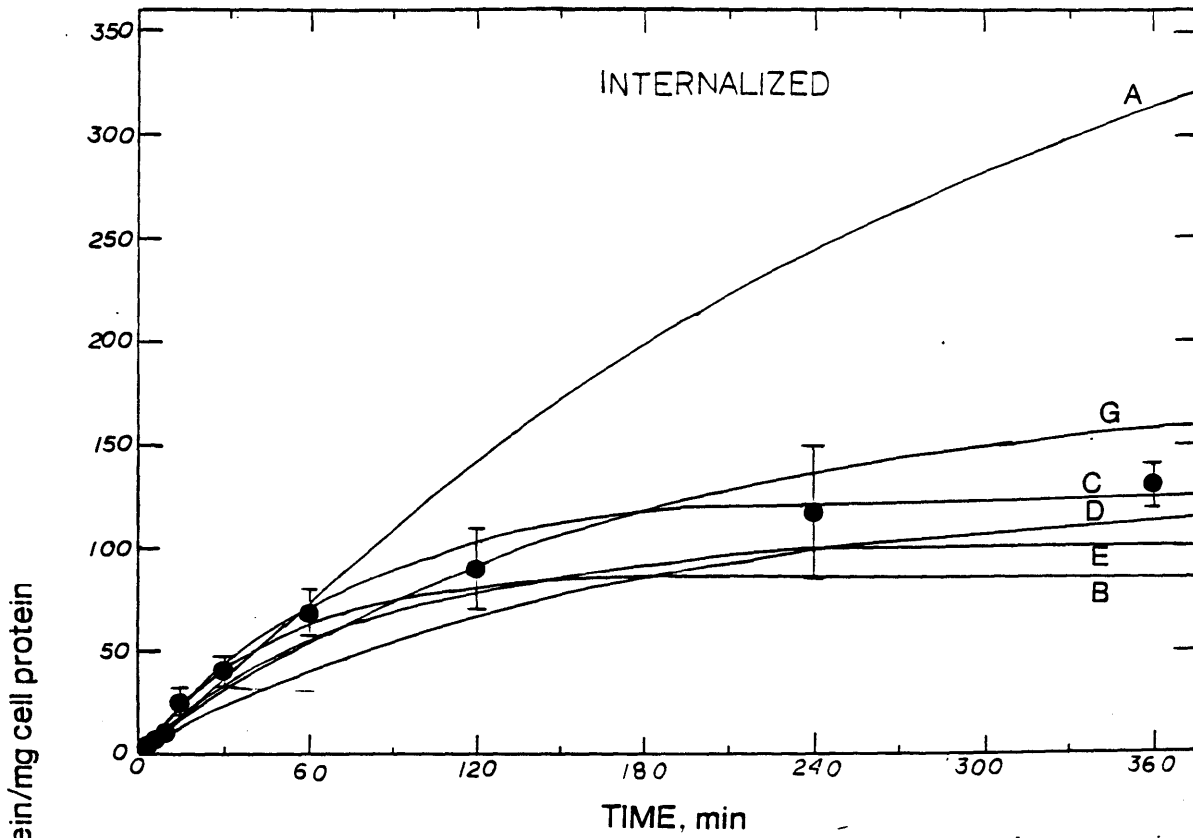
and R_T are different than the values obtained using all three responses with any model. Fitting internalization and degradation separately gives estimates with large standard deviations; rate constants and number of receptors per cell estimated from degradation alone differ significantly from estimates with all responses. When two responses are fit the parameter standard deviations are reduced.

Parameter estimates obtained by fitting internalization data alone yields fits in excellent agreement with data for internalized LDL (Figure 2-6) but the predicted values for degradation are poor. The situation is improved only slightly by fitting bound and internalized LDL. Likewise, rate constants estimated from fits of degradation alone and binding and degradation together give good fits for degraded LDL but poor fits for internalized LDL. Fitting all response reduces parameter correlations compared with the fits of individual responses. For example, fitting degradation alone yields a correlation of 0.906 between k_2 and k_3 . The correlation drops to -0.40 for bound and degraded together, -0.71 for internalized and degraded together, and -0.20 for all three responses.

Parameter estimates determined from fits of individual and combined responses indicates that: 1) parameter standard deviations and correlations are reduced by fitting all responses simultaneously (cases D and E, Table 2-V); 2) fitting separate responses fails to yield a consistent set of parameters; and 3) simultaneous regression of all three responses produces a consistent set of parameters which requires inclusion of exocytosis. The necessity of including exocytosis is examined further by fitting individual experiments.

Results from six individual experiments are presented in Figures 2-7 to 2-12. Each point represents the average of three dishes, except for experiments BSMC29 and BSMC33 in which each point represents the average of two dishes. Error bars are equal to the standard deviation. Each experiment was fit to the lumped single

Figure 2-6: Comparison of model fits obtained from individual responses, two responses, and all responses with data for internalized and degraded LDL. Lumped model without exocytosis was fit to internalization and degradation data separately, and to combinations of binding and internalization data, binding and degradation data, internalization and degradation data, and binding, internalization, and degradation data.



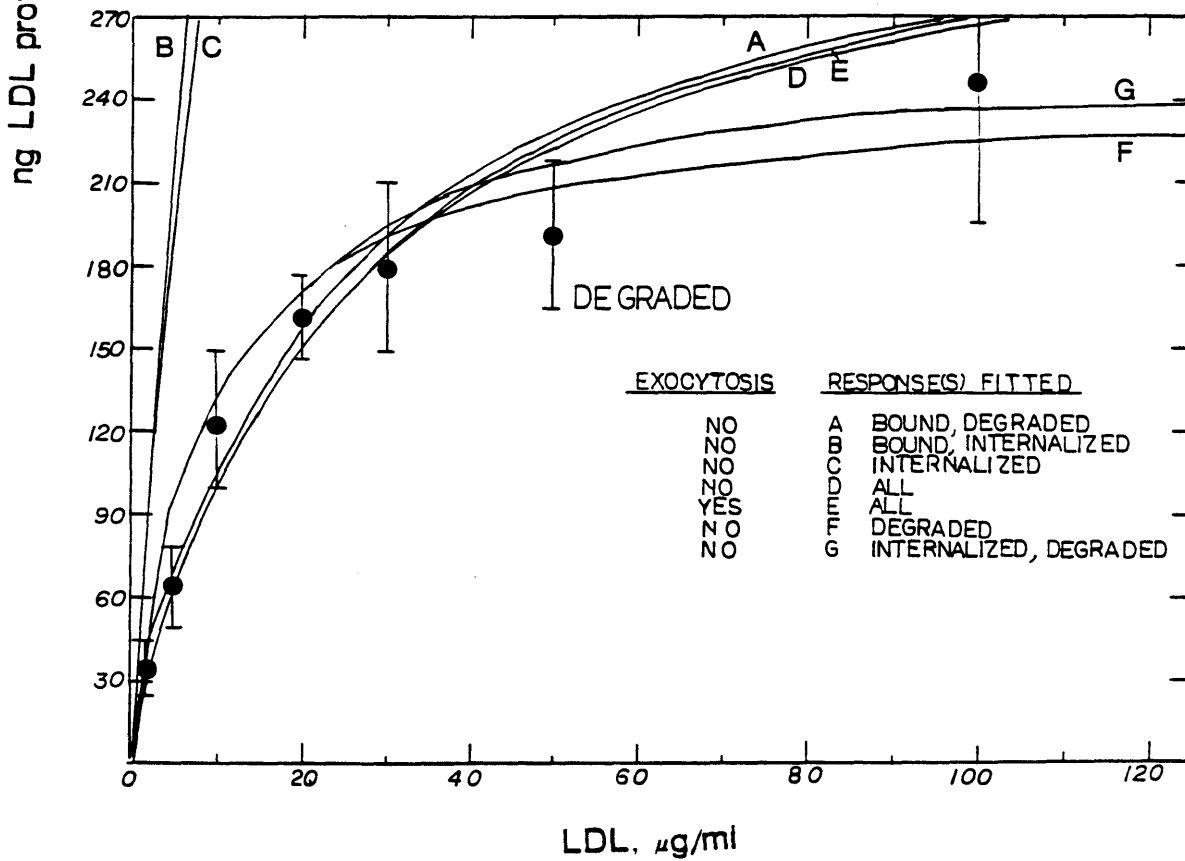
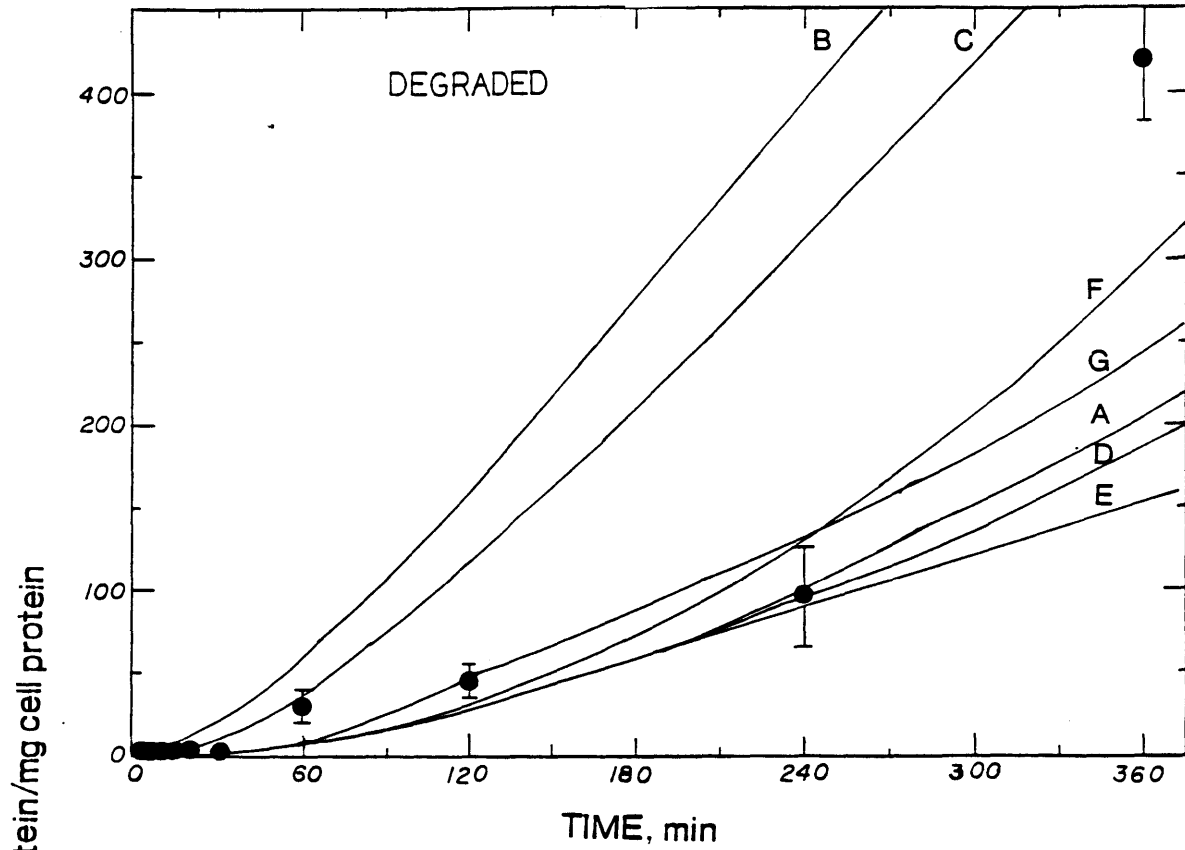


**Table 2-V: Rate Constants for Receptor-Mediated
LDL Metabolism from Individual Responses or two Responses**

	Curve in Figure 2-6	$k_1, M^{-1} \text{ min}^{-1} \times 10^{-7}$	$k_2, \text{ min}^{-1}$	$k_3, \text{ min}^{-1}$	$k_5, \text{ min}^{-1}$	$R_T, \text{ receptors/cell}$	$\text{det}(\mathbf{F}) \times 10^5$
Bound Alone	not shown	0.22 ± 0.12	0.14 ± 0.07			9100 ± 1100	0.037
Internalized Alone	C	0.9 ± 5.5	0.24 ± 1.54	0.014 ± 0.011	0 (fixed)	7200 ± 50000	20.6
Degraded Alone	F	6.1 ± 7.2	1.01 ± 1.19	$8.3 \pm 155 \times 10^5$	0 (fixed)	$41000 \pm (7.0 \times 10^6)$	9.27
Bound and Internalized	B	0.50 ± 0.10	0.40 ± 0.13	0.0234 ± 0.0008	0 (fixed)	9900 ± 1200	244
Bound and Degraded	A	0.56 ± 0.32	0.24 ± 0.13	0.0031 ± 0.0021	0 (fixed)	7500 ± 7200	210
Internalized and Degraded	G	1.0 ± 5.2	0.18 ± 0.99	0.0064 ± 0.0004	0 (fixed)	4700 ± 2600	1.06×10^5
All Responses	D	0.32 ± 0.01	0.15 ± 0.01	0.0067 ± 0.0004	0 (fixed)	7500 ± 700	1.44×10^6
Bound and Degraded	not shown	0.40 ± 0.08	0.16 ± 0.07	0.0113 ± 0.0092	0.0082 (fixed)	7400 ± 700	202
All Responses	E	0.50 ± 0.17	0.25 ± 0.07	0.0057 ± 0.0006	0.0082	7800 ± 770	1.35×10^6

compartment model with and without exocytosis and the rate constants are presented in Table 2-VI.

The most significant difference among the models is in fitting LDL internalization as a function of time; the four parameter model without exocytosis underestimates the amount internalized prior to the establishment of a steady state. Including exocytosis results in a considerable decrease in $\det(\mathbf{F})$ and an improvement in the fit.

Both models give poor asymptotic values for LDL binding as a function of time in experiments BSMC10 (Figure 2-8a), BSMC29 (Figure 2-9a), and BSMC40 (Figure 2-12a). This error in the fit is not an artifact of the regression routine since each response is weighted equally by the other two responses. In addition, asymptotic values for bound LDL for the other three experiments are in good agreement with data (Figures 2-7a, 2-10a, 2-11a). Possibly the poor fits are a result of considerable scatter in data for bound LDL in these experiments.

Rate constants for binding and internalization are larger when exocytosis is included in the model. As a result, binding and internalization occur more rapidly, resulting in better agreement with data. Exocytosis compensates for the increase in binding and internalization resulting in a steady state level similar to that for the case of no exocytosis. Average values from fits of individual experiments have larger standard deviations and are different from values obtained by fitting all data together. The difference in the values is probably due to differences in the number of measurements among the experiments.

The results indicate that exocytosis must be included in the model in order to obtain reasonable agreement with data. Exocytosis of LDL has been observed in fibroblasts and smooth muscle cells (Aulinskas et al. [1981, 1985], Greenspan and St. Clair [1984]). Further evidence for exocytosis is presented below.

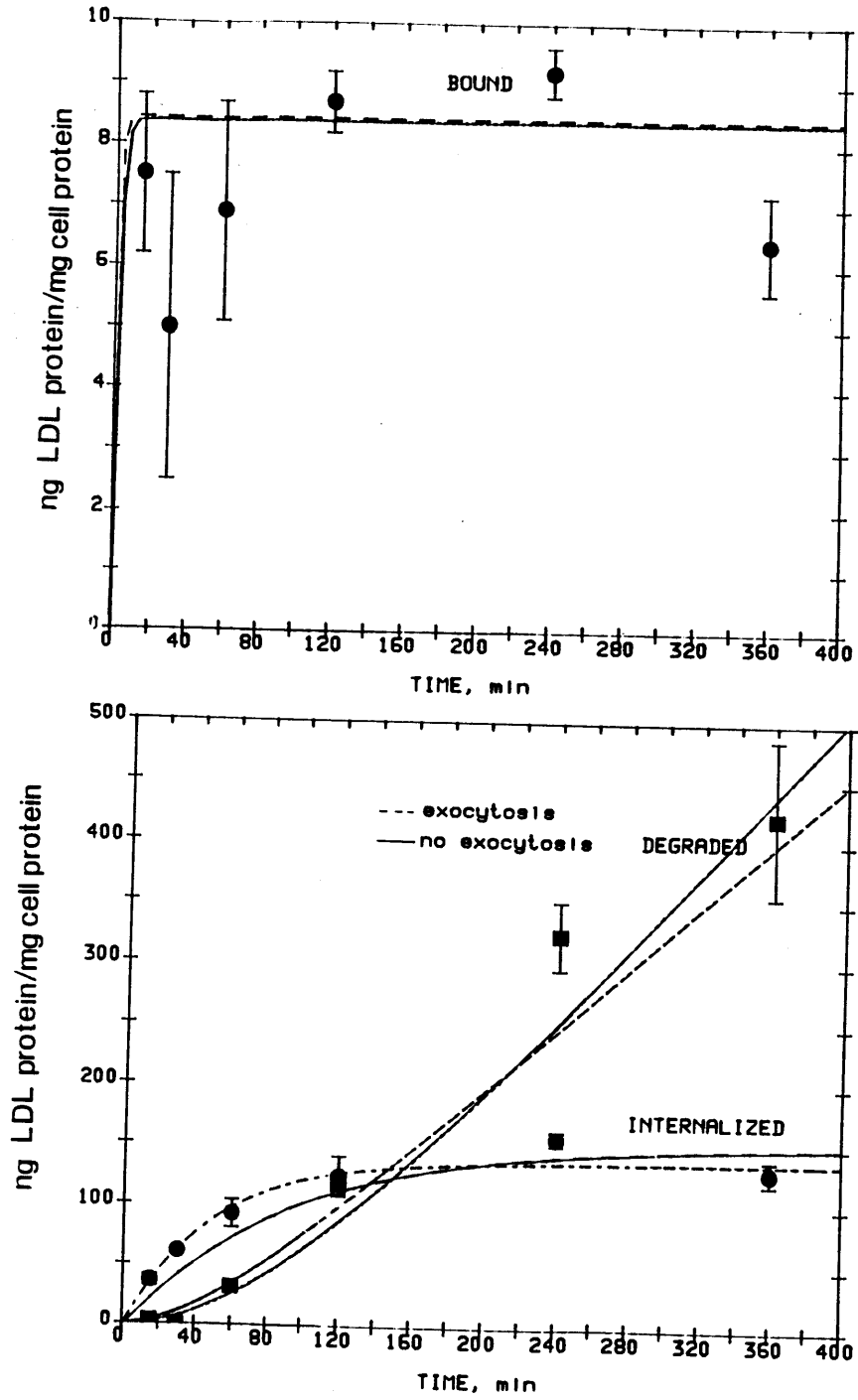


Figure 2-7: Expt. BSMC6: LDL metabolism as a function of time. Smooth muscle cells were incubated with 10 $\mu\text{g}/\text{ml}$ for indicated times.

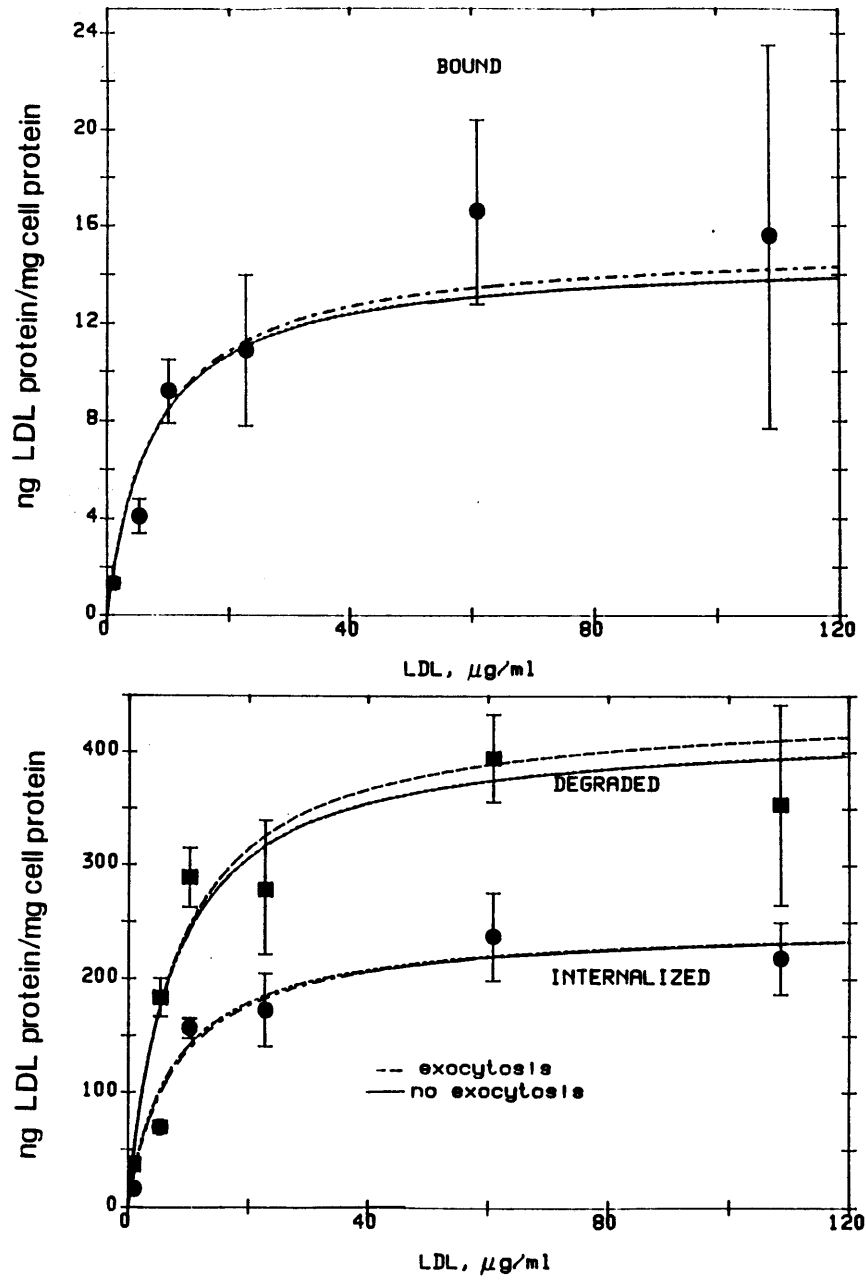


Figure 2-7 (cont.) Expt. BSMC6: LDL metabolism as a function of concentration at 4 hr.

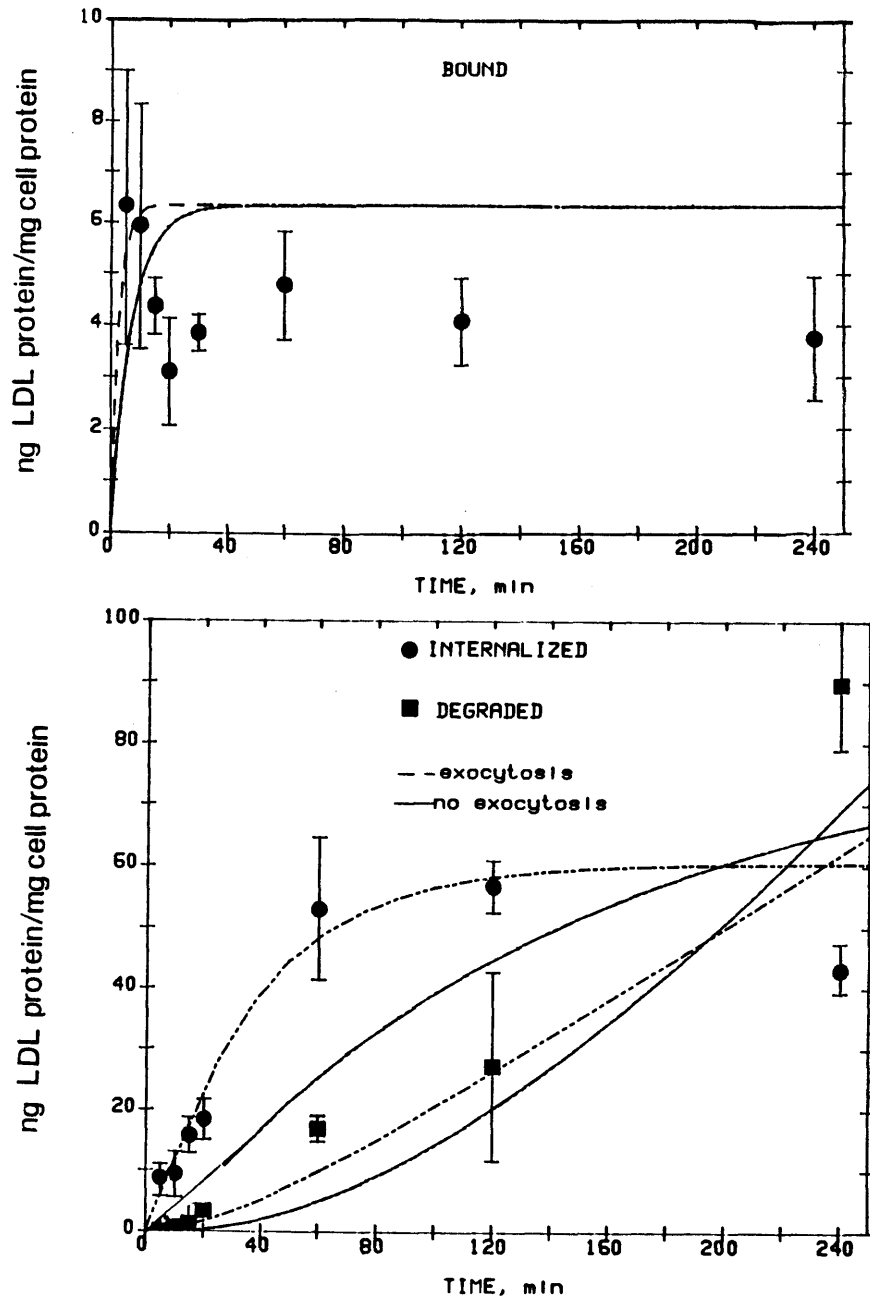


Figure 2-8: Expt. BSMC10: LDL metabolism as a function of time. Smooth muscle cells were incubated with $10.4 \mu\text{g/ml}$ for indicated times.

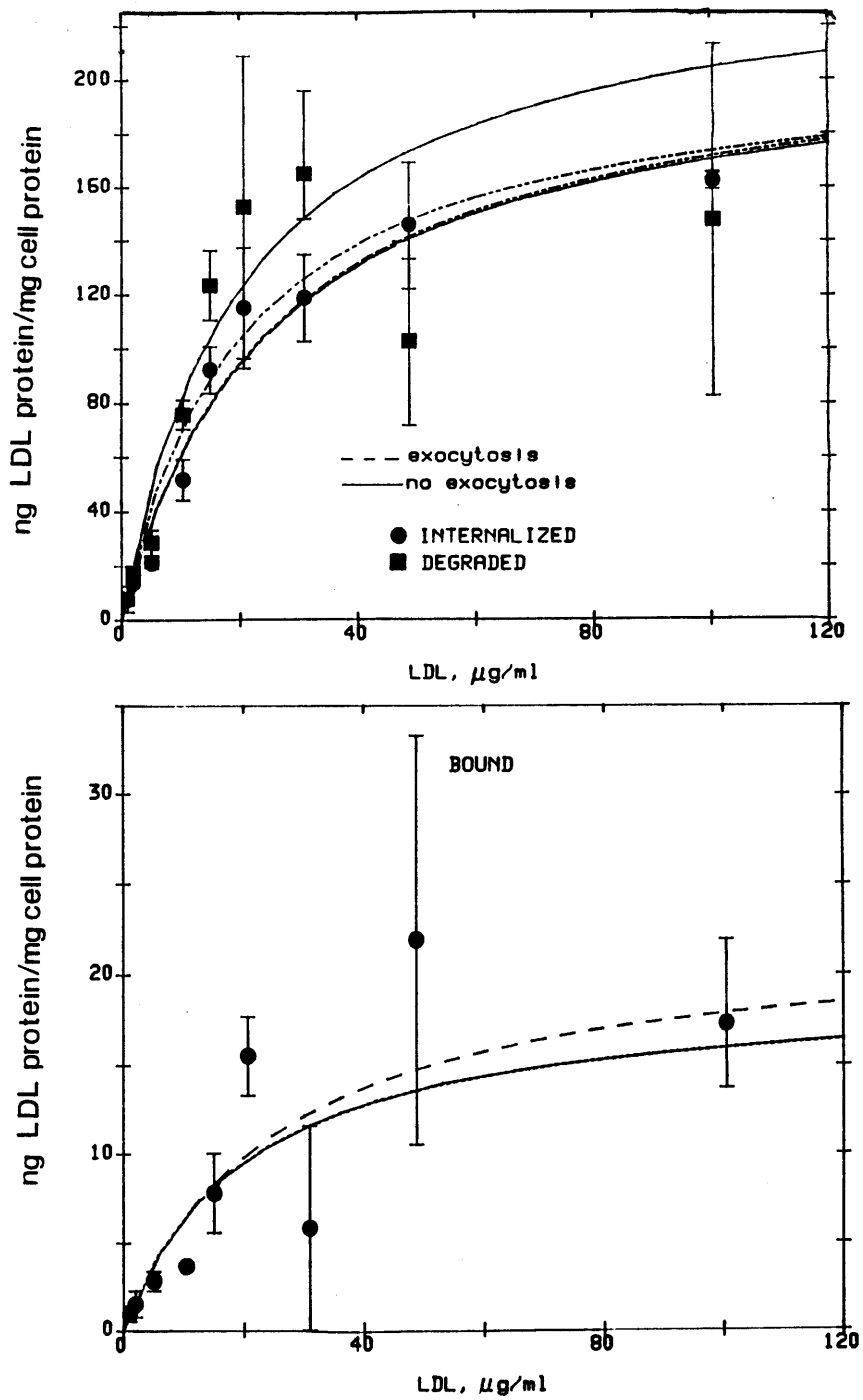


Figure 2-8 (cont.) Expt. BSMC10: LDL metabolism as a function of concentration at 4 hr.

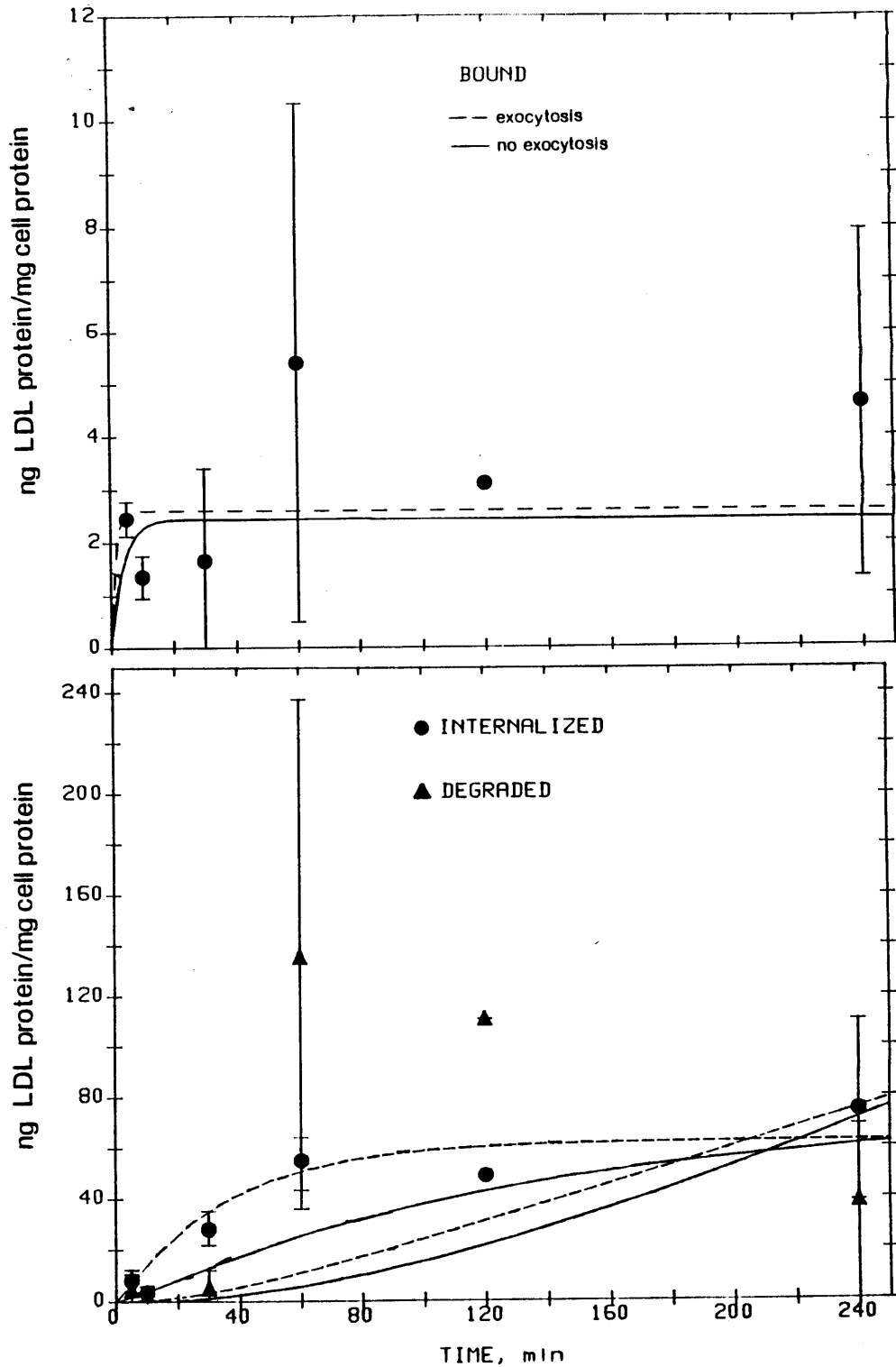


Figure 2-9: Expt. BSMC29: LDL metabolism as a function of time. Smooth muscle cells were incubated with $10 \mu\text{g/ml}$ for indicated times.

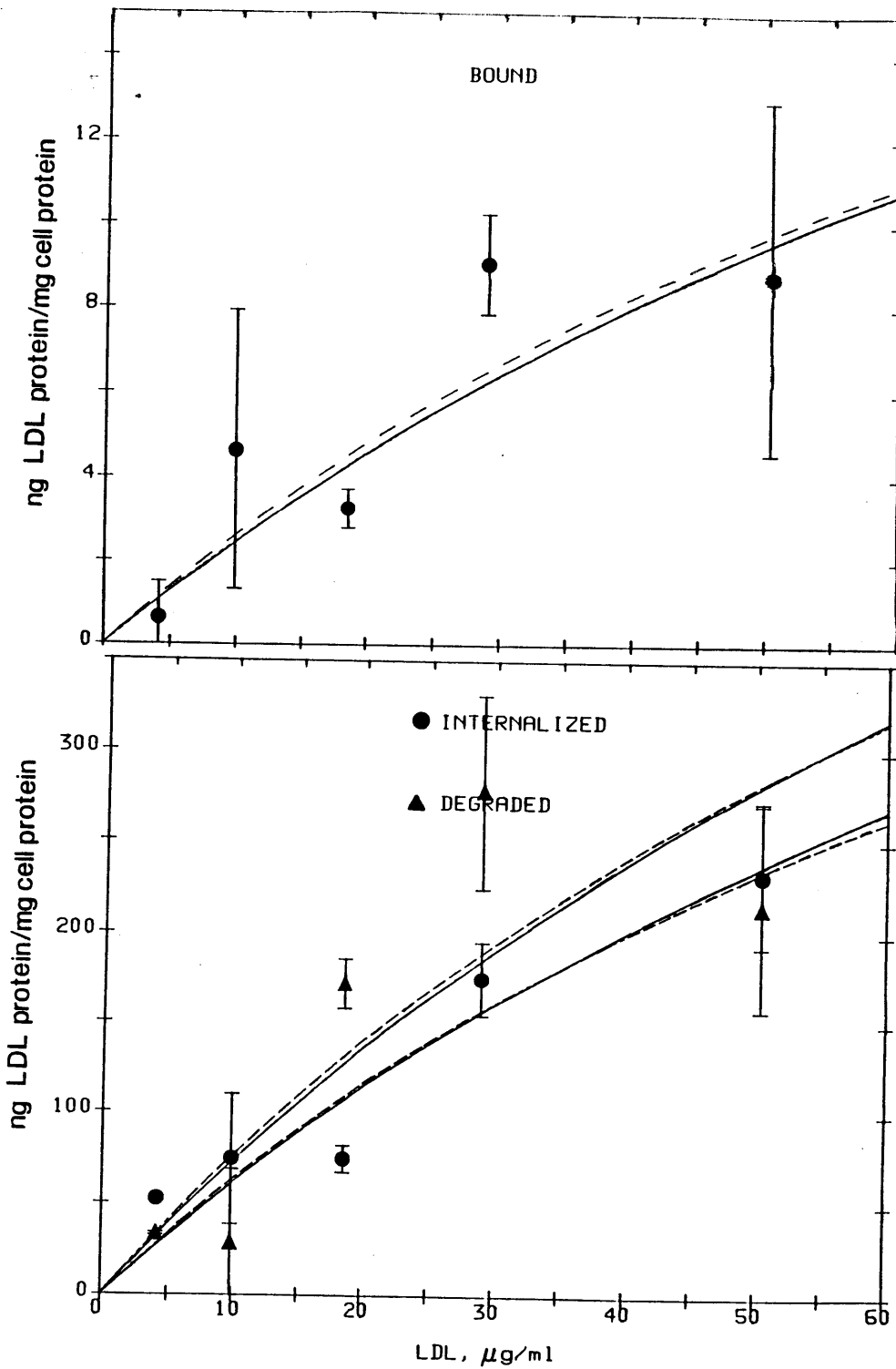


Figure 2-9 (cont.) Expt. BSMC29: LDL metabolism as a function of concentration at 4 hr.

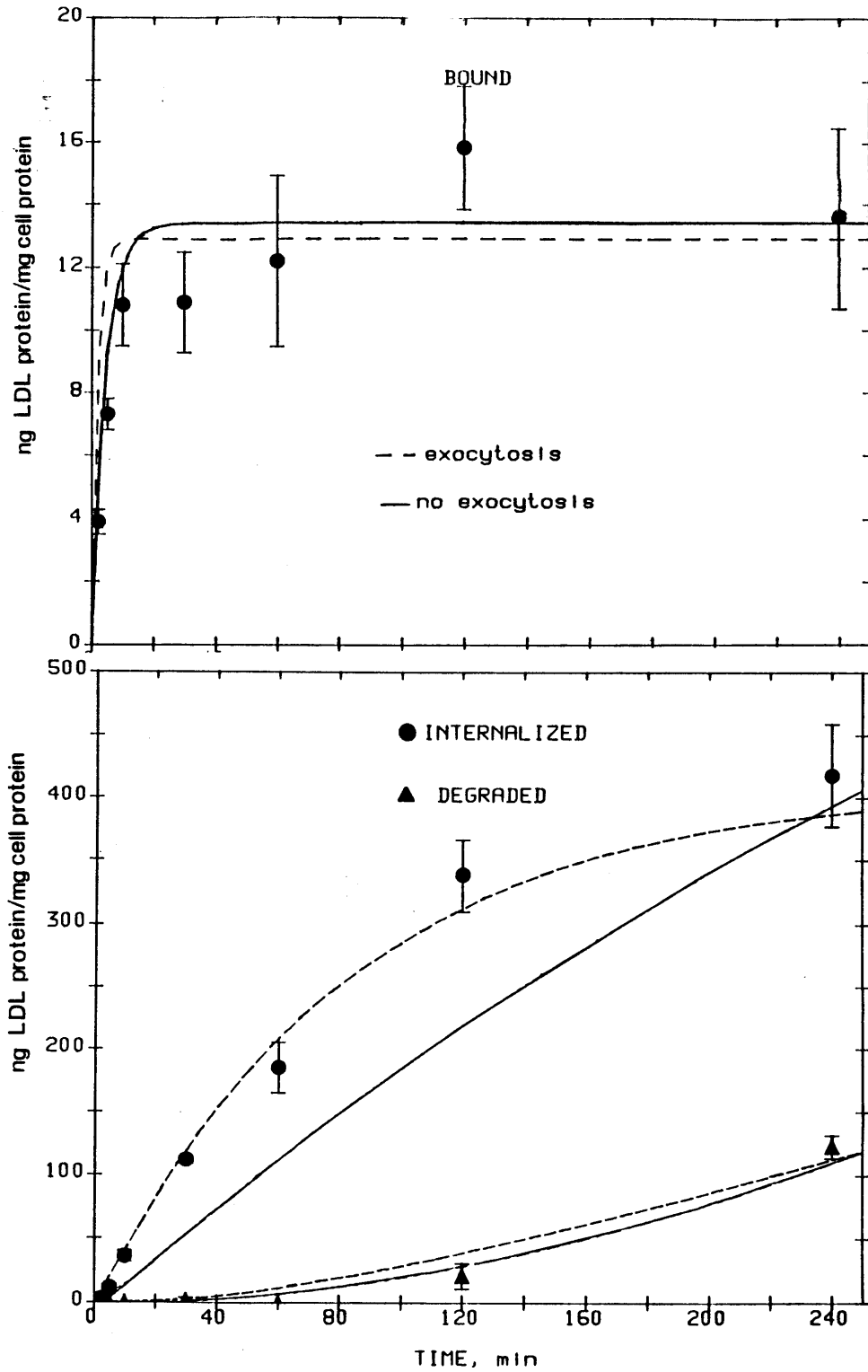


Figure 2-10: Expt. BSMC33: LDL metabolism as a function of time. Smooth muscle cells were incubated with $12 \mu\text{g/ml}$ for indicated times.

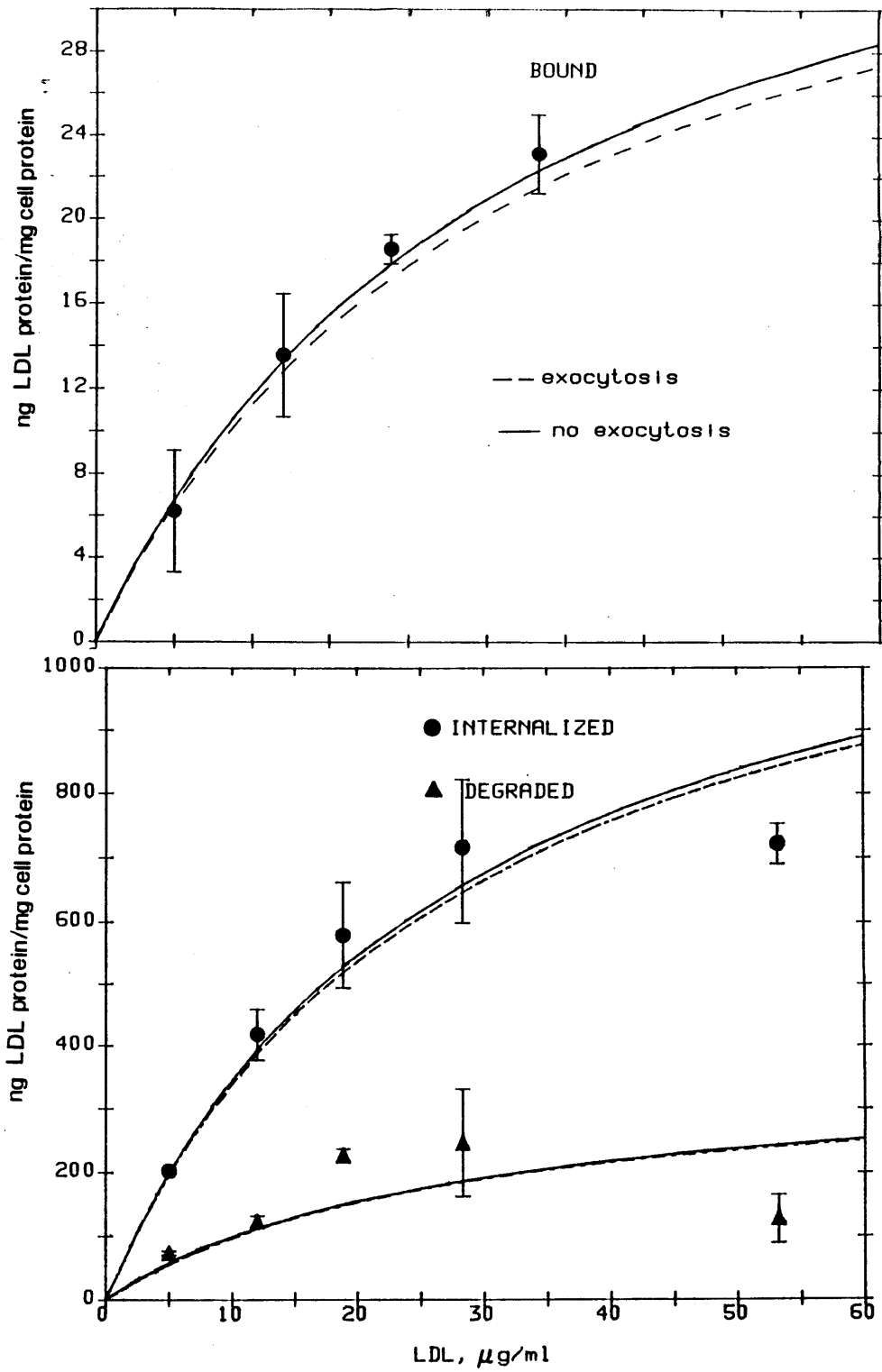


Figure 2-10 (cont.) Expt. BSMC33: LDL Metabolism as a Function of concentration at 4 hr.

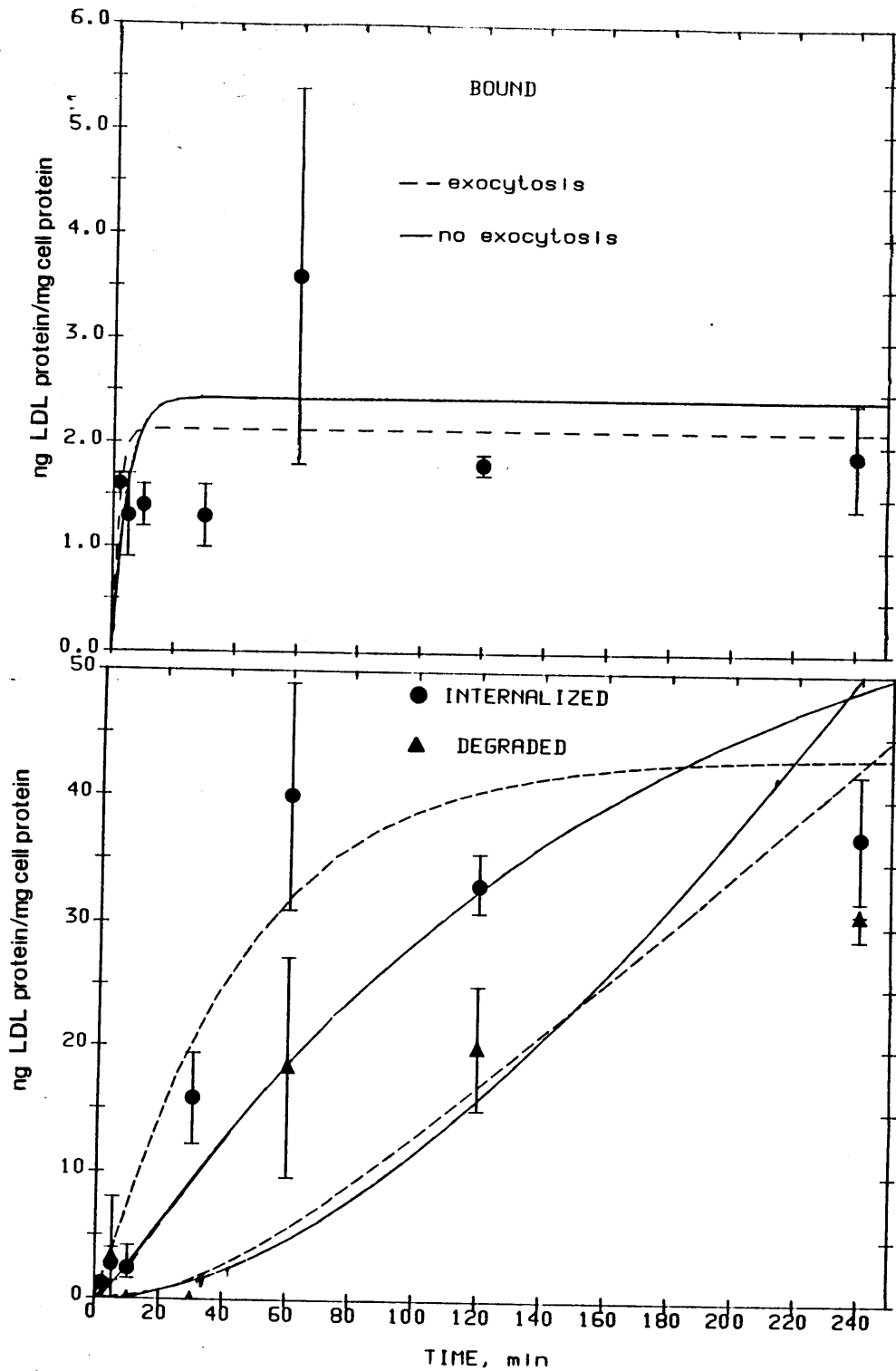


Figure 2-11: Expt. BSMC35: LDL metabolism as a function of time. Smooth muscle cells were incubated with $8 \mu\text{g}/\text{ml}$ for indicated times.

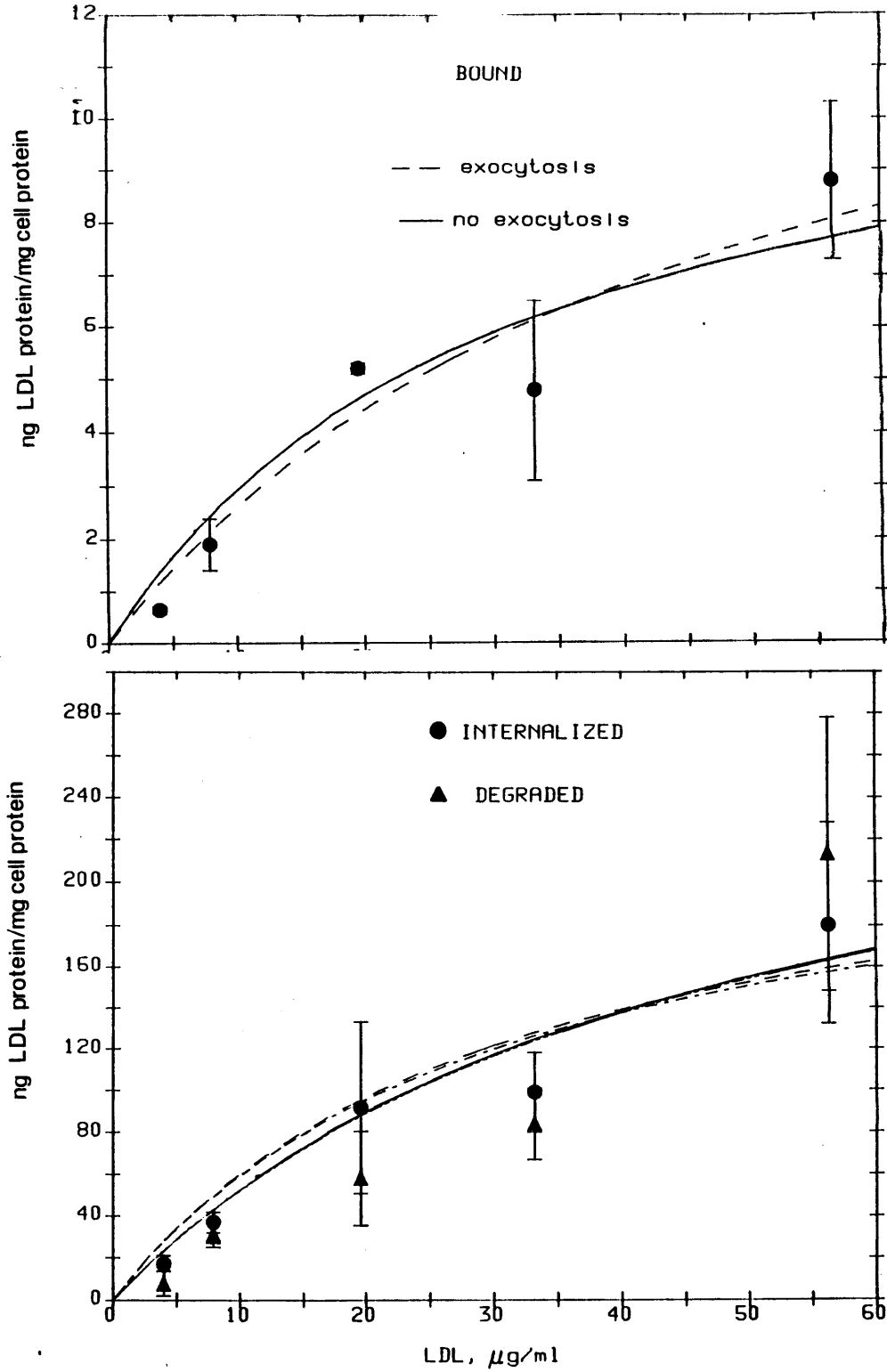


Figure 2-11 (cont.) Expt. BSMC35: LDL metabolism as a function of concentration at 4 hr.

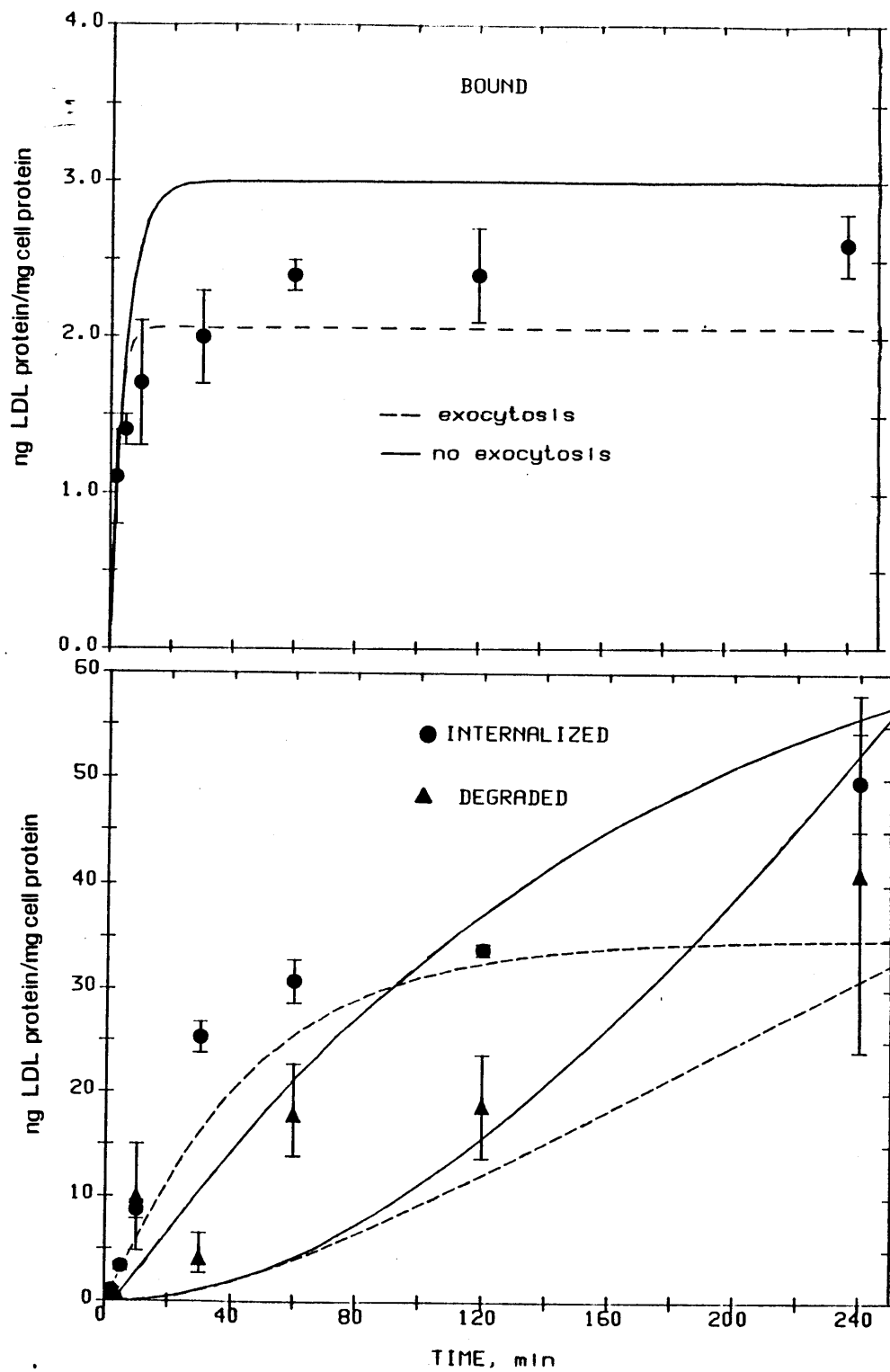


Figure 2-12: Expt. BSMC40: LDL metabolism as a function of time. Smooth muscle cells were incubated with $10.8 \mu\text{g/ml}$ for indicated times.

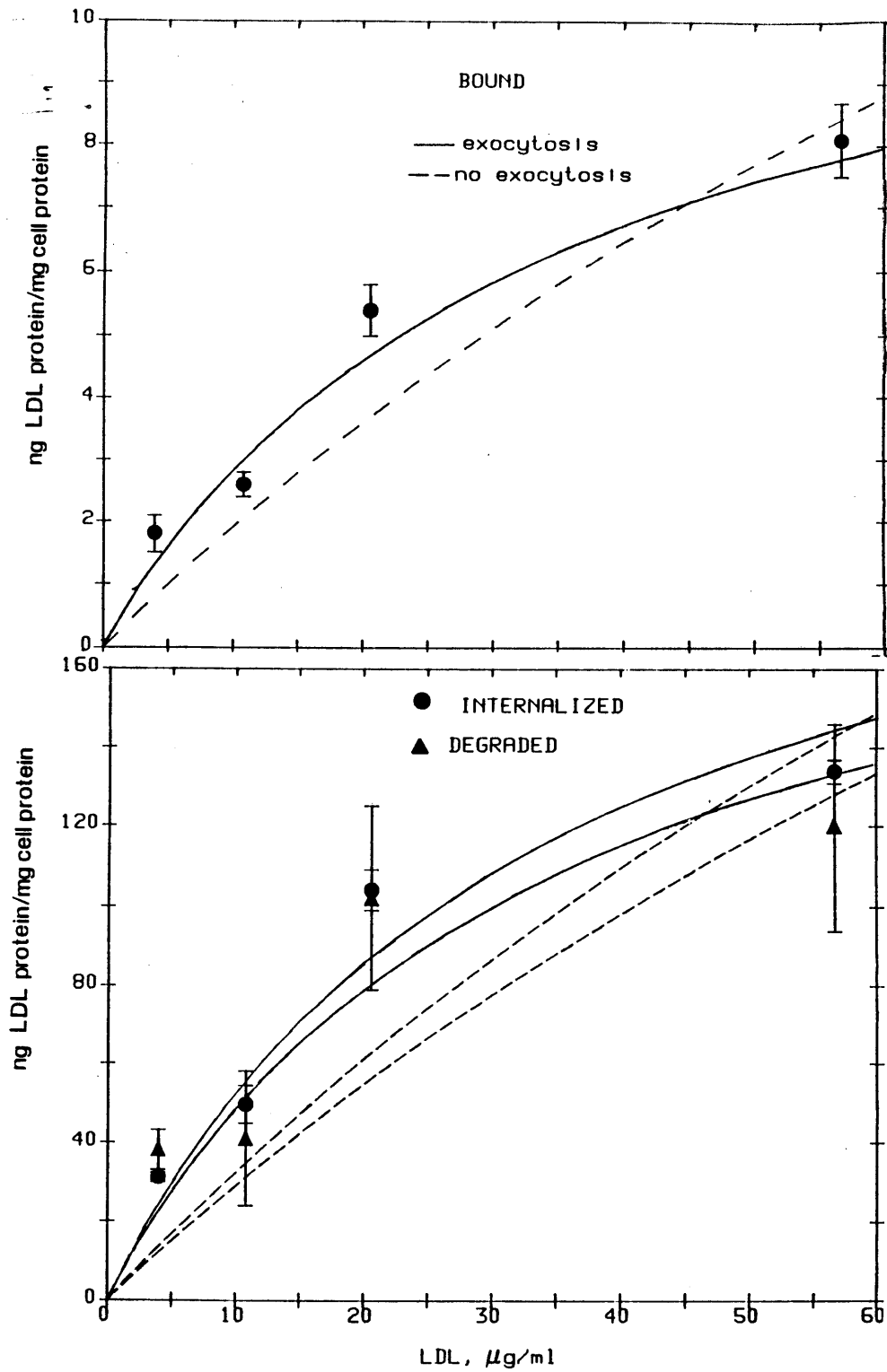


Figure 2-12 (cont.) Expt. BSMC40: LDL metabolism as a function of concentration at 4 hr.)

Table 2-VI: Rate Constants for Receptor-Mediated LDL Metabolism from Fits of Individual Experiments

Expt.	Model	$k_1, M^{-1}min^{-1} \times 10^{-7}$	k_2, min^{-1}	k_3, min^{-1}	k_5, min^{-1}	R_T , receptors/cell	$det(F) \times 10^{-8}$
BSMC6	no exocytosis	1.29 ± 0.19	0.20 ± 0.01	0.0107 ± 0.0003	--	5900 ± 400	2.28
	exocytosis	2.04 ± 0.34	0.33 ± 0.04	0.0093 ± 0.0003	0.011 ± 0.003	6100 ± 400	1.17
BSMC10	no exocytosis	0.23 ± 0.04	0.09 ± 0.01	0.0071 ± 0.0003	--	7600 ± 800	1.96
	exocytosis	0.53 ± 0.08	0.27 ± 0.03	0.0050 ± 0.0003	0.023 ± 0.004	8900 ± 800	0.73
BSMC29	no exocytosis	0.10 ± 0.07	0.23 ± 0.02	0.0078 ± 0.0008	--	13000 ± 8000	1.19
	exocytosis	0.34 ± 0.19	0.70 ± 0.24	0.0059 ± 0.0008	0.023 ± 0.005	12000 ± 5000	0.79
BSMC33	no exocytosis	0.29 ± 0.05	0.16 ± 0.01	0.0022 ± 0.0012	--	17500 ± 1600	8.82
	exocytosis	0.70 ± 0.10	0.39 ± 0.04	0.0017 ± 0.0002	0.011 ± 0.002	17000 ± 1500	2.40
BSMC35	no exocytosis	0.28 ± 0.07	0.17 ± 0.01	0.0067 ± 0.0003	--	4800 ± 600	0.057
	exocytosis	0.49 ± 0.16	0.46 ± 0.16	0.0051 ± 0.0005	0.018 ± 0.008	5900 ± 1000	0.042
BSMC40	no exocytosis	0.22 ± 0.03	0.15 ± 0.01	0.0063 ± 0.0002	--	5000 ± 400	0.00203
	exocytosis	0.13 ± 0.05	0.39 ± 0.07	0.0046 ± 0.0003	0.017 ± 0.004	12500 ± 4100	0.0015
Average	no exocytosis	0.40 ± 0.40	0.17 ± 0.05	0.007 ± 0.003	--	8900 ± 5000	
	exocytosis	0.71 ± 0.68	0.41 ± 0.17	0.0053 ± 0.0024	0.017 ± 0.006	10000 ± 4200	
Table 2-III	no exocytosis	0.32 ± 0.06	0.15 ± 0.01	0.0067 ± 0.0004	--	7500 ± 700	1440
	exocytosis	0.50 ± 0.17	0.25 ± 0.07	0.0057 ± 0.0006	0.008 ± 0.005	7800 ± 800	1420

2.5.3 Comparison of Receptor-Mediated Metabolism in Rabbit and Bovine Smooth Muscle Cells

Since rabbits were used in the in vivo experiments discussed in Chapter 4 it was necessary to determine if LDL metabolism of rabbit and bovine aortic smooth muscle cells are similar. Rabbit aortic smooth muscle cells were isolated by enzymatic digestion (Chamley-Campbell et al. [1979]). A single experiment (BSMC38) was performed in which quiescent bovine and rabbit smooth muscle cells were incubated for 4 hr with LDL concentrations ranging from 2 to 70 $\mu\text{g/ml}$. At the end of the incubation receptor-mediated binding, internalization, and degradation were determined. Results are presented in Figure 2-13. Each point is the average of three dishes and the error bars represent the standard deviation.

Qualitatively, LDL binding, internalization, and degradation are similar for both types of smooth muscle cells. Although all of the rate constants cannot be determined independently in this experiment, the kinetic models can be used to compare the data. Based upon the estimates of the rate constants presented in Table 2-III) for the lumped model including exocytosis, it is evident that steady state is reached by about 4 hr. At steady state, equations (2-24) to (2-26) reduce to:

$$[LR] = \frac{[R_T][L_o]}{K_{int} + [L_o]} \quad (2-49)$$

$$[LR_i] = \frac{k_2}{k_x} \left[\frac{[R_T][L_o]}{K_{int} + [L_o]} \right] \quad (2-50)$$

$$[L_d] = \frac{k_2 k_3}{k_x} \left[t - \frac{1}{k_x} \left(\frac{[R_T][L_o]}{K_{int} + [L_o]} \right) \right] \quad (2-51)$$

Regression of equations (2-49) to (2-51) using the minimization criterion of equation (2-41) results in estimates for four parameter groups: $[R_T]$, K_{int} , $\frac{k_2}{k_x}$, and

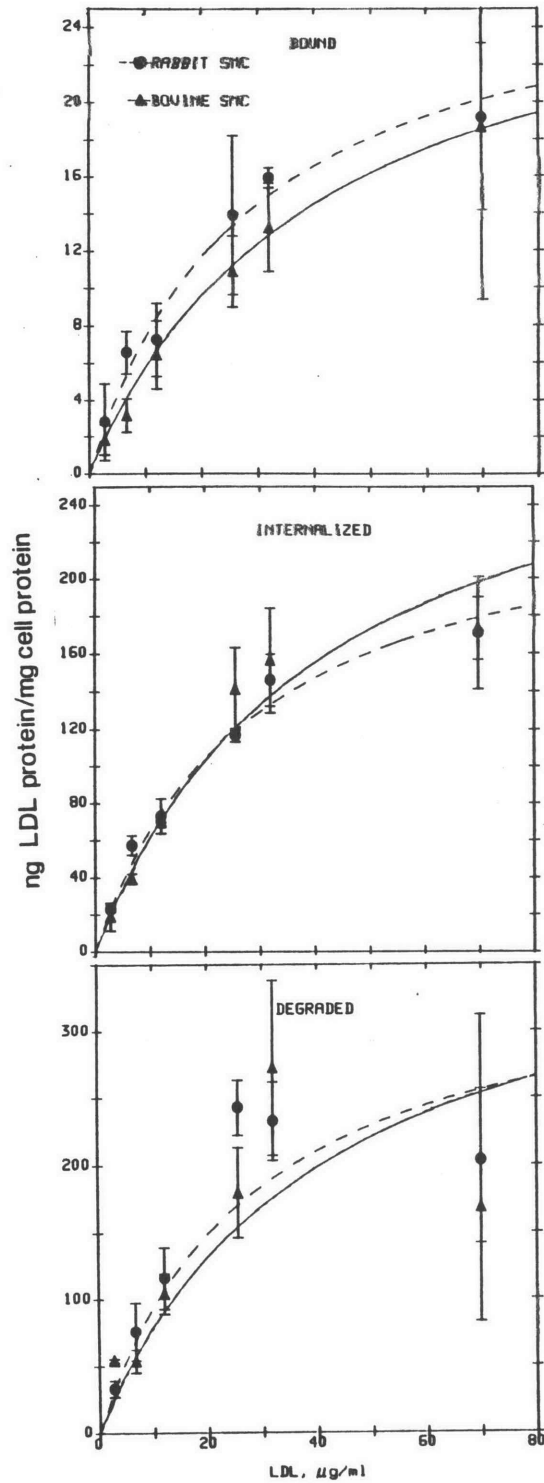


Figure 2-13: LDL binding, internalization, and degradation by rabbit and bovine aortic smooth muscle cells. Smooth curves represent the best fits of equations (2-49) to (2-51) to data for bovine (\blacktriangle) and rabbit (\bullet) smooth muscle cells.

$k_3[t - 1/k_x]$. The fits are presented in Figure 2-13 and the parameters are listed in columns 1 and 2 of Table 2-VII. For comparison, the values of the parameter groups calculated from fits of the pooled data (Table 2-III) are presented in column 3 of Table 2-VII. At the 95% confidence level there is no statistical difference between the two cell types in the estimates of $[R_T]$ and K_{int} . (Reckless et al. [1979] report that K_{int} is 43 nM for rabbit LDL metabolism by rabbit smooth muscle cells). $\frac{k_2}{k_x}$ ($p < 0.02$) and $k_3(t - 1/k_x)$ ($p < 0.05$) for bovine and rabbit smooth muscle cells are significantly different. The relative difference between these two groups is not large, suggesting that the rate constants measured using bovine cells are a reasonable approximation of the rate constants describing LDL metabolism by rabbit smooth muscle cells.

Table 2-VII: Comparison of Parameter Groups for Bovine and Rabbit Smooth Muscle Cells

	Bovine SMC	Rabbit SMC	From Table 2-III
$[R_T]$, receptors/cell	11681 ± 1430	11165 ± 1109	7754 ± 768
K_{int} , M x 10^9	82.0 ± 18.6	56.2 ± 7.6	50.0 ± 9.6
k_2/k_x	10.7 ± 0.5	8.9 ± 0.5	18.0 ± 10.4
$k_3(t - 1/k_x)$	1.28 ± 0.10	1.43 ± 0.07	0.96 ± 0.16

2.5.4 Pulse-Chase Experiments

In order to examine exocytosis in more detail, pulse-chase experiments were performed. Quiescent bovine smooth muscle cells were incubated with either 10 or 20 $\mu\text{g/ml}$ ^{125}I -LDL for 2 hr at 37 °C (pulse), after which they were washed and incubated with heparin as described in Materials and Methods. At the end of the 4 °C incubation the cells were washed one additional time and warm medium

containing unlabeled LDL was added. The cells were then incubated at 37 °C for times ranging from 15 min to 2 hr (chase). At the end of the chase period, the medium was removed for assay of degradation products, the cells were rinsed three times, and cell-associated ^{125}I was measured. The protocol is identical to that of Aulinskas et al. [1981].

Three pulse chase experiments were performed with smooth muscle cells. In two of these (BSMC15 and BSMC21) cells were incubated with 10 $\mu\text{g}/\text{ml}$ ^{125}I -LDL, and in the third (BSMC26) 20 $\mu\text{g}/\text{ml}$ was used. In experiment BSMC26 exocytosis was determined by measuring the TCA insoluble radioactivity released into the medium during the chase period.

A semilogarithmic plot of the disappearance of the normalized intracellular LDL concentration is presented in Figure 2-14. (Data were corrected for nonspecific internalization). Loss of intracellular LDL is first order, which is in agreement with predicted behavior for the single compartment model. The slope is $0.0071 \pm 0.0005 \text{ min}^{-1}$ which is equal to k_x , the sum of the rate constants for degradation and exocytosis. This is significantly less than the value k_x (0.0139 ± 0.0047) determined from regression of data for bound, internalized, and degraded LDL presented in Table 2-III.

In order to examine whether the reduction in k_x depended upon the cell type, two experiments were also performed with human skin fibroblasts. (Cells were incubated with 20 $\mu\text{g}/\text{ml}$ ^{125}I -LDL for 2 hr at 37 °C.) Again, loss of intracellular ligand is first order (Figure 2-15) with k_x equal to $0.0096 \pm 0.0007 \text{ min}^{-1}$.

The single compartment model can be used to analyze the pulse-chase experiments. During the chase period, the concentration of LDL on the cell surface is zero and LDL is removed by exocytosis and degradation. For this case equations

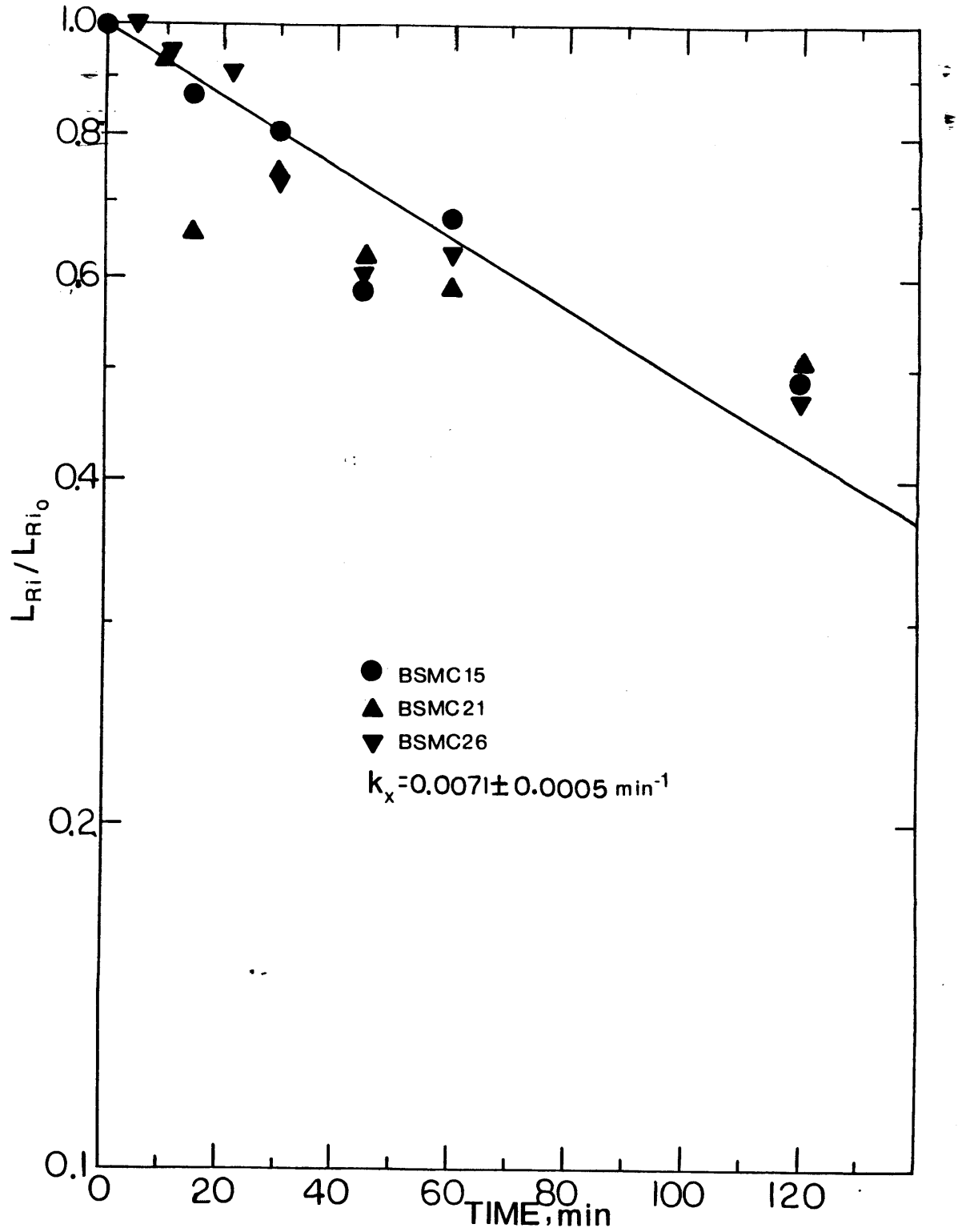


Figure 2-14: Semilogarithmic Plot of the Disappearance of Intracellular LDL from Bovine Smooth Muscle Cells.

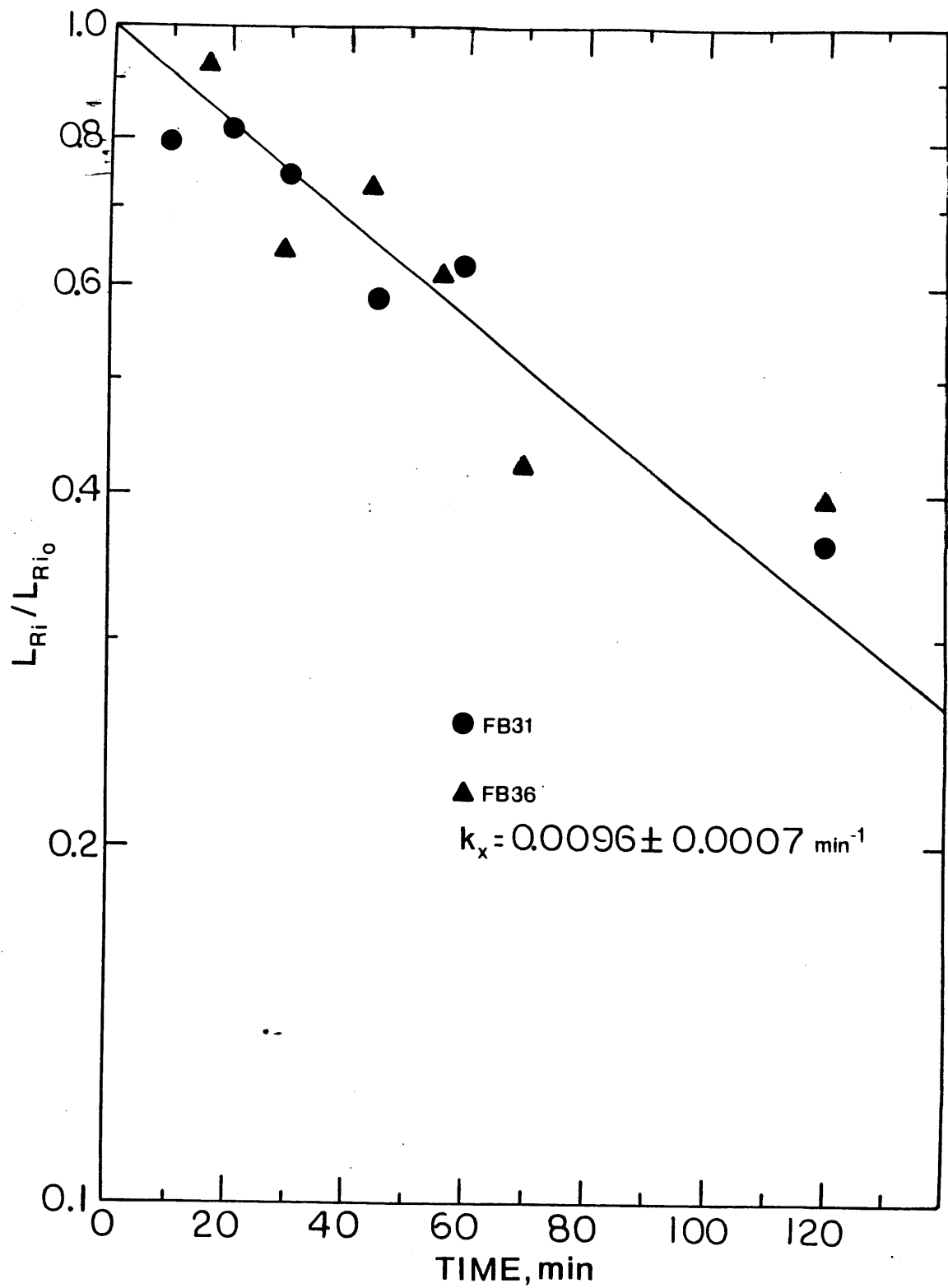


Figure 2-15: Semilogarithmic Plot of the Disappearance of Intracellular LDL from Human Skin Fibroblasts.

(2-22) and (2-23) reduce to:

$$\frac{d[L_{Ri}]}{dt} = -(k_3 + k_5)[L_{Ri}] \quad (2-52)$$

$$\frac{d[L_{Rd}]}{dt} = k_3[L_{Ri}] \quad (2-53)$$

At the start of the chase incubation, $[L_{Ri}] = [L_{Rio}]$ and $[L_{Rd}] = 0$. The solution of the equations (2-52) and (2-53) are:

$$[L_{Ri}] = [L_{Rio}]e^{-k_x t} \quad (2-54)$$

$$[L_{Rd}] = [L_{Rio}]\frac{k_3}{k_x}(1 - e^{-k_x t}) \quad (2-55)$$

Internalization and degradation were simultaneously fit to equations (2-54) and (2-55) by minimization of the determinant of the **F** matrix. Fitted curves are presented in Figure 2-16 for smooth muscle cells and Figure 2-17 for fibroblasts. The rate constants are presented in columns 1 and 2 of Table 2-VIII. There is good agreement between fitted curves and data (Figures 2-16 and 2-17) for internalized and degraded LDL and predicted and experimental data for exocytosis.

Table 2-VIII: Rate Constants Estimated from Pulse-Chase Experiments

	Bovine SMC	Human Fibroblasts	from Table 2-III
k_3, min^{-1}	0.0038 ± 0.0005	0.0075 ± 0.0004	0.0057 ± 0.0006
k_5, min^{-1}	0.0034 ± 0.0011	0.0021 ± 0.0008	0.0082 ± 0.0047

From the pulse-chase experiments, the rate constant for LDL degradation is about two times larger for fibroblasts than for smooth muscle cells. Values of k_3 and k_5 from Table 2-III are presented in column 3 of Table III for comparison. Values of k_3 and k_5 calculated from pulse-chase experiments with bovine smooth

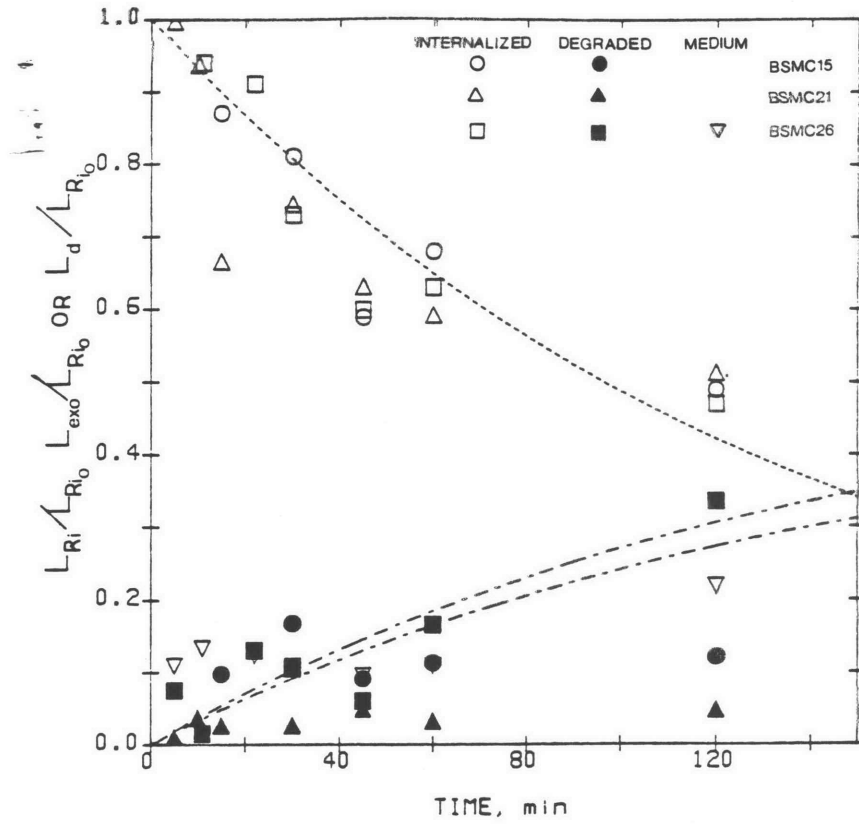


Figure 2-16: Fitting Pulse-Chase Experiments: Bovine Smooth Muscle Cells.

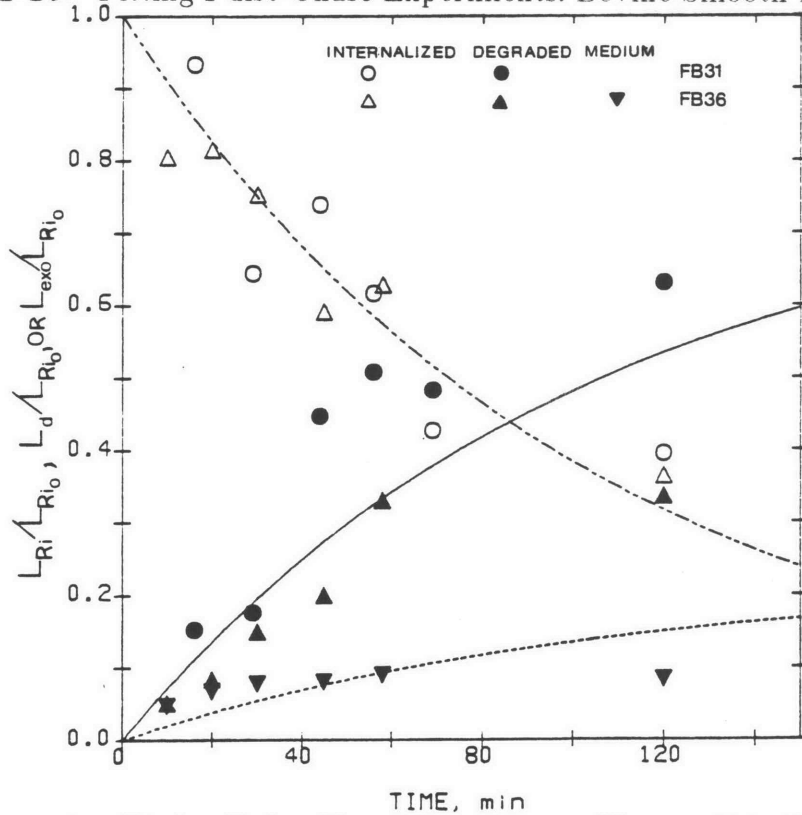


Figure 2-17: Fitting Pulse-Chase Experiments: Human Skin Fibroblasts.

muscle cells are less than the values presented in Table 2-III. For human fibroblasts, k_3 is larger than the value presented in Table 2-III whereas k_5 is less than the value in Table 2-III. Estimates of the rate constant for exocytosis from pulse-chase experiments are close to the values estimated from the pulse-chase experiments of Aulinskas et al. [1981] with bovine smooth muscle cells ($k_5 = 0.0020 \pm 0.0006$).

The difference between estimates of k_3 and k_5 from pulse-chase experiments and kinetic experiments presented in Figure 2-V is probably due to some general metabolic alteration as a result of the pulse-chase protocol. Vesicles involved in exocytosis may be vesicles which have recently detached and are close to the cell membrane (Adams et al. [1982]). Upon cooling to 4 °C vesicle-membrane fusion is inhibited, but vesicle diffusion continues at a much lower speed. Vesicles involved in exocytosis move away from the cell membrane such that, upon warming they are less likely to fuse with the cell membrane and k_5 would be smaller than if determined from an experiment in which the cells are maintained at 37 °C throughout.

2.5.5 Regulation of the LDL Receptor by LDL

In order to study LDL receptor regulation by LDL, quiescent smooth muscle cells were preincubated for 24 hr with 0 to 100 $\mu\text{g/ml}$ human LDL in 5% LPDS. Following the incubation cells were washed and incubated with 5% LPDS for 30 min at 37 °C in order to allow cells to internalize any residual receptor-bound unlabeled LDL. Smooth muscle cells were then incubated for 2 hr at 37 °C with either 10 $\mu\text{g/ml}$ ^{125}I -LDL or 10 $\mu\text{g/ml}$ ^{125}I -LDL and 500 $\mu\text{g/ml}$ LDL after which receptor-mediated binding, internalization, and degradation were determined. Results from two experiments (BSMC37 and BSMC42) are presented in Figures 2-18

and 2-19. Each point represents the average of four dishes in experiment BSMC37 and three dishes in experiment BSMC42. The error bars are equal to the standard deviation.

^{125}I -LDL binding and internalization decrease as the preincubation concentration of LDL increases (Figures 2-18 and 2-19). For preincubation concentrations above 30 $\mu\text{g}/\text{ml}$, binding and internalization do not decrease further. This minimum is about 30% to 40% of the amount bound or internalized when the cells are preincubated without LDL. LDL degradation is more erratic, decreasing with increasing preincubation concentration until 50 $\mu\text{g}/\text{ml}$ when degradation increases. The cause of the erratic behavior of degraded LDL is not known.

In experiment BSMC42, rabbit and human LDL were used. (Rabbit LDL was used to determine if receptor regulation is influenced by the type of LDL used and to mimic the interstitial environment to which the smooth muscle cells are exposed.) Preincubation with either rabbit or human LDL resulted in about the same decrease in binding, internalization, and degradation (Figure 2-19). The minimum level of binding, internalization, and degradation is less than in the results presented in Figure 2-18, but the results are qualitatively similar. The results are qualitatively similar to those obtained by Witte et al. [1982] with quiescent human skin fibroblasts.

Results in Figures 2-18 and 2-19 have been used to estimate the number of receptors on rabbit aortic smooth muscle cells exposed to rabbit LDL in the interstitial fluid. The plasma concentration of rabbit LDL in New Zealand white rabbits is about 290 μg LDL protein/ml (Shore and Shore [1975]). The concentration of native human LDL in the inner media of the human aorta ($\mu\text{g}/\text{cm}^3$ tissue) is reported to be 0.6% of plasma concentration (Smith and Staples [1980]). The interstitial concentration (C_f/ϵ_w) is simply:

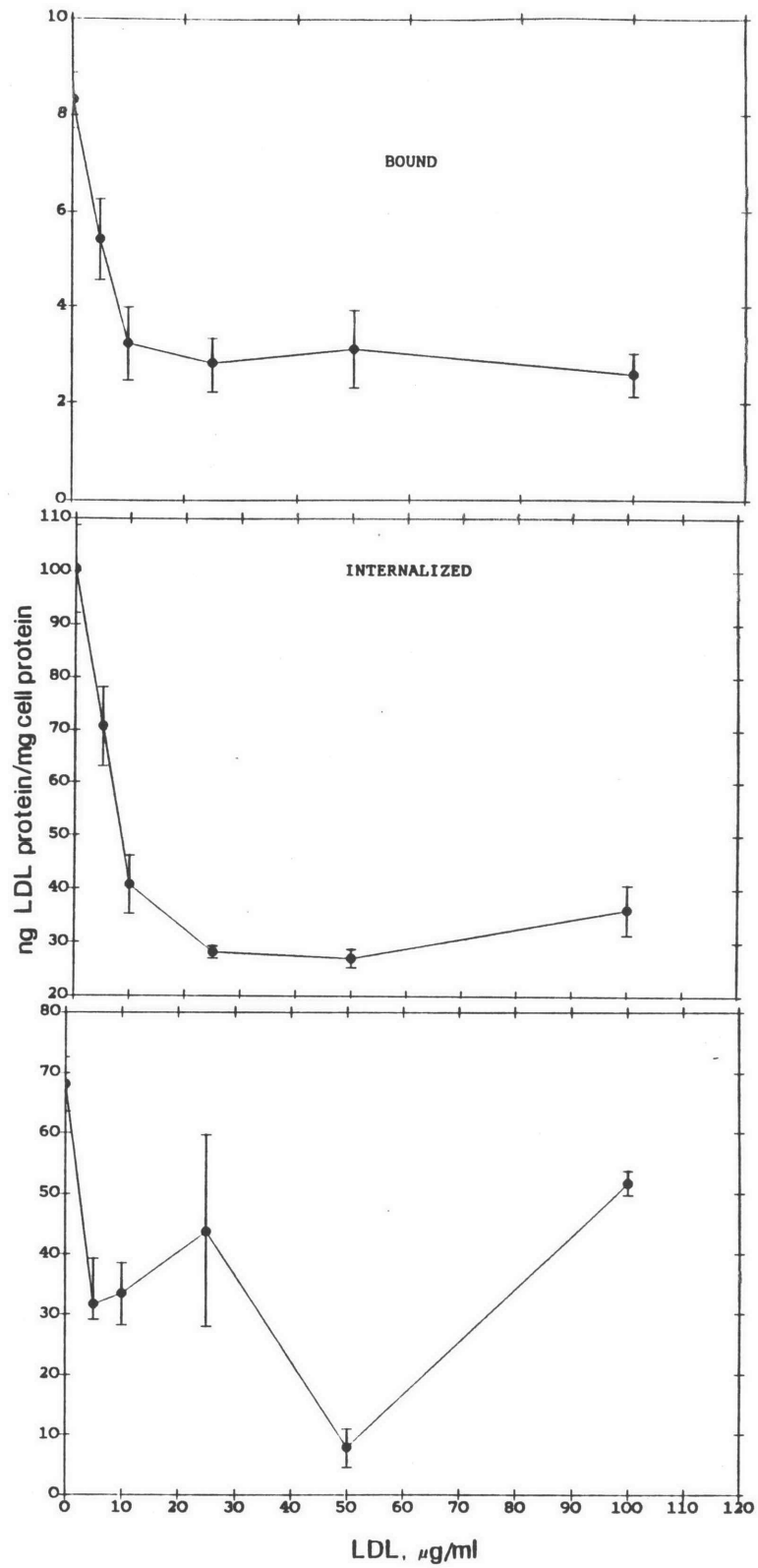


Figure 2-18: Regulation of the LDL Receptor on Bovine Smooth Muscle Cells (Expt. BSMC37).

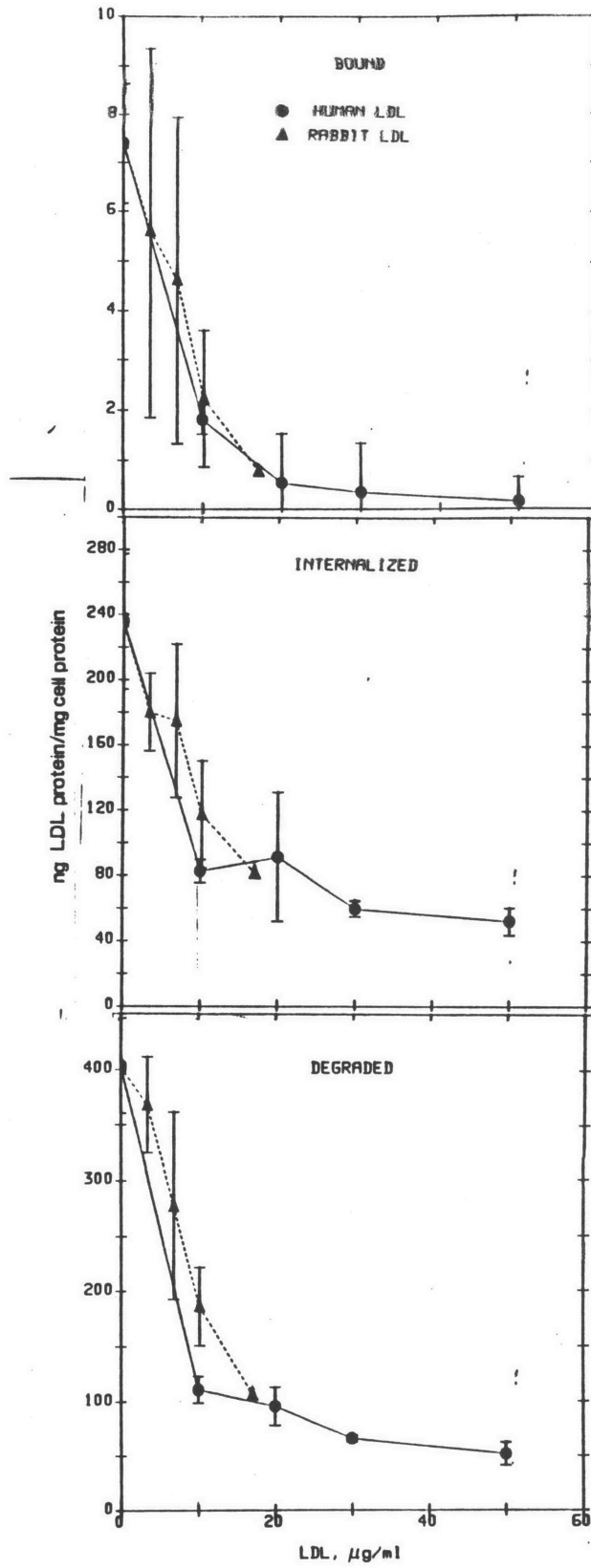


Figure 2-19: Regulation of the LDL Receptor by Rabbit and Human LDL (Expt. BSCM42).

$$\frac{C_f}{\epsilon_w C_{p_0}} = \frac{0.006}{\epsilon_w} \quad (2-56)$$

Smith and Staples [1980] estimated ϵ_w to be 0.30 for which the interstitial concentration is 2% of the plasma concentration. In the rabbit this corresponds to about 6 $\mu\text{g}/\text{ml}$. For this concentration, the data in Figures 2-18 and 2-19 indicate that the LDL receptors are reduced to about 45% of the maximum value (7800 receptors/cell) or 3500 receptors/cell. Another estimate can be made from the LDL concentration in lymph which is assumed to be in equilibrium with the interstitial fluid. The lymph concentration of LDL is 10% of the plasma concentration (Reichl et al. [1975]) and the interstitial concentration would then be 29 $\mu\text{g}/\text{ml}$. For this concentration, the results in Figures 2-18 and 2-19 indicate that the receptor number on quiescent bovine smooth muscle cells is 23% of its value when the cells are incubated in 5% LPDS, which corresponds to 1800 receptors/cell. (These estimates are reconsidered in Chapter 5 in light of the in vivo experiments presented in Chapter 4.)

2.5.6 Effect of NH_4Cl on LDL Metabolism

In order to examine the effect of an alteration in LDL metabolism upon the rate constants, smooth muscle cells were incubated with either 5% LPDS or 10 mM NH_4Cl in 5% LPDS for one hr after which they were incubated with ^{125}I -LDL with or without NH_4Cl . (NH_4Cl raises the lysosomal pH and inhibits degradation (Seglen [1983]). NH_4Cl may have additional effects, such as raising the endosomal pH and inhibiting receptor recycling (Tietze et al. [1980]).) Receptor-mediated LDL binding, internalization, and degradation were measured as a function of time with 12 $\mu\text{g}/\text{ml}$ ^{125}I -LDL or as a function of concentration at four hr. Results are presented in Figure 2-20. Experiment BSMC33 (Figure 2-10) is the control

experiment. Each point is the average of two dishes and error bars represent standard deviation.

In the presence of 10 mM NH_4Cl , LDL binding and internalization are reduced relative to the control and degradation is essentially zero. After incubation with 10 mM NH_4Cl , intracellular LDL reaches a steady state. Since degradation is blocked, LDL must leave the cell by exocytosis. (If exocytosis did not occur, the intracellular concentration would increase linearly with time at steady state.)

Table 2-IX: Effect of 10 mM NH_4Cl on Rate Constants for Receptor-Mediated LDL Metabolism

	Control	10 mM NH_4Cl
$k_1, \text{M}^{-1}\text{min}^{-1} \times 10^{-7}$	0.69 ± 0.10	2.68 ± 0.48
k_2, min^{-1}	0.39 ± 0.04	0.54 ± 0.08
k_3, min^{-1}	0.0017 ± 0.0002	0.000041 ± 0.000034
k_5, min^{-1}	0.011 ± 0.002	0.008 ± 0.002
$R_T, \text{receptors/cell}$	17050 ± 1590	2820 ± 280

Equations (2-24) to (2-26) were fit to the data in Figure 2-20 and rate constants are presented in Table 2-IX. As expected, the degradation rate constant (k_3) is significantly reduced. In addition, there are several secondary changes in LDL metabolism. When smooth muscle cells are incubated with 10 mM NH_4Cl the number of receptors is reduced, the association rate constant (k_1) and the internalization rate constant (k_2) increase, and the rate constant for receptor-mediated exocytosis (k_5) decreases. The decrease in the number of receptors may reflect inhibition of receptor recycling as a result of an increase in endosomal pH. The change in k_5 is small and is probably not significant. Changes in k_1 and k_2 are

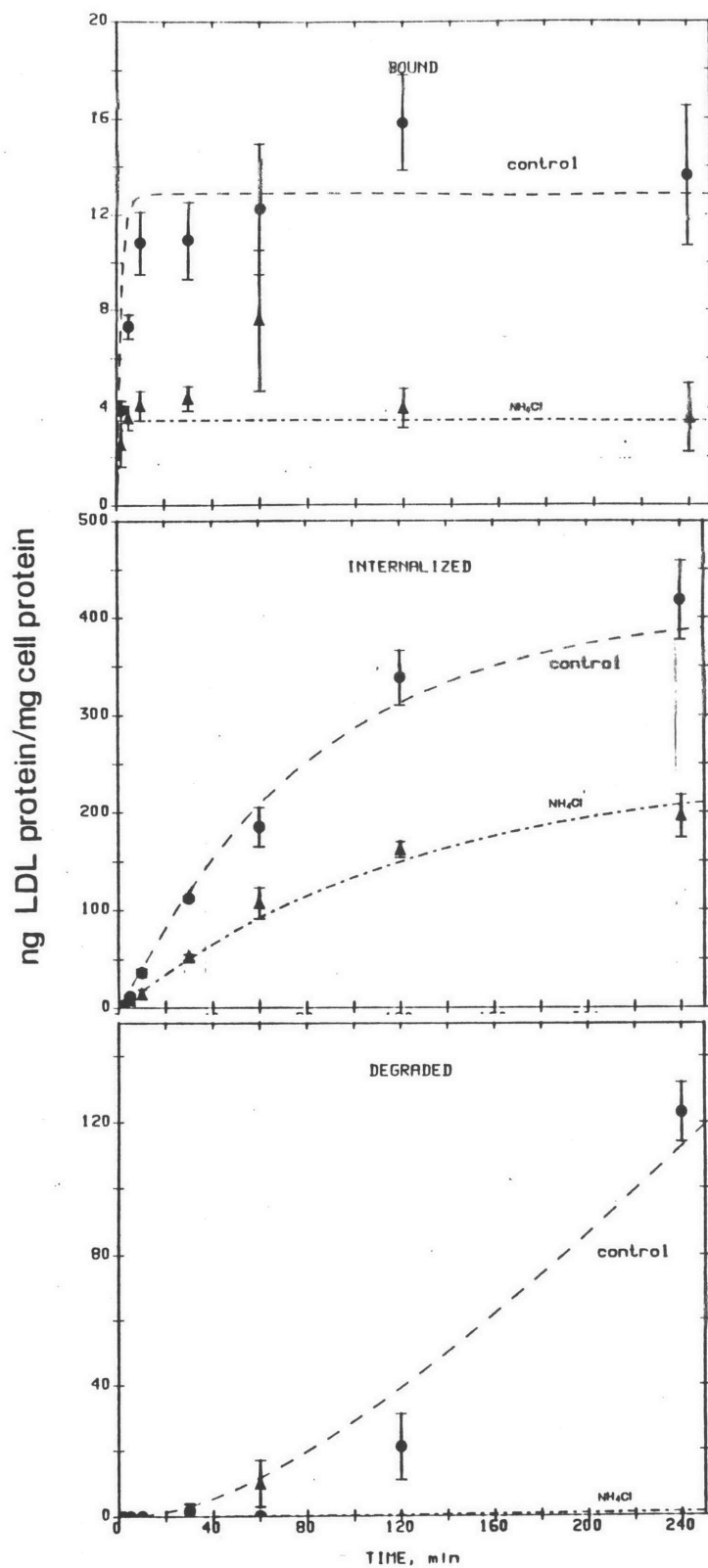


Figure 2-20: Effect of NH₄Cl on the kinetics of LDL metabolism for 12 μ g/ml LDL.

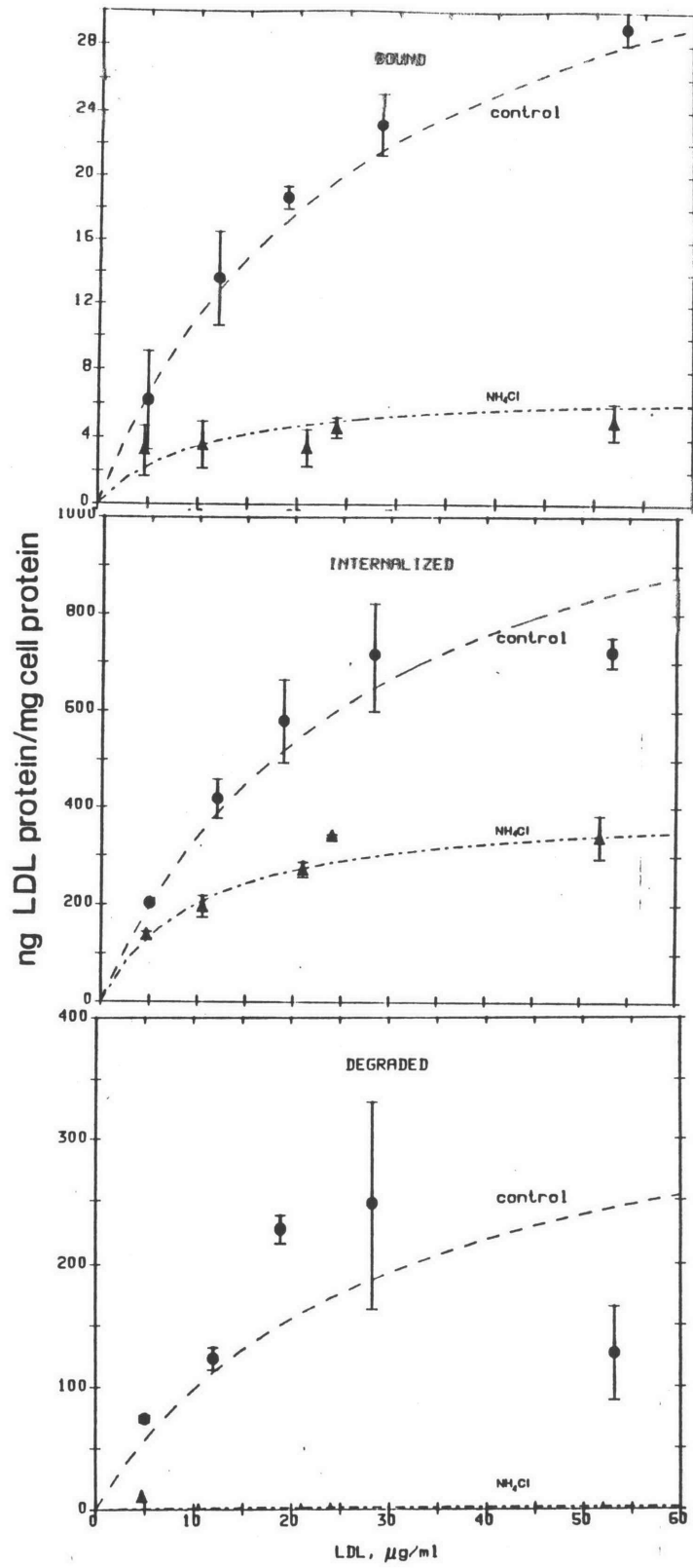


Figure 2-20 (cont.) Effect of NH_4Cl on LDL metabolism as a function of concentration at 4 hr.

rather large but the values are within the range of rate constants presented in Table 2-VI.

2.5.7 Determination of Rate Constants for Receptor-Independent LDL

Metabolism

To determine rate constants for receptor-independent LDL metabolism, cells were incubated with 500 $\mu\text{g}/\text{ml}$ unlabeled LDL and 1 to 110 $\mu\text{g}/\text{ml}$ ^{125}I -LDL. These experiments correspond to those described for receptor-mediated LDL metabolism. Binding, internalization, and degradation were determined as described in Materials and Methods. Results from the six experiments were averaged and are presented in Figure 2-21. Error bars are equal to the standard error of the mean for the pooled samples.

The kinetic behavior of receptor-independent and receptor-mediated internalization and degradation at 10 $\mu\text{g}/\text{ml}$ are similar, although the magnitude of receptor-independent metabolism is lower. Internalization and degradation are linear functions of LDL concentration at 4 hr.

Receptor-independent internalization and degradation were fit to the three models analogous to those described for receptor-mediated metabolism: 1) a model with endosomal and lysosomal compartments with exocytosis from the endosomal compartment (curve A in Figure 2-21); 2) a single compartment lumped model with exocytosis (curve B in Figure 2-21); and 3) a lumped model without exocytosis (curve C in Figure 2-21). These models are presented as the smooth curves in Figure 2-21 and the rate constants are listed in Table 2-X. The lumped model without exocytosis (curve C) tends to underestimate internalized LDL as a function of time, whereas the other two models fit data for internalized LDL much better. The estimated parameter standard deviations for the two compartment model are

larger than those for the single compartment model. For the available data, it is likely that a single compartment model adequately describes the data.

The correlation matrices for fits obtained with three models (curves A,B,C) are presented in Table 2-XI. The correlation matrices are very high even when only one intracellular compartment was used which explains why the standard deviation of k_7 is large. The values of k_4 and k_6 change when k_7 is set to zero, suggesting that exocytosis is important. The high correlations indicate that additional data are required in order to accurately estimate k_7 .

For the lumped model with exocytosis, k_7 (0.0071 ± 0.0091) is very similar to k_5 (0.0082 ± 0.0047) min^{-1} (curve D), the rate constant for exocytosis of LDL internalized by receptor-mediated mechanisms. When the pooled data for receptor-independent metabolism are fit with $k_7 = k_5 = 0.0082$, the resulting values of k_4 and k_6 (row 4 of Table 2-X) are similar to those obtained when k_7 is allowed to vary (row 2 of Table 2-X). k_6 for the lumped model with exocytosis is 63% of the value of k_3 obtained with pooled data for receptor-mediated metabolism.

Internalization and degradation were also fit separately by nonlinear regression with k_7 fixed at 0.0082. (Examination of equations (2-37) and (2-38) indicates that internalization depends on k_4 and $k_6 + k_7$ and degradation depends upon $k_4 k_6$ and $k_6 + k_7$ which indicates that it is not possible to fit the individual responses to all three rate constants.) The rate constants are listed in Table 2-X (rows 5 and 6) and the fits are plotted in Figure 2-21 (curves E and F). When internalization is fit alone, k_4 is close to the value obtained from fits of both responses, but k_6 is about twice as large as the value obtained when both responses are fit. When degradation is fit, k_4 and k_6 are quite different than the values obtained with both responses. Parameter standard deviations are larger for estimates obtained from fits of individual responses than from fits of both responses

**Table 2-X : Rate Constants for Combined Data of
Receptor-Independent Metabolism**

Model	Curve in Figure 2-21	k_4 , ml/(mg · min) x 10 ⁵	k_{6l} (or k_6), min ⁻¹	k_{6d} , min ⁻¹	k_7 , min ⁻¹	det(
2 Compartments	A	3.11 ± 1.97	0.0016 ± 0.0006	0.77 ± 6.87	0.0084 ± 0.0078	2.30
Lumped Model	B	3.22 ± 2.00	0.0036 ± 0.0007		0.0071 ± 0.0091	2.28
Lumped Model	C	1.86 ± 0.07	0.0042 ± 0.0002		0.0 (fixed)	2.30
Lumped Model	D	3.48 ± 0.13	0.0035 ± 0.0002		0.0082 (fixed)	2.30
Lumped Model (Internalization Only)	E	3.89 ± 2.36	0.0134 ± 0.0095		0.0082 (fixed)	0.02
Lumped Model (Degradation Only)	F	0.80 ± 0.90	0.0802 ± 0.6697		0.0082 (fixed)	0.00

by the method of Box and Draper [1965]. The fits for the individual responses are quite good, but the predicted values for the response not fit are poor. The value of $\det(\mathbf{F})$ is lower for cases E and F because only a single response has been fit.

Nonspecific binding was also measured as a function of time and concentration. The average results from all six experiments are presented in Figure 2-22. The error bars are equal to the standard error of the mean. Nonspecific binding reaches a steady state after 40 min, is slower than receptor-mediated binding and is a linear function of concentration. Nonspecific binding represents LDL bound to the cell surface and the extracellular matrix. It is not known what fraction of nonspecifically bound LDL is internalized. Consequently, nonspecifically bound LDL has not been incorporated directly into the model. Nevertheless, nonspecific binding qualitatively resembles nonspecific internalization and has been fit to the following function:

$$[L_b] = a[L_o](1 - e^{-bt}) \quad (2-57)$$

where $[L_b]$ is the concentration of nonspecifically bound LDL and a and b are empirical constants. Equation (2-57) was fit to data for nonspecifically bound LDL by nonlinear regression. The best fit curves are displayed in Figure 2-22 and the rate constants are:

$$a = 3.01 \pm 1.67 \times 10^{-4} \text{ ml mg}^{-1}$$

$$b = 0.0813 \pm 0.0668 \text{ min}^{-1}$$

The fit of binding as a function of concentration is quite good, but there is a systematic overestimate of bound LDL between 40 and 240 min. It is possible that LDL is binding to more than one class of sites, some of which bind rapidly and others which bind more slowly. The scatter in the data precluded examination of this with the available data. The relationship between a and k_4 is considered in the

Figure 2-21: Fits of combined data for receptor-independent metabolism of LDL from six experiments. Internalization and degradation were measured as a function of time for an ^{125}I -LDL concentration of $10 \mu\text{g/ml}$ (2-21a) and as a function of LDL concentration at 4 hr (2-21b). Smooth curves represent best fits of data by minimization of the determinant of the matrix \mathbf{F} : A. complete model with two intracellular compartments and exocytosis; B. lumped model with one intracellular compartment and including exocytosis; C. lumped model without exocytosis; D. lumped model with $k_7 = k_5$; E. internalization only with $k_7 = k_5$; and F. degradation only with $k_7 = k_5$.

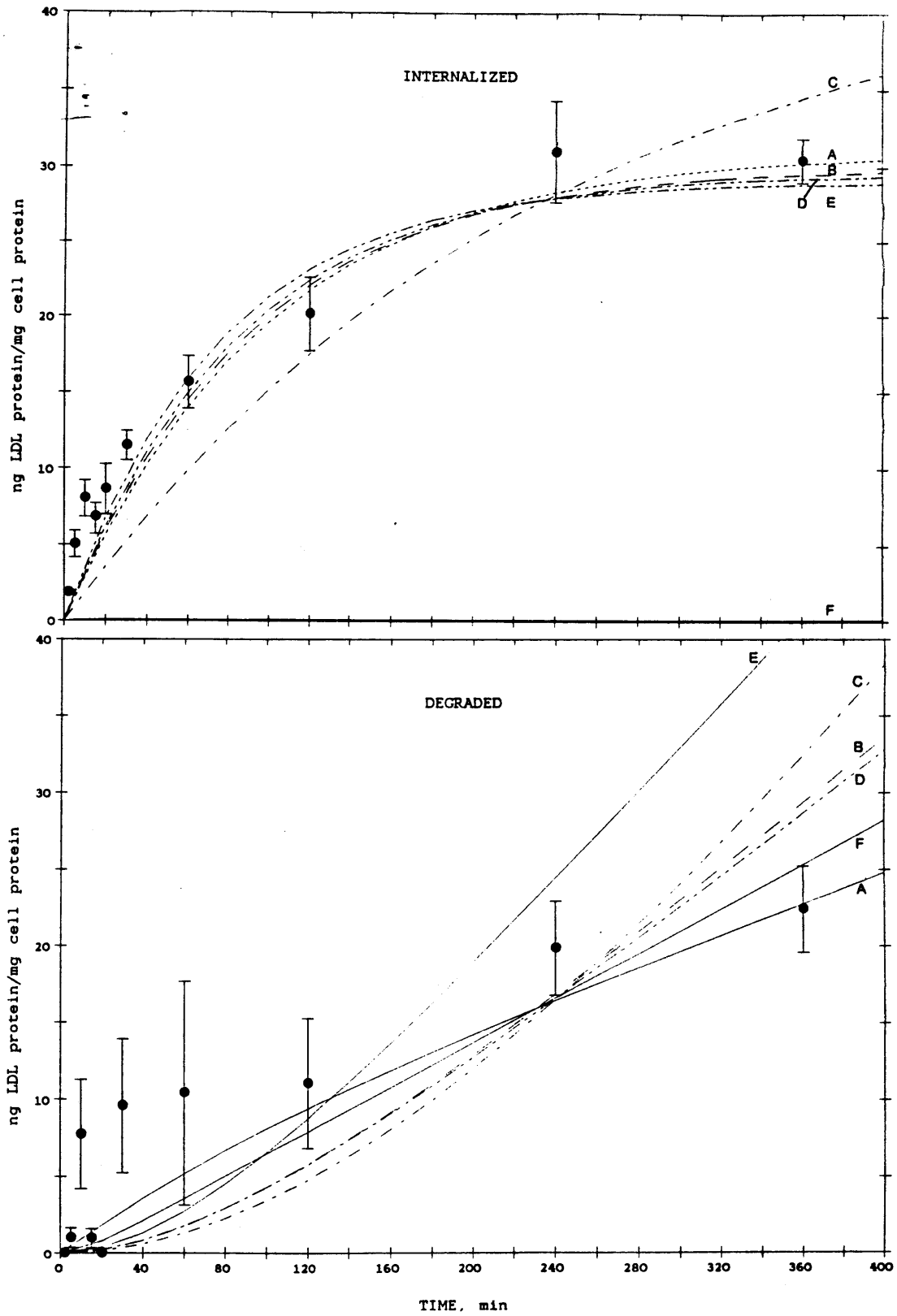


Figure 2-21: Nonspecific metabolism as a function of time.

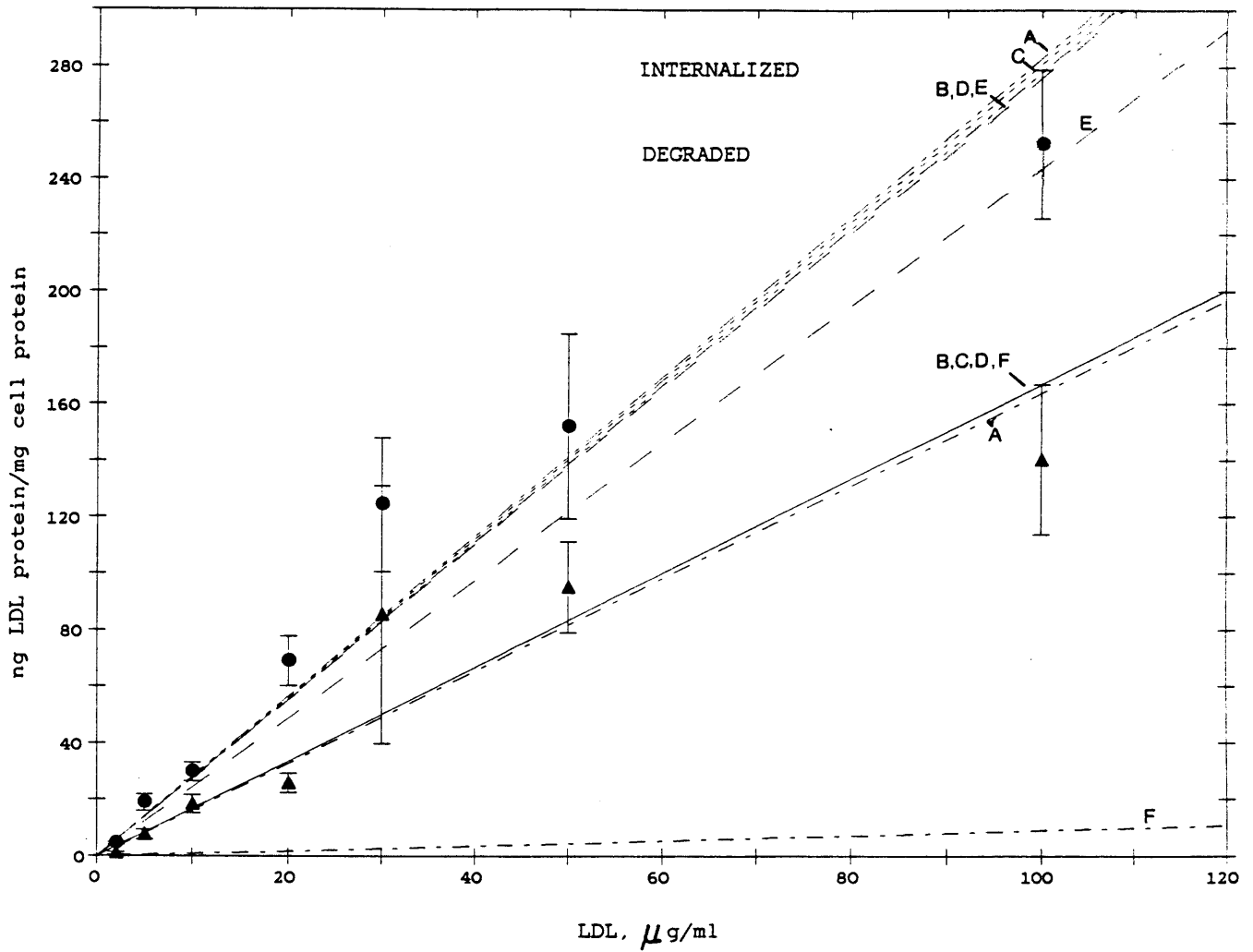


Figure 2-21: Nonspecific metabolism as a function of concentration.

Table 2-XI: Matrix of Correlation Coefficients for Receptor-Independent Metabolism

Complete Two Compartment Model with Exocytosis

	k_4	k_{6l}	k_{6d}	k_7
k_4	1.000	0.949	0.215	0.998
k_{6l}	0.949	1.000	-0.039	0.957
k_{6d}	0.215	-0.039	1.000	0.196
k_7	0.918	0.957	0.196	1.000

Lumped Model with Exocytosis

	k_4	k_6	k_7
k_4	1.000	-0.957	0.998
k_6	-0.954	1.000	-0.956
k_7	0.998	-0.956	1.000

Lumped Model without Exocytosis

	k_4	k_6
k_4	1.000	0.698
k_6	0.689	1.000

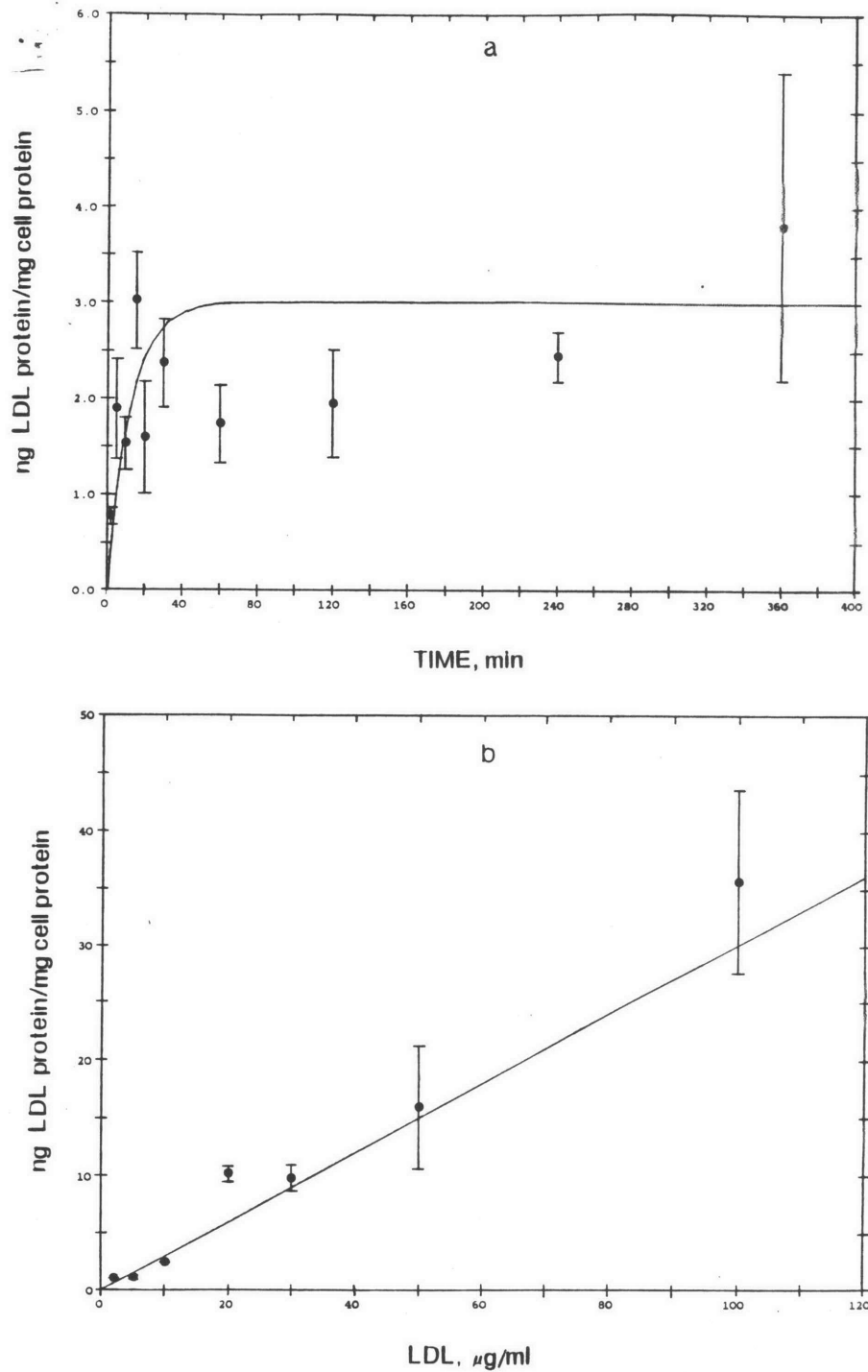


Figure 2-22: Combined data for receptor-independent binding of LDL from six experiments. Binding was measured as a function of time for $10 \mu\text{g/ml}$ ^{125}I -LDL (2-22a) and as a function of LDL concentration at 4 hr (2-22b). Smooth curve represents best fit of data to equation (2-56) by nonlinear regression.

Discussion.

The six individual experiments are presented in Figures 2-23 to 2-28. Data were fit to the lumped model (equations (2-36) and (2-37)) with exocytosis, with $k_7 = k_5$, and without exocytosis ($k_7 = 0$). Fits of the models to data are also presented in Figures 2-23 to 2-28 and the rate constants are listed in Table 2-XII.

The range of values for the rate constant for nonspecific degradation (k_6) and exocytosis (k_7) are similar to the range of values observed for receptor-mediated degradation (k_3) and exocytosis (k_5). It appears likely that the rate-limiting step for LDL degradation is the same for receptor-mediated and receptor-independent degradation, although receptor-independent cholesterol metabolism does not regulate cellular cholesterol and LDL receptor expression. When k_7 is fixed to the value of k_5 determined for receptor-mediated metabolism in the individual experiments, experiments BSMC6, 10, 35, and 40 give fits virtually identical to those obtained when k_7 is not fixed, which suggests that the mechanism of ligand exocytosis is the same for receptor-mediated and receptor-independent pathways.

2.5.8 Metabolism of Methylated LDL

Methylated LDL (mLDL) metabolism was examined in order to verify that mLDL does not bind to the LDL receptor and that mLDL internalization and degradation occur by receptor-independent processes. In two experiments quiescent bovine smooth muscle cells were incubated for two hr with 10 $\mu\text{g}/\text{ml}$ ^{125}I -LDL and 0 to 500 $\mu\text{g}/\text{ml}$ unlabeled LDL or mLDL, after which binding, internalization and degradation were determined. Results are presented in Figures 2-29 and 2-30 for experiments BSMC38 and BSMC41, respectively. Each point is the average of three dishes, and the error bars are equal to the standard deviation. ^{125}I -LDL binding, internalization, and degradation decrease as the concentration of LDL increases,

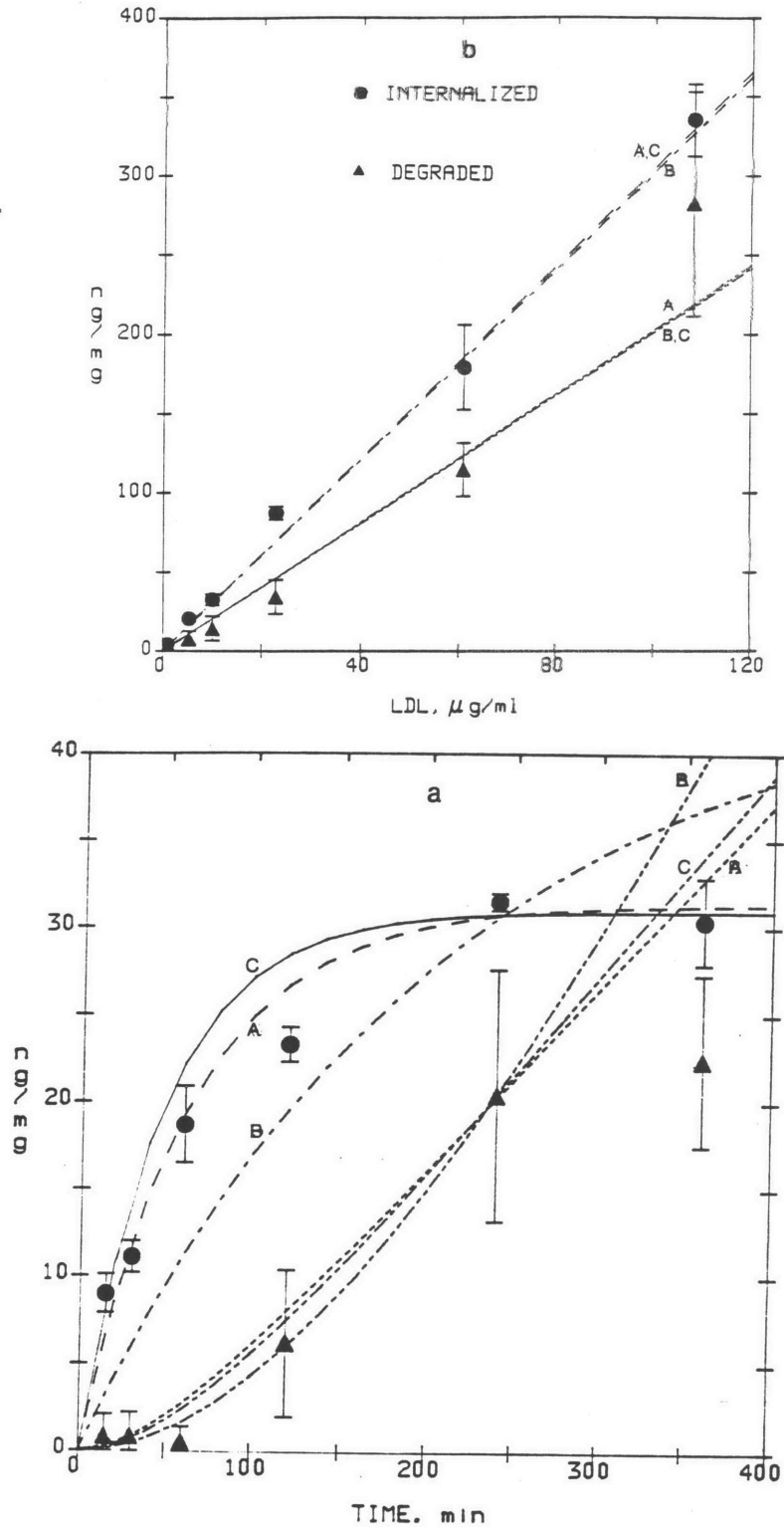


Figure 2-23: Expt. BSMC6: Receptor-Independent LDL internalization and degradation as a function of time at $10.0 \mu\text{g/ml}$ ^{125}I -LDL (a) and as a function of concentration at 4 hr (b). Smooth curves represent: A) lumped model with exocytosis; B) lumped model with no exocytosis; and C) lumped model with $k_7 = k_5$.

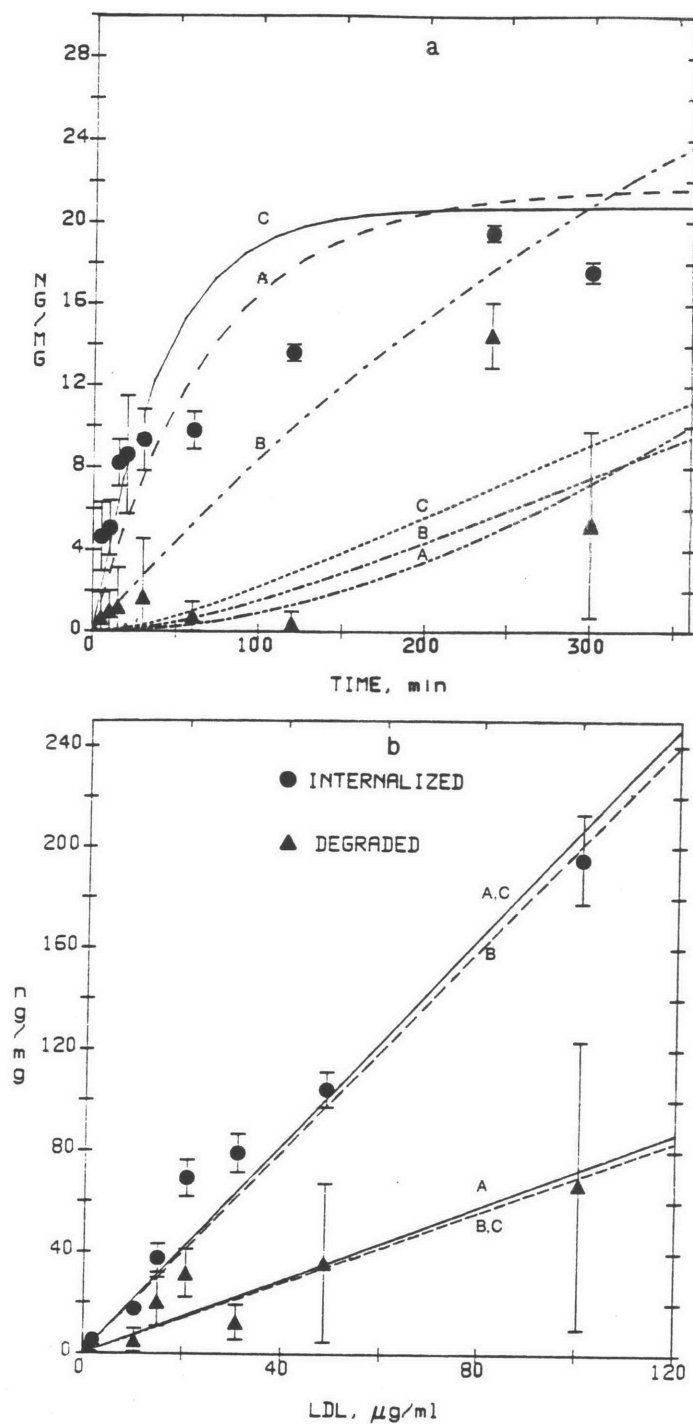


Figure 2-24: Expt. BSMC10: Receptor-Independent LDL internalization and degradation as a function of time at $10.4 \mu\text{g/ml}$ ^{125}I -LDL (a) and as a function of concentration at 4 hr (b). Smooth curves represent: A) lumped model with exocytosis; B) lumped model with no exocytosis; and C) lumped model with $k_7 = k_5$.

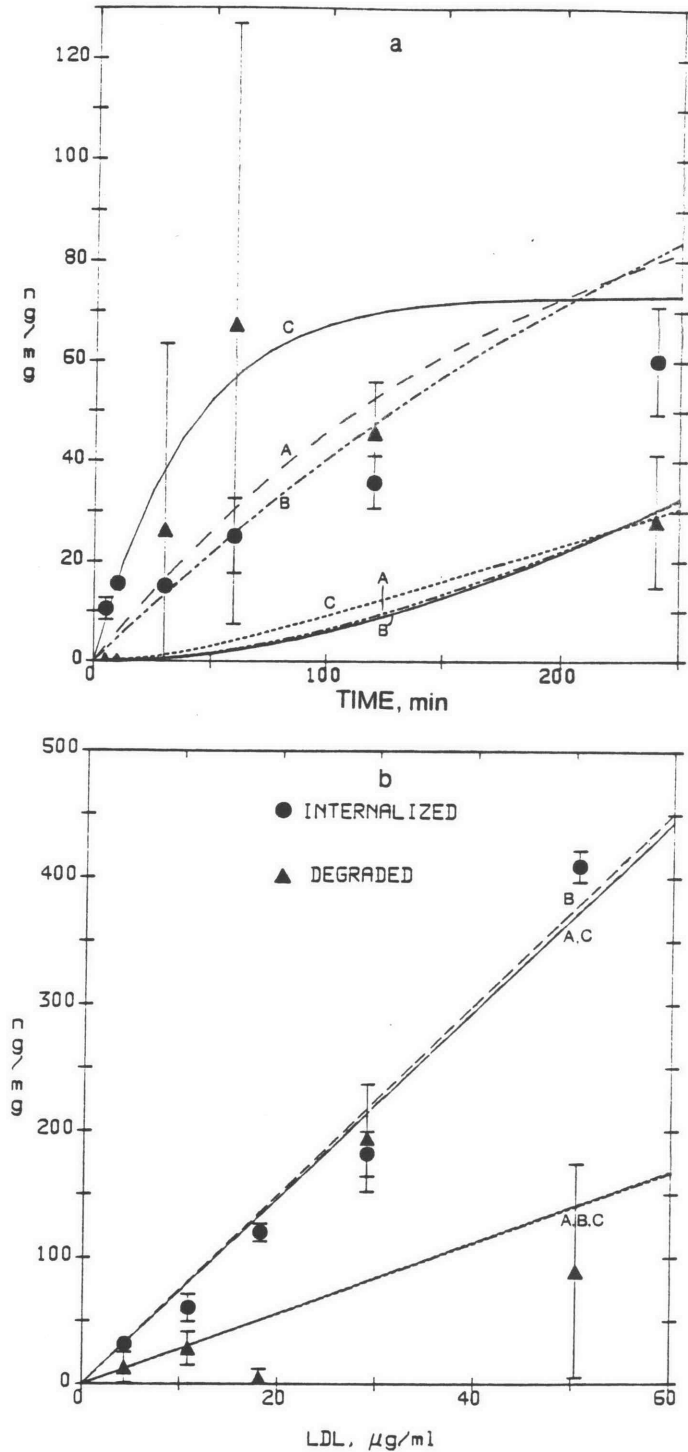


Figure 2-25: Expt. BSMC29: Receptor-Independent LDL internalization and degradation as a function of time at $10.0 \mu\text{g/ml}$ ^{125}I -LDL (a) and as a function of concentration at 4 hr (b). Smooth curves represent: A) lumped model with exocytosis; B) lumped model with no exocytosis; and C) lumped model with $k_7 = k_5$.

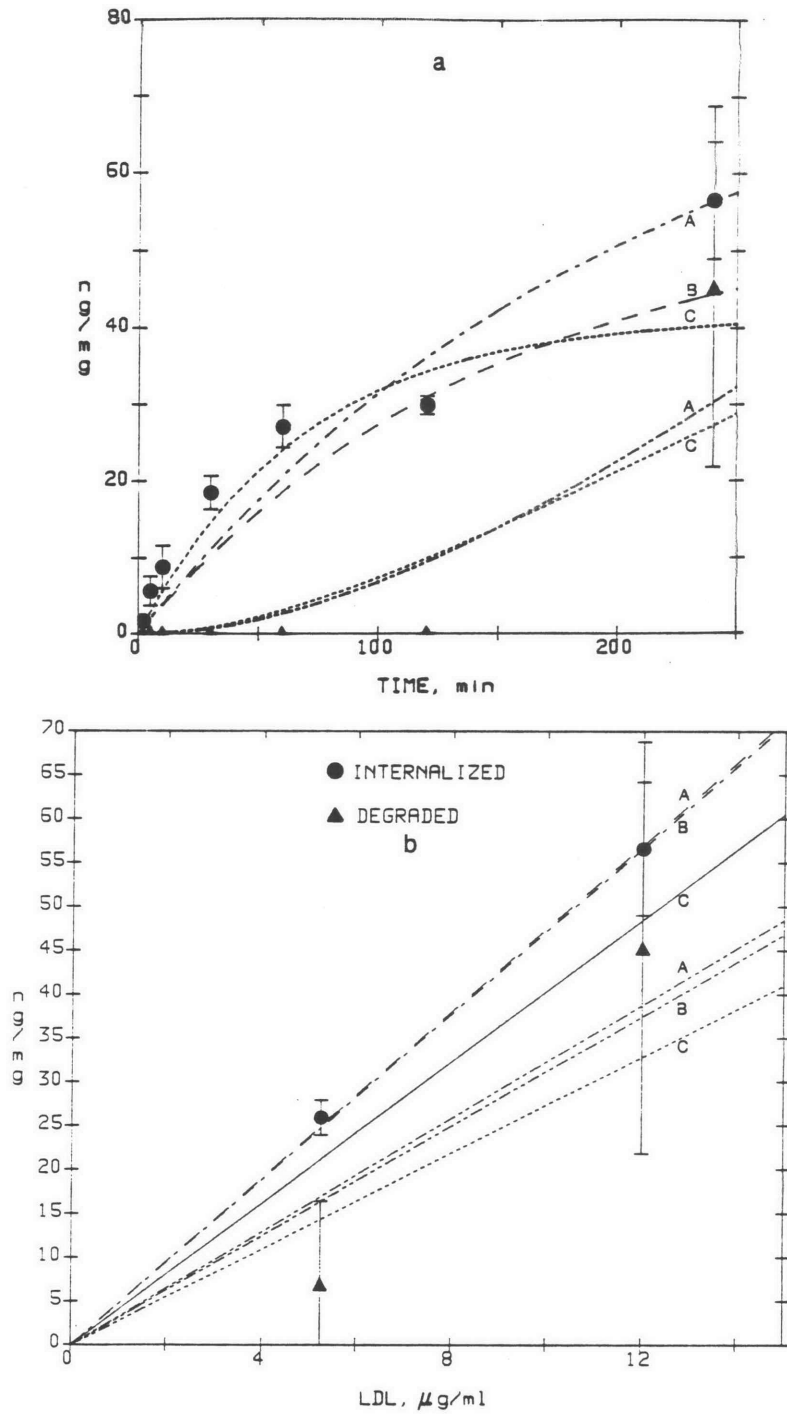


Figure 2-26: Expt. BSMC33: Receptor-Independent LDL internalization and degradation as a function of time at $12.0 \mu\text{g/ml}$ ^{125}I -LDL (a) and as a function of concentration at 4 hr (b). Smooth curves represent: A) lumped model with exocytosis; B) lumped model with no exocytosis; and C) lumped model with $k_7 = k_5$.

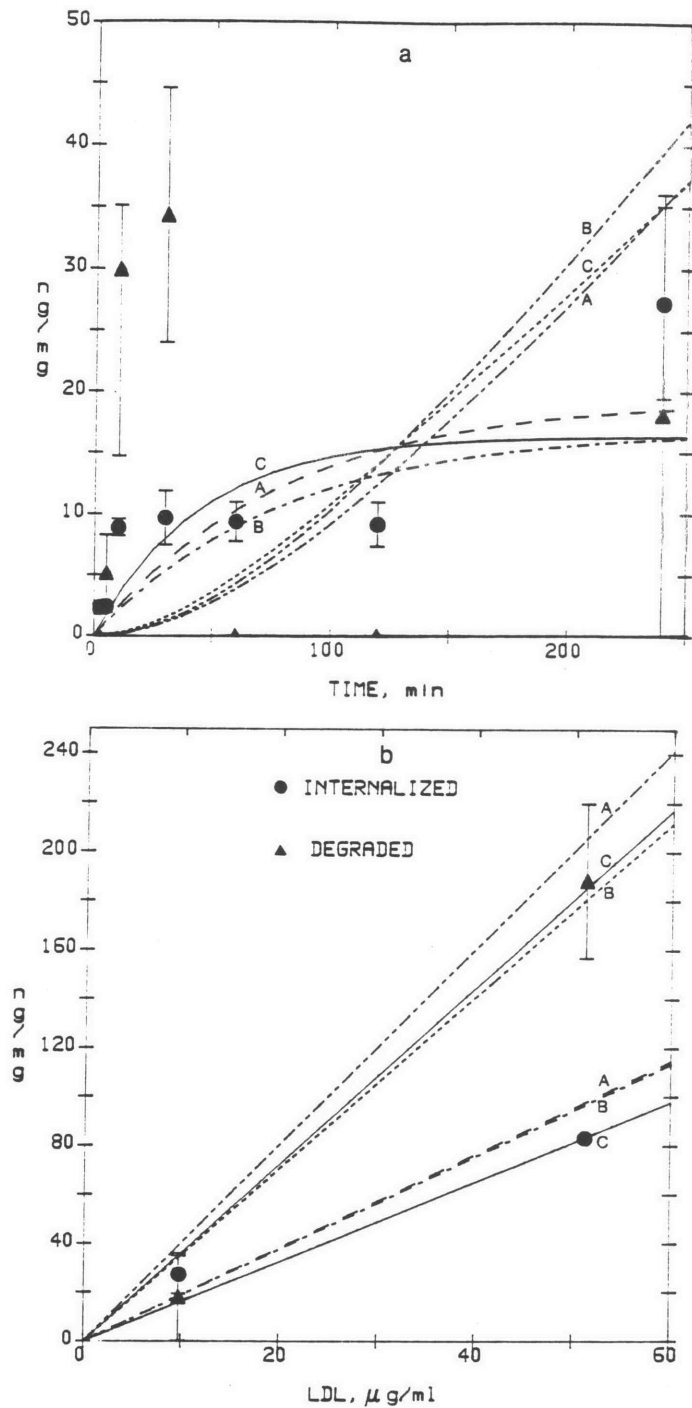


Figure 2-27: Expt. BSMC35: Receptor-Independent LDL internalization and degradation as a function of time at $8.0 \mu\text{g/ml}$ ^{125}I -LDL (a) and as a function of concentration at 4 hr (b). Smooth curves represent: A) lumped model with exocytosis; B) lumped model with no exocytosis; and C) lumped model with $k_7 = k_5$.

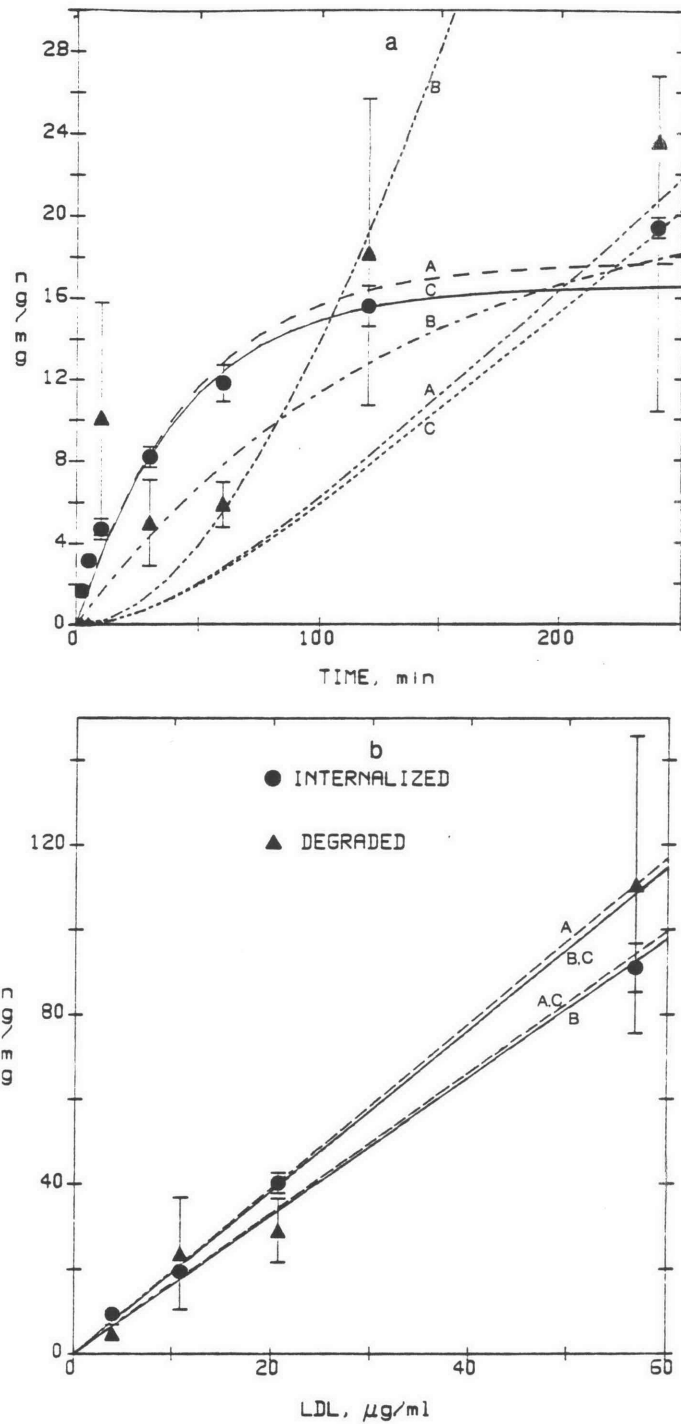


Figure 2-28: Expt. BSMC40: Receptor-Independent LDL internalization and degradation as a function of time at $10.8 \mu\text{g/ml}$ ^{125}I -LDL (a) and as a function of concentration at 4 hr (b). Smooth curves represent: A) lumped model with exocytosis; B) lumped model with no exocytosis; and C) lumped model with $k_7 = k_5$.

Table 2-XII: Rate Constants for Receptor-Independent Metabolism in Individual Experiments

Expt.	k_4 , ml/(mg · min) x 10 ⁵	k_6 , min ⁻¹ x10 ³	k_7 ,min ⁻¹	det(F)
BSMC6	4.7 ± 1.6	3.7 ± 0.3	0.0113 ± 0.0058	9.3 x 10 ⁵
	2.1 ± 0.1	4.7 ± 0.1	0 (fixed)	11.2 x 10 ⁵
	6.5 ± 1.1	3.4 ± 0.1	0.0176 (fixed)	9.8 x 10 ⁵
BSMC10	3.1 ± 1.4	1.9 ± 0.3	0.0126 ± 0.0074	10.0 x 10 ⁵
	1.2 ± 0.1	2.6 ± 0.2	0 (fixed)	11.5 x 10 ⁵
	5.1 ± 0.1	1.7 ± 0.2	0.0229 (fixed)	11.1 x 10 ⁵
BSMC29	5.5 ± 0.2	2.6 ± 0.7	0.0028 ± 0.0042	20.7 x 10 ⁵
	4.3 ± 0.3	2.8 ± 0.7	0 (fixed)	22.3 x 10 ⁵
	18.3 ± 0.6	2.0 ± 0.5	0.023 (fixed)	34.6 x 10 ⁵
BSMC33	3.9 ± 0.6	4.5 ± 0.8	0.0024 ± 0.0024	0.38 x 10 ⁵
	3.3 ± 0.2	4.8 ± 0.7	0 (fixed)	0.43 x 10 ⁵
	6.0 ± 0.4	3.8 ± 0.7	0.0106 (fixed)	0.56 ± 10 ⁵
BSMC35	2.5 ± 1.2	12.2 ± 1.7	0.0023 ± 0.0093	2.8 x 10 ⁵
	2.2 ± 0.1	12.6 ± 0.8	0 (fixed)	2.5 x 10 ⁵
	3.7 ± 0.2	11.0 ± 0.9	0.0116 (fixed)	2.5 x 10 ³
BSMC40	3.5 ± 0.6	6.0 ± 0.4	0.0153 ± 0.0043	0.41 x 10 ⁵
	1.5 ± 0.1	7.6 ± 0.4	0 (fixed)	0.67 x 10 ⁵
	3.8 ± 0.7	5.9 ± 0.4	0.0170 (fixed)	0.42 x 10 ⁵

whereas increasing concentrations of mLDL have little effect on ¹²⁵I-LDL binding, internalization, and degradation. In experiment BSMC41 (Figure 2-30) with different batches of LDL and cells, the trends are less clear but ¹²⁵I-LDL internalization and degradation do not appear to be affected by mLDL concentration.

Total ¹²⁵I-LDL binding, internalization, and degradation in the presence of 0

Table 2-XIII: ^{125}I -LDL Metabolism in the Presence of 500 $\mu\text{g}/\text{ml}$ LDL or mLDL

	mg ^{125}I -LDL protein/mg cell protein		
	Bound	Internalized	Degraded
Expt. BSMC38 (n=3)			
0 $\mu\text{g}/\text{ml}$ LDL	8.2 \pm 0.5	212 \pm 15	48 \pm 8
500 $\mu\text{g}/\text{ml}$ LDL	1.4 \pm 0.5	20.7 \pm 1.3	0
500 $\mu\text{g}/\text{ml}$ mLDL	7.4 \pm 2.4	222 \pm 82	16 \pm 7
Expt. BSMC41 (n=3)			
0 $\mu\text{g}/\text{ml}$ LDL	6.5 \pm 1.7	75 \pm 20	45 \pm 9
500 $\mu\text{g}/\text{ml}$ LDL	2.1 \pm 0.7	17.9 \pm 4.1	5.6 \pm 6.1
500 $\mu\text{g}/\text{ml}$ mLDL	5.1 \pm 1.1	91.5 \pm 24.1	41.8 \pm 11.4

or 500 $\mu\text{g}/\text{ml}$ LDL or mLDL are presented in Table 2-XIII for two experiments. Incubation with 500 $\mu\text{g}/\text{ml}$ LDL results in decreased ^{125}I -LDL binding, internalization, and degradation, whereas mLDL has little effect, indicating that mLDL does not bind to the LDL receptor.

mLDL and receptor-mediated and receptor-independent LDL binding, internalization, and degradation by bovine smooth muscle cells were determined following a four hr incubation with 2.5-55 $\mu\text{g}/\text{ml}$ ^{125}I -mLDL or ^{125}I -LDL (Expt. BSMC41). For determination of receptor-independent LDL metabolism, smooth muscle cells were also incubated with ^{125}I -LDL in the presence of 500 $\mu\text{g}/\text{ml}$ unlabeled LDL. Results are presented in Figure 2-31. Each point is the average of three dishes, and the error bars are equal to the standard deviation. mLDL binding, internalization, and degradation are linear in mLDL concentration and are qualitatively similar to nonspecific LDL metabolism, although, in this experiment, mLDL internalization is greater than nonspecific LDL internalization.

Nonspecific LDL and mLDL metabolism presented in Figure 2-31 were fit to

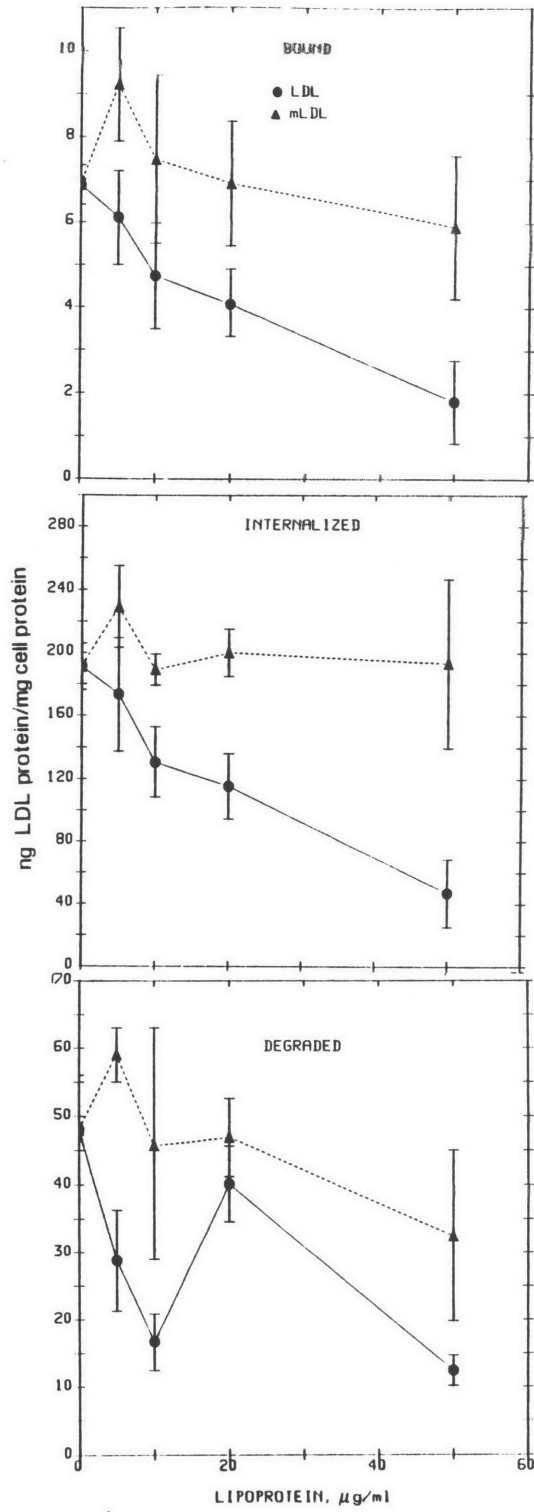


Figure 2-29: Expt. BSMC38. LDL and mLDL Competition Experiment

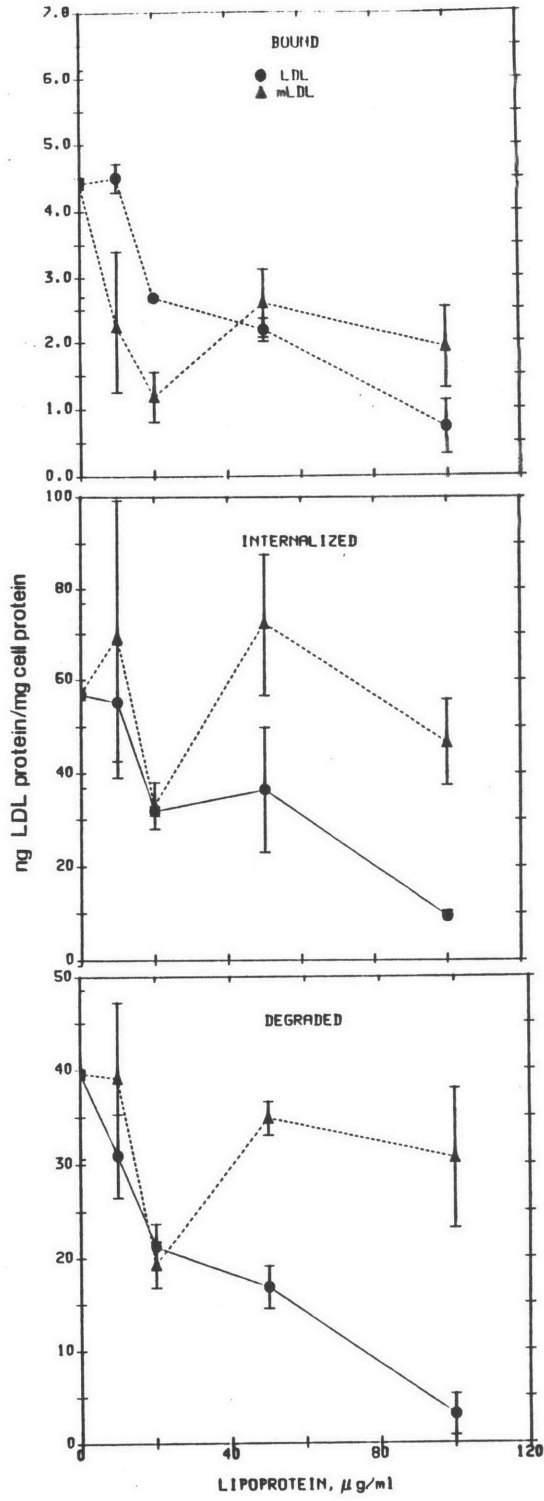


Figure 2-30: Expt. BSMC41. LDL and mLDL Competition Experiment

Table 2-XIV: Rate Constants for mLDL Metabolism

	k_4 , ml mg ⁻¹ min ⁻¹ x 10 ⁵	k_6	k_7
LDL	1.76 ± 0.07	0.0023 ± 0.0002	0.0082 (fixed)
mLDL	3.12 ± 0.09	0.00077 ± 0.00015	0.0082 (fixed)
LDL (Table 2-XI)	3.22 ± 2.00	0.0036 ± 0.0007	0.007 ± 0.009

the model for nonspecific LDL metabolism, equations (2-37) and (2-38). Since measurements were made at a single time, it was not possible to determine all three constants. As a result k_7 was fixed at 0.0082 min⁻¹. Fitted curves are displayed in Figure 2-31 and the rate constants are listed in Table 2-XIV. For LDL, k_4 is less than estimates obtained from pooled data and individual experiments, and k_6 is within the range of estimated values. For mLDL, k_4 is close to the value obtained from the pooled data, and k_6 is much less than any other estimate. Additional experiments would be required in order to examine variability of rate constants for mLDL metabolism.

2.5.9 Comparison with Other Models

Kinetic models are reported in the literature for receptor-mediated metabolism of epidermal growth factor (Wiley and Cunningham [1981, 1982]), chemotactic peptides (Zigmond et al. [1982]), and transferrin (Ciechanover et al. [1983a]) as well as fluid endocytosis of sucrose (Besterman et al. [1981]). Determination of the rate constants usually involved analysis of a single response under limiting conditions. For example, Wiley and Cunningham [1982] and Zigmond et al. [1982] have determined k_2 when binding is at steady state and little degradation has occurred. For this case, the rate of internalization is equal to $k_2[LR]$, which is approximately

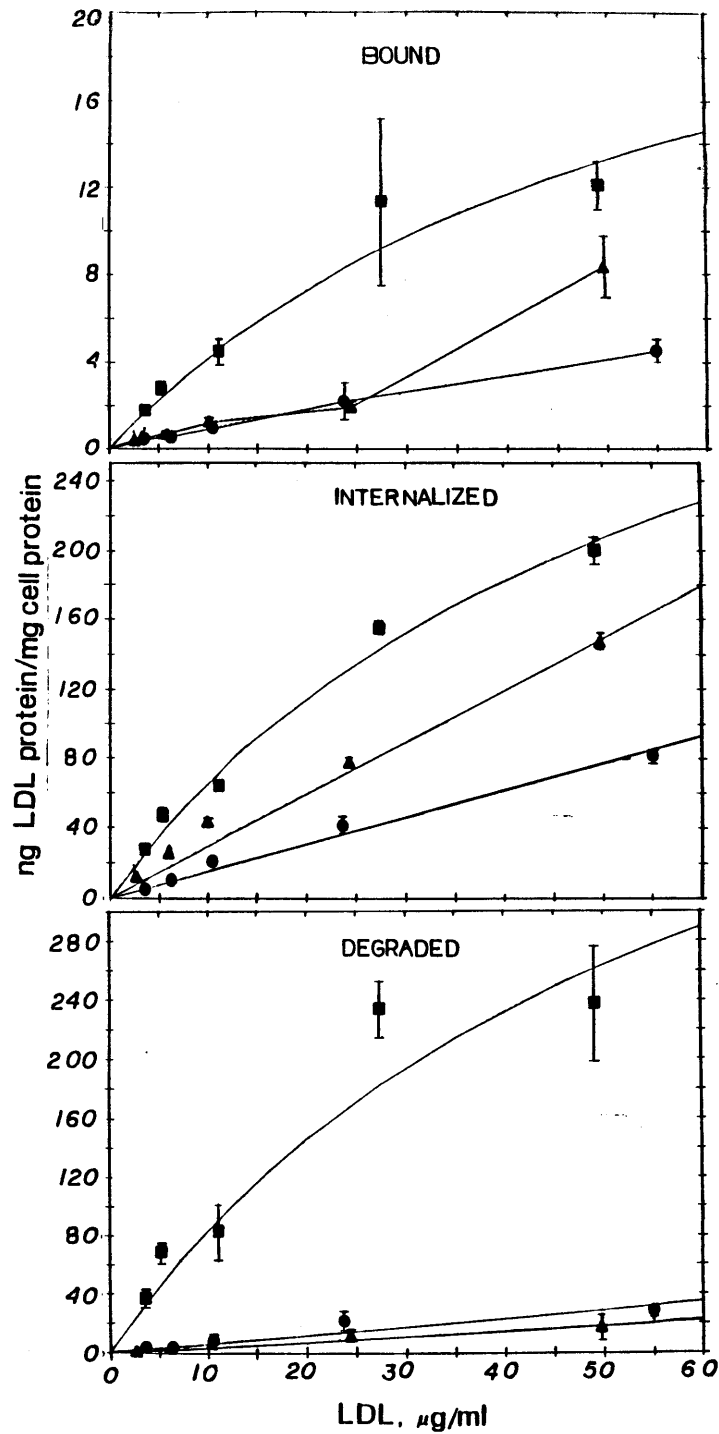
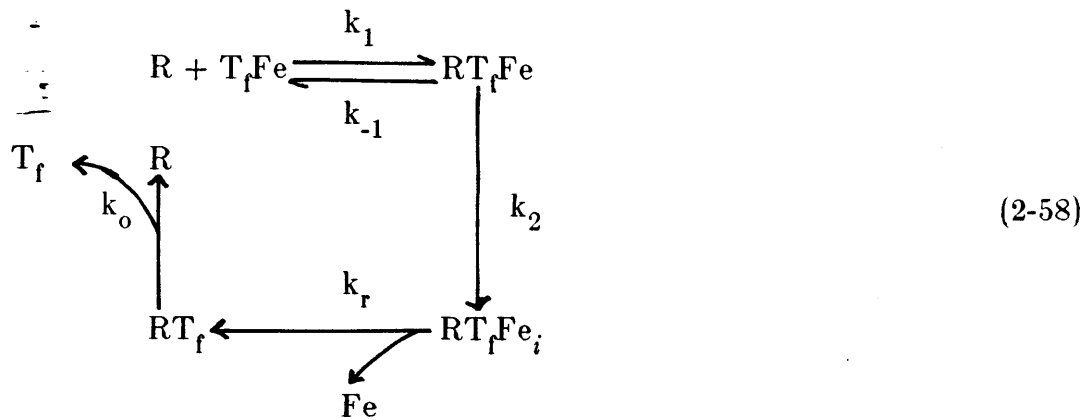


Figure 2-31: LDL and mLDL binding, internalization, and degradation following four hr incubation. (■): Receptor-mediated LDL binding, internalization, and degradation; (●) Receptor-independent LDL metabolism; (▲) mLDL binding, internalization, and degradation.

constant, and a plot of the rate of internalization versus receptor occupancy is linear (Zigmond et al. [1982]). Schwartz et al. [1982] and Ciechanover et al. [1983a] have measured binding at 37 °C in the presence of metabolic inhibitors which block internalization and determined k_1 and k_{-1} . The limitations of these approaches are: 1) each rate constant must be measured independently which may increase the error associated with the resulting parameters; and 2) the use of metabolic inhibitors or other perturbations may alter the very process which is being measured. Although the approach developed in this chapter must be used carefully, it does permit determination of a consistent set of rate constants with fewer experiments. Not all rate constants may be uniquely determined, only those which have a significant effect upon the responses.

As an example of the advantages and limitations of regression of multiple response data, consider receptor-mediated metabolism of transferrin. Transferrin consists of a ferrous ion complexed to an apoprotein and is involved in the delivery of iron to peripheral tissues. Transferrin binds reversibly to its receptor on the cell surface. The transferrin-receptor complex is internalized during the formation of a coated vesicle. Within the acidified endosome, iron dissociates from the apoprotein and is stored in the cell. Unlike LDL, apotransferrin does not dissociate from its receptor at acid pH (Dautry-Varsat et al. [1983]). The receptor-apotransferrin complex is recycled back to the cell surface. At physiological pH the apoprotein dissociates from the receptor, and unless iron is present to reform transferrin, does not reassociate.

Based upon this qualitative picture, Ciechanover et al. [1983a] have developed a kinetic model of transferrin internalization and recycling in a human hepatoma cell line (HepG2).



where $T_f Fe$ represents transferrin, T_f represents apotransferrin, Fe represents iron, R represents the receptor, $RT_f Fe$ and $RT_f Fe_i$ represent the receptor-transferrin complex on the cell surface and within the cell, respectively, and RT_f represents the surface concentration of receptor-apoprotein complex. k_1 , k_{-1} , and k_2 are the same as defined in Section 2.3.1. k_r (min^{-1}) is the rate constant for receptor recycling and k_o is the rate constant for dissociation of apotransferrin from its receptor. k_r is identical to k_x of Ciechanover et al. [1983a]. Implicit in the model represented by equation (2-58) is the assumption that, once within the endosomes, iron dissociates rapidly from the receptor-transferrin complex and essentially all of the intracellular transferrin is apotransferrin.

Ciechanover et al. [1983] measured all rate constants, except k_r , in separate experiments. In one experiment cells were incubated with ^{125}I -transferrin at 4 °C in the presence of metabolic inhibitors. The cells were washed and incubated at 37 °C with unlabeled transferrin and metabolic inhibitors which blocked internalization. k_{-1} was determined from the slope of a semi-logarithmic plot of the fractional amount bound versus time at 37 °C. The same experiment was repeated in the absence of metabolic inhibitors and the sum of k_{-1} and k_2 was determined from the slope of a semi-logarithmic plot of the fractional amount bound versus time at 37 °C. k_2 was determined using the known value of k_{-1} . Binding was measured at 37

$^{\circ}\text{C}$ in the presence of metabolic inhibitors and from the known value of k_{-1} , k_1 was calculated. In order to measure dissociation of apotransferrin from the receptor, cells were incubated with ^{125}I -transferrin at 4°C in the presence of metabolic inhibitors, after which cells were washed to remove unbound ligand. Iron was dissociated from apotransferrin by incubation at 4°C at pH 5 and desferrioxamine in the presence of metabolic inhibitors. Under these conditions, apotransferrin remained bound to the receptor (Dautry-Varsat et al. [1983]). The medium was then replaced with fresh medium at pH 7.3 containing unlabeled transferrin, metabolic inhibitors, and desferrioxamine and dissociation of ^{125}I -apotransferrin at 37°C was determined. k_o was determined from the slope of a semilogarithmic plot of the fractional amount bound versus time. The only constant which was not directly measured was k_r which was estimated by comparing fits of the model to results of a pulse-chase experiment similar to the one described in Figure 2-2. The resulting rate constants are listed in Table 2-XV.

The pulse-chase results of Figure 2 of Ciechanover et al. [1983] were fit using the minimization criterion for multiple response data (equation (2-41)). Briefly, HepG2 cells were incubated with ^{125}I -transferrin at 4°C , after which cells were washed to remove unbound ligand and were incubated at 37°C in medium containing unlabeled transferrin. At various times, ^{125}I -protein on the cell surface, within the cell, and in the medium was determined.

During the chase period, the medium concentration of labeled transferrin is initially zero. The amount of ^{125}I -transferrin dissociated from the cell is much less than the amount of unlabeled transferrin and there is little reassociation of ^{125}I -transferrin. Consequently, k_1 can not be determined from this experiment. Material balances for cell surface transferrin and cell surface and intracellular apotransferrin are:

$$\frac{d[RT_fFe]}{dt} = -(k_{-1} + k_2)[RT_fFe] \tag{2-59}$$

$$\frac{d[RT_fFe_i]}{dt} = k_2[RT_fFe] - k_r[RT_fFe_i] \tag{2-60}$$

$$\frac{d[RT_f]}{dt} = k_r[RT_fFe_i] - k_o[RT_f] \tag{2-61}$$

The rate of appearance of protein-bound radioactivity into the medium is the sum of the rates of transferrin and apotransferrin dissociation from the receptor:

$$\frac{d[T_fFe]_m}{dt} + \frac{d[T_f]_m}{dt} = k_{-1}[RT_fFe] + k_o[RT_f] \tag{2-62}$$

Equation (2-62) is the sum of equations (2-59) - (2-61), and is not an independent relationship.

Table 2-XV: Rate Constants for Receptor-Mediated Metabolism of Transferrin

	Regression of Multiple Response Data		Ciechanover et al. [1983]
k_{-1}, min^{-1}	0.08 ± 0.01	0.05 ± 0.01	0.09/0.11
k_2, min^{-1}	0.24 ± 0.02	0.20 ± 0.02	0.20/0.30
k_r, min^{-1}	0.14 ± 0.01	0.14 ± 0.01	0.14
k_o, min^{-1}	0.42 ± 0.07	2.6 (fixed)	2.6
$\det(\mathbf{F}) \times 10^{10}$	9.35	18.81	

The integrated forms of equations (2-59)-(2-62) were fit to the data of Figure 2 of Ciechanover et al. [1983a] using the criterion of equation (2-41) and the results are presented in Figure 2-32. The rate constants are presented in Table 2-XIV. k_{-1} , k_2 , and k_r are identical to the values obtained by Ciechanover et al. [1983] (column

3 of Table 2-XV). k_0 is significantly less than the value obtained by Ciechanover et al. [1983]. This may arise from differences in the experimental procedure. Fitting the data with k_0 fixed at 2.6 min^{-1} produced the set of values listed in column 2 of Table 2-XV. The resulting fit is plotted in Figure 2-32. k_1 decreases in order to compensate for the value of k_0 . k_2 also decreases resulting in slower internalization of RT_fFe from the cell surface which partly compensates for the increased removal of RT_f from the cell surface. Fixing k_0 at 2.6 min^{-1} results in a larger value of $\det(\mathbf{F})$ and poorer fits of surface and intracellular concentrations (Figure 2-32). (The parameter correlation matrix is listed in Table 2-XVI.)

Most likely, the rate limiting step for apotransferrin release into the medium is the recycling of the receptor. Thus three of the five rate constants (k_{-1} , k_2 , and k_r) can be accurately determined from the pulse chase experiments. Furthermore, this comparison also demonstrates that metabolic inhibitors do not significantly alter the rate constants.

Table 2-XVI: Parameter Correlation Matrix for Fit of Data of Ciechanover et al. [1983a]

	k_{-1}	k_2	k_r	k_0
k_{-1}	1.000	0.664	-0.006	-0.658
k_2	0.664	1.000	0.127	-0.530
k_3	-0.006	0.127	1.000	-0.665
k_0	-0.658	-0.530	-0.665	1.000

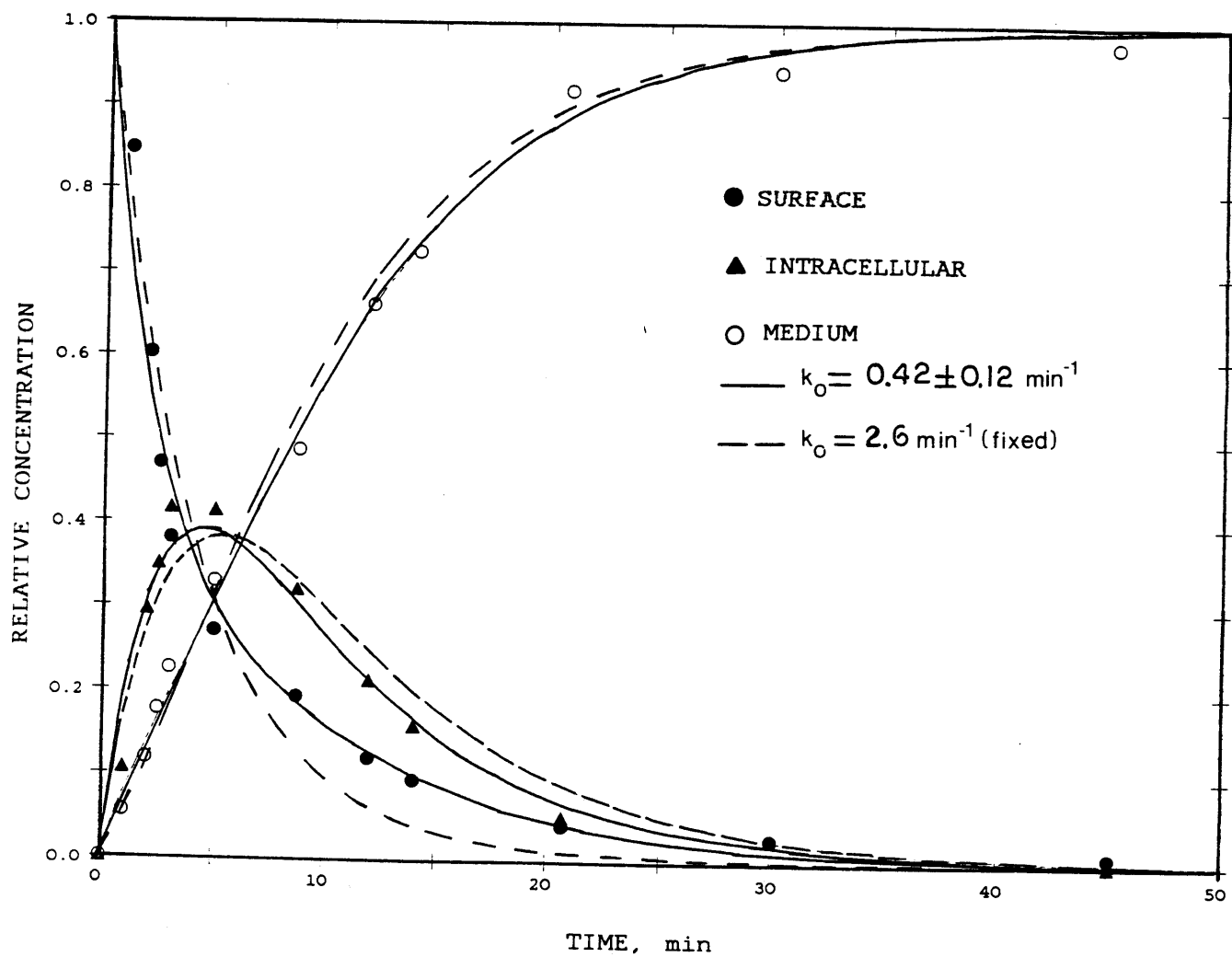


Figure 2-32: Pulse-chase experiment with ^{125}I -transferrin, data from Ciechanover et al. [1983a]. Integrated forms of equations (2-59) to (2-62) were fit to data by minimization of equation (2-41).

2.6 DISCUSSION

Kinetic studies provide a useful method to understand the dynamics of the endocytosis and degradation of proteins. Such studies permit the formulation of mechanisms from which mathematical models are developed. The proposed mechanisms are then tested by comparing model-generated results with experimental data. Ideally, a predictive model is desired, in which all of the rate constants are known. Generally, this is not possible and regression techniques are required to estimate the rate constants as well as test the adequacy of the model.

In this chapter, general models of receptor-mediated and receptor-independent metabolism have been developed and applied to LDL metabolism by quiescent bovine aortic smooth muscle cells to determine rate constants. Because measured values of bound, internalized, and degraded ligand are multiple responses to a single input, the Bayesian estimation technique developed by Box and Draper [1965] was used to determine a consistent set of rate constants from all of the data. Results obtained with this method support the model of receptor-mediated endocytosis of LDL developed by Brown and Goldstein. In addition, new insights have been obtained with regard to receptor-mediated and receptor-independent degradation and exocytosis.

Although data exist in the literature to estimate the rate constants (Appendix A), no single set of experimental data is available from which all rate constants can be determined. In order to maximize the accuracy of the estimates using the Bayesian parameter estimation technique and reduce the number of experiments, transient and steady state binding, internalization, and degradation were measured as a function of incubation time and ^{125}I -LDL medium concentration. As a result, all of the significant rate constants were determined from a single experiment.

Replicate experiments were used to examine the variability in the rate constants.

Several alternative methods are available for parameter estimation with complex kinetic models: 1) each constant can be estimated separately by proper choice of experimental conditions such that a single reaction is dominant; or 2) parameters can be determined by minimization of $\det(\mathbf{F})$ from a single set of experimental multiresponse data. Both methods have advantages and disadvantages. Independent measurement of rate constants provides unambiguous values of the parameters, as long as the experimental conditions do not influence the value of the rate constant (e.g. metabolic inhibitors applied to cells in order to measure k_1 (Ciechanover et al. [1983a])). It may not, however, be possible to measure all of the rate constants because product concentrations are too low or two products cannot be easily distinguished.

Minimization of $\det(\mathbf{F})$ to estimate the rate constants provides a consistent set of parameters which provide agreement between model predictions and data for all responses over a range of experimental conditions (time, concentration, temperature, etc.). Such a fitting procedure, if successful, serves to demonstrate that the parameter is constant for all conditions studied which supports the underlying model. Minimization of $\det(\mathbf{F})$ also allows determination of constants not easily accessible to measurement (e.g. exocytosis, k_5). As a result, minimization of multiple response data to estimate rate constants, requires fewer experiments and makes greater use of available data. The major drawback to this technique is that the data may not be sensitive to all parameters in the model. Thus, an optimal parameter estimation strategy would use both methods.

Several models of receptor-mediated and receptor-independent metabolism have been considered and the model which yields the best fit of the data includes exocytosis from a single lumped intracellular compartment. Fitting all responses

simultaneously leads to a consistent set of parameters with standard deviations less than those obtained from fits of one or two responses. Degradation alone cannot explain the transient behavior of internalized LDL. The results suggest that exocytosis transports a significant amount of internalized LDL back to the medium. Although the model is somewhat simplistic, more complicated models cannot be evaluated until kinetic data are available for the individual intracellular compartments.

Rate constants for exocytosis of LDL internalized by receptor-mediated and receptor-independent metabolism (k_5 and k_7 , respectively) are very similar, which indicates that the receptor is not involved in exocytosis. Furthermore, free receptors return to the cell surface with a half-time of less than three minutes (Brown et al. [1983]) which is significantly faster than the half-time for exocytosis, 85 min. It is unlikely that LDL undergoes exocytosis attached to the receptor. Taken together, these observations suggest that exocytosis occurs via an undissociated form of LDL.

Aulinskas et al. [1981, 1985] and Greenspan and St. Clair [1984] have observed exocytosis of intracellular LDL in pulse-chase experiments, but their results indicate a significantly smaller amount of exocytosis relative to degradation, except in the presence of the lysosomotropic agents chloroquine and methylamine. A value of k_5 close to the value estimated from the data of Aulinskas was obtained by pulse-chase experiments suggesting a fundamental alteration in the kinetics as a result of the different experimental protocols.

The model for receptor-mediated LDL metabolism readily explains the kinetic behavior of LDL metabolism. The lumped rate constant for binding to the receptors is $k_1[L_o] + k_{-1} + k_2$ which is equal to $k_1([L_o] + K_{int})$. For ligand concentrations much less than K_{int} , receptor-mediated endocytosis is limited by

binding of LDL to its receptor. At LDL concentrations much greater than K_{int} , binding reaches steady state very rapidly and the rate of receptor-mediated endocytosis is limited by the rate of vesicle formation.

The rate of degradation is initially zero, increasing to its steady state value when the intracellular concentration is constant. Two limiting cases exist. For slow binding and internalization relative to degradation, the rate of degradation is limited by the rate of binding and internalization. Conversely, the rate of degradation is limited by the rate of lysosomal hydrolysis (k_3) when binding and internalization are rapid relative to degradation. For LDL the latter case is true and the lag time in degradation results from slow lysosomal hydrolysis (Table 2-III). Furthermore, rate constants for degradation of LDL internalized by receptor-mediated and receptor-independent mechanisms are similar which suggests that there is a common mechanism of LDL protein degradation.

Receptor-independent internalization is by fluid phase endocytosis and nonspecific adsorptive endocytosis. Conversion of k_4 into units of the endocytotic index yields a value of 616 ± 390 nl/(10^6 cells · hr). The endocytotic index for fluid phase endocytosis by smooth muscle cells ranges from from 27 to 50 nl/(10^6 cells · hr) (see Section 1.3.2) 12 to 23 times less than the endocytotic index for LDL. Thus, the primary mechanism for nonspecific uptake is by nonspecific adsorptive endocytosis. Over the concentration range studied (0 to 100 μ g/ml), the rate of nonspecific adsorptive endocytosis is first order in ligand concentration; presumably the adsorption sites are saturated at much higher concentrations. Miller et al. [1977] and van Hinsbergh et al. [1983] have also proposed that adsorptive endocytosis plays a significant role in the nonspecific uptake of LDL.

If the results for nonspecific binding are to be consistent with those for nonspecific internalization and degradation, then binding to sites involved in

adsorptive endocytosis must be rapid. This implies that there are several classes of nonspecific binding sites. At steady state, an expression for nonspecific binding analogous to the steady state form of equation (2-24) for receptor-mediated binding is:

$$[L_b] = \frac{[S_T][L_o]}{K'_{int} + [L_o]} \quad (2-63)$$

where $[S_T]$ is the total concentration of nonspecific sites involved in adsorptive endocytosis, and K'_{int} is analogous to K_{int} for receptor-mediated binding. Over the concentration range 0 to 100 $\mu\text{g/ml}$, binding is a linear function of concentration (Figure 2-22). Hence, $K'_{int} \gg [L_o]$ and $[L_b] \approx [S_T][L_o]/K'_{int}$ which is equal a in equation (2-57). The rate of nonspecific adsorptive endocytosis is simply $k'_2[L_b] = k'_2[S_T][L_o]/K'_{int}$. Subtracting the contribution due to fluid endocytosis, $k'_2[S_T]/K'_{int}$ ranges from 2.95 to 3.08×10^{-5} ml/(mg cell protein \cdot min). If $k'_2 = k_2 = 0.25 \text{ min}^{-1}$, then $[S_T]/K'_{int}$ is 38% of the value of the constant a determined in fitting nonspecific binding to equation (2-57). Since the value of k'_2 is not known, it is also possible that k'_2 is 38% of the value of k_2 . Additional data are required to determine the fraction of nonspecific binding sites involved in adsorptive endocytosis.

Rate constants estimated from individual experiments show considerable variability which may be due to variations among the population of bovine smooth muscle cells as well as effects associated with growth state, subculture, morphological state, and cell density. Cells were incubated in PDS and growth-factor deficient 5% LPDS. ^3H -Thymidine labeling of these cells was low (see the Results section of Chapter 3) indicating that the cells were quiescent. Cells were derived from at least 18 different bovine thoracic aortae in subcultures 2 and 3, but no attempt was made to record the subculture used in a particular experiment.

Gallop et al. [1981] have observed that late subcultures (20 to 50) have fewer receptors than earlier subcultures (1 to 10) with no change in K_{int} .

All experiments were performed with subconfluent cells. Every attempt was made to maintain constant cell densities in all experiments. In four experiments (BSMC6, BSMC10, BSMC35, and BSMC40) cell densities ranged from 0.75 to 0.84×10^6 cells/dish but in experiments BSMC29 and BSMC33 cell densities were 0.19×10^6 and 0.57×10^6 cells/dish, respectively. Kenagy et al. [1983] have observed that LDL binding, internalization, and degradation by human fibroblasts decreases with increasing cell density when data are presented in terms of cells/cm² dish. This effect is likely due to a decrease in the number of receptors at higher cell densities, but effects of cell density on rate constants could not be determined. Davies and Ross [1980] and Davies [1980] observed that fluid phase endocytosis by quiescent monkey arterial smooth muscle cells and 3T3 fibroblasts is unaffected by cell density.

In order to determine if the cell density had any effect upon the rate constants or receptor number, the cell protein, cell numbers per dish, and cell densities are presented in Table 2-XVII along with the rate constants. Cell number was calculated based upon an experimentally determined correlation between cell number and cell protein (0.33 mg cell protein/ 10^6 cells) presented in Appendix F. Cell densities were calculated based upon the area of the 35 mm diameter dishes. In contrast with the results of Kenagy et al. [1983], cell density does not appear to affect LDL receptor number. k_2 appears to decrease with increasing cell density; all other rate constants do not seem to be affected by cell density. Since there was no systematic attempt to vary the cell density, it is premature to draw definitive conclusions.

Rate constants for pooled data are compared with estimates obtained from

Table 2-XVII: Effect of Cell Density Upon Rate Constants and Receptor Number

	BSMC29	BSMC33	BSMC40	BSMC10	BSMC6	BSMC35
Ave. Cell Protein, mg	0.06 ± 0.01	0.19 ± 0.04	0.25 ± 0.03	0.25 ± 0.05	0.27 ± 0.02	0.28 ± 0.07
Cells/dish x 10 ⁻⁶	0.19 ± 0.05	0.57 ± 0.11	0.75 ± 0.08	0.76 ± 0.15	0.83 ± 0.06	0.84 ± 0.20
Cells/cm ² x 10 ⁻⁴	2.0 ± 0.4	5.9 ± 1.1	7.8 ± 0.8	7.9 ± 1.6	8.6 ± 0.6	8.7 ± 2.1
k ₁ , M ⁻¹ min ⁻¹ x 10 ⁻⁷	0.34 ± 0.19	0.70 ± 0.10	0.13 ± 0.05	0.53 ± 0.08	2.04 ± 0.34	0.49 ± 0.16
k ₂ , min ⁻¹	0.70 ± 0.24	0.39 ± 0.04	0.39 ± 0.07	0.27 ± 0.03	0.33 ± 0.04	0.46 ± 0.16
k ₃ , min ⁻¹	0.0059 ± 0.0008	0.0017 ± 0.0002	0.0046 ± 0.0003	0.0050 ± 0.0003	0.0093 ± 0.0003	0.0051 ± 0.0005
k ₅ , min ⁻¹	0.023 ± 0.011	0.011 ± 0.002	0.017 ± 0.004	0.023 ± 0.004	0.011 ± 0.003	0.018 ± 0.008
R _T , receptors/cell	11800 ± 4900	16900 ± 1500	12500 ± 4100	8900 ± 900	6100 ± 400	5900 ± 1000
k ₄ , ml/min x 10 ⁵	5.5 ± 0.2	3.9 ± 0.6	3.5 ± 0.6	3.1 ± 1.4	4.7 ± 1.6	2.5 ± 1.2
k ₆ , min ⁻¹	0.0026 ± 0.0007	0.0045 ± 0.0008	0.0060 ± 0.0004	0.0029 ± 0.0003	0.0037 ± 0.0003	0.0122 ± 0.0017
k ₇ , min ⁻¹	0.0028 ± 0.0042	0.0024 ± 0.0024	0.0153 ± 0.0043	0.0126 ± 0.0074	0.0113 ± 0.0058	0.0023 ± 0.0093

Table 2-XVIII: Average Value of Rate Constants for Receptor-Mediated LDL Metabolism and Comparison with Estimates from Published Data

$k_1, M^{-1} \text{ min}^{-1} \times 10^{-7}$	$k_{-1}, \text{ min}^{-1}$	$k_2, \text{ min}^{-1}$	$k_3, \text{ min}^{-1}$	$k_5, \text{ min}^{-1}$	Cell Type	Growth State	LDL	Reference
0.50 ± 0.17		0.25 ± 0.07	0.0057 ± 0.0006	0.0082 ± 0.0047	Bovine Aortic Smooth Muscle	Quiescent, Subconfluent	Human	This Study
		0.20 ± 0.02	0.015 ± 0.002		Human Skin Fibroblasts	Growing, Subconfluent	Human	Brown and Goldstein [1976]
		0.015 ± 0.001			Human Skin Fibroblasts	Growing, Subconfluent	Human	Goldstein et al. [1977]
		0.008 ± 0.001			Human Skin Fibroblasts	Growing, Subconfluent	Human	Brown and Goldstein [1976]
			0.25 ± 0.02			Human Skin Fibroblasts	Growing, Subconfluent	Human
1.7 ± 0.5		0.20 ± 0.02			Human Skin Fibroblasts	Growing, Subconfluent	Human	Goldstein et al. [1976]
			0.007 ± 0.001	0.0020 ± 0.0006	Bovine Aortic Smooth Muscle	Confluent	Human	Aulinkas et al. [1981]
0.26 ± 0.04		0.10 ± 0.02	0.013 ± 0.001		Bovine Heart Endothelial Cells	Growing, Subconfluent	Human	Vlodavsky et al. [1978]
0.24 ± 0.05		0.02 ± 0.01	0.0022 ± 0.0005	0.0048 ± 0.0015	Rabbit Aortic Endothelial Cells	Growing, Subconfluent	Rabbit	Reckless et al. [1978]
0.40 ± 0.07		0.05 ± 0.01	0.0071 ± 0.0009		Monkey Aortic Smooth Muscle	Confluent	Monkey	Eisele et al. [1980]

published data in Table 2-XVIII for receptor-mediated metabolism and in Table 2-XIX for receptor-independent metabolism. (Estimation of the rate constants from literature data is presented in Appendix A.) k_1 and k_3 estimated from literature data are within the variability observed for these rate constants. k_2 for growing, subconfluent human fibroblasts is similar to the value estimated in this study for quiescent, subconfluent bovine smooth muscle cells. For bovine and rabbit endothelial cells and monkey smooth muscle cells, k_2 is much smaller than k_2 determined from pooled data in this study. Estimates of k_{-1} are 3% to 6% of the value of k_2 determined in this study, which validates the assumption that dissociation is slower than internalization. k_5 estimated from the data of Aulinskas et al. [1981] is less than the value of k_5 from pooled data but is similar to values estimated from pulse-chase experiments (Table 2-VIII). The total number of receptors per cell (7750 ± 770) is significantly less than typical values reported in the literature for growing cells (15,000 to 70,000 on human fibroblasts (Goldstein and Brown [1977])). This is due to differences in the growth state of the cultured cells. In this study, cells are maintained in a quiescent state during measurement of LDL metabolism, whereas others have used actively growing cells which consequently have a high demand for cholesterol and increase their expression of receptors.

Rate constants for receptor-independent metabolism calculated from pooled data are compared with estimates from published data in Table 2-XIX. Published data were obtained at a single time (5 hr). As a result, all of the rate constants cannot be determined. k_7 was set equal to the value of k_5 obtained in this study (0.0082 min^{-1}) and k_4 and k_6 were calculated by iterative solution of equations (2-37) and (2-38). The value of k_4 determined in this study is similar to the values estimated from published data for normal fibroblasts and fibroblasts from patients

homozygous for familial hypercholesterolemia. k_6 for fibroblasts from patients with familial hypercholesterolemia, is, however, larger than values for normal human fibroblasts or bovine smooth muscle cells. Possibly these cells have developed an adaptation whereby they have increased the concentration of hydrolytic enzymes to more effectively degrade LDL.

Table 2-XIX: Average Value of Rate Constants for Receptor-Independent Metabolism and Comparison with Estimates from Published Data

Reference	k_4 , ml/(mg · min) x 10^5	k_6 , min ⁻¹	k_7 , min ⁻¹
This Study	3.22 ± 2.00	0.0036 ± 0.0007	0.0071 ± 0.0091
Brown and Goldstein [1976]*	4.3	0.008	0.0082 (fixed)
Brown and Goldstein [1976]#	6.4	0.0102	0.0082 (fixed)
Stone et al.[1977]#	1.9	0.0116	0.0082 (fixed)

* Normal human fibroblasts

Fibroblasts from patients homozygous for familial hypercholesterolemia

Under the experimental conditions reported herein, receptor-mediated endocytosis is quantitatively more important than receptor-independent endocytosis. It is instructive to compare the steady state rates of internalization by receptor-mediated and receptor-independent endocytosis. The ratio (r) of these rates is:

$$r = \frac{k_2[R_T]/(K_{int} + [L_o])}{k_4} \quad (2-64)$$

r is unity when the two rates are equal. For the values presented in Tables 2-III and 2-X, r is unity at an LDL concentration of about 127 μ g/ml. For LDL

concentrations much less than $127 \mu\text{g/ml}$ receptor-mediated endocytosis dominates, and at concentrations much greater than $127 \mu\text{g/ml}$, receptor-independent endocytosis dominates. In vivo, aortic smooth muscle cells are bathed in an interstitial fluid containing LDL, which results in down-regulation of the receptors. If down-regulation reduces the receptor number by 55% to 77% (Figures 2-18 and 2-19), r is unity at an LDL concentration between 10 and $30 \mu\text{g/ml}$. In section 2.5.6 it was estimated that the interstitial LDL concentration in the rabbit aorta is between 10 and $73 \mu\text{g/ml}$. Thus, it is likely that both receptor-mediated and receptor-independent metabolism contribute significantly to LDL metabolism in the rabbit arterial wall in vivo. This is examined in detail in Chapters 4 and 5.

Chapter 3

The Effects of Endothelial Cell-Smooth Muscle Cell Interactions on Smooth Muscle Cell LDL Metabolism

3.1 Introduction

Metabolic interactions between endothelial cells and smooth muscle cells are likely to be involved in the pathogenesis of atherosclerosis. Endothelial cells produce platelet derived growth factor and other growth factors which stimulate smooth muscle cell proliferation (Gadjusek et al. [1980], DiCorleto et al. [1983], DiCorleto and Bowen-Pope [1983], DiCorlet [1984], Fox and DiCorleto [1984]) and lipoprotein metabolism (Witte et al. [1982], Davies et al. [1983, 1985]). Smooth muscle cell growth can be regulated by heparan sulfate cleaved from the endothelial cell surface (Castellot et al. [1981]). Conditioned media derived from porcine aortic endothelial cells stimulates human fibroblast proliferation and LDL binding and internalization in fibroblasts. LDL degradation is, however, inhibited as a result of ammonia production by porcine endothelial cells, which raises lysosomal pH, inactivating lysosomal enzymes (Witte et al. [1982], Cornicelli et al. [1983]).

The close apposition between vascular endothelial and smooth muscle cells in vivo may result in bidirectional interactions. Medium conditioned by endothelial cells permits only unidirectional communication and cannot be used to examine interactions requiring the simultaneous presence of both cell types or the production of short-lived intermediates, which can potentially modulate target cell metabolism.

In order to circumvent limitations associated with the use of conditioned media, Davies [1982] has grown endothelial cells on microcarriers and has studied

the coculture of endothelial cell and smooth muscle cells. This arrangement allows metabolic cooperation to occur. Furthermore the ratio of endothelial cells to smooth muscle cells can be adjusted to examine the effect of cell number. Davies et al. [1983] have observed that following a period of coculture with endothelial cells, smooth muscle cells proliferate and increase their metabolism of LDL.

In this study the effects of endothelial cell/smooth muscle cell coculture and endothelial cell conditioned medium upon LDL metabolism by smooth muscle cells are examined. Kinetic studies were performed to determine rate constants for LDL metabolism by smooth muscle cells following coculture. In addition, experiments were conducted to: 1) examine the effect of endothelial cell number upon smooth muscle cell LDL metabolism; 2) measure ammonia production by endothelial cells and smooth muscle cells; and 3) examine growth-factor independent stimulation of LDL metabolism by endothelial cells.

3.2 Previous Results with Platelet-Derived Growth Factor, Conditioned Media, and Coculture

3.2.1 Platelet-Derived Growth Factor

Platelet-derived growth factor (PDGF) is the principle mitogen in serum and is released from platelet α granules upon platelet aggregation. PDGF is cationic with a molecular weight between 29,000 and 32,000 (Westermarck et al. [1983]). Exposure of fibroblasts and smooth muscle cells to PDGF results in stimulation of cell growth (Westermarck et al. [1983]), fluid endocytosis (Davies and Ross [1978]), and LDL metabolism (Chait et al. [1980], Witte and Cornicelli [1980]). Studies with purified mitogen show that cells which are committed to the cell cycle exhibit increased LDL metabolism (Davies and Kuczera [1982]), although stimulation of LDL metabolism precedes entry into the cell cycle as measured by nuclear uptake of

^3H -thymidine (Chait et al. [1980]). The primary effect of PDGF upon LDL metabolism appears to be an increase in the number of LDL receptors (Chait et al. [1980], Witte et al. [1982]), although kinetic studies have not been performed to examine changes in the rate constants.

3.2.2 Endothelial Cell Conditioned Media

Cultured endothelial cells secrete a number of growth factors, some of which are related to PDGF. Most published reports have examined PDGF-like growth factor production, since its activity can be easily measured. The growth factor is cationic with a molecular weight between 25,000 and 40,000 g/mole (DiCorleto et al. [1983]) and competes with PDGF for binding sites on the PDGF receptor on human fibroblasts (Fox and DiCorleto [1984]). In culture, the rate of growth factor production by bovine aortic endothelial cells is constant with time (0.69 ± 0.11 ng/ 10^6 cells/day) for as long as three weeks (Fox and DiCorleto [1984]).

Witte et al. [1982] have examined LDL metabolism by human fibroblasts incubated with conditioned media derived from porcine aortic endothelial cells. Confluent monolayers of endothelial cells in 75 cm^2 flasks were each incubated with 14 ml of 5% lipoprotein-deficient serum (LPDS) for 96 hr. The conditioned media was diluted with 5% LPDS, and volume fractions of conditioned media from 0 to 1 were incubated with fibroblasts for 72 hr after which LDL metabolism was determined following a 2 hr incubation with $20\ \mu\text{g/ml}$ ^{125}I -LDL. Results from this study are presented in Figure 3-1.

In fibroblasts incubated with endothelial cell conditioned media, binding and internalization increase as the volume fraction of conditioned media increases (Figure 3-1a,b). Degradation of LDL and esterification of cholesterol increase at low concentrations of conditioned media, but reach a maximum at 20% conditioned

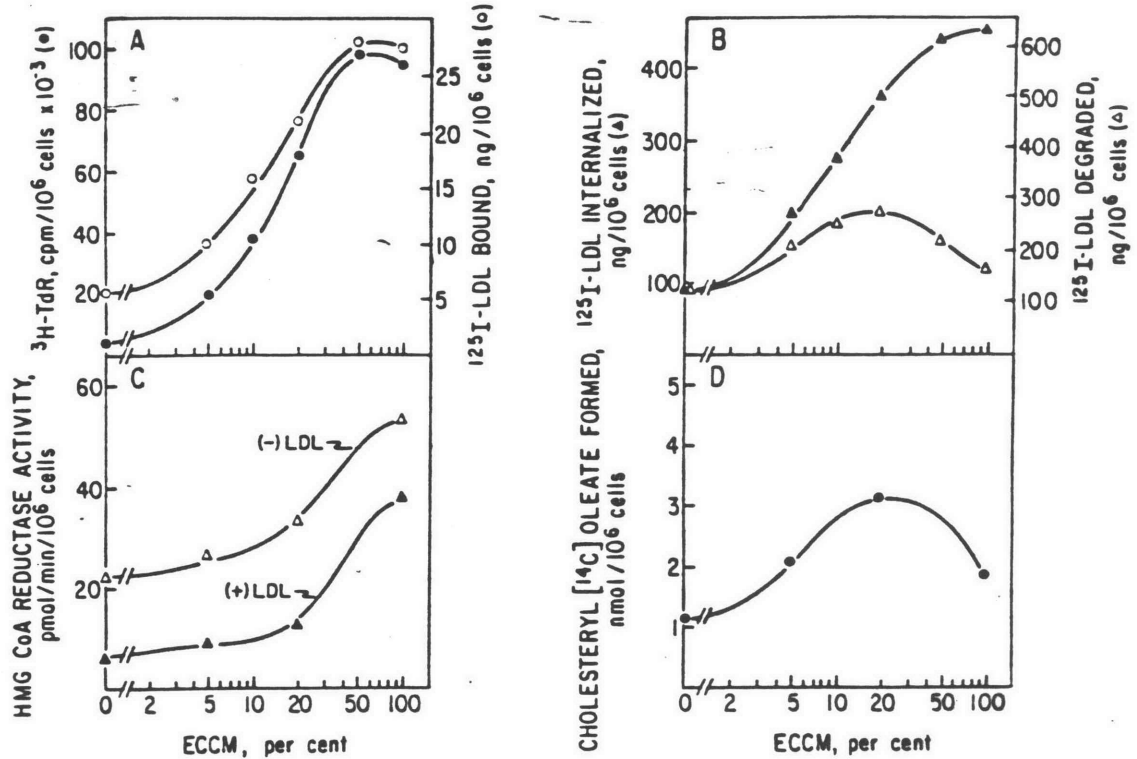


Figure 3-1: LDL metabolism by fibroblasts following incubation with conditioned media (from Witte et al. [1982]).

media and then decrease as the concentration of conditioned media is increased further (Figure 3-1b,d). The activity of HMG-CoA reductase, the rate-limiting enzyme for the endogenous synthesis of cholesterol, increases as the concentration of conditioned media increases (Figure 3-1c) even after incubation with LDL (data labeled (+) LDL in Figure 3-1c), suggesting that cholesterol delivery from LDL is insufficient to meet the cellular demand for cholesterol. These results indicate that LDL degradation is inhibited by endothelial cell conditioned media. Inhibition of LDL degradation increases with increasing time for endothelial cell conditioning of media (Cornicelli et al. [1983]).

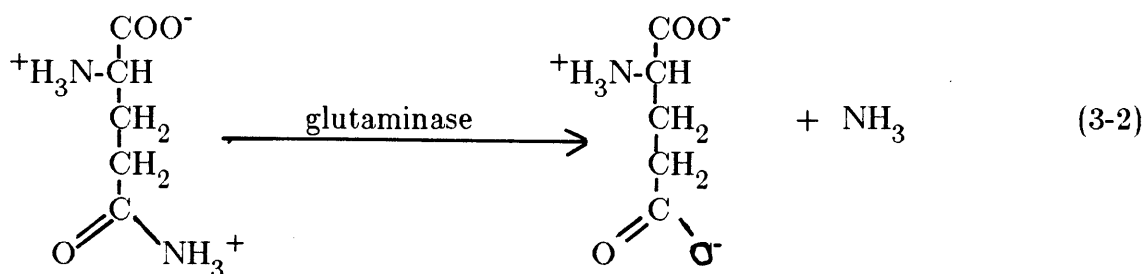
Cornicelli et al. [1983] found that this inhibitor is distinct from the endothelial cell derived growth factors, and they present evidence which suggests that degradation is inhibited by the production of ammonia (measured as the

concentration of ammonium ion in the medium) by porcine endothelial cells (Table 3-I). Ammonium ion raises the lysosomal pH, inactivating lysosomal enzymes. The concentration of ammonium ion is correlated with the inhibition of LDL degradation, which Cornicelli et al. [1983] have quantified in terms of the inhibitory index (Ix).

$$Ix = 1 - \frac{D/(D + I)_{cm}}{D/(D + I)_c} \quad (3-1)$$

where D and I are, respectively, the amounts degraded and internalized following a 2 hr incubation with 20 $\mu\text{g/ml}$ ^{125}I -LDL. The subscripts *cm* and *c* refer to conditioned medium and control measurements. The inhibitory index is a rather complicated function of all the rate constants for LDL metabolism, and k_3 is a more appropriate measure of degradation but it cannot be estimated from the data of Witte et al. [1982] and Cornicelli et al. [1983].

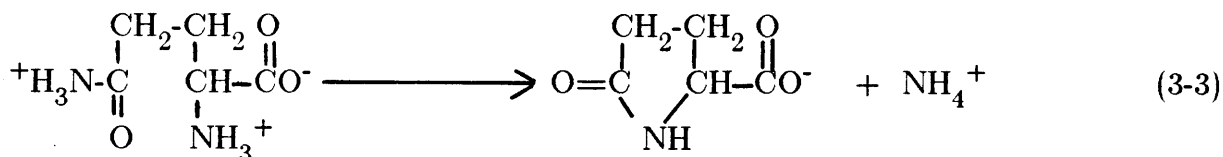
Ammonia is derived from the cellular metabolism of glutamine to glutamic acid in the presence of the enzyme glutaminase (White et al. [1978]).



At physiological pH (7.4) ammonia is present largely as ammonium ion which can be determined spectrophotometrically. Epithelial cells, especially those in the kidney, produce significant amounts of ammonia (Butler et al. [1983], Glacken and Sinskey [1985]). In addition to cellular metabolism, glutamine present in the culture medium spontaneously decomposes to pyrrolidine-carboxylic acid and ammonium ion at pH 7.4.

Table 3-I: Production of Ammonia by Endothelial Cells and Inhibition of Degradation (From Cornicelli et al. [1983])

Hours of Conditioning	NH ₄ ⁺ in Media, mM	Cell-Specific NH ₄ ⁺ , mM	Inhibitory Index, Ix
0	0.08	0.08	0.012
8	0.80	0.73	0.043
24	1.18	0.96	0.081
48	2.96	2.55	0.133
72	3.14	2.56	0.175
96	3.64	2.90	0.283
144	3.77	2.77	0.343



The decomposition reaction is first order in glutamine concentration, and at 37 °C the rate constant is 0.0048 hr⁻¹ (Glacken and Sinskey [1985]). Subtracting the ammonium ion concentration due to decomposition yields ammonium ion concentration resulting from cellular production of ammonia which is also presented in Table 3-I. At long incubation times, as much as 25% of the ammonium ion present in the medium can be attributed to the breakdown of glutamine.

Both total and cell-associated ammonium ion concentrations increase rapidly during the first 48 hours of the conditioning period and then increase more slowly at

later times (Figure 3-2). The slowdown may represent depletion of glutamine from the medium. The ammonium ion concentrations are similar to those produced by kidney epithelial cells after similar incubation periods (Glacken et al. [1985]).

Cornicelli et al. [1983] have measured the effect of NH_4Cl concentration on ^{125}I -LDL degradation by human fibroblasts. Their results are summarized in Figure 3-3. Inhibition of LDL degradation in fibroblasts, measured in terms of the inhibitory index, increases as NH_4Cl concentration increases, reaching a plateau at about 7 mM. The nonlinear relationship between inhibition of degradation and NH_4Cl concentration may be due to the nonlinear relationship between lysosomal pH and the concentration of weak base (Poole and Ohkuma [1981]).

3.2.3 Coculture of Endothelial Cells and Smooth Muscle Cells

Microcarrier-Bound Endothelial Cells Bovine aortic endothelial cells readily grow to confluence on solid plastic microcarriers (Figure 3-4). Davies [1981, 1982] has extensively characterized these cells and has found that they are identical to cells grown on plastic dishes in terms of cell growth, morphological appearance, ultrastructural characteristics, and prostaglandin I_2 production. At confluence, there are about 150 cells/bead.

In coculture, greater than 90% of the endothelial cells exclude trypan blue. Lactate dehydrogenase release into the medium by microcarrier-bound endothelial cells is less than 1% of the lactate dehydrogenase of an equivalent lysed cell population (Davies et al. [1983]). Thus, endothelial cells are stable when grown on microcarriers.

Growth Stimulation of Smooth Muscle Cells by Endothelial Cells Dr. Henry Warren, a postdoctoral fellow in the laboratory of Dr. Peter Davies at Brigham and Women's Hospital (Boston, MA), studied the growth of bovine smooth muscle cells

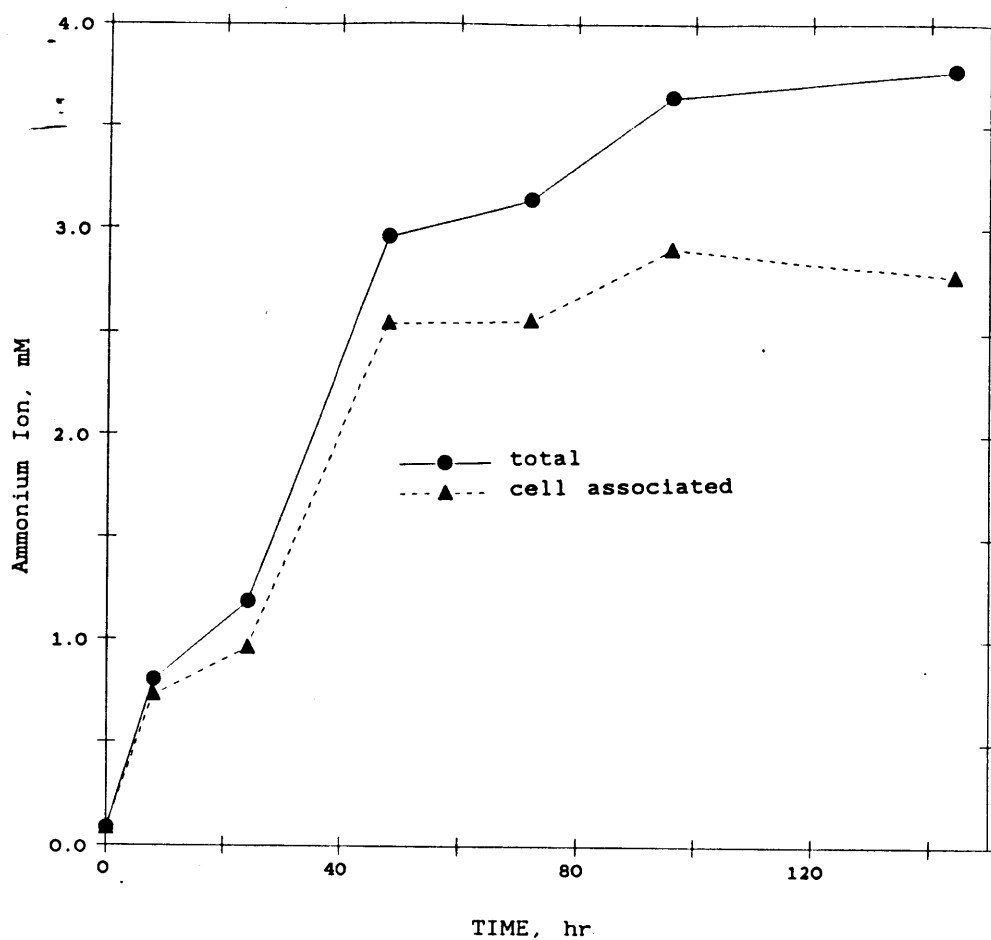


Figure 3-2: Total (●) and Cell-Associated (▲) Ammonia Production in Endothelial Cell Conditioned Media (Data from Table 3-I).

cocultured with bovine aortic endothelial cells. In these experiments, smooth muscle cells in 2% PDS were seeded onto plastic Petri dishes. The cells were incubated in 2% PDS for 72 hr at 37 °C in order to arrest cell growth. On the third day following seeding, all dishes received fresh 2% PDS and the cells were divided into three groups. One group was incubated with microcarrier-bound endothelial cells, a second with micorcarrier-bound smooth muscle cells, and a third with empty microcarrier beads. The number of smooth muscle cells per dish was measured at 2 day intervals.

The results of a typical experiment are presented in Figure 3-5. Each point is

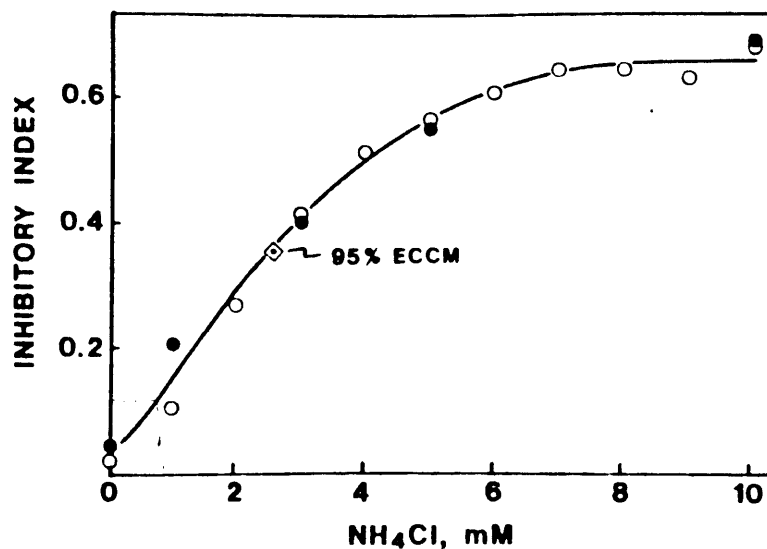


Figure 3-3: Relationship between ammonium ion concentration and inhibitory index. Human fibroblasts were incubated for 2 hr with 20 $\mu\text{g}/\text{ml}$ ^{125}I -LDL and the indicated concentration of NH_4Cl with (○) or without (●) 1 $\mu\text{g}/\text{ml}$ PDGF. Inhibitory index was calculated according to equation (3-1). The symbol ◊ represents the estimated NH_4Cl concentration in 95% (v/v) endothelial cell conditioned medium for an inhibitory index of 0.328.

the mean of 4 dishes and standard deviations are within 20% of the mean. Coculture of smooth muscle cells with microcarrier-bound smooth muscle cells or empty beads does not stimulate growth of smooth muscle cells. Coculture of smooth muscle cells with microcarrier-bound endothelial cells results in a significant stimulation of smooth muscle cell growth. Growth curves for endothelial cell conditioned media are similar.

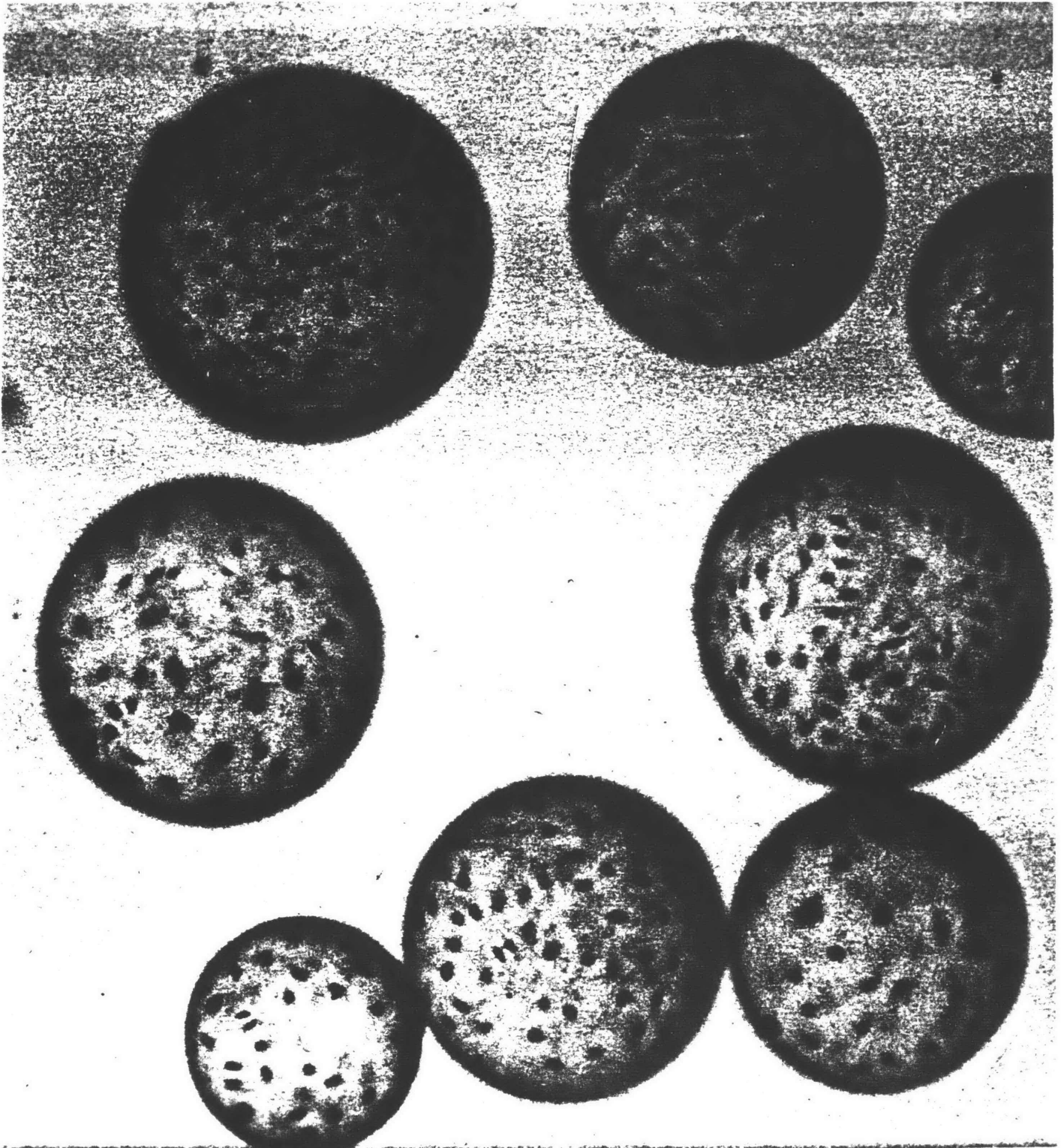


Figure 3-4: Confluent Bovine Aortic Endothelial Cells Cultured on Solid Plastic Microcarriers. x 480

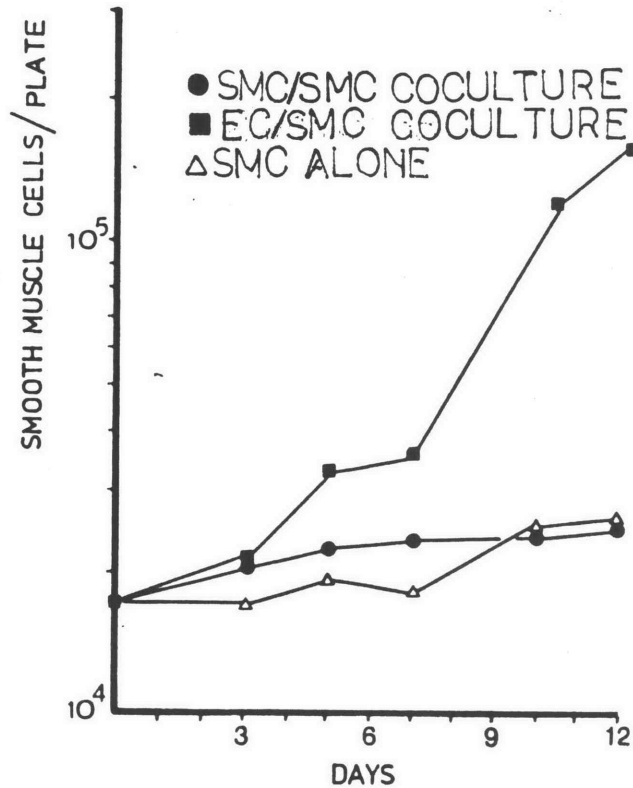


Figure 3-5: Growth Curves of Bovine Aortic Smooth Muscle Cells.
(From Davies et al. [1985])

By varying the number of microcarriers, the effect of endothelial cell mass on the growth of smooth muscle cells was studied. The results of such an experiment (performed by Dr. Warren) are presented in Figure 3-6. The protocol was identical to that for the growth studies, except that all measurements were made three days after start of cocultivation. There are significant increases in smooth muscle number with increasing endothelial cell mass, whereas growth increases slightly as the mass of smooth muscle cells on microcarriers increases. For reference, 0.1 mg cell protein is equal to approximately 4.3×10^5 endothelial cells and 3.3×10^5 smooth muscle cells.

Data were fit to the following lines by least squares linear regression:

Endothelial Cell Coculture $y = 23.6 \times 10^4 x + 6.4 \times 10^4$ (3-4)

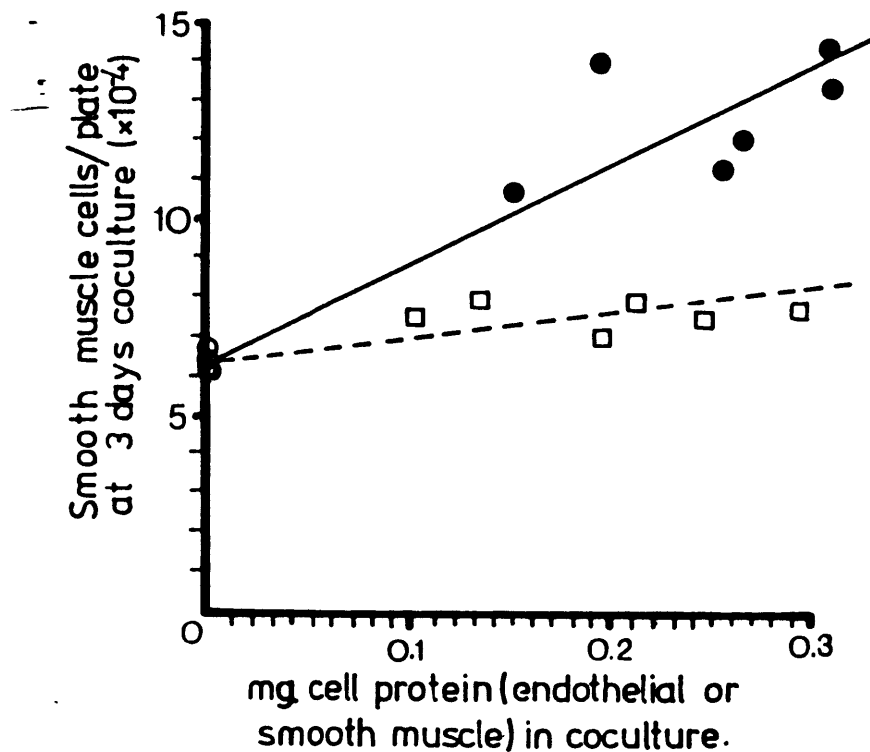


Figure 3-6: Effect of Endothelial Cell Number on Smooth Muscle Cell Growth. (From Davies et al. [1985]); (●) EC/SMC coculture; (□) SMC/SMC coculture.

$$\text{Smooth Muscle Cell Coculture} \quad y = 4.5 \times 10^4 x + 6.2 \times 10^4 \quad (3-5)$$

where x is the mass (mg) of endothelial cells or smooth muscle on microcarriers and y is the number of smooth muscle cells. The correlation coefficients are respectively 0.89 and 0.66 for endothelial cell and smooth muscle coculture with smooth muscle cells. The slope in equation (3-4) is statistically significant ($p < 0.025$) whereas the slope in equation (3-5) is not ($p > 0.20$).

LDL Metabolism by Smooth Muscle Cells Incubated with Endothelial Cells

Davies et al. [1983] examined LDL metabolism by bovine smooth muscle cells following coculture incubations with microcarrier-bound endothelial cells or smooth muscle cells. Smooth muscle cells ($2 \times 10^5/35$ mm dish) were preincubated with 2% PDS for 24 hr, in order to arrest cell growth, and then with 5% growth-factor

deficient LPDS for 48 hr to increase receptor expression. Microcarrier-bound endothelial and smooth muscle cells were incubated under the same conditions. 10 $\mu\text{g}/\text{ml}$ ^{125}I -LDL and ^{14}C -sucrose were added at 0, 15, 30, 44, and 54 hr after the start of coculture and smooth muscle cells and microcarrier-bound cells were incubated for an additional six hr after which binding, internalization, degradation and fluid endocytosis were determined. Nonspecific binding, internalization, and degradation were measured separately by incubating cells with 10 $\mu\text{g}/\text{ml}$ ^{125}I -LDL and an excess of unlabeled LDL and the results were subtracted from total binding, internalization, and degradation to yield the receptor-mediated contribution.

The results are presented in Figure 3-7. Each point is the average of four dishes and standard deviations were less than 20% of the mean. Binding, internalization, and degradation by smooth muscle cells cocultured with endothelial cells increase as the incubation time increases. Binding reaches a plateau 10 hr after the onset of coculture, whereas internalization and fluid endocytosis continue to increase throughout the experiment. Coculture with smooth muscle cells has no effect upon LDL metabolism.

3.3 MATERIALS AND METHODS

Plasma-Derived and Lipoprotein-Deficient Serum Plasma-derived serum (PDS) was prepared by the method of Vogel et al. [1978]. Cationic growth factors were removed by passage over a carboxymethyl-Sephadex (CM-50, Pharmacia Fine Chemicals, Piscataway, NJ) chromatography column. The resulting PDS was dialyzed against phosphate buffered saline, pH 7.4, concentrated to 50 mg protein/ml by ultrafiltration, and stored frozen. Protein concentrations were measured by the method of Lowry et al. [1951].

Lipoprotein-deficient medium (LPDS) was prepared by a modification of the

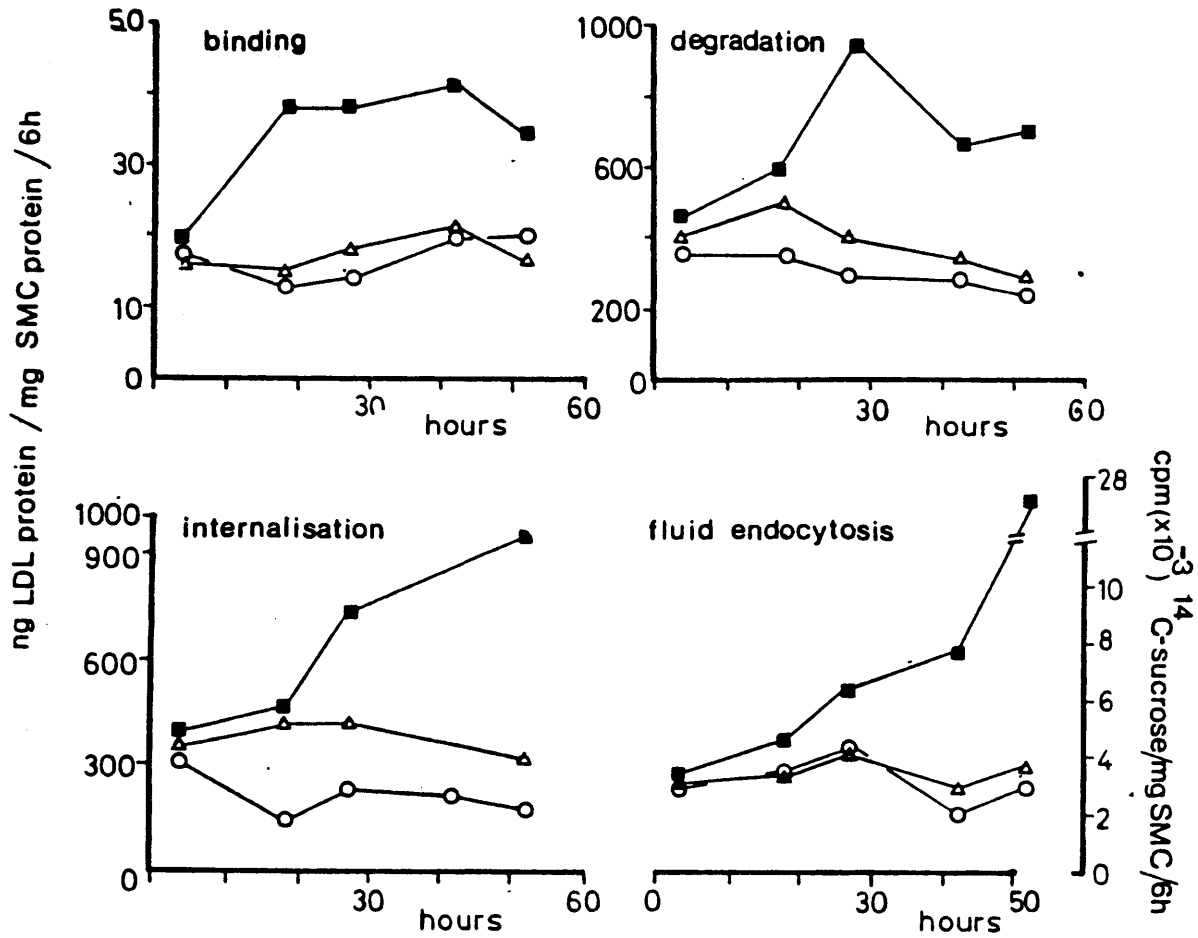


Figure 3-7: LDL metabolism by smooth muscle cells alone (○) or cocultured with microcarrier-bound endothelial cells (■) or smooth muscle cells (Δ) (from Davies et al. [1983]).

method of Weinstein et al. [1976]. Human plasma (American Red Cross, Boston, MA), was dialyzed against 0.15 M NaCl 0.001 M Na₂EDTA, pH 8.6, at 4°C. The density was adjusted to 1.25 g/cm³ by addition of NaBr (Hatch and Lees [1968]). The solution was centrifuged for 48 hours at 60,000 rpm in a Beckman Ti 60 rotor. The bottom fraction was isolated and dialyzed against 0.1 M Tris buffer, pH 7.4, at 4 °C. The solution was then passed over a CM-50 column to remove cationic growth factors, concentrated (50 mg protein/ml), and dialyzed against phosphate buffered saline, pH 7.4.

Isolation and Radiolabeling of LDL LDL was isolated from recovered human plasma (American Red Cross) by a modification of conventional precipitation techniques (Cornwall and Krueger [1961], Burstein et al. [1970]). Purity was assessed by double radial immunodiffusion, immunoelectrophoresis, and cellulose acetate electrophoresis. Protein content was measured by the method of Lowry et al. [1951]. Additional details are discussed in Chapter 2.

LDL was iodinated with Na¹²⁵I (New England Nuclear, Boston, MA) by the method of McFarlane [1958] as modified by Bilheimer et al. [1972]. Non-protein-bound radioactivity was removed by passing over a PD-10 column (G-50, Pharmacia Fine Chemicals) which was followed by dialysis against 0.15 M NaCl, 0.001 M Na₂EDTA, pH 8.6, at 4 °C. Greater than 97% of the total ¹²⁵I was precipitable in 10% trichloroacetic acid. By chloroform-methanol extraction (Folch et al. [1957]) only 2% of label was associated with lipid. Specific activities ranged from 100 to 400 cpm/ng protein (65-260 μCi/mg LDL protein).

Isolation of Endothelial Cells Endothelial cells were isolated from bovine aorta by the method of Gimbrone et al. [1976]. A sterile cotton swab was applied to the luminal surface of the aorta following a 10 minute exposure to crude collagenase (Type 1, 1 mg/ml; Worthington Biochemicals, Freehold, NJ) at 37 °C. The swab,

with attached cells, was rotated in a 25 cm² plastic dish containing 5% PDS in Dulbecco's modified Eagle's medium (DMEM) (M.A. Bioproducts, Gaithersburg, MD) to release the sheets of endothelial cells. PDS inhibits growth of occasional contaminating smooth muscle cells, without affecting endothelial cell proliferation. Beginning at the third subculture, cells were maintained in 10% calf serum in DMEM (10% CS-DMEM). Endothelial cells which were used in these experiments have been designated SOC-1 and were in subcultures 5 to 20 at the time of the experiments.

Microcarrier Cultures of Endothelial Cells Endothelial cells were loaded onto microcarrier beads by the method of Davies [1981]. Briefly, negatively charged polystyrene beads (Trade name: Biosilon (A.S. Nunc, Denmark); Vanguard Intl., Neptune, NJ) were incubated with 10% CS-DMEM for 30 minutes at room temperature. This apparently results in adsorption of cold-insoluble globulin to the beads, a necessary step in the attachment of endothelial cells to beads (Davies [1981]). 10⁸ cells in 10 ml 10% CS-DMEM were added to 2 g of beads (3.7 x 10⁵ beads/g) in a 10 cm plastic Petri dish, the surface of which was treated with hydroxyethyl methacrylate (Hydron Laboratories; New Brunswick, NJ; 1.2% (w/v) solution in ethanol) in order to prevent attachment of endothelial cells to the dish surface. The cells attached to the beads in 2-3 hours (Davies [1981]). Medium was changed every 2 days. All cultures were incubated at 37 °C in a humidified 5% CO₂-95% air atmosphere.

Cells were dissolved in 0.1% (w/v) sodium dodecyl sulfate (SDS) and cell protein was determined by the method of Lowry et al. [1951]. Endothelial cells were detached from plastic microcarriers by trypsinization (3 ml of 2.5% trypsin in modified Hanks' balanced salt solution (M.A. Bioproducts)) and cell number was determined in a Coulter Counter (Coulter Electronics, Hialeh, FL). Data are

presented as cell protein mass since this is easier to determine. 10^6 endothelial cells are equivalent to 0.43 mg endothelial cell protein (H.B. Warren, unpublished observations).

Smooth Muscle Cell Culture Bovine smooth muscle cells were cultured from explant outgrowths by the method of Ross [1971]. All cells were in subcultures 2 or 3 at the time of the experiment. Cells were plated at 5×10^4 cells/35mm dish in 10% CS-DMEM. After 48 hr, the cells were washed once with Hanks' balanced salt solution (HBSS) and the medium was replaced with 5% (v/v) plasma derived serum in Dulbecco's modified Eagle's medium to arrest cell growth. Additional details are presented in Chapter 2.

Coculture System A microcarrier coculture system was used based upon the design of Davies and Kerr [1982a]. Briefly, the device consists of a shallow plastic cylinder attached to the underside of a petri dish lid (Figure 3-8). The lower end of the cylinder was covered with a silicon-treated nylon mesh (1 μ m pore size; Spectramesh, Spectrum Medical Industries, Los Angeles). A sterile plastic 10 ml pipet was used to load microcarrier cells into the cylindrical chamber which was then attached to the petri dish lid with grease. The lid was placed in a culture dish containing 2.5 ml of medium in which smooth muscle cells were grown. Thus, the culture medium was shared by both cell populations allowing communication to occur without direct contact.

Dialysis Membrane Barrier between Cells In some coculture experiments, growth factors (molecular weight between 25,000 and 40,000 (DiCorleto et al. [1983])) were prevented from reaching smooth muscle cells by replacing the nylon mesh with a dialysis membrane with a nominal molecular weight cutoff of 3500 (Spectra/Por 3, Spectrum Medical Industries; Fisher Scientific Co., Medford, MA). The membrane was secured across the opening of the cylinder with a tight fitting

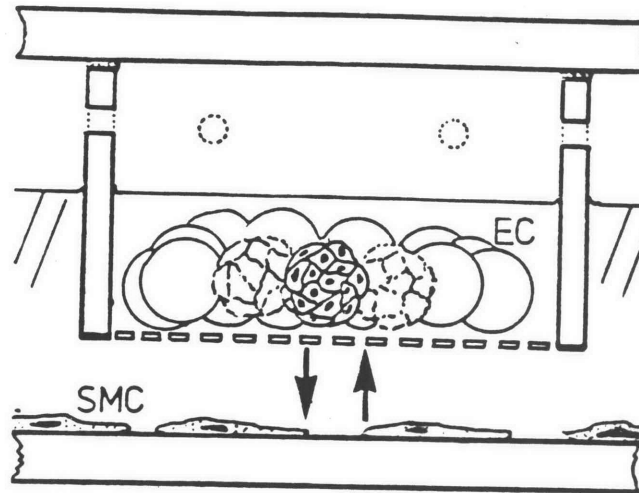


Figure 3-8: Microcarrier Coculture Apparatus

plastic ring. The effectiveness of the membrane was tested by measuring the amount of ^{125}I -labeled proteins with molecular weights ranging from 6,000 to 66,200 which passed from one side of the membrane to the other after 24 hr (Davies et al. [1985]).

Incorporation of ^3H -Thymidine into DNA Smooth muscle cells were incubated with $0.1 \mu\text{Ci/ml}$ ^3H -Thymidine (specific activity 6-7 Ci/mmol; New England Nuclear, Boston) for 20 hr at 37°C after endothelial cell coculture. At the end of the incubation the cells were rinsed two times with phosphate buffered saline and fixed in 2% glutaraldehyde overnight. Following fixation, the dishes were dipped in Kodak NTB2 emulsion (Kodak; Rochester, NY). Following exposure in the dark at 4°C for 10 days, the autoradiographs were developed and stained with hemotoxylin and eosin. 1000 nuclei were counted on each dish from which the percent of labeled nuclei was determined.

Lipoprotein Metabolism Binding, internalization, and degradation of ^{125}I -LDL were determined using standard procedures (Brown et al. [1983]). Quiescent smooth muscle cells alone or cocultures of smooth muscle cells and endothelial cells were incubated with 5% growth factor-deficient LPDS for 48 hr (Figure 3-9). At the end of the coculture incubation, coculture baskets were removed along with the endothelial cells, and smooth muscle cells were incubated with ^{125}I -LDL at 37 °C for periods appropriate to each experiment. At the end of the experiment, the dishes were rapidly chilled to 4 °C and the medium was removed for determination of LDL degradation. Cells were washed seven times with HBSS containing 2 mg/ml bovine serum albumin, followed by one rinse with HBSS alone. The cells were incubated for one hour at 4 °C with HBSS containing 10 mg/ml sodium heparin (Grade 1, Sigma Chemical Co., St. Louis, MO) to release LDL from its receptors on the cell surface (Goldstein et al. [1976]). The heparin-containing medium was removed and counted to determine the amount of binding. The cells were then rinsed in HBSS and dissolved in 0.1% (w/v) sodium dodecyl sulfate for determination of cell associated ^{125}I (internalized LDL) and total cellular protein. LDL degradation was determined as trichloroacetic acid-soluble ^{125}I -tyrosine activity in the culture medium. Free ^{125}I was removed by oxidation to iodine and partition into chloroform (Bierman et al. [1974]). Endothelial cells were dissolved in 0.1% sodium dodecyl sulfate and protein was determined by the method of Lowry et al. [1951].

In all experiments, receptor-independent LDL binding, internalization, and degradation were determined by incubation of ^{125}I -LDL with 500 $\mu\text{g}/\text{ml}$ unlabeled LDL. Receptor-mediated metabolism was determined by subtracting receptor-independent binding, internalization, and degradation from total binding, internalization, and degradation. Cell free dishes were incubated with ^{125}I -LDL in parallel to the above and the amount degraded was subtracted from the specific and

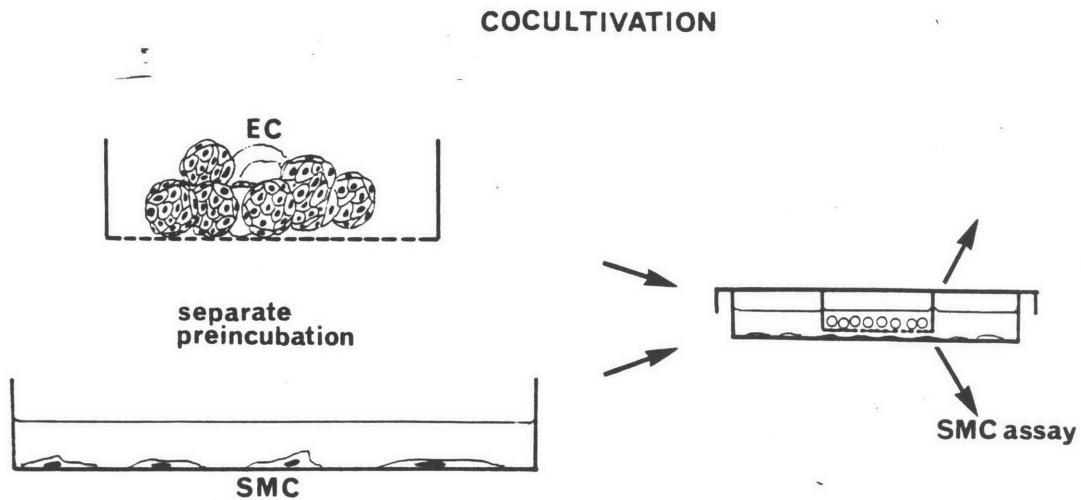


Figure 3-9: Experimental Protocol for Coculture nonspecific contributions.

3.4 Results

3.4.1 ^3H -Thymidine Autoradiography of Smooth Muscle Cells Cocultured with Endothelial Cells

Proliferation of smooth muscle cells cocultured with endothelial cells is inhibited in the presence of 5% lipoprotein deficient serum, presumably because of a limited supply of exogenous sterols which prevents completion of mitosis (Davies, P.F.; unpublished observations). Nevertheless, cells still enter the synthetic phase of the cell cycle and this was measured by ^3H -thymidine autoradiography. Smooth muscle cells (2 to $5 \times 10^5/35$ mm dish) were incubated in 2% PDS for 48 hr to arrest cell growth followed by an incubation in 5% LPDS for 48 hr to increase receptor expression. Smooth muscle cells then received fresh 5% LPDS and were incubated for either 20 hr or 45 hr alone, with microcarrier-bound smooth muscle cells or endothelial cells, or with endothelial cell or smooth muscle conditioned

media. (Conditioned media was prepared by incubating 10^8 smooth muscle cells or endothelial cells with 14 ml of 5% LPDS for 96 hr. The medium was centrifuged to remove cells, and diluted 50% with 5% LPDS.) At the end of this incubation ^3H -thymidine was added and the cells were incubated for an additional 20 hr. The cells were fixed and processed for autoradiography as described in Materials and Methods.

The results are presented in Table 3-II. Each value is the average from two dishes. Smooth muscle cells incubated alone, cocultured with smooth muscle cells, or incubated with smooth muscle cell conditioned media show a low level of labeling indicating that the cells are nongrowing. Coculture with endothelial cells or incubation with endothelial cell conditioned media stimulates a significant percentage of cells to enter the synthetic phase of the cell cycle. Similar results were obtained with 2% PDS and 0.4% calf serum (Davies et al. [1985]). These results are consistent with the growth studies performed by Dr. Warren using 2% PDS.

Table 3-II: ^3H -Thymidine Labeling of Smooth Muscle Cells

Treatment (Expt. BSMC5) (n=2)	Percent Labeled Nuclei (\pm SD)	
	20 hr	45 hr
Endothelial Cell Conditioned Media	62.3 \pm 5.4	39.5 \pm 3.5
Smooth Muscle Cell Conditioned Media	2.1 \pm 0.1	0.9 \pm 0.1
Endothelial Cell Coculture		63.4 \pm 4.4
Smooth Muscle Cell Coculture		4.6 \pm 3.2
SMC alone	2.3 \pm 0.4	2.3 \pm 0.1

3.4.2 Endothelial Cell Specific Stimulation of LDL Metabolism

Davies et al. [1983] demonstrated that coculture of endothelial cells with smooth muscle cells stimulates receptor-mediated metabolism of LDL by bovine smooth muscle cells. In order to verify these results, receptor-mediated metabolism was measured in smooth muscle cells alone, smooth muscle cells incubated with conditioned media from endothelial cells or smooth muscle cells, and smooth muscle cells cocultured with microcarrier-bound endothelial cells or smooth muscle cells. The protocol is the same as that described for the ^3H -thymidine uptake experiment (Table 3-II) except that, after 20 hr and 45 hr incubations, media and any microcarrier-bound cells were removed, and cells received fresh media containing either $10\ \mu\text{g}/\text{ml}$ ^{125}I -LDL or $10\ \mu\text{g}/\text{ml}$ ^{125}I -LDL and $500\ \mu\text{g}/\text{ml}$ LDL. Cells were incubated for 4 hr after which receptor-mediated binding, internalization, and degradation were measured.

Results are presented in Table 3-III for receptor-mediated binding, internalization, and degradation. Each value is the average of two dishes. The results presented in Tables 3-II and 3-III are from the same experiment (BSMC5).

At 20 hr endothelial cell conditioned media stimulates LDL metabolism. After 45 hr, endothelial cell conditioned media and endothelial cell coculture stimulate LDL metabolism. Smooth muscle cell conditioned media has no effect at either time, although smooth muscle cell coculture does stimulate LDL metabolism, but not to the extent of endothelial cell coculture or conditioned media. Davies et al. [1983] obtained similar results except that coculture of smooth muscle cells with microcarrier-bound smooth muscle cells did not stimulate LDL metabolism of smooth muscle cells.

The 45 hr incubation experiment was repeated three additional times with different batches of cells and LDL. Average values of receptor-mediated and

Table 3-III: Effect of Coculture and Conditioned Media on LDL Metabolism by Smooth Muscle Cells

Treatment (Expt. BSMC5) (n=2)	ng ¹²⁵ I-LDL protein/mg cell protein (\pm SD)		
	Bound	Internalized	Degraded
20 hr			
Endothelial Cell Conditioned Media	78.6 \pm 4.2	542 \pm 80	597 \pm 110
Smooth Muscle Cell Conditioned Media	25.1 \pm 9.5	104.5 \pm 1.1	111.9 \pm 2.9
None	17.4 \pm 8.5	146.3 \pm 13.6	123.8 \pm 8.8
45 hr			
Endothelial Cell Conditioned Media	31.4 \pm 6.8	592 \pm 89	521 \pm 64
Smooth Muscle Cell Conditioned Media	5.0 \pm 2.2	84.5 \pm 1.1	49.6 \pm 20.1
Endothelial Cell Coculture	37.3 \pm 0.5	489 \pm 34	285 \pm 19
Smooth Muscle Cell Coculture	17.1 \pm 8.6	341 \pm 109	180 \pm 95
None	6.7 \pm 5.6	93.0 \pm 8.8	28.7 \pm 8.6

receptor-independent metabolism calculated from all four experiments, including BSMC5 (Table 3-III) are presented in Table 3-IV. In all experiments, incubation of smooth muscle cells with endothelial cell conditioned media or microcarrier-bound endothelial cells results in stimulation of receptor-mediated binding, internalization, and degradation and receptor-independent internalization and degradation. There is greater stimulation of receptor-mediated than receptor-independent metabolism. Results obtained with coculture and conditioned media are similar, except for LDL

degradation. Stimulation of LDL degradation following smooth muscle cell incubation with endothelial cell conditioned media are in contrast with the results obtained by Witte et al. [1982] (Figure 3-I). Data presented in Tables 3-I, 3-II, 3-III and 3-IV are consistent with growth factor induced stimulation of LDL metabolism. (The possibility of growth factor independent stimulation of LDL metabolism is discussed below.)

Table 3-IV: LDL Metabolism by Smooth Muscle Cells Following a 45 hr Coculture Incubation

(n=11)	Treatment		
	SMC alone (n=7)	ECCM ¹ (n=11)	EC Coculture ²
Receptor-Mediated (\pm SEM), ng LDL protein/mg cell protein			
Bound	10.6 \pm 4.3	39.4 \pm 11.8	46.6 \pm 8.7
Internalized	94 \pm 10	385 \pm 70	422 \pm 58
Degraded	79 \pm 17	523 \pm 117	226 \pm 56
Receptor-Independent (\pm SEM), ng LDL protein/mg cell protein			
Bound	9.2 \pm 2.2	5.2 \pm 1.6	8.9 \pm 1.4
Internalized	54 \pm 3	67 \pm 21	78 \pm 11
Degraded	12 \pm 4	33 \pm 11	99 \pm 34

1. Endothelial cell conditioned media

2. endothelial cell coculture

Changes in LDL metabolism by smooth muscle cells incubated with microcarrier-bound endothelial cells or endothelial cell conditioned media as a function of incubation time was investigated. In order to maintain cell to volume ratios for conditioned media similar to those in coculture, the collection process for conditioned media was changed and approximately 5×10^5 microcarrier-bound

endothelial-cells were incubated with 2.5 ml 5% LPDS per 35 mm plastic dish for 48 hr. The conditioned media was then diluted 1:1 (v/v) with 5% LPDS in order to insure that smooth muscle cells received sufficient nutrients. Quiescent smooth muscle cells were incubated with microcarrier-bound endothelial cells or endothelial cell conditioned media for times ranging from 2 to 44 hr. At the end of the incubation, endothelial cells and medium were removed, and bovine smooth muscle cells were incubated for 2 hr with 10 $\mu\text{g/ml}$ ^{125}I -LDL or 10 $\mu\text{g/ml}$ ^{125}I -LDL and 500 $\mu\text{g/ml}$ LDL (for determination of nonspecific metabolism) after which receptor-mediated binding, internalization, and degradation are determined. The results are summarized in Figures 3-10 and 3-11 for receptor-mediated and receptor-independent metabolism, respectively. For coculture and conditioned media, each point in Figures 3-10 and 3-11 is the average of three dishes, whereas for smooth muscle cells incubated alone, each point is the average of two dishes. Error bars represent the standard deviation.

By 16 hr after the onset of the incubation, receptor-mediated LDL binding and internalization were stimulated by endothelial cell coculture and conditioned media. Stimulation of receptor-mediated degradation did not occur until at least 24 hr after onset of incubations. At all times results with conditioned media and coculture are similar. As incubation time increases, the difference in LDL metabolism between smooth muscle control experiments and coculture and conditioned media experiments becomes greater. At 48 hr stimulation appears to be increasing, suggesting that the growth factor has not been depleted from the medium.

In contrast with the results in table 3-IV for receptor-mediated and receptor-independent metabolism, there is little stimulation of receptor-independent metabolism (Figure 3-11). At all times nonspecific binding, internalization, and

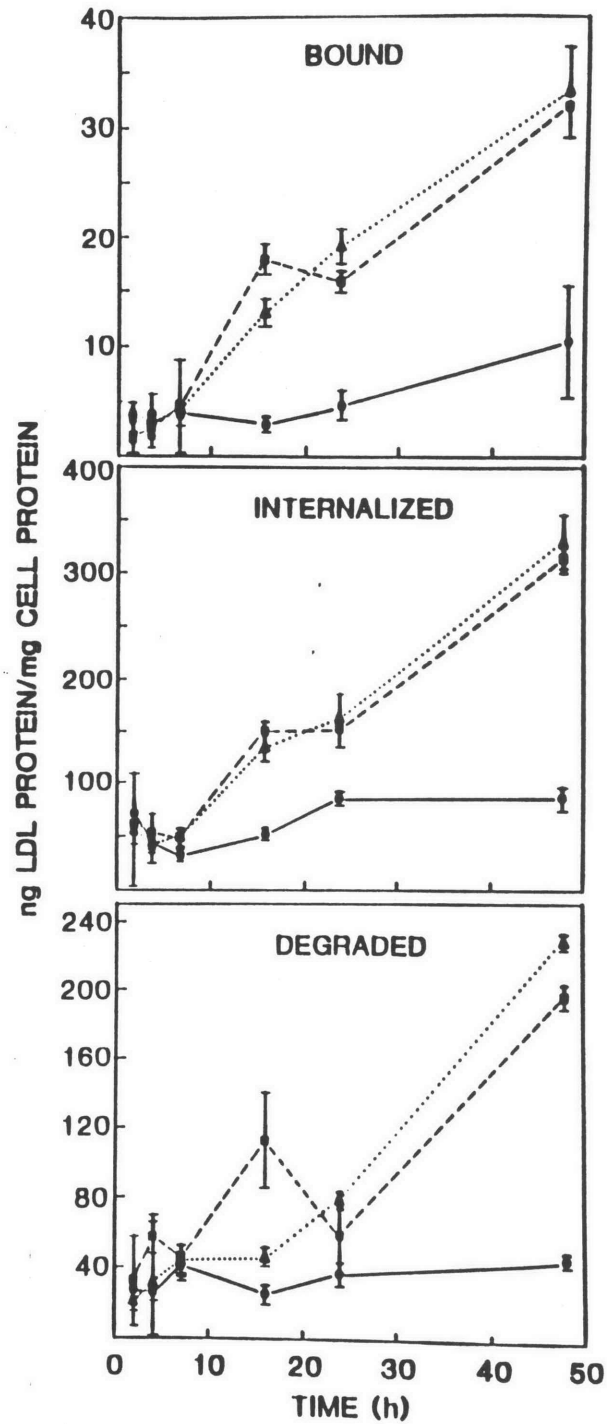


Figure 3-10: Expt. BSMC30: Receptor-Mediated LDL metabolism by smooth muscle cells incubated with endothelial cell conditioned media or cocultured with endothelial cells.

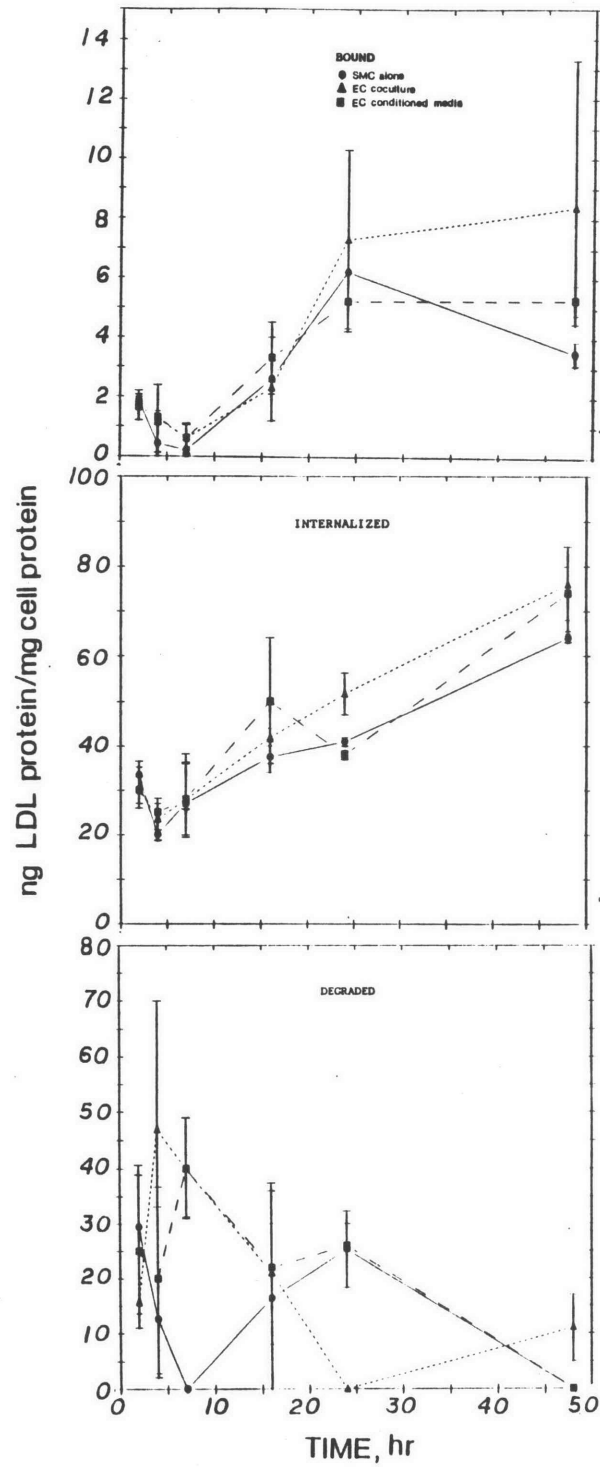


Figure 3-11: Expt. BSMC30: Receptor-Independent LDL metabolism by smooth muscle cells incubated with endothelial cell conditioned media or cocultured with endothelial cells.

degradation by smooth muscle cells incubated with endothelial cell conditioned media or microcarrier-bound endothelial cells are similar to those for smooth muscle cells incubated with 5% LPDS. Values for control experiments (smooth muscle cells incubated alone) are not constant with time. Consequently, no definitive conclusions can be drawn from this experiment for receptor-independent metabolism.

Although the results suggest that coculture is at least as potent as conditioned media in stimulating LDL metabolism, direct comparison of coculture and conditioned media is difficult. Conditioned media represents an endpoint in growth factor production by the endothelial cells, whereas, in coculture, growth factor production is initially zero and increases linearly with time (Fox and DiCorleto [1984]). At the beginning of the experiment presented in Figures 3-10 and 3-11, smooth muscle cells which receive endothelial cell conditioned media are exposed to the cumulative amount of growth factor produced after 48 hr. Smooth muscle cells cocultured with endothelial cells are initially exposed to low concentrations of growth factor relative to smooth muscle cells incubated with conditioned media. The similarity in changes of LDL metabolism by smooth muscle cells exposed to coculture and conditioned media suggests that either very low concentrations of endothelial cell derived growth factors are required to stimulate LDL metabolism or additional cell-cell interactions are occurring.

3.4.3 Effect of Endothelial Cell Number

If stimulation of smooth muscle cell LDL metabolism following coculture with endothelial cells is a result of a molecule(s) secreted by endothelial cells then LDL binding, internalization, and degradation should be a function of the number of endothelial cells incubated with smooth muscle cells. To examine this, bovine aortic

smooth muscle cells were incubated with varying numbers of endothelial cells for 48 hr. At the end of the incubation the endothelial cells were removed, the smooth muscle cells were washed and incubated with 20 $\mu\text{g/ml}$ ^{125}I -LDL for 4 hr after which receptor-mediated binding, internalization, and degradation have been measured. The results are presented in Figure 3-12. Each point is the average of two dishes, except for the point at 0.23 mg endothelial cells, which is the value from a single dish.

LDL binding, internalization, and degradation by smooth muscle cells increases with increasing endothelial cell mass, although at higher endothelial cell masses, the rate of increase is less. Data were fit to the following empirical function:

$$y = y_0 + \frac{a_1 x}{a_2 + x} \quad (3-6)$$

where y is the amount of LDL bound, internalized, or degraded per mg smooth muscle cells, x is the mass of endothelial cells, y_0 is the amount of LDL bound, internalized, or degraded per mg smooth muscle cell in the absence of endothelial cells, and a_1 and a_2 are empirical constants. Equation (3-6) was fit to data in Figure 3-12 by nonlinear regression and the best fit parameters are listed in Table 3-V. For internalized and degraded LDL, the half saturation value, a_2 , is between 0.08 and 0.09 mg endothelial cells which corresponds to 1.9 to 2.1×10^5 endothelial cells. Data for binding are best represented by a step change in the amount bound as a function of endothelial cell mass. Bound LDL could be fit with a_2 fixed at 0.086 (the average value for internalized and degraded) with only a small 23% increase in the sums of squares.

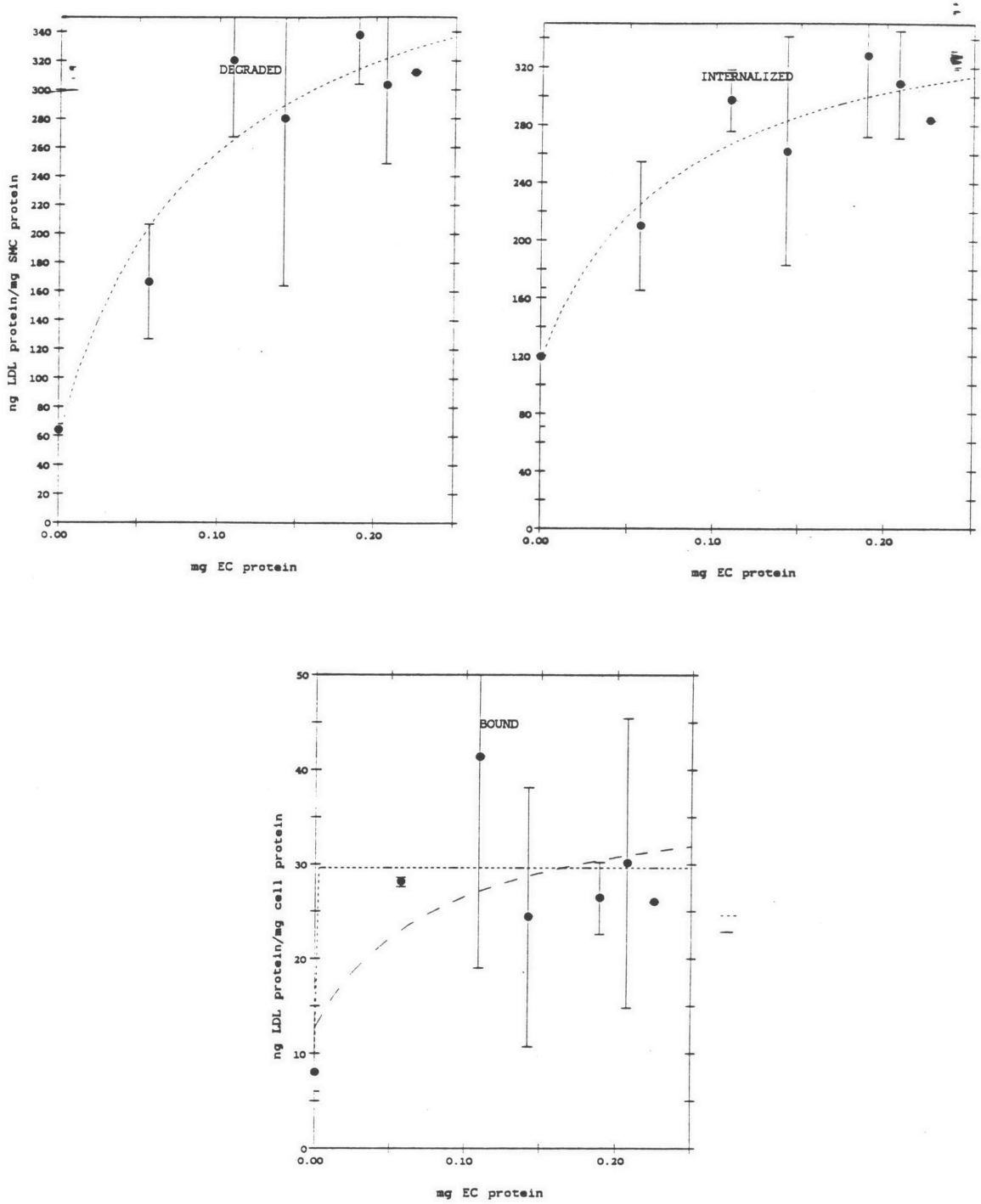


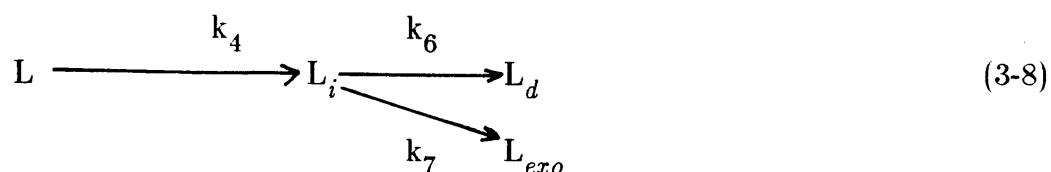
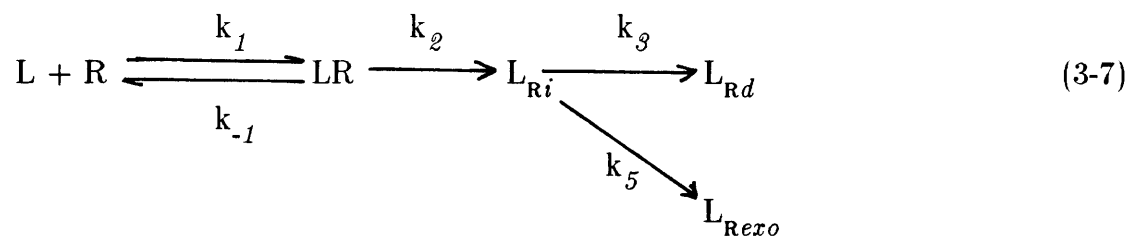
Figure 3-12: Smooth muscle cell LDL metabolism as a function of endothelial cell mass. Smooth curves represent best fit of equation (3-6) to data.

Table 3-V: Best Fit Parameters of Equation (3-6) to Data in Figure 3-12

	y_0	a_1	a_2
Bound	7.8 ± 5.8	21.8 ± 8.3	$10^{-8} \pm 2.1$
	12.7 ± 7.3	25.8 ± 12.5	0.086 (fixed)
Internalized	117 ± 28	259 ± 71	0.079 ± 0.067
Degraded	59 ± 38	380 ± 108	0.092 ± 0.076

3.4.4 Kinetic Analysis of LDL Metabolism in Smooth Muscle Cells Cocultured with Endothelial Cells

Kinetic models of receptor-mediated and receptor-independent LDL metabolism developed in Chapter 2 were used to examine the effect of coculture on LDL receptor number and rate constants for smooth muscle cells. The results presented in Chapter 2 indicate that the best models consist of a single intracellular compartment from which LDL is either degraded or removed by exocytosis. These models are represented schematically as:



where L represents the ligand, R represents the receptor, LR represents the receptor-ligand complex on the cell surface, L_{Ri} and L_i represent ligand internalized

by receptor-mediated and receptor-independent processes, respectively, L_d represents degraded ligand and L_{exo} represents ligand returned to the medium by exocytosis. The rate constants are as follows: k_1 ($M^{-1}min^{-1}$), receptor-ligand association; k_2 (min^{-1}), receptor-ligand dissociation; k_3 (min^{-1}), receptor-mediated internalization; k_4 ($ml/(mg \cdot min)$), nonspecific internalization; and k_5 and k_6 (min^{-1}), degradation and exocytosis, respectively, of ligand internalized by receptor-mediated endocytosis; k_7 and k_8 (min^{-1}), degradation and exocytosis, respectively, of ligand internalized by nonspecific mechanisms. Throughout the experiment the ligand concentration is approximately constant and is represented by $[L_0]$. The governing differential equations and solutions are presented in Chapter 2.

In order to determine the rate constants, the following experiment was performed. Quiescent smooth muscle cells were incubated either alone or with micorcarrier-bound endothelial cells for 48 hr after which the endothelial cells were removed. The smooth muscle cells were washed and incubated with either 10 $\mu g/ml$ ^{125}I -LDL (with and without 500 $\mu g/ml$ LDL) for times ranging from 5 min to 4 hr or with varying concentrations of ^{125}I -LDL (with and without 500 $\mu g/ml$ LDL) for 4 hr at 37 °C, after which receptor-mediated and receptor-independent binding, internalization, and degradation were determined.

Two experiments were performed, BSMC17 and BSMC29. In experiment BSMC17 binding, internalization, and degradation were measured as a function of LDL concentration at 4 hr whereas, in experiment BSMC29, LDL metabolism was measured as a function of time and concentration. Results are presented in Figures 3-13 and 3-14 for experiment BSMC17 and in Figures 3-15 and 3-16 for BSMC29. For experiment BSMC17 each point in Figures 3-13 and 3-14 is the average of 3 dishes, while for experiment BSMC29 each point in Figures 3-15 and 3-16 is the average of two dishes. The control experiment in Figure 3-15 was discussed in

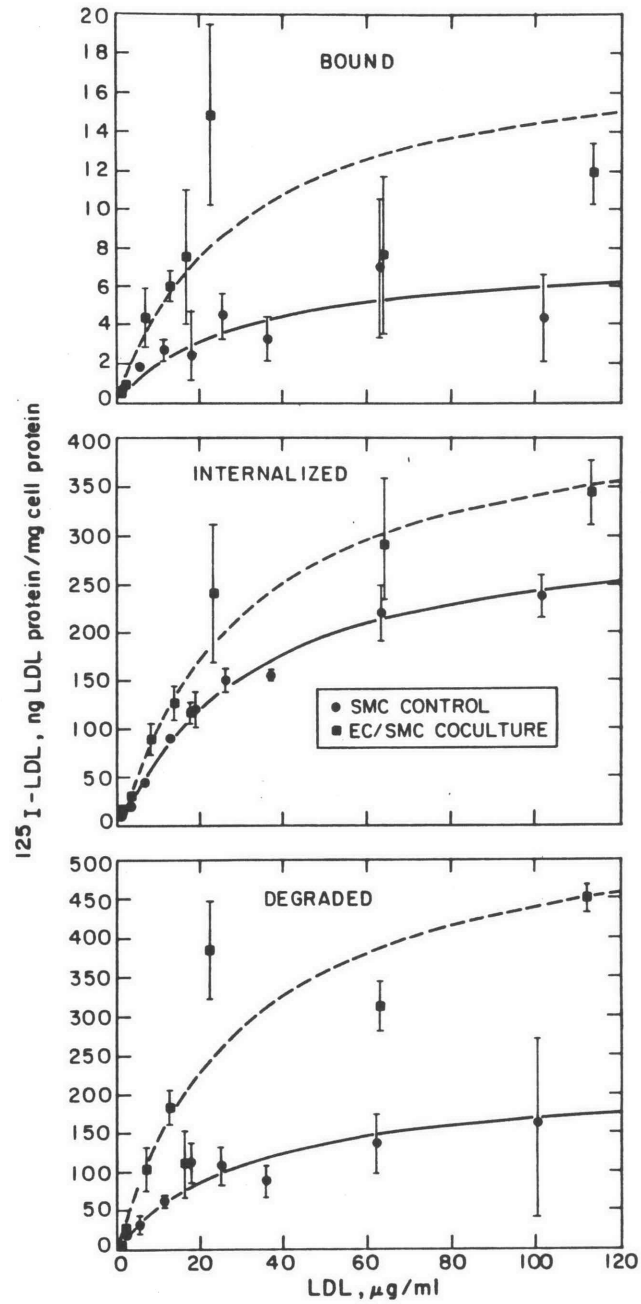


Figure 3-13: Expt. BSMC17: Receptor-mediated metabolism in smooth muscle cells following coculture with endothelial cells. Smooth muscle cells were incubated alone or with microcarrier-bound endothelial cells for 48 hr after which smooth muscle cells were incubated with ^{125}I -LDL for 4 hr.

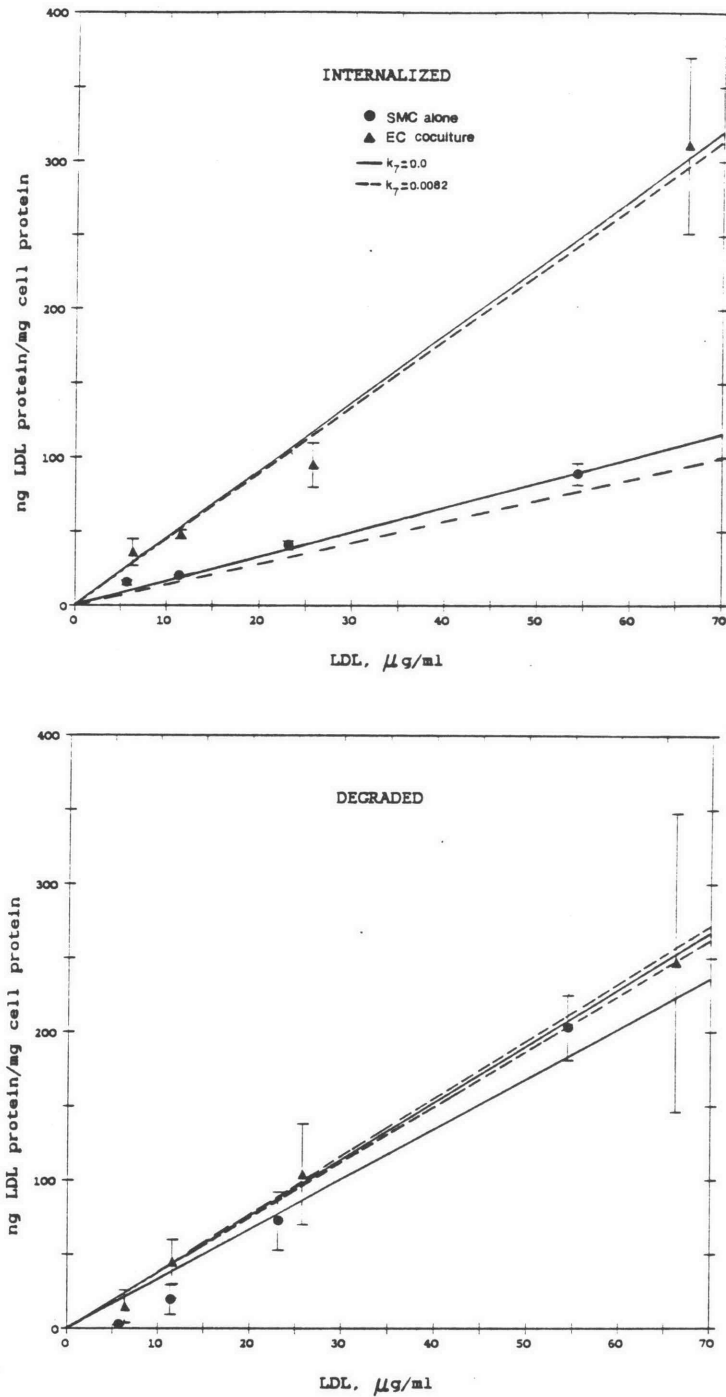


Figure 3-14: Expt. BSMC17: Receptor-independent metabolism in smooth muscle cells following coculture with endothelial cells. Smooth muscle cells were incubated alone or with microcarrier-bound endothelial cells for 48 hr after which smooth muscle cells were incubated with ^{125}I -LDL for 4 hr.

Chapter 2.- The error bars represent the standard error of the mean.

For experiment BSMC17 it is not possible to determine all of the rate constants independently, although the kinetic model can still be used to compare data. As noted in Chapter 2, receptor-mediated binding, internalization, and degradation have reached steady state by 4 hr and equations (2-24) to (2-26) reduce to:

$$[LR] = \frac{[R_T][L_o]}{K_{int} + [L_o]} \quad (3-9)$$

$$[LR_{Ri}] = \frac{k_2}{k_x} \left(\frac{[R_T][L_o]}{K_{int} + [L_o]} \right) \quad (3-10)$$

$$[L_d] = \frac{k_2 k_3}{k_x} \left(t - \frac{1}{k_x} \right) \quad (3-11)$$

where $K_{int} = \frac{k_1 + k_2}{k_1}$

Simultaneous regression of equations (3-9) to (3-11) by minimization of the determinant of the **F** matrix (equation (2-41)) results in estimates for four parameter groups: $[R_T]$, K_{int} , $\frac{k_2}{k_x}$, and $k_3[t - 1/k_x]$. The fits are presented in Figure 3-13 and the parameter estimates along with standard deviations are listed in Table 3-VI.

The number of LDL receptors on smooth muscle cells approximately doubles following coculture. This is consistent with the effect of purified PDGF on LDL receptor expression (Chait et al. [1980], Witte et al. [1982]). K_{int} is unchanged ($p > 0.50$), k_2/k_x decreases 37% ($p < 0.001$), and $k_3[t - 1/k_x]$ increases 60% ($p < 0.001$). The results suggest that some of the rate constants (k_2 , k_3 , and k_5) may change following coculture of smooth muscle cells with endothelial cells.

In experiment BSMC17 nonspecific internalization by smooth muscle cells increases following coculture whereas nonspecific degradation is unchanged (Figure

3-13). Data for nonspecific internalization and degradation were fit to equations (2-37) and (2-38) by minimization of the determinant of \mathbf{F} . Not all of the rate constants could be determined from the data, so k_4 and k_6 were determined for two values of k_7 , 0.0082 min^{-1} and 0.0 min^{-1} . Results are plotted in Figure 3-13 and the rate constants are listed in Table 3-VII. Regardless of the value chosen for k_7 , k_4 is larger and k_6 is smaller in smooth muscle cells following coculture than in smooth muscle cells incubated alone. It is also possible that k_7 changes following coculture. The value of k_6 in smooth muscle cells after coculture is within the range observed for k_6 (see Table 2-XI), whereas the value of k_4 in smooth muscle cells following coculture is outside the range of values observed.

Table 3-VI: Expt. BSMC17: Parameter Groups for Receptor-Mediated Metabolism of LDL by Smooth Muscle Cells Cocultured with Endothelial Cells

	SMC alone	EC/SMC Coculture
$[R_T]$, receptors/cell	3160 ± 330	7600 ± 990
K_{int} , $M \times 10^9$	64.2 ± 9.2	60.0 ± 15.8
k_2/k_x	37.5 ± 4.4	23.6 ± 1.8
$k_3(t-1/k_x)$	0.77 ± 0.06	1.28 ± 0.06

In order to examine possible changes in the rate constants, experiment BSMC29 was performed in which receptor-mediated and receptor-independent LDL metabolism by smooth muscle cells following 48 hr of coculture with endothelial cells was examined as a function of time and concentration (Figures 3-15 and 3-16). Data were fit to equations (2-24) to (2-26) using the minimization criterion of Box and Draper [1965]. The fits are plotted in Figure 3-15 and 3-16 and the rate constants are listed in Table 3-VIII.

Table 3-VII: Expt. BSMC17: Parameter Groups for Receptor-Independent Metabolism of LDL by Smooth Muscle Cells Cocultured with Endothelial Cells

	k_4 ml/mg·min x 10^5	k_6, min^{-1}	k_7, min^{-1}
SMC alone	2.0 ± 0.1	0.0135 ± 0.0011	0 (fixed)
	3.4 ± 0.1	0.0122 ± 0.0010	0.0082 (fixed)
EC/SMC Coculture	3.5 ± 0.3	0.0057 ± 0.0004	0 (fixed)
	6.1 ± 0.4	0.0048 ± 0.0003	0.0082 (fixed)

In experiment BSMC29, there are seven times as many receptors present on smooth muscle cells cocultured with endothelial cells than on cells incubated alone. k_1 and k_2 are very similar to values determined in control experiments. K_{int} is reduced by 25%, but this difference is not statistically significant at the 95% confidence level. k_3 and k_5 are significantly larger in smooth muscle cells following coculture ($p < 0.005$) for k_3 and ($p < 0.001$) for k_5 . The change in k_3 falls within the range of values obtained with smooth muscle cells (Table 2-VI) whereas k_5 falls outside this range. Increases in k_3 and k_5 are consistent with the results obtained in experiment BSMC17.

In experiment BSMC29, rate constants for receptor-independent internalization (k_4) and degradation (k_6) increase following coculture whereas the rate constant for exocytosis (k_7) decreases and becomes essentially zero. The values for k_6 and k_7 in smooth muscle cells cocultured with endothelial cells are within the range of values obtained with smooth muscle cells alone (Table 2-XI), but k_4 falls outside this range.

These results suggest that, following coculture of smooth muscle cells with endothelial cells, there is an increase in the number of receptors as well as increases

in the rate constants for receptor-mediated exocytosis and receptor-independent internalization.

Table 3-VIII: Expt. BSMC29: Rate Constants for LDL Metabolism Following Coculture

	SMC alone	EC/SMC Coculture
$k_1, M^{-1}min^{-1} \times 10^{-7}$	0.70 ± 0.18	0.79 ± 0.18
k_2, min^{-1}	0.42 ± 0.12	0.36 ± 0.06
k_3, min^{-1}	0.0053 ± 0.0004	0.0072 ± 0.0004
k_5, min^{-1}	0.017 ± 0.006	0.042 ± 0.008
$[R_T], receptors/cell$	10340 ± 2758	77080 ± 6730
$K_{int}, M \times 10^9$	60.3 ± 23.6	45.6 ± 12.9
$k_4, ml/(mg \cdot min) \times 10^5$	5.5 ± 0.2	8.3 ± 0.7
k_6, min^{-1}	0.0026 ± 0.0007	0.0047 ± 0.0002
k_7, min^{-1}	0.0028 ± 0.0042	$(3.45 \pm 76.3) \times 10^{-5}$

3.4.5 Production of Ammonium Ion by Bovine Endothelial Cells and its Effect upon LDL Degradation

Unlike the results of Witte et al. [1982] with porcine endothelial cells and human fibroblasts, media conditioned by incubation with bovine endothelial cells does not inhibit LDL degradation by bovine smooth muscle cells. Rather, incubation of bovine smooth muscle cells with endothelial cell conditioned media or microcarrier-bound endothelial cells results in an increase in degradation due to an increase in receptor number. There is no significant change in the rate constants

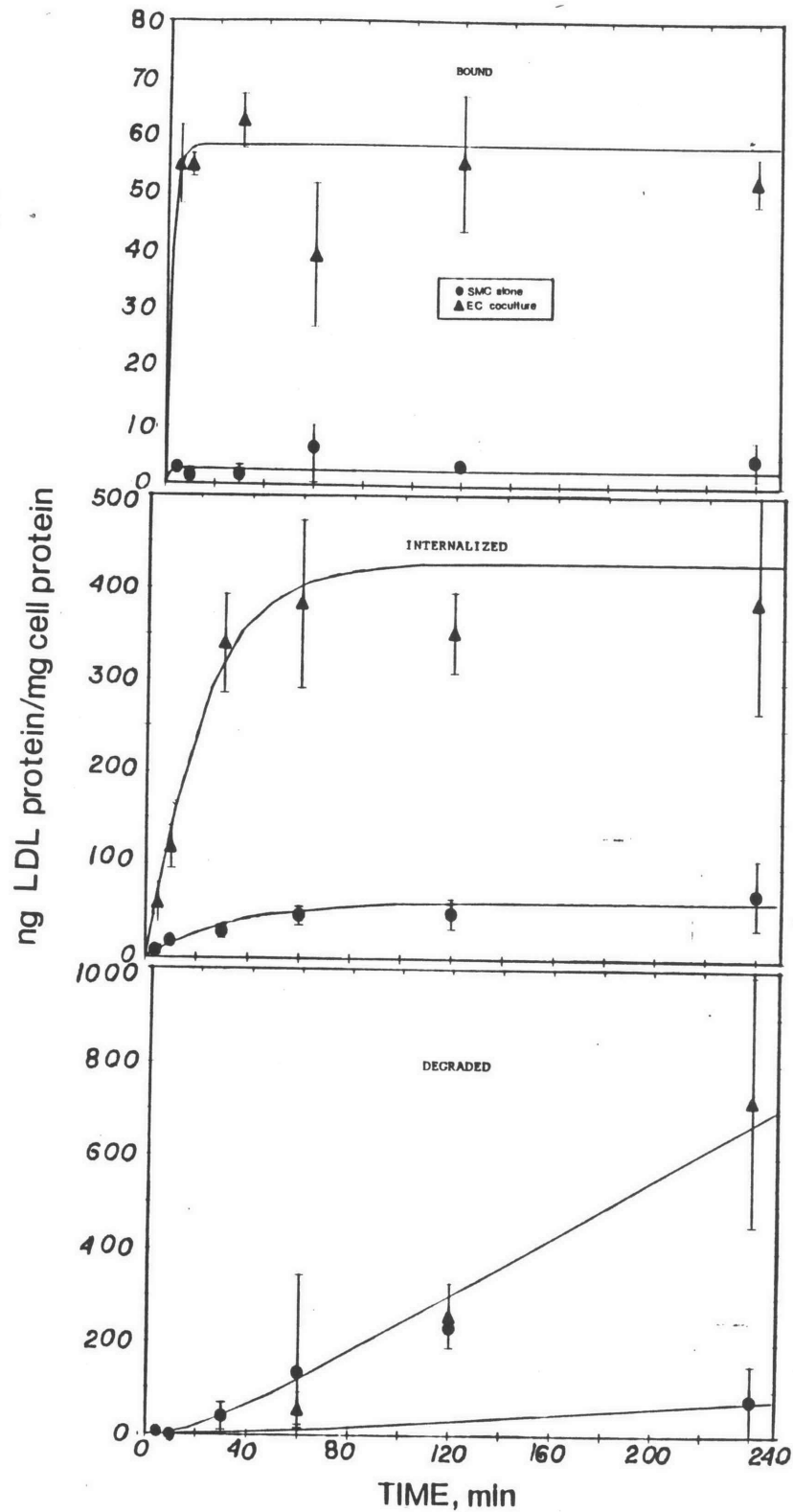


Figure 3-15: Expt. BSMC29: Receptor-mediated LDL metabolism by smooth muscle cells following 48 hr of coculture with endothelial cells. Smooth curves represent best fit of equations (2-24) to (2-26) to data.

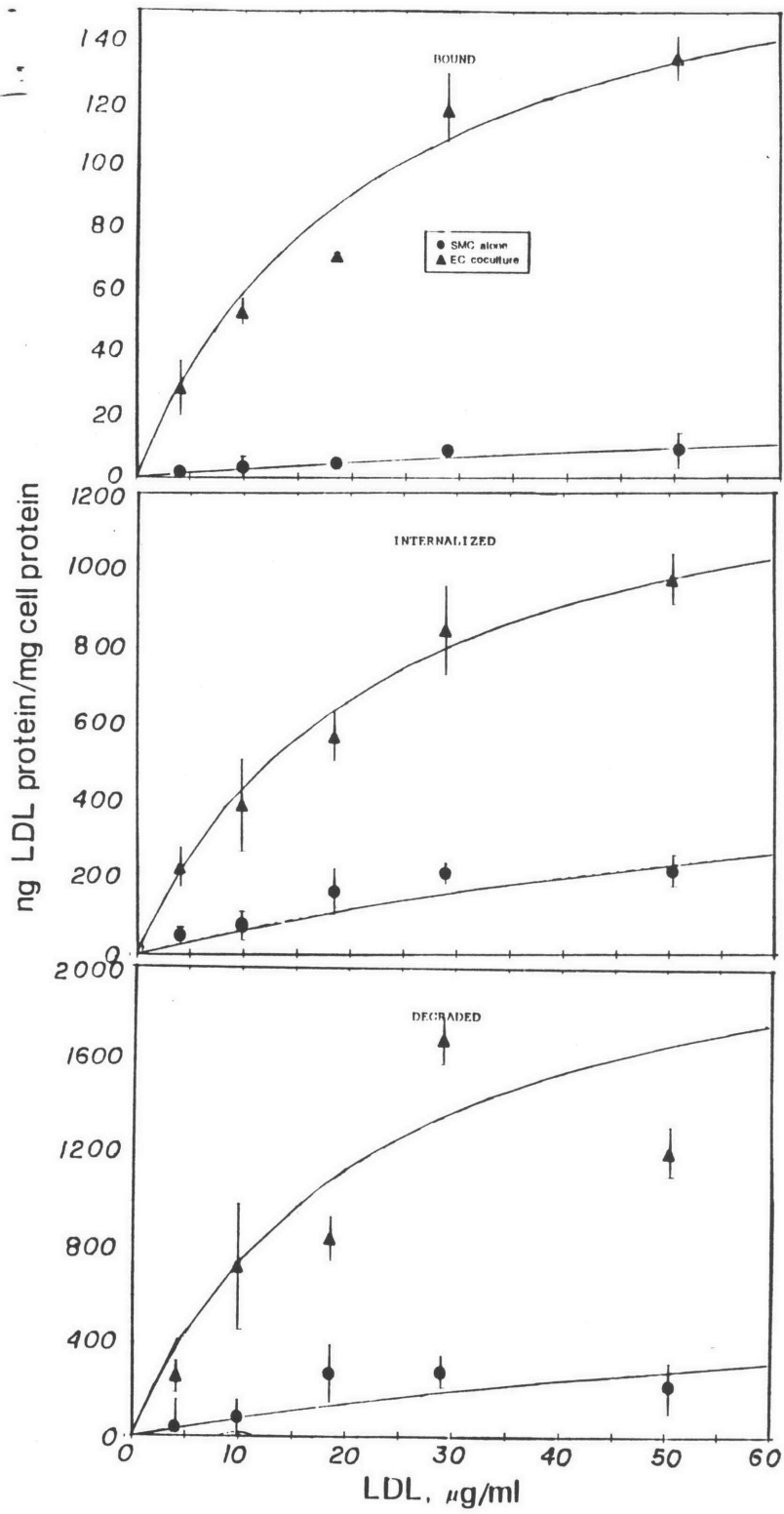


Figure 3-15: (continued)

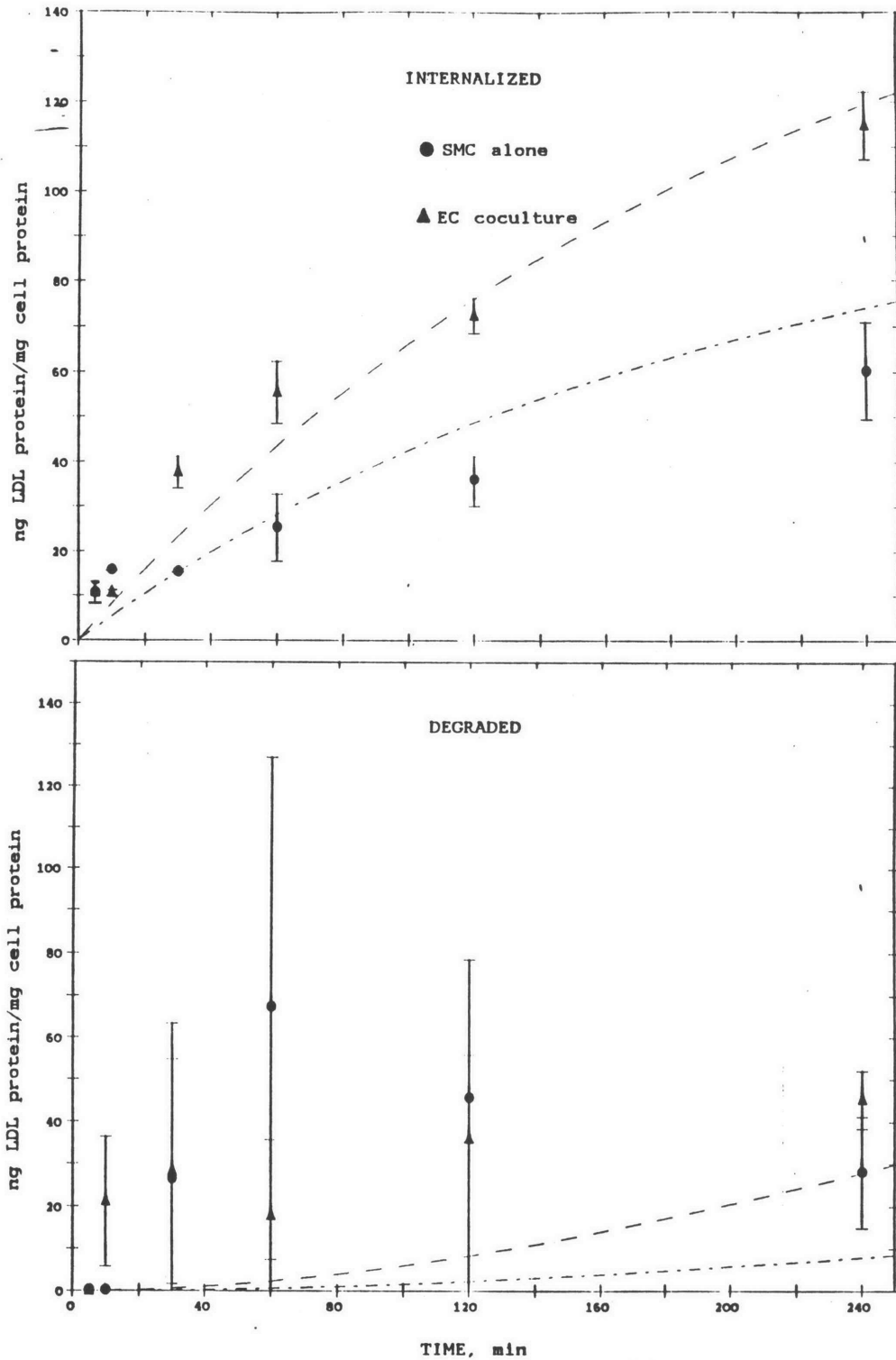


Figure 3-16: Expt. BSMC29: Receptor-independent LDL metabolism by smooth muscle cells following 48 hr of coculture with endothelial cells. Smooth curves represent best fit of equations (2-37) and (2-38) to data.

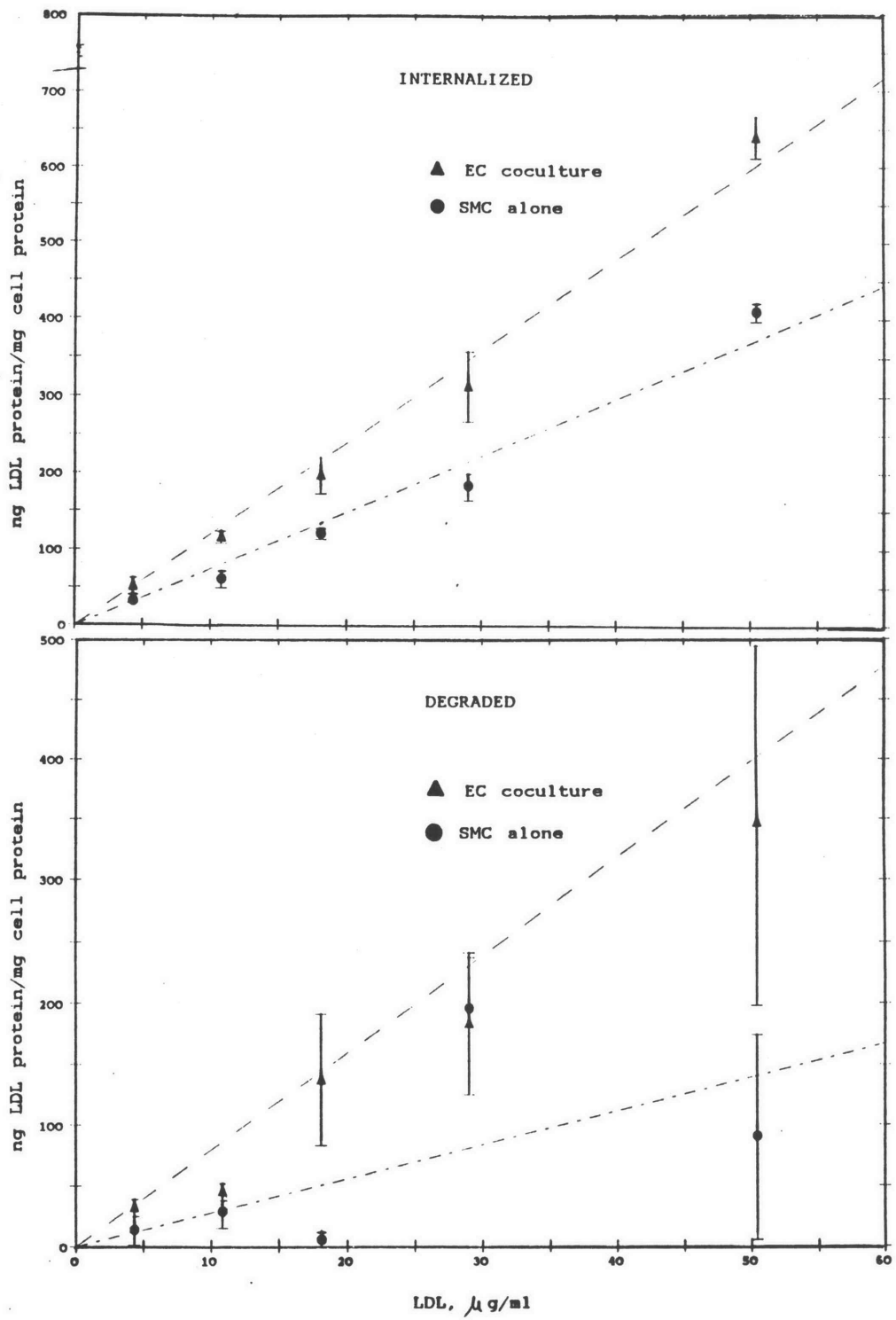
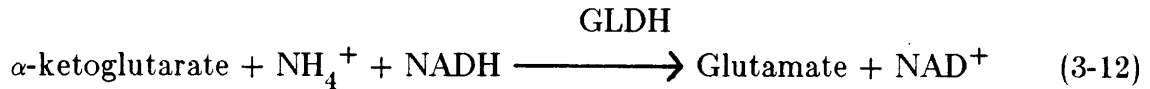


Figure 3-16: (continued) Expt. BSMC29. Receptor-independent metabolism.

for degradation, k_3 and k_6 . It was therefore of interest to measure ammonium ion concentrations in the various media. The production of ammonia by bovine aortic endothelial cells and smooth muscle cells was measured in three experiments (BSMC5, BSMC5, and BSMC8) using a spectrophotometric technique involving the reductive amination of α -ketoglutarate (Sigma Diagnostic Kit 170-UV):



where GLDH is L-glutamate dehydrogenase. The decrease in absorbance (at 340 nm) of a solution following reaction is proportional to the ammonium ion concentration. Cornicelli et al. [1983] have used the same method.

Media conditioned by endothelial cells, smooth muscle cells, and endothelial cell-smooth muscle cell cocultures was collected after a 48 hr incubation. The number of cells (10^7) and medium volumes (14 ml) for endothelial and smooth muscle cell conditioned media are similar to those used by Cornicelli et al. [1983]. The initial concentration of glutamine was 2 mM, the same concentration used by Cornicelli et al. [1983]. Total ammonium ion concentration and the ammonium ion concentration due to cell specific production of ammonia are listed in Table 3-IX. (Cell specific ammonium ion concentrations were calculated by subtracting the concentration of ammonium ion generated by the breakdown of glutamine (equation (3-3)) using the first-order rate constant of 0.0048 hr^{-1} .) Bovine endothelial cells produce very little ammonium whereas bovine smooth muscle cells produce significantly more. Nevertheless, ammonium ion concentrations are less than those obtained by Cornicelli et al. [1983] following 48 hr incubations with porcine endothelial cells. The low levels of ammonium ion are consistent with the absence of inhibition of degradation (Truskey and Davies [1985]).

Table 3-IX: Ammonium Ion Production

	NH ₄ ⁺ Concentration, mM	
	Total	Cell Specific
Endothelial Cell Conditioned Media	0.62 ± 0.18	0.22 ± 0.18
Smooth Muscle Cell Conditioned Media	1.65 ± 0.38	1.25 ± 0.39
Endothelial Cell/ Smooth Muscle Cell Coculture (BSMC8 Only)	0.51	0.11

3.4.6 Growth Factor Independent Stimulation of LDL Metabolism

Growth factors secreted by endothelial cells are responsible, in part, for the stimulation of LDL metabolism. Endothelial cell derived growth factors are believed to have molecular weights between 25,000 and 40,000 (DiCorleto et al. [1983]). In order to separate growth factor dependent stimulation of LDL metabolism from the effect of lower molecular weight agents, the coculture system was modified. The 1 μ m pore size mesh was replaced with a dialysis membrane (3500 molecular weight cutoff) as described in Materials and Methods.

Interposition of the dialysis membrane between microcarrier-bound endothelial cells and target smooth muscle cells successfully blocks DNA synthesis as measured by ³H-thymidine autoradiography (Figure 3-17). Following 48 hr coculture with endothelial cells, 42% of smooth muscle cell nuclei are labeled, whereas only 4% are labeled when dialysis membrane is present. Thus, the dialysis membrane effectively blocks the passage of the high molecular weight growth factors.

LDL metabolism following 48 hr of coculture using the modified apparatus has

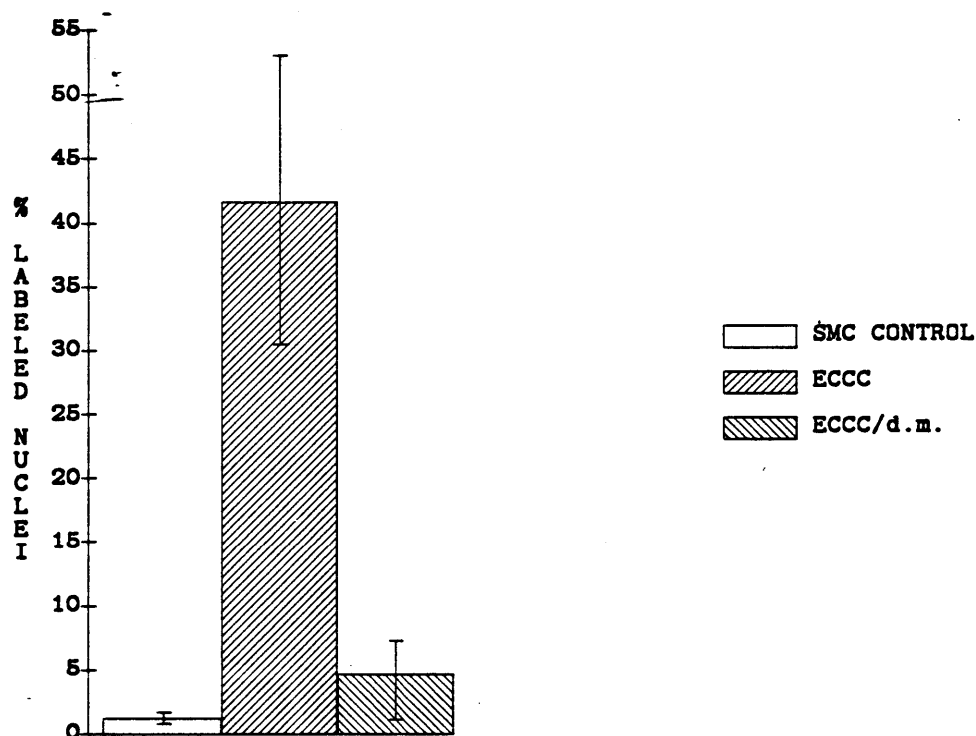


Figure 3-17: Dialysis membrane prevents growth factors from reaching smooth muscle cells

also been examined and the results are presented in Table 3-X. In experiments BSMC17 and BSMC24 smooth muscle cells were incubated with $10 \mu\text{g/ml}$ ^{125}I -LDL for 4 hr whereas in experiment BSMC32 the incubation time was 2 hr. Although replacement of the $1 \mu\text{m}$ mesh with dialysis membrane prevents growth factors from reaching smooth muscle cells, LDL metabolism is stimulated. The increase is less than that observed if dialysis membrane were absent. Regardless of the presence of the dialysis membrane, Dunnett's test for comparing a control mean to other group means (Zar [1984]) indicates that LDL metabolism by smooth muscle cells cocultured with endothelial cells is significantly different from LDL metabolism by smooth muscle cells incubated alone (BSMC17: $p < 0.001$; BSMC24: $p < 0.01$; BSMC32 $p < 0.01$).

Endothelial cell conditioned media was also examined to determine if

Table 3-X: Growth factor independent stimulation of LDL metabolism

	ng ¹²⁵ I-LDL protein/mg cell protein (± SD)		
	Bound	Internalized	Degraded
<hr/>			
Experiment BSMC17 (n=3)			
EC/SMC Coculture	5.92± 0.81	127± 18	184± 22
EC/SMC Coculture (dialysis membrane)	7.54± 1.39	191± 22	163± 59
SMC	2.64± 0.53	88.0± 3.3	60.6± 7.8
<hr/>			
BSMC24 (n=4)			
EC/SMC Coculture	8.87± 2.53	130± 8	207± 16
EC/SMC Coculture (dialysis membrane)	5.31± 1.46	86.6± 11.0	145± 20
SMC	3.58± 1.18	63.6± 2.3	82.7± 9.3
<hr/>			
BSMC32 (n=8)			
EC Coculture	16.3± 4.2	170± 35	151± 63
EC/SMC Coculture (dialysis membrane)	9.4± 2.5	128± 32	43± 29
SMC/SMC Coculture (dialysis membrane)	6.7± 0.9	114± 18	34± 22
SMC (n=14)	4.2± 0.8	93± 9	78± 11

nonmitogenic factors are also present. Again the mesh was replaced with dialysis tubing and conditioned media was obtained by incubating 6.7×10^5 endothelial cells bound to microcarriers with 2.5 ml 5% growth factor free LPDS for 48 hr. Smooth muscle cells were then incubated for 48 hr with this conditioned media as well as

with endothelial cells in coculture. LDL metabolism was determined after a 2 hr incubation with 20 $\mu\text{g/ml}$ ^{125}I -LDL. Endothelial cell conditioned media prepared in the modified coculture apparatus does not stimulate smooth muscle cell DNA synthesis (Davies et al. [1985]).

While LDL metabolism is stimulated following coculture in the modified apparatus, LDL metabolism is unaltered following incubation with endothelial cell conditioned media prepared in the same manner (Table 3-XI). Davies et al. [1985] have found that concentration of this conditioned media five times (by ultrafiltration) does not stimulate LDL metabolism (Figure 3-18). These results indicate that growth factor independent stimulation of LDL metabolism requires the presence of coculture, which suggests that the active agents have short half-lives or require cell-cell interactions to become active.

Table 3-XI: Growth Factor Independent Stimulation of LDL Metabolism Requires Coculture (\pm SD)

	Bound, ng/mg	Internalized, ng/mg	Degraded, ng/mg
BSMC39 (n=4)			
EC/SMC Coculture (dialysis membrane)	13.4 \pm 3.5	153 \pm 34	63 \pm 21
EC Conditioned Media (dialysis membrane)	6.96 \pm 1.18	114 \pm 12	37 \pm 15
SMC Conditioned Media (dialysis membrane)	10.0 \pm 3.5	123 \pm 20	37 \pm 13
SMC	7.53 \pm 1.27	114 \pm 13	30 \pm 16

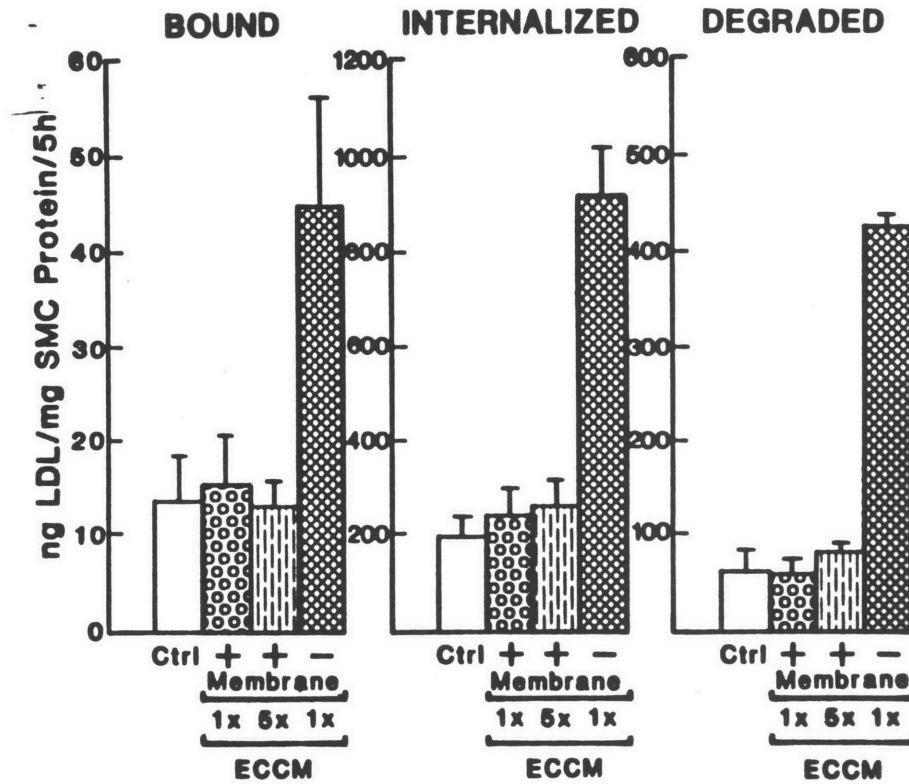


Figure 3-18: Absence of mitogen-independent stimulation of LDL metabolism in smooth muscle cells incubated with endothelial cell conditioned media (from Davies et al. [1985]).

3.5 Discussion

The complexity of interactions between the cells of the vessel wall, as well as interactions between cells and the extracellular matrix necessitates the development of simplified in vitro model systems. In the coculture system developed by Davies, endothelial cells and smooth muscle cells are bathed in the same solution and are maintained in close apposition. In this system cell-cell interactions may occur and this offers a major advantage over the use of conditioned media.

Smooth muscle cell LDL metabolism increases and cells are stimulated to grow after coculture incubations with endothelial cells. Changes in LDL metabolism are dependent upon the coculture incubation time and the number of endothelial cells.

The results are qualitatively consistent with stimulation of LDL metabolism, in part, by endothelial cell derived growth factors. Purified growth factors appear to act by increasing the number of LDL receptors (Chait et al. [1980], Witte et al. [1982]), although changes in the rate constants have not been studied.

LDL binding and internalization in smooth muscle cells incubated with microcarrier-bound endothelial cells or endothelial cell conditioned media are similar to those obtained by Witte et al. [1982] with endothelial cell conditioned media. In contrast, LDL degradation, measured in this study, is stimulated following coculture or conditioned media incubations, whereas Witte et al. [1982] observed a decrease in degradation following exposure of fibroblasts to conditioned media. Cornicelli et al. [1983] have shown that inhibition is due to NH_4^+ produced by porcine endothelial cells. In this study, measured levels of ammonium ion in endothelial cell conditioned medium or following coculture are less than 1 mM, which are not high enough to cause appreciable inhibition of degradation. (Results presented in Chapter 2 indicate that 10 mM NH_4^+ completely inhibits degradation.) Rather, the results obtained in this study are consistent with the effects of growth factors on LDL metabolism.

The stimulation of LDL binding, internalization, and degradation as a result of coculture also depends upon the number of endothelial cells. Stimulation is saturable at high numbers of endothelial cells and, from fits of data in Figure 3-12, 0.08 to 0.09 mg endothelial cell protein or 1.8 to 2.1×10^5 endothelial cells are required for half-maximal stimulation.

The production rate of endothelial cell derived growth factors in culture is about $0.69 \text{ ng}/10^6 \text{ cells/hr}$ and is constant for up to three weeks (Fox and DiCorleto [1984]). At half-maximal stimulation of LDL metabolism, 2.0×10^5 endothelial cells produce about 6.6 ng of growth factor after 48 hr (i.e at the time of the assay for

LDL metabolism) and the concentration is 2.6 ng/ml. From the data of Witte et al. [1982] presented in Figure 3-1 half-maximal stimulation of binding occurs with 10% endothelial cell conditioned media. The conditioned media was prepared with about $1 \pm 0.2 \times 10^7$ endothelial cells incubated in 10 ml 5% LPDS for 72 hr. The cumulative amount of growth factor produced is 500 ng and the concentration initially present in 10% conditioned media is 5.0 ± 1.4 ng/ml. Within the errors inherent in this calculation, these values are quite similar. Nevertheless, this calculation is a rough approximation and does not account for degradation of growth factor by smooth muscle cells, which should be substantial (Heldin et al. [1982], Singh et al. [1983]). It is interesting to note that these values correspond to the concentration of PDGF required to cause half-maximal binding to the PDGF receptor (Stiles [1983]) and LDL metabolism (Witte et al. [1982]).

Kinetic analysis of receptor-mediated and receptor-independent LDL metabolism by smooth muscle cells following a period of coculture indicates that the primary response is an increase in the number of receptors. Maximum increase in receptor number range from two to sevenfold. This variability is partly due to variations in endothelial cell number as well as to variations in the expression of receptors for growth factors. (Literature estimates for the number of PDGF receptors per cell ranges from 7,200 on bovine smooth muscle cells (DiCorleto and Bowen-Pope [1983] to 79,000 on monkey smooth muscle cells (Bowen-Pope and Ross [1982]. PDGF receptors increase with subculture (DiCorleto and Bowen-Pope [1983].)

In addition to changes in the number of cell surface receptors, rate constants for receptor-mediated exocytosis (k_5) and receptor-independent internalization (k_4) increase. The increase in k_5 results in lower intracellular LDL concentrations than would be expected for the number of receptors expressed. Alterations in exocytosis

may indicate that LDL is being used in other nondegradative metabolic pathways (such as in the Golgi). The increase in the value of k_4 in smooth muscle cells following coculture is consistent with results of Davies (Davies and Ross [1978, 1980], Davies et al. [1980]) in which the rate of fluid endocytosis is greater in growing than nongrowing cells. Changes in k_4 may result from an increase in the rate of vesicle formation or an increase in the total number of vesicles being formed. The rate constant for receptor-mediated internalization (k_2) increased to a much smaller extent, suggesting that receptor-mediated endocytosis occurs in a subpopulation of vesicles.

Increases in LDL metabolism following endothelial cell coculture are dependent, in part, upon low molecular weight species which do not stimulate growth. Since growth factor-independent stimulation of LDL metabolism is not observed with endothelial cell conditioned media, the agent (or agents) must either be short-lived or require cell-cell interactions to be produced.

Bounds can be placed on the half-life of any biologically active molecule involved in the growth factor-independent stimulation of LDL metabolism. The absence of a growth-factor independent response in endothelial cell conditioned media when the dialysis membrane is present may be due to a molecule with a very short half-life. Processing of conditioned media for addition to smooth muscle cells typically requires about one hour. If this low molecular weight species is not active in conditioned media, its half-life can be no more than 30 min. The low molecular weight agent is active in coculture, where the endothelial cells are separated from the smooth muscle cells by about 1 mm. Typical diffusion coefficients for low molecular weight solutes in water range from 5×10^{-6} cm²/s for sucrose (342 g/mole) to 2×10^{-6} cm²/s for inulin (4000 g/mole) (Colton et al. [1971]) and the characteristic time required for these solutes to diffuse the distance separating

smooth muscle cells and endothelial cells in coculture ranges from 30 to 83 min. These diffusion times are greater than the upper-limit of the half-life of any active low molecular weight solute. It is thus unlikely that a short-lived intermediate is responsible for growth factor-independent stimulation of LDL metabolism.

This line of reasoning implies that growth factor-independent stimulation of LDL metabolism requires cell-cell interactions. If true, a plausible scheme consistent with data is as follows. Since endothelial cell conditioned media does not contain an active agent which stimulates LDL metabolism in the absence of cell growth, then the actual presence of endothelial cells is required, suggesting that endothelial cells alter a molecule produced (or modified) by smooth muscle cells. Following endothelial cell alteration, the molecule is biologically active and causes smooth muscle cells to increase production of LDL receptors. Based upon diffusion times, at least one hr is required before activation of smooth muscle cells. According to this hypothesis, conditioned media obtained from endothelial cell/smooth muscle cell coculture using the modified coculture apparatus with dialysis membrane would contain these non-mitogenic factors.

Although production of endothelial cell derived growth factors has not been examined *in vivo*, mRNA hybridization techniques have demonstrated the presence of PDGF-like growth factor mRNA in human umbilical vein endothelial cells and adult bovine aortic endothelial cells (Barrett et al. [1984]). (These methods are semi-quantitative and, at present, no relationship has been developed between mRNA levels and growth factor production rates.) mRNA levels are much lower than in cultured cells and mRNA levels are less in adult cells than in developing cells. Barrett et al. [1984] speculate that endothelial cell derived growth factors play a role in normal growth and development as well as in the maintenance of the vessel wall. Although mRNA or growth factor production has not been examined in

vivo under pathological conditions, it is interesting to note that, in culture, tumor promoting agents and endotoxins can stimulate growth factor production (Fox and DiCorleto [1984]).

Based upon the limited in vivo data available, it is likely that, in the normal vessel wall, endothelial cell derived growth factor production is sufficiently low that there is little stimulation of LDL metabolism by arterial smooth muscle cells. results in Table 3-X suggest that growth factor independent stimulation of smooth muscle cells by endothelial cells may, however, result in a 20% to 50% increase in LDL metabolism above that which would be expected based upon studies with smooth muscle cells alone. This stimulation may be nonuniform, affecting those smooth muscle cells closest to the intima more than cells farther away. If such a phenomenon is occurring in vivo, then current models (Chapter 5) must be modified in order to account for spatial variations in cellular metabolism. Under pathological conditions, growth factor production may increase which would stimulate smooth muscle cell growth and LDL metabolism. If the increase in growth factor production is persistent then changes in LDL metabolism, in concert with other changes in the vessel wall, might result in the formation of foam cells.

Chapter 4

An Experimental Investigation of Receptor-Mediated and Receptor-Independent Accumulation and Degradation of LDL in the Rabbit Arterial Wall In Vivo

4.1 INTRODUCTION

Numerous studies have demonstrated that ^{125}I -LDL enters and accumulates within the vessel wall (Okishio [1961], Duncan et al. [1963], Calvert et al. [1975], Ghosh et al. [1976], Bratzler et al. [1977b]), and transmural concentration profiles indicate that entry is from the vessel lumen as well as the vasa vasorum (Bratzler et al. [1977a,b]). The intimal endothelium accounts for a significant amount of the total mass transfer resistance in the arterial wall (Bratzler et al. [1977a,b,c], Truskey et al. [1981], Ramirez et al. [1984]). Although the mechanisms governing LDL transport in the arterial wall have been, in part, elucidated, the extent of lipoprotein metabolism, the role of receptor-mediated and receptor-independent mechanisms in transendothelial transport and cellular metabolism, and the effect of diffusion and transendothelial transport on the rates of smooth muscle uptake and degradation are poorly understood.

The objectives of this part of the thesis were to examine receptor-mediated and receptor-independent LDL accumulation and degradation in the rabbit arterial wall in vivo and assess the importance of receptor-mediated processes in the transendothelial transport and cellular metabolism of LDL. Receptor-mediated and receptor-independent pathways can be distinguished by chemical modification of

lysine and arginine residues of the LDL protein. Methylated LDL (mLDL) was used in this study because the reaction conditions are mild (Weisgraber et al. [1978]), the reaction is irreversible (Mahley et al. [1980]), and the charge is unchanged following reaction (Weisgraber et al. [1978]).³ Transmural concentration profiles of ¹²⁵I-LDL and ¹²⁵I-mLDL across the rabbit aortic wall were measured as a function of time by frozen serial sectioning microtomy.

Measurement of protein degradation in vivo has required modification of existing radioactive labels. Proteins are commonly labeled with ¹²⁵I which results in the attachment of ¹²⁵I to the tyrosine residue. Protein-bound radioactivity in the tissue represents undegraded protein which is either freely diffusible, bound to the extracellular matrix or cell membrane, or intracellular. The major radioactive degradation product is ¹²⁵I-tyrosine, which is rapidly excreted from the cell (Figure 4-1) and equilibrates between the interstitial fluid and the plasma (Donovan [1980]). Therefore tissue concentrations of ¹²⁵I-tyrosine do not represent degradation in individual tissues.

Pittman et al. [1978, 1979a] have developed a ¹⁴C-sucrose label which is retained intracellularly. Sucrose is a suitable marker for degradation since it is not hydrolyzed by lysosomes and does not leak from the cells at an appreciable rate (Pittman et al. [1978, 1979a]). ¹⁴C-sucrose-labeled protein degradation within the lysosomes leaves behind a product containing ¹⁴C-sucrose attached to a polypeptide fragment (Pittman et al. [1979a]). The difference between tissue associated ¹⁴C and ¹²⁵I activity represents the amount of protein degraded by the tissue (Figure 4-1). Using ¹²⁵I-tyramine-cellobiose conjugated LDL, which behaves the same as

³Increasing the positive charge by acetylation, cyclohexanedione treatment, and carbamylation inhibits binding between LDL and glycosaminoglycans (Iverius [1972], Mahley et al. [1979b]). Binding of mLDL to heparin is 85% of LDL binding, whereas cyclohexanedione-treated LDL binding is 10% of LDL binding (Mahley et al. [1979]).

^{14}C -sucrose-LDL but has much higher specific activities, Carew et al. [1984] report that LDL degradation by the rabbit aorta occurs primarily in the intima, and the luminal endothelium is responsible for 40% of the total degradation. Based upon the difference in the concentration of LDL and mLDL degradation products in the tissue, Carew et al. [1984] estimated that between 40% and 50% of this degradation is due to the receptor-mediated pathway.

In this study experiments were conducted to measure transmural profiles of ^{125}I -LDL and ^{125}I -mLDL degradation in the rabbit thoracic aorta as a function of time. ^{125}I and ^{14}C -sucrose labeled LDL and mLDL activities in the rabbit aorta were measured at various times following injection. Cumulative degradation was determined from the difference between ^{125}I and ^{14}C -sucrose concentrations.

Following a bolus injection, radiolabeled LDL and mLDL plasma concentrations decay at different rates. Consequently, LDL and mLDL driving forces for entry into the arterial wall are different. This difference in driving forces, in turn, influences accumulation and metabolism within the vessel wall. In order to account for differences in the plasma decay, linear systems theory (Himmelblau and Bischoff [1968], pp. 98-137) was applied to the in vivo results and steady state tissue concentrations and rates of degradation in response to a step change in plasma concentration were calculated from data for tissue concentrations and amounts degraded in response to a decaying plasma concentration.

4.2 MATERIALS AND METHODS

Preparation of LDL and mLDL Human LDL was isolated from fresh plasma by a modification of conventional precipitation techniques (Cornwall and Kruger [1961], Burstein et al. [1970]). (Details are presented in Chapter 2.) Purity was

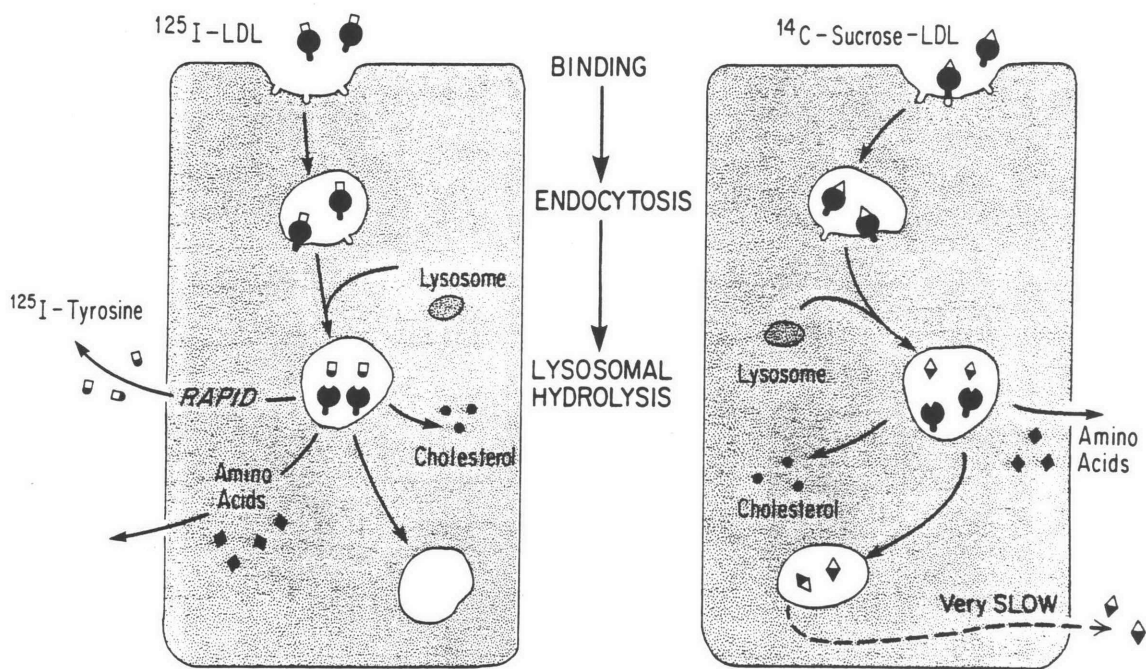


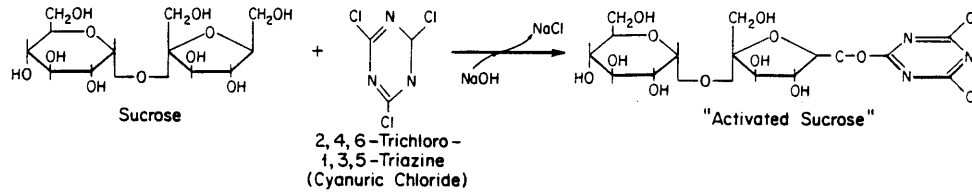
Figure 4-1: ^{125}I and ^{14}C -Sucrose Labels as Markers of LDL Uptake and Degradation.

assessed by double radial immunodiffusion, immunoelectrophoresis, and cellulose acetate gel electrophoresis (Hatch and Lees [1968]). Protein was determined by the method of Lowry et al. [1951]. Reductive methylation of LDL was performed by the method of Weisgraber et al. [1978] and the extent of methylation was assessed by the trinitrobenzenesulfonic acid test (Habeeb [1961]).

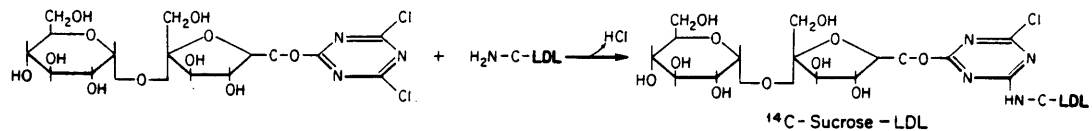
Radioiodination of LDL and mLDL LDL and mLDL were iodinated with Na^{125}I (New England Nuclear, Boston, MA) by the method of McFarlane [1958] as modified by Bilheimer et al. [1972]. Nonprotein-bound radioactivity was removed by equilibrium dialysis against 10 to 12 changes of 0.15 M NaCl, 0.001 M Na_2EDTA , pH 8.6 at 4 °C for four days. After dialysis, greater than 97% of the total ^{125}I was precipitable in 10% (w/v) trichloroacetic acid (TCA). By chloroform-methanol extraction (Folch et al. [1957]), only 6% of label was associated with lipid. For experiments in which transmural profiles were determined, specific activities of ^{125}I -LDL and ^{125}I -mLDL ranged from 120 to 320 $\mu\text{Ci}/\text{mg}$ protein. For experiments in which rabbits were injected with both ^{14}C -sucrose and ^{125}I -labeled lipoproteins, specific activities of ^{125}I -LDL and ^{125}I -mLDL ranged from 3.5 to 45 $\mu\text{Ci}/\text{mg}$ protein (Navarro [1984]).

Derivatization of LDL with ^{14}C -sucrose ^{14}C -sucrose was covalently attached to LDL by a modification of the method of Pittman et al. [1979a] (Figure 4-2). 250 μCi [^{14}C]sucrose in 3% ethanol solution (specific activity 552 $\mu\text{Ci}/\text{mmol}$, Amersham Corporation, Arlington Heights, IL) were lyophilized and rehydrated in 10 μl distilled water followed by the addition of 10 μl of 0.13 M NaOH. 10 μl of 0.066 M twice recrystallized 2,4,5-trichloro-1,3,5-triazine (cyanuric chloride, Aldrich Chemical Co., Milwaukee, WI) in acetone was added to the NaOH-sucrose solution. After 10-15 min, the reaction was quenched by the addition of 10 μl 0.176 M acetic acid. The resulting ^{14}C -sucrose-dichlorotriazine adduct ("activated sucrose") was

• **SUCROSE ACTIVATION: ALKALINE CONDITIONS IN NONAQUEOUS SOLVENT**



• **COVALENT ATTACHMENT TO LDL**



From Pittman et al. (1979) *J. Biol. Chem.* 254: 6876-6879.

Figure 4-2: Covalent Attachment of ¹⁴C-Sucrose to LDL

added to LDL (20-35 mg LDL protein/ μ mole sucrose) which was dialyzed against 20 mM sodium phosphate, 1 mM Na₂EDTA, 0.15 M NaCl (Buffer A), pH 7.4. The activated sucrose was used within 30 min of its preparation. The solution was allowed to react for 1 hr at room temperature with gentle mixing. Unreacted ligand and side products were removed using a PD-10 column (Sephadex G-25, Pharmacia, Piscataway, NJ) eluted with Buffer A, pH 6.8, and dialyzed against Buffer A, pH 7.4, until greater than 94% of the label was precipitable in 10% TCA. Labeling efficiencies were typically 20% and specific activities ranged from 3.2 to 13.5 μ Ci ¹⁴C/mg LDL.

Animal Procedures and Tissue Preparation Two separate sets of experiments were performed: 1) ¹²⁵I-LDL and ¹²⁵I-mLDL transmural profiles were measured as a function of time; and 2) ¹²⁵I- and ¹⁴C-sucrose-labeled LDL and mLDL concentrations in glutaraldehyde-fixed aortic samples were measured as a function of time after injection.

For determination of transmural profiles, 0.8 to 1.2 mCi of either ^{125}I -LDL or ^{125}I -mLDL in 0.15 M NaCl, 0.001 M Na_2EDTA , pH 8.6, were filtered (sterile 0.22 μm filter; Millipore, Bedford, MA) and injected through a catheter into the marginal ear vein of normal conscious male New Zealand white rabbits (2.5-3.5 kg) placed in a restraining cage. Blood samples were taken from the marginal ear vein five min postinjection and at specified times thereafter for determination of plasma protein-bound radioactivity. For experiments of more than four hr duration, rabbits were placed in a cage and food and water were taken ad libitum. Rabbits were returned to the restraining cage only for blood sampling.

After 0.5, 4, 24, and 72 hr the animals were sacrificed with an overdose of sodium pentobarbital. The thoracic cavity was quickly opened and the aorta from arch to diaphragm was exposed. The thoracic aorta was excised immediately, rinsed with isotonic saline to remove remnants of blood, gently sandwiched flat between two glass slides, and then rapidly frozen in order to prevent further solute diffusion. The elapsed time between sacrifice and freezing was between five and six min, and the tissue was stored frozen (1-5 days) until further processing.

Samples of frozen aorta were sectioned (10 μm in thickness) parallel to the intimal surface on a refrigerated microtome (Harris, Needham Heights, MA) by the method of Bratzler et al. [1977a]. A sample of frozen aorta was warmed, transferred to a separate slide, refrozen, and trimmed to remove intercostal arteries and deposits of fatty or bloody tissues around the sides. Samples of about 0.4 cm^2 to 0.9 cm^2 luminal surface area were mounted, intimal side down, on a layer of embedding medium beneath a piece of Evans blue dyed filter paper, which had first been leveled with the microtome knife. This ensured that samples were sectioned in a plane parallel to the intimal surface. The sample edges were trimmed of any overhanging material, and additional embedding material was applied to buttress the

tissue on all sides.

After thermal equilibration at -20°C , slicing proceeded from the adventitial side to the luminal side. After every slice the upper and lower edges of the knife blade were cleaned with absorbent paper. Groups of two adjacent $10\ \mu\text{m}$ slices were placed in precooled test tubes and set aside for radioactive assay. Slices exhibiting visible blood contamination were excluded from further analysis, although their position was noted.

The transition from adventitia to media was marked by a change from a curled, deformable slice to a flat rigid slice, and by a change of opacity. The intimal surface was noted by the appearance of dyed filter paper. Positions of the intimal surface and the medial-adventitial border were noted, and the total thickness (L) between them was estimated to within $\pm 10\ \mu\text{m}$. Similarly, the distance (x) from the intimal surface to the midpoint of each tissue slice is noted and the position of the slice designated x/L .

Each sample ranged in thickness from $210\ \mu\text{m}$ to $260\ \mu\text{m}$ and between five and seven samples were obtained from each aorta. As sections near the intimal surface were taken, the subjacent tissue sometimes fractured down to the mounting medium and the slice included portions of tissue that should have been parts of subsequent slices. Visual estimates were made to correct the slice volumes. Slices that took more than 30% extra tissue were excluded from data analysis, as were slices with less than 40% of the original tissue surface area.

The volume of each slice was estimated from the thickness and the measured cross-sectional area. The shape of the stained filter paper was outlined on a transparent plastic sheet (Ramirez [1979]). The plastic section was weighed and the surface area was determined by comparing the weight with that of plastic of $1\ \text{cm}^2$ area. An estimate of the in vivo thickness of the media was obtained by dividing

the medial thickness by 1.72 (Schneiderman et al. [1983]).

Each tissue slice was extracted twice in 10% TCA to remove non-protein bound radioactivity before radioassay. Two TCA washes were sufficient to remove all non protein-bound radioactivity (Bratzler [1974]). All slices were counted for at least 20 min, and almost all had counting rates in excess of 10 cpm above background. The tissue concentrations were expressed as the TCA-precipitable concentration of labeled solute in tissue (cpm/ml tissue) divided by its initial concentration in plasma. These normalized concentrations were plotted versus relative position of each slice between intima and medial-adventitial border.

For studies of LDL and mLDL uptake and degradation, lipoproteins were separately labeled with ^{125}I and ^{14}C -sucrose. Approximately equal amounts of activity of ^{125}I and ^{14}C -sucrose labeled LDL or mLDL were pooled and injected into rabbits as described above. The activity of the injectate ranged from 20 to 50 μCi each for ^{125}I and ^{14}C . Blood samples were taken five min postinjection and at various times thereafter. After 0.5, 4, 15, 24, 48, and 72 hr the animals were sacrificed, and the aortic arch was cannulated and perfused with 2.5% (w/v) glutaraldehyde in 0.1 M cacodylate buffer. Typically, 7 to 10 min elapsed between sacrifice and start of perfusion. Following 30 min of pressure perfusion, the thoracic and abdominal aortae were removed and placed in 2.5% glutaraldehyde. The fixative was changed several times over a 24 hr period, after which the adventitia and branches of the aorta were removed. The samples were blotted dry of excess fixative, weighed several times, placed in a test tube containing fresh fixative, and counted in a gamma counter for 100 min. Generally, the ^{125}I content of the thoracic aorta (0.20-0.25 g fixed weight) ranged from 200 to 300 cpm above background. The ^{125}I content of the abdominal aorta (0.15-0.20 g fixed weight) ranged from 100-250 cpm above background.

After gamma counting, samples were dissolved in 2 ml NCS tissue solubilizer (Amersham Corp., Arlington Heights, IL) by incubation at 55 °C for approximately 18 hr. To reduce color quenching, samples were bleached by adding 20% (w/v) benzoyl peroxide in toluene and incubating at 55 °C for 30 min. All samples were counted in a Tri-Carb liquid scintillation spectrometer (Packard Instruments, Downers Grove, IL) with automatic external standard capability. The efficiency of counting aortic samples varied from 30% to 60%. The external standard channel ratio method (Navarro [1984]) was used for quench correction and isotope separation. Quench correction curves were constructed using a known amount of isotope (^{125}I or ^{14}C) and either unlabeled solubilized tissue (to mimic color quenching in tissue digests) or water and acetic acid (to mimic plasma samples) (Navarro [1984]). Experimental determination of ^{14}C -sucrose activity and calculation of cumulative degradation were performed by Maria Navarro as part of her Masters Thesis.

4.3 RESULTS

4.3.1 Plasma Decay of Radiolabeled LDL and mLDL

Plasma decay curves for ^{125}I -LDL and ^{125}I -mLDL from two representative experiments are presented in Figure 4-3. (These correspond to experiment 24C2 for LDL and 24M2 for mLDL.) Data were fit to double exponential functions using Marquardt's method (Marquardt [1963]):

$$\frac{C_p}{C_{p_0}} = C_1 e^{-b_1 t} + C_2 e^{-b_2 t} \quad (4-1)$$

where t is in hours. The fits for LDL and mLDL are displayed in Figure 4-3.

All experiments of 24 and 72 hr duration are well represented by equation

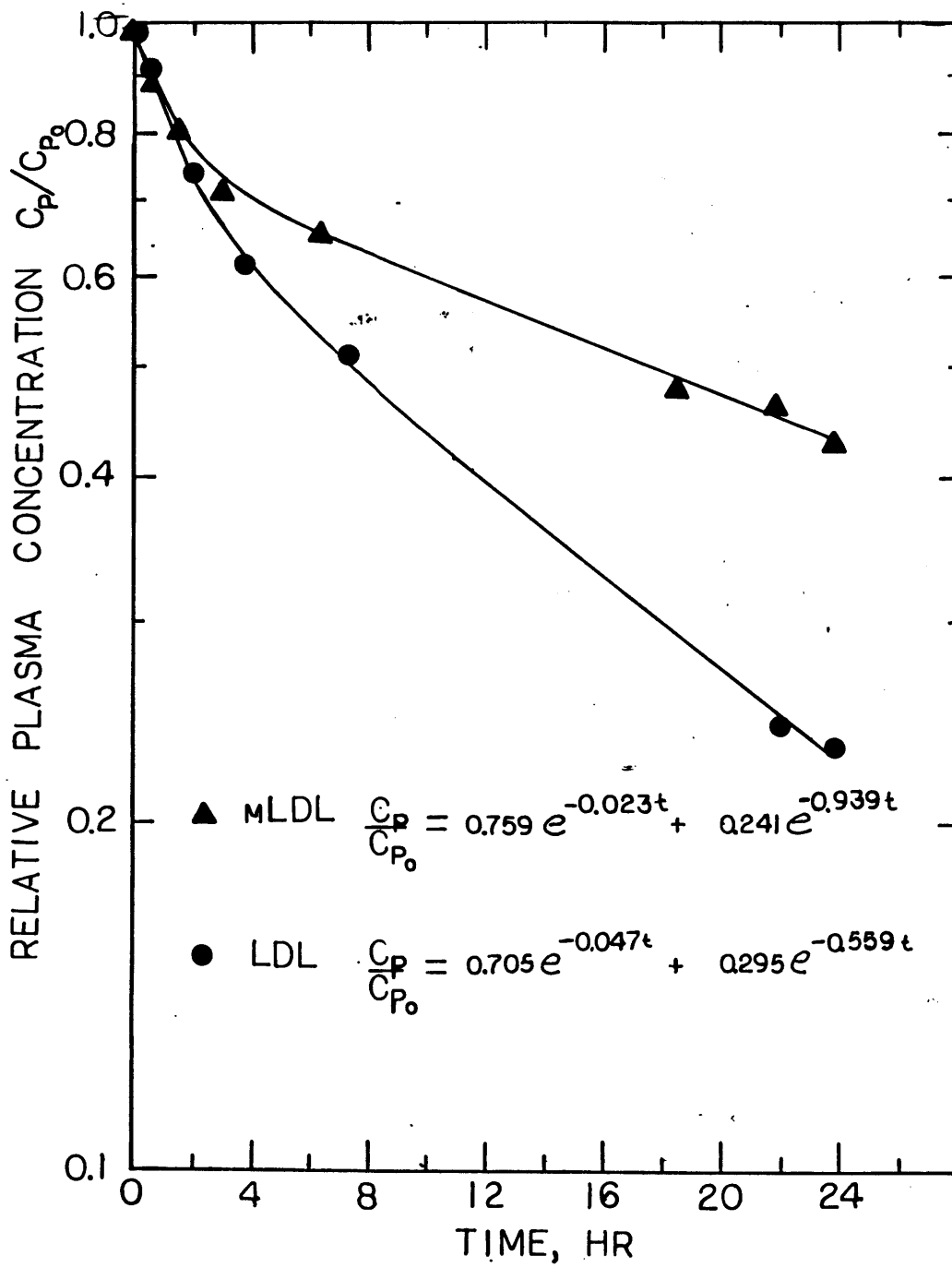


Figure 4-3: Representative plasma decay curves of ^{125}I -LDL (Expt. 24C2) and ^{125}I -mLDL (Expt. 24M2)

(4-1). Experiments of 0.5 hr and 4 hr duration were fit to a single exponential. Equation (4-1) is consistent with the predicted form of the plasma decay curve for a two compartment model (see Appendix D). One parameter, which is widely reported in the literature, is the fractional catabolic rate (FCR), which is the inverse of the mean time a molecule remains in the plasma before it is removed irreversibly. It is defined as (Berman [1979]):

$$FCR = \frac{1}{C_1/b_1 + C_2/b_2} \quad (4-2)$$

The fractional catabolic rate was calculated for all experiments of 24 hr and 72 hr duration and the results are presented in Table 4-I. The average fractional catabolic rates are $0.100 \pm 0.031 \text{ hr}^{-1}$ for LDL and $0.033 \pm 0.013 \text{ hr}^{-1}$ for mLDL. The difference in the fractional catabolic rates is statistically significant ($p < 0.001$). Navarro [1984] obtained average fractional catabolic rates (for experiments of 15 hr, 24 hr, 48 hr, and 72 hr duration) of $0.111 \pm 0.014 \text{ hr}^{-1}$ for LDL and $0.042 \pm 0.025 \text{ hr}^{-1}$ for mLDL. There are no statistical differences between the fractional catabolic rates obtained by Navarro [1984] and those presented in Table 4-I.

Figure 4-4 shows the relative change in plasma ^{125}I -LDL and ^{125}I -mLDL concentrations with time for all experiments of four hr or longer duration in which transmural profiles were obtained. The initial ^{125}I -LDL and ^{125}I -mLDL concentrations in plasma (C_{p_0}) ranged from 1.4 to 7.1×10^7 dpm/(ml plasma). Data were fit to double-exponential functions by nonlinear regression (Table 4-2). The FCR is $0.096 \pm 0.014 \text{ hr}^{-1}$ for LDL and $0.036 \pm 0.004 \text{ hr}^{-1}$ for mLDL ($p < 0.001$). These estimates for FCR are statistically indistinct from the average of individual 24 hr and 72 hr experiments.

The plasma decay curves obtained in this study were combined with those obtained by Navarro [1984] and the combined set of data were fit to equation fit to

Table 4-I: Fractional Catabolic Rates

Time, hr	FCR, hr ⁻¹			
	Expt.	LDL	Expt.	mLDL
24	24C1	0.0787	24M1	0.0426
24	24C2	0.0648	24M2	0.0307
24	24C3	0.0760	24M3	0.0141
24	24C4	0.1364	24M4	0.0243
72	72C1	0.123	72M1	0.0335
72	72C2	0.123	72M3	0.0515

equation (4-1) by nonlinear regression. Data and best-fit regression curves are display in Figure 4-5. and the parameters are listed in Table 4-II. The fractional catabolic rates are 0.113 ± 0.016 for LDL and 0.035 ± 0.004 . The difference between the FCR of LDL and mLDL is statistically significant ($p < 0.001$).

The hypothesis that two regression equations are estimating the same underlying population can be tested by means of the following F statistic(Zar [1984], p. 347):

$$F = \frac{(SS_t - SS_p)/[(m+1)(k-1)]}{SS_p/DF_p} \quad (4-3)$$

where SS_t is the sum of squares of the residuals for the fit of the combined data, SS_p is the sum of the residual sums of squares for the separate fits for the k regression equations, DF_p is the sum of the degrees of freedom from separate fits of the two sets of data, m is the number of independent variables, and k is the number of individual regression equations. The F statistic has degrees of freedom $(m+1)(k-1)$ and DF_p . The F statistic in equation (4-3) is calculated from the data and

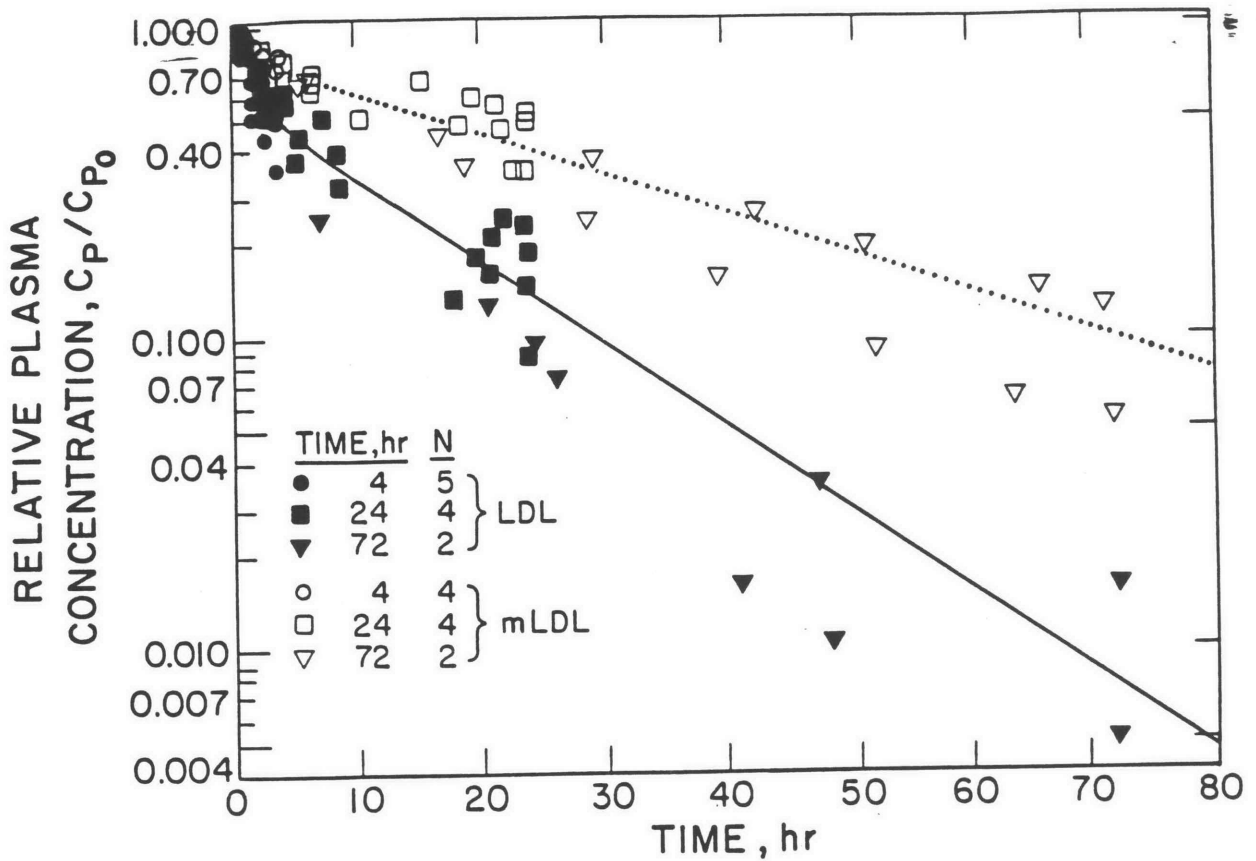


Figure 4-4: Plasma decay curves for all experiments 4 hr or longer. Best fit parameters are presented in Table 4-II.

compared with the tabulated value of the F statistic at the 95% confidence level with degrees of freedom $(m+1)(k-1)$ and DF_p (denoted $F_{0.05(1),(m+1)(k-1),DF_p}$). If the calculated value of F is greater than $F_{0.05(1),(m+1)(k-1),DF_p}$, then the two regression equations do not estimate the same population. If, however, the calculated value of F is less than $F_{0.05(1),(m+1)(k-1),DF_p}$, then the two regression equations estimate the same underlying population and pooling is acceptable. The F statistic defined in equation (4-3) is a measure of whether the fit of the combined data is as good as the fits of the individual sets of data. The statistic is exact for linear and multiple regression problems and is only approximate for nonlinear regression.

Table 4-II: Best Fit Parameters of Plasma Decay Curves
for ^{125}I -Labeled LDL and mLDL

	C_1	C_2	b_1, hr^{-1}	b_2, hr^{-1}
<hr/>				
This Study				
LDL	0.407 ± 0.061	0.593 ± 0.061	0.673 ± 0.167	0.0606 ± 0.0067
mLDL	0.176 ± 0.037	0.824 ± 0.037	0.651 ± 0.266	0.0298 ± 0.0025
<hr/>				
Navarro [1984]				
LDL	0.446 ± 0.063	0.554 ± 0.063	0.756 ± 0.194	0.0696 ± 0.010
mLDL	0.342 ± 0.088	0.658 ± 0.088	0.284 ± 0.090	0.0234 ± 0.0049
<hr/>				
Combined Data				
LDL	0.433 ± 0.052	0.567 ± 0.052	0.689 ± 0.133	0.0688 ± 0.0079
mLDL	0.224 ± 0.045	0.776 ± 0.045	0.487 ± 0.171	0.0277 ± 0.0026

The F statistic defined in equation (4-3) was used to compare the plasma decay curves obtained in this study with those of Navarro [1984]. Time is the only independent variable ($m=1$) for the two regression equations ($k=2$). Sums of squares of the residuals for the individual fits are listed in Table 4-III. The pooled sums of squares of the residuals (SS_p) listed in row three is the sum of rows one and two. The total sum of squares (SS_t) listed in row four represents the sums of squares of the residuals for the fit of the combined data presented in Figure 4-5. The F statistic was then calculated according to equation (4-3) and compared with the tabulated value listed in Table 4-III. For LDL the two sets of plasma decay curves are significantly different ($p < 0.001$), whereas for mLDL the plasma decay curves are not different ($0.05 < p < 0.10$). The source of the difference in the LDL plasma decay curves is not known, since the same preparation and iodination

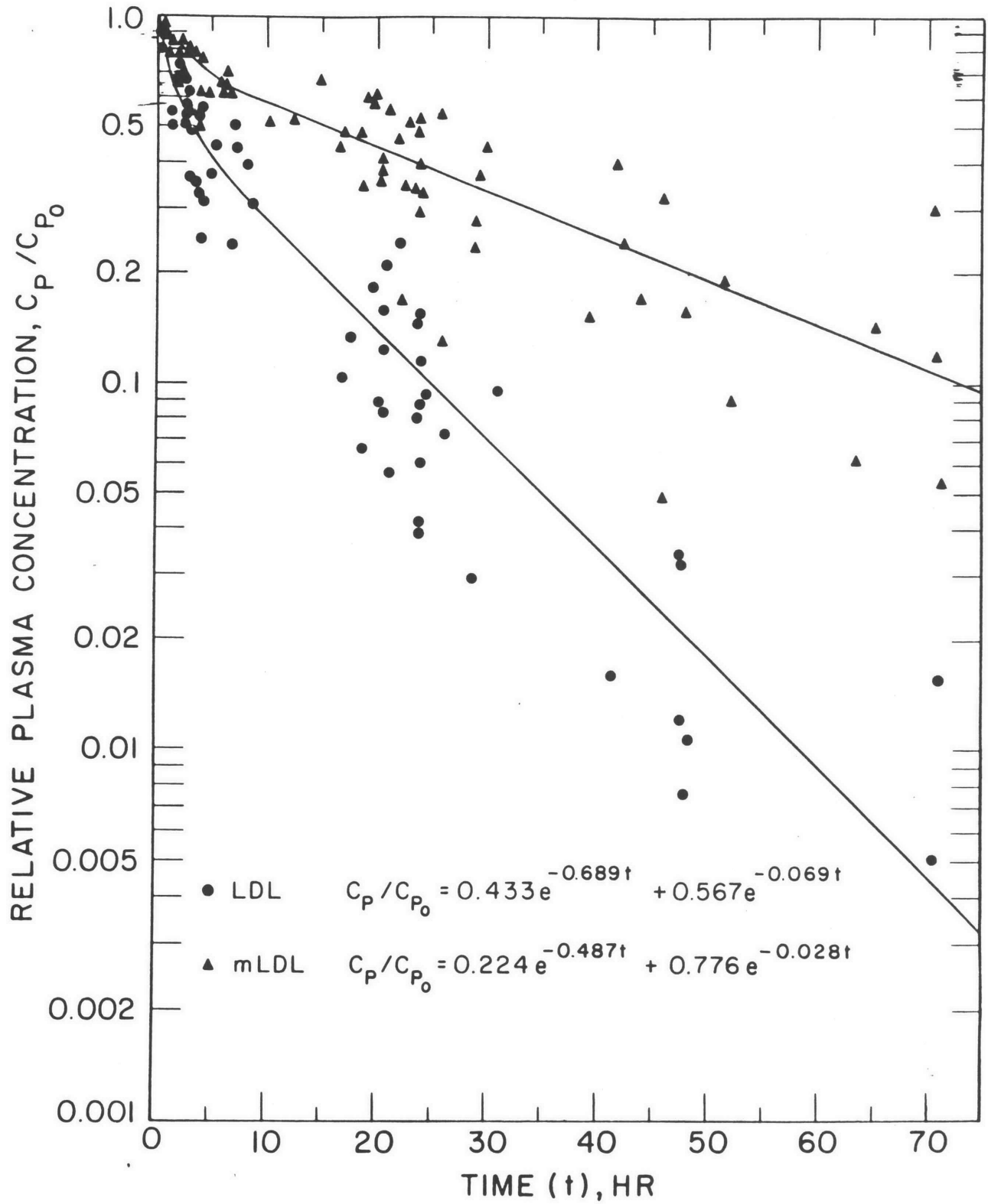


Figure 4-5: Combined Plasma Decay Curves of Navarro [1984] and This Study.

Table 4-III: Comparison of Plasma Decay Curves

	LDL		mLDL	
	SS _{res}	DF	SS _{res}	DF
This Study (SS ₁)	0.32	64	0.25	66
Navarro [1984] (SS ₂)	0.30	66	0.45	57
Pooled Data (SS _p)	0.62	130	0.71	123
Total (SS _t)	0.70	133	0.74	126

$$F = \frac{(SS_t - SS_p)/[(m+1)(k-1)]}{SS_p/DF_p}$$

For LDL $F=8.91$ with associated degrees of freedom 2 and 130.

Since $F_{0.05(1),2,130} \approx 3.07$ reject null hypothesis
($p < 0.001$)

For mLDL $F=3.05$ with associated degrees of freedom 2 and 133.

Since $F_{0.05(1),2,130} \approx 3.07$ accept null hypothesis
($0.05 < p < 0.10$)

techniques were used in both studies.

The fits of LDL and mLDL data listed in Table 4-II are plotted in Figure 4-6. The curves for mLDL are very similar, but the best fit values for LDL obtained by Navarro [1984] yields a curve which decays faster than the one for the best fit values for LDL plasma decay obtained in this study.

In order to measure degradation in the aorta, LDL and mLDL were labeled separately with ^{125}I and ^{14}C -sucrose, and samples of similar total activity were pooled and injected into rabbits. The initial plasma concentration of ^{125}I -LDL and ^{125}I -mLDL ranged from 5 to 25 x 10⁵ dpm/(ml plasma) and the initial plasma concentration of ^{14}C -sucrose labeled LDL and mLDL ranged from 3 to 14 x 10⁵

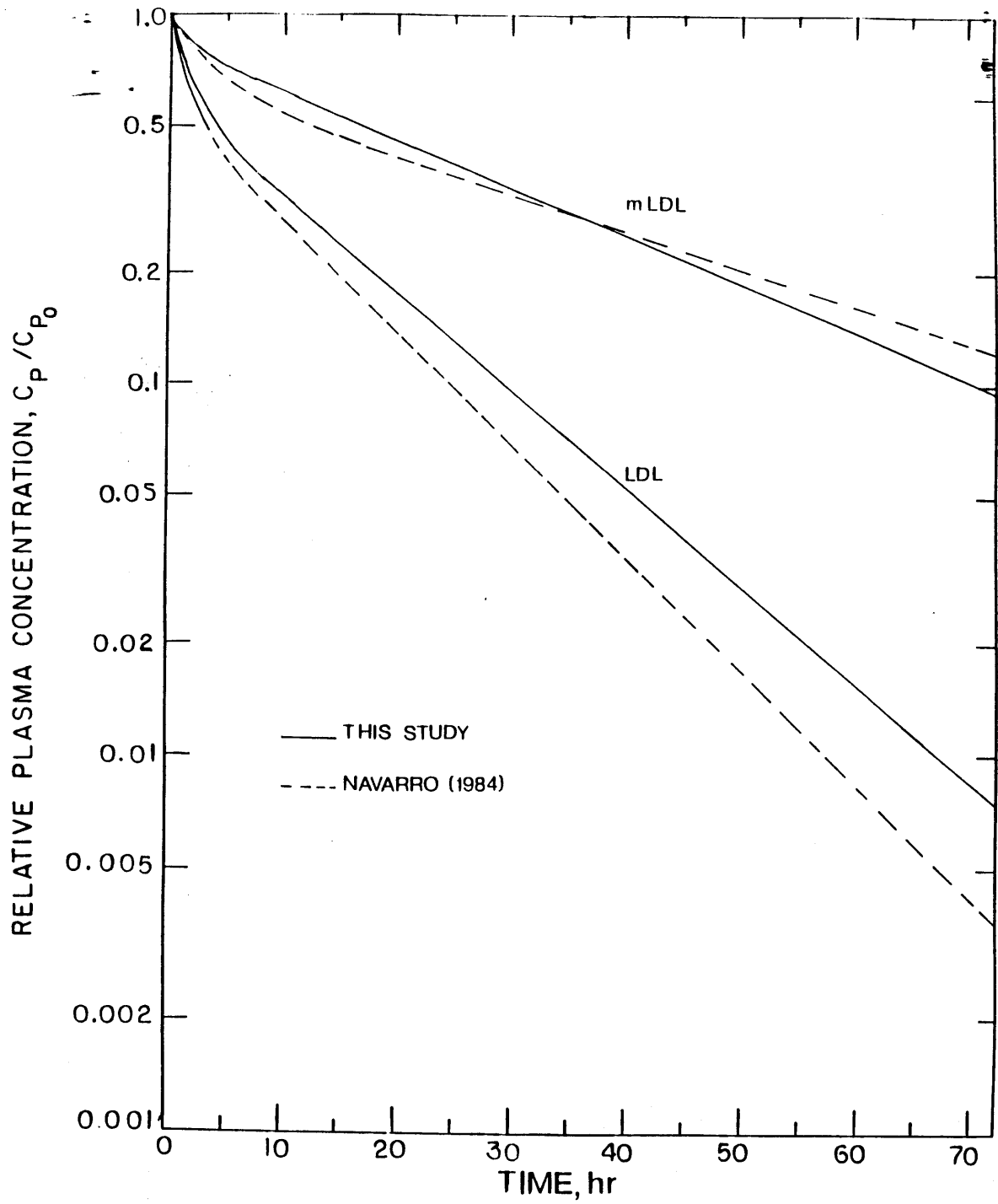


Figure 4-6: Comparison of the best fit values for plasma decay curves. Parameter values are listed in Table 4-II.

dpm/(ml plasma).

Plasma decay curves of ^{125}I - and ^{14}C -sucrose labeled LDL or mLDL are very similar (Figure 4-7). Comparison of the fitted curves for combined ^{125}I - and ^{14}C -sucrose plasma decay curves with the individual profiles indicates that there are no statistically significant differences between ^{125}I - and ^{14}C -sucrose labeled proteins. The fractional catabolic rates are $0.134 \pm 0.028 \text{ hr}^{-1}$ and $0.117 \pm 0.020 \text{ hr}^{-1}$ for ^{125}I and ^{14}C -sucrose labeled LDL, respectively ($p > 0.5$), and are 0.036 ± 0.007 and $0.031 \pm 0.010 \text{ hr}^{-1}$ for ^{125}I and ^{14}C -sucrose labeled mLDL, respectively ($p > 0.20$).

4.3.2 Transmural and Average Tissue Concentrations

Transmural concentration profiles of ^{125}I -LDL and ^{125}I -mLDL were determined by frozen serial section microtomy. Each animal yielded from five to seven sections with thicknesses ranging from 210 to 260 μm . Tissue concentrations were normalized by the initial plasma concentration. Results are presented as a function of normalized depth x/L where x is the distance from the intimal surface and L is the medial thickness.

Individual section and average profiles from two representative experiment are presented in Figures 4-8 and 4-9. Additional results are presented in Appendix G. The individual profiles are similar in shape and magnitude, although there is greater variability among sections near the medial-adventitial and intimal interfaces. There is no discernable trend in concentration among sections from various parts of the thoracic aorta. The average profiles resemble the individual profiles and represent a smoothed distribution.

Animal average and grand average profiles for all LDL and mLDL experiments are presented in Figures 4-10 to 4-17. For each solute, profiles at each circulation time are very similar, except for 4 hr and 24 hr LDL experiments. For each of these

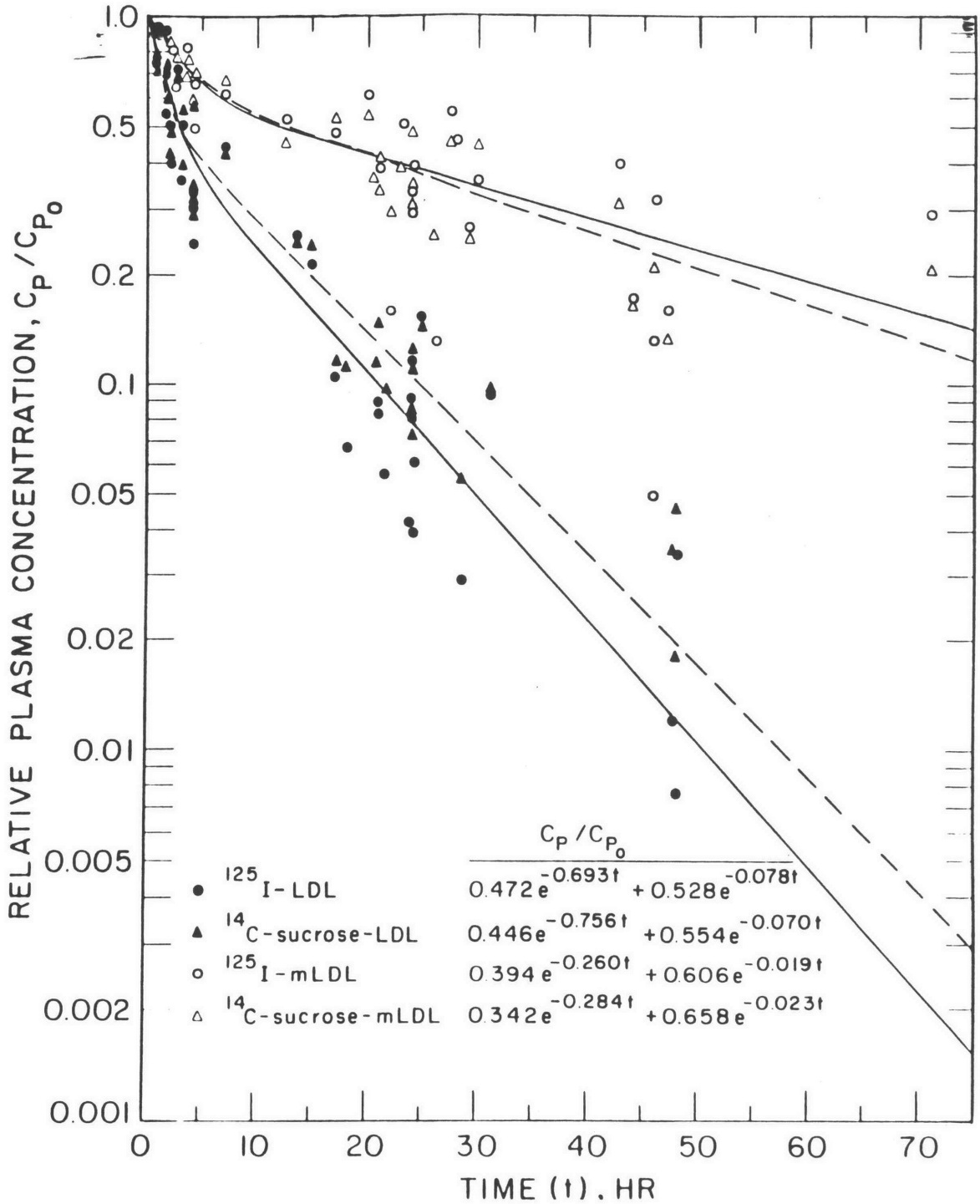


Figure 4-7: Plasma decay curves of ^{125}I - and ^{14}C -sucrose labeled LDL and mLDL

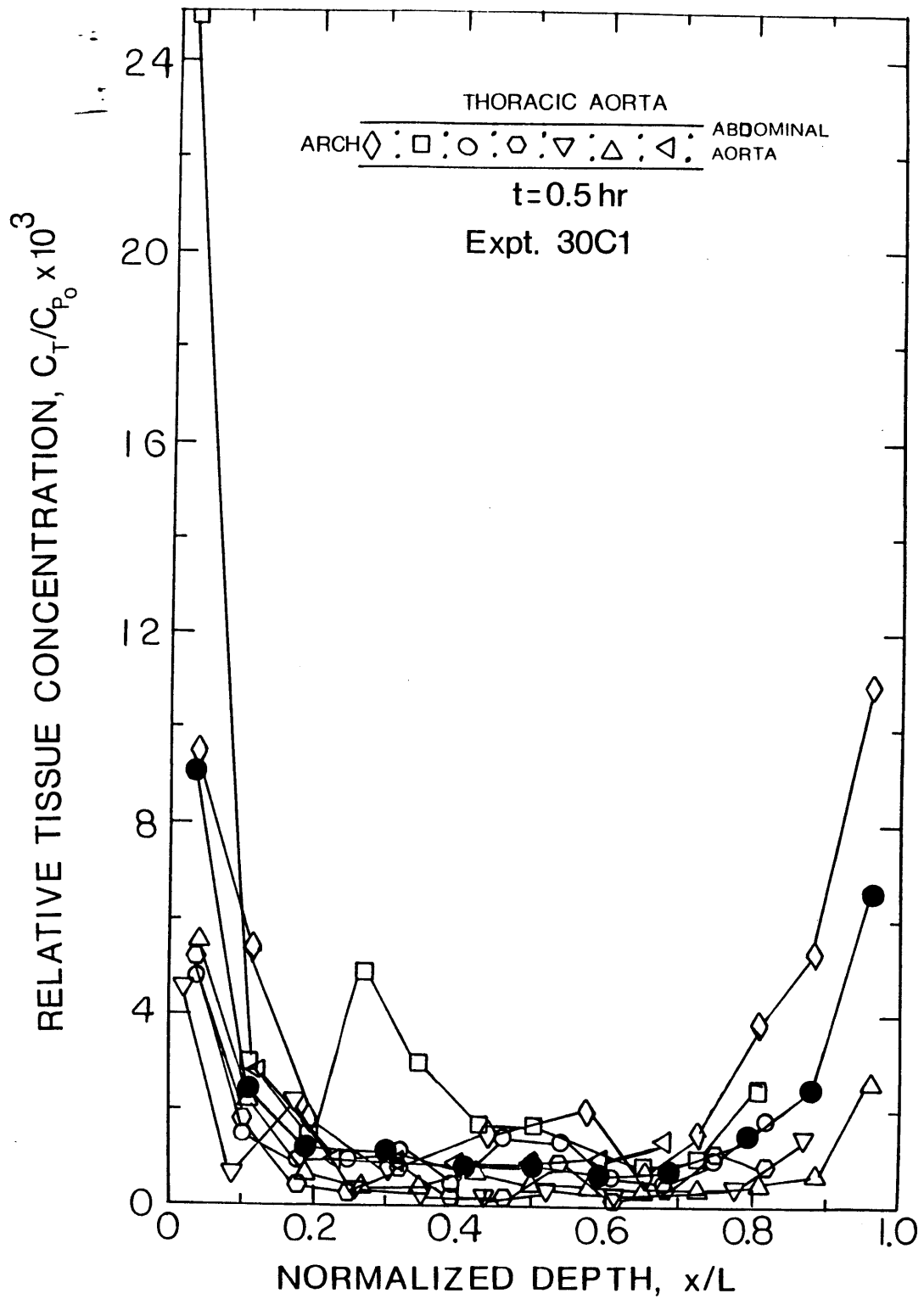


Figure 4-8: Individual Section Profiles and Animal Average for Expt. 30C1.

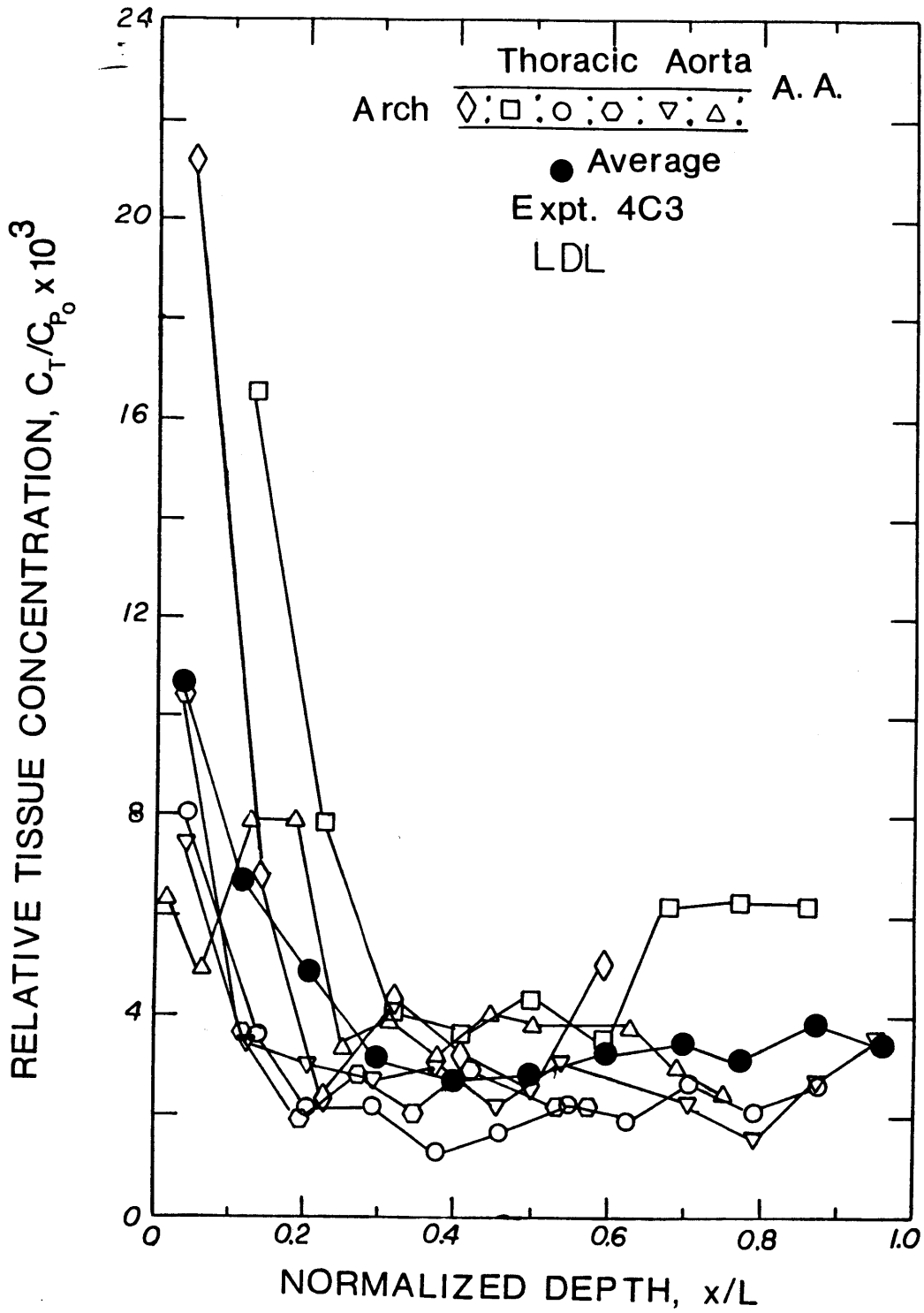


Figure 4-9: Individual Section Profiles and Animal Average for Expt. 4C3.

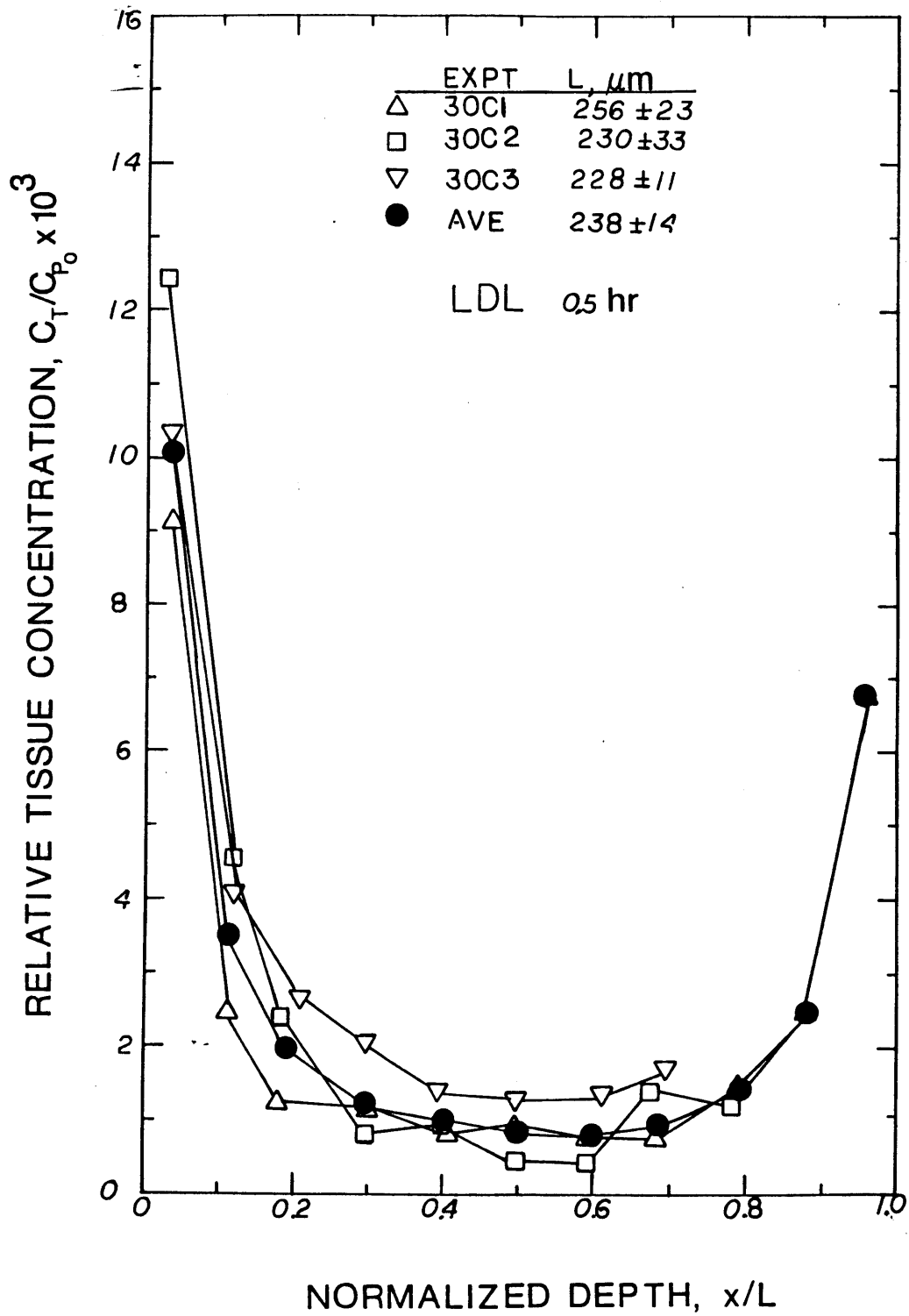


Figure 4-10: Animal Average Profiles for 0.5 hr LDL Experiments.

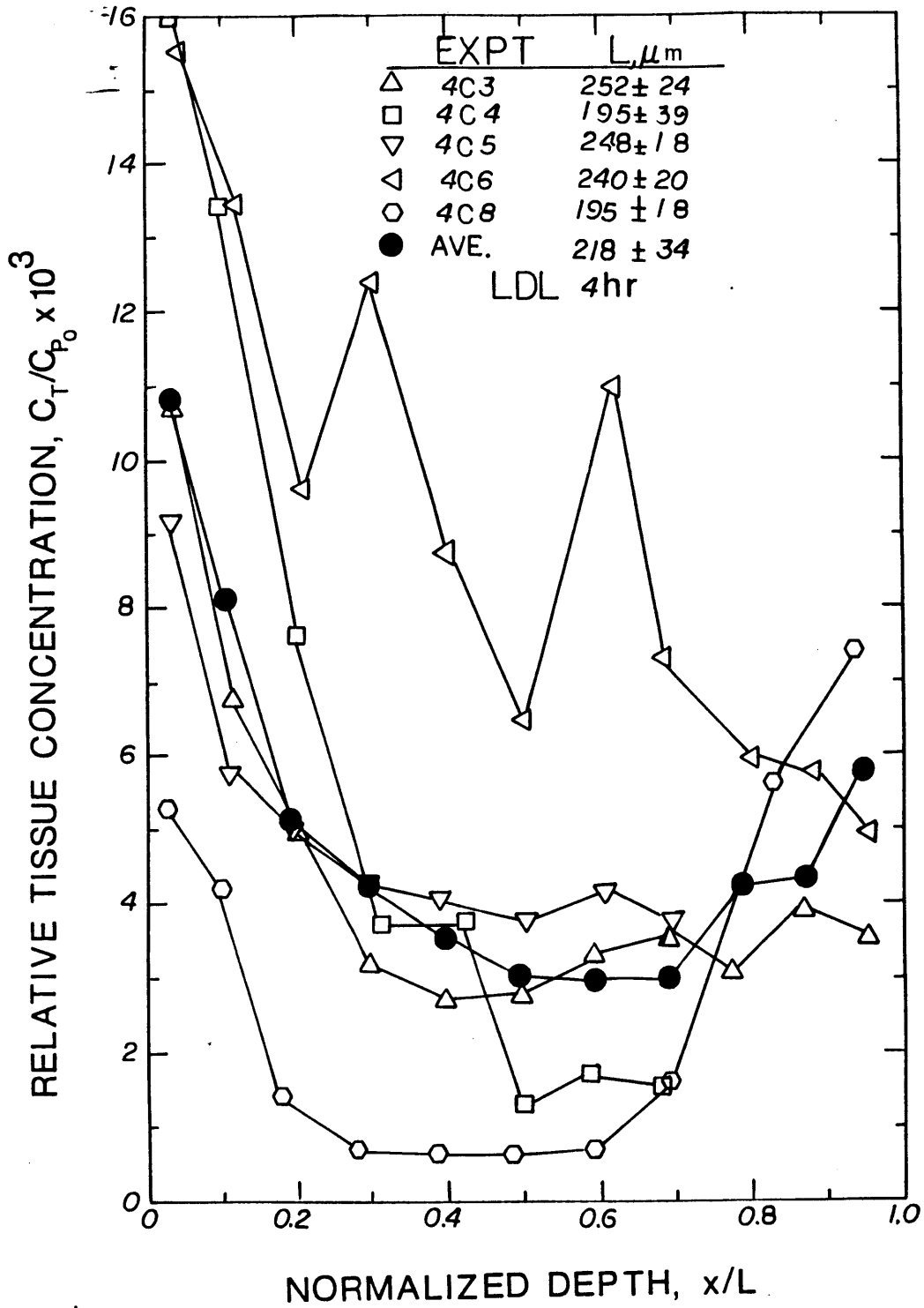


Figure 4-11: Animal Average Profiles for 4 hr LDL Experiments.

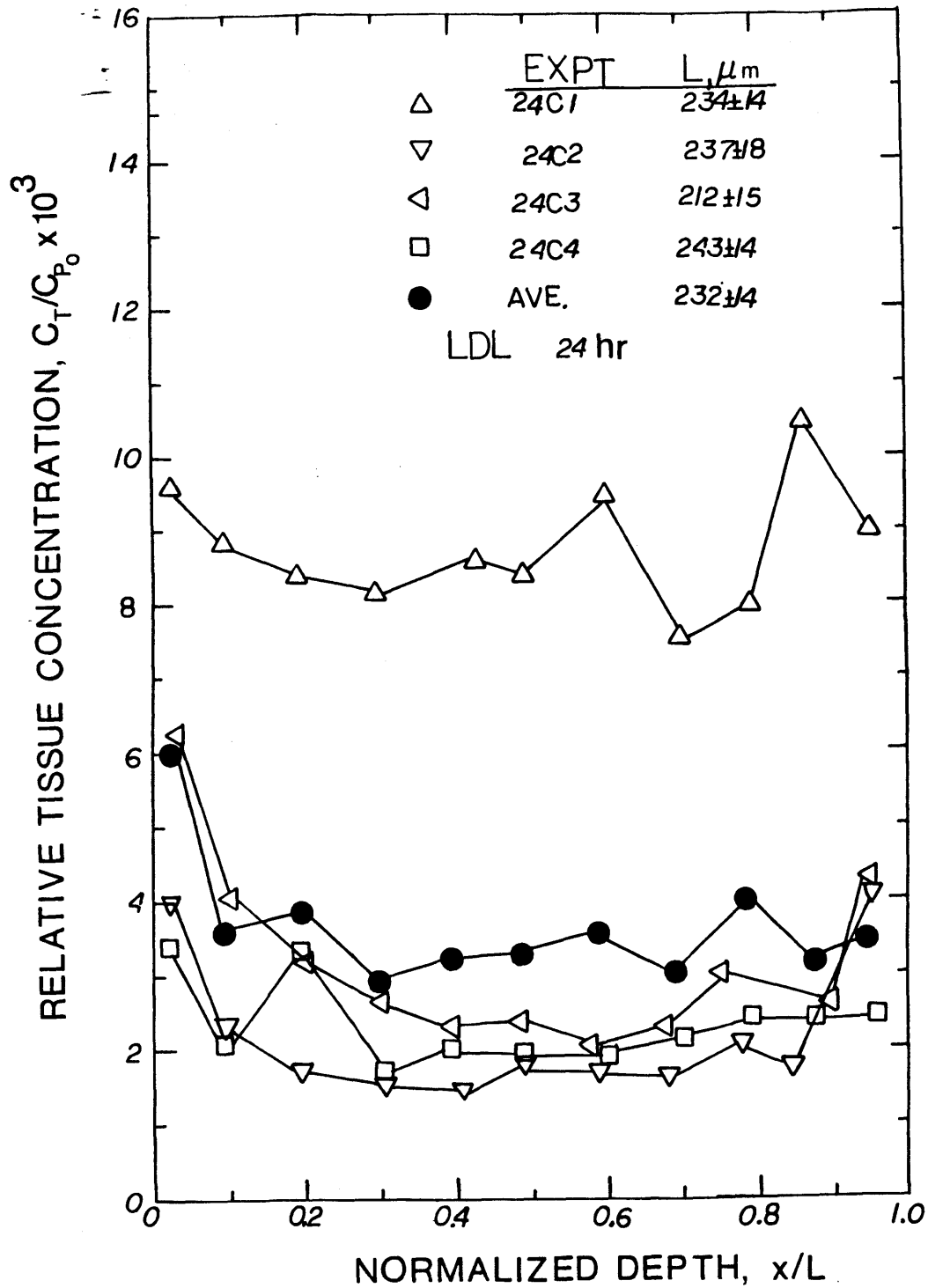


Figure 4-12: Animal Average Profiles for 24 hr LDL Experiments.

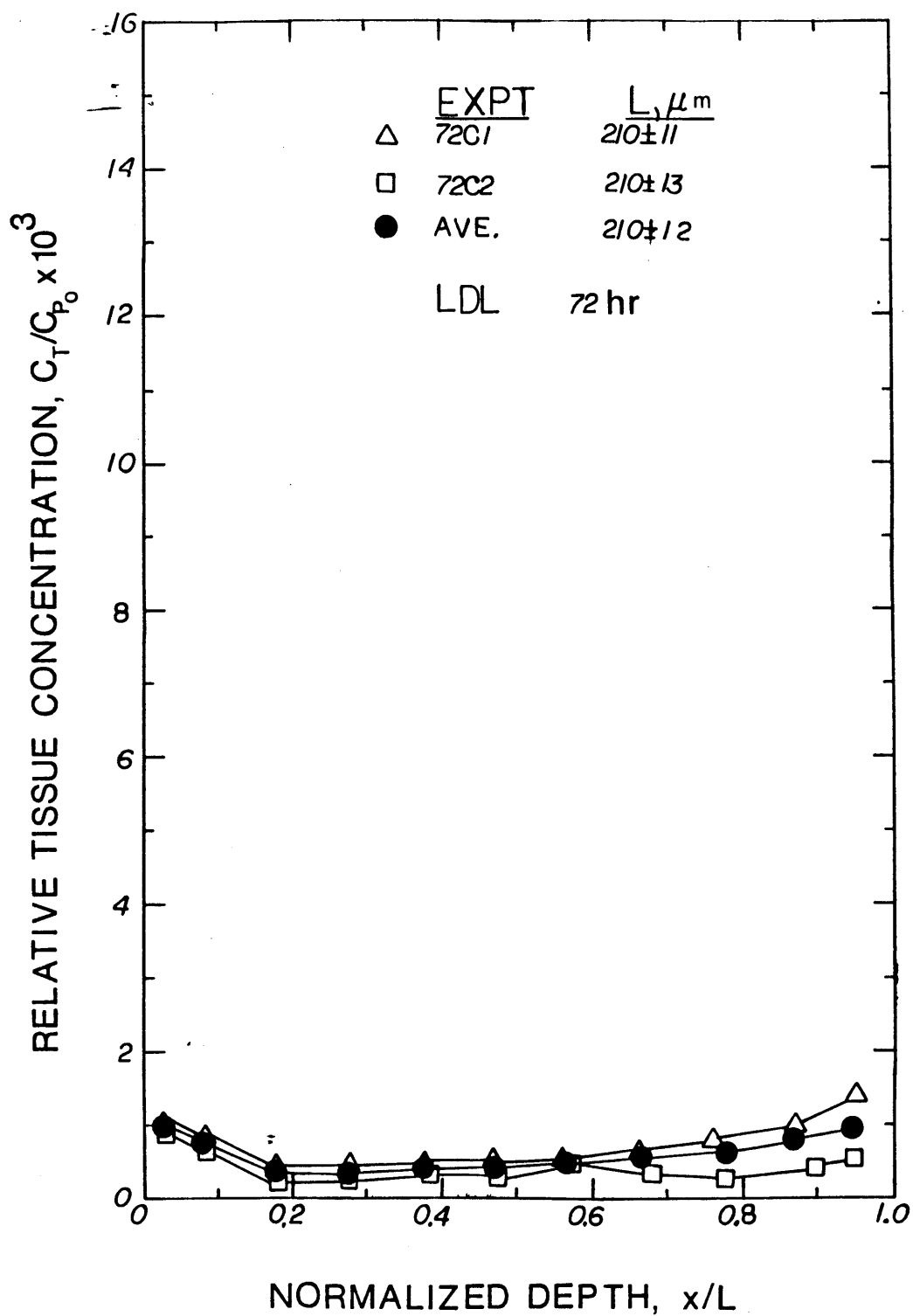


Figure 4-13: Animal Average Profiles for 72 hr LDL Experiments.

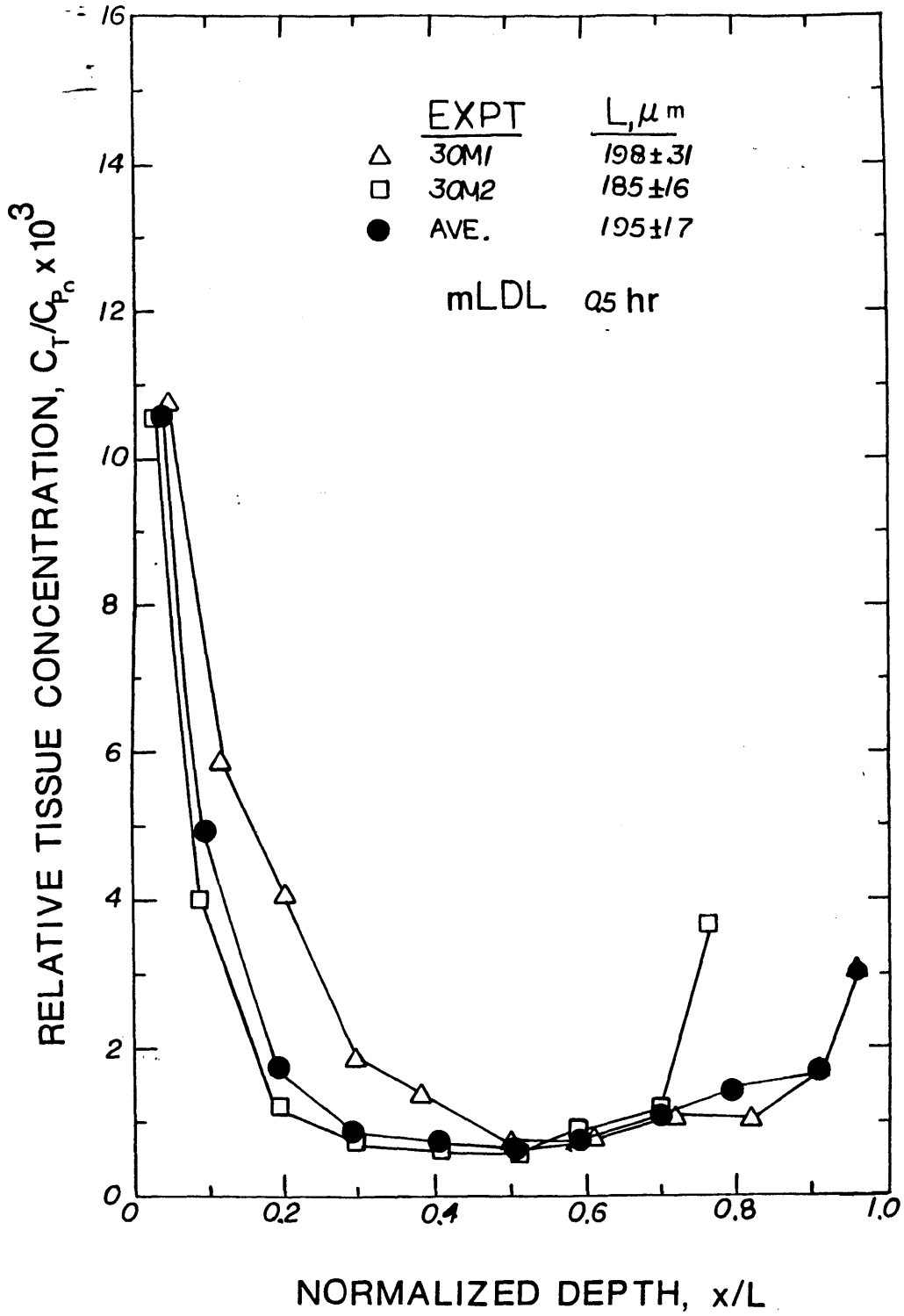


Figure 4-14: Animal Average Profiles for 0.5 hr mLDL Experiments.

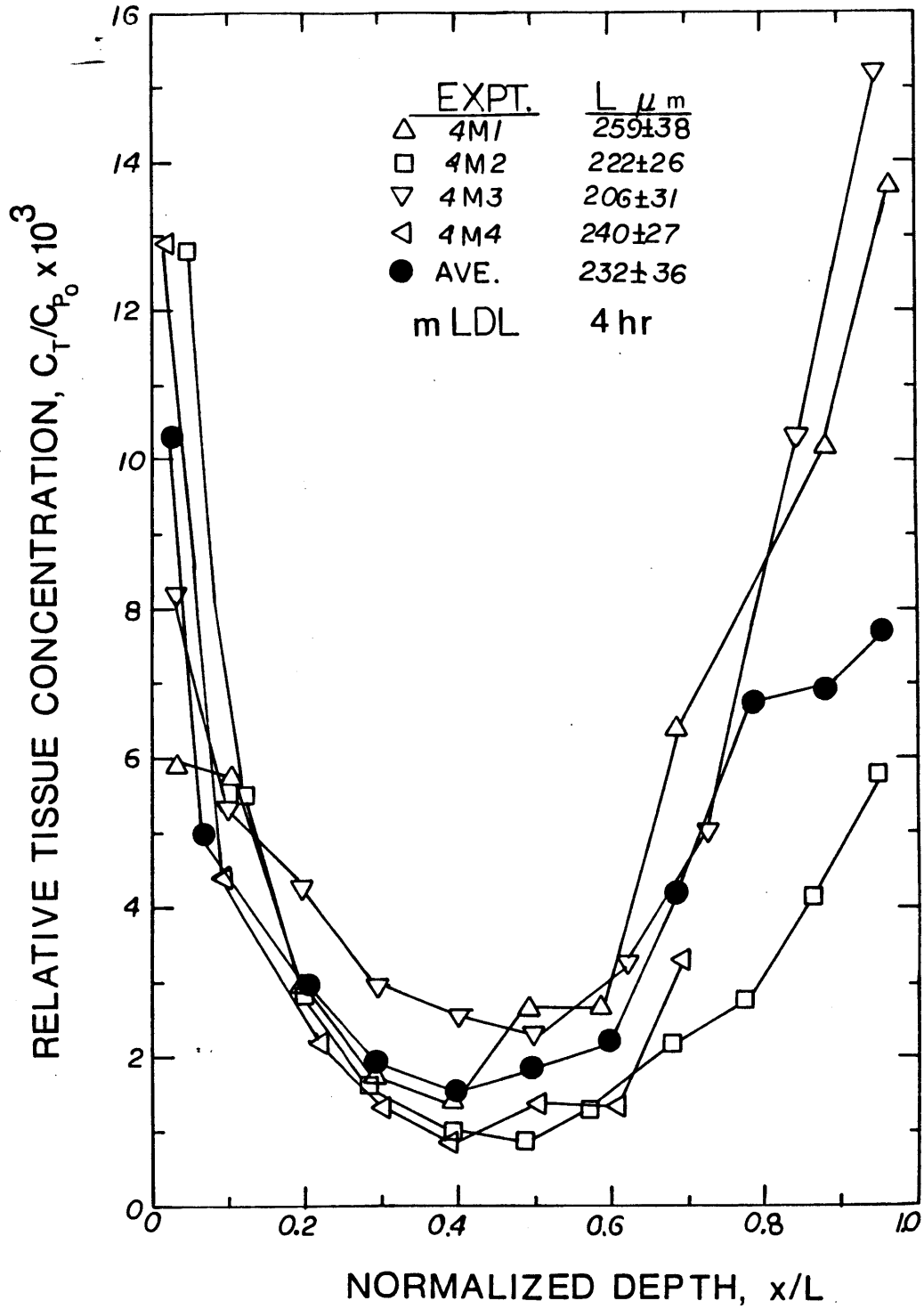


Figure 4-15: Animal Average Profiles for 4 hr mLDL Experiments.

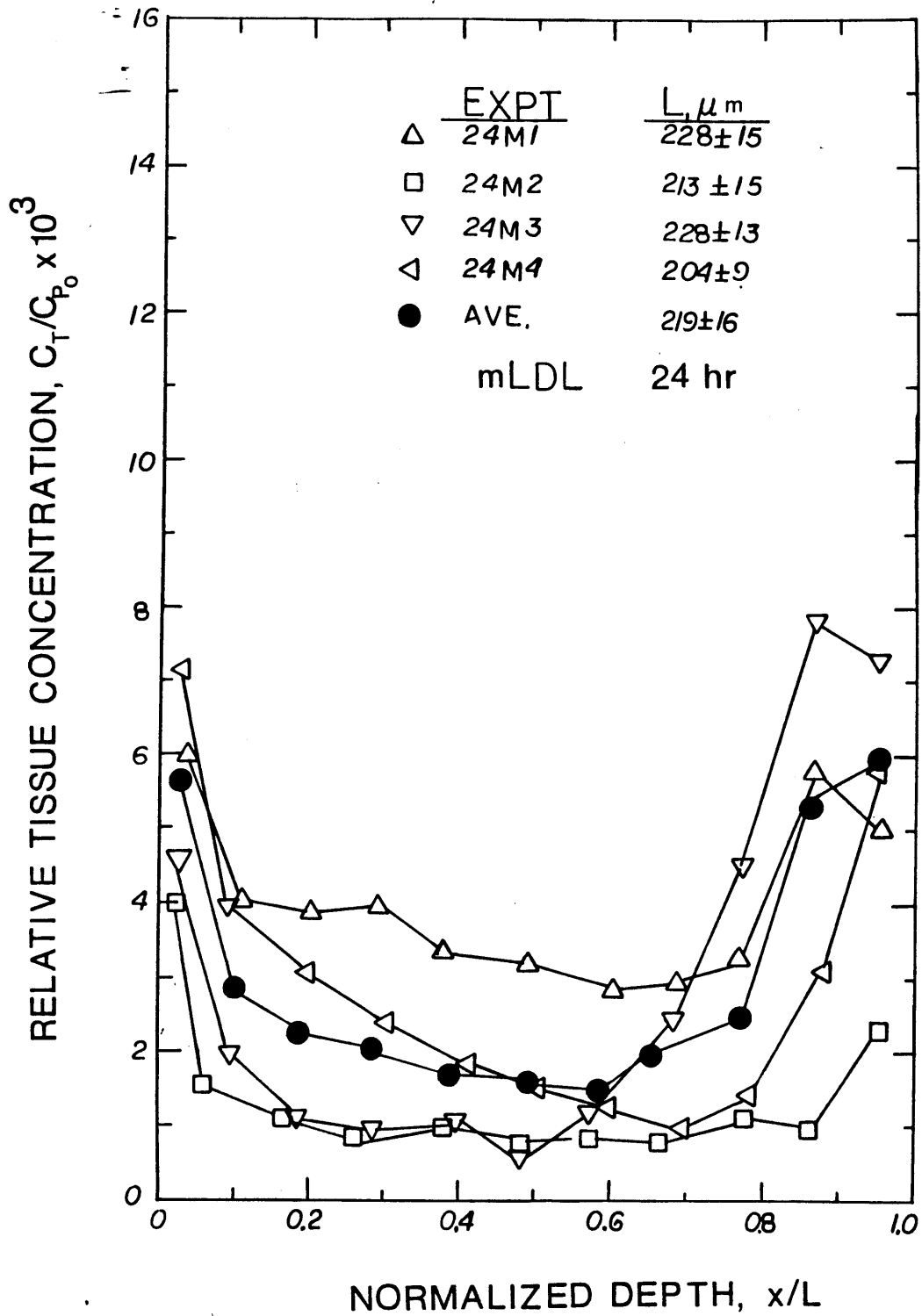


Figure 4-16: Animal Average Profiles for 24 hr mLDL Experiments.

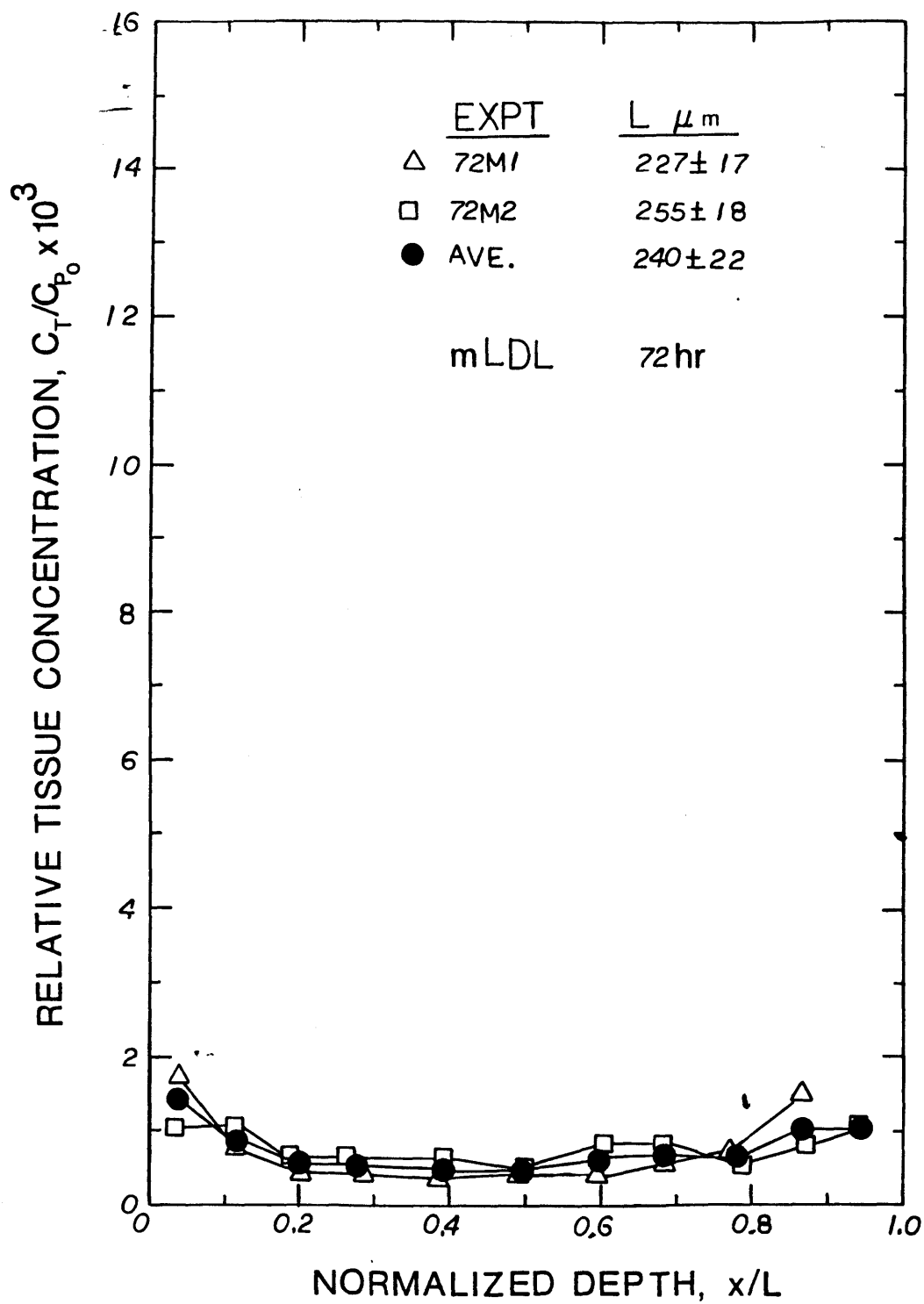


Figure 4-17: Animal Average Profiles for 72 hr mLDL Experiments.

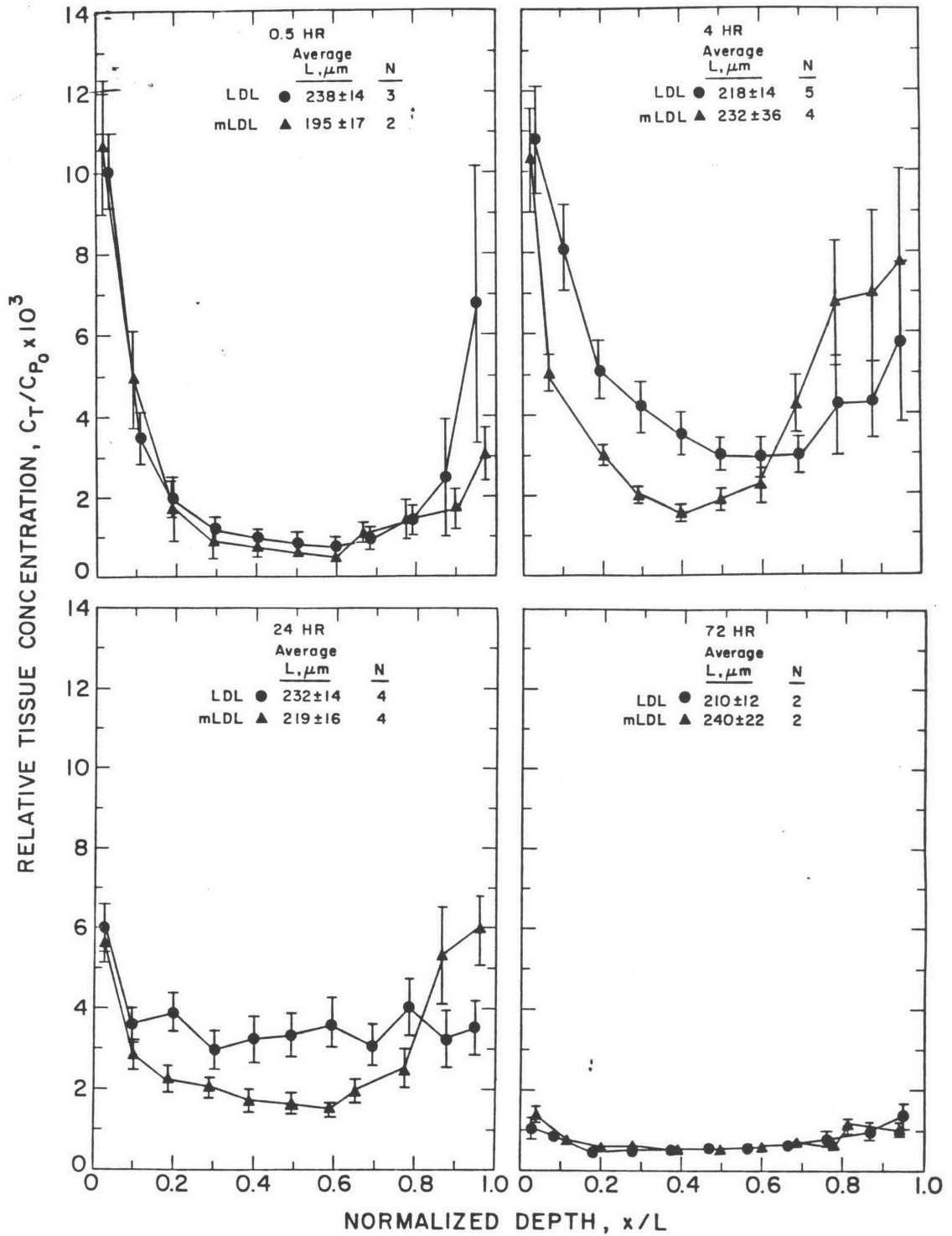


Figure 4-18: Grand Average Profiles for LDL and mLDL.

two circulation times, one profile is significantly different from the others.

At each circulation time the animal average profiles were averaged to obtain grand average profiles (Figure 4-18). The points represent averages of all data points and error bars represents standard errors of the mean. At 0.5 hr, relative tissue concentrations range from 0.0002 to 0.002 at the middle of the media and are about 5 to 15-fold higher near the luminal surface. The steep intimal ($x=0$) and adventitial ($x=L$) gradients at 0.5 hr suggest solute entry from both the vessel lumen as well as the adventitia. At four hr, the gradients have decreased and the mid-medial concentrations have increased. By 24 hr, the LDL gradients have flattened, with mid-medial values similar to those at four hr. There are still significant intimal and medial-adventitial gradients for mLDL at 24 h. At 72 h, both profiles are flat, with concentrations ranging from 0.0002 at the middle of the media to 0.0012 at both ends. At all times studied, the mid-medial concentrations in all animals are significantly different from zero ($p < 0.05$).

At each circulation time, the shapes of the mLDL transmural profiles are similar to those for LDL. At 0.5 hr and 72 hr LDL and mLDL profiles are virtually identical. At 4 and 24 hr the LDL and mLDL concentrations at the intimal surface are the same, but with increasing distance into the wall the mLDL concentrations are less than those for LDL until a normalized depth of 0.7-0.8 where the mLDL concentrations exceed those for LDL.

Statistical comparisons between grand average LDL and mLDL profiles at each circulation time were performed using Student's t test (Table 4-IV) for tissue concentrations at comparable depths. At four hr significant differences between LDL and mLDL were detected for normalized depths between 0.10 and 0.50; at 24 hr significant differences between LDL and mLDL concentrations exist at depths between 0.19 and 0.59 and at a depth of 0.96.

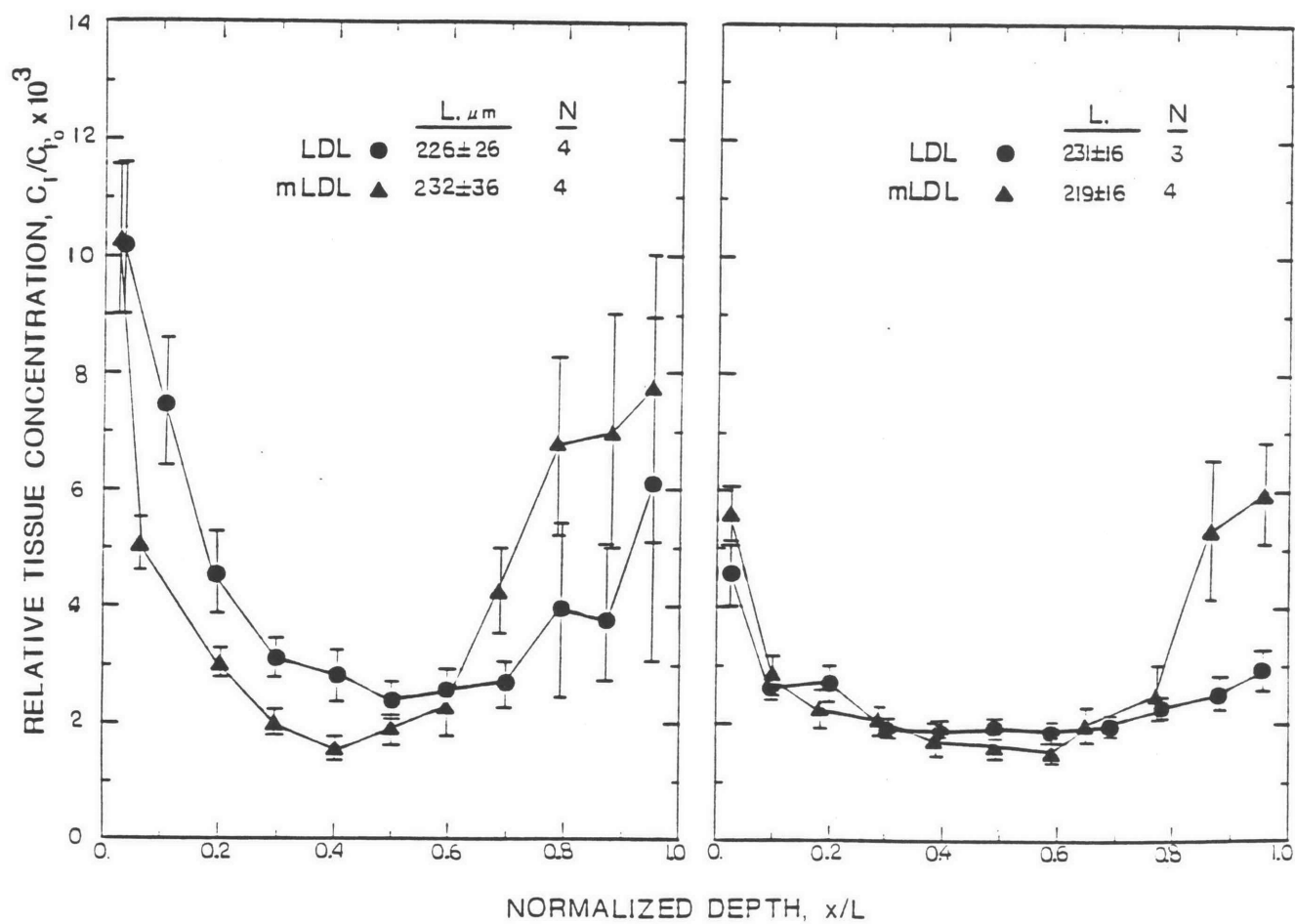


Figure 4-19: Comparison of 4 hr and 24 hr Grand Average LDL and mLDL Transmural Profiles without Aberrant Profiles (4C6 and 24c1).

For LDL transmural profiles at 4 and 24 hr (Figures 4-11 and 4-12) there is a single profile that is drastically different from all others (Experiment 4C6 at 4 hr and experiment 24C1 at 24 hr). The grand averages were recalculated without these two experiments and the results are presented in Figure 4-19. As a result, the mid-medial concentrations are similar to those obtained with mLDL. Differences between LDL and mLDL profiles are much smaller. Nevertheless, significant differences between LDL and mLDL profiles still exist at 4 hr for normalized depths between 0.11 and 0.40 and at 24 hr at a normalized depth of 0.96. At 24 hr mLDL concentrations near the medial-adventitial interface are higher than LDL concentrations. Excluding experiment 24C1 had little effect upon this difference near the medial-adventitial interface. The differences between LDL and mLDL profiles at 24 hr are due largely to experiment 24C1. At 4 hr there are still statistically significant differences between LDL and mLDL concentrations even when experiment 4C6 is excluded from the grand average, although the level of significance has decreased (Table 4-V).

The mean relative tissue concentration as a function of time is obtained by numerical integration of transmural profiles (Figure 4-20A):

$$\frac{C_T}{C_{p_o}} = \sum_{i=1}^{11} \frac{C_{T_i}}{C_{p_o}} \Delta\eta_i \quad (4-4)$$

where $\Delta\eta_i$ is the normalized interval thickness $\Delta x_i/L$. The vessel wall was divided into 11 intervals; the first and last interval have relative thicknesses of 0.05, all others have thicknesses of 0.10. (See Appendix G and Bratzler [1974] for sample calculations.) The mean relative concentration was calculated for each animal, and, at each circulation time, all animals injected with the same lipoprotein were averaged together. The error bars represent the standard error of the mean.

The mean relative tissue concentration reaches a maximum at around four hr

Table 4-IV: Comparison of LDL and mLDL Grand Average Profiles

t=0.5 hr			t=0.5 hr			
η	$\theta_T \times 10^3$	LDL n	η	$\theta_T \times 10^3$	mLDL n	
0.036	10.07 ± 6.51	16	0.025	10.66 ± 3.94	7	$p > 0.50$
0.118	3.48 ± 1.98	16	0.100	4.80 ± 3.44	11	$p > 0.10$
0.194	1.96 ± 1.23	17	0.198	1.72 ± 1.30	13	$p > 0.20$
0.300	1.21 ± 1.07	26	0.295	1.02 ± 1.27	10	$p > 0.50$
0.406	0.97 ± 0.52	16	0.401	0.87 ± 0.89	11	$p > 0.50$
0.502	0.85 ± 0.48	20	0.508	0.61 ± 0.44	12	$p > 0.50$
0.599	0.76 ± 0.60	13	0.599	0.80 ± 0.80	8	$p > 0.50$
0.687	0.97 ± 0.55	13	0.673	0.92 ± 0.65	8	$p > 0.50$
0.792	1.42 ± 1.08	9	0.789	1.44 ± 1.17	6	$p > 0.50$
0.880	2.47 ± 2.52	3	0.911	1.69 ± 0.98	4	$p > 0.50$
0.962	6.77 ± 5.93	2	0.958	3.07 ± 1.31	2	$p > 0.20$

t=4 hr			t=4 hr			
0.035	10.97 ± 6.46	22	0.029	10.55 ± 4.97	14	$p > 0.50$
0.111	8.03 ± 5.18	28	0.099	4.90 ± 2.33	25	$p < 0.01$
0.198	5.11 ± 3.73	27	0.204	2.95 ± 1.44	29	$p < 0.01$
0.300	4.20 ± 3.74	34	0.298	1.96 ± 1.15	30	$p < 0.002$
0.401	3.49 ± 2.88	27	0.399	1.54 ± 0.80	31	$p < 0.001$
0.499	2.99 ± 2.19	31	0.502	1.87 ± 1.52	29	$p < 0.05$
0.600	2.92 ± 2.40	23	0.595	2.06 ± 1.70	22	$p > 0.10$
0.694	2.97 ± 1.93	16	0.690	4.25 ± 3.21	20	$p > 0.10$
0.797	4.23 ± 3.43	7	0.789	6.76 ± 4.60	9	$p > 0.20$
0.875	4.34 ± 1.92	4	0.883	6.97 ± 4.92	6	$p > 0.20$
0.960	5.82 ± 3.90	4	0.957	7.75 ± 4.60	4	$p > 0.20$

Table 4-IV (continued)

t=24 hr LDL			t=24 hr mLDL			
η	$\theta_T \times 10^3$	n	η	$\theta_T \times 10^3$	n	
0.026	5.63 ± 3.10	24	0.031	5.62 ± 2.19	19	$p > 0.50$
0.097	3.48 ± 2.50	35	0.101	3.08 ± 1.48	22	$p > 0.50$
0.200	3.90 ± 2.91	34	0.190	2.24 ± 1.49	20	$p < 0.05$
0.305	3.18 ± 2.87	30	0.294	2.06 ± 1.31	23	$p < 0.05$
0.400	3.29 ± 3.29	24	0.395	1.73 ± 1.14	21	$p < 0.05$
0.493	3.36 ± 2.92	24	0.493	1.71 ± 1.18	20	$p < 0.05$
0.595	3.62 ± 3.49	30	0.589	1.49 ± 0.82	21	$p < 0.01$
0.695	3.09 ± 2.66	25	0.653	1.94 ± 1.26	20	$p < 0.02$
0.786	3.78 ± 2.82	16	0.778	2.50 ± 1.90	17	$p > 0.10$
0.879	3.24 ± 2.40	12	0.870	5.15 ± 4.05	13	$p > 0.10$
0.957	3.54 ± 2.12	10	0.955	5.82 ± 2.29	9	$p < 0.05$
t=72 hr			t=72 hr			
0.029	1.07 ± 0.75	8	0.040	1.41 ± 0.46	12	$p > 0.50$
0.087	0.87 ± 0.57	12	0.116	0.74 ± 0.44	13	$p > 0.50$
0.184	0.45 ± 0.23	12	0.200	0.57 ± 0.32	14	$p > 0.20$
0.280	0.51 ± 0.51	12	0.282	0.55 ± 0.25	14	$p > 0.50$
0.379	0.55 ± 0.39	13	0.392	0.50 ± 0.32	15	$p > 0.20$
0.474	0.55 ± 0.36	11	0.499	0.47 ± 0.23	19	$p > 0.20$
0.568	0.56 ± 0.26	11	0.602	0.61 ± 0.33	12	$p > 0.50$
0.667	0.63 ± 0.34	10	0.687	0.69 ± 0.28	11	$p > 0.50$
0.764	0.80 ± 0.31	10	0.780	0.64 ± 0.23	7	$p > 0.20$
0.871	0.99 ± 0.44	6	0.816	1.10 ± 0.41	5	$p > 0.20$
0.951	1.39 ± 0.62	4	0.958	1.03 ± 0.15	3	$p > 0.20$

Table 4-V: Comparison of LDL and mLDL Grand Average Profiles at 4 and 24 hr without Experiments 4C6 and 24C1

t=4 hr LDL			t=4 hr mLDL			
η	$\bar{\theta}_T \times 10^3$	n	η	$\bar{\theta}_T \times 10^3$	n	
0.034	10.19 ± 6.38	19	0.029	10.55 ± 4.97	14	$p > 0.50$
0.209	7.49 ± 5.55	25	0.099	4.90 ± 2.33	25	$p < 0.05$
0.197	4.55 ± 3.54	24	0.204	2.95 ± 1.44	29	$p < 0.05$
0.299	3.10 ± 1.93	30	0.298	1.96 ± 1.15	30	$p < 0.01$
0.401	2.82 ± 2.26	24	0.399	1.54 ± 0.80	31	$p < 0.01$
0.499	2.40 ± 1.60	27	0.502	1.87 ± 1.52	29	$p > 0.20$
0.599	2.55 ± 1.68	22	0.595	2.06 ± 1.70	22	$p > 0.20$
0.697	2.68 ± 1.59	15	0.690	4.25 ± 3.21	20	$p > 0.05$
0.795	3.95 ± 3.67	13	0.789	6.76 ± 4.60	9	$p > 0.20$
0.872	3.86 ± 2.03	3	0.883	6.97 ± 4.92	6	$p > 0.20$
0.949	6.12 ± 4.72	3	0.957	7.75 ± 4.60	4	$p > 0.50$
t=24 hr			t=24 hr			
0.026	4.58 ± 2.46	19	0.031	5.62 ± 2.19	19	$p > 0.10$
0.101	2.63 ± 1.04	29	0.101	3.08 ± 1.48	22	$p > 0.20$
0.201	2.73 ± 1.70	27	0.190	2.24 ± 1.49	20	$p > 0.20$
0.306	1.93 ± 0.65	24	0.294	2.06 ± 1.31	23	$p > 0.20$
0.401	1.88 ± 0.55	19	0.395	1.73 ± 1.14	21	$p > 0.50$
0.493	1.93 ± 0.60	21	0.493	1.71 ± 1.18	20	$p > 0.20$
0.593	1.84 ± 0.51	23	0.589	1.49 ± 0.82	21	$p > 0.05$
0.693	1.99 ± 0.51	20	0.653	1.94 ± 1.26	20	$p > 0.50$
0.782	2.30 ± 0.70	11	0.778	2.50 ± 1.90	17	$p > 0.50$
0.880	2.58 ± 0.83	11	0.870	5.15 ± 4.05	13	$p > 0.05$
0.957	2.94 ± 0.98	9	0.955	5.82 ± 2.29	9	$p < 0.005$

and decays thereafter. At 4 and 24 hr, the mean relative concentration of mLDL is less than the value for LDL, but the differences are not statistically significant at the 95% confidence level (Table 4-VI). When experiments 4C6 and 24C1 are excluded from the analysis, the mean relative tissue concentrations of LDL and mLDL are identical at all times (Figure 4-20B).

Table 4-VI: Comparison of LDL and mLDL Mean Relative Concentrations

t, hr	LDL $\theta_T \times 10^3$		mLDL $\theta_T \times 10^3$	
0.5	30C1	1.962	30M1 2.512	
	30C2	1.816	30M2 2.105	
	30C3	2.519		
	Ave.	2.10 ± 0.37	$p > 0.50$	Ave. 2.31 ± 0.29
4	4C3	4.086	4M1 5.281	
	4C4	5.405	4M2 3.072	
	4C5	4.641	4M3 5.732	
	4C6	9.100	4M4 2.887	
	4C8	2.644		
	Ave.	5.18 ± 2.42	$p > 0.50$	Ave. 4.24 ± 1.47
	Ave without 4C6	4.20 ± 1.17	$p > 0.50$	
24	24C1	8.612	24M1 3.315	
	24C2	1.942	24M2 1.200	
	24C3	2.953	24M3 2.597	
	24C4	2.264	24M4 2.764	
	Ave.	3.94 ± 3.14	$p > 0.20$	Ave. 2.47 ± 0.90
	Ave. without 24C1	2.38 ± 0.56	$p > 0.50$	
72	72C1	0.912	72M1 0.677	
	72C2	0.409	72M3 0.730	
	Ave.	0.66 ± 0.36	$p > 0.50$	Ave. 0.70 ± 0.04

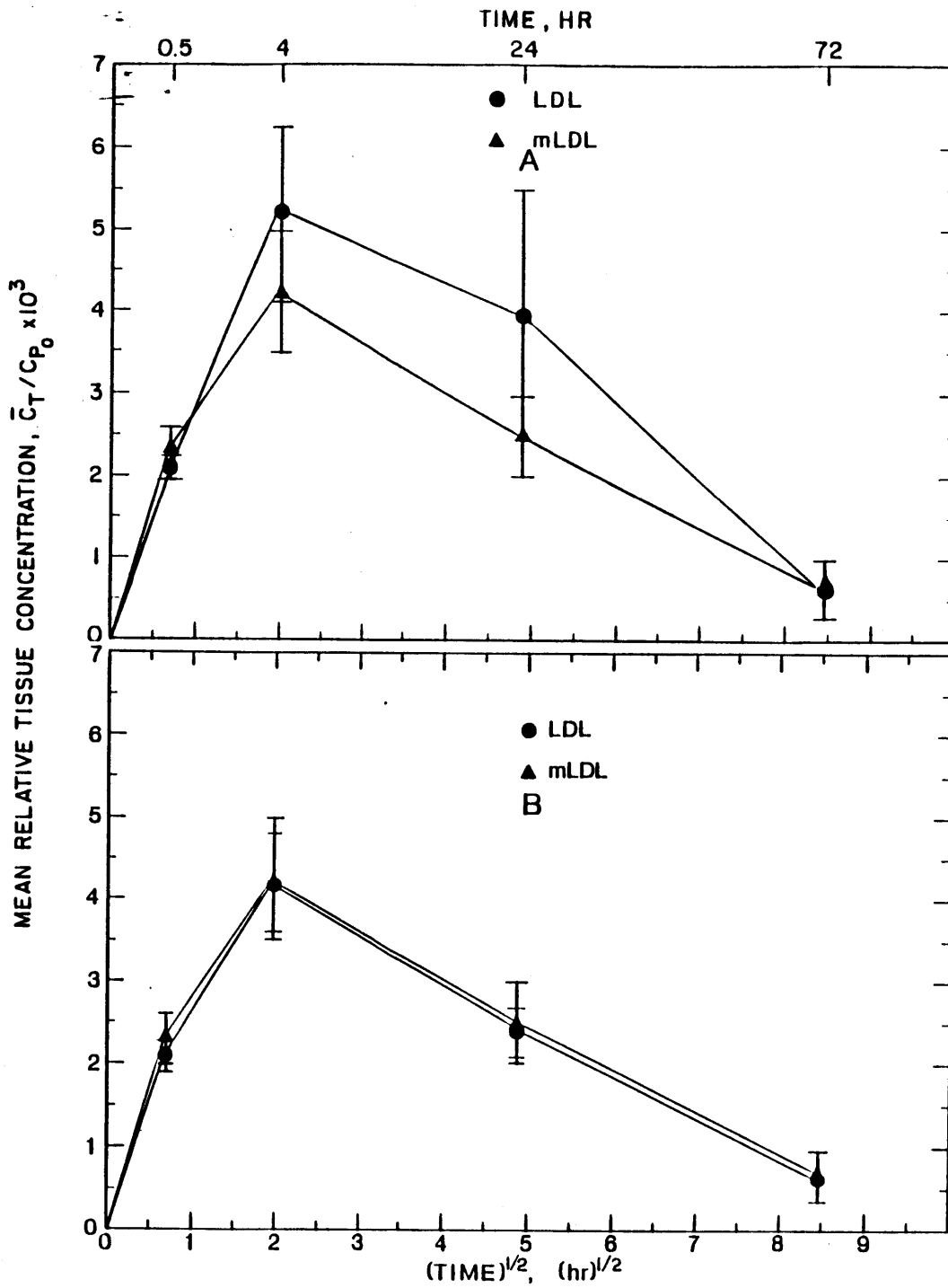


Figure 4-20: Mean Relative Average Concentrations of LDL and mLDL. B) Experiments 4C6 and 24C1 were excluded from the average values for LDL.

4.3.3 LDL- and mLDL Accumulation and Degradation in the Aorta

In experiments performed by Navarro [1984], lipoproteins were labeled separately with ^{125}I - and ^{14}C -sucrose and samples of similar total activity were pooled and injected into rabbits. Specific activities of ^{14}C -sucrose labeled lipoproteins were too low to permit frozen serial sectioning. Consequently, whole tissue samples were analyzed. Glutaraldehyde-fixed thoracic and abdominal segments were stripped of adventitia and counted in a gamma counter of known efficiency (68%) to determine the ^{125}I content. The tissues were solubilized and the amount of radioactivity was determined by liquid scintillation, the degree of quench was determined, and the ^{14}C contribution was calculated after subtracting any contribution by ^{125}I . In this manner the content of ^{14}C and ^{125}I in each sample, of known weight, was calculated. A density of 1.09 g/ml was assumed for glutaraldehyde-fixed tissue (Fry et al. [1980]). Tissue concentrations of each isotope are expressed as dpm/cm³ of fixed tissue relative to the initial plasma concentration of that isotope.

In each experiment two samples were obtained, one each from the thoracic and abdominal aortae. Although LDL and mLDL concentrations of ^{125}I - and ^{14}C -sucrose- labeled lipoproteins are slightly higher in the abdominal aorta than in the thoracic aorta, the differences are not significant and the samples were pooled. Results are presented in Figure 4-21 and the error bars represent the standard error of the mean. ^{125}I -LDL levels reach a maximum at around four hr and decrease thereafter. ^{125}I -mLDL levels behave in a similar fashion except that the maximum lies between four and 24 hr. At each time, differences between ^{125}I -LDL and ^{125}I -mLDL are not significant. ^{125}I -LDL and ^{125}I -mLDL concentrations determined from transmural profiles (Figure 4-20) and whole sample counting of fixed tissue (Figure 4-21) are not significantly different, except for mLDL at 72 hr (Table 4-VII).

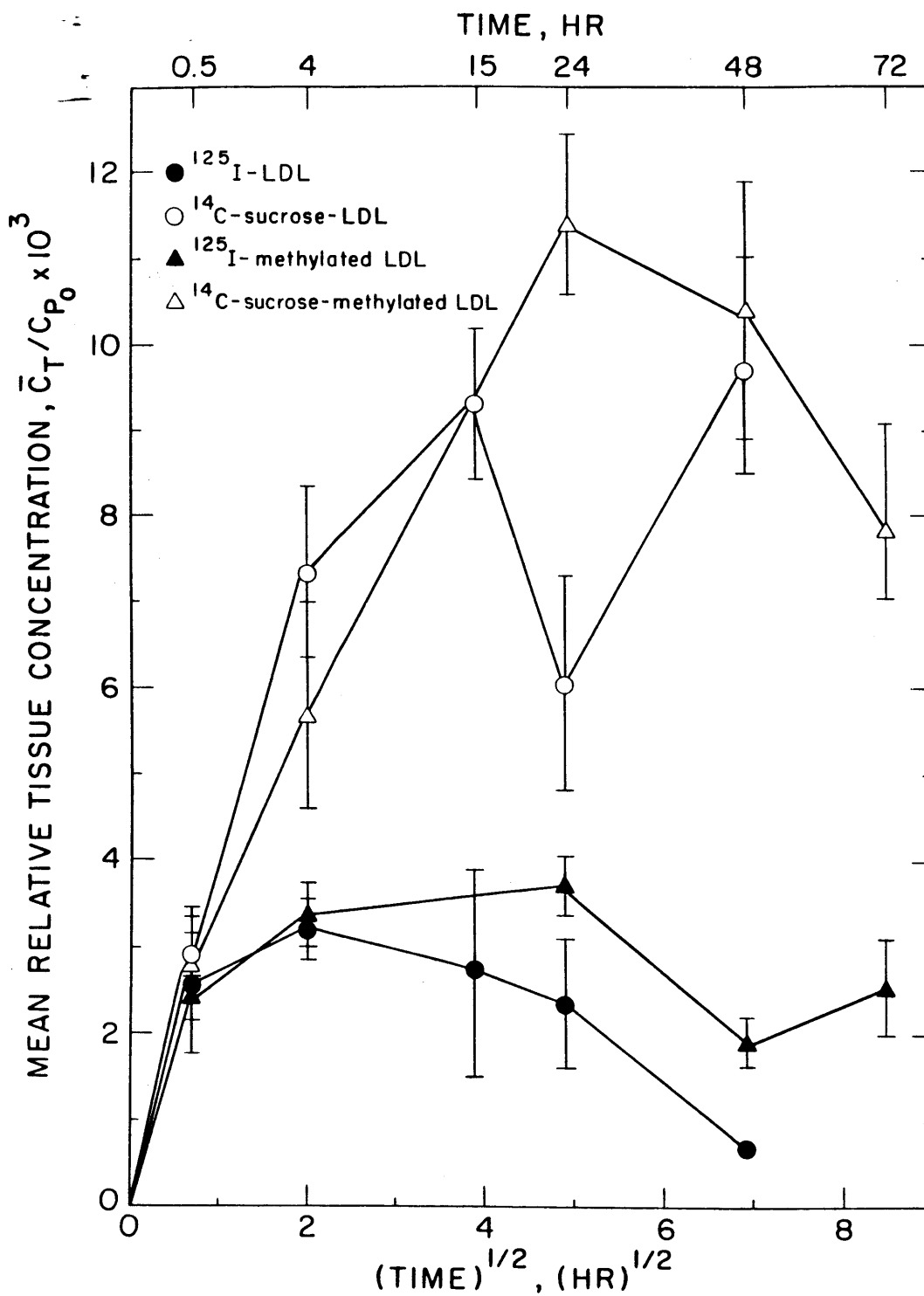


Figure 4-21: ^{125}I and ^{14}C -Sucrose Labeled LDL and mLDL Mean Relative Concentrations in the Rabbit Aorta

Table 4-VII: Comparison of Mean Relative ^{125}I Tissue Concentrations

t, hr	This Study $\bar{\theta}_T \times 10^3$	N		Navarro [1984] $\bar{\theta}_T \times 10^3$	N
LDL					
0.5	2.10 ± 0.37	3	$p > 0.20$	2.56 ± 0.63	2
4.0	5.18 ± 2.42	5	$p > 0.10$	3.19 ± 0.72	4
24	3.94 ± 3.14	4	$p > 0.20$	2.20 ± 1.17	3
mLDL					
0.5	2.31 ± 0.29	2	$p > 0.50$	2.40 ± 0.50	2
4.0	4.24 ± 1.47	4	$p > 0.20$	3.37 ± 0.75	2
24	2.47 ± 0.90	4	$p > 0.50$	3.70 ± 0.60	3
72	0.70 ± 0.04	2	$p < 0.02$	2.54	1

Mean relative ^{14}C -sucrose labeled LDL and mLDL concentrations are very similar at 0.5, 4, and 48 h. Mean relative concentrations of all solute-tracer combinations are statistically indistinct at 0.5 hr, suggesting that, although LDL may have entered the cells of the vessel wall, degradation has not occurred. This is in accord with results presented in Chapter 2 with cultured cells, in which there is a 15 to 30 min lag time before degradation occurs. In vivo, mass transfer resistances offered by transendothelial transport and medial diffusion should lengthen this lag time. ^{14}C -sucrose-LDL and ^{125}I -LDL are significantly different at four hr ($p < 0.02$), whereas ^{14}C -sucrose-mLDL and ^{125}I -mLDL concentrations do not differ significantly until 24 hr. The difference between ^{14}C -sucrose and ^{125}I concentrations increases with circulation time. This is consistent with the accumulation of ^{14}C -sucrose-labeled degradation products within the cell. The decrease in the mean relative concentration of ^{14}C -sucrose-mLDL between 48 and 72 hr probably reflects animal to animal variability.

The above data permit direct evaluation of LDL degradation. The tissue concentration of ^{14}C at time t , C_{T+d} , represents the sum of the concentrations of undegraded (C_T) and degraded protein (C_d):

$$(C_{T+d})_{14C} = (C_T)_{14C} + (C_d)_{14C} \quad (4-5)$$

where $(C_{T+d})_{14C}$, $(C_T)_{14C}$, and $(C_d)_{14C}$ are in units of dpm/cm^3 tissue. $(C_T)_{14C}$ refers to the concentration of intact undegraded protein in the interstitial fluid, bound to the extracellular matrix, and cell associated.

Protein-bound ^{125}I , denoted by $(C_T)_{125I}$ with units of dpm/cm^3 , also represents undegraded solute in all forms. For the experimental conditions used in the study of Navarro [1984] and presented in Figure 4-21, the specific activities of ^{125}I and ^{14}C -sucrose labeled lipoproteins were different and different activities of ^{125}I - and ^{14}C -sucrose-labeled lipoproteins were injected into the rabbits. Consequently, $(C_T)_{14C}$ is not equal to $(C_T)_{125I}$. ^{125}I - and ^{14}C -sucrose-labeled LDL and mLDL behave as tracers in the arterial wall, and the relative concentrations of ^{14}C and ^{125}I in the tissue are related by:

$$(C_T)_{14C} = (C_{p_o})_{14C} \left[\frac{C_T}{C_{p_o}} \right]_{125I} \quad (4-6)$$

Substitution of equation (4-6) into equation (4-5) yields:

$$(C_{T+d})_{14C} = (C_{p_o})_{14C} \left[\frac{C_T}{C_{p_o}} \right]_{125I} + (C_d)_{14C} \quad (4-7)$$

By division of equation (4-7) by $(C_{p_o})_{14C}$ and rearrangement, a relation for C_d is obtained:

$$\left[\frac{C_d}{C_{p_o}} \right]_{14C} = \left[\frac{C_{T+d}}{C_{p_o}} \right]_{14C} - \left[\frac{C_T}{C_{p_o}} \right]_{125I} \quad (4-8)$$

Thus, $(C_d/C_{p_o})_{^{14}\text{C}}$ represents the relative amount of ^{14}C -sucrose-labeled LDL (or mLDL) which has been degraded. In the presentation to follow, the subscript ^{14}C is dropped, and it is understood that C_d/C_{p_o} refers to the relative concentration of degraded ^{14}C -sucrose-labeled lipoproteins. Equations (4-5) through (4-8) are equally valid for the tissue concentration at a point or the mean relative tissue concentration. For purposes of distinction, mean relative concentrations are denoted with an overbar.

Also of interest is the rate of degradation which is simply the derivative with respect to time of the cumulative amount degraded:

$$r_d = \frac{dC_d}{dt} \quad (4-9a)$$

The rate in equation (4-9a) is expressed in units of $\text{dpm}/(\text{cm}^3 \cdot \text{hr})$. Alternatively, equation (4-9a) can be expressed in terms of the dimensionless concentration of degraded protein:

$$R_d = \frac{dC_d/C_{p_o}}{dt} \quad (4-9b)$$

For each animal, mean relative tissue concentrations of ^{125}I and ^{14}C were measured from which C_d/C_{p_o} was calculated. Calculation of C_d/C_{p_o} for each animal cancels out animal to animal variability in ^{125}I and ^{14}C tissue concentrations, and there is a single error due just to the animal to animal variability in C_d/C_{p_o} . Alternatively, ^{125}I and ^{14}C tissue concentrations for a given lipoprotein at a given time could be averaged and then C_d/C_{p_o} calculated. The two methods yield the same average value for C_d/C_{p_o} , but the error associated with the estimate calculated from the animal averages contains errors associated with animal to animal variability for ^{125}I and ^{14}C mean relative concentrations and this error is

larger than the error associated with C_d/C_{p_0} calculated for each animal. Data for protein-bound ^{125}I tissue concentrations and cumulative degradation are summarized in Figure 4-22. (The smooth curves in Figure 4-22 are discussed below). Error bars are equal to the standard error of the mean. Cumulative degradation represents the average of C_d/C_{p_0} calculated for individual animals at each time. (Note that since mean relative concentrations obtained by frozen serial section microtomy were not used to calculate cumulative degradation, the deviant profiles at 4 and 24 hr have no effect upon degradation.) The mean relative tissue concentration of ^{125}I -labeled protein represents the average from all experiments (i.e., those of this study and Navarro [1984]). At all times, both quantities are similar for LDL and mLDL. At 0.5 hr, degradation is negligible. Cumulative degradation increases rapidly between 4 and 24 hr and reaches a plateau between 24 and 48 hr.

Of particular interest is when degradation becomes statistically significant. Analysis of variance for LDL and mLDL indicated that there are significant differences among the dimensionless concentrations as a function of time, $p < 0.001$ for LDL and $p < 0.003$ for mLDL. The pooled estimate of the variance (σ_p) obtained from the analysis of variance was used to calculate a t statistic for each concentration, $t = \frac{C_d/C_{p_0}}{\sigma_p}$, from which the hypothesis that the concentrations are different than zero was tested (H. Chernoff, MIT Statistics Center, personal communication). LDL degradation becomes statistically significant at 4 hr whereas mLDL degradation does not become significant until 24 hr.

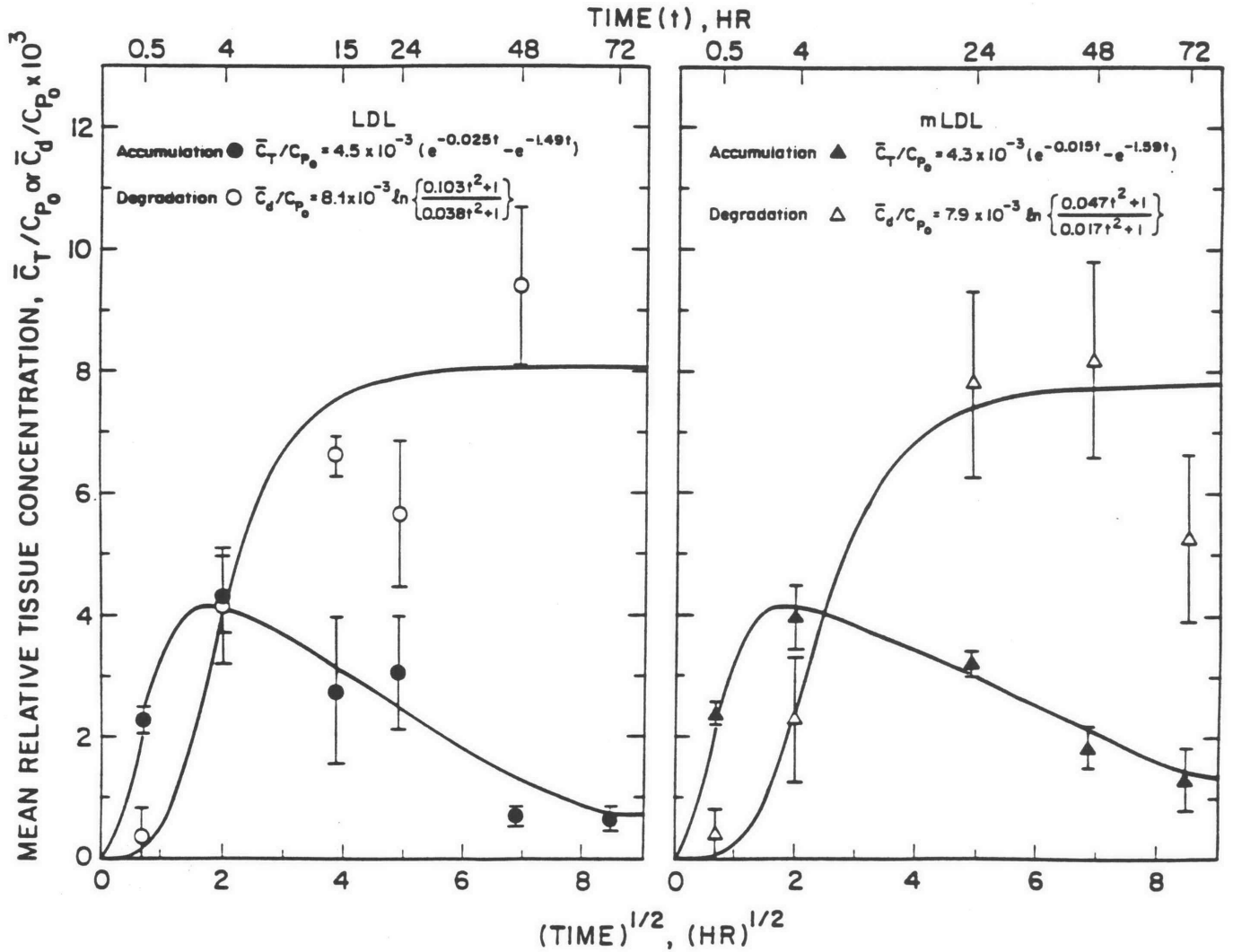


Figure 4-22: LDL and mLDL tissue concentrations and cumulative degradation in the rabbit aorta. Open symbols refer to the mean relative concentration of degradation products calculated according to equation (4-8) using data of Navarro [1984]; filled symbols represent mean relative ¹²⁵I-LDL and ¹²⁵I-mLDL tissue concentrations calculated from the data of this study and Navarro [1984].

4.3.4 Steady State Tissue Concentration and Rate of Degradation in Response to a Step Input

Data presented for LDL and mLDL accumulation and degradation include effects associated with differences in the plasma decay of LDL and mLDL. In order to remove these effects and estimate the contribution of receptor-mediated and receptor-independent pathways, it is necessary to manipulate the data so that the results represent an idealized experiment in which the plasma concentrations of LDL and mLDL are the same. This is done by taking advantage of the linearity of tracer experiments.

For a linear system, the tissue concentration in response to a time varying plasma concentration can be determined from the convolution integral:

$$\theta_T(t) = \int_0^t H(\tau)\theta_p(t-\tau)d\tau \quad (4-10)$$

where $\theta_T(t)$ is the relative tissue concentration (C_T/C_{p_0}), $\theta_p(t)$ is the relative plasma concentration (C_p/C_{p_0}), and $H(t)$ is the relative tissue concentration in response to a Dirac delta function (instantaneous pulse). $\theta_T(t)$ can be either the transmural concentration at a given normalized position or the mean relative concentration (denoted by an overbar).

In order to compare tissue concentrations of radiolabeled LDL and mLDL in which the plasma decay curves are different, one would like to estimate the time-varying tissue concentration in response to either an impulse or step change in plasma concentration (Hildebrand [1976], pp. 53-92). Techniques for determination of the impulse response, known as numerical deconvolution, require repeated differentiation of data, an inaccurate procedure, especially for scattered data. An alternative approach is to determine the steady state tissue concentration in

response to a step change in plasma concentration. This is done by a second integration of the convolution integral to yield:

$$\psi_T(\infty) = FCR \int_0^{\infty} \theta_T(t) dt \quad (4-11)$$

where $\psi_T(\infty)$ is the mean relative steady state tissue concentration in response to a step change in plasma concentration and FCR is the fractional catabolic rate. Derivation of equation (4-11) is presented in Appendix C.

Cumulative degradation of LDL and mLDL can be corrected for differences in plasma decay in a manner similar to that for undegraded protein. The result is the steady state rate of degradation in response to a step change in plasma concentration:

$$r_d = C_d(\infty) FCR \quad (4-12a)$$

where C_d is the cumulative amount of ^{14}C -sucrose-labeled lipoprotein which has been degraded per cm^3 of tissue (dpm/cm^3). r_d has units of $\text{dpm}/(\text{cm}^3 \cdot \text{hr})$. In terms of the relative concentration of degraded protein defined in equation (4-8), equation (4-12a) becomes:

$$R_d = \theta_d(\infty) FCR \quad (4-12b)$$

where $\theta_d(\infty)$ is the normalized cumulative degradation at long times defined in equation (4-8).

In order to facilitate application of equations (4-11) and (4-12a,b) to the data, the following functions were assumed for $\theta_T(t)$ and $\theta_d(t)$:

$$\bar{\theta}_T(t) = \alpha(e^{-\beta_1 t} - e^{-\beta_2 t}) \quad (4-13)$$

$$\bar{\theta}_d(t) = a \ln \left[\frac{edt^2 + 1}{dt^2 + 1} \right] \quad (4-14)$$

where α , β_1 , β_2 , a , and d are empirical constants determined by nonlinear regression of data and e is 2.7183.

These functions are the simplest ones which mimic the general behavior of the data. Equation (4-13) is zero at $t=0$ and $t=\infty$, and there is a single maximum at $\ln(\beta_2/\beta_1)/(\beta_2-\beta_1)$. Equation (4-14) has an initial slope of zero (indicating an initial rate of degradation of zero) and reaches an asymptote at long times which is equal to parameter a . The parameters in equations (4-13) and (4-14) were obtained by nonlinear regression of data (Marquardt [1963]) and the best fit parameters along with the resulting curves are presented in Figure 4-22. The steady state mean relative concentrations and rates of degradation in response to a step change in plasma concentration were determined from the best fits of data and are presented in Table 4-VIII.

For pooled data with and without aberrant profiles, the steady state mean relative concentration of LDL is twice as large as the value for mLDL Navarro's data, however, indicates that there is essentially no difference between $\bar{\psi}_T(\infty)$ for LDL and mLDL. This is largely due to the high mLDL tissue concentration at 72 hr which results in the slow decay of $\bar{\theta}_T$ and an increased value of $\bar{\psi}_T(\infty)$. Excluding the 72 hr data point results in $\bar{\psi}_T(\infty)$ equal to 0.012 ± 0.007 . The steady state rate of degradation of LDL is about three times larger than the value for mLDL even though the cumulative amounts degraded are similar. The difference in the steady state estimates arises from differences in the fractional catabolic rate. The steady state rate of LDL degradation in response to a step change in plasma concentration

Table 4-VIII: Steady State Tissue Concentration and Rate of Degradation in Response to a Step Change in Plasma Concentration

		LDL	mLDL
Steady State Tissue Concentration			
Pooled Data	$\bar{\psi}_T(\infty)$	0.020 ± 0.008	0.010 ± 0.003
without 4C6 and 24C1	$\bar{\psi}_T(\infty)$	0.018 ± 0.007	
Navarro [1984]	$\bar{\psi}_T(\infty)$	0.017 ± 0.005	0.015 ± 0.008
Steady State Rate of Degradation			
	$R_d, \text{hr}^{-1} \times 10^4$	9.2 ± 1.6	2.8 ± 0.4
Fractional Catabolic Rate			
	FCR, hr^{-1}	0.11 ± 0.02	0.036 ± 0.004
Cumulative Relative Degradation			
	$\bar{\theta}_d(\infty) \times 10^3$	8.1 ± 0.8	7.9 ± 0.9

is the sum of the steady state rates of receptor-mediated and receptor-independent degradation.

The steady state rate of LDL degradation in response to a step change in plasma concentration is the sum of the rates of receptor-mediated, R_{dRM} , and receptor-independent, R_{dRI} , degradation:

$$R_d = R_{dRM} + R_{dRI} \quad (4-15a)$$

Pittman and colleagues (Pittman et al. [1979b, 1982a,b], Carew et al. [1984]) have assumed that the rate of mLDL degradation per cm^3 tissue represents the receptor-independent contribution:

$$R_{dRI} = (R_d)_{mLDL} \quad (4-15b)$$

Assuming that equation (4-15b) is valid, substitution of equation (4-15b) into (4-15a) and rearrangement yields:

$$\frac{R_{dRM}}{(R_d)_{LDL}} = \frac{(R_d)_{LDL} - (R_d)_{mLDL}}{(R_d)_{LDL}} \quad (4-15c)$$

where $R_d = (R_d)_{LDL}$. Applying equation (4-15c) to the results presented in Table 4-VIII indicates that about 67% of LDL degradation in the arterial wall is by receptor-independent mechanisms. The validity of the assumption used to derive equation (4-15c) is examined in Chapter 5.

The use of other functions to fit data for $\bar{\theta}_T$ and $\bar{\theta}_d$ was investigated. For $\bar{\theta}_T$, data in Figure 4-22 were fit to the following four parameter model (equation (4-16)) by nonlinear regression:

$$\bar{\theta}_T = \alpha_1 e^{-\beta_1 t} - \alpha_2 e^{-\beta_2 t} \quad (4-16)$$

which resulted in the following parameters:

	$\alpha_1 \times 10^3$	$\alpha_2 \times 10^3$	β_1, hr^{-1}	β_2, hr^{-1}
LDL	7.4 ± 6.1	5.6 ± 5.9	0.039 ± 0.030	0.25 ± 0.30
mLDL	5.2 ± 1.1	3.3 ± 1.2	0.020 ± 0.006	0.35 ± 0.24

Although these parameter values yield excellent fits of data, the initial concentration, which is equal to $\alpha_1 - \alpha_2$, is nonzero which is not physically reasonable. Consequently, this model was not used to calculate $\bar{\psi}_T$. If, however, the point (0,0) is included with the data, then the fitted values of α_1 and α_2 are the same and equal to a , and β_1 and β_2 are equal to the values obtained using equation (4-13).

For $\bar{\theta}_d$, two other models were examined:

$$\bar{\theta}_d = a \tanh(bt) \quad (4-17a)$$

$$\bar{\theta}_d = \frac{dt}{b+t} \quad (4-17b)$$

Fits of $\bar{\theta}_d$ using equations (4-14), (4-17a), and (4-17b) are similar (Figure 4-23) although equation (4-17b) yields higher estimates of $\bar{\theta}_d(\infty)$ and R_d (Table 4-IX). Derivatives of equations (4-17a) and (4-17b) are nonzero at t equal to zero, and these equations cannot be used to estimate the rate of degradation as a function of time.

Table 4-IX: Comparison of Estimated Values of $\bar{\theta}_d(\infty)$ and R_d for Various Functions

Molecule	Function	$\bar{\theta}_d(\infty)$	$R_d, \text{hr}^{-1} \times 10^4$
LDL	eqn. (4-14)	8.1 ± 0.8	9.2 ± 1.6
	eqn. (4-17a)	8.0 ± 0.8	9.0 ± 1.5
	eqn. (4-17b)	9.5 ± 1.3	10.8 ± 2.1
mLDL	eqn. (4-14)	7.9 ± 0.9	2.8 ± 0.4
	eqn. (4-17a)	7.7 ± 0.8	2.8 ± 0.5
	eqn. (4-17b)	9.0 ± 1.7	3.3 ± 0.8

Equation (4-13) was applied to the mean relative tissue concentrations obtained by frozen serial section microtomy (Figure 4-20). The best fits of equation (4-13) to these data are presented in Figure 4-24 and the best fit parameters are listed in Table 4-X along with the fractional catabolic rate and steady state tissue concentration in response to a step change in concentration. The steady state tissue concentration of LDL is 3.5 times larger than the value for mLDL, which is larger than the ratio of 2.0 obtained using combined data from this study and Navarro [1984] (Table 4-VIII).

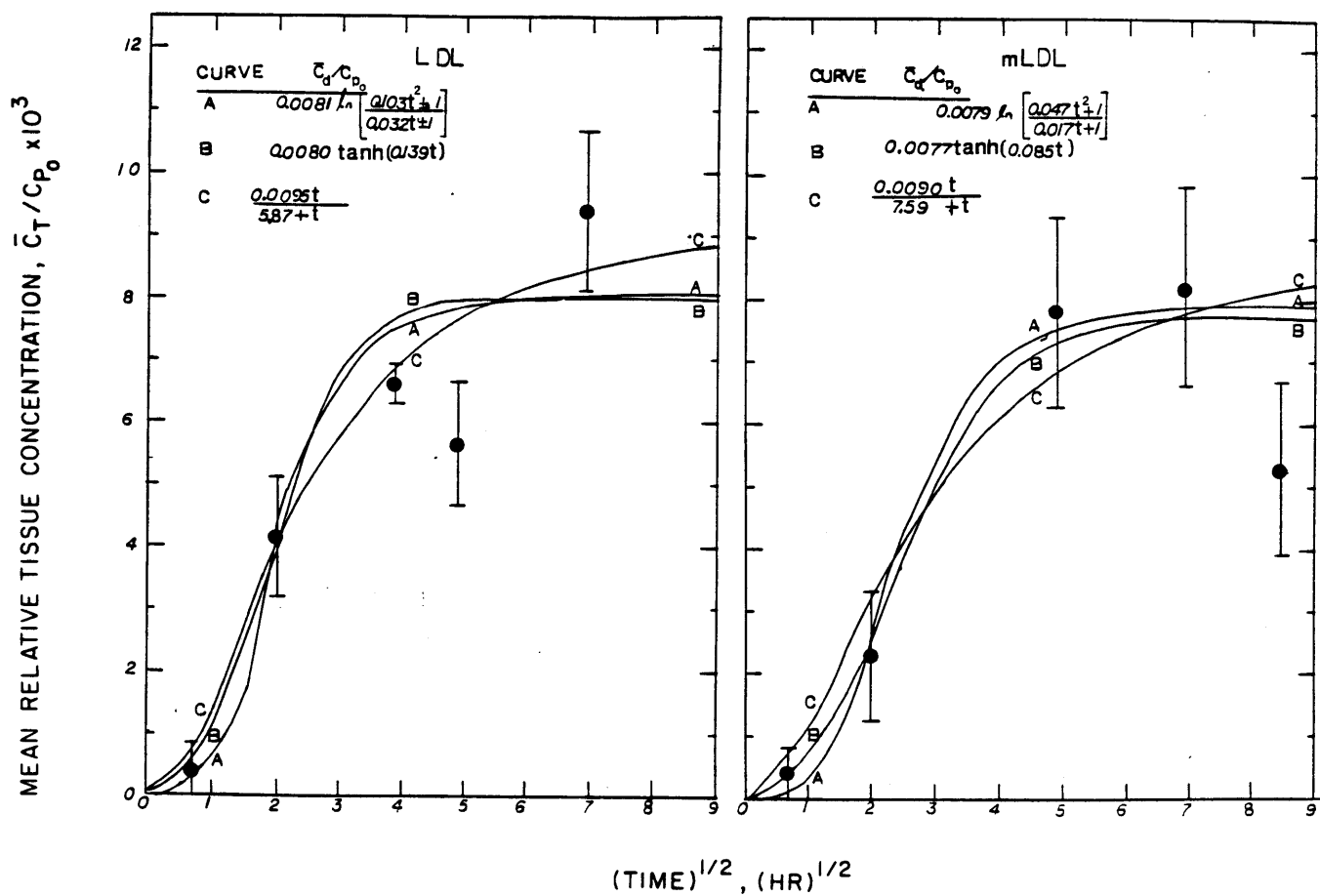


Figure 4-23: Comparison of Fits of Empirical Functions to Data for LDL Degradation.

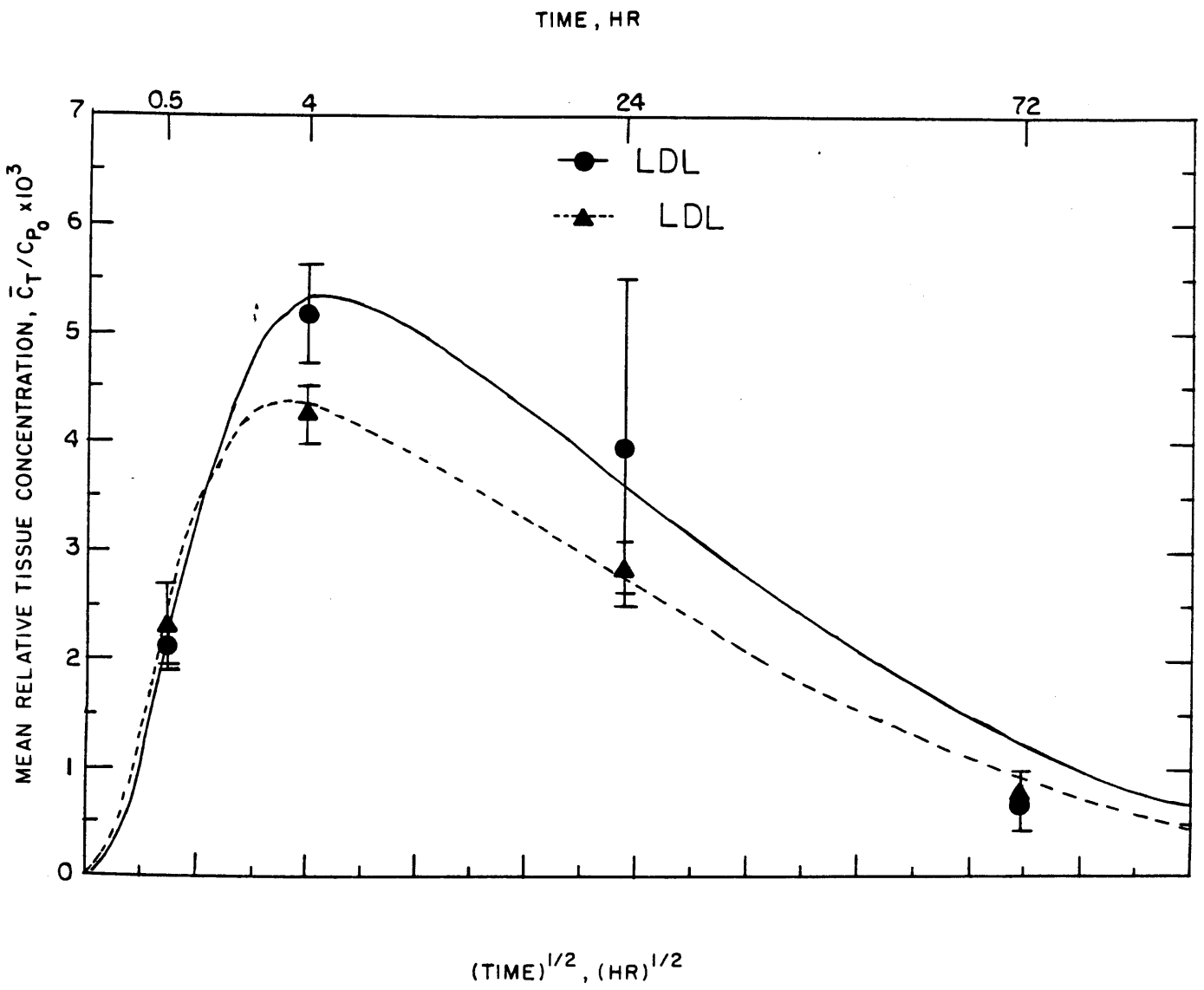


Figure 4-24: Best Fits of Equation (4-13) to Mean Relative Tissue Concentrations Obtained by Frozen Serial Section Microtomy.

Table 4-X: Steady State Tissue Concentration in Response to a Step Change in Plasma Concentration

		LDL	mLDL
Grand Average from Transmural Profiles			
Steady State Tissue Concentration	$\bar{\psi}_T(\infty)$	0.026 ± 0.020	0.0073 ± 0.0027
without 4C6 and 24C1	$\bar{\psi}_T(\infty)$	0.016 ± 0.006	
Fractional Catabolic Rate	FCR, hr^{-1}	0.096 ± 0.014	0.036 ± 0.004
Best Fit Parameters	$\alpha \times 10^3$	6.08 ± 1.76	4.73 ± 0.57
without 4C6 and 24C1		4.72 ± 0.53	
of Equation (4-13)	β_1, hr^{-1}	0.022 ± 0.015	0.023 ± 0.007
without 4C6 and 24C1		0.028 ± 0.008	
	β_2, hr^{-1}	0.82 ± 0.79	1.38 ± 0.59
without 4C6 and 24C1		1.23 ± 0.40	

Fits of the mean relative tissue concentrations for pooled data, Navarro's data and values obtained from transmural profiles are compared in Figure 4-25. The fits are qualitatively similar for LDL, but the pooled data (curve C) leads to lower estimates of the tissue concentrations than those calculated from the mean relative concentrations obtained from all of the transmural profiles (curve A) and Navarro's data (curve E). Consequently, $\int_0^\infty \bar{\theta}_T(t) dt$ calculated from pooled data, curve C, (0.18) is less than the value obtained from mean relative concentrations determined from transmural profiles (0.26). When experiments 4C6 and 24C1 are excluded from the fitting (curves B and D), the fitted curves of the mean relative tissue concentrations are similar to curve C for pooled data. The fits for mLDL are much

closer, but at long times, the fits of pooled data (curve C) and Navarro's data (Curve E) yield higher concentrations than curve A obtained from data in Figure (4-24).

The difference between LDL and mLDL concentrations can also be demonstrated in the transmural profiles at steady state following a step change in plasma concentration (Figure 4-26), which were calculated by application of equation (4-11) to the best fit of equation (4-13) to data at each value of the normalized depth (Figure 4-18). (Fits at each dimensionless depth are presented in Appendix G.) At comparable values of normalized depth, the LDL concentration is two to four times larger than the value for mLDL ($p > 0.02$). The rate of LDL degradation is three times greater than the rate of mLDL degradation (Table 4-VIII). Consequently, LDL tissue concentrations should be less than those for mLDL, unless binding to the cell membrane or intracellular accumulation is greater for LDL than mLDL. Thus, differences in the steady state concentrations presumably reflect differences in the cellular accumulation of LDL and mLDL.

The steady state LDL transmural profile in response to a step change in plasma concentration was calculated without experiments 4C6 and 24C1 and the results are plotted in Figure 4-27 along with the profile obtained using all transmural profiles. The gradient at $x = 0$ is similar for both profiles, although the concentration at the intimal surface is lower when calculated without experiments 4C6 and 24C1. Excluding the two aberrant profiles leads to lower mid-medial concentrations and a steeper gradient near the medial-adventitial interface.

The estimated transmural profiles of LDL and mLDL at steady state following a step change in plasma concentration are concave, suggesting mass transfer limitations. The steady state rate of LDL degradation is greater than the value for mLDL which indicates that any mass transfer limitations would be more significant

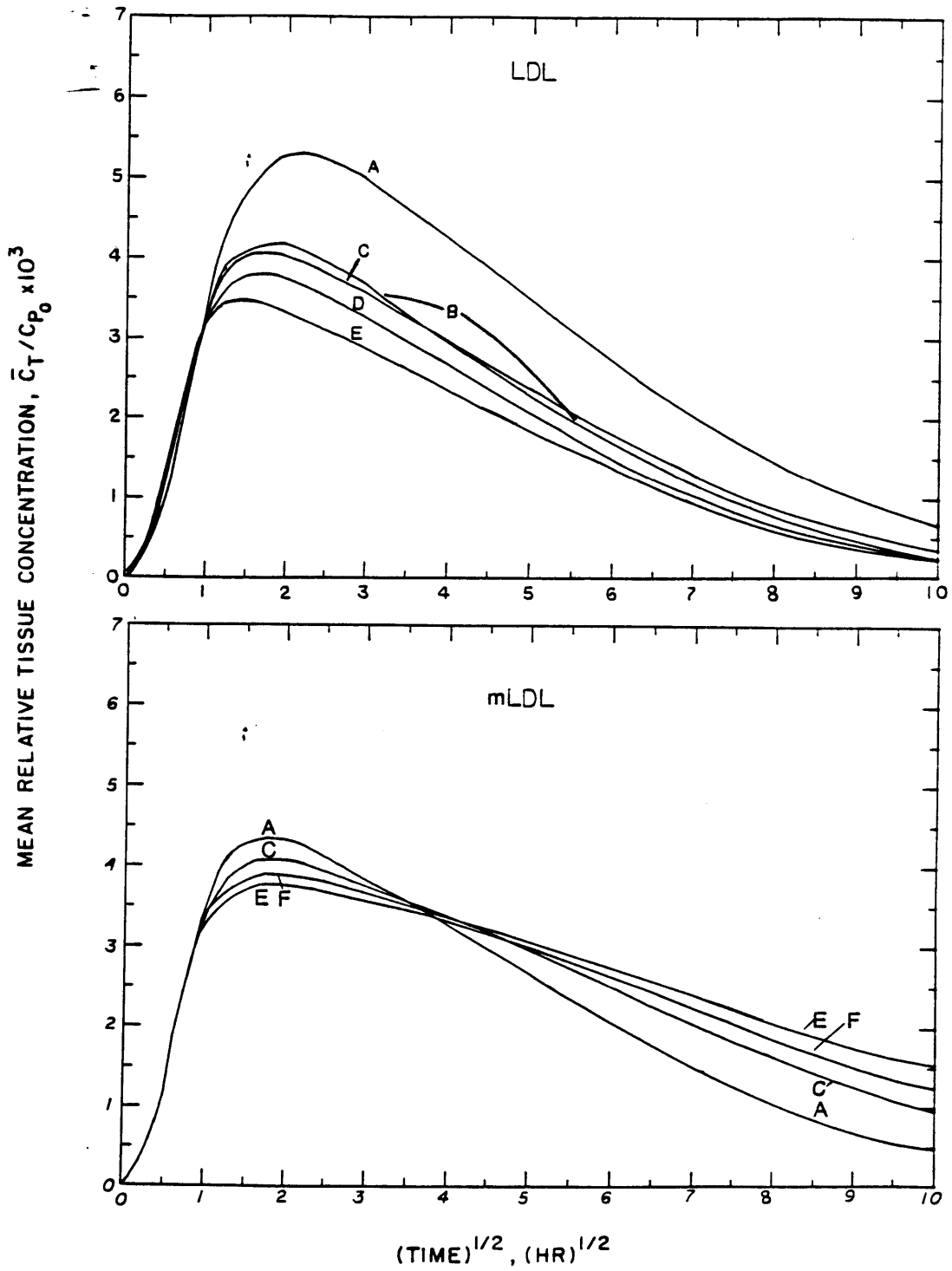


Figure 4-25: Comparison of fits of mean relative concentrations: A. all transmural profiles (Figure 4-24); B. transmural profiles without 4C6 and 24C1; C. pooled data from this study and Navarro [1984]; D. pooled data without experiments 4C6 and 24C1; E. Navarro [1984].

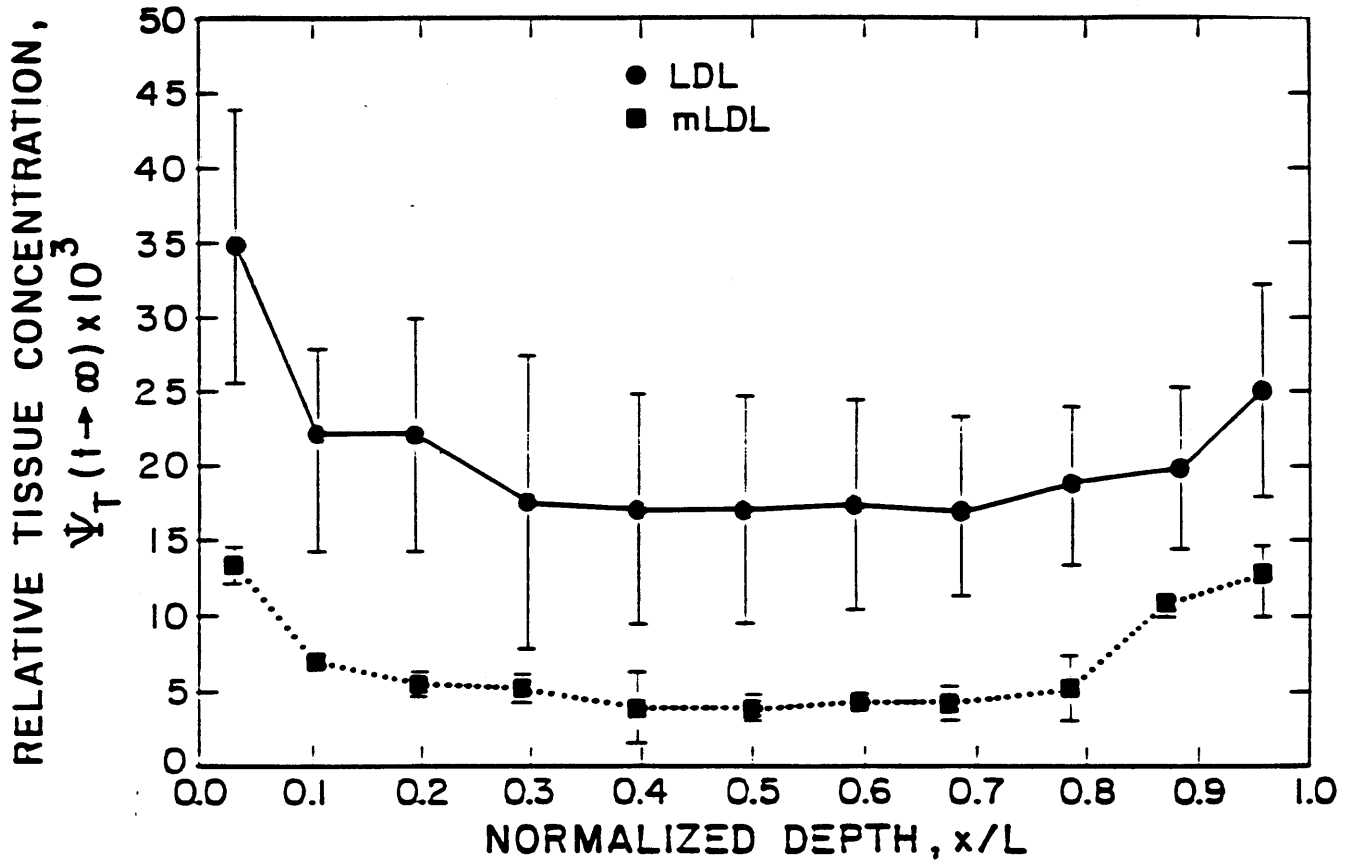


Figure 4-26: Transmural Profiles of LDL (●) and mLDL (■) at Steady State Following a Step Change in Plasma Concentration. At each normalized depth data were fit to equation (4-13) from which $\Psi_T(\eta, \infty)$ was determined.

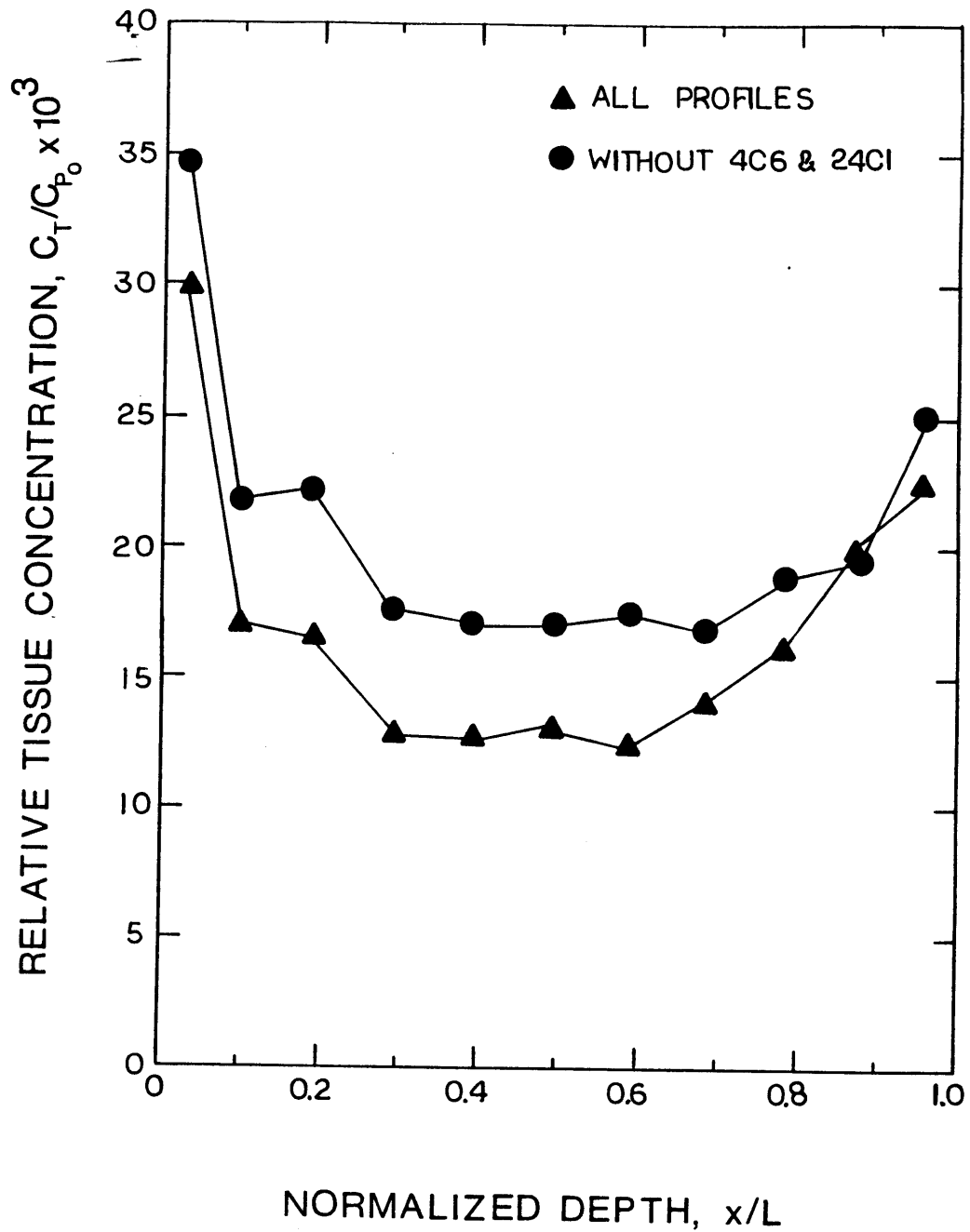


Figure 4-27: Transmurial Profiles of LDL at Steady State Following a Step Change in Plasma Concentration. Profiles were calculated with (●) and without (▲) experiments 4C6 and 24C1.

for LDL than mLDL. Although LDL concentration gradients at the intima and medial-adventitial interface are steeper than those for mLDL (dimensionless gradients for LDL are -0.182 and 0.070 at $x/L = 0$ and 1, respectively, and dimensionless gradients for mLDL are -0.088 and 0.021 at $x/L = 0$ and 1, respectively, the gradient of LDL concentrations flattens out in mid-media at a concentration about four times greater than the mLDL concentration. This behavior is not expected when degradation is more significant for LDL than mLDL, and mass transfer limitations are present. Rather one would expect to observe a continuously decreasing gradient over the inner media. (The profile calculated without experiments 4C6 and 24C1 is closer to the expected behavior.) This discrepancy between expected and observed behavior may be due to greater cellular accumulation of LDL than mLDL or to differences in the transport properties of the two lipoproteins.

4.3.5 Estimated Transendothelial Transport Mass Transfer Coefficients

The mass transfer coefficient (k_E) was estimated from ^{125}I -LDL and ^{125}I -mLDL data at 0.5 hr and ^{14}C -sucrose-LDL and ^{14}C -sucrose-mLDL data at all circulation times. The mass transfer coefficient is a lumped parameter accounting for transendothelial transport into the vessel wall from both the vessel lumen and the vasa vasorum.

Tissue concentrations of ^{14}C -sucrose, C_{T+d} , represent the sum of the concentrations of undegraded and degraded protein. Changes in tissue concentrations of ^{14}C -sucrose are a result of changes in the flux of the diffusing species, and a material balance on a tissue element yields (see Chapter 5):

$$\frac{\partial C_{T+d}}{\partial t} = \frac{\partial C_T}{\partial t} + \frac{\partial C_d}{\partial t} = -\frac{\partial N}{\partial x} \quad (4-18)$$

where C_T and C_d represent the tissue concentration of undegraded and degraded ^{14}C -sucrose-labeled solutes and N is the solute flux ($\text{dpm}/(\text{cm}^2 \cdot \text{s})$). C_T can be expressed in terms of ^{125}I -labeled proteins by use of equation (4-6). Equation (4-18) states that the time rate of change of uptake is equal to the negative of the gradient of the flux.

Integration of equation (4-18) from x equals 0 to L yields:

$$\frac{d\bar{C}_{T+d}}{dt} = -\frac{1}{L}(N|_{x=L} - N|_{x=0}) \quad (4-19)$$

The solute fluxes at $x=0$ and $x=L$ are (see Chapter 5):

$$N|_{x=0} = k_{E_1} \left(C_p - \frac{C_f}{\epsilon_f} \right) \quad (4-20a)$$

$$N|_{x=L} = -k_{E_2} \left(C_p - \frac{C_f}{\epsilon_f} \right) \quad (4-20b)$$

where k_{E_1} and k_{E_2} are mass transfer coefficients (cm/s) for transport across intimal endothelial cells and the medial-adventitial interface, respectively, and ϵ_f is the volume fraction of interstitial fluid accessible to solute. The fluxes in equations (4-18) to (4-20a,b) are based upon the luminal surface area. At the medial-adventitial interface transport is across the vasa vasorum, the surface area of which is unknown. Hence, k_{E_2} is the product of a true mass transfer coefficient and the ratio of the surface area of the vasa vasorum to surface area of the vessel lumen. Substitution of equations (4-20a) and (4-20b) into (4-19) yields:

$$\frac{d\bar{C}_{T+d}}{dt} = \frac{k_{E_2}}{L} \left(C_p - \frac{C_f(x=L)}{\epsilon_f} \right) + \frac{k_{E_1}}{L} \left(C_p - \frac{C_f(x=0)}{\epsilon_f} \right) \quad (4-21)$$

Inspection of Figures 4-5 and 4-18 indicates that the tissue concentration is generally less than the plasma concentration. Therefore, a reasonable assumption is

that $\frac{C_f}{\epsilon_f} \ll C_p$ and equation (4-21) reduces to:

$$\frac{d\bar{C}_{T+d}}{dt} = \frac{1}{L}(k_{E_1} + k_{E_2})C_p = \frac{k_E}{L}C_p \quad (4-22)$$

where k_E is the lumped mass transfer coefficient.

For short circulation times (e.g. 0.5 hr) there is little degradation and \bar{C}_{T+d} is approximately equal to \bar{C}_T and equation (4-22) reduces to:

$$\frac{d\bar{C}_T}{dt} = \frac{k_E}{L}C_p \quad (4-23)$$

If C_p is assumed to be constant for the initial 0.5 hr of the experiment, then integration of equation (4-23) yields:

$$k_E \approx \frac{\bar{C}_T L}{C_{p_0} t} \quad (4-24a)$$

The tissue thickness L is equal to the ratio of the tissue volume, V , to the luminal area, A , and k_E can also be written as:

$$k_E \approx \frac{\bar{C}_T V}{C_{p_0} t A} \quad (4-24b)$$

The mass transfer coefficient used in equations (4-20) to (4-24) is identical to the mass transfer coefficient defined by Bratzler et al. [1977a,b]. Note that the derivation of equations (4-24a,b) embodies two assumptions: 1) $C_d \ll C_T$ and 2) $C_p \approx C_{p_0}$.

The mass transfer coefficient for ^{125}I -labeled lipoproteins at a circulation time of 0.5 hr was estimated from the mean relative tissue concentrations obtained in this study, the results of Navarro [1984], and the combined results presented in Figure 4-22. Measured tissue thicknesses from frozen serial section microtomy were converted to in vivo dimensions by dividing by 1.72 ± 0.15 (Schneiderman et al.

[1983]). For transmural profiles, estimated in vivo thicknesses of $138 \pm 15 \mu\text{m}$ and $113 \pm 14 \mu\text{m}$ were used for LDL and mLDL, respectively. Tissue thicknesses were not measured in the study of Navarro [1984]. As a result, the mass transfer coefficient was estimated from Navarro's data and pooled data using a thickness of $130 \mu\text{m}$ calculated from the average of all transmural profiles. The results are presented in Table 4-XI. All three sets of data yield similar estimates. The mass transfer coefficients of LDL and mLDL are virtually identical, implying that transendothelial transport is by receptor-independent processes.

Table 4-XI: Mass Transfer Coefficients for LDL and mLDL
at 0.5 hr

		$k_E, \text{cm/s} \times 10^8$
This Study	LDL	1.51 ± 0.33
	mLDL	1.45 ± 0.22
Navarro [1984]	LDL	1.86 ± 0.35
	mLDL	1.83 ± 0.49
Combined Data	LDL	1.67 ± 0.37
	mLDL	1.68 ± 0.30

The mass transfer coefficients obtained from the combined data are compared with those of others for circulation times less than one hour (Table 4-XII). Except for the data of Ghosh et al. [1976], all values are from in vivo experiments. The mass transfer coefficient for LDL obtained in this study is similar to the values of Bratzler et al. [1977b] and Carew et al. [1984], but are about five times smaller than the value of Ghosh et al. [1976] and twice as large as the estimates obtained by Wiklund et al. [1985] and whole sample data of Morrel [1983], and Schnitzer [1983].

⁴ Results obtained with rabbit LDL (Carew et al. [1984], Wiklund et al. [1985]) are similar to those obtained with human LDL.

The relative contributions of luminal endothelium to the overall mass transfer coefficient was determined by calculating the mean relative concentration at 0.5 hr for normalized depths between 0.0 and 0.5 from grand average profiles presented in Figure 4-18. The mean relative concentrations in the inner media are $1.32 \pm 0.27 \times 10^{-3}$ for LDL and $1.58 \pm 0.22 \times 10^{-3}$ for mLDL which are 63% and 68%, respectively, of the mean relative concentrations for the entire tissue. Using these values, the mass transfer coefficients for the luminal endothelium are $0.95 \pm 0.21 \times 10^{-8}$ cm/s for LDL and $0.99 \pm 0.19 \times 10^{-8}$ cm/s for mLDL. The similarity in the values of the luminal mass transfer coefficients for LDL and mLDL strongly suggests that transport across the luminal endothelium is by receptor-independent mechanisms.

For circulation times longer than 0.5 hr, ¹²⁵I-labeled proteins are degraded and tissue concentrations of ¹²⁵I do not represent accumulation. Thus, protein-bound ¹²⁵I cannot be used to estimate the mass transfer coefficient at longer circulation times. k_E can be estimated from data by using the integrated form of equation (4-22) only when k_e is constant with time. Otherwise, a generalized mass transfer coefficient, k_E' , can be defined such that:

⁴Estimates from Morrel [1983] and Schnitzer [1983] are averages from whole sample gamma counting (see legend of Table 4-XII). As noted in Chapter 1 (Section 1.5.2) the arterial wall consists of focal regions of high permeability. These regions occupy from 1% to 5% of the luminal surface area (Morrel [1983]). The mass transfer coefficients presented in Table 4-XII are whole sample averages which represent average values for high and low permeability regions. Tompkins [1983] found that low permeability regions have mass transfer coefficients of about 1.7×10^{-9} cm/s (range: $0.9-3.0 \times 10^{-9}$ cm/s), whereas high permeability regions have mass transfer coefficients of $60 \pm 120 \times 10^{-9}$ cm/s with values as high as 600×10^{-9} cm/s.

Table 4-XII: Comparison of Mass Transfer Coefficients in the Rabbit Arterial Wall Estimated for Short Circulation Times

Reference	Molecule	Time, hr	k_E , cm/s x 10^8
Ghosh et al. [1976]	LDL	1.0	5.70
Bratzler et al. [1977b]	LDL	0.167	3.60 ¹
		0.50	2.74 ¹
Carew et al. [1984]	LDL	1.0	1.95
Morrel [1983]	LDL	0.5	0.88 ± 0.20^2
Schnitzer [1983]	LDL	0.5	0.86 ± 0.28^3
Wiklund et al. [1985]	LDL	0.5	0.72 ± 0.20
		1.0	0.66 ± 0.34
	mLDL	0.5	0.75 ± 0.12
		1.0	0.69 ± 0.37
This Study	LDL	0.5	1.67 ± 0.37
	mLDL	0.5	1.68 ± 0.30

- ¹ Estimates of L in vivo were 98 and 105 μm at 0.167 and 0.5 hr, respectively
- ² Mean relative tissue concentration calculated from whole sample counting (Table 4 of Morrel [1983]). A value of L = 130 μm , the average thickness calculated from all frozen serial section microtomy experiments, was used.
- ³ Mean relative tissue concentration calculated from whole sample counting (Table V-10 of Schnitzer [1983]). A value of L = 138 μm was used based upon average value calculated by Schnitzer [1983] for perfused-fixed tissue.

$$k_E' = L \frac{\overline{C}_{T+d}/C_{p_0} \text{ }^{14}\text{C}}{\int_0^t C_p/C_{p_0} d\tau} = \frac{\overline{C}_{T+d}}{\int_0^t C_p d\tau} \quad (4-25)$$

k_E' is a weighted mass transfer coefficient. If k_E is constant then k_E is equal to k_E' .

Equation (4-25) was applied to raw data for ^{14}C -sucrose uptake and k_E' was determined. Results are plotted in Figure 4-28. The mass transfer coefficient is not constant with time, but decreases with increasing time. Consequently, the values in Figure 4-28 represent the weighted mass transfer coefficient defined in equation (4-25). At 0.5 hr, the weighted mass transfer coefficients of LDL and mLDL are similar ($2.28 \pm 0.56 \times 10^{-8}$ cm/s for LDL vs. $2.06 \pm 0.56 \times 10^{-8}$ cm/s for mLDL), although the values are about 40% larger than estimates obtained using ^{125}I . The weighted mass transfer coefficient for LDL at 48 hr is 21% of its value at 0.5 hr, whereas the mass transfer coefficient for mLDL at 72 hr is 7% of its value at 0.5 hr.

The assumption that $\frac{C_f}{\epsilon_f} \ll C_p$ was examined by assuming that $C_f(x=0) = C_f(x=L) \approx \overline{C}_T$. With this assumption, equation (4-21) becomes:

$$\frac{d\overline{C}_{T+d}}{dt} = \frac{k_E}{L} \left(C_p - \frac{\overline{C}_T}{\epsilon_f} \right) \quad (4-26)$$

and

$$k_E' = L \frac{(\overline{C}_{T+d}/C_{p_0}) \text{ }^{14}\text{C}}{\int_0^t (C_p/C_{p_0} - C_T/\epsilon_f C_{p_0}) dt} \quad (4-27)$$

\overline{C}_T probably overestimates C_f since not all solute is in the interstitial fluid. \overline{C}_T was estimated from the analytical fits of the mean relative concentrations of LDL and mLDL presented in Figure 4-22. A value of ϵ_f equal to 0.17 was used (Bratzler and

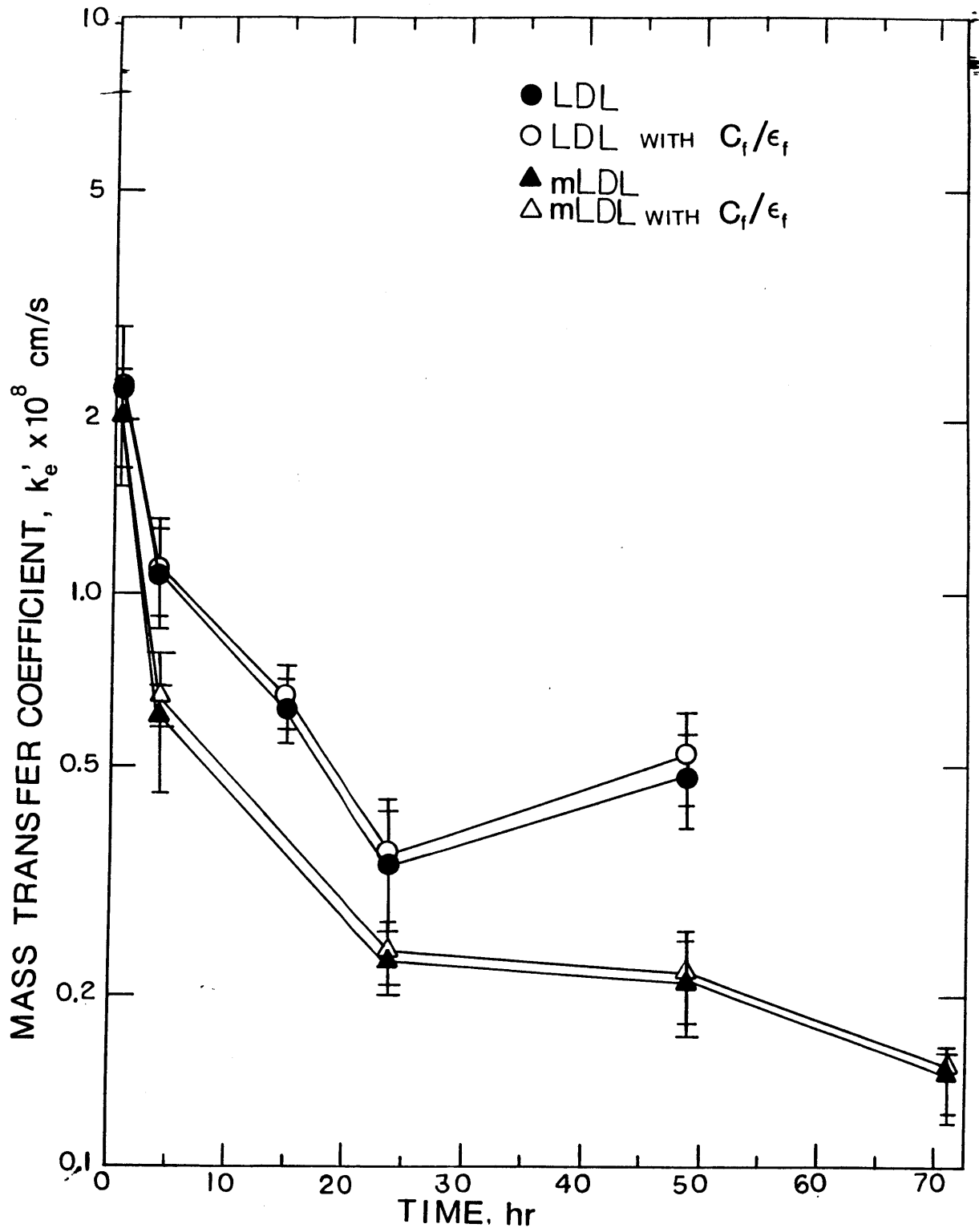


Figure 4-28: Weighted Mass Transfer Coefficient as a Function of Time

Schwarz [1977]).

Including this correction had little effect upon the estimates of k_E' (Figure 4-29). The largest increase in k_E' is 10% for LDL at 48 hr. Thus, the original assumption that $\frac{C_f}{\epsilon_f} \ll C_p$ appears to be reasonable.

Based upon the behavior of k_E' , the following function was assumed for k_E :

$$k_E = k_{E_0} [1 - f(1 - e^{-\gamma t})] \quad (4-28)$$

where k_{E_0} is the initial value of k_E , $k_{E_0}(1-f)$ is the asymptotic value of the mass transfer coefficient and γ is the time constant. Equations (4-27) and (4-1) (for C_p/C_{p_0}) were substituted into equation (4-21). Integration of the result from t equals 0 to t yields:

$$\left[\frac{\bar{C}_{T+d}}{C_{p_0}} \right]_{14C} = \frac{k_{E_0}}{L} (1-f) \sum_{i=1}^2 \frac{C_i}{b_i} (1 - e^{-b_i t}) + f \sum_{i=1}^2 \frac{C_i}{b_i + \gamma} (1 - e^{-(b_i + \gamma)t}) \quad (4-29)$$

Equation (4-29) was fit by nonlinear regression to data for mean relative tissue concentrations of ^{14}C -sucrose as a function of time, Figure 4-21. Fitted curves are presented in Figure 4-29. k_{E_0} , f , and γ are presented in Table 4-XIII, and equation (4-28) is displayed in Figure 4-30. Initially the mass transfer coefficients are almost identical, suggesting, that, at least initially, uptake is by receptor-independent processes. Comparison of estimated and predicted values of k_E' are presented in Figure 4-31.

Asymptotic values of the mass transfer coefficients for LDL and mLDL are 13.4% and 1.9%, respectively, of the initial values. The time constant for changes in the mass transfer coefficient of LDL is two times the value for mLDL.

k_E' was also estimated using the fitted functions for \bar{C}_T/C_{p_0} and \bar{C}_d/C_{p_0} ,

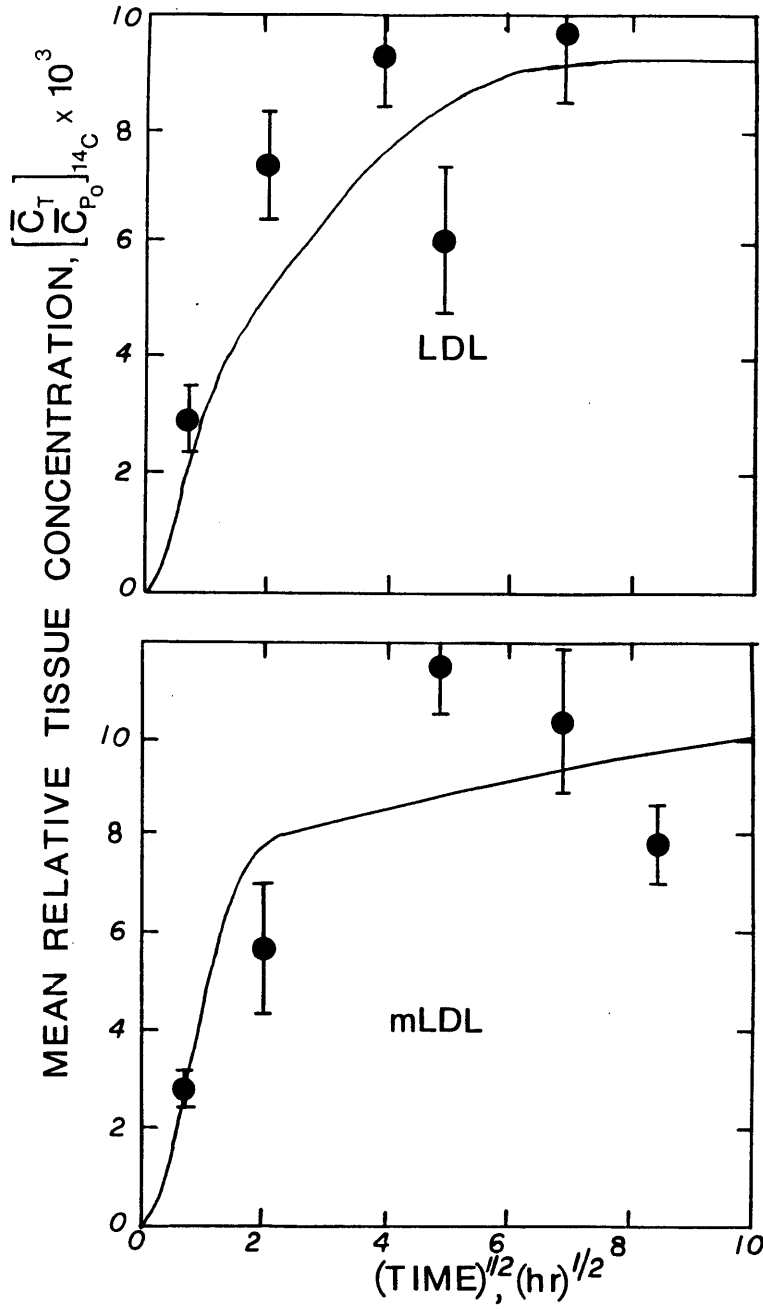


Figure 4-29: Determination of k_E as a Function of time by Fitting equation (4-26) to ^{14}C -Sucrose Data.

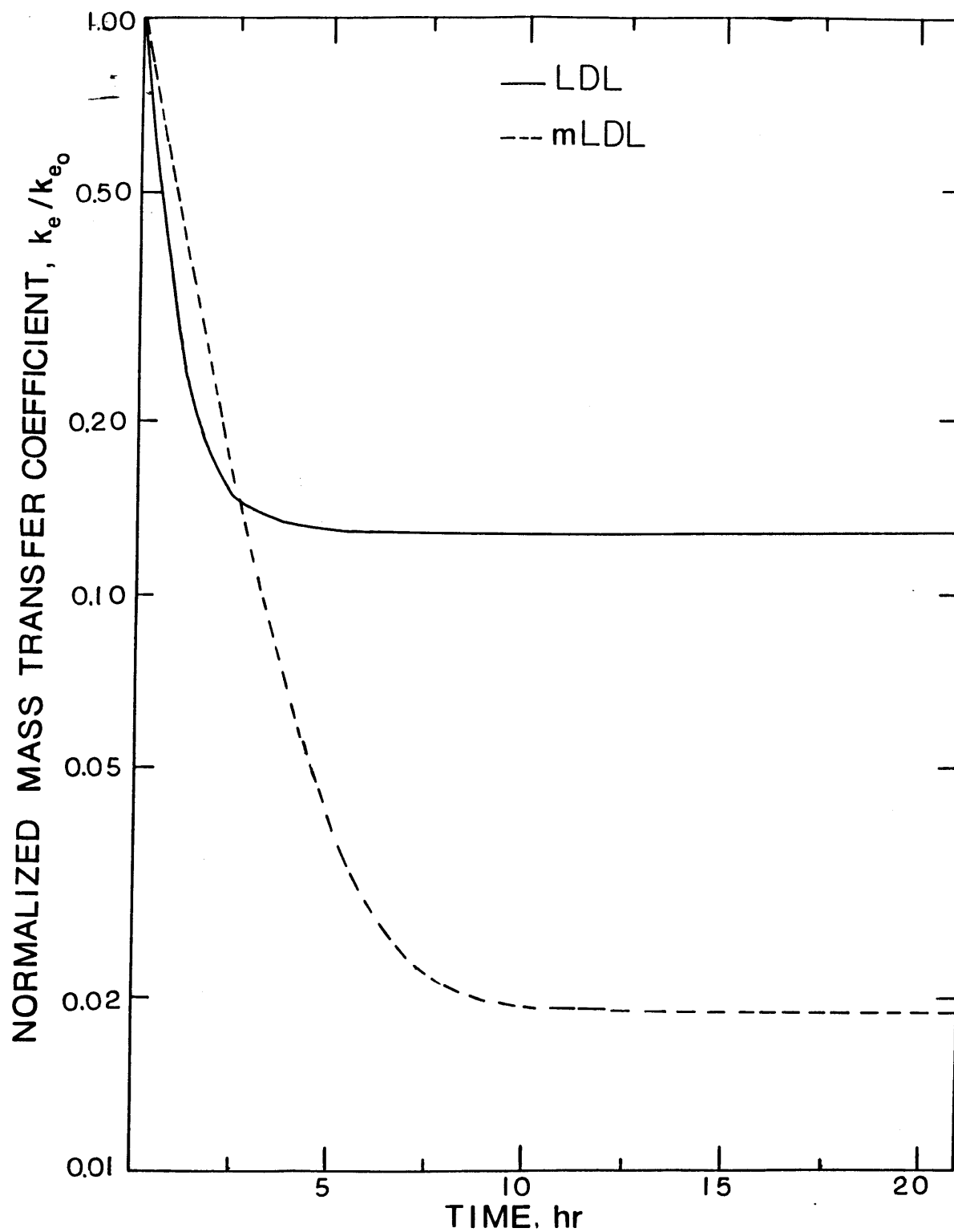


Figure 4-30: Normalized Mass Transfer Coefficient for LDL and mLDL

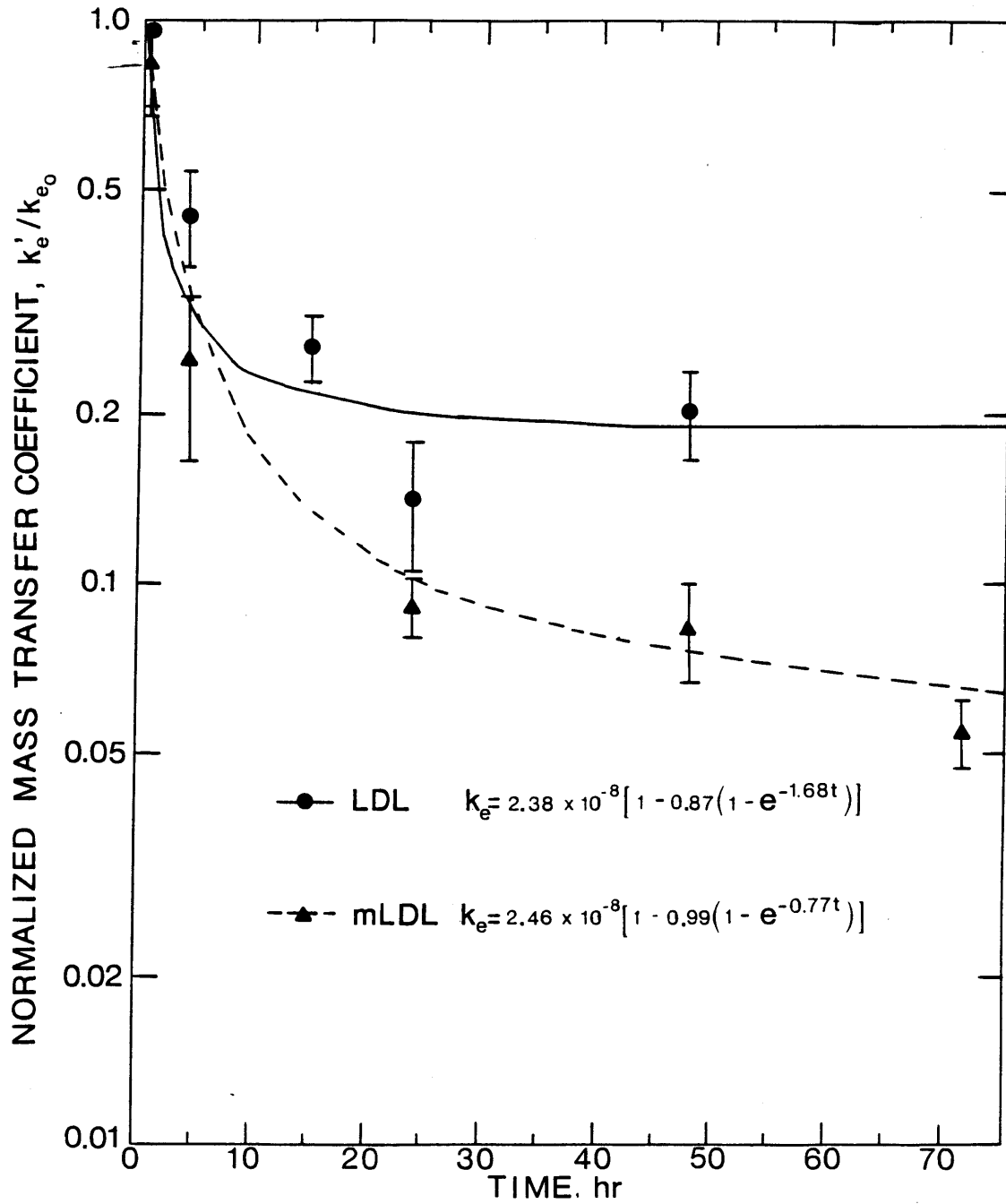


Figure 4-31: Comparison of Calculated and Predicted Values of k'_E .

Table 4-XIII: Fitting Equation 4-29 to ^{14}C -Sucrose Uptake Data

	k_{E_0} , cm/sx10 ⁸	f	γ , hr ⁻¹
LDL	2.38 ± 0.36	0.866 ± 0.054	1.68 ± 1.13
mLDL	2.46 ± 0.23	0.981 ± 0.023	0.77 ± 0.27

equations (4-13) and (4-14), respectively, to represent \bar{C}_{T+d}/C_{p_0} . Both fitted functions for \bar{C}_T/C_{p_0} and \bar{C}_d/C_{p_0} were calculated from Navarro's data. The resulting estimate of k_E' is plotted in Figure 4-32. The curve is similar to that obtained using equation (4-28) to represent k_E except for LDL between 2 and 30 hr. Attempts to use fits of \bar{C}_T/C_{p_0} and \bar{C}_d/C_{p_0} to directly calculate k_E were unsuccessful for the calculated value of k_E became less than zero for times greater than 12 hr. This is probably due to the fit of \bar{C}_d/C_{p_0} since equation (4-14), as well as equations (4-17a,b), reached the asymptotic value before data.

4.3.6 Characterization of LDL

LDL was characterized by high performance liquid chromatography (HPLC) and quasi-elastic light scattering (QLS) in order to verify that LDL used was homogeneous. (The assistance of Dr. David Yarmush and Ms. Regina Murphy in performing the characterizations is gratefully acknowledged.) HPLC was performed on a Beckman Model 330 with a Superose 6 column (molecular weight cutoff of 4×10^7 g/mole, optimal range: 5×10^3 to 5×10^6 ; Pharmacia). Using a flow rate of 0.3 ml/min LDL eluted as a single peak after about 45 min (Figure 4-33). The elution profile contains a tail which may be due to dispersion of the sample or the presence of low molecular contaminants. The molecular weight was not be calculated because the column had not been calibrated.

Quasi-elastic light scattering (Coulter Model N4, submicron particle analyzer;

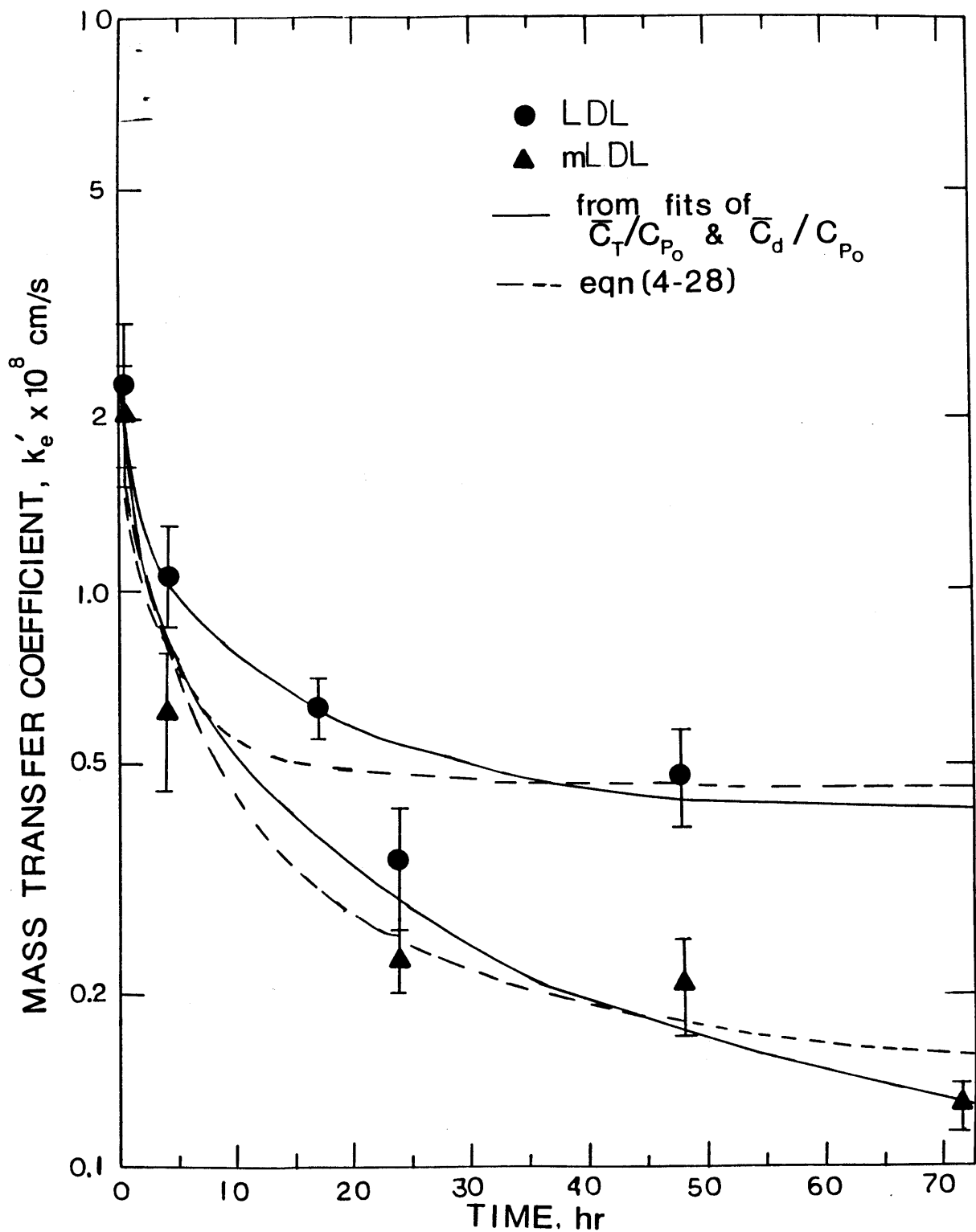


Figure 4-32: Comparison of Calculated and Predicted Values of k'_E based upon fits of \bar{C}_T/C_{p_0} and \bar{C}_d/C_{p_0} and equation (4-28).

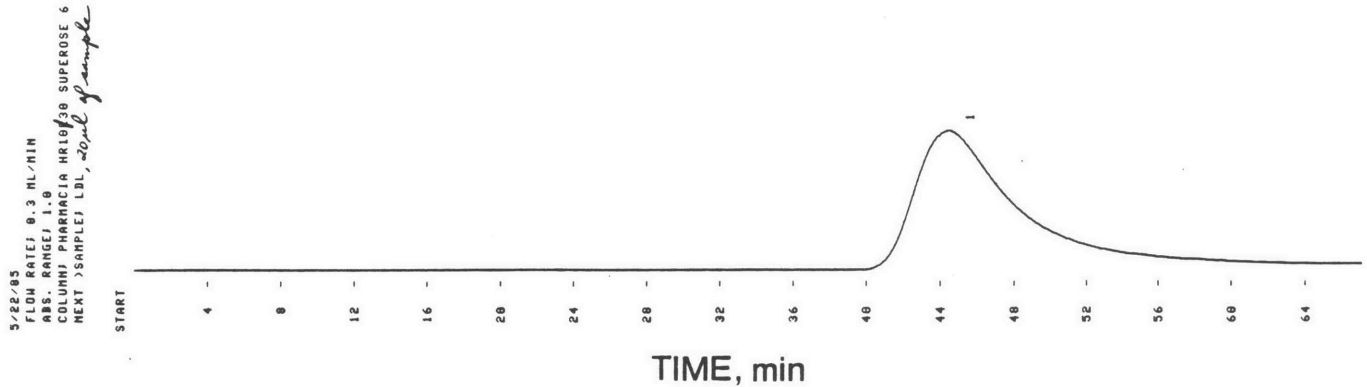


Figure 4-33: Elution Profile of LDL on a Superose 6 HPLC column.

Coulter Electronics; Hialeh, FL) of a different sample of LDL from the same preparation indicated a homogeneous population with a mean Stokes-Einstein radius of 10.40 nm (95% confidence interval of ± 0.35 nm) and a diffusion coefficient of 2.06×10^{-7} cm²/s. The particle radius is very close to values reported by others for LDL prepared by differential ultracentrifugation (Schumaker [1973], Crossley et al. [1981], Mitterer et al. [1982]). These results indicate that the LDL used is a single homogeneous population with hydrodynamic properties similar to those obtained by others. Thus, changes in k_E with time must be due to alterations of either LDL or the endothelial cells which occur subsequent to injection of LDL.

4.4 Discussion

This study represents the first detailed data on the spatial distribution of ^{125}I -mLDL and the temporal behavior of LDL and mLDL degradation in the rabbit aorta. A detailed analysis of this nature provides insight into the relative importance of cellular metabolism, transendothelial transport, and medial diffusion. The use of linear systems theory has demonstrated that such data are required in order to properly compare receptor-mediated and receptor-independent metabolism in terms of the steady state accumulation and rate of degradation in response to a step change in plasma concentration.

The FCR for LDL is the sum of contributions from the receptor-mediated (FCR_{RM}) and receptor-independent pathways (FCR_{RI}):

$$(\text{FCR})_{\text{LDL}} = \text{FCR}_{\text{RM}} + \text{FCR}_{\text{RI}} \quad (4-30)$$

It has commonly been assumed that the receptor-independent contribution to the FCR (FCR_{RI}) is equal to the FCR for mLDL (Mahley et al. [1980], Slater et al [1982a,b,c]) and the fraction of the FCR attributed to the receptor-mediated pathway can be determined by rearrangement of equation (4-30):

$$\frac{\text{FCR}_{\text{RM}}}{(\text{FCR})_{\text{LDL}}} = \frac{(\text{FCR})_{\text{LDL}} - \text{FCR}_{\text{mLDL}}}{(\text{FCR})_{\text{LDL}}} \quad (4-31)$$

Based upon the assumption that $(\text{FCR})_{\text{mLDL}} = \text{FCR}_{\text{RI}}$, the fractional catabolic rates calculated from fits of pooled LDL and mLDL data in Figure 4-5 indicate that about 70% of all LDL removed from the plasma is by the receptor-mediated pathway.

Equations (4-30) and (4-31) have been frequently used in the literature without examination of their validity. When degradation is occurring in both plasma and tissues, the FCR can be represented as (see equation (D-15), Appendix D):

$$FCR = k_{2p} + \frac{k_{1p}k_{3t}}{k_{1t} + k_{3t}} \quad (4-32)$$

where k_{2p} and k_{3t} are first order rate constants for degradation in the plasma and tissues, respectively, and k_{1p} and k_{1t} are first order rate constants for transport from the plasma into tissue and from tissue into plasma, respectively. In its most general form, equation (4-32), the FCR is a lumped constant reflecting degradation in the plasma and tissues, as well as transport in and out of tissues. If tissue degradation is negligible then k_{3t} is approximately equal to zero and equation (4-32) reduces to:

$$FCR = k_{2p} \quad (4-33)$$

For this case the difference between the fractional catabolic rates of LDL and mLDL reflects the activity of the receptor-mediated pathway. If, however, degradation in the plasma is small relative to degradation in the tissue (i.e. $k_{2p} \approx 0$), the FCR depends upon tissue degradation as well as transport in and out of tissues.

Plasma decay curves of normal and methylated LDL were compared, in terms of the fractional catabolic rate, with results obtained in rabbits by a number of investigators (Table 4-XIV). The fractional catabolic rates of LDL modified by reductive methylation, cyclohexanedione treatment, and glycosylation are about one-third the fractional catabolic rate of LDL suggesting that about two-thirds of all LDL removed from the plasma is by the receptor-mediated pathway.

Fractional catabolic rates obtained in this study are larger than those obtained by other investigators. In this study, LDL was isolated by a precipitation method; all other investigators used differential ultracentrifugation. Smooth muscle cells metabolize LDL prepared by these two different methods in exactly the same manner (see Chapter 2, Section 2.4.1), and analysis of a single preparation of LDL

Table 4-XIV: Fractional Catabolic Rates of Normal and Modified LDL in Rabbits

Type of LDL	FCR, hr ⁻¹		Reference
	LDL	modified LDL	
Human	0.113 ± 0.016	0.035 ± 0.004 ¹	This Study
Human	0.0512		Bratzler et al. [1977b]
Human	0.071 ± 0.008	0.027 ± 0.007 ²	Sasaki and Cottam [1982]
Human		0.033 ± 0.009 ³ 0.015 ± 0.005 ¹	Slater et al. [1982b]
Human	0.063 ± 0.020	0.035 ± 0.005 ³	Slater et al. [1982c]
Rabbit	0.086	0.021 ²	Steinbrecher et al. [1983]
Rabbit	0.063 ± 0.013	0.016 ¹	Carew et al. [1984]
Rabbit	0.069 ± 0.004	0.023 ± 0.004 ¹	Bilheimer et al. [1982]

¹ methylated LDL² glycosylated LDL³ cyclohexandione-treated LDL

by HPLC and QLS showed that LDL is homogeneous with hydrodynamic properties similar to those obtained by others. A detailed comparison of the physicochemical properties of LDL prepared by precipitation and differential ultracentrifugation has not been performed (Lee [1976]). Except for the results of this study, there is little difference between fractional catabolic rates for rabbit and human LDL.

Further support for the importance of receptor-mediated metabolism in vivo can be obtained by comparing the fractional catabolic rates of LDL in normal and a mutant form of rabbits which lack functional LDL receptors (Attie et al. [1981],

Kita et al. [1981]) (Table 4-XV). In these mutant or Watanabe rabbits (WHHL), the fractional catabolic rate of LDL is about 30% of its value in normal rabbits. This reduction in fractional catabolic rate is similar to that observed with modified forms of LDL.

Table 4-XV: Fractional Catabolic Rates of LDL in Normal and WHHL Rabbits

Type of LDL	FCR, hr ⁻¹		Reference
	Normal	WHHL Rabbits	
Rabbit	0.063 ± 0.026	0.024 ± 0.010	Pittman et al. [1982b]
Rabbit	0.069 ± 0.004	0.020 ± 0.003	Bilheimer et al. [1982]
Rabbit	0.086	0.010	Steinbrecher et al. [1983]

In Figures 4-34 to 4-36 transmural profiles obtained in this study are compared with results obtained by Bratzler et al. [1977b]. (Error bars represent the standard error of the mean calculated from all data points at a given normalized depth.) The major difference between this study and that of Bratzler et al. [1977b] is the method of LDL isolation. Bratzler et al. [1977b] isolated LDL by differential ultracentrifugation. Differences in the plasma decay curves have already been noted (Table 4-XIV). The shapes of the transmural profiles obtained in this study are similar to those obtained by Bratzler et al. [1977b]. At 0.5 hr, ¹²⁵I-LDL tissue concentrations are 1.5 to 2 times less than those obtained by Bratzler et al. [1977b]. At 4 and 24 hr, the magnitudes of the tissue concentrations are comparable. Nevertheless, the mean relative tissue concentrations are consistently less than those obtained by Bratzler et al. [1977b] (Figure 4-37).

The mean relative tissue concentrations of ¹²⁵I-LDL in the arterial wall

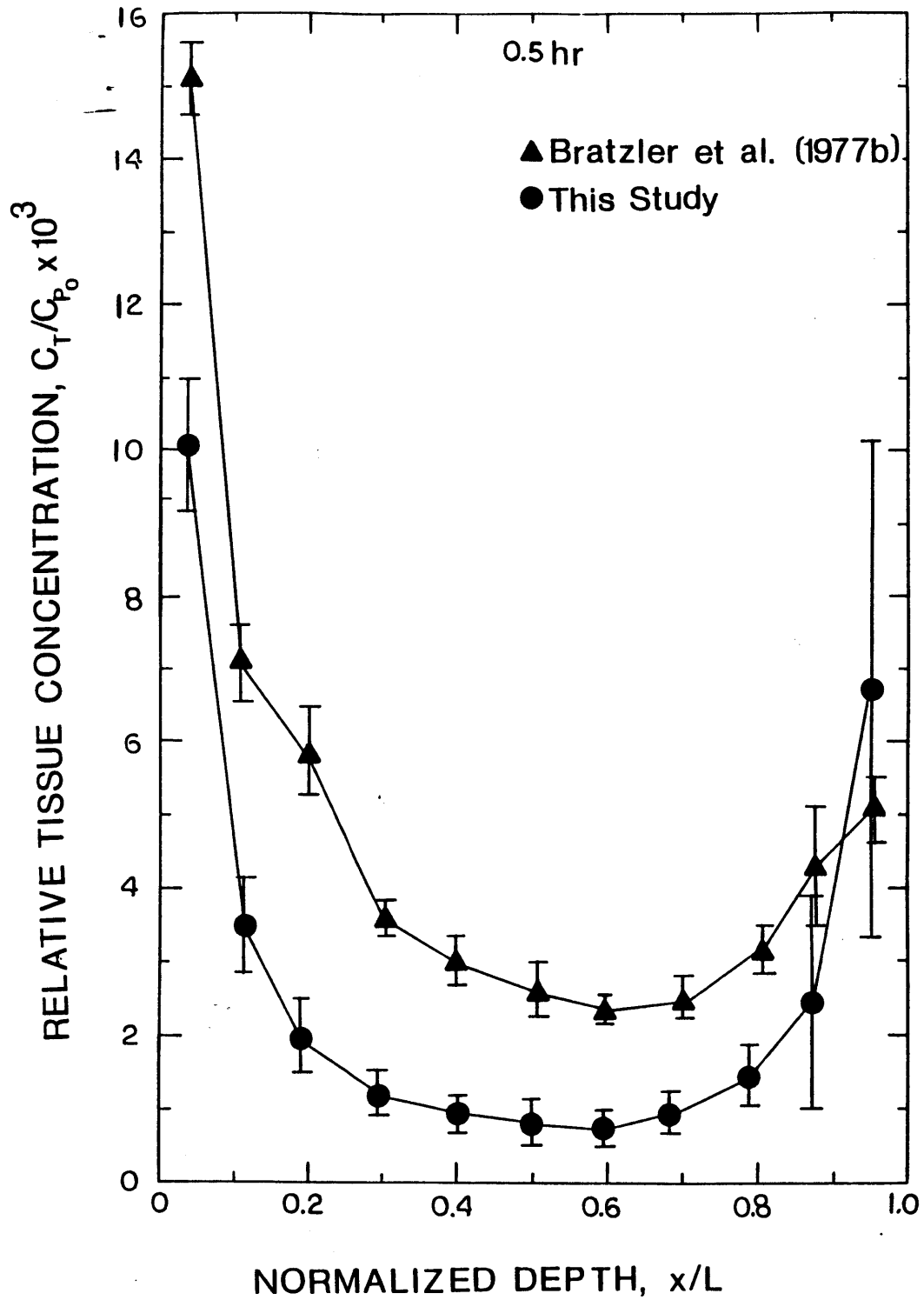


Figure 4-34: Comparison of 0.5 hr ^{125}I -LDL Transmural Profiles with the Results of Bratzler et al. [1977b].

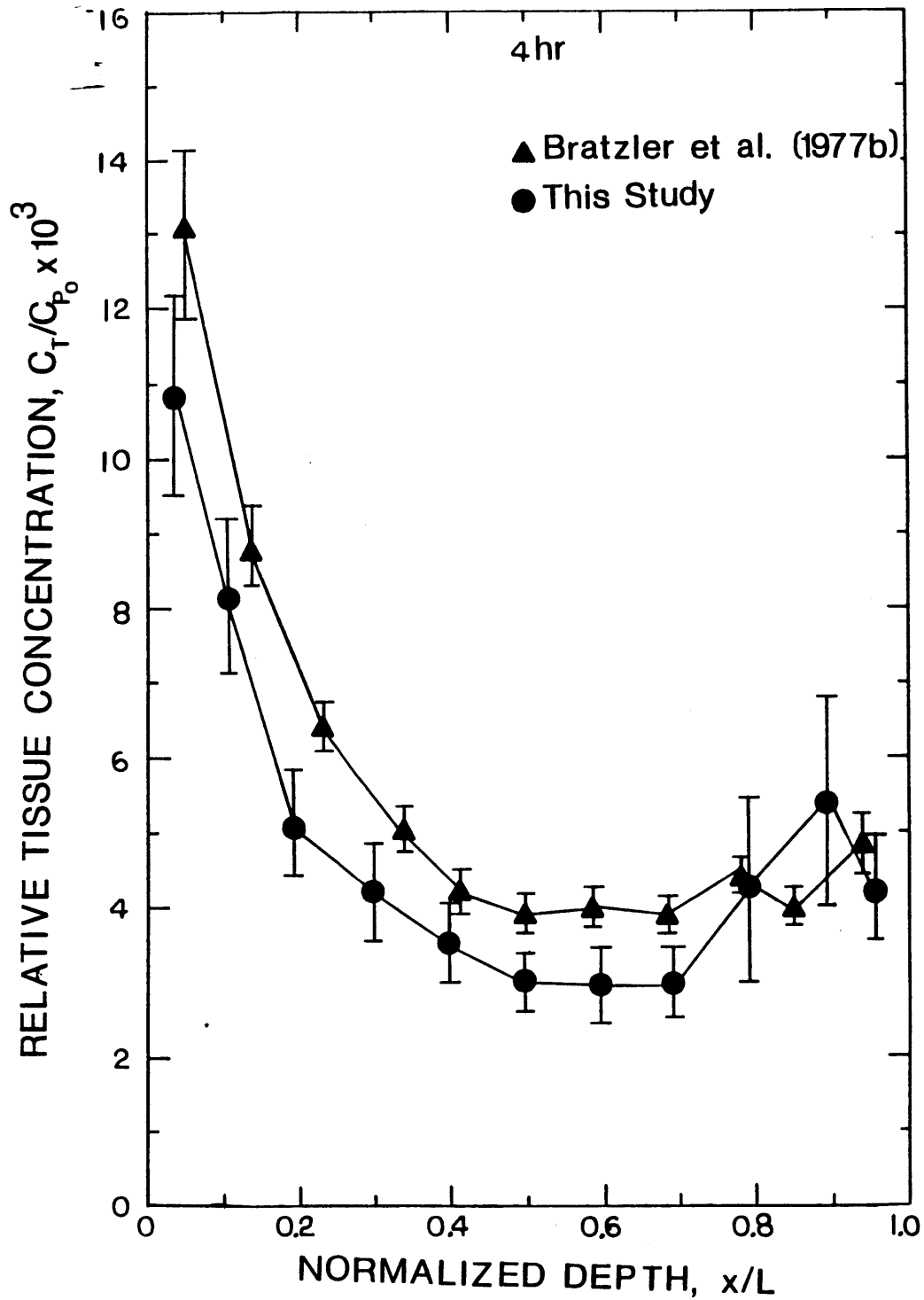


Figure 4-35: Comparison of 4 hr ^{125}I -LDL Transmural Profiles with the Results of Bratzler et al. [1977b].

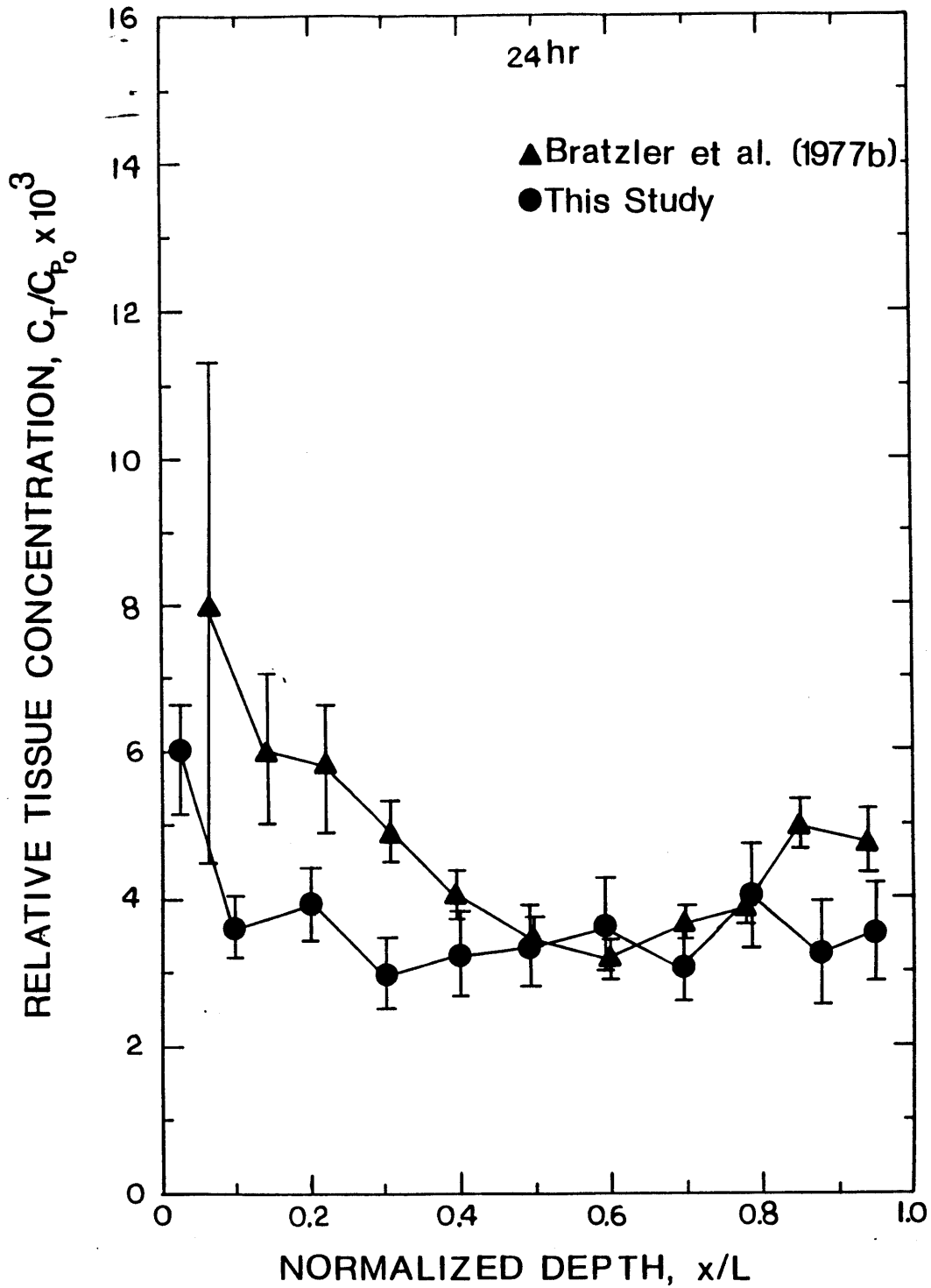


Figure 4-36: Comparison of 24 hr ^{125}I -LDL Transmural Profiles with the Results of Bratzler et al. [1977b].

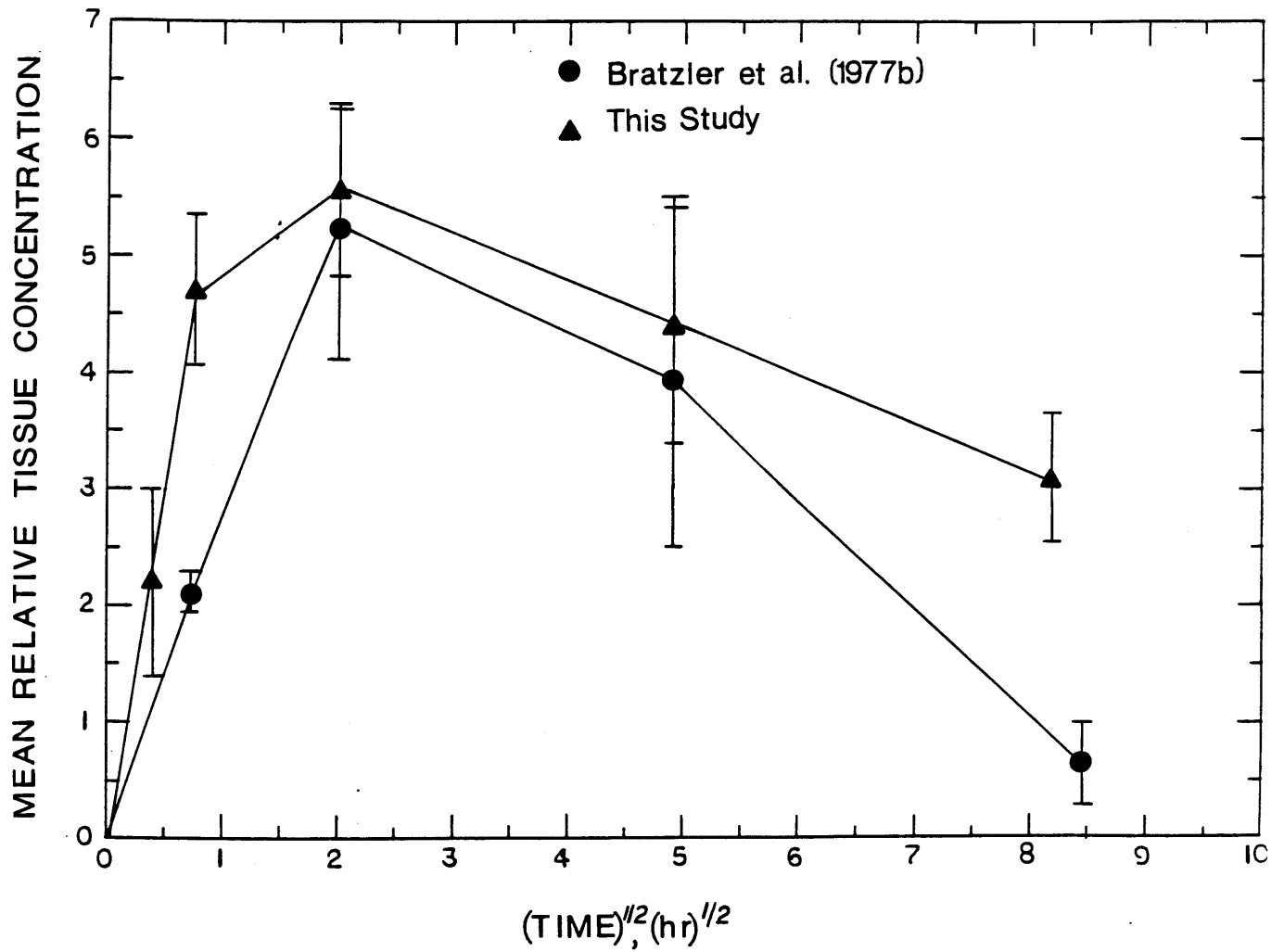


Figure 4-37: Comparison of ^{125}I -LDL Mean Relative Tissue Concentrations with the Results of Bratzler et al. [1977b].

obtained by a number of investigators are summarized in Table 4-XVI. There is general agreement among values for the mean relative tissue concentration in the descending thoracic aorta of the rabbit except for the studies of Virag et al. [1968]. The experiments by Virag et al. [1968] were conducted in vitro and the results may reflect a disrupted endothelial monolayer or contamination by TCA-soluble radioactivity. In all other experiments TCA soluble radioactivity was removed.

Morrel [1983], Schnitzer [1983], and Tompkins [1983] have used quantitative autoradiography to measure transmural profiles, from which mean relative tissue concentrations were calculated. The values of Schnitzer and Tompkins presented in Table 4-XIV are for low permeability regions of the vessel wall; the values obtained by Morrel [1983] are for low and high permeability regions. Morrel [1983] is the first to systematically compare LDL concentrations in low and high permeability regions. His estimates of the fractional area occupied by the high permeability regions suggests that they might account for the discrepancy between results obtained by frozen serial section microtomy and quantitative autoradiography.

Previous studies of receptor-mediated and receptor-independent LDL metabolism in the arterial wall have been limited to one or two circulation times and steady state tissue concentrations in response to a step input cannot be determined. Nevertheless, comparisons can still be made. A number of investigations have presented their data in terms of the tissue concentration (dpm/(g tissue)) divided by the injected dose of tracer (dpm). This quantity is related to \bar{C}_T/C_{p_0} as follows:

$$\frac{\bar{C}_T}{C_{p_0}} = \frac{(dpm/g \text{ tissue})V_p\rho}{(\text{plasma dpm at } t=0)} \quad (4-34)$$

where ρ is the tissue density (1.07 g/cm³ for unfixed tissue (Bell et al. [1974a]) and 1.09 g/cm³ for fixed tissue (Fry et al. [1980])), and V_p is the plasma volume.

Table 4-XVI: Comparison of Mean Relative Tissue Concentration of Radioiodinated LDL from Various Studies with Normal Animals. (Modified from Bratzler et al. [1977b])

Reference	Animal	Position in Aorta	Time After Injection	\bar{C}_T/C_{p_0}	
Virag et al. [1968] ^a	Rabbit (in vitro)	descending thoracic (DT)	2 hr	0.085	
				(inner layer)	
Okishio [1961] ^c	Rabbit (in vivo)	whole aorta	24 hr	0.0012	
			72 hr	0.0012	
				(inner layer)	
Duncan et al. [1963]	dog (in vivo)	DT	6 hr	0.013	
				(outer layer)	
				0.001	
				(inner layer)	(outer layer)
Calvert et al. [1975] ^d	pig (in vivo)	DT	24 hr	0.0076	0.0064
			49 hr	0.0053	0.0054
			72 hr	0.0033	0.0035
				(inner layer)	(outer layer)
Scott and Hurley [1977]	human (in vivo)	DT	0.2 days	0.046	0.19
			1.1 days	0.023	0.017
			1.7 days	0.054	0.0078
			1.9 days	0.014	0.0095
			4.3 days	0.011	0.0047
Bretherton et al. [1976] ^b	rabbit (in vivo)	DT	6 hr	0.0059	

Table 4-XIV: continued

Reference	Animal	Position in Aorta	Time After Injection	\bar{C}_T/C_{p_0}
Tompkins [1983]	Squirrel	Ascending Arch	0.5 hr	0.000221
	Monkey & highest DT (in vivo)	DT	0.5 hr	0.000183
		Abdominal Aorta	0.5 hr	0.000414
Schnitzer [1983]	Rabbit (in vivo)	DT	0.5 hr	0.000535
Morrel [1983]	Rabbit	DT	0.5 hr	0.00035 ^e 0.0301 ^f
Bratzler et al. [1977]	Rabbit (in vivo)	DT	0.167 hr	0.0022
			0.5 hr	0.0047
			4 hr	0.0055
			24 hr	0.0044
			67 hr	0.0031
This Study	Rabbit (in vivo)	DT	0.5 hr	0.0021
			4 hr	0.0052
			24 hr	0.0039
			72 hr	0.00066

a. Calculated by assuming 70% counting efficiency.

b. Calculated from uptake data in Table 2 and mean serum protein concentration in Table 1 of Bretherton et al. [1976]; and by assuming double exponential decay of serum plasma of Bratzler et al. [1977b] is valid for calculating C_p/C_{p_0} ; and

specific gravity of 1.07 (Bell et al. [1974a]) for aortic tissue and TCA precipitable radioactivity 88% of measured value.

c. Calculated from data for C_T/C_p and C_p/C_{p_0} .

d. Calculated from Table 9 of Calvert et al. [1975] by assuming specific gravity of 1.07 for aortic tissue and TCA precipitable radioactivity 88% of measured value.

e. HRP impermeable regions.

f. HRP permeable regions.

Equation (4-27) was used to convert the results of Packard et al. [1982], Pittman et al. [1982b], Slater et al. [1982c], and Carew et al. [1984] into C_T/C_{p_0} . The plasma volume was computed using a tabulated value for the average plasma volume in rabbits (38.8 ml/(kg body weight) (Spector [1956], p. 306)) and assuming that animal weights were similar to those found for rabbits in this study and the study of Navarro [1984] (3 kg).

Mean relative tissue concentrations of ^{125}I - and ^{14}C -sucrose-labeled LDL and modified LDL in the rabbit aorta are presented in Table 4-XVII. Uptake represents mean relative ^{14}C -sucrose-labeled lipoprotein concentrations, except for the study of Carew et al. [1984] in which ^{125}I -tyramine-cellobiose was used. In general, the agreement is quite good, except for total uptake in the WHHL rabbit aorta. The large error associated with the value for WHHL rabbits makes it difficult to determine if arterial LDL metabolism has changed in these animals. For the other studies listed in Table 4-XVII, there does not appear to be any significant difference between the metabolism of human and rabbit LDL.

The contribution of the receptor-mediated pathway to LDL tissue concentrations and cumulative degradation was analyzed using linear systems theory. This was necessary because differences in the plasma decay of LDL and mLDL influence the tissue concentrations of the two lipoproteins. The effect of the plasma decay has been recognized by others (Pittman et al. [1982a,b], Carew et al. [1984]), who have used heuristic arguments to derive a quantity termed the tissue catabolic rate (TCR):

$$TCR = \frac{(dpm \text{ } ^{14}\text{C}/g \text{ tissue})FCR}{(\text{plasma } dpm \text{ at } t = 0)f_d} \quad (4-35)$$

where f_d is the mass fraction degraded by all tissues and can be determined using the pharmacokinetic model described in Appendix D (equation (D-23)):

Table 4-XVII: Mean Relative Tissue Concentrations of ^{125}I - and ^{14}C -sucrose-labeled Lipoproteins in Rabbits

Reference	Time	Lipoprotein	$\left[\frac{\bar{C}_T}{C_{p_o}} \right]_{^{125}\text{I}} \times 10^3$	$\left[\frac{\bar{C}_{T+d}}{C_{p_o}} \right]_{^{14}\text{C}} \times 10^3$
Carew et al. [1984]	24 hr	rabbit LDL	1.5 ± 0.5^1	6.3 ± 1.0^2
		(rabbit) mLDL	2.8 ± 0.8	10.5 ± 2.2
Pittman et al. [1982b]	24 hr	rabbit LDL		11.8 ± 12.9
		rabbit LDL (WHHL rabbit)		56.4 ± 50.7
Slater et al. [1982c]	48 hr	human LDL	2.4 ± 0.7	
		(human) CHD-LDL ³	6.4 ± 1.9	
Packard et al. [1982]	48 hr	(human) mLDL		11.8 ± 2.6
		(human) CHD-LDL ³		11.2 ± 1.2
This study	24 hr	human LDL	3.1 ± 2.5	6.1 ± 2.2
		(human) mLDL	3.2 ± 0.6	11.5 ± 2.3
	48 hr	human LDL	0.71 ± 0.15	9.7 ± 3.0
		(human) mLDL	1.9 ± 0.60	10.4 ± 3.7

1. ^{125}I -labeled lipoproteins
2. ^{125}I -tyramine-cellobiose used in place of ^{14}C -sucrose
3. cyclohexanedione treated LDL

$$f_d = \frac{b_2(1 - e^{-b_1 t})}{b_2 - b_1} - \frac{b_1(1 - e^{-b_2 t})}{b_2 - b_1} \quad (4-36)$$

where b_1 and b_2 are obtained from the plasma decay curve, equation (4-1). Carew et al. used equations (4-34) and (4-35) to compare receptor-mediated and receptor-independent metabolism in the rabbit arterial wall in much the same way as equation (4-15c) was used.

The use of the tissue catabolic rate to correct for differences in the plasma

decay of LDL and mLDL appears reasonable on heuristic grounds. At long circulation times, TCR is related to the steady state rate of degradation in response to a step change in plasma concentration, R_d . To see this, note that dpm $^{14}\text{C}/\text{g}$ tissue is equal to \bar{C}_{T+d}/ρ and the dpm in the plasma at $t = 0$ is equal to $C_{p_0} V_p$. Making these substitutions, equation (4-35) becomes:

$$TCR = \frac{\bar{C}_{T+d} FCR}{\rho C_{p_0} V_p f_d} \quad (4-37)$$

In the limit as $t \rightarrow \infty$, $f_d \rightarrow 1$, all radioactivity in the tissues represents degradation products (i.e., $\bar{C}_{T+d} = \bar{C}_d$), and equation (4-36) becomes:

$$\lim_{t \rightarrow \infty} TCR = \frac{\bar{C}_d FCR}{\rho C_{p_0} V_p} = \frac{\bar{\theta}_d(\infty) FCR}{\rho V_p} \quad (4-38a)$$

$$= \frac{R_d}{\rho V_p} \quad (4-38b)$$

The mass transfer coefficient for transendothelial transport was estimated from tissue concentrations of ^{14}C . The most intriguing result obtained in this study is that transendothelial permeabilities to LDL and mLDL decrease with time. In order to determine if the same phenomenon also occurred in other studies of lipoprotein uptake, the weighted mass transfer coefficient, k_E' was estimated from the data presented in Table 4-XVII. Plasma decay curves in the original references were fit to equation (4-1) and $\int_0^t C_p dt$ calculated. (Carew et al. [1984] and Pittman et al. [1982b] present representative plasma decay curves, so the estimate for the integral may be in error.)

Estimated values of the weighted mass transfer coefficients are presented in Table 4-XVIII. Values obtained at 24 and 48 hr are similar to those obtained in this study. The mass transfer coefficient of mLDL is consistently smaller than the value

for LDL. The mass transfer coefficients at 24 and 48 hr are substantially less than values at 0.5 hr (Table 4-XII), except for the value for receptor-deficient WHHL rabbits. These results indicate that the reduction in the mass transfer coefficient is not an artifact of this study, but is a general phenomenon. Nor is the effect an artifact of using ^{14}C -sucrose labeled lipoprotein; Carew et al. [1984] used ^{125}I -tyramine-cellobiose to measure uptake. In addition, results from cell culture studies indicate that LDL labeled with ^{14}C -sucrose or ^{125}I -tyramine-cellobiose behaves the same as ^{125}I -LDL (Pittman et al. [1979, 1983]).

Table 4-XVIII: Weighted Mass Transfer Coefficient Estimated from Mean Relative Tissue Concentrations of ^{14}C -Sucrose

Reference	Molecule	Time, hr	k_E' , cm/s x 10^8
Carew et al. [1984]	LDL	24	0.22 ± 0.05
	mLDL	24	0.14 ± 0.03
Pittman et al. [1982b]	LDL	24	0.37 ± 4.2
	LDL	24	1.31 ± 1.18
	(WHHL rabbit)		
Packard et al. [1982]	mLDL	48	0.19 ± 0.05
	CHD-LDL	48	0.16 ± 0.02
This study	LDL	24	0.34 ± 0.12
	mLDL	24	0.23 ± 0.05
	LDL	48	0.48 ± 0.15
	mLDL	48	0.21 ± 0.07

As noted above, analysis of LDL by HPLC and QLS indicates that the hydrodynamic properties are normal. Nevertheless, the decreasing mass transfer coefficient may be an artifact of handling LDL (e.g. isolation and radiolabeling). LDL is cytotoxic to cultured bovine and porcine endothelial cells and human skin fibroblasts. Cytotoxicity is probably the result of lipid peroxidation (Morel et al. [1983], van Hinsbergh [1984]), and the presence of 1 mM EDTA is sufficient to

inhibit peroxidation (Hessler et al. [1983]). 1 mM EDTA was present in all solutions containing LDL or mLDL in this study, and it was used in all studies cited. Thus, LDL cytotoxicity is not a likely explanation.

Another possible artifact may result from self-aggregation of LDL. Bratzler [1974] reisolated human ^{125}I -LDL 0.5, 4, and 24 hr following injection into rabbits and found that 93.8% to 95.1% of plasma protein bound radioactivity was associated with LDL; the remaining plasma protein bound radioactivity was associated with VLDL and HDL. In other experiments, Bratzler [1974] tested for the presence of aggregates by means of a "screening" experiment. ^{125}I -LDL was injected into one rabbit and, after 17 min, the animal was exsanguinated and plasma recovered. ^{131}I -LDL was added to the plasma which was then injected into a second rabbit. The ratio of TCA precipitable ^{125}I to ^{131}I was constant with time indicating that both "screened" and "unscreened" LDL were being removed from the plasma in the same fashion. Transmural profiles of ^{125}I -LDL and ^{131}I -LDL, determined after 4 hr circulation time, were virtually identical, suggesting that few, if any, aggregates were present.

Sniderman et al. [1975] used sucrose density ultracentrifugation to compare the density distribution of porcine ^{125}I -LDL before and after injection into pigs. There was a slight skewing of the density of LDL allowed to circulate for times ranging from 4 to 24 hr, but no significant increase in radioactivity at either density extreme was observed.

Gel chromatography of LDL isolated by dextran sulfate precipitation, a method similar to the precipitation method used in this study, yields a single symmetrical peak with a molecular weight of 3.5×10^6 and a Stokes-Einstein radius of 13 nm (Margolis [1967]). Aggregation of LDL was induced by heating (65 °C for 5 min), partial delipidation, and pronase digestion which resulted in a skewed and

broadened-elution profile.

Although these results are not conclusive, they do suggest that conventional methods of LDL isolation and handling are unlikely to result in aggregation or lipid peroxidation. Nevertheless, additional studies are needed to conclusively demonstrate this.

If the time varying permeability cannot be attributed to experimental artifact, then two possible biological explanations should be considered. One possibility is that endothelial cells are reacting to LDL and altering, in a time dependent fashion, either the LDL molecule itself or their metabolism of LDL. Endothelial cells are known to modify LDL such that it binds to the acetyl-LDL receptor (Henriksen et al. [1982]). Endothelial cells possess receptors for acetylated LDL, but their role in transendothelial transport is unknown.

Another possible explanation is that radiolabeled LDL and mLDL are binding to another protein in the plasma and this complex has a lower permeability. Albumin is a possible candidate since it is believed to bind to LDL (Lee [1976]). Binding of LDL to circulating heparin is unlikely since the plasma concentration of heparin is believed to be about 0.1 $\mu\text{g}/\text{ml}$ (Guyton [1976]), far less than the amount required to cause any aggregation (Pan et al. [1978]).

The injectate containing radiolabeled lipoproteins is usually a salt solution, and since LDL is present in high purity (as judged by immunodiffusion, immunoelectrophoresis, and electrophoresis), then the initial permeability represents that of the LDL molecule alone. As LDL binds to this other protein in the plasma, permeability is decreased either as a result of either steric interactions with the stalk of the endothelial cell vesicle or decreased affinity for nonspecific adsorption sites on the cell membrane. Differences in LDL and mLDL permeabilities may reflect differences in binding to the protein. This hypothesis can be tested by incubating

radiolabeled lipoproteins with either albumin, other plasma proteins, or serum for several hours prior to injection.

It is instructive to calculate limits on the transendothelial permeability. A lower bound can be obtained from cell culture data for fluid endocytosis. The endocytotic index for endothelial cells is typically 50 nl/(10⁶ cells · hr) (Davies et al. [1980], Davies [1984]). Typical endothelial cell surface areas range from 500 μm² to 1000 μm² (Reidy and Bowyer [1977], Cornhill et al. [1980]). The endocytotic index (EI) is related to the mass transfer coefficient as follows:

$$k_E = EI \cdot S_c \quad (4-39)$$

where S_c is the luminal surface area per cell. Using the above values for EI and S_c , k_E ranges from 1.4 to 2.8 x 10⁻⁹ cm/s.

Based upon the cell culture results obtained with bovine smooth muscle cells, the endocytotic index of LDL internalized by nonspecific mechanisms (largely adsorptive endocytosis) is 614 nl/(10⁶ cells · hr) and the estimated mass transfer coefficient ranges from 3.4 to 6.8 x 10⁻⁸ cm/s.

These estimates are quite speculative since fluid and adsorptive endocytosis measured in culture represent uptake by the cell and do not reflect transcellular transport. Nevertheless, the estimated mass transfer coefficient based upon uptake by fluid endocytosis is close to the asymptotic value of the mass transfer coefficient (3.2 x 10⁻⁹ cm/s for LDL and 0.5 x 10⁻⁹ cm/s for mLDL), and the estimated mass transfer coefficient for adsorptive endocytosis is close to the initial value of the mass transfer coefficient (2.38 x 10⁻⁸ cm/s for LDL and 2.46 x 10⁻⁸ cm/s for mLDL). These results are consistent with the hypothesis that the change in the mass transfer coefficient is a result of binding to a plasma protein which inhibits adsorptive endocytosis.

Theoretical investigations of LDL transport in the arterial wall indicate that transendothelial transport is the major transport resistance and the diffusion coefficient in the arterial media is about 50 times smaller than in aqueous solution (Bratzler et al. [1977], Truskey et al. [1981]). The characteristic diffusion time in the media, using a diffusion coefficient of $7.5 \times 10^{-9} \text{ cm}^2/\text{s}$ (Truskey et al. [1981]) and a tissue thickness of $130 \text{ }\mu\text{m}$, is about 6.3 hr whereas results obtained with cultured cells (Chapter 2) indicate that receptor-mediated internalization and degradation occur with half-times of 2.8 min and 2.0 hr, respectively. Therefore, metabolic phenomena in vivo should be limited by transendothelial transport and medial diffusion. In Chapter 5, mathematical models are developed in order to assess the effect of transport upon metabolism.

Chapter 5

Mathematical Models of LDL Transport and Metabolism in the Rabbit Arterial Wall In Vivo

5.1 Introduction

In order to obtain a more detailed understanding of LDL transport and metabolism in the arterial wall, a mathematical model has been developed. The model describes the behavior of radiolabeled LDL protein and is an extension of previous models (Bratzler et al. [1979], Ramirez [1979], Truskey et al. [1981], Fry [1985]). Radiolabeled LDL protein behaves as a tracer in the vessel wall and constitutive relations describing metabolic events can be represented by linear relationships rather than the nonlinear relationships applicable to unlabeled LDL. Expressions for cellular uptake and degradation of LDL presented in earlier models have been replaced with linearized forms of the kinetic models developed in Chapter 2. In addition, LDL metabolism by endothelial cells and time-varying endothelial permeabilities have been included.

The resulting equations were solved by the method of Laplace transforms, and transport parameters were determined by nonlinear regression of the model solution to transmural profiles of ^{125}I -LDL and ^{125}I -methylated LDL (mLDL) at 0.5 hr. Rate constants from cell culture experiments together with the transport parameters for constant and time-varying permeabilities, described in Chapter 4, were used to compare model predictions with transmural profiles, average tissue concentrations, and cumulative uptake. The importance of binding to the extracellular matrix was estimated by comparing the effect of these terms on the model predictions. The

sensitivity of model predictions was examined by varying parameters. The results of this analysis were compared with estimates obtained from linear systems theory.

5.2 Mechanisms of LDL Transport and Metabolism in the Arterial Wall

Based upon the literature review in Chapter 1 and the results presented in Chapters 2, 3, and 4, a conceptual framework of transport and metabolic pathways of LDL in the arterial wall is shown schematically in Figure 5-1. LDL can enter the vessel wall from the luminal surface by crossing the layer of intact endothelium. Diffusion and/or convection through the intercellular junctions are unlikely for a molecule as large as LDL. Rather, vesicular transport is the primary route for the transendothelial transport of LDL. In principle, vesicular transport may involve fluid, adsorptive, and receptor-mediated endocytosis. Estimates of the permeabilities of the vessel wall to LDL and mLDL are similar (Chapter 4 and Wiklund et al. [1985]). Furthermore, in situ morphological studies with rat aortic endothelium (Vasile et al. [1983]) indicate that receptor-mediated endocytosis is not involved in vesicular transport. Together, these results indicate that vesicular transport is solely by nonspecific mechanisms. In addition to transcellular transport, endothelial cells in vivo may degrade LDL in order to supply their cholesterol needs and this may occur by receptor-mediated mechanisms.

The arterial media can be conceptualized as a heterogeneous medium consisting of smooth muscle cells embedded in a gel formed by the extracellular matrix and the interstitial fluid. LDL which enters the media diffuses through the interstitial fluid in a direction consistent with its local concentration gradient. Since there is a pressure difference between the vessel lumen and the adventitial capillaries and lymphatics, the volume flow convects LDL towards the adventitia.

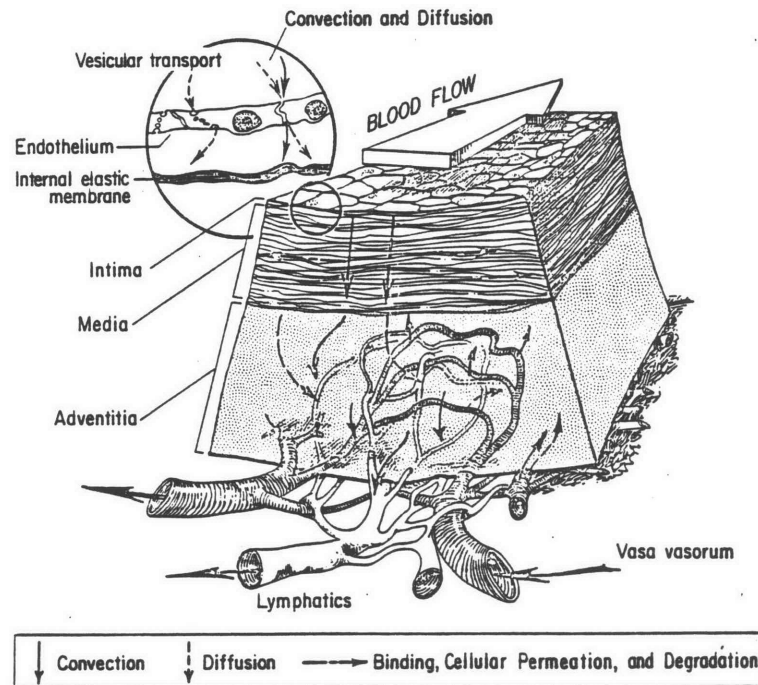


Figure 5-1: Schematic illustration of arterial wall showing modes of LDL transport and reaction thought to occur in the rabbit thoracic aorta. (from Truskey et al. [1981])

Due to hydrodynamic interactions between LDL and the extracellular matrix, diffusion within the media is slower than in free solution and the convective solute velocity is less than that of the mean interstitial velocity.

LDL can also enter the vessel wall by transport across the adventitial capillaries. Transport mechanisms are similar to those occurring at the luminal endothelium, except that Starling's flow results in the convection of LDL from the arteriolar to venular end of the capillaries (Guyton [1976], p. 395). In addition, LDL is removed from the tissue by lymphatic drainage.

LDL interactions with the extracellular matrix and metabolism by arterial smooth muscle cells may influence the uptake and distribution of LDL.

Glycosaminoglycans, collagen, and elastin can all bind to LDL. For a tracer experiment few binding sites are occupied and the association reactions are pseudo-first order.

Smooth muscle cells metabolize LDL by receptor-mediated and receptor-independent mechanisms. Kinetic models developed in Chapter 2 were adapted for LDL transport and metabolism in the arterial wall. For a tracer experiment, the receptor concentration can be assumed constant and binding becomes a pseudo-first order reaction.

5.3 Model Development

5.3.1 Interstitial Concentration

In order to develop a model amenable to interpretation, the arterial wall is assumed to be statistically homogeneous over volumes sufficiently large that local heterogeneities are unimportant. Concentrations associated with freely diffusible, bound, and intracellular solute represent quantities averaged over these volumes. The averaging volume cannot be so large, however, that the concentration changes appreciably within the volume (Whitaker [1969]). Although the exact dimensions of the averaging volume need not be specified, the volume must be much less than that of the tissue volume, but larger than the molecular dimensions of the extracellular matrix and smooth muscle cells.

Average concentrations can be defined in terms of the volume of all phases or the volume of the particular phase in which the solute is located. For freely diffusible solute in the interstitial fluid the following average concentration can be defined:

$$C_f = \frac{1}{V} \int_V C dV \quad (5-1)$$

where C is the local interstitial concentration and the integration volume is over the interstitial, extracellular matrix, and cellular phases. Since C is nonzero only in the interstitial phase $\int_V C dV$ is equivalent to $\int_{V_w} C dV$ where V_w is the interstitial fluid volume. Equation (5-1) represents the average concentration which is experimentally measurable for freely diffusible solute which is not bound to the extracellular matrix and is not metabolized by smooth muscle cells.

Alternatively, the concentration can be averaged only over the interstitial volume, V_w :

$$C'_f = \frac{1}{V_w} \int_{V_w} C dV \quad (5-2)$$

where C'_f is the interstitial concentration based on the interstitial volume. Since the integrals in equations (5-1) and (5-2) are equivalent, division of (5-1) by (5-2) yields:

$$\frac{C_f}{C'_f} = \frac{V_w}{V} = \epsilon_w \quad (5-3)$$

where ϵ_w is the interstitial volume fraction or porosity.

Solute molecules with dimensions approaching the molecular dimensions of the extracellular matrix cannot occupy all positions within the interstitial fluid. C is zero for some regions of V_w and a third volume average may be defined:

$$C''_f = \frac{1}{V_s} \int_{V_s} C dV \quad (5-4)$$

where V_s is the interstitial volume accessible to solute and C''_f is the interstitial solute concentration based upon V_f . C''_f is related to both C_f and C'_f :

$$\frac{C_f}{C''_f} = \frac{V_s}{V} = \epsilon_f \quad (5-5a)$$

and

$$\frac{C'_f}{C''_f} = \frac{V_s}{V_w} = \frac{\epsilon_f}{\epsilon_w} = K_p \quad (5-5b)$$

where K_p is the partition coefficient.

Equations (5-2) and (5-4) define two different interstitial concentrations, but only one definition is consistent with the equilibrium relation between interstitial and plasma concentrations:

$$\frac{\langle C \rangle}{C_p} = K_p \quad (5-6)$$

where $\langle C \rangle$ represents the interstitial concentration based upon an, as yet, unspecified volume. To determine whether equation (5-2) or (5-4) is the appropriate interstitial concentration, let $\langle C \rangle$ be equated with C'_f . Using equation (5-3), equation (5-6) becomes:

$$\frac{C'_f}{C_p} = \frac{C_f}{\epsilon_w C_p} = K_p \quad (5-7a)$$

Multiplication of equation (5-7a) by ϵ_w and noting that $\epsilon_w K_p = \epsilon_f$ (equation (1-2)) yields:

$$\frac{C_f}{C_p} = \epsilon_w K_p = \epsilon_f \quad (5-7b)$$

Equation (5-7b) defines ϵ_f , the volume fraction of tissue accessible to solute.

Equating $\langle C \rangle$ with $C' = C_f/\epsilon_w$ provides a consistent definition of the interstitial concentration. If, however, $\langle C \rangle$ is equated with $C''_f = C_f/\epsilon_p$, then equation (5-6) becomes:

$$\frac{C_f}{C_p} = \epsilon_f K_p \quad (5-7c)$$

which differs from (5-7b) by a factor of K_p . Equations (5-7b) and (5-7c) are consistent only for $K_p = 1$. This corresponds to the limiting case in which the solute size is very small relative to the characteristic dimensions of the extracellular matrix (i.e. $\epsilon_f = \epsilon_w$). Equation (5-2) is consistent with the definition of ϵ_f and K_p , whereas equation (5-4) is not.

C_f/ϵ_w is, therefore, the appropriate definition of the interstitial concentration to be used in the formulation of the material balances and is the same equation derived by Fry [1983]. Anderson and Quinn [1974] and Brenner and Gaydos [1977] have also used this definition in their models of restricted solute transport in cylindrical pores.

The molecular structure of the extracellular matrix is not known and it is conceivable that regions of interstitial fluid may exist which are separated from continuous channels by micropores. Such micropores are too small for large solute molecules to diffuse through, effectively preventing these solutes from occupying the separated regions. If there are a significant number of these regions, an estimate of the interstitial concentration based upon C_f/ϵ_w underestimates the concentration in the interstitial fluid accessible to solute.

The existence of these isolated regions presents additional complications when considering metabolic reactions. For example, suppose that part of a smooth muscle plasma membrane bounds the region inaccessible to solute. LDL receptors,

nonspecific binding sites, and vesicles would not interact with LDL and the rate constants would require modification in order to account for the fraction of cell membrane surface which contacts the isolated regions.

The arterial wall is constantly subjected to time-varying compressive forces due to pressure oscillations. These forces tend to stretch the tissue and may alter the local geometry of the extracellular matrix gel. Consequently, the dimensions of any micropores may change with time, allowing entry of large solutes during part of the cardiac cycle. Isolated regions of interstitial fluid, which are inaccessible to large solutes, may not exist.

The existence of such isolated regions, whether solute is completely excluded from these regions, and the extent to which smooth muscle cells and binding sites on the extracellular matrix bound these regions are not known. Thus, a simpler view of solute exclusion is invoked, in which the isolated regions are assumed not to exist, and exclusion is entirely a result of partitioning due to the overlap of solute with components of the interstitial gel (Giddings et al. [1968]).

In addition to freely diffusible LDL in the interstitial fluid, LDL may exist bound to the extracellular matrix, bound to the cell membrane, or within smooth muscle cells. For simplicity, all forms of LDL bound to the extracellular matrix are lumped into a single concentration. The smooth muscle cells are assumed to be a single well-mixed compartment although intracellular concentrations of LDL derived from receptor-mediated and receptor-independent endocytosis are viewed as distinct. The total concentration of labeled LDL in the tissue, C_T , is:

$$C_T = C_f + C_b + C_{LR} + C_{L_{Ri}} + C_{L_i} \quad (5-8)$$

where C_f , C_b , C_{LR} , $C_{L_{Ri}}$, and C_{L_i} are, respectively, labeled LDL concentrations which are freely diffusible, bound to the extracellular matrix, bound to cell surface

receptors, internalized by receptor-mediated endocytosis, and internalized by nonspecific mechanisms. The units of the concentrations are either mol/cm³ total tissue volume, g/cm³ total tissue volume, or dpm/cm³ total tissue volume. C_{LR} and C_{LRi} are zero for mLDL, since it cannot be internalized by receptor-mediated mechanisms.

In Chapter 2, cell associated concentrations measured in culture were reported in units of ng protein/mg cell protein. In order to convert these units to mol/cm³ total tissue volume, the concentrations are multiplied by the reciprocal of the molecular weight of the protein, M_w , times the product of the cell protein density, ρ_c (mg cell protein/cm³ cell volume), times the volume fraction of aortic tissue occupied by cells, ϵ_c (cm³ total cell volume/cm³ tissue volume), which for receptor-bound LDL on the cell surface is:

$$C_{LR} = \frac{[LR]\rho_c\epsilon_c}{M_w \times 10^9} \quad (5-9)$$

where [LR] is the concentration in units of ng protein/mg cell protein. Similar relations can be written for C_{LRi} and C_{Li} . Estimates of the values of ρ_c and ϵ_c are presented in Section 5.4.2.

As discussed in Chapter 4, ¹⁴C-sucrose label present in the tissue represents the sum of ¹⁴C-sucrose-labeled protein and ¹⁴C-sucrose-labeled degradation products trapped in the lysosomes, and is represented by C_{T+d} :

$$C_{T+d} = C_T + C_d \quad (5-10)$$

where C_{T+d} represents the total amount of solute, in degraded and undegraded forms, at a particular position in the tissue at a given time. ¹⁴C-sucrose labeled protein present in the tissue cannot be measured, but is related to the tissue concentration of ¹²⁵I-labeled protein. As long as the labeled proteins behave as

tracers (or the metabolic relationships are linear), then the relative tissue concentration of ^{125}I -labeled protein is equal to the relative tissue concentration of ^{14}C -sucrose-labeled protein (equation (4-6)). As shown in Chapter 4, the use of ^{125}I - and ^{14}C -sucrose-labeled proteins permits determination of the concentration of ^{14}C -sucrose-labeled degradation products, C_d .

5.3.2 Constitutive Relations

The rabbit aortic wall is approximately $150\ \mu\text{m}$ thick whereas the radius of the vessel is about $2000\ \mu\text{m}$. Since the vessel wall thickness is much less than the vessel radius, the curvature of the vessel wall can be neglected and a Cartesian coordinate system can be used.

Solute Flux Diffusion and convection of LDL occur only within the interstitial fluid. For volume averaged concentrations, the flux is one dimensional and can be written as:

$$N_s = -D_e \frac{\partial C_f / \epsilon_w}{\partial x} - \chi \frac{v}{\epsilon_w} \frac{C_f}{\epsilon_w} \quad (5-11)$$

where N_s is the average solute flux in terms of the interstitial area (mol/cm^2 interstitial area \cdot s), D_e is the effective diffusion coefficient, v is the superficial fluid velocity, and χ is the retardation factor which accounts for the reduction in the solute velocity as a result of interactions with the extracellular matrix (Anderson and Quinn [1974]). v/ϵ_w is the interstitial velocity. The diffusive flux is expressed as a partial derivative because concentrations are functions of position and time.

The effective diffusion coefficient is less than the diffusion coefficient in free solution (D_o) as a result of two effects: 1) hydrodynamic and electrostatic interactions between solute and the extracellular matrix; and 2) the increased diffusional path length due to the presence of obstructions. A consistent definition

of the effective diffusion coefficient and its relationship to D_o is (Satterfield et al. [1973]):

$$D_e = \frac{D_o K_r}{\tau^*} \quad (5-12)$$

where K_r represents the reduction in the diffusion coefficient due to the first effect and τ^* is the tortuosity which accounts for the second effect.

Binding to the Extracellular Matrix All binding reactions are lumped into a single reversible reaction:



where F and B represent free and bound solute, respectively, S represents binding sites in the extracellular matrix, and k'_a ($\text{cm}^3 \text{mol}^{-1} \text{min}^{-1}$) and k_b (min^{-1}) are the association and dissociation constants. The rate of binding of lipoprotein to the extracellular matrix, r_b , is:

$$r_b = k'_a C_s \frac{C_f}{\epsilon_w} - k_d C_b \quad (5-14)$$

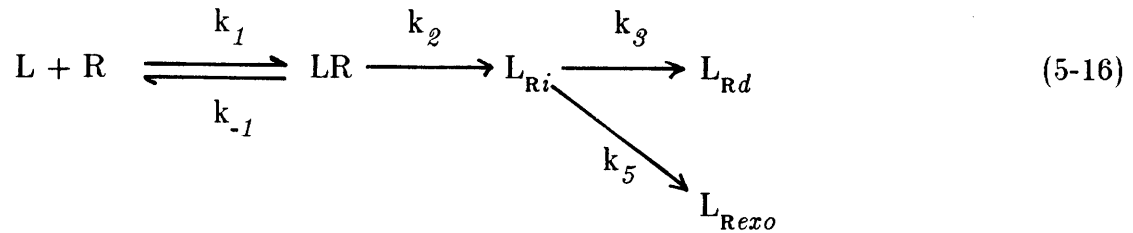
where C_s is the concentration of binding sites (mol/cm^3 tissue). For a tracer experiment C_s is approximately constant and a pseudo-first order rate constant can be defined:

$$k_a = \frac{k'_a C_s}{\epsilon_w} \quad (5-15a)$$

Substituting equation (5-15a) into (5-14) yields:

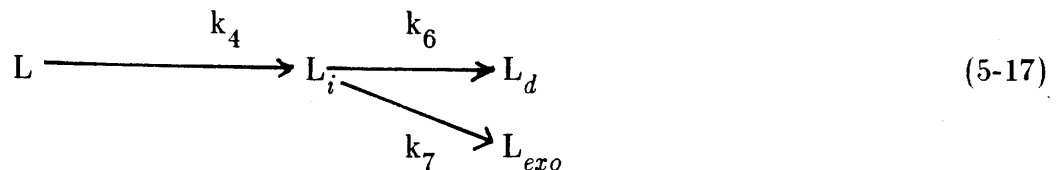
$$r_b = k_a \left(C_f - \frac{k_d}{k_a} C_b \right) \quad (5-15b)$$

Receptor-Mediated and Receptor-Independent Metabolism Kinetic models for receptor-mediated and receptor-independent binding, internalization, and degradation discussed in Chapter 2 have been incorporated into the in vivo model. The model for receptor-mediated metabolism is represented schematically as:



where L represents freely diffusible LDL in the interstitial fluid; R represents the receptor on the cell surface; L_{Ri} , represents intracellular LDL; L_{Rexo} represents ligand returned to the interstitial fluid by exocytosis; and L_{Rd} , degraded ligand. The notation L_R is used to denote ligand which is metabolized by the receptor-mediated pathway as opposed to ligand which is metabolized by the receptor-independent pathway. k_1 ($M^{-1}min^{-1}$) is the rate constant for receptor-ligand association, k_{-1} (min^{-1}) is the rate constant for receptor-ligand dissociation, k_2 (min^{-1}) is the rate constant for receptor-mediated internalization, k_3 (min^{-1}) is the rate constant for lysosomal degradation of ligand and k_5 (min^{-1}) is the rate constant for exocytosis.

The model for receptor-independent metabolism is represented schematically as:



where L_i represents intracellular protein internalized by receptor-independent mechanisms, L_d represents degraded solute, and L_{exo} represents solute which has

been returned to the interstitial fluid by exocytosis. k_4 (ml interstitial fluid)/(mg cell protein · min) is the rate constant for receptor-mediated internalization, and k_6 (min^{-1}) and k_7 (min^{-1}) are, respectively, rate constants for degradation and exocytosis of protein internalized by receptor-independent mechanisms. Although the results presented in Chapter 2 indicate that k_6 and k_7 are approximately equal to their respective receptor-mediated counterparts, k_3 and k_5 , the model has been developed for the more general case in which rate constants for receptor-mediated and receptor-independent degradation and exocytosis are different.

In Chapter 2, cell associated concentrations ($[LR]$, $[L_{Ri}]$, $[L_{Rexo}]$, $[L_i]$, $[L_d]$ and $[L_{exo}]$) are expressed as ng protein/mg cell protein. Using equation (5-9), the concentrations are expressed in terms of moles/cm³ total tissue:

$$C_{LR} = \frac{[LR]\rho_c \epsilon_c}{M_w \times 10^9} \quad (5-18a)$$

$$C_{L_{Ri}} = \frac{[L_{Ri}]\rho_c \epsilon_c}{M_w \times 10^9} \quad C_{L_i} = \frac{[L_i]\rho_c \epsilon_c}{M_w \times 10^9} \quad (5-18b,c)$$

$$C_{L_{Rd}} = \frac{[L_{Rd}]\rho_c \epsilon_c}{M_w \times 10^9} \quad C_{L_d} = \frac{[L_d]\rho_c \epsilon_c}{M_w \times 10^9} \quad (5-18d,e)$$

$$C_{L_{Rexo}} = \frac{[L_{Rexo}]\rho_c \epsilon_c}{M_w \times 10^9} \quad C_{L_{exo}} = \frac{[L_{exo}]\rho_c \epsilon_c}{M_w \times 10^9} \quad (5-18f,g)$$

In Chapter 2, $[R]$ was presented in units of receptors/cell. C_R is related to $[R]$ as follows:

$$C_R = \frac{[R]\epsilon_c}{V_c N} \quad (5-18h)$$

where V_c is the smooth muscle cell volume and N is Avogadro's number (6.02×10^{23} molecules/mole).

Binding of LDL to its receptor is bimolecular and the rate of binding, r_{LR} , per unit of tissue volume is:

$$r_{LR} = k_1 C_R \frac{C_f}{\epsilon_w} - k_{-1} C_{LR} \quad (5-19)$$

LDL is assumed to behave as a tracer in the arterial wall. Consequently, the receptor concentration, C_R is approximately constant and equal to the total number of receptors, C_{RT} , and a pseudo-first order rate constant, k_1' , is defined:

$$k_1' = \frac{k_1 C_{RT}}{\epsilon_w} \quad (5-20)$$

which, when substituted into equation (5-19) yields:

$$r_{LR} = k_1' \left(C_f - \frac{k_{-1}}{k_1'} C_{LR} \right) \quad (5-21)$$

The rate of internalization, r_i , is the sum of the rates of receptor-mediated (r_{LR_i}) and nonspecific endocytosis (r_{L_i}):

$$r_i = r_{LR_i} + r_{L_i} \quad (5-22a)$$

where

$$r_{LR_i} = k_2 C_{LR} \quad (5-22b)$$

$$r_{L_i} = k_4 \rho_c \epsilon_c \frac{C_f}{\epsilon_w} \quad (5-22c)$$

In order to simplify notation, a new constant, k_4' (min^{-1}), can be defined, such that:

$$k_4' = \frac{\rho_c \epsilon_c k_4}{\epsilon_w} \quad (5-23)$$

The rates of degradation and exocytosis per unit of total tissue volume (r_d and r_{exo} , respectively) are the sums of the respective rates for solute internalized by receptor-

mediated and receptor-independent mechanisms.

$$-r_d = k_3 C_{L_{Ri}} + k_6 C_{L_i} \quad (5-24)$$

$$r_{exo} = k_5 C_{L_{Ri}} + k_7 C_{L_i} \quad (5-25)$$

5.3.3 Species Conservation Relations

A conservation relation for freely diffusible solute is obtained from a material balance expressed in words as

$$\begin{aligned} \left[\begin{array}{l} \text{Rate of} \\ \text{accumulation} \\ \text{of free protein} \end{array} \right] &= \left[\begin{array}{l} \text{Mass transport} \\ \text{rate by} \\ \text{diffusion} \end{array} \right] + \left[\begin{array}{l} \text{Mass transport} \\ \text{rate by} \\ \text{convection} \end{array} \right] - \left[\begin{array}{l} \text{Rate of} \\ \text{binding} \\ \text{to matrix} \end{array} \right] \\ &\quad - \left[\begin{array}{l} \text{Rate of} \\ \text{binding} \\ \text{to cells} \end{array} \right] - \left[\begin{array}{l} \text{Rate of} \\ \text{nonspecific} \\ \text{endocytosis} \\ \text{by cells} \end{array} \right] + \left[\begin{array}{l} \text{Rate of} \\ \text{exocytosis} \\ \text{by cells} \end{array} \right] \quad (5-26) \end{aligned}$$

Expressing equation (5-26) mathematically over a differential volume element of width Δx and cross-sectional area of A yields:

$$\frac{\partial(C_f/\epsilon_w)}{\partial t} \Delta x A \epsilon_w = \left\{ \left[-D e \frac{\partial^2(C_f/\epsilon_w)}{\partial x^2} \right]_x - \left[-D e \frac{\partial^2(C_f/\epsilon_w)}{\partial x^2} \right]_{x+\Delta x} \right\} \epsilon_w A + \left\{ \left[\frac{\chi v C_f}{\epsilon_w} \right]_x - \left[\frac{\chi v C_f}{\epsilon_w} \right]_{x+\Delta x} \right\} \epsilon_w A - r_b A \Delta x - r_{LR} A \Delta x - r_{L_i} A \Delta x + r_{exo} A \Delta x \quad (5-27)$$

Dividing equation (5-27) by $A \Delta x$ and taking the limit as Δx goes to zero yields the differential formulation of the material balance:

$$\frac{\partial C_f}{\partial t} = D e \frac{\partial^2 C_f}{\partial x^2} - \frac{\chi v}{\epsilon_w} \frac{\partial C_f}{\partial x} - r_b - r_{LR} - r_i + r_{exo} \quad (5-28)$$

Substituting for r_b , r_{LR} , r_{L_i} , and r_{exo} with equations (5-15b), (5-21), (5-22c), and (5-25), respectively, yields:

$$\begin{aligned} \frac{\partial C_f}{\partial t} = & D e \frac{\partial^2 C_f}{\partial x^2} - \frac{\chi v}{\epsilon_w} \frac{\partial C_f}{\partial x} - k_a \left(C_f - \frac{k_d}{k_a} C_b \right) \\ & - k_1' \left(C_f - \frac{k_{-1}}{k_1'} C_{LR} \right) - k_4' C_f + k_5 C_{LR} + k_7 C_{L_i} \end{aligned} \quad (5-29)$$

Similar material balances can be written for lipoprotein bound to the extracellular matrix, bound to cell membrane receptors, internalized, and degraded.

$$\frac{\partial C_b}{\partial t} = k_a \left(C_f - \frac{k_d}{k_a} C_b \right) \quad (5-30)$$

$$\frac{\partial C_{LR}}{\partial t} = k_1' \left(C_f - \frac{k_{-1} + k_2}{k_1'} C_{LR} \right) \quad (5-31)$$

$$\frac{\partial C_{L_{Ri}}}{\partial t} = k_2 C_{LR} - (k_3 + k_5) C_{L_{Ri}} \quad (5-32)$$

$$\frac{\partial C_{L_i}}{\partial t} = k_4' \left(C_f - \frac{k_6 + k_7}{k_4'} C_{L_i} \right) \quad (5-33)$$

$$\frac{\partial C_d}{\partial t} = k_3 C_{L_{Ri}} + k_6 C_{L_i} \quad (5-34)$$

Addition of equations (5-29) to (5-34) together leads to:

$$\frac{\partial C_f}{\partial t} + \frac{\partial C_b}{\partial t} + \frac{\partial C_{LR}}{\partial t} + \frac{\partial C_{L_{Ri}}}{\partial t} + \frac{\partial C_{L_i}}{\partial t} + \frac{\partial C_d}{\partial t} = D e \frac{\partial^2 C_f}{\partial x^2} - \frac{\chi v}{\epsilon_w} \frac{\partial C_f}{\partial x} \quad (5-35)$$

Noting that $C_T = C_f + C_b + C_{LR} + C_{L_{Ri}} + C_{L_i}$ (equation (5-8)) and $C_{T+d} = C_T + C_d$ (equation (5-10)), equation (5-35) becomes:

$$\frac{\partial C_{T+d}}{\partial t} = D e \frac{\partial^2 C_f}{\partial x^2} - \frac{\chi v}{\epsilon_w} \frac{\partial C_f}{\partial x} \quad (5-36)$$

Making use of the definition of the solute flux, equation (5-11), the right hand side of equation (5-36) is simply the negative of the gradient of the flux:

$$\frac{\partial C_{T+d}}{\partial t} = - \frac{\partial N_s}{\partial x} \quad (5-37)$$

The rate of accumulation of ^{14}C -sucrose in the tissue is equal to the negative of gradient of the flux. Equation (5-37) is identical to equation (4-17) which was used to analyze ^{14}C -sucrose tissue concentrations and evaluate the time-varying permeabilities.

5.3.4 Boundary Conditions

Although endothelial cells metabolize LDL to supply their cholesterol needs, it is likely that transendothelial transport and degradation are two distinct and separate processes. Transendothelial transport is a rapid process, limited by vesicle attachment and detachment (Rubin [1977], Arminski et al. [1980]). Vesicles diffuse across the endothelial cell in less than a minute (Rubin [1977], Arminski et al. [1980]); LDL degradation is much slower ($t_{1/2} = \ln 2/k_3 = 85$ min) and is probably limited by vesicle-lysosome fusion (Herman and Albertini [1984]). Although it is not known whether degradation and transendothelial transport occur in different vesicles, cell metabolism of LDL and transendothelial transport were examined

separately. The effect of endothelial cell metabolism is considered in the Results section.

Since vesicular transport across the intimal endothelium is rapid relative to subsequent events in the vessel wall, transendothelial transport is in a quasi-steady state. The intimal boundary condition is derived from a balance which equates the total rate of lipoprotein transport by transendothelial vesicular transport and simultaneous convection and diffusion through the transcellular junctions.

The flux of lipoprotein across the endothelial cell, N_v (mol/cm² luminal area · s) is proportional to the difference in vesicle concentrations at the luminal and abluminal faces.

$$N_v = k_e(C_{0^-} - C_{0^+}) \quad (5-38)$$

where C_{0^-} and C_{0^+} refer to the concentrations of solute in vesicles at the luminal and abluminal sides, respectively, and k_e is the mass transfer coefficient (cm/s). Bratzler [1974] has pointed out that k_e is equal to the product of the vesicle flux (S_v , vesicles/cm² luminal area · s) times the vesicle volume (V_v).

At the vessel lumen the plasma adjacent to the endothelial cells is assumed to be in equilibrium with the vesicle contents. Due to steric effects and nonspecific adsorption to the cell membrane, partitioning results and the vesicle concentration is related to the plasma concentration in terms of a partition coefficient ($K_{e/p}$):

$$\frac{C_{0^-}}{C_p} = K_{e/p} \quad (5-39a)$$

Likewise, at the abluminal surface the vesicle concentration is related to the medial concentration in terms of a second partition coefficient ($K_{e/i}$):

$$\frac{C_{0+}}{C_f/\epsilon_w} = K_{e/i} \quad (5-39b)$$

If the tissue is at equilibrium with the plasma, then there are no gradients across the endothelial cell, $C_{0+} = C_{0-}$ and equations (5-39a) and (5-39b) are related:

$$\frac{C_f}{C_p} = \frac{\epsilon_w K_{e/p}}{K_{e/i}} \quad (5-40c)$$

The left hand side of equation (5-40c) is equal to $\epsilon_w K_p$ or ϵ_f . Thus, the ratio of the partition coefficients, $\frac{K_{e/p}}{K_{e/i}}$, is equal to K_p .

Substituting for C_{0+} and C_{0-} in equation (5-38) yields:

$$N_v = k_e (K_{e/p} C_p - K_{e/i} \frac{C_f}{\epsilon_w}) \quad (5-41a)$$

By multiplying and dividing the right hand side of equation (5-41a) by $K_{e/p}$, the flux can be expressed in terms of $K_{e/p}$ and ϵ_f .

$$N_v = k_e K_{e/p} (C_p - \frac{C_f}{\epsilon_f}) \quad (5-41b)$$

The rate of solute transport through the junctions per unit total luminal surface area, N_j , is:

$$N_j = v C_p (1-R) \quad (5-42)$$

where R is the endothelial cell rejection coefficient and v is the superficial velocity. R is a measure of the hindrance of solute convective and diffusive transport through the junctions and can range from zero for a solute which is not hindered to one for a solute which is completely rejected.

The complete initial boundary condition is obtained by equating the rates of vesicular and junction transport to the rates of diffusive and convective transport in the media:

$$A(N_v + N_j) = N_s A \epsilon_w \quad (5-43a)$$

$$A \left[v C_p (1-R) + k_e K_{e/p} \left(C_p - \frac{C_f}{\epsilon_f} \right) \right] = \left[-D_e \frac{\partial C_f / \epsilon_w}{\partial x} + \chi \frac{v}{\epsilon_w} \frac{C_f}{\epsilon_w} \right] A \epsilon_w \quad (5-43b)$$

Dividing by A, the luminal surface area, yields:

$$v C_p (1-R) + k_e K_{e/p} \left(C_p - \frac{C_f}{\epsilon_f} \right) = -D_e \frac{\partial C_f}{\partial x} + \chi \frac{v}{\epsilon_w} C_f \quad (5-43c)$$

The results in Chapter 4 indicate that the permeabilities are decreasing with time, and k_e can be represented by:

$$k_e = k_{e_0} [1 - f(1 - e^{-\gamma t})] \quad (5-43d)$$

Changes in the permeabilities may be due to an alteration in LDL as a result of aggregation, binding to other plasma proteins, or interaction with the endothelial cell surface.

Qualitatively similar phenomena occur in the transport of solute between the media and capillaries and lymphatic vessels in the adventitia. The nonvascular adventitial tissue is assumed to have a relatively small capacity for accumulation and is at a quasi-steady state. A material balance on the adventitia is obtained by equating the rate of convection and diffusion in the tissues to the rates of convective and vesicular transport across the lymphatics, arterioles and venules.

$$N_s A \epsilon_w = N_l A_l - N_a A_a + N_c A_c + N_v A_v \quad (5-44)$$

where N_l , N_a , N_c , and N_v represent the fluxes for solute transport across lymphatic

endothelium, arteriolar endothelium, capillary endothelium, and venular endothelium, respectively, and A_l , A_a , A_c , and A_v represent the surface areas of the lymphatic, arteriolar, capillary, and venular endothelium, respectively.

The flux across the lymphatic vessels is the sum of convective transport through the junctions and vesicular transport across the endothelium:

$$N_l = v_l \frac{C_f}{\epsilon_w} (1 - R_l) + k_l K_{lv/l} \left(\frac{C_f}{\epsilon_f} - C_l \right) \quad (5-45a)$$

where v_l is the superficial convective velocity into the lymphatics, based upon the lymphatic area, A_l , R_l is the rejection coefficient for junctional transport, k_l is the mass transfer coefficient for vesicular transport across the lymphatic vessels, and $K_{lv/l}$ is analogous to $K_{e/p}$ and is the partition coefficient between the lymphatic vesicles (lv) and the lymphatic fluid.

Transport across the entire capillary network is divided among three fluxes: 1) convective transport into the adventitia across the arteriolar capillaries, N_a ; 2) convective transport out of the adventitia across the venular capillaries, N_v ; and 3) vesicular transport across all of the capillaries, N_c . The resulting fluxes are:

$$N_a = v_a C_p (1 - R_a) \quad (5-45b)$$

$$N_v = v_v \frac{C_f}{\epsilon_w} (1 - R_v) \quad (5-45c)$$

$$N_c = k_c K_{c/p} \left(\frac{C_f}{\epsilon_f} - C_p \right) \quad (5-45d)$$

where v_a and v_v are the superficial velocities across the arterial and venular ends of the capillaries, R_a and R_v are the corresponding rejection coefficients, and k_c and

$K_{c/p}$ are, respectively, the mass transfer coefficients and partition coefficients for vesicular transport across the capillaries.

Substitution of equation (5-11) for N_s , and equations (5-45a), (5-45b), (5-45c) and (5-45d) for N_l , N_a , N_v , and N_c , respectively, into equation (5-44) yields:

$$A_{\epsilon_w} \left[-D e \frac{\partial C_f / \epsilon_w}{\partial x} + \chi \frac{v C_f}{\epsilon_w} \right] = v_l A_l \frac{C_f}{\epsilon_w} (1 - R_l) - v_a A_a C_p (1 - R_a) \\ + v_v A_v \frac{C_f}{\epsilon_w} (1 - R_v) + k_l K_{lv/l} A_l \left(\frac{C_f}{\epsilon_f} - C_l \right) + k_c K_{c/p} A_c \left(\frac{C_f}{\epsilon_f} - C_p \right) \quad (5-46)$$

For simplicity, the lymphatic concentration, C_l is assumed to be zero.

The lymphatic and capillary mass transfer coefficients are assumed to vary with time in the same fashion as the luminal endothelium mass transfer coefficient.

$$k_l = k_{l_o} [1 - f(1 - e^{-\gamma t})] \quad (5-47a)$$

$$k_c = k_{c_o} [1 - f(1 - e^{-\gamma t})] \quad (5-47b)$$

The initial conditions are:

$$t < 0 \quad C_p = C_T = C_f = C_b = C_{LR} = C_{L_{Ri}} = C_{L_i} = C_e = 0 \quad (5-48a)$$

$$t \geq 0 \quad C_p = C_p(t) \quad (5-48b)$$

where the time dependence of the plasma concentration is represented by a biexponentially decaying function, equation (4-1).

5.3.5 Nondimensionalization

In order to generalize the mathematical solution and interpretation of the results, the conservation relations (equations (5-29) - (5-34)), boundary conditions (equations (5-43c) and (5-46)), and initial conditions (equations (5-48a,b)) are cast into dimensionless form.

Conservation Relations

$$\frac{\partial \theta_f}{\partial \tau} = \frac{\partial \theta_f^2}{\partial \eta^2} - Pe \frac{\partial \theta_f}{\partial \eta} - \phi_b^2 (\theta_f - m\theta_b) - \phi_r^2 (\theta_f - (K-\beta)\theta_{LR}) - \phi_i^2 \theta_f + \phi_{e_1}^2 \theta_{LRi} + \phi_{e_2}^2 \theta_{Li} \quad (5-49)$$

$$\frac{\partial \theta_b}{\partial \tau} = \phi_b^2 (\theta_f - m\theta_b) \quad (5-50)$$

$$\frac{\partial \theta_{LR}}{\partial \tau} = \phi_r^2 (\theta_f - K\theta_{LR}) \quad (5-51)$$

$$\frac{\partial \theta_{LRi}}{\partial \tau} = \phi_r^2 \beta \theta_{LR} - (\phi_{d_1}^2 + \phi_{e_1}^2) \theta_{LRi} \quad (5-52)$$

$$\frac{\partial \theta_{Li}}{\partial \tau} = \phi_i^2 \theta_f - (\phi_{d_2}^2 + \phi_{e_2}^2) \theta_{Li} \quad (5-53)$$

$$\frac{\partial \theta_d}{\partial \tau} = \phi_{d_1}^2 \theta_{LRi} + \phi_{d_2}^2 \theta_{Li} \quad (5-54)$$

Boundary Conditions

$$\eta = 0 \quad \frac{Pe\theta_p}{\chi K_p} (1-R) + Bi(\theta_p - \frac{\theta_f}{\epsilon_f}) = \frac{1}{\epsilon_f} (-\frac{\partial \theta_f}{\partial \eta} + Pe\theta_f) \quad (5-55)$$

$$\eta = 1 \quad -\frac{\partial \theta_f}{\partial \eta} + Pe\theta_f = Pe_l \theta_f (1-R_l) - Pe_a \epsilon_w \theta_p (1-R_a) + Pe_v \theta_f (1-R_v) + Bi_l \theta_f + \epsilon_f Bi_c (\frac{\theta_f}{\epsilon_f} - \theta_p) \quad (5-56)$$

Initial Conditions

$$\tau < 0 \quad \theta_p = 0 \quad (5-57a)$$

$$\theta_f = \theta_b = \theta_{LR} = \theta_{LRi} = \theta_{Li} = \theta_d = 0 \quad (5-57b)$$

$$\tau \geq 0. \quad \theta_p = \theta_p(\tau) \quad (5-57c)$$

Definitions of the dimensionless groups are summarized in Table 5-I. Distance is normalized by medial thickness and each concentration by the initial plasma concentration. The dimensionless time, or Fourier number, is a measure of the elapsed time of the experiment divided by the relaxation time, L^2/D_e for diffusion in the media. The Peclet number is a measure of the relative rates of convection and diffusion in the media. Unlike previous definitions of the Peclet number (Ramirez [1979], Truskey et al. [1981]), the definitions presented here correctly define the interstitial velocity, v/ϵ_w . Each Biot number is a measure of the diffusive mass transfer resistance in the media, $L/D_e \epsilon_f$, divided by the the resistance at a specific boundary associated with transendothelial vesicular transport. Each Thiele modulus is a measure of the relaxation time for diffusion in the media divided by the relaxation time for a specific reaction. The binding equilibrium ratio m represents the ratio of the rate constants for binding to and dissociation from the extracellular matrix. K is the ratio of the rate constants for dissociation of ligand from the receptor and receptor-mediated internalization to the rate constant for binding. The relationship between K and K_{int} defined in Chapter 2 can be determined by substituting for k_1' .

$$K = \frac{(k_{-1} + k_2)\epsilon_w}{k_1 C_R} = \frac{K_{int}\epsilon_w}{C_R} \quad (5-58)$$

β represents the ratio of the rate constant for receptor-mediated internalization to the rate constant for receptor-ligand binding. For the case of slow dissociation of the ligand from its receptor (i.e. $k_{-1} \ll k_2$), β is approximately equal to K .

The adventitial boundary condition, equation (5-56), can be written in a simpler form:

Table 5-I: Dimensionless Groups Used in Transport Model

<u>Position</u>	$\eta = \frac{x}{L}$	<u>Time</u>	$\tau = \frac{D_e t}{L^2}$		
<u>Concentration</u>					
$\theta_p = \frac{C_p}{C_{p_0}}$	$\theta_T = \frac{C_T}{C_{p_0}}$	$\theta_f = \frac{C_f}{C_{p_0}}$	$\theta_b = \frac{C_b}{C_{p_0}}$	$\theta_{LR} = \frac{C_{LR}}{C_{p_0}}$	
$\theta_{L_{Ri}} = \frac{C_{L_{Ri}}}{C_{p_0}}$	$\theta_{L_i} = \frac{C_{L_i}}{C_{p_0}}$	$\theta_d = \frac{C_d}{C_{p_0}}$			
<u>Peclet Numbers</u>			<u>Biot Numbers</u>		
Medial	$Pe = \frac{\chi v L}{D_e \epsilon_w}$	Intimal	$Bi = \frac{k_e K_{e/p} L}{D_e \epsilon_f}$		
Lymphatic	$Pe_l = \frac{v_l LA_l}{D_e \epsilon_w A}$	Lymphatic	$Bi_l = \frac{k_l K_{lv/l} LA_l}{D_e \epsilon_f A}$		
Venular	$Pe_v = \frac{v_v LA_v}{D_e \epsilon_w A}$	Capillary	$Bi_c = \frac{k_c K_{c/p} LA_v}{D_e \epsilon_f A}$		
Arteriolar	$Pe_a = \frac{v_a LA_a}{D_e \epsilon_w A}$				

Table 5-I: (continued)Thiele Moduli

$$\phi_b^2 = \frac{k_a L^2}{D_e}$$

$$\phi_r^2 = \frac{k_1' L^2}{D_e}$$

$$\phi_{d_1}^2 = \frac{k_3 L^2}{D_e}$$

$$\phi_{e_1}^2 = \frac{k_5 L^2}{D_e}$$

$$\phi_i^2 = \frac{k_4' L^2}{D_e}$$

$$\phi_{d_2}^2 = \frac{k_6 L^2}{D_e}$$

$$\phi_{e_2}^2 = \frac{k_7 L^2}{D_e}$$

Plasma Decay Constant

$$b_i = \frac{b_i' L^2}{D_e}$$

Binding Equilibrium

Matrix $m = \frac{k_d}{k_a}$

Receptors $K = \frac{k_{-1} + k_2}{k_1}$

Rate Constant Ratio

$$\beta = \frac{k_2}{k_1'}$$

Time Dependent Biot Numbers

$$\gamma' = \frac{\gamma L^2}{D_e}$$

$$\eta = 1 \quad K_2 \theta_p - K_1 \theta_f = - \frac{\partial \theta_f}{\partial \eta} \quad (5-59a)$$

$$K_1 = Pe - Pe_l(1-R_l) - Pe_v(1-R_v) - Bi_l - Bi_c \quad (5-59b)$$

$$K_2 = -Pe_a(1-R_a)\epsilon_w - Bi_c \epsilon_f \quad (5-59c)$$

In fitting 0.5 hr LDL transmural profiles in the squirrel monkey, Tompkins found that the adventitial boundary condition, equation (5-59a), was best represented by a single parameter.

$$\eta = 1 \quad \epsilon_f Bi_c \left(\theta_p - \frac{\theta_f}{\epsilon_f} \right) = \frac{\partial \theta_f}{\partial \eta} \quad (5-60)$$

Equation (5-60) can be derived from equations (5-59b) and (5-59c) by assuming that $Pe = Pe_l = Pe_a = 0$ and $Bi_l \ll Bi_c$. Equation (5-60) has been used in the estimation of transport parameters in this study, although the equations are solved using the more general boundary condition, equation (5-59a).

5.3.6 Solution

Equations (5-48) to (5-53) were solved by the method of Laplace transforms. Solutions were first obtained for a step input (i.e., $\theta_p(\tau) = 1$) to yield solutions for ψ_T .

$$\psi_T = \psi_f + \psi_b + \psi_{LR} + \psi_{L_{Ri}} + \psi_{Li} \quad (5-61)$$

Duhamel's superposition integral was applied to the solution for a step response to obtain the solution for a time-varying plasma concentration. For mobile solute the integral is:

$$\theta_f(\eta, \tau) = \psi_f(\eta, \tau)D(0) + \int_0^\tau \psi_f(\eta, \tau - \tau') \frac{dD(\tau')}{d\tau'} d\tau' \quad (5-62)$$

where $D(\tau)$ is the disturbance function. Two cases were considered: 1) the mass transfer coefficient is constant and θ_p is represented by equation (4-1); and 2) the mass transfer coefficients are decreasing with time according to equation (5-45c) and the plasma concentration is represented by equation (4-1). For the first case equation (5-62) becomes:

$$D(\tau) = \theta_p(\tau) = \sum_{i=1}^2 a_i e^{-b_i \tau} \quad (5-63a)$$

For the second case equation (5-62) is:

$$D(\tau) = [1 - f(1 - e^{-\gamma \tau})] \theta_p(\tau) = [1 - f(1 - e^{-\gamma \tau})] \sum_{i=1}^2 a_i e^{-b_i \tau} \quad (5-63b)$$

The average tissue concentration are also of interest (represented by an overbar) and they can be obtained by analytically integrating the solutions for the tissue concentration over the tissue thickness:

$$\bar{\theta}_T(\tau) = \int_0^1 \theta_T(\eta, \tau) d\eta \quad (5-64)$$

Similar relations can be obtained for θ_f , θ_b , θ_{LR} , θ_{LRi} , and θ_{Li} as well as θ_d . Details of the solution are presented in Appendix E.

5.4 Results

Comparison of model predictions with data (concentration profiles and cumulative degradation) requires estimates for the various dimensionless groups listed in Table 5-I. Transport parameters were estimated from fits of 0.5 hr LDL and mLDL transmural profiles by nonlinear regression. Rate constants for receptor-mediated and receptor-independent LDL metabolism obtained from fits of pooled cell culture data (Chapter 2) served as estimates for these rate constants in vivo. Rate constants for LDL binding to the extracellular matrix were not available and were determined by fitting the model to transmural profiles. Finally, the model sensitivity to the various parameters and the assumption of linearization were examined.

5.4.1 Determination of Transport Parameters

The results presented in Chapter 4 indicate that little, if any, degradation has occurred by 0.5 hr, although LDL may have entered the smooth muscle cells. In order to estimate the transport parameters, freely diffusible LDL and mLDL were assumed to represent the major contribution to the total tissue concentration at 0.5 hr, for which equations (5-61) reduces to:

$$\theta_T(\eta, \tau) \approx \theta_f(\eta, \tau) \quad (5-65)$$

Equation (5-65) implies that metabolic phenomena are unimportant at short circulation times and the conservation equations ((5-49) to (5-55)) reduce to:

$$\frac{\partial \theta_f}{\partial \tau} = \frac{\partial^2 \theta_f}{\partial \eta^2} - Pe \theta_f \quad (5-66)$$

LDL is probably too large to fit through the endothelial cell junctions. Therefore, R is equal to 1 and the boundary condition at $\eta = 0$ reduces to:

$$\eta=1 \quad Bi\epsilon_f\left(\theta_p - \frac{\theta_f}{\epsilon_f}\right) = -\frac{\partial\theta_f}{\partial\eta} \quad (5-67)$$

The boundary condition at $\eta = 1$ is represented by the generalized boundary condition, equations (5-59a,b,c).

The solution to equation (5-66) for constant mass transfer coefficients and subject to boundary conditions represented by equations (5-59) and (5-67) is a limiting case of equation (E-61) in which $\phi_r^2 = \phi_b^2 = \phi_i^2 = 0$ and $K_1\epsilon_f = K_2 = -Bi$. For this case, the solution is:

$$\theta_f(\eta,\tau) = A(\eta) \left\{ B(\eta) \sum_{i=1}^2 a_i e^{-b_i\tau} - 2 \sum_{m=1}^{\infty} \frac{Q_m}{s_m} \left(e^{s_m\tau} + \sum_{i=1}^2 \frac{a_i b_i (e^{s_m\tau} - e^{-b_i\tau})}{s_m + b_i} \right) \right\} \quad (5-68)$$

where $A(\eta)$, $B(\eta)$, and Q_m are defined in equations (E-33) and (E-40).

There are five parameters to be estimated: Bi , K_1 , K_2 , Pe , and τ (or D_e). A value of ϵ_f equal to 0.17 was used, based upon the interstitial volume fraction accessible to albumin (Bratzler and Schwarz [1977]). The five parameters were determined by minimizing the sums of the squared residuals between theoretical prediction and experimental data through the use of the nonlinear least squares method of Marquardt [1963]. (This method is discussed in Chapter 2 and the computer codes are presented in Appendix H.) Output from a typical fit includes the best fit parameter values, the linearized estimate of the standard deviation, the sums of squares of the residuals, the parameter correlation matrix and the residuals.

In addition to the five parameter model, two simpler cases were also fit: 1) a four parameter model in which Pe was set equal to zero; and 2) a three parameter

model in which Pe is set equal to zero, and the boundary condition at $\eta = 1$ is represented by equation (5-60):

$$\eta = 1 \quad \epsilon_f Bi_c \left(\theta_p - \frac{\theta_f}{\epsilon_f} \right) = \frac{\partial \theta_f}{\partial \eta} \quad (5-60)$$

Parameter estimates for the three models were obtained by fitting all LDL and mLDL profiles at 0.5 hr (Figure 5-2). All three models give essentially identical fits and the sums of squares of the residuals are similar (Table 5-II). The Peclet number is close to zero for both LDL and mLDL, suggesting that convection can be neglected. The values of D_e and Bi are not significantly different in the three, four, and five parameter models, and the parameter standard deviations are lower in the three parameter model than in the five or four parameter models. (The four parameter model failed to converge for mLDL, possibly because of an insufficient number of data points near the medial-adventitial interface.) Thus, the three parameter model adequately represents the data, and the simplified boundary condition at $\eta = 1$ and $Pe = 0$ were used in all subsequent calculations.

In addition to fitting the pooled LDL and mLDL data at 0.5 hr (Figure 5-2) to the three parameter model, fits were also obtained for all profiles at 0.5 hr (Figure 5-3) as well as the individual profiles (Figures 5-4 and 5-5 for LDL and mLDL, respectively). For three of the experiments, of the experiments (30C2, 30C3, and 30M2) the model fit yields mid-medial concentrations much less than the measured concentrations and the fits resemble a penetration solution. In these three experiments the intimal gradients are very steep and mid-medial concentrations are about 0.001. No fit could be obtained which exhibited this behavior. This discrepancy between model fits and data may reflect heterogeneities in vessel wall permeability (Morrel [1983]) and/or a nonuniform distribution of binding sites. Fits

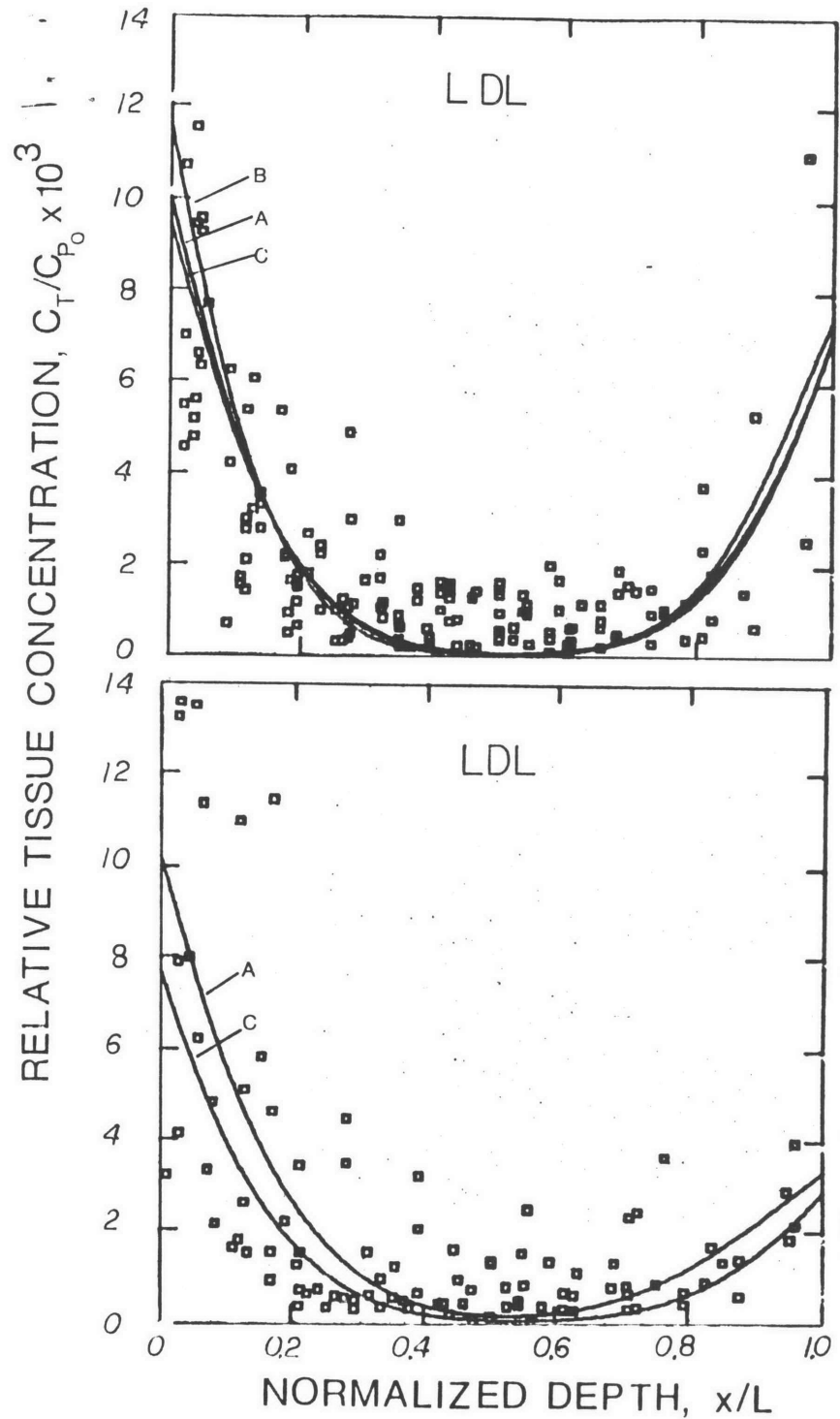


Figure 5-2: Model fits of all 0.5 hr LDL and mLDL transmural profiles for three (A), four (B), and five (C) parameter models. Each point represents a single section. Best fit values of parameters are listed in Table 5-II.

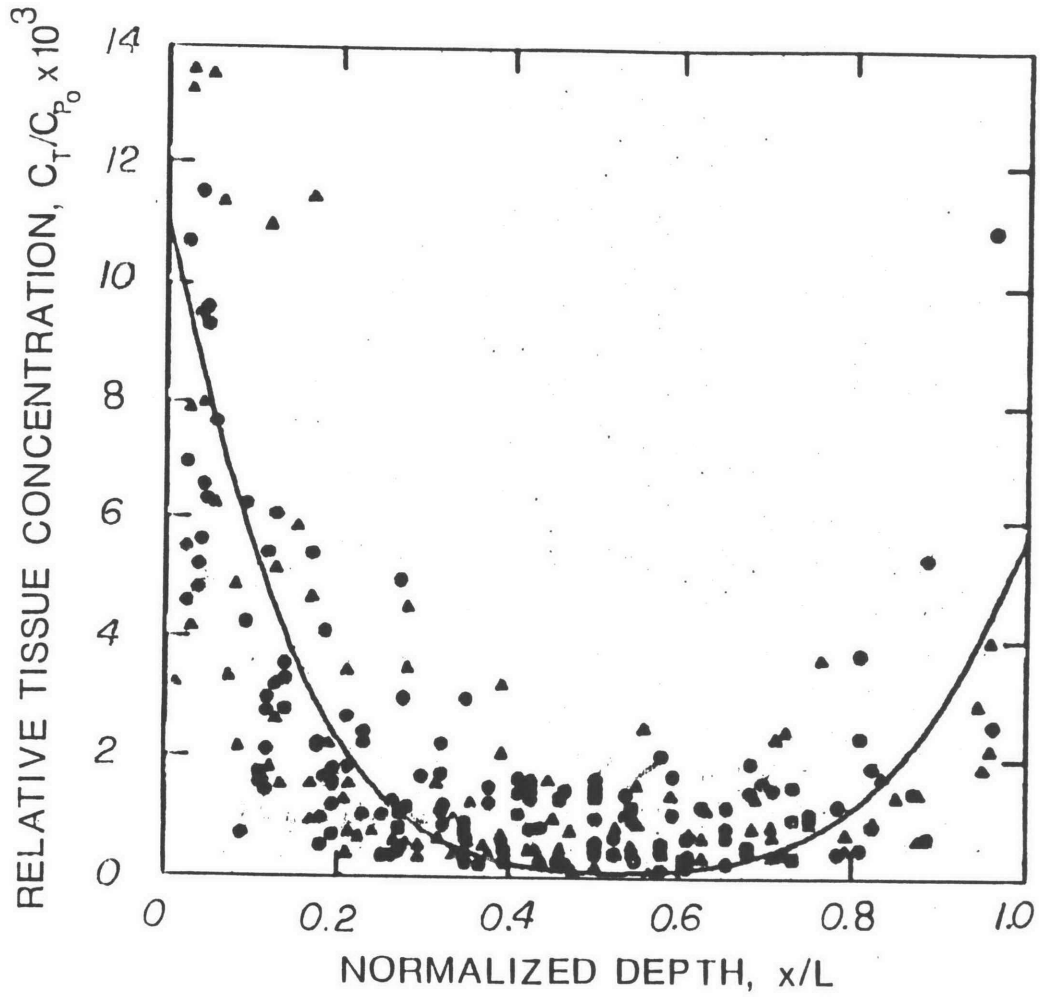


Figure 5-3: Model fits of combined 0.5 hr LDL (●) and mLDL (▲) transmural profiles for the three parameter model. Each point represents a single section. Best fit values of parameters are listed in Table 5-II.

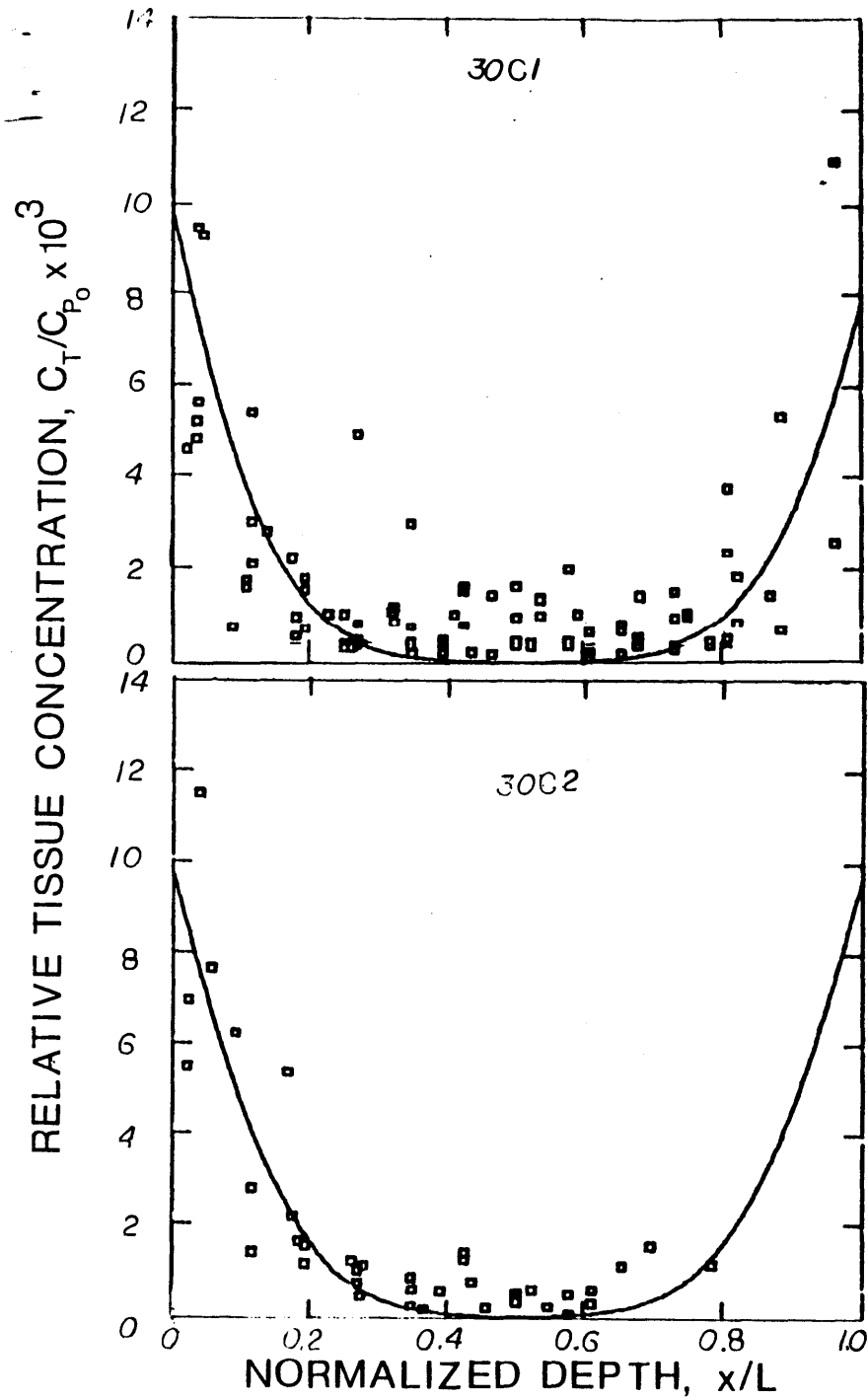


Figure 5-4: Model fits of individual animal 0.5 hr LDL transmurial profiles to the three parameter model. Each point represents a single section. Transport groups are listed in Table 5-II.

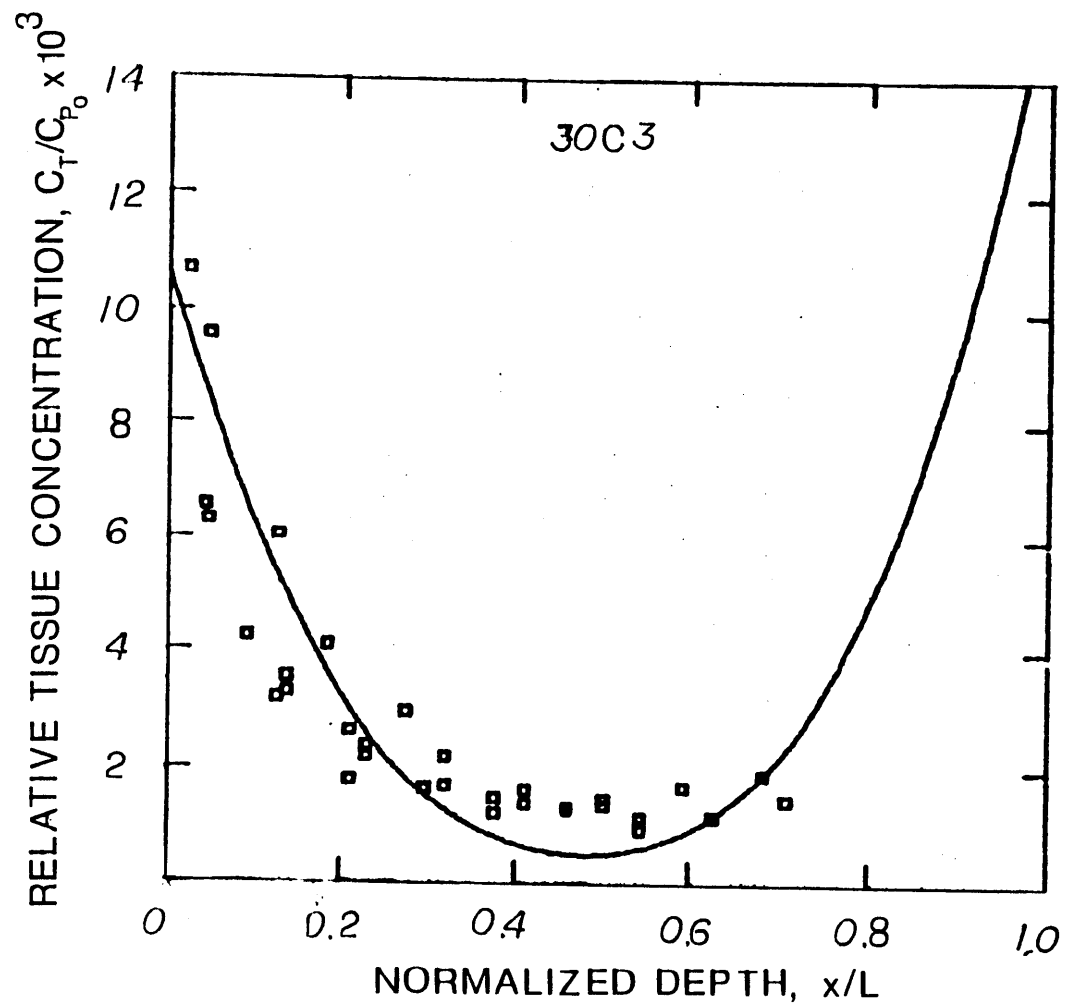


Figure 5-4: (continued)

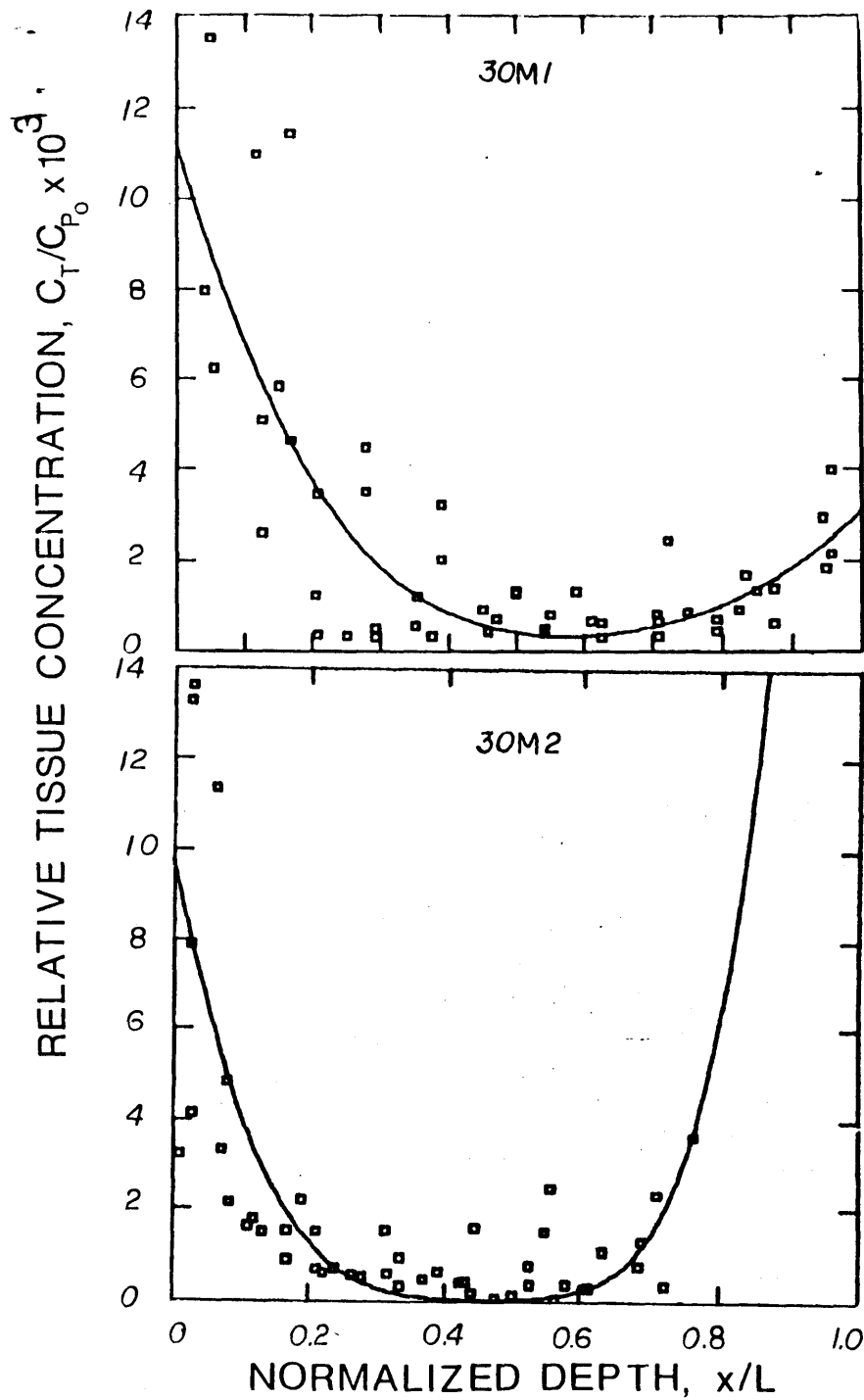


Figure 5-5: Model fits of individual animal 0.5 hr mLDL transmural profiles to the three parameter model. Each point represents a single section. Transport groups are listed in Table 5-II.

of pooled data presented in Figures 5-2 and 5-3 also underestimated the mid-medial concentrations.

Best fit parameters for the results presented in Figures 5-3 to 5-5 are listed in Table 5-II. Estimates of D_e and Bi among the individual LDL experiments are quite similar. The effective diffusion coefficients for LDL and mLDL are similar, implying that methylation does not influence diffusion. The intimal Biot numbers differ for LDL and mLDL, but this is due to differences in the tissue thickness ($113 \pm 13 \mu\text{m}$ for mLDL and $138 \pm 11 \mu\text{m}$ for LDL). Because the partition coefficient, $K_{e/p}$, is not known, k_e cannot be calculated, but rather, a lumped quantity, $k_E = k_e K_{e/p}$ can be determined. Values of k_E for LDL and mLDL from fits of pooled LDL and mLDL data are identical indicating that transendothelial transport is by receptor-independent mechanisms. Fitting all LDL and mLDL 0.5 hr data together yields values of k_E and D_e similar to estimates obtained fitting all LDL and mLDL data separately. These results are consistent with the calculations of k_E based upon mean relative tissue concentrations of ^{125}I -labeled LDL and mLDL at 0.5 hr discussed in Chapter 4.

Estimates for the Biot number at the medial-adventitial interface, Bi_c , are more variable, reflecting differences in capillary and lymphatic supply among the different animals. In experiments 30C2 and 30C3 for LDL and 30M2 for mLDL, the errors associated with Bi_c are quite large, resulting from the lack of data points between dimensionless depths of 0.8 and 1.0.

Additional insight concerning the relationship among the transport groups and the effect of methylation upon the various groups can be obtained by examination of the parameter correlation matrix for pooled data presented in Table 5-III. The correlation matrices for LDL and mLDL are very similar indicating that the parameters are influenced in the same fashion. There is a large negative correlation

Table 5-II: Transport Parameters Determined from Nonlinear Regression of 0.5 hr LDL and mLDL Transmural Profiles

Four and Five Parameter Models								
	$L, \mu\text{m}$	Bi	K_2	K_3	Pe	τ	$D_e \times 10^9, \text{cm}^2/\text{s SS} \times 10^4$	
LDL	138 ± 11	0.64 ± 0.23	0.39 ± 1.56	-0.063 ± 0.025	0.006 ± 3.6	0.013 ± 0.004	1.40	2pm 0.42 9.1
LDL	138 ± 11	0.76 ± 0.14	-16 ± 76	-0.23 ± 0.72	0 (fixed)	0.013 ± 0.019	1.35 ± 2.94	9.4
mLDL	113 ± 13	0.44 ± 0.46	-34.5 ± 949	-0.16 ± 3.86	-0.068 ± 8.5	0.030 ± 0.033	2.1 ± 2.3	4.5
Three Parameter Model								
Expt.	$L, \mu\text{m}$	Bi	τ	Bi_c	$D_e, \text{cm}^2/\text{s} \times 10^9$	$K_E, \text{cm}/\text{s} \times 10^9$	SS $\times 10^4$	
LDL Experiments								
30C1	149 ± 19	0.59 ± 0.17	0.011 ± 0.004	0.46 ± 0.17	1.4 ± 0.5	0.9 ± 0.6	4.91	
30C2	134 ± 23	0.71 ± 0.27	0.013 ± 0.006	0.72 ± 0.33	1.3 ± 0.6	1.3 ± 0.6	3.30	
30C3	133 ± 13	0.35 ± 0.06	0.030 ± 0.006	0.48 ± 0.29	2.9 ± 0.7	1.3 ± 0.4	0.77	
Combined	138 ± 11	0.58 ± 0.10	0.014 ± 0.003	0.42 ± 0.12	1.5 ± 0.3	1.1 ± 0.3	9.33	
mLDL Experiments								
30M1	119 ± 21	0.37 ± 0.08	0.034 ± 0.008	0.093 ± 0.032	2.6 ± 0.8	1.4 ± 0.5	1.62	
30M2	108 ± 13	0.67 ± 0.18	0.009 ± 0.003	3.9 ± 3.8	0.6 ± 0.2	0.6 ± 0.3	2.08	
Combined	113 ± 13	0.36 ± 0.07	0.025 ± 0.006	0.13 ± 0.05	1.8 ± 0.5	1.0 ± 0.3	4.55	
Combined LDL and mLDL	128 ± 16	0.58 ± 0.07	0.017 ± 0.003	0.29 ± 0.07	1.6 ± 0.2	1.2 ± 0.3	14.3	

between Bi_c and τ indicating that increases in the effective diffusion coefficient are offset by decreases in Bi_c . Correlations between Bi_c and τ and Bi_c and Bi are much lower.

5.4.2 Estimation of Transmural Profiles and Cumulative Degradation at Long Circulation Times

The estimated transport parameters together with rate constants from cell culture data were used to compare model predictions for transmural profiles and cumulative degradation. The dimensional quantities used are listed in Table 5-IV. The transport parameters are those determined from 0.5 hr data and ϵ_f is based upon the measured interstitial volume fraction of albumin (Bratzler and Schwarz [1977]). The rate constants for receptor-mediated and receptor-independent LDL metabolism are from fits of pooled cell culture data (Tables 2-III and 2-X, respectively). The receptor number, R_T , represents a reduction of 45% to 77% of the maximum number of receptors on smooth muscle cells as a result of receptor down-regulation.

In order to calculate C_{R_T} , k_1' , and k_4' values for the protein density (ρ_c) and cellular volume fraction (ϵ_c) of aortic smooth muscle are needed. These values are not known for rabbit aortic smooth muscle cells in vivo, and were estimated from measurements obtained for rat smooth muscle cells.

The cell protein density is the product of the protein mass per 10^6 cells (M_p) times the cell volume (V_c):

$$\rho_c = M_p V_c \quad (5-69)$$

M_p is 0.33 mg protein/ 10^6 cells for cultured bovine smooth cells (Appendix F). The cell volume of rat aortic smooth muscle cells is about $1000 \mu\text{m}^3$ (Bucher et al.

Table 5-III: Parameter Correlation Matrix for Pooled
LDL and mLDL Data

LDL			
	Bi	τ	Bi _c
Bi	1.000	-0.934	-0.599
τ	-0.934	1.000	0.642
Bi _c	-0.599	0.642	1.000
mLDL			
	Bi	τ	Bi _c
Bi	1.000	-0.932	-0.493
τ	-0.932	1.000	0.592
Bi _c	-0.493	0.592	1.000

Table-5-IV: Values of Dimensional Constants Used in Model Calculations for Constant Mass Transfer Coefficients

<u>Transport Parameters</u>	<u>Source</u>
$k_E = 1.19 \times 10^{-8} \text{ cm/s}$	Pooled Data in Table 5-II
$k_{E_c} = 0.60 \times 10^{-8} \text{ cm/s}$	Pooled Data in Table 5-II
$D_e = 1.55 \times 10^{-9} \text{ cm}^2/\text{s}$	Pooled Data in Table 5-II
$\epsilon_f = 0.17$	Bratzler and Schwarz [1977]
$\epsilon_w = 0.42$	Harrison and Massaro [1976]
$L = 0.013 \text{ cm}$	Pooled Data in Table 5-II
<hr/>	
<u>Metabolic Parameters</u>	
<u>Receptor-Mediated Metabolism</u>	
$k_1 = 0.50 \times 10^7 \text{ M}^{-1}\text{min}^{-1}$	Table 2-III
$k_1' = 0.0089\text{-}0.0174 \text{ min}^{-1}$	Section 5.4.2
$k_{-1} = 0.0 \text{ min}^{-1}$	Table 2-III
$k_2 = 0.25 \text{ min}^{-1}$	Table 2-III
$k_3 = 0.0057 \text{ min}^{-1}$	Table 2-III
$k_5 = 0.0082 \text{ min}^{-1}$	Table 2-III
$R_T = 1800\text{-}3500 \text{ receptors/cell}$	Table 2-III and Figs. 2-18, 2-19
$C_{R_T} = 0.75\text{-}1.45 \times 10^{-13} \text{ mol/cm}^3 \text{ tissue}$	Section 5.4.2
<u>Receptor-Independent Metabolism</u>	
$k_4 = 3.22 \times 10^{-5} \text{ ml/mg}\cdot\text{min}$	Table 2-X
$k_4' = 0.0063 \text{ min}^{-1}$	Section 5.4.2
$k_6 = 0.0036 \text{ min}^{-1}$	Table 2-X
$k_7 = 0.0071 \text{ min}^{-1}$	Table 2-X
<hr/>	
$\rho_c = 330 \text{ mg protein/cm}^3 \text{ cell}$	Section 5.4.2
$\epsilon_c = 0.25$	Gerrity and Cliff [1975]

[1982]) and the smooth muscle cells occupy 25% of the rat aorta (Gerrity and Cliff : [1975]). The estimated protein density, ρ_c , for smooth muscle cells is 330 mg protein/cm³ cell and $\rho_c \epsilon_c$ is 82.5 mg protein/cm³ tissue.

C_{R_T} can be calculated from the receptor numbers listed in Table 5-IV from equation (5-18h):

$$C_{R_T} = \frac{R_T \epsilon_c}{N V_c} \quad (5-18h)$$

where N is Avagadoro's number, 6.02×10^{23} molecules/mole. For the values of R_T and ϵ_c listed in Table 5-IV and a smooth muscle cell volume of $1000 \mu\text{m}^3$ (or 10^{-9}cm^3), C_{R_T} ranges from $0.75 \times 10^{-12} \text{mol/cm}^3$ tissue to $1.45 \times 10^{-12} \text{mol/cm}^3$ tissue.

Using this range of values for C_{R_T} , k_1' can be calculated from equation (5-20):

$$k_1' = \frac{k_1 C_{R_T}}{\epsilon_w} \quad (5-20)$$

and ranges in value from 0.0089min^{-1} to 0.0174min^{-1} .

In a similar manner k_4' can be determined using equation (5-23):

$$k_4' = \frac{k_4 \rho_c \epsilon_c}{\epsilon_w} \quad (5-23)$$

to yield a value of 0.0063min^{-1} .

The values of the dimensional constants listed in Table 5-IV were used to calculate the dimensionless groups listed in Table 5-I and their values are listed in Table 5-V. The Biot numbers represent the values estimated from fits of pooled 0.5 hr LDL data. The values listed for ϕ_r^2 , β , and ω represent the the extreme values for the different number of receptors. Thus, for 1800 receptors/cell ϕ_r^2 is 16.5, β (and

K) is 28.9; for 3500 receptors per cell ϕ_r^2 is 32.1 and β (and K) is 14.9. Not listed in Table 5-V are parameters for binding to the extracellular matrix, m and ϕ_b^2 , and the functional forms for the time varying Biot numbers. These groups are discussed below.

Table 5-V: Dimensionless Groups Used in Model Calculations

$Bi = 0.56$	$Bi_c = 0.39$
$\gamma_r^2 = 16.5, 32.1$	$\phi_i^2 = 11.6$
$\phi_{d_1} = 10.5$	$\phi_{d_2} = 6.8$
$\phi_{e_1}^2 = 14.9$	$\phi_{e_2} = 12.9$
$\beta = K = 28.9, 14.9$	

Constant Permeabilities The case of constant mass transfer coefficients with no binding to the extracellular matrix ($\phi_b^2 = 0.0$) was examined first. Model predictions for LDL and mLDL are compared with data for transmural profiles, mean relative concentrations, and cumulative degradation in Figures 5-6 to 5-9. For LDL, values of $\phi_r^2 = 16.5$, $\beta = K = 28.9$ were used to generate model predictions; all other parameters are listed in Table 5-V. Transmural profiles and mean relative concentrations were calculated using the pooled plasma decay curve for LDL obtained in this study (Figure 4-4) whereas cumulative degradation was calculated using pooled plasma decay curves from the data of Navarro [1984] (Figure 4-7).

Model predictions of LDL tissue concentrations overestimate data at 4 and 24 hr although mid-medial concentrations are similar (Figure 5-6). At 72 hr, model predictions underestimate tissue concentrations, suggesting that binding to the extracellular matrix may be important at long circulation times. The shapes of the transmural profiles are qualitatively similar to experimentally derived profiles at 4 and 72 hr, whereas at 24 hr the model predicts steeper gradients than those

observed experimentally. The model also predicts higher mean relative concentrations of undegraded and degraded LDL (Figure 5-7) than experimentally observed; $\theta_d(\infty)$ calculated from the model is 0.033 vs. 0.0081 ± 0.0008 estimated from data.

Model predictions for mLDL were generated by neglecting the receptor-mediated pathway (i.e. $\phi_r^2 = 0.0$). Model-generated tissue concentrations are greater than experimentally determined values at 4, 24, and 72 hr (Figure 5-8), due to the slower plasma decay and degradation of mLDL ($\phi_{d_2}^2 = 6.8$). Differences between model predictions and experimental observations are also apparent in the plot of the mean relative tissue concentration (Figure 5-9). Although mLDL is removed from the tissue by receptor-independent mechanisms only, predicted values for cumulative degradation is greater than data as well as predictions for LDL (Figure 5-9).

Model predictions for constant mass transfer coefficients highlight an apparent paradox, namely that improved agreement between model predictions and data for one set of results (either cumulative degradation or tissue concentrations) are obtained at the expense of poorer agreement between data and theory for the other response. Furthermore, a consistent parameter set is desired such that the same constants which yield reasonable predictions for LDL also yield reasonable predictions for mLDL (with ϕ_r^2 set equal to 0.0).

In order to examine if such a parameter set existed, nonlinear regression was used to fit LDL transmural profiles to determine ϕ_r^2 and $\phi_{d_1}^2$. Parameter values are listed in Table 5-VI. As a result of fitting for ϕ_r^2 and $\phi_{d_1}^2$ there is an improved fit of the LDL transmural profile (Figure 5-10), although the model overestimates the tissue concentration at 4 hr. Nevertheless, the model still predicts significantly more degradation than observed experimentally (Figure 5-11). The discrepancy between

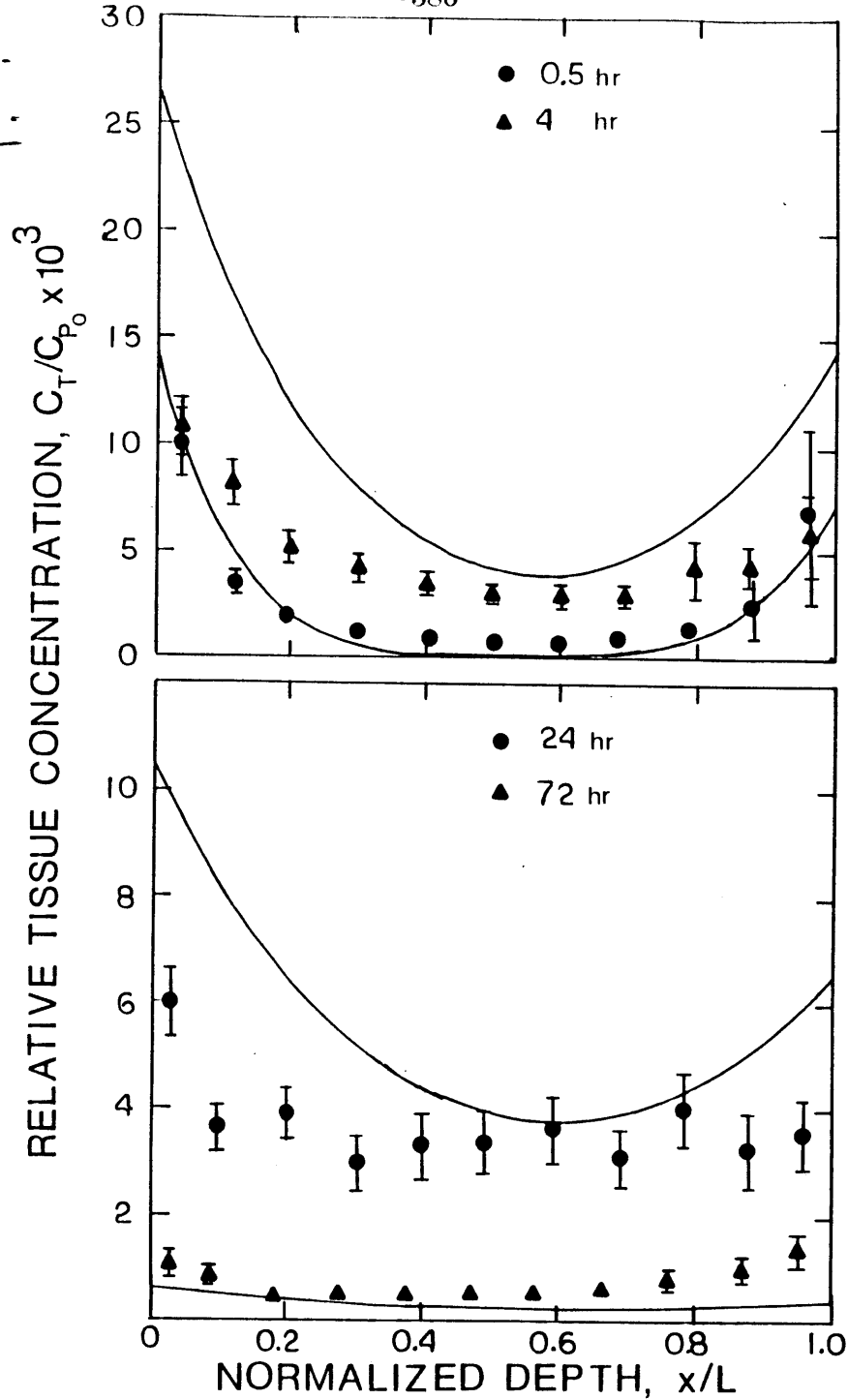


Figure 5-6: Comparison between model predictions and LDL transmural profiles for constant mass transfer coefficients and no binding to the extracellular matrix ($\phi_b^2 = 0.0$). For model predictions $\phi_r^2 = 16.5$, $\phi_{d_1}^2 = 10.5$, $\phi_{e_1}^2 = 14.9$, $\beta = K = 28.9$, $\phi_i^2 = 11.6$, $\phi_{d_2}^2 = 6.8$, $\phi_{e_2}^2 = 12.9$, $Bi = 0.58$, $Bi_c = 0.29$, $D_e = 1.55 \times 10^{-9} \text{ cm}^2/\text{s}$, $L = 0.013 \text{ } \mu\text{m}$.

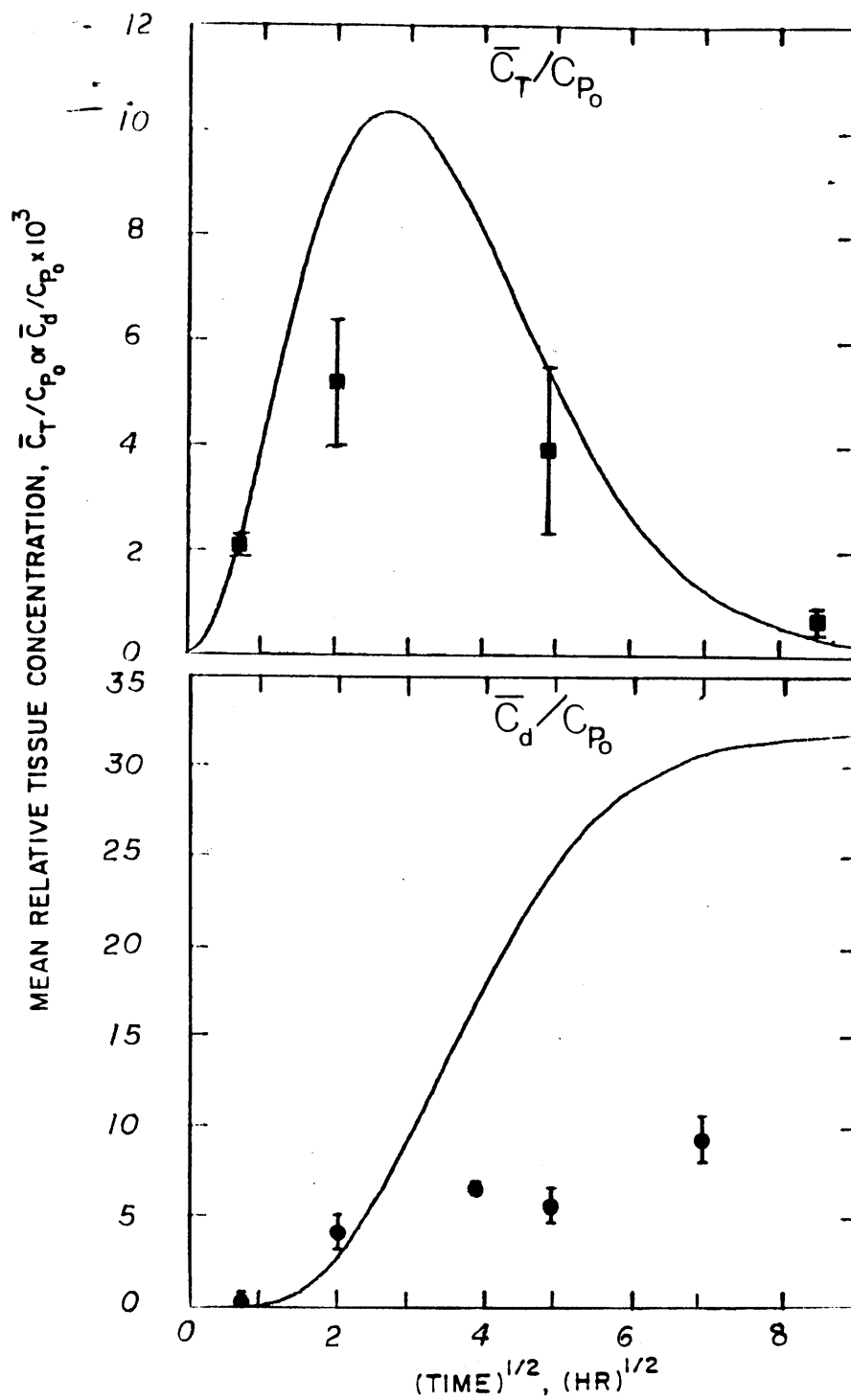


Figure 5-7: Comparison between model predictions and LDL mean relative concentrations and cumulative degradation for constant mass transfer coefficients and no binding to the extracellular matrix ($\phi_b^2 = 0.0$).

Parameter values are listed in the legend to Figure 5-6.

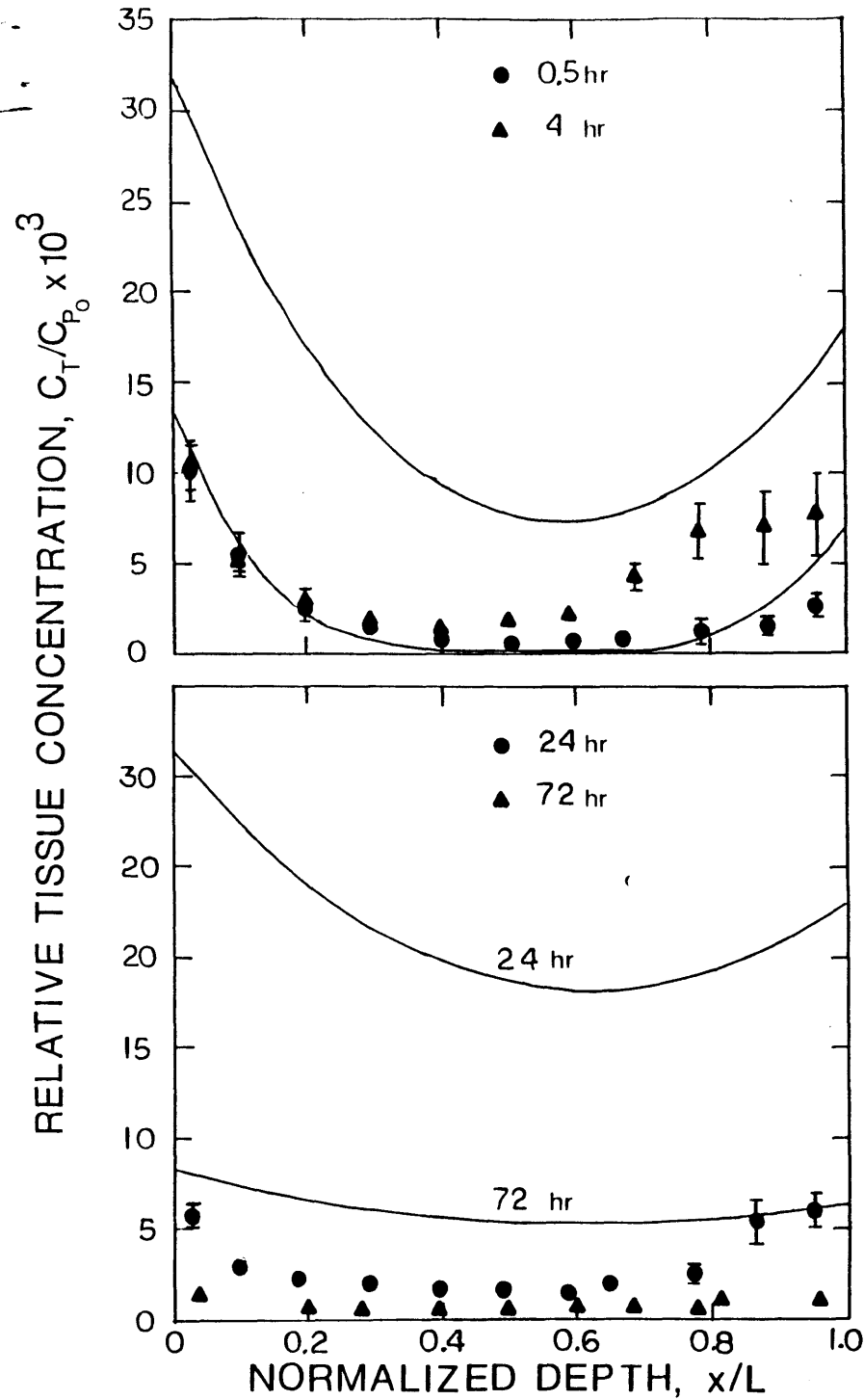


Figure 5-8: Comparison between model predictions and mLDL transmural profiles for constant mass transfer coefficients and no binding to the extracellular matrix ($\phi_b^2 = 0.0$). For model predictions $\phi_r^2 = 0.0$, $\phi_i^2 = 11.6$, $\phi_{d_2}^2 = 6.8$, $\phi_{e_2}^2 = 12.9$, $Bi = 0.58$, $Bi_c = 0.29$, $D_e = 1.55 \times 10^{-9} \text{ cm}^2/\text{s}$, $L = 0.013 \text{ } \mu\text{m}$.

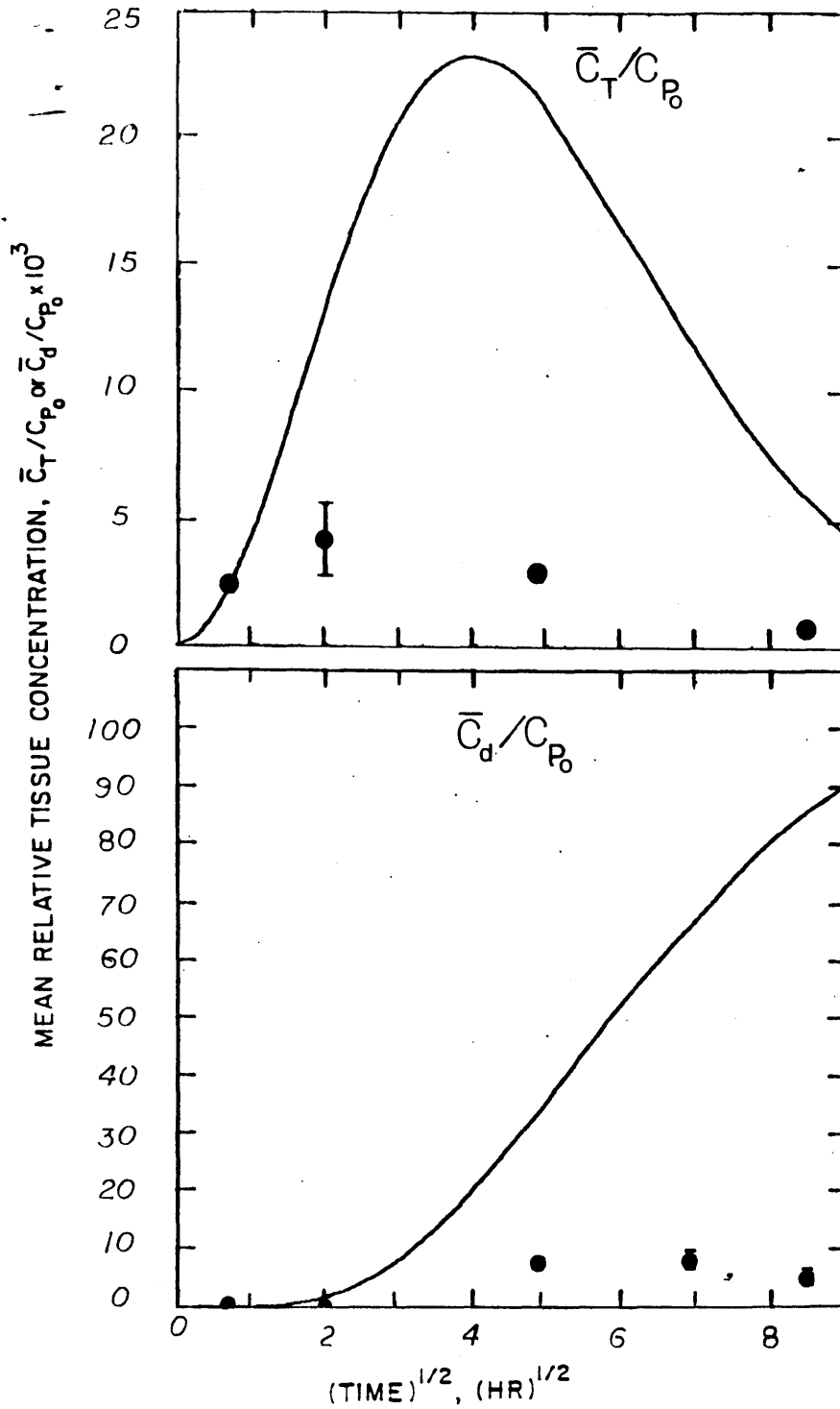


Figure 5-9: Comparison between model predictions and mLDL mean relative concentrations and cumulative degradation for constant mass transfer coefficients and no binding to the extracellular matrix ($\phi_b^2 = 0.0$).

Parameter values are listed in the legend to Figure 5-8.

model predictions and data for cumulative degradation is reduced slightly by fitting for ϕ_i^2 and $\phi_{d_2}^2$ and holding ϕ_r^2 and $\phi_{d_1}^2$ fixed at 16.5 and 10.5, respectively (Figure 5-11).

Fitting mLDL to determine ϕ_i^2 and $\phi_{d_2}^2$ (Figures 5-12 and 5-13) gives good fits of the transmural profiles, but model predictions overestimate experimentally determined values for cumulative degradation. In addition, the values obtained for ϕ_i^2 and $\phi_{d_2}^2$ (Table 5-VI) are very different than the values obtained for LDL.

Table 5-VI: Best Fit Parameters Obtained by Nonlinear Regression of Model for Constant Mass Transfer Coefficients to Transmural Profiles

	ϕ_r^2	$\phi_{d_1}^2$	ϕ_i^2	$\phi_{d_2}^2$	SS x 10 ⁴
LDL	8.5 ± 3.1	300 ± 60	11.6 (fixed)	6.8 (fixed)	1.44
LDL	16.5 (fixed)	10.5 (fixed)	17 ± 3	46 ± 8	1.30
mLDL	0.0		27 ± 2	(1.8 ± 0.1) x 10 ¹⁰	0.71

Fixed values

$$Bi = 0.58$$

$$Bi_c = 0.29$$

$$\phi_{e_1}^2 = 14.9$$

$$\phi_{e_2}^2 = 12.9$$

$$\phi_b^2 = 0$$

$$\beta = 476/\phi_r^2$$

$$D_e = 1.55 \times 10^{-9} \text{cm}^2/\text{s}$$

$$L = 130 \mu\text{m}$$

One parameter which can cause a decrease in both the tissue concentration and cumulative degradation is ϵ_f . The value used in the above calculations is based upon the interstitial volume fraction accesible to albumin; the value for LDL may be even lower. (Attempts to measure ϵ_f for LDL have been unsuccessful due to binding and tissue swelling (Scott [1984]).) The influence of this parameter on the mean

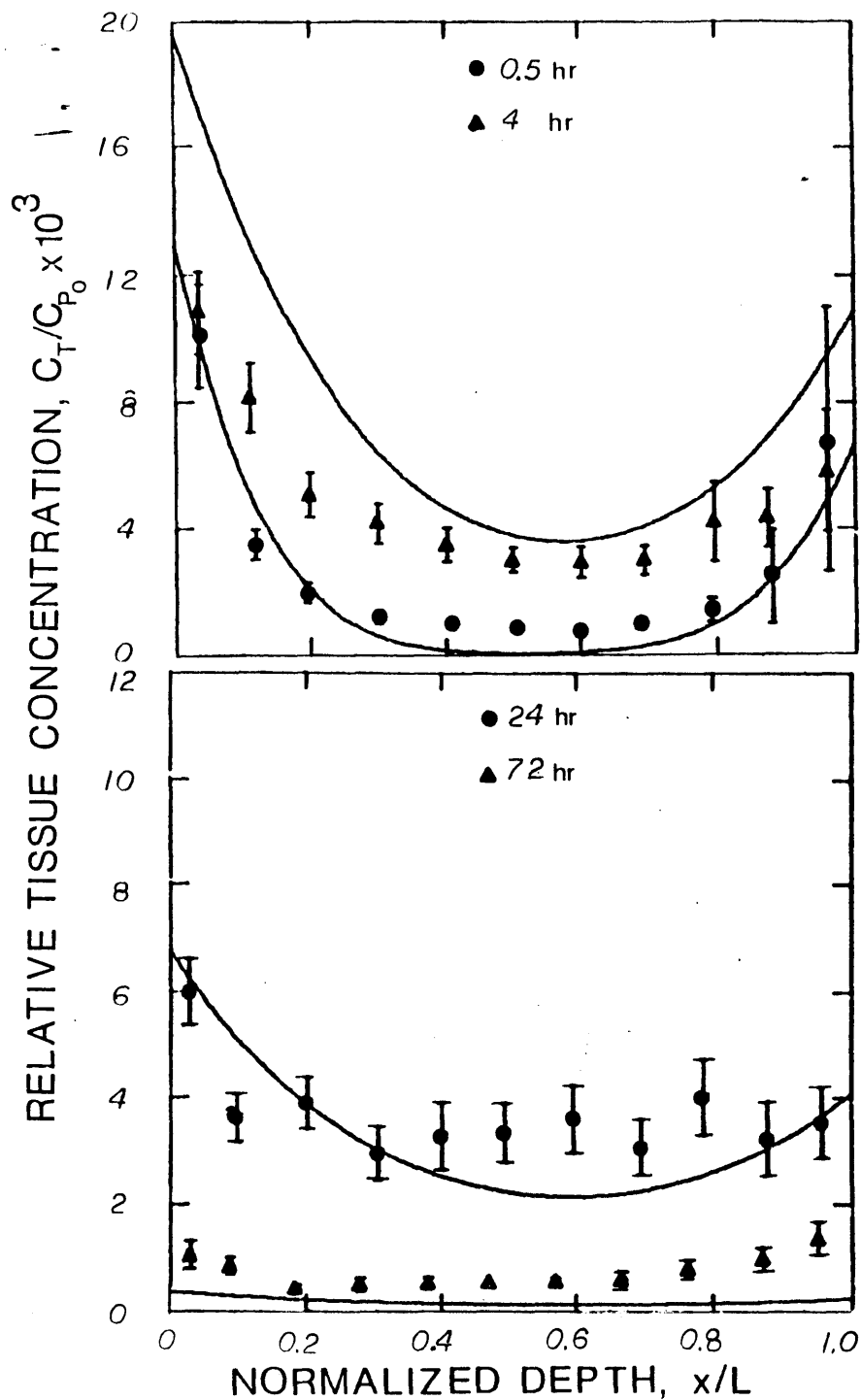


Figure 5-10: Best fit of LDL transmural profiles for constant mass transfer coefficients and no binding to the extracellular matrix ($\phi_b^2 = 0.0$).

Model was fit to data yielding $\phi_r^2 = 8.5 \pm 3.1$ and $\phi_{d_1}^2 = 303 \pm 58$, $\beta = K = 56.0 \pm 20.0$. All other parameters are as listed in Table 5-V.

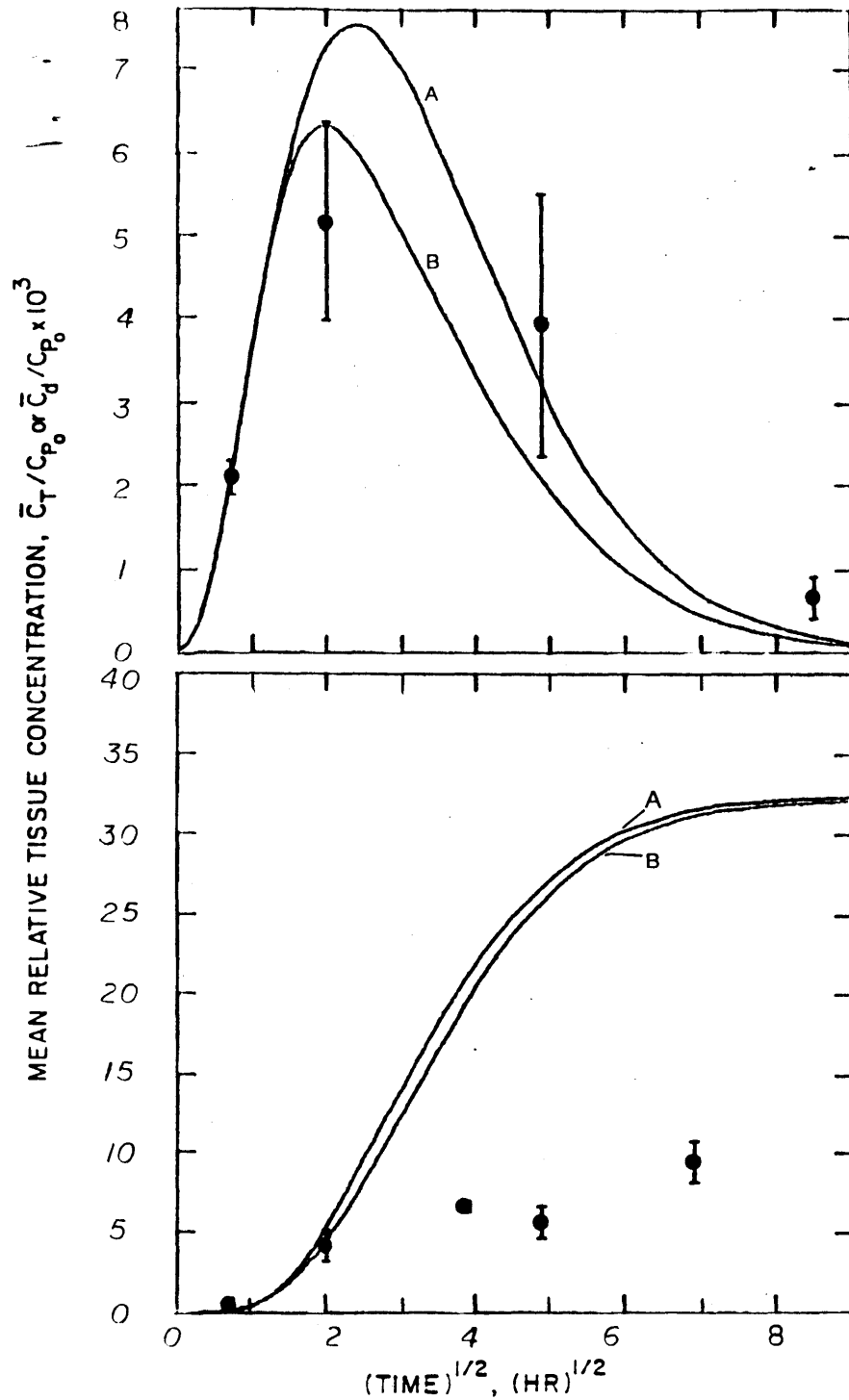


Figure 5-11: Comparison between model predictions and LDL mean relative concentrations and cumulative degradation for constant mass transfer coefficients and no binding to the extracellular matrix ($\phi_b^2 = 0.0$). Best fit parameter values are (A) $\phi_r^2 = 8.5 \pm 3.1$ and $\phi_{d_1}^2 = 300 \pm 60$, $\beta = K = 56 \pm 20$; (B) $\phi_i^2 = 17 \pm 3$, $\phi_{d_2}^2 = 46 \pm 8$. All other parameter values are as listed in Table 5-VI.

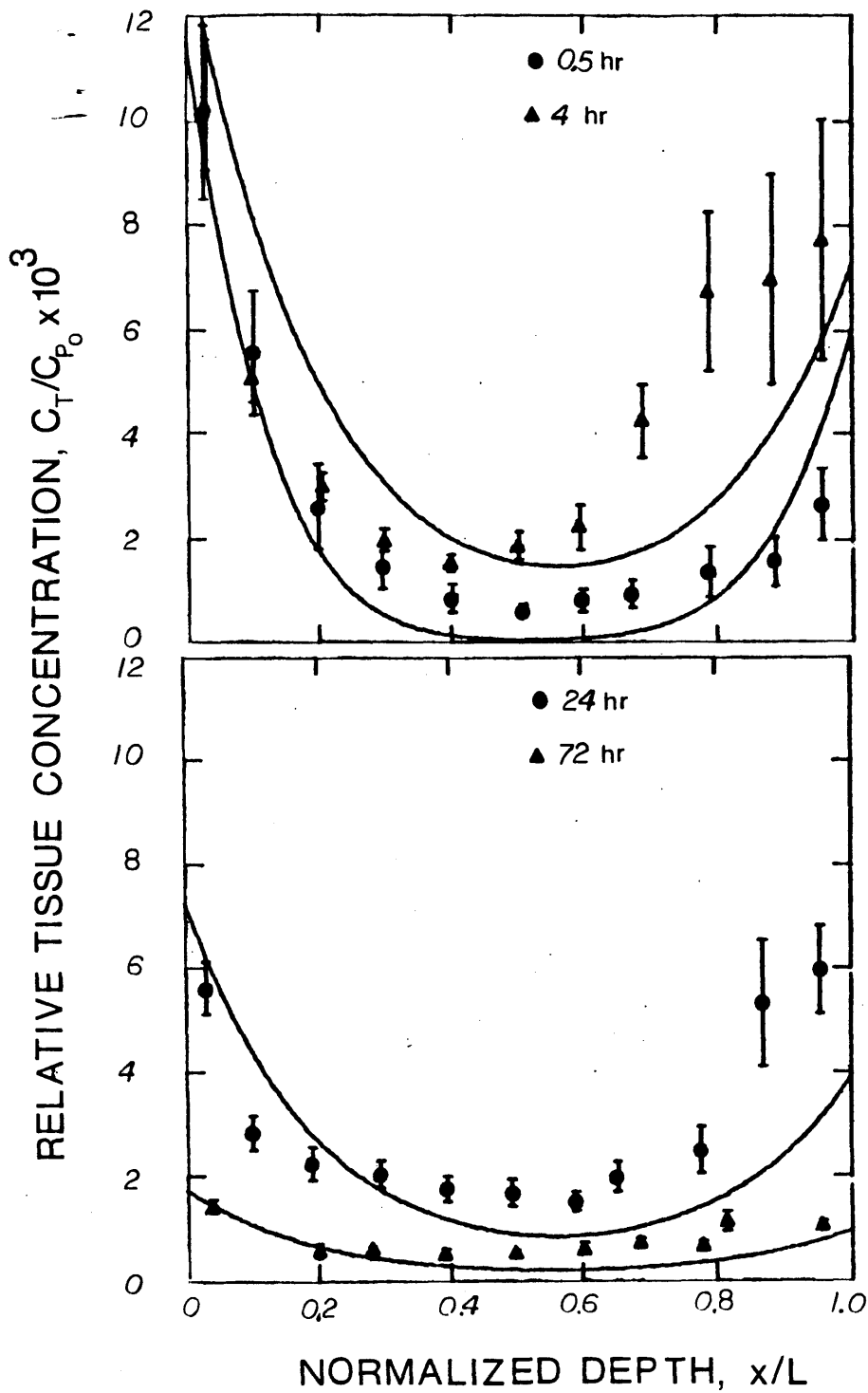


Figure 5-12: Best fit of mLDL transmural profiles for constant mass transfer coefficients and no binding to the extracellular matrix ($\phi_b^2 = 0.0$).

Best fit parameter values are $\phi_i^2 = 27 \pm 2$, $\phi_{d_2}^2 = (2 \pm 0.1) \times 10^{10}$.

All other parameter values are as listed in Table 5-VI.

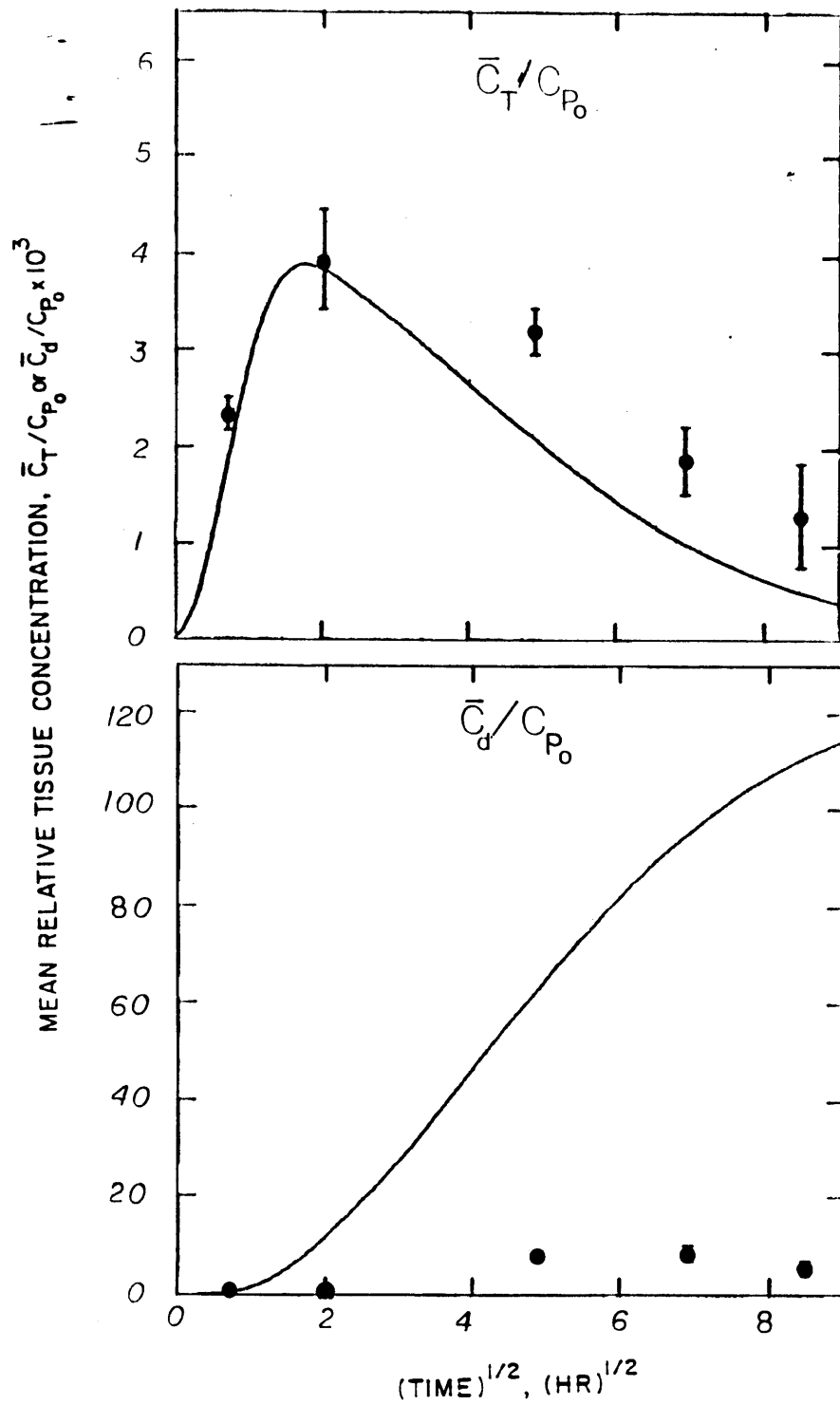


Figure 5-13: Comparison between model predictions and mLDL mean relative concentrations and cumulative degradation for constant mass transfer coefficients and no binding to the extracellular matrix ($\phi_b^2 = 0.0$).

Parameter values are listed in the legend to Figure 5-12.

relative concentrations and cumulative degradation of LDL and mLDL was examined by varying its value from 0.02 to 0.17. Results are presented in Figures 5-14 and 5-15 for LDL and mLDL, respectively. All other parameters are as listed in Table 5-V ($\phi_r^2 = 16.5$, $\beta = K = 28.9$). For all values of ϵ_f examined, model predictions for mean relative concentration and cumulative degradation are insensitive to ϵ_f for times less than about one hour. Decreasing ϵ_f results in better agreement between model predictions and LDL mean relative tissue concentrations, but the model overestimates $\theta_d(\infty)$ even at ϵ_f equal to 0.02. Similar trends are observed for mLDL, but even at ϵ_f equal to 0.02, model predictions overestimate both mLDL mean relative tissue concentrations and cumulative degradation (Figure 5-15). Although the estimate of ϵ_f equal to 0.17 may be in error, these results suggest that simply decreasing ϵ_f cannot explain the discrepancy between model predictions and data.

Time-Varying Permeabilities The analysis of model results for constant mass transfer coefficients indicates that no single parameter set could give reasonable agreement between theory and data. Consequently, the effect of time-varying permeabilities was examined, for which Bi and Bi_c are represented by:

$$Bi = Bi_o [1 - f(1 - e^{-\gamma' \tau})] \quad (5-70a)$$

$$Bi_c = Bi_{c_o} [1 - f(1 - e^{-\gamma' \tau})] \quad (5-70b)$$

where $\gamma' = \frac{\gamma D_e}{L^2}$ and γ is the time constant for time-varying mass transfer coefficients defined in equation (4-25). Estimates of γ' and f were obtained from fits of ^{14}C -sucrose tissue concentrations (Table 4-XIII) and are listed in Table 5-VII. Bi_o and Bi_{c_o} were obtained by fitting 0.5 hr data using equations (5-69a,b) to represent

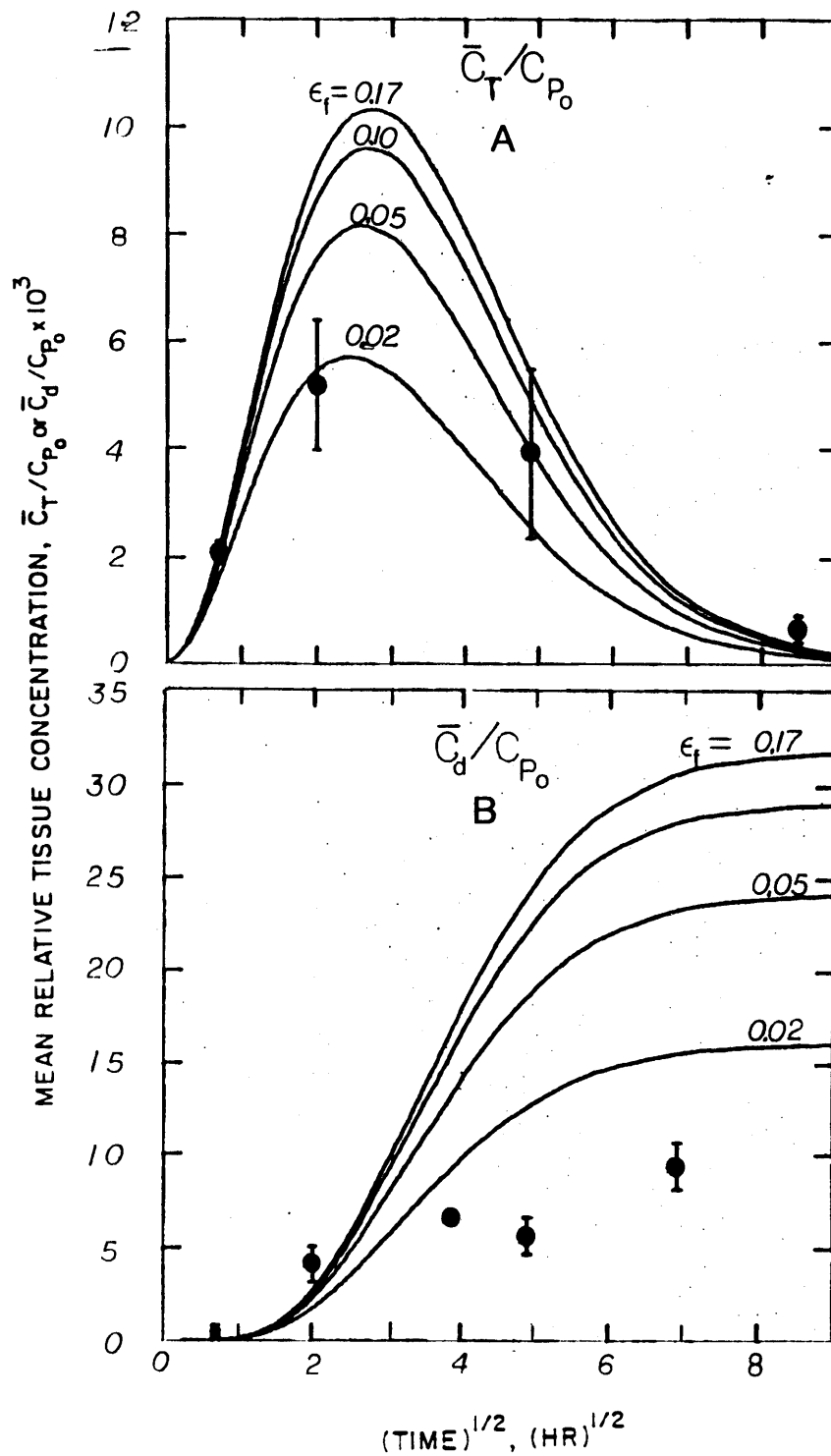


Figure 5-14: Effect of ϵ_f on model predictions for LDL (A) mean relative tissue concentrations and (B) cumulative degradation for constant mass transfer coefficients. $\phi_r^2 = 16.5$, $\beta = K = 28.9$ and all other parameters are as listed in Table 5-V.

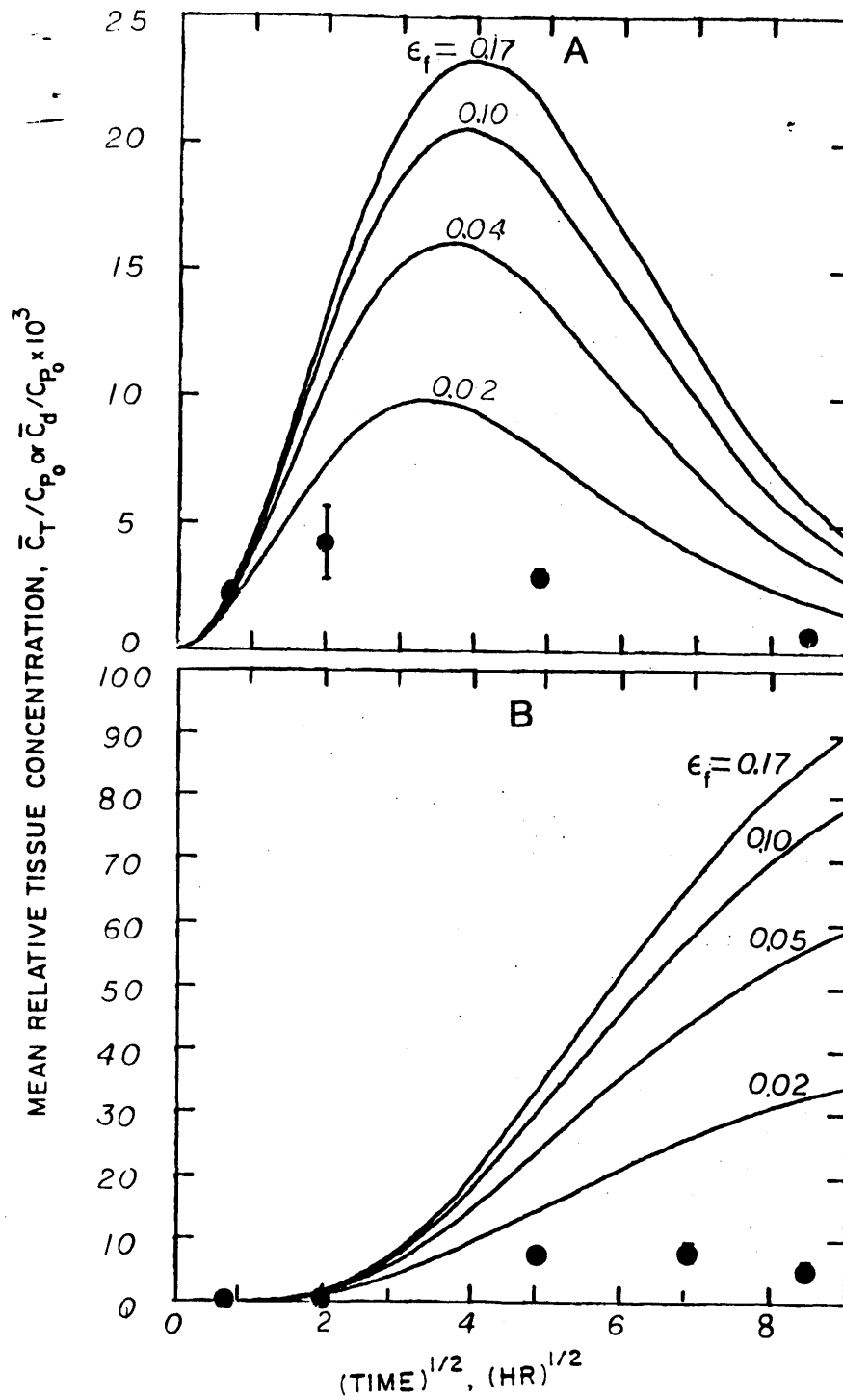


Figure 5-15: Effect of ϵ_f on model predictions for mLDL (A) mean relative tissue concentrations and (B) cumulative degradation for constant mass transfer coefficients. $\phi_r^2 = 0.0$ and all other parameters are as listed in Table 5-V.

time-varying permeabilities using the values of γ' and f listed in Table 5-VII. The resulting fits are presented in Figure 5-16 and the values of Bi_o and Bi_c and the sums of squares are listed in Table 5-VII (D_e was fixed at 1.55×10^{-9} cm²/s). The fitted curves are similar to those obtained using constant mass transfer coefficients.

Table 5-VII: Best Fit Values of Bi_o and Bi_c from Fitting 0.5 hr Data

	γ, hr^{-1}	γ'	f	Bi_o	Bi_c	$SS \times 10^4$
LDL	1.68	52.6	0.866	0.98 ± 0.03	0.60 ± 0.15	9.61
mLDL	0.77	24.1	0.981	0.79 ± 0.03	0.22 ± 0.07	4.61

The parameters for binding to the extracellular matrix, ϕ_b^2 and m , and the Thiele moduli for receptor-mediated binding, ϕ_r^2 , and degradation, $\phi_{d_1}^2$, were determined by nonlinear least squares regression of the model to the grand average transmural profiles using Marquardt's method (Marquardt [1963]). In order to keep k_2 constant, the value of β was set equal to $476/\phi_r^2$. mLDL was fit for m and ϕ_b^2 only, since $\phi_r^2 = 0$. All other metabolic parameters used are those listed in Table 5-V. Four cases were examined for LDL: A) m and ϕ_b^2 were fit, and ϕ_r^2 and $\phi_{d_1}^2$ were held fixed at 16.5 and 10.5, respectively; B) m , ϕ_b^2 , and ϕ_r^2 were fit and $\phi_{d_1}^2$ was held fixed at 10.5; C) m , ϕ_b^2 , and $\phi_{d_1}^2$ were fit and ϕ_r^2 was held fixed at 16.5; and D) m , ϕ_b^2 , and $\phi_{d_1}^2$, and ϕ_r^2 were fit. Each of the four cases was examined for grand average profiles with and without the aberrant profiles (4C6 and 24C1). The best fit values of m , ϕ_b^2 , ϕ_r^2 , and $\phi_{d_1}^2$ were used to calculate model predictions for the mean relative tissue concentration, cumulative degradation, and the steady state tissue concentration in response to a step change in plasma concentration.

Model fits of LDL grand average transmural profiles calculated from all

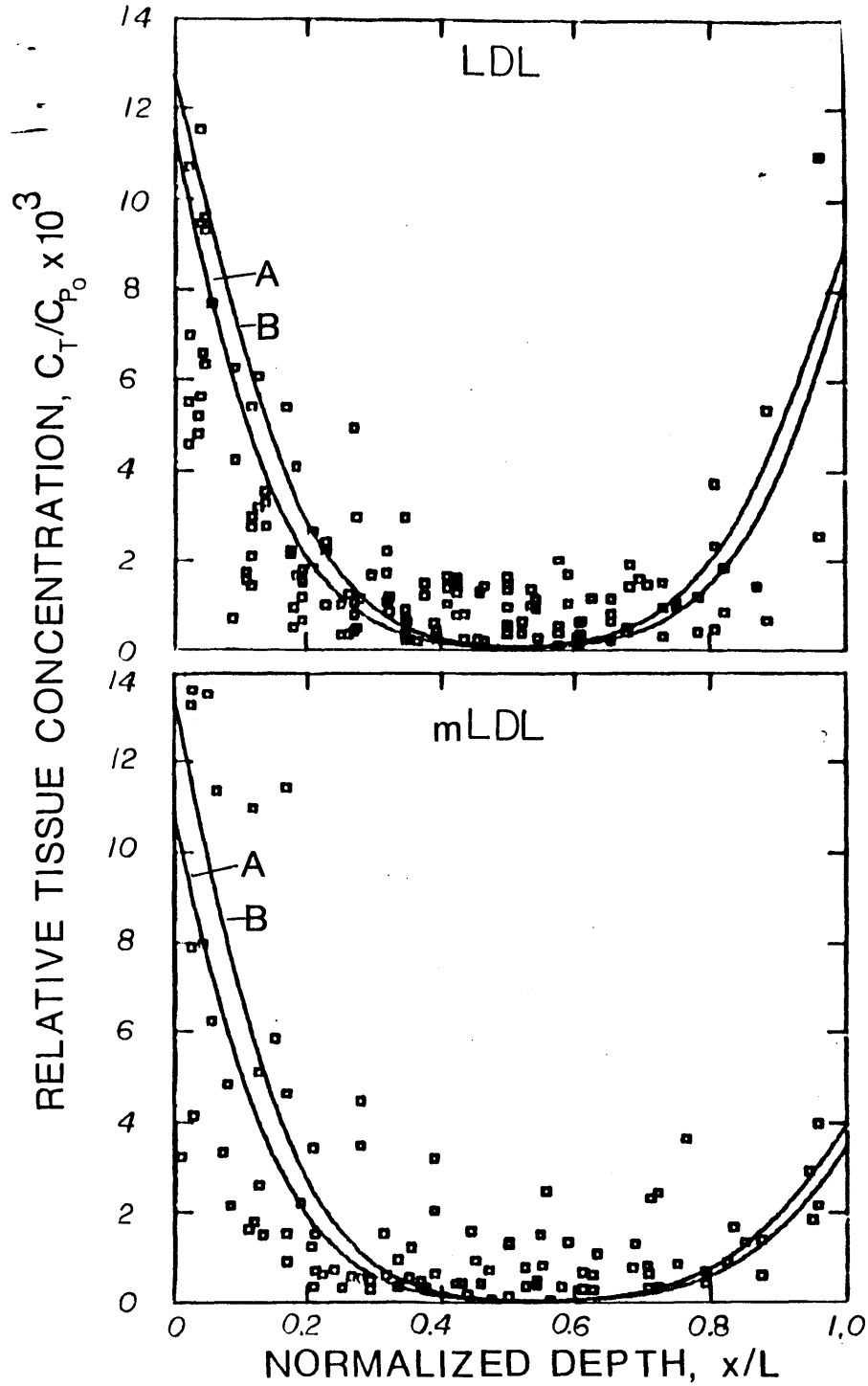


Figure 5-16: Comparison of fits of LDL and mLDL for (A) constant and (B) time-varying permeabilities. Parameter values for cases (A) and (B) are listed in Tables 5-II and 5-VII, respectively.

transmural profiles are presented in Figure 5-17 and best fit values of m , ϕ_b^2 , ϕ_r^2 and $\phi_{d_2}^2$ are listed in Table 5-VIII along with the sums of the squared residuals. When m and ϕ_b^2 alone were fit, gradients are steeper than experimentally observed and the mid-medial concentrations underestimate measured values. When ϕ_r^2 and/or $\phi_{d_1}^2$ are also fit (cases B,C,D), the sum of the squared residuals drops and the fits at 24 hr and 48 hr decrease relative to case A. For all cases, the fitted curve at 72 hr has less curvature than data. For cases B,C, and D (Table 5-VIII) the sums of squares are similar, but the resulting parameter values are very different, suggesting that the data are insensitive to these parameters.

Model predictions of mean relative concentration and cumulative degradation are presented in Figure 5-18. Model predictions for cases B,C,D are in good agreement with measured values of the mean relative concentrations although the model underestimates mean relative concentration at 24 hr. This may result from the inclusion of aberrant profiles at 4 and 24 hours (see below). Model predictions agree reasonably well with data for cumulative degradation although $\theta_d(\infty)$ is overestimated; θ_d ranges from 0.0091 (case D) to 0.0102 (case A) vs. experimentally estimated value of 0.0081 ± 0.0008 .

As noted in Chapter 4, two LDL profiles (4C6 at 4 hr and 24C1 at 24 hr) were significantly different than all other profiles at their respective circulation times. The model was fit to grand average transmural profiles excluding these aberrant profiles and the results are presented in Figure 5-19 and the best fit parameter values are listed in table 5-VIII. The sums of squares of the residuals are similar for all four cases examined and are lower than the values obtained from fitting the complete data set (Table 5-VIII). The data at 24 hr has greater curvature when experiment 24C1 is excluded from the grand average resulting in improved agreement with the model. At 72 hr, model fits show greater curvature (Figure

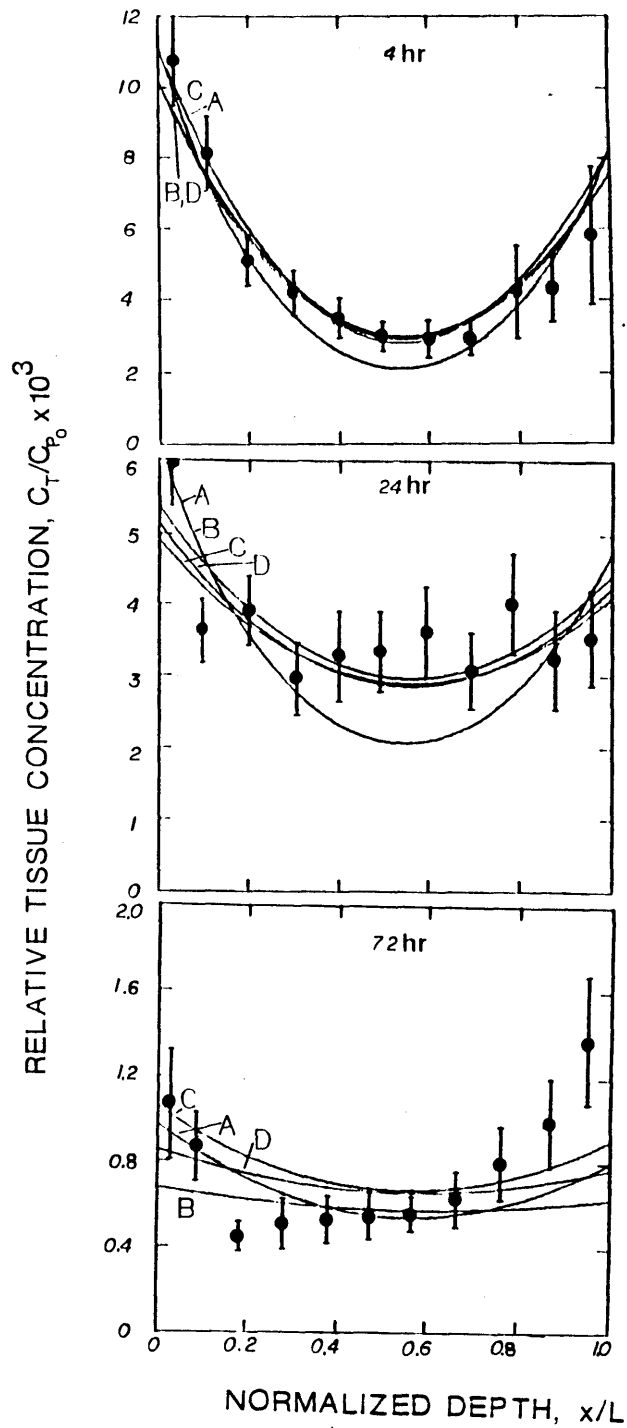


Figure 5-17: Comparison of model fits with time-varying permeabilities to grand average transmural profiles using all LDL profiles. Parameter values corresponding to cases A,B,C, and D are listed in Table 5-VIII.

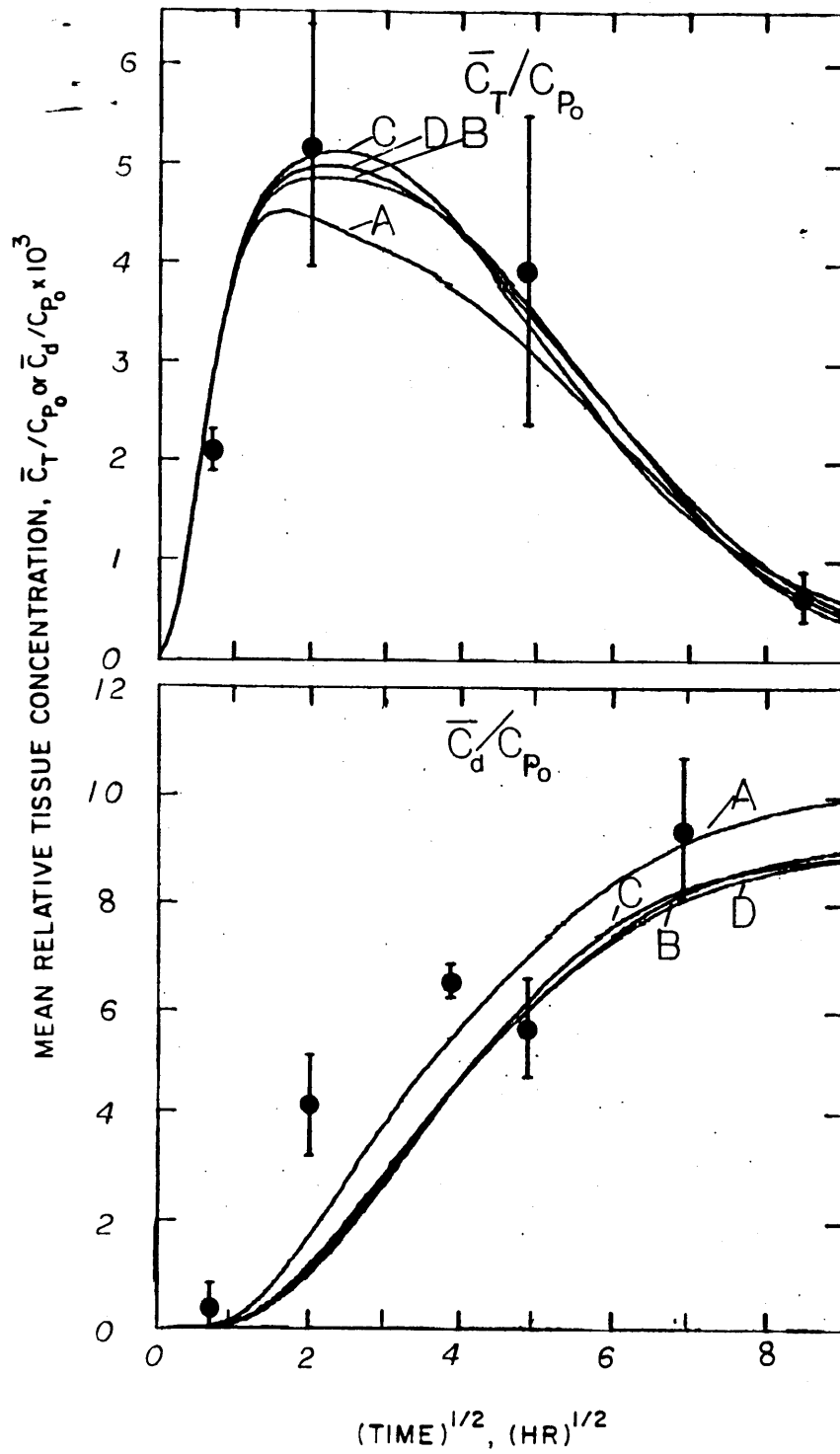


Figure 5-18: Predicted values of mean relative tissue concentrations and cumulative degradation. Parameter values are those obtained from best fit of grand average profiles presented in Figure 5-17.

Table 5-VIII: Metabolic Parameters Obtained by Nonlinear Regression of Model to Transmural Profiles for Time-Varying Mass Transfer Coefficients

	m	ϕ_b^2	ϕ_r^2	$\phi_{d_1}^2$	SS x 10 ⁵
LDL: all profiles (Figure 5-17)					
A	0.35 ± 0.06	5.8 ± 1.7	16.5 (fixed)	10.5 (fixed)	3.5
B	0.67 ± 0.18	4.5 ± 1.7	4.3 ± 2.7	10.5 (fixed)	2.7
C	0.93 ± 0.69	0.6 ± 1.1	16.5 (fixed)	1.9 ± 1.2	2.8
D	0.82 ± 0.41	2.1 ± 2.1	8.5 ± 5.4	3.3 ± 3.6	2.7
LDL: without aberrant profiles (Figure 5-19)					
A	0.43 ± 0.09	2.5 ± 0.6	16.5 (fixed)	10.5 (fixed)	1.87
B	0.40 ± 0.10	2.8 ± 0.7	19 ± 4	10.5 (fixed)	1.85
C	0.45 ± 0.12	2.3 ± 0.9	16.5 (fixed)	9.7 ± 2.6	1.86
D	0.41 ± 0.12	2.1 ± 0.9	22 ± 5	8.3 ± 2.1	1.82
mLDL: (Figure 5-21)					
	0.39 ± 0.16	4.0 ± 2.4			12.5

Fixed Values

$\beta = 476/\phi_r^2$	LDL	$Bi_o = 0.98$	$\gamma' = 52.6$
$\phi_i^2 = 11.6$		$Bi_{c_o} = 0.66$	$f = 0.866$
$\phi_{e_1}^2 = 14.9$	mLDL	$Bi_o = 0.79$	$\gamma' = 24.1$
$\phi_{e_2}^2 = 12.9$		$Bi_{c_o} = 0.22$	$f = 0.981$
$\phi_{d_2}^2 = 6.8$			
$D_e = 1.6 \times 10^{-9} \text{ cm}^2/\text{s}$			
$L = 0.013 \text{ } \mu\text{m}$			

5-19) than obtained with fits of grand average profiles which included aberrant profiles (Figure 5-17). This is probably because the fitted values of ϕ_r^2 and $\phi_{d_1}^2$ are larger than the values obtained from fitting grand average profiles which included aberrant profiles. Unlike fits obtained with aberrant profiles, the parameter estimates obtained without the aberrant profiles are similar for all four cases studied and are close to estimated values obtained using cell culture data (case A, Table 5-VIII).

Model predictions of mean relative concentration and cumulative degradation are presented in Figure 5-20. As a result of omitting experiments 4C6 and 24C1, the model prediction of the mean relative concentration at 24 hr is closer to measured value. Cumulative degradation is similar to the results obtained with the complete data set. All four cases listed in Table 5-VII give essentially identical values for mean relative concentration and cumulative degradation.

mLDL profiles were fit by nonlinear regression with $\phi_r^2 = 0$ to obtain estimates of m and ϕ_b^2 . Best fit parameters are listed in Table 5-VIII and the fitted transmural profiles are presented in Figure 5-21. The sums of the squares of the residuals is considerably larger than any value obtained with LDL (Table 5-VIII), largely due to the poor fit of the 4 hr profile (Figure 5-21). At normalized depths between 0 and 0.3, the tissue concentrations at 4 hr are very similar to those at 0.5 hr, resulting in similar intimal gradients at both times. The model predicts a decreasing gradient between 0.5 and 4 hr and is unable to fit concentrations near the intimal surface at 4 hr. Only near the medial-adventitial interface are tissue concentrations close to observed values at 4 hr. The gradient near the medial-adventitial interface at 0.5 hr is much steeper than data as a result of using Bi_{c_0} based upon LDL data. At 24 and 72 hr the fitted curves are much flatter than data.

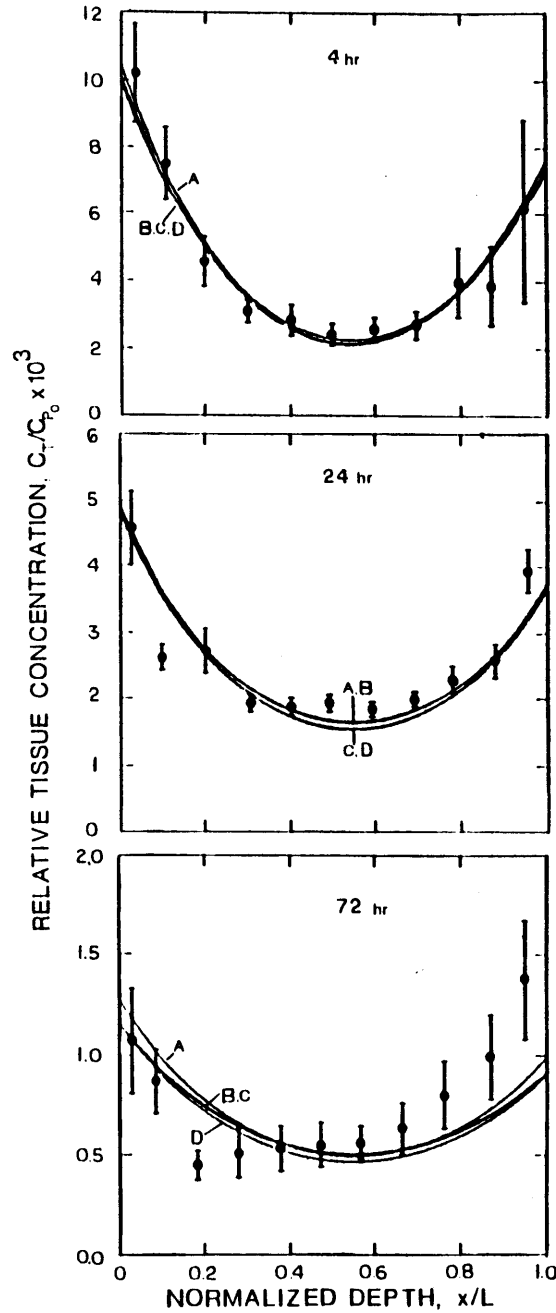


Figure 5-10: Comparison of model fits with time-varying permeabilities to grand average transmural profiles without experiments 4C6 and 24C1. Best fit values of m , ϕ_b^2 , ϕ_r^2 , and $\phi_{d_1}^2$ for cases A, B, C, and D are listed in Table 5-VIII along with values of parameters held fixed.

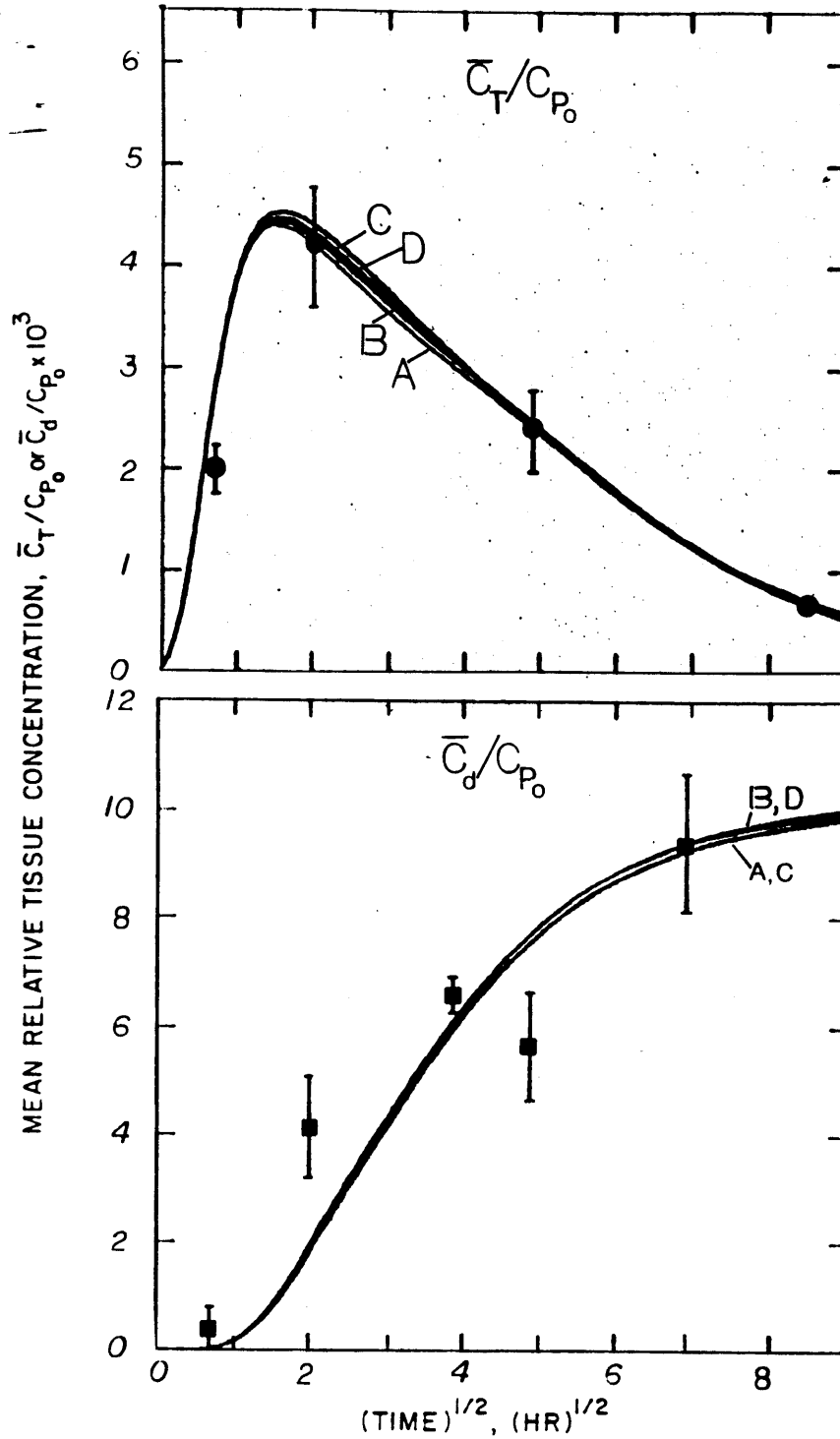


Figure 5-20: Predicted values of mean relative tissue concentrations and cumulative degradation using parameter estimates obtained by fitting grand average transmural profiles without experiments 4C6 and 24C1. Parameter values corresponding to cases A, B, C, and D are listed in Table 5-VIII.

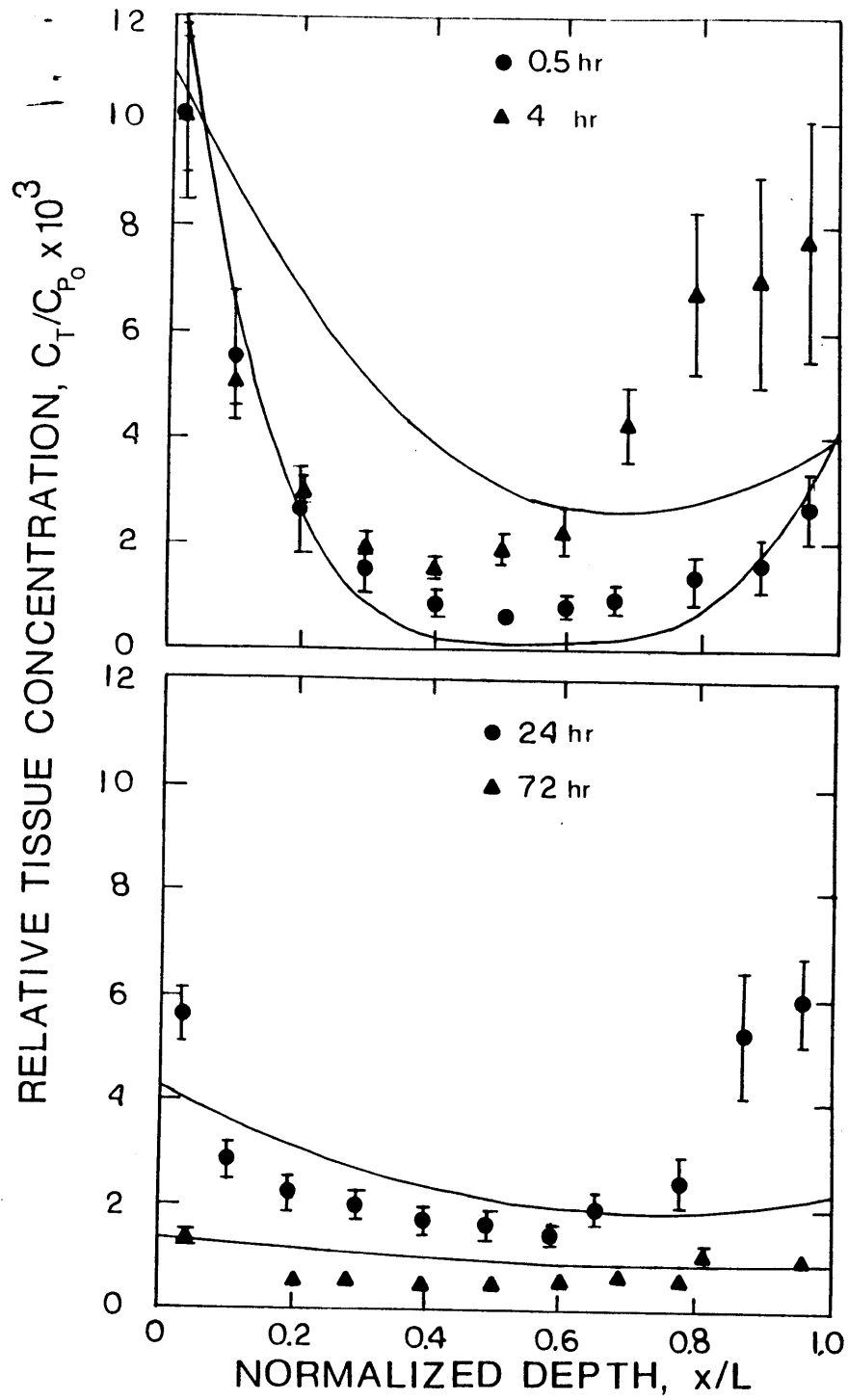


Figure 5-21: Comparison of model fits with time-varying permeabilities to grand average mLDL transmural profiles. Best fit values of m and ϕ_b^2 for $\phi_r^2 = 0$ are listed in table 5-VIII.

Comparisons between model predictions and data for mean relative concentrations and cumulative degradation are presented in Figure 5-22. Using the values of m and ϕ_b^2 from best fit of mLDL transmural profiles, model results overestimate mean relative concentration at 4 hr, but agree reasonably well with data at 24 and 72 hr. Cumulative degradation increases with time more slowly than data, but the value of $\theta_d(\infty)$ (0.0099) is larger than the value estimated from data (0.0079 ± 0.0009).

The values of m and ϕ_b^2 obtained from fitting LDL grand average profiles with and without the aberrant profiles are different, although, for both data sets binding is generally faster than diffusion ($\phi_b^2 > 1$), and dissociation is slower than binding ($m < 1$). For values obtained with grand average profiles excluding aberrant profiles, the value of ϕ_b^2 indicates that binding is about two to three times faster than the characteristic diffusion time (L^2/D_e) and, at steady state, the concentration bound to the extracellular matrix ($1/m$) is 1.5 to 2.4 times the free concentration. The values are also similar to the estimates obtained from fits of mLDL data (although ϕ_b^2 is larger for mLDL), suggesting that methylation does not influence the binding of LDL to the extracellular matrix.

The values of ϕ_r^2 obtained by fitting LDL transmural profiles with and without aberrant profiles are quite different. ϕ_r^2 for the complete data set is significantly lower than the estimated values of ϕ_r^2 based upon receptor down-regulation in culture (Table 5-V). Assuming that k_1 is unchanged, then ϕ_r^2 obtained by fitting the complete data set yields values of $[R_T]$ ranging from 470 to 930 receptors/cell. The values of ϕ_r^2 obtained from fits of transmural profiles without the aberrant profiles are much closer to estimates based on cell culture data, and yield values for the receptor number ranging from 1800 to 2300 receptors/cell.

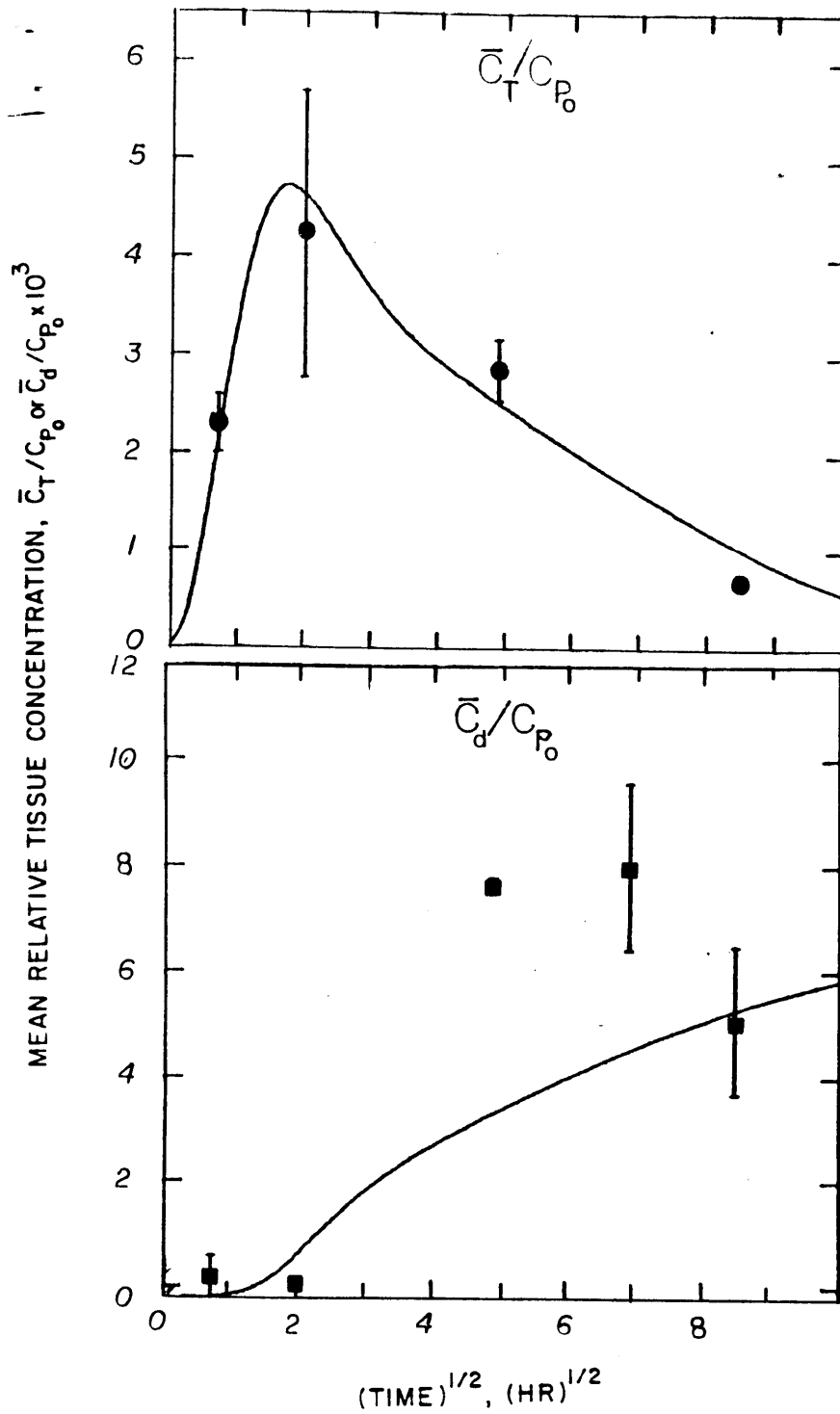


Figure 5-22: Predicted values of mLDL mean relative tissue concentrations and cumulative degradation. Parameter values are those obtained from best fit of grand average mLDL profiles presented in Figure 5-21.

Steady state tissue concentrations in response to a step change in plasma concentration were obtained from the complete solutions (equations (E-61) to (E-72)) by setting b_1 and b_2 to unity. For freely diffusible LDL, the resulting steady state solution of equation (E-61) is (for $Pe = 0$, $R = 1$, and $K_2 = \epsilon_f K_1 = -Bi_c$):

$$\Psi_f(\eta) = (1-f)\epsilon_f \left[\frac{[Bi_o(Bi_{c_o} \sinh(\alpha_o) + \alpha_o \cosh(\alpha_o)) + \alpha_o Bi_{c_o}] \cosh(\alpha_o \eta) + [Bi_o(Bi_{c_o} \cosh(\alpha_o) + \alpha_o \sinh(\alpha_o)) + Bi_o Bi_{c_o}] \sinh(\alpha_o \eta)}{[(Bi_o Bi_{c_o} + \alpha_o^2) \sinh(\alpha_o) + \alpha_o (Bi_o + Bi_{c_o}) \cosh(\alpha_o)]} \right] \quad (5-71)$$

where α_o^2 is:

$$\alpha_o^2 = \frac{\beta \phi_{d_1}^2 \phi_r^2}{K(\phi_{d_1}^2 + \phi_{e_1}^2)} + \frac{\phi_{d_2}^2 \phi_i^2}{\phi_{d_2}^2 + \phi_{e_2}^2} \quad (5-72)$$

Ψ_{f_o} is governed by five groups, $(1-f)$, ϵ_f , Bi_o , Bi_{c_o} , and α_o . $(1-f)$ and ϵ_f simply shift the magnitudes of the concentrations, but do not influence the curvature. α_o behaves as a global Thiele modulus. To see this note that at steady state, $\frac{\partial \theta_b}{\partial \tau}$, $\frac{\partial \theta_{LR}}{\partial \tau}$, $\frac{\partial \theta_{L_{Ri}}}{\partial \tau}$, and $\frac{\partial \theta_i}{\partial \tau}$ are equal to 0, and for $Pe = 0$ equations (5-50) to (5-53) reduce to:

$$\Psi_b = \frac{\Psi_f}{m} \quad (5-73)$$

$$\Psi_{LR} = \frac{\Psi_f}{K} \quad (5-74)$$

$$\Psi_{L_{Ri}} = \frac{\phi_r^2 \beta \Psi_{LR}}{\phi_{d_1}^2 + \phi_{e_1}^2} = \frac{\phi_r^2 \beta \Psi_f}{K(\phi_{d_1}^2 + \phi_{e_1}^2)} \quad (5-75)$$

$$\Psi_{L_i} = \frac{\phi_i^2 \Psi_f}{\phi_{d_2}^2 + \phi_{e_2}^2} \quad (5-76)$$

The steady-state form of the conservation relation for freely diffusible LDL is:

$$\begin{aligned} -\frac{d\Psi_f^2}{d\eta^2} = & \phi_b^2(\Psi_f - m\Psi_b) + \phi_r^2(\Psi_f - (K-\beta)\Psi_{LR}) \\ & + \phi_i^2\Psi_f - \phi_{e_1}^2\Psi_{LRi} - \phi_{e_2}^2\Psi_{Li} \end{aligned} \quad (5-77)$$

Substituting equations (5-73) to (5-76) into equation (5-77) yields:

$$\frac{d\Psi_f^2}{d\eta^2} = \left[\frac{\beta\phi_{d_1}^2\phi_r^2}{K\phi_{d_1}^2 + \phi_{e_1}^2} + \frac{\phi_{d_2}^2\phi_i^2}{\phi_{d_2}^2 + \phi_{e_2}^2} \right] \Psi_f \quad (5-78)$$

The total tissue concentration is:

$$\Psi_T = \Psi_f + \Psi_b + \Psi_{LR} + \Psi_{LRi} + \Psi_{Li} \quad (5-79a)$$

Substituting equations (5-73) to (5-76) into equation (5-79a) yields:

$$\Psi_T(\eta) = \Psi_f(\eta) \left[1 + \frac{1}{m} + \frac{1}{K} + \frac{\beta\phi_r^2}{(\phi_{d_1}^2 + \phi_{e_1}^2)K} + \frac{\phi_i^2}{\phi_{d_2}^2 + \phi_{e_2}^2} \right] \quad (5-79b)$$

Binding to the extracellular matrix increases the concentration by $1/m$, binding to the cell surface receptors increases the concentration by $1/K$, and LDL internalized by receptor-mediated and receptor-independent mechanisms increases the tissue concentration by $\beta\phi_r^2/(\phi_{d_1}^2 + \phi_{e_1}^2)K$ and $\phi_i^2/(\phi_{d_2}^2 + \phi_{e_2}^2)$, respectively.

For mLDL, $\Psi_{LR_o} = \Psi_{LRi_o} = 0$ and equation (5-79b) reduces to:

$$\Psi_T(\eta) = \Psi_f(\eta) \left[1 + \frac{1}{m} + \frac{\phi_i^2}{\phi_{d_2}^2 + \phi_{e_2}^2} \right] \quad (5-79c)$$

In Figures 5-23 and 5-24 model predictions for the transmural profile at steady

state in response to a step input are compared with the estimated profiles calculated using linear-systems theory. Parameter values obtained from fits of grand average LDL transmural profiles including all data results in underestimation of the tissue concentrations and the curvature of the profile (Figure 5-23a). Excluding the aberrant profiles leads to better agreement between model predictions and data (Figure 5-24b), although the model tends to underestimate the tissue concentrations. The curvature of the model generated profile is increased as a result of the larger value of ϕ_r^2 .

There is much poorer agreement between model predictions and data for mLDL steady state profiles (Figure 5-24). Model predictions show much less curvature than data due to the decrease in the value of α_o ($=2.00$) relative to LDL ($\alpha_o = 2.35$ to 3.29 for all data and 3.29 to 3.46 for data without aberrant profiles). Model predictions of the steady state profile are probably biased by the poor fits of the transmural profiles.

Calculations of cumulative degradation presented in Figures 5-18, 5-20, and 5-22 have neglected endothelial cell degradation. Kinetic models developed for LDL metabolism by cultured cells were used to model LDL metabolism by endothelial cells. Endothelial cells are exposed to the plasma concentration of LDL ($290 \mu\text{g/ml}$) and the receptors are likely to be down-regulated. In addition, LDL receptor expression on confluent endothelial cells is reduced further (Vlodavsky et al. [1978]). Thus, endothelial cells probably degrade LDL by receptor-independent processes which are assumed to be linear in the plasma concentration of radiolabeled LDL and mLDL. Material balances yield:

$$\frac{\partial C_{L_{ie}}}{\partial t} = k_4 \rho_c C_f - (k_6 + k_7) C_{L_{ie}} \quad (5-80a)$$

$$\frac{\partial C_{d_e}}{\partial t} = k_6 C_{L_{ie}} \quad (5-80b)$$

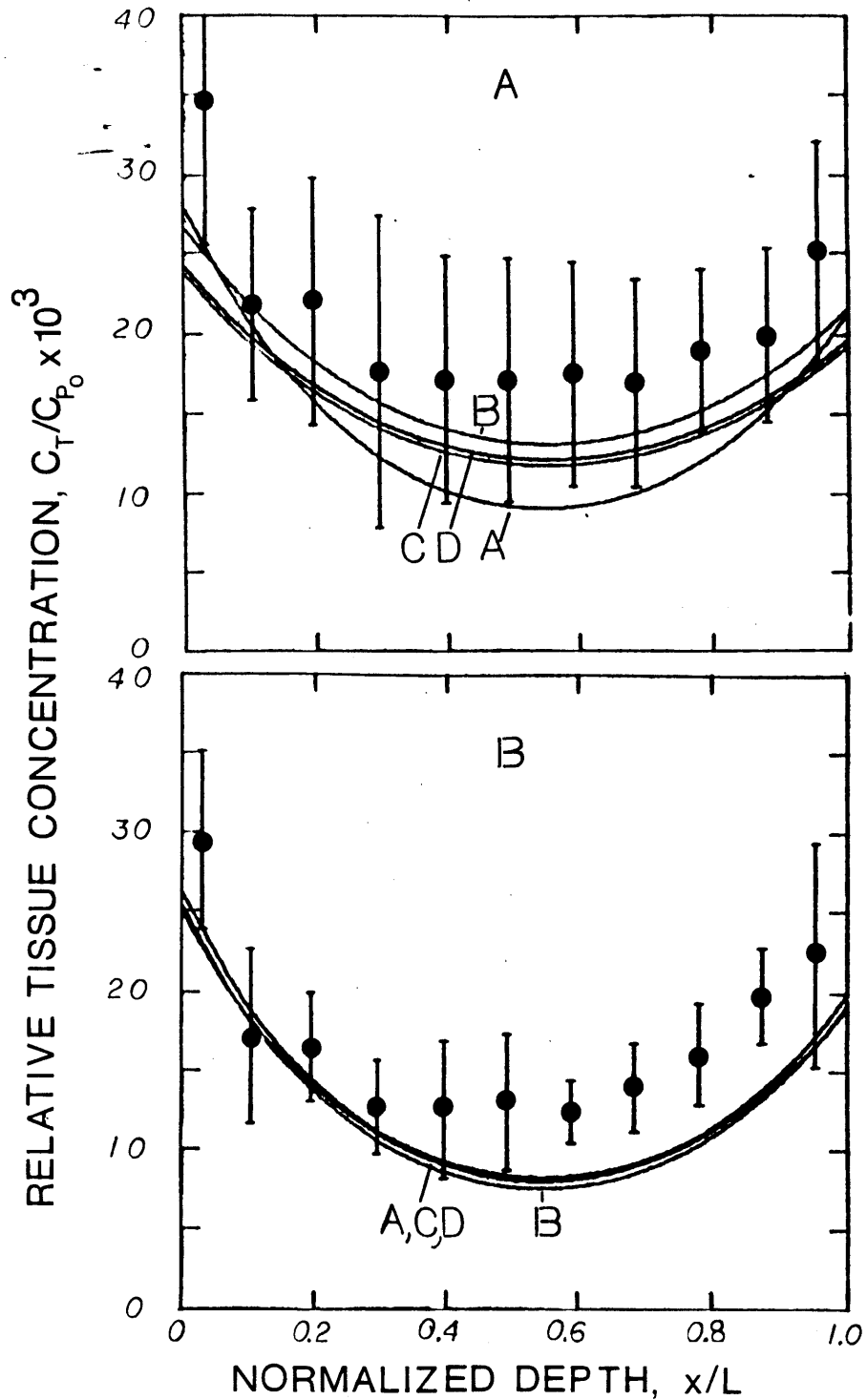


Figure 5-23: Comparison of model predictions with estimated steady state profile in response to a step change in plasma concentration. (A) profiles calculated from all transmural profiles; (B) profiles calculated without experiments 4C6 and 24C1. Parameter values are listed in Table 5-VIII.

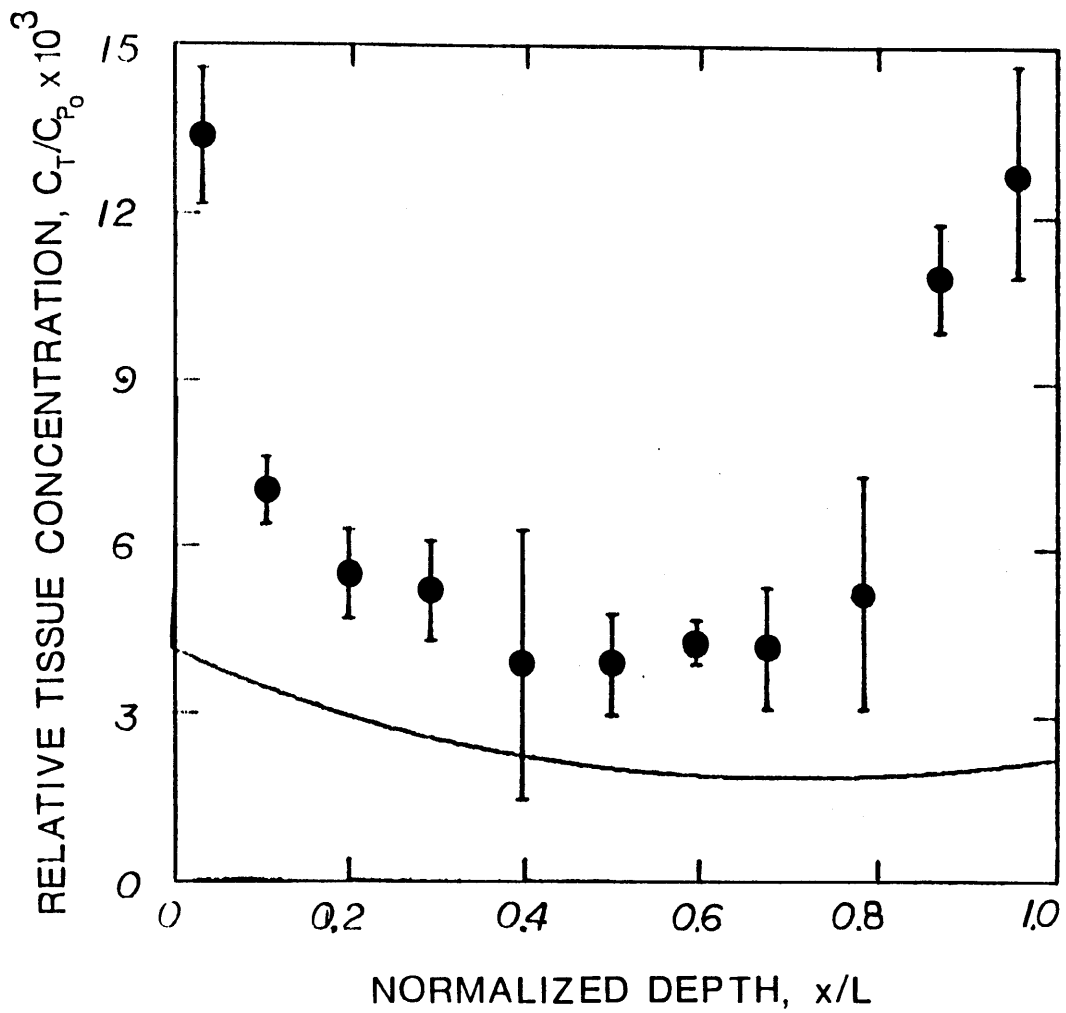


Figure 5-24: Comparison of model predictions with estimated steady state profile of mLDL in response to step change in plasma concentration. Parameter values are listed in Table 5-VIII.

where the subscript e refers to the moles of lipoprotein internalized or degraded by endothelial cells per cm^3 tissue (i.e. $C_{L_{ie}} = [L_{ie}] \rho_e \epsilon_e / M_w$ where ρ_e and ϵ_e are, respectively, the cell protein density and the volume fraction occupied by endothelial cells). A new constant, k_4'' , can be defined such that:

$$k_4'' = k_4 \rho_e \epsilon_e \tag{5-81}$$

This model of endothelial cell metabolism neglects concentration gradients and assumes the cells are well-mixed. Vesicle diffusion is rapid relative to vesicle attachment and detachment, solute concentration gradients are probably confined to a region near the the plasma membrane, and the concentration is approximately uniform within the region in which degradation is occurring.

It is also possible that the same process affecting the mass coefficients is also affects the rate constant for nonspecific internalization, k_4'' , which can be represented by an equation similar to equations (5-69a,b).

$$k_4'' = k_{4_0}'' [1 - f(1 - e^{-\gamma t})] \tag{5-82}$$

where k_{4_0}'' represents the rate constant for adsorptive endocytosis. Use of equation (5-82) implies that LDL and mLDL are altered either in the plasma or on the endothelial cell surface, and that this alteration affects all cellular uptake processes.

Equations (5-80) to (5-82) can be rewritten in dimensionless form:

$$\frac{\partial \theta_e}{\partial \tau} = \phi_{ie}^2 \theta_p - (\phi_{d_2}^2 + \phi_{e_2}^2) \theta_e \tag{5-83}$$

$$\frac{\partial \theta_{de}}{\partial \tau} = \phi_{d_2}^2 \theta_e \tag{5-84}$$

$$\phi_{ie}^2 = \phi_{ie_0}^2 [1 - f(1 - e^{-\gamma \tau})] \tag{5-85}$$

where $\theta_e = \bar{C}_{ie}/C_{p_0}$, $\phi_{ie}^2 = k_4''L^2/D_e$, and $\phi_{ie_0}^2 = k_{4_0}''L^2/D_e$.

The solution of equations (5-83) to (5-85) for a decaying plasma concentration is:

$$\theta_e = \phi_{ie_0}^2 \sum_{i=1}^2 a_i \left[\frac{(1-f)(e^{-b_i\tau} - e^{-(\phi_{d_2}^2 + \phi_{e_2}^2)\tau})}{\phi_{d_2}^2 + \phi_{e_2}^2 - b_i} + \frac{f(e^{-(b_i + \gamma')\tau} - e^{-(\phi_{d_2}^2 + \phi_{e_2}^2)\tau})}{\phi_{d_2}^2 + \phi_{e_2}^2 - (b_i + \gamma')} \right] \quad (5-86)$$

$$\theta_{de} = \phi_{ie_0}^2 \phi_{d_2}^2 \sum_{i=1}^2 a_i \left[\frac{(1-f)}{\phi_{d_2}^2 + \phi_{e_2}^2 - b_i} \left(\frac{1 - e^{-b_i\tau}}{b_i} - \frac{1 - e^{-(\phi_{d_2}^2 + \phi_{e_2}^2)\tau}}{\phi_{d_2}^2 + \phi_{e_2}^2} \right) + \frac{f}{\phi_{d_2}^2 + \phi_{e_2}^2 - (b_i + \gamma')} \left(\frac{1 - e^{-(b_i + \gamma')\tau}}{b_i + \gamma'} - \frac{1 - e^{-(\phi_{d_2}^2 + \phi_{e_2}^2)\tau}}{\phi_{d_2}^2 + \phi_{e_2}^2} \right) \right] \quad (5-87)$$

ρ_e and ϵ_e can be estimated from published data for cell surface area and endothelial cell protein content. For cultured bovine aortic endothelial cells M_p is 0.42 mg protein/ 10^6 cells (H.B. Warren, unpublished results). Estimates of the rabbit aortic endothelial cell surface area in vivo range from $290 \pm 50 \mu\text{m}^2$ (Reidy and Bowyer [1977]) to $780 \pm 110 \mu\text{m}^2/\text{cell}$ (Cornhill et al. [1980]). (Part of this variability may be attributed to location. Nerem et al. [1981] found that the endothelial cell surface area proximal to a flow divide is larger than distal to the flow divider.) Eskin et al. [1984] have measured a surface area of $590 \mu\text{m}^2$ for cultured bovine endothelial cells. Arterial endothelial cells are about $1 \mu\text{m}$ thick (Chien [1978]) and the cell volume can be estimated as the product of the surface

area times the thickness. For this range of endothelial cell surface areas ρ_e ranges from 540 to 1440 mg/cm³ cell. An estimate of ϵ_e equal to 0.0077 can be obtained from the ratio of the cell thickness relative to the medial thickness (130 μ m), which yields estimates of $\rho_e \epsilon_e$ ranging from 4.2 to 11.1 mg/cm³ tissue. An alternate estimate of $\rho_e \epsilon_e$ can be obtained from the results of Carew et al. [1984] in which they report a protein concentration of 1.98 mg/g tissue for the rabbit intima. Endothelial cells comprise the bulk of the rabbit intima and the intimal protein is approximately equal to the cell protein in the intima. For a tissue density of 1.07 g/cm³ (Bell et al. [1974a]), $\rho_e \epsilon_e$ is 2.1 mg/g tissue. Using the value of k_4 from cell culture, and estimates of ρ_e and ϵ_w listed in Table 5-IV, k_4'' ranges in value from 6.8 x 10⁻⁵ min⁻¹ to 35.7 x 10⁻⁵ min⁻¹, and $\phi_{ie_0}^2$ ranges from 0.12 to 0.64.

The total amount of LDL or mLDL degraded per unit volume of tissue is the sum of lipoprotein degraded by the endothelial cells and smooth muscle cells:

$$\bar{\theta}_{dT} = \bar{\theta}_d + \bar{\theta}_{de} \quad (5-88)$$

Model results are presented in Figure 5-25 for values of $\phi_{ie_0}^2$ ranging from 0.0 to 0.50. Increasing the value of $\phi_{ie_0}^2$ leads to an increase in total tissue degradation. For values of $\phi_{ie_0}^2$ equal to 0.1, 0.2, and 0.5, respectively, $\bar{\theta}_d(\infty)$ for LDL increases by 15%, 31%, and 78% above the value of $\bar{\theta}_d(\infty)$ for no endothelial cell degradation. For mLDL, the increase above the value of $\bar{\theta}_d(\infty)$ for no endothelial cell degradation is 13%, 32%, and 89% for $\phi_{ie_0}^2$ equal to 0.1, 0.2, and 0.5, respectively. Endothelial cell degradation has a greater effect upon mLDL degradation because of the slower plasma decay of mLDL relative to LDL. For comparison, Carew et al. [1984] reported that the rabbit aortic intima accounts 31% to 55% of total LDL degradation at 24 hr. For values of $\phi_{ie_0}^2$ equal to 0.1 and 0.5 the corresponding values of θ_{ie} are 0.0010 and 0.00011 4 hr and 24 hr, respectively.

θ_{ie} raises the mean relative tissue concentration by 19-24% at 4 hr and 2.7-4.4% at 24 hr. Corresponding concentrations at $\eta = 0$ (θ_{ie}/ϵ_e) are 0.13 and 0.014. Thus, the endothelial cell can potentially account for a significant fraction of the tissue concentration near the intimal surface.

Calculations were also performed for constant ϕ_{ie}^2 (Figure 5-26). In order to obtain reasonable agreement with data, ϕ_{ie}^2 must be about an order of magnitude smaller than $\phi_{ie_0}^2$ used for time-varying mass transfer coefficients. This implies that, if ϕ_{ie}^2 is constant, then the major route of cellular uptake by endothelial cells is by fluid phase endocytosis.

Model Sensitivity Calculations were performed to assess the relative importance of metabolic parameters and the manner in which they influence the predicted concentrations of degraded and undegraded lipoprotein. Parameters were varied about the base case which corresponds to case D obtained by fitting grand average profiles without aberrant profiles (Table 5-VIII). Of particular interest is the model sensitivity to the parameters for binding to the extracellular matrix (m , ϕ_b^2), receptor-mediated binding (ϕ_r^2), and receptor-mediated and receptor-independent internalization (β and ϕ_i^2), exocytosis ($\phi_{e_1}^2$ and $\phi_{e_2}^2$), and degradation ($\phi_{d_1}^2$ and $\phi_{d_2}^2$). The effect of the transport parameters on tissue concentrations was not examined since these parameters have been thoroughly analyzed by Bratzler [1974] and Truskey et al. [1981].

Figures 5-27 and 5-28 show the effect of binding to the extracellular matrix on the mean relative concentration and cumulative degradation. Increasing ϕ_b^2 at a constant value of m equal to 0.41 results in increased tissue concentrations for times greater than four hr (Figure 5-27). At low values of ϕ_b^2 the increase occurs only at longer times (24 hr or later), but as ϕ_b^2 increases, bound solute concentrations increase even at earlier times. The value of m indicates that dissociation is two and

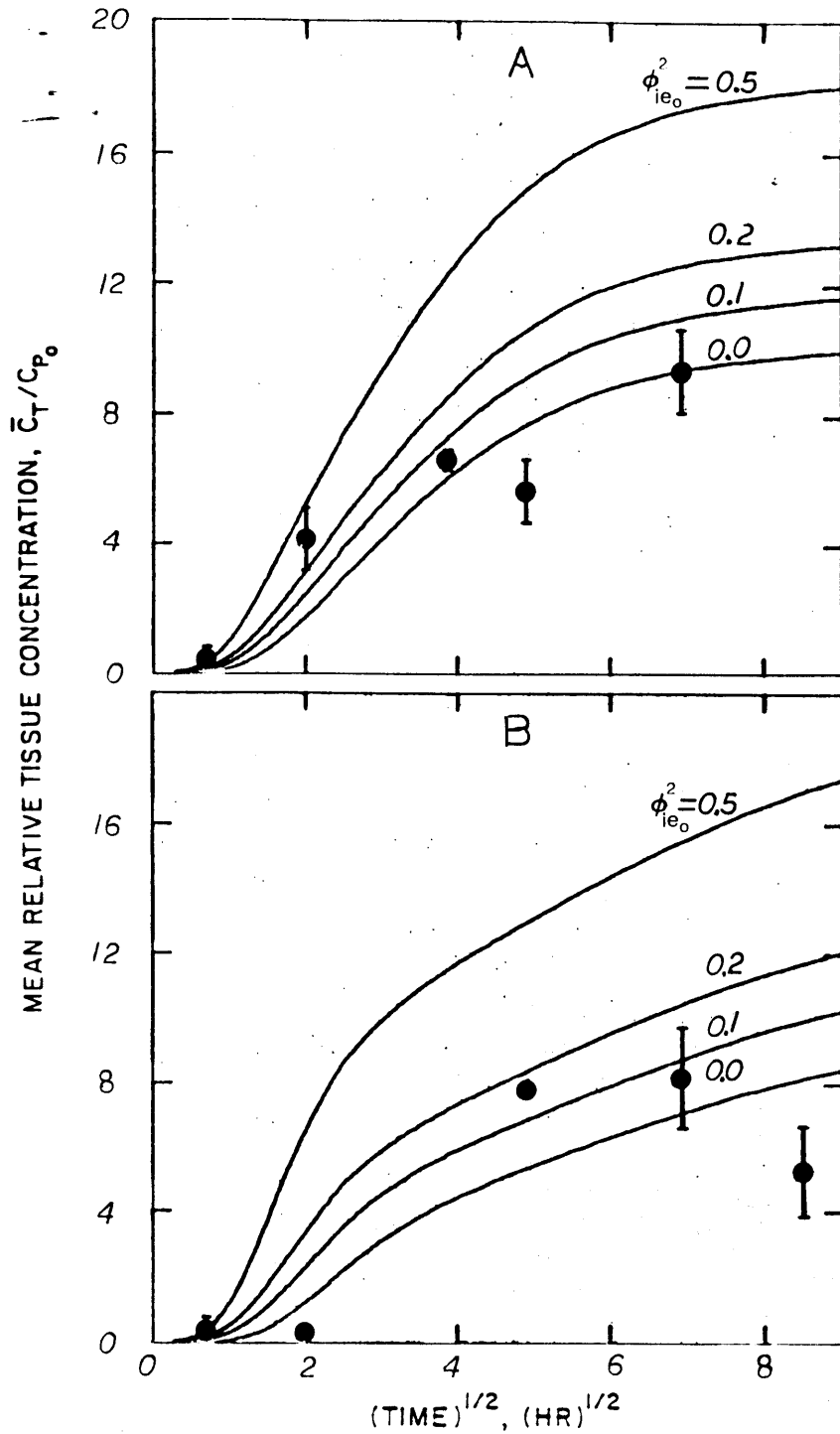


Figure 5-25: Effect of endothelial cell degradation upon cumulative LDL (A) and mLDL (B) degradation. ϕ_{ie}^2 is assumed to vary with time according to equation (5-85). Model predictions were calculated using parameter values obtained with case D from the fit of the grand average profiles without aberrant profiles (Table 5-VIII).

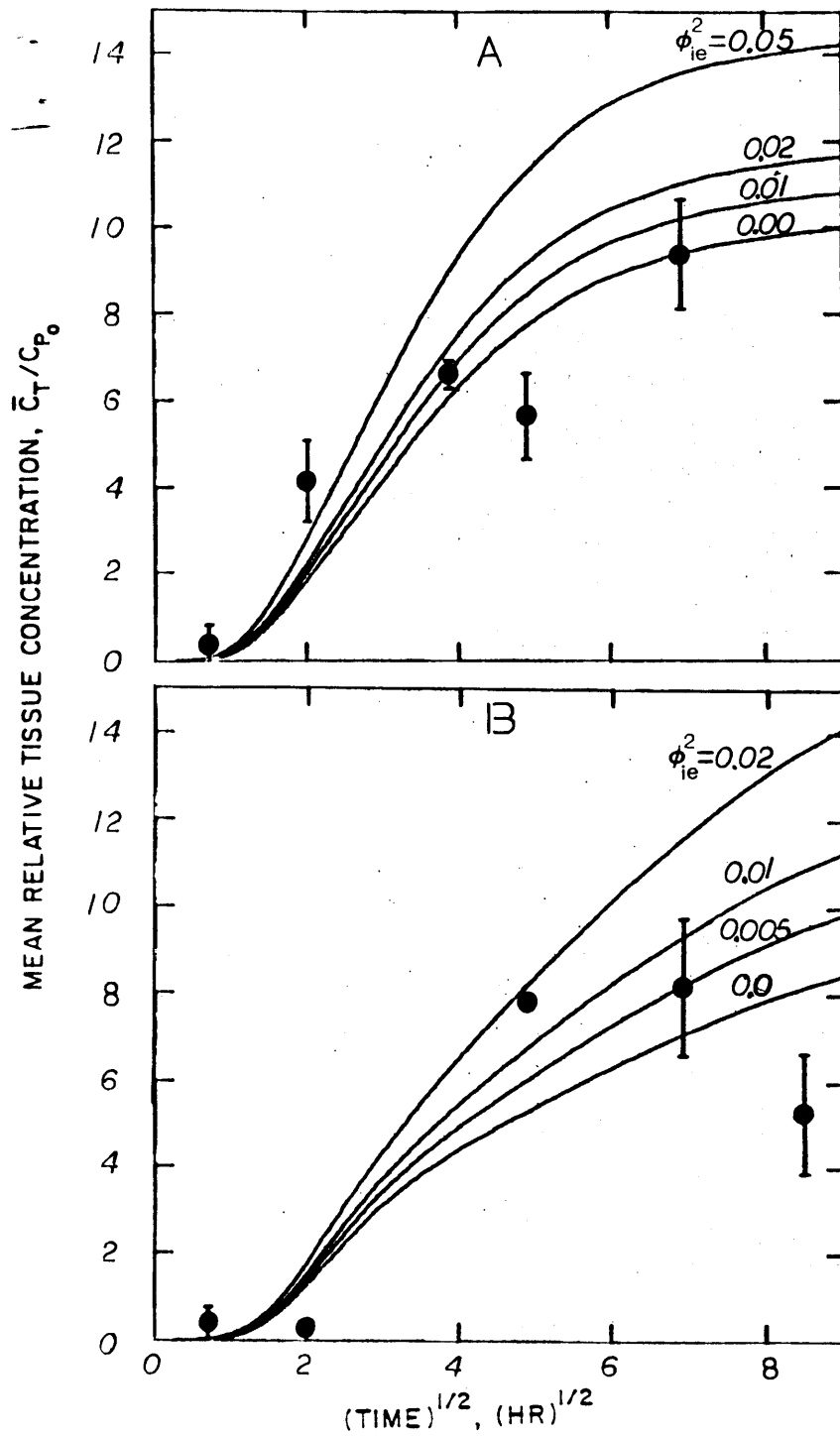


Figure 5-26: Effect of endothelial cell degradation upon cumulative LDL (A) and mLDL (B) degradation for constant ϕ_{ie}^2 . Model predictions were calculated using parameter values obtained with case D from the fit of the grand average profiles without aberrant profiles (Table 5-VIII).

a half times slower than binding resulting in the decreased loss of solute from the tissues at later times. As ϕ_b^2 increases, dissociation ($m\phi_b^2$) also increases, resulting in the more rapid removal of solute at later times. Increasing ϕ_b^2 slows down the rate of degradation but does not influence the value of $\bar{\theta}_d(\infty)$ (Figure 5-27). As t goes to ∞ , equation (E-71) reduces to:

$$\bar{\theta}_d(\infty) = \frac{\alpha_o^2 \bar{\psi}_f(\infty)}{(1-f)} \left[(1-f) \sum_{i=1}^2 \frac{a_i}{b_i} + f \sum_{i=1}^2 \frac{a_i}{\gamma' + b_i} \right] \quad (5-89)$$

where $\bar{\psi}_f(\infty)$ is obtained by analytically integrating the expression for $\bar{\psi}_f(\eta)$ (equation (E-43)). Since α_o^2 and $\bar{\psi}_f(\infty)$ are independent of m and ϕ_b^2 , $\bar{\theta}_d(\infty)$ is independent of binding to the extracellular matrix.

As the value of ϕ_b^2 increases, the rate of degradation slows down for early times, but increases at later times. The increase in the rate of degradation at later times for large ϕ_b^2 is a result of the increased rate of dissociation ($m\phi_b^2$) of LDL from the matrix.

Plotted in Figure 5-28 is the effect of m on the mean relative tissue concentration and cumulative degradation for ϕ_b^2 equal to 2.11. Decreasing m increases the amount bound at longer times since the lower the value of m , the more slowly solute dissociates from the matrix. As m decreases in value, the rate of degradation is slowed down at later times, since solute remains bound to the matrix for longer periods of time.

The effect of the number of receptors was studied by varying the value of ϕ_r^2 from 0 to 100 (Figure 5-29). A value of ϕ_r^2 equal to zero corresponds to no receptors and cellular uptake is by receptor-independent mechanisms only; a value of ϕ_r^2 equal to 100 is equal to about 10,000 receptors/cell, assuming k_1' is constant. Increasing ϕ_r^2 results in decreased tissue concentrations and increased degradation

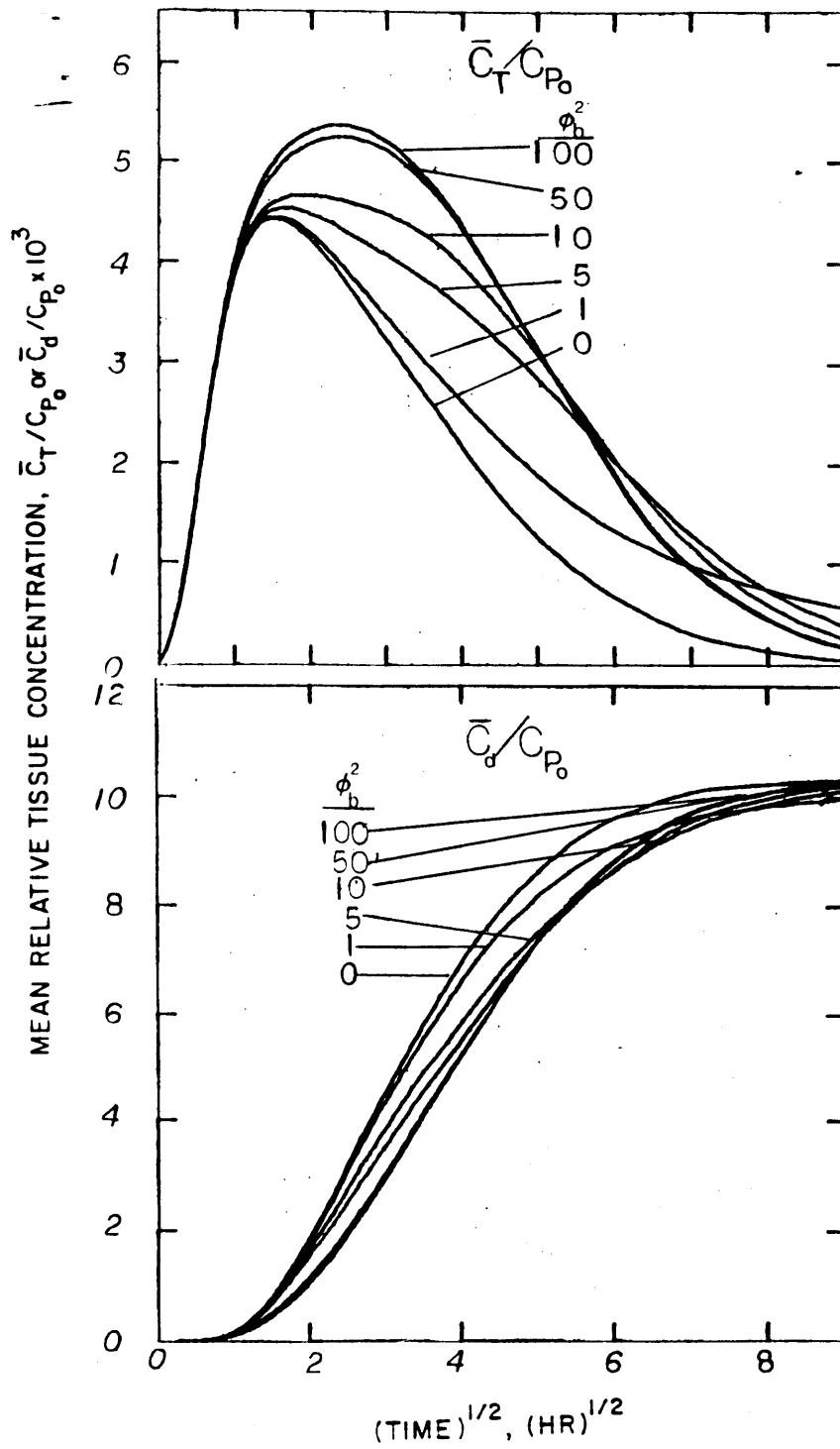


Figure 5-27: Effect of ϕ_b^2 on mean relative LDL tissue concentration and cumulative degradation. All other parameters are listed in Table 5-VIII for case D for data without aberrant profiles.

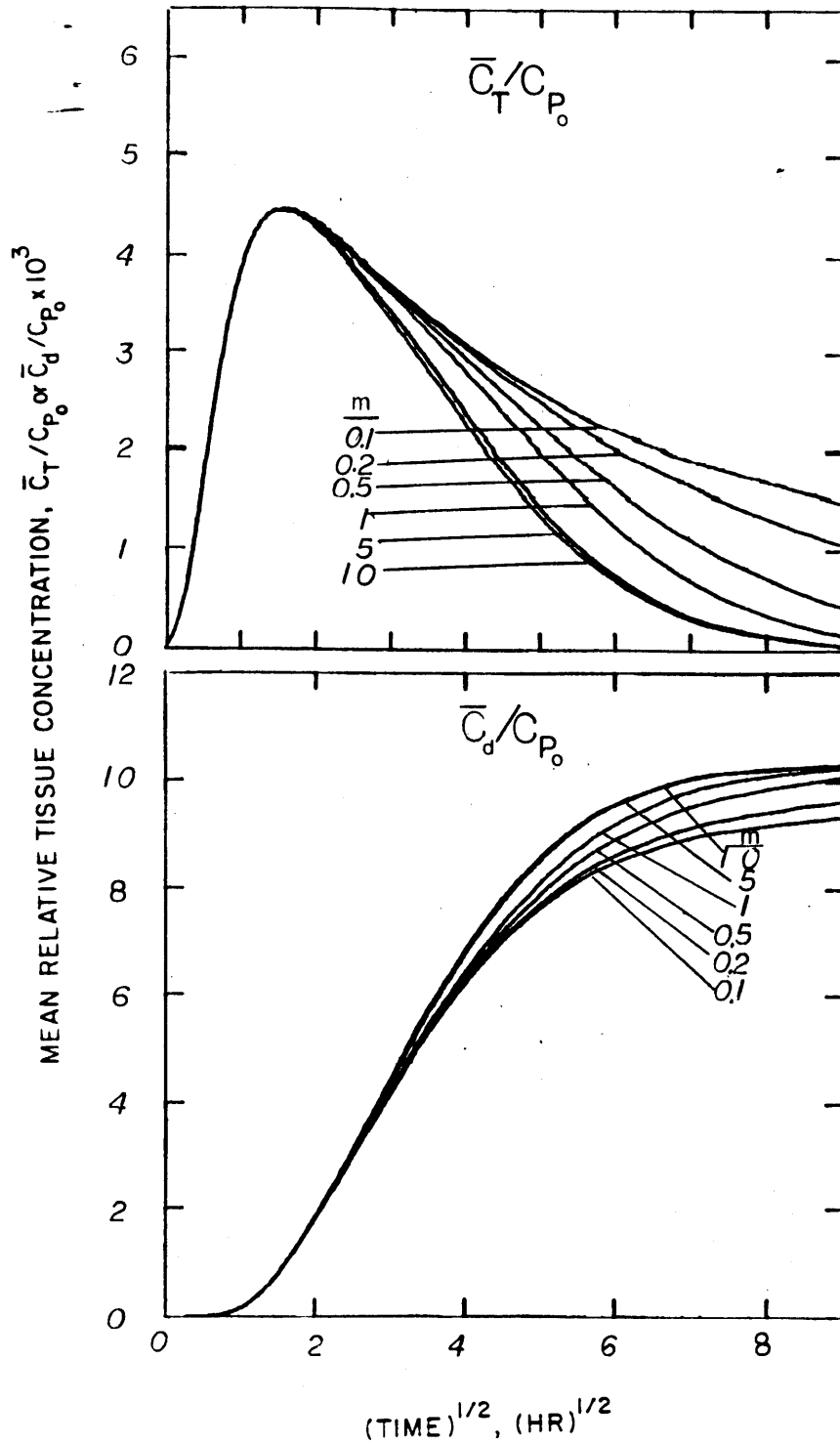


Figure 5-28: Effect of m on mean relative LDL tissue concentrations and cumulative degradation for ϕ_b^2 equal to 2.11. All other parameters are listed in Table 5-VIII for case D for data without aberrant profiles.

(Figure 5-29). For all receptor numbers examined, the receptor number does not influence the total tissue concentration for times less than about two hours and there is a lag time of at least one hr before degradation occurs. This suggests that binding and degradation of LDL by smooth muscle cells do not influence the concentration profiles during the first several hours of the experiment.

Transmural profiles at 4 and 24 hr as a function of ϕ_r^2 are presented in Figure 5-30. At both times, increasing ϕ_r^2 increases the curvature in the profiles. At 4 hr, changing ϕ_r^2 has little effect upon the concentrations near the intimal and medial-adventitial surfaces. The value of the Thiele modulus for receptor-mediated internalization ($\beta\phi_r^2$) was held fixed at a value of 476, based upon the cell culture estimate of k_2 . Consequently, receptor-mediated internalization is about 45 times faster than degradation ($\phi_{d_1}^2$) and intracellular solute has not reached quasi-steady state by 4 hr. By 24 hr, intracellular solute has reached a quasi-steady state with solute in the interstitial fluid and increasing ϕ_r^2 causes the entire profile to shift downward.

The effect of, β , the ratio of the rate constants for receptor-binding (k_1) and receptor-mediated internalization (k_2) upon LDL mean relative tissue concentrations and cumulative degradation is presented in Figure 5-31). For β greater than 5, internalization is sufficiently rapid that model predictions are insensitive to its value. For β equal to or less than 2, LDL begins to accumulate on the cell surface and the linearization assumption (i.e. $C_R \approx C_{R_T}$) begins to break down.

The effect of $\phi_{d_1}^2$ upon mean relative concentrations and cumulative degradation is similar to the effect of ϕ_r^2 (Figure 5-32). Increasing $\phi_{d_1}^2$ results in decreasing mean relative concentrations for times greater than four hours and increased rates and absolute concentrations of degraded LDL. At very high values of $\phi_{d_1}^2$, the intracellular concentration of LDL internalized by receptor-mediated

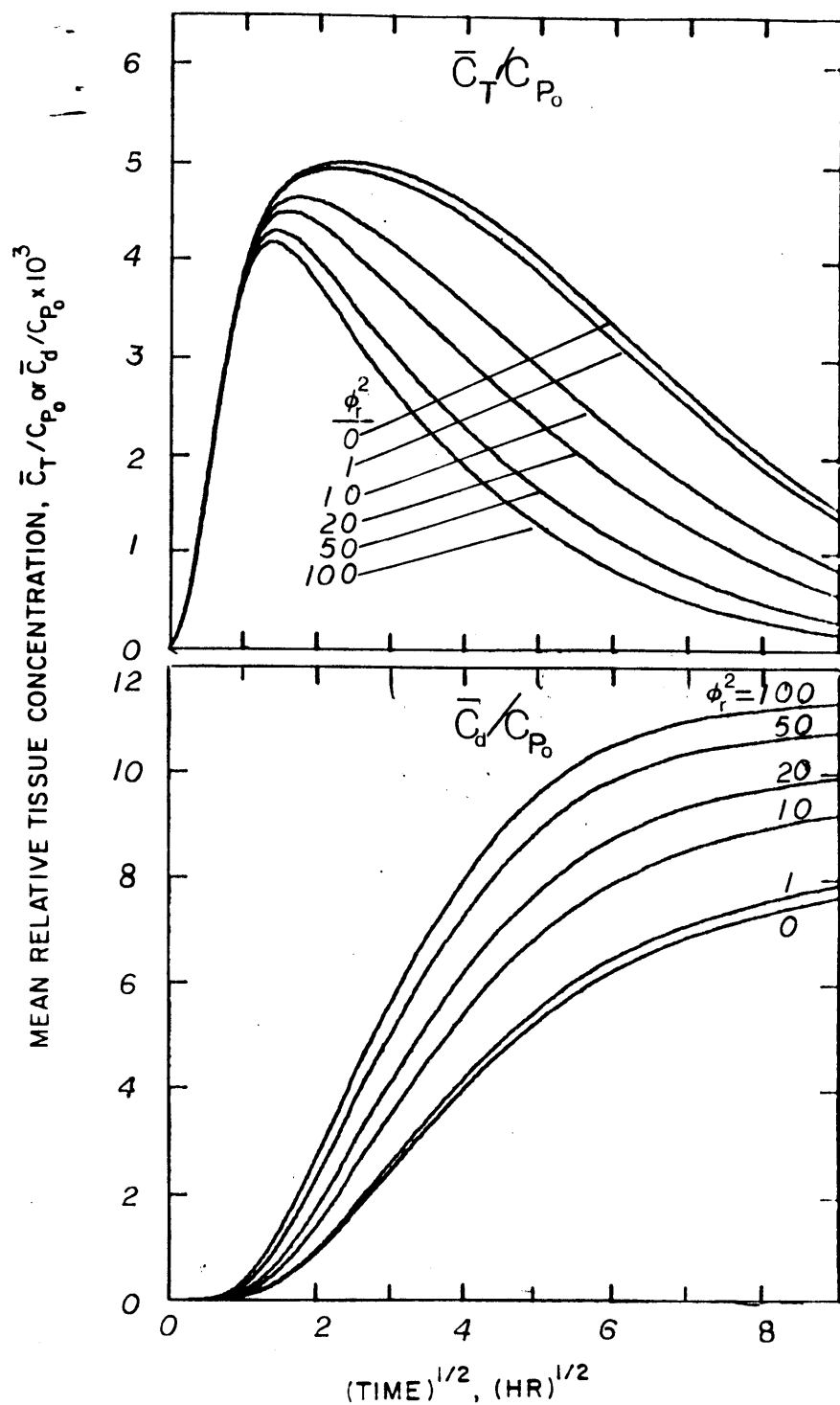


Figure 5-29: Effect of binding to the receptors (ϕ_r^2) on mean relative LDL tissue concentrations and cumulative degradation. All other parameters are listed in Table 5-VIII for case D for data without aberrant profiles.

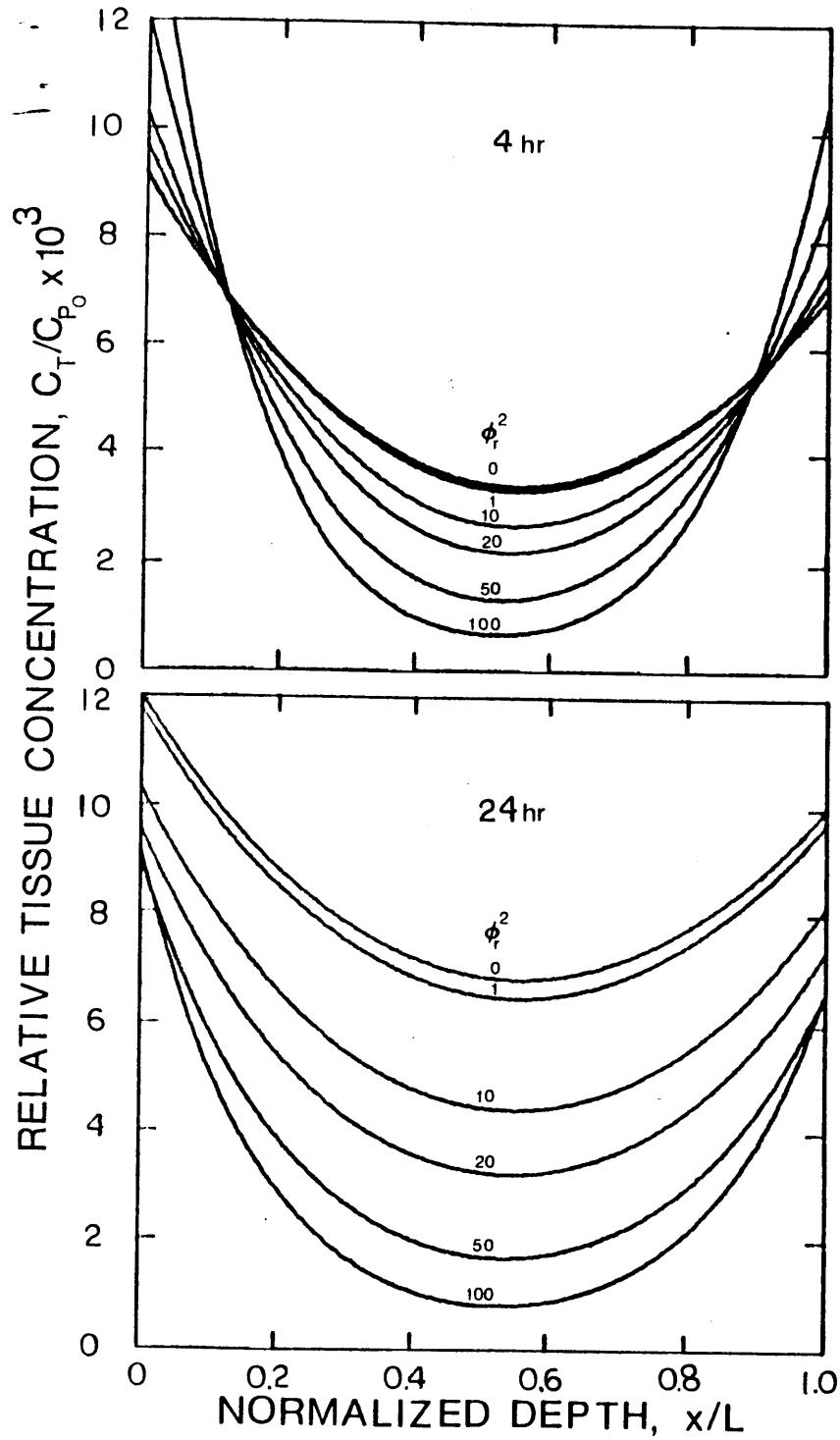


Figure 5-30: Effect of receptor binding (ϕ_r^2) on LDL transmural profiles at 4 and 24 hr. All other parameters are listed in Table 5-VIII for case D from fits of data without aberrant profiles.

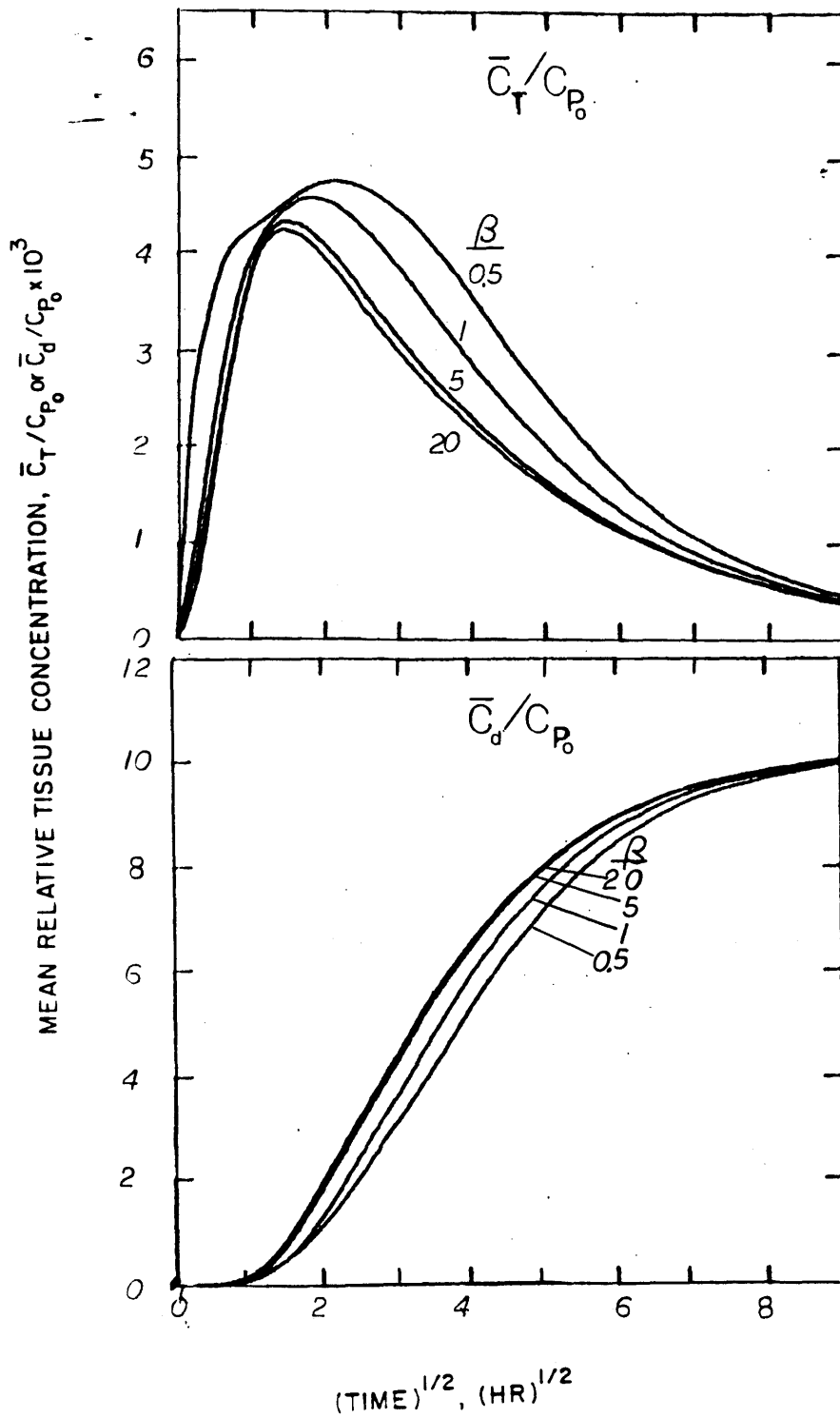


Figure 5-31: Effect of receptor-mediated internalization (β) on LDL transmural profiles at 4 and 24 hr. All other parameters are listed in Table 5-VIII for case D from fits of data without aberrant profiles.

mechanisms is low and degradation is limited by the rate of binding to the receptors.

Tissue concentrations and cumulative degradation are also influenced by exocytosis. Shown in Figure 5-33 is the effect of $\phi_{e_1}^2$ on the mean relative tissue concentration and cumulative degradation. Increasing the value of $\phi_{e_1}^2$ results in return of intracellular solute to the interstitial fluid. As a result, the intracellular concentration and the concentration of receptor-mediated degradation products decrease. At very high values of $\phi_{e_1}^2$ relative to ϕ_{d_1} , LDL internalized by receptor-mediated endocytosis is rapidly returned to the medium, receptor-mediated degradation is negligible, and LDL is degraded by receptor-independent mechanisms only.

The effect of parameters for receptor-independent metabolism was investigated with mLDL. Results are presented in Figures 5-34, 5-35, and 5-36 for the ϕ_i^2 , $\phi_{d_2}^2$, and $\phi_{e_2}^2$, respectively. The results are similar to those observed with receptor-mediated metabolism for LDL except that, at very low values of ϕ_i^2 and $\phi_{d_2}^2$, degradation is negligible. LDL degradation never dropped to zero in the above calculations because LDL could still be degraded by receptor-independent mechanisms.

5.5 Discussion

This study represents the first detailed attempt to model LDL transport and metabolism in the arterial wall in vivo and assess the role of metabolic phenomenon. Previous studies by Ramirez [1979], Schnitzer [1983], and Tompkins [1983] were concerned with estimating transport parameters by fitting transmural profiles following short time circulations during which metabolic phenomenon were

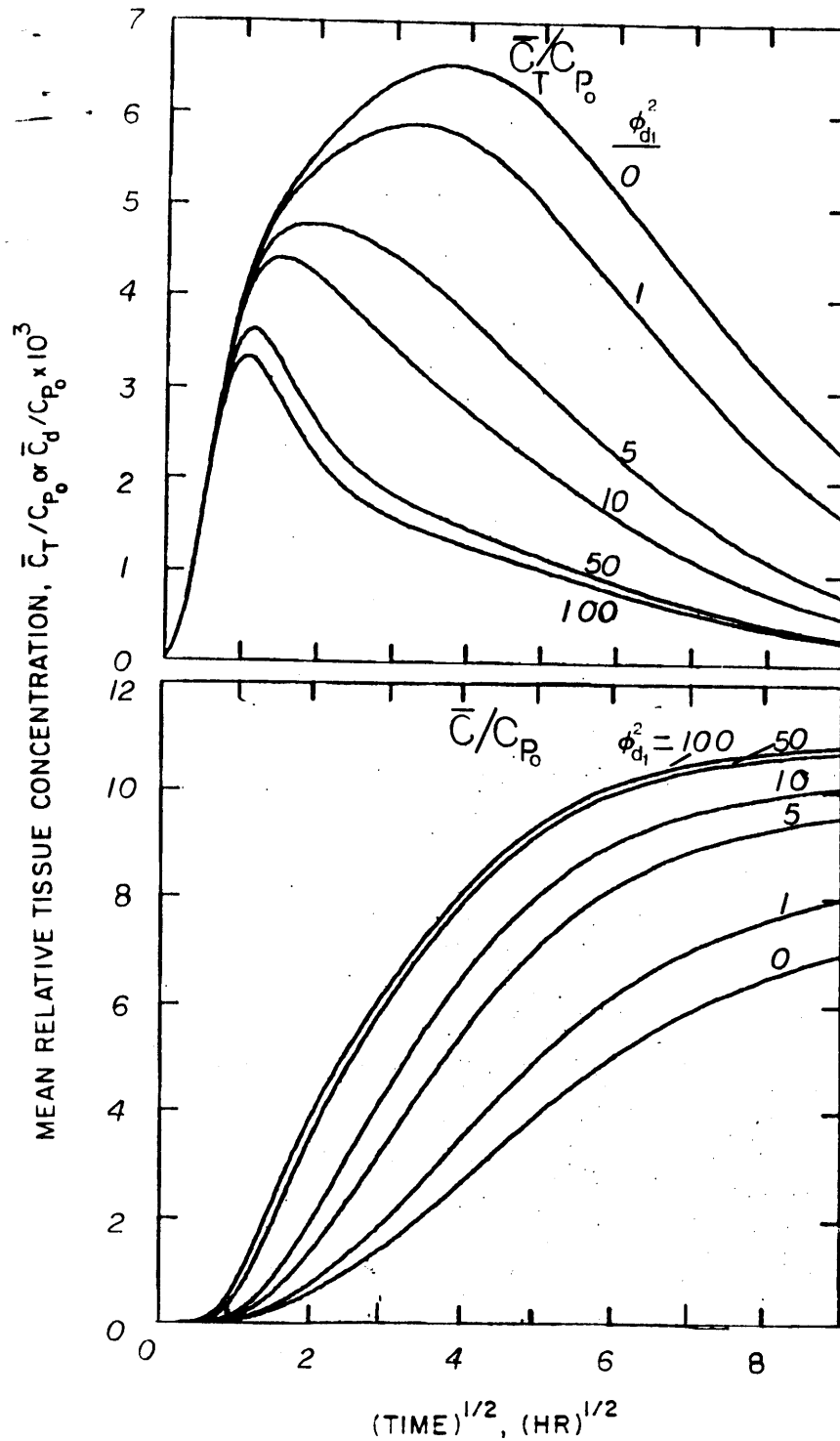


Figure 5-32: Effect of receptor-mediated degradation, $\phi_{d_1}^2$, on LDL mean relative tissue concentrations and cumulative degradation. All other parameters are listed in Table 5-VIII for case D from fits of data without aberrant profiles.

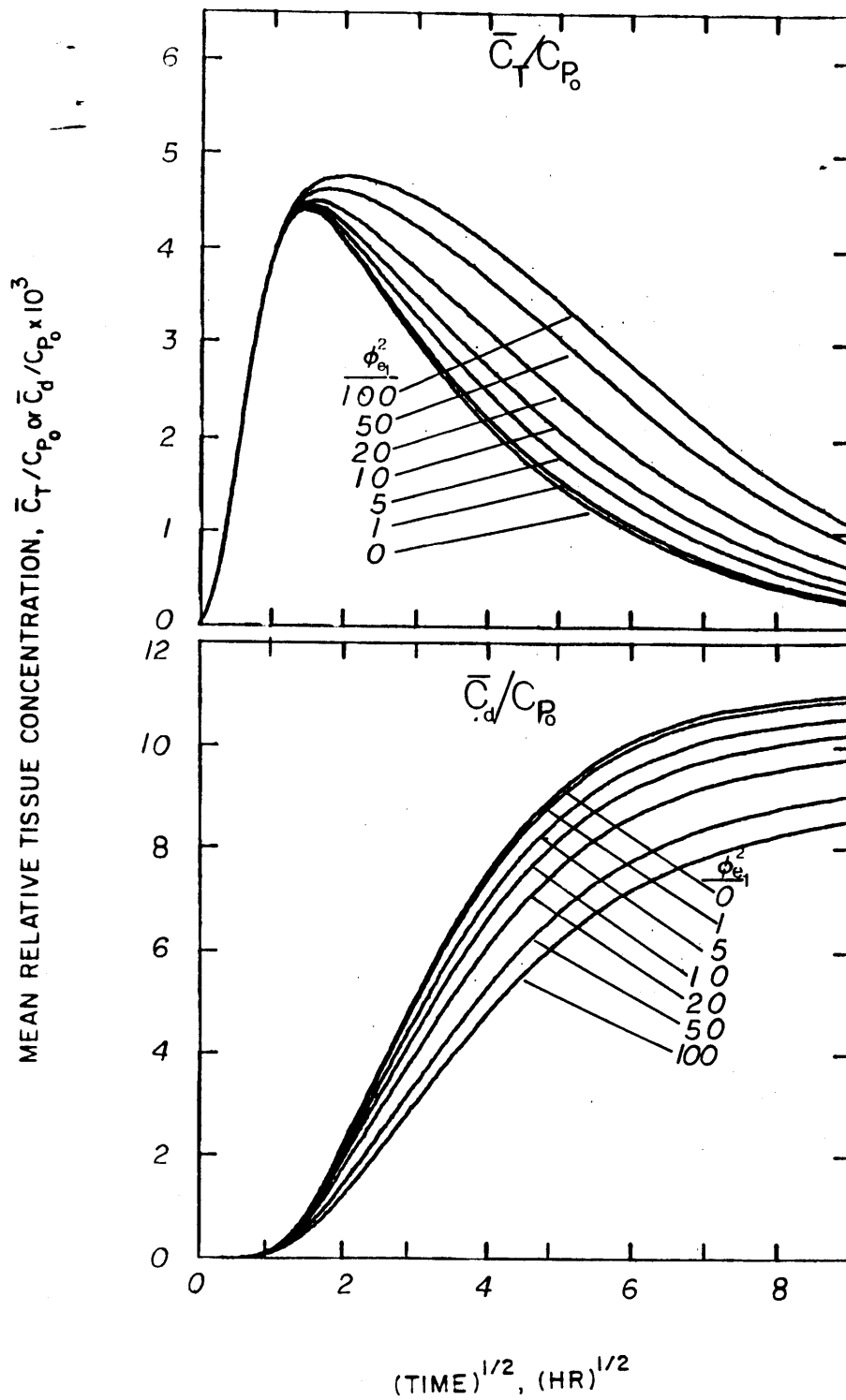


Figure 5-33: Effect of $\phi_{e_1}^2$ on LDL mean relative tissue concentrations and cumulative degradation. All other parameters are listed in Table 5-VIII for case D from fits of data without aberrant profiles.

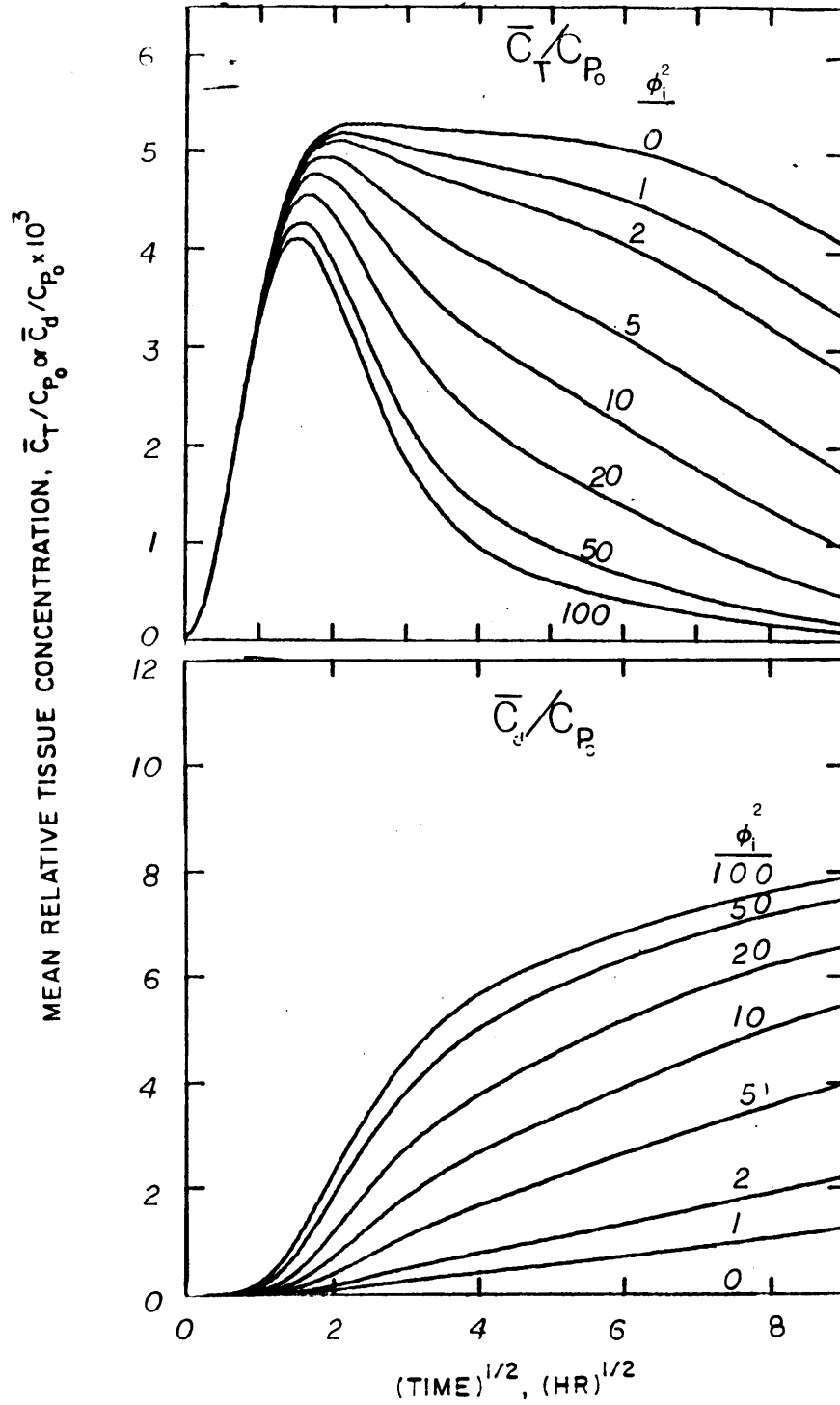


Figure 5-34: Effect of ϕ_i^2 on mLDL mean relative tissue concentrations and cumulative degradation. All other parameters are listed in Table 5-VIII for case D from fits of data without aberrant profiles.

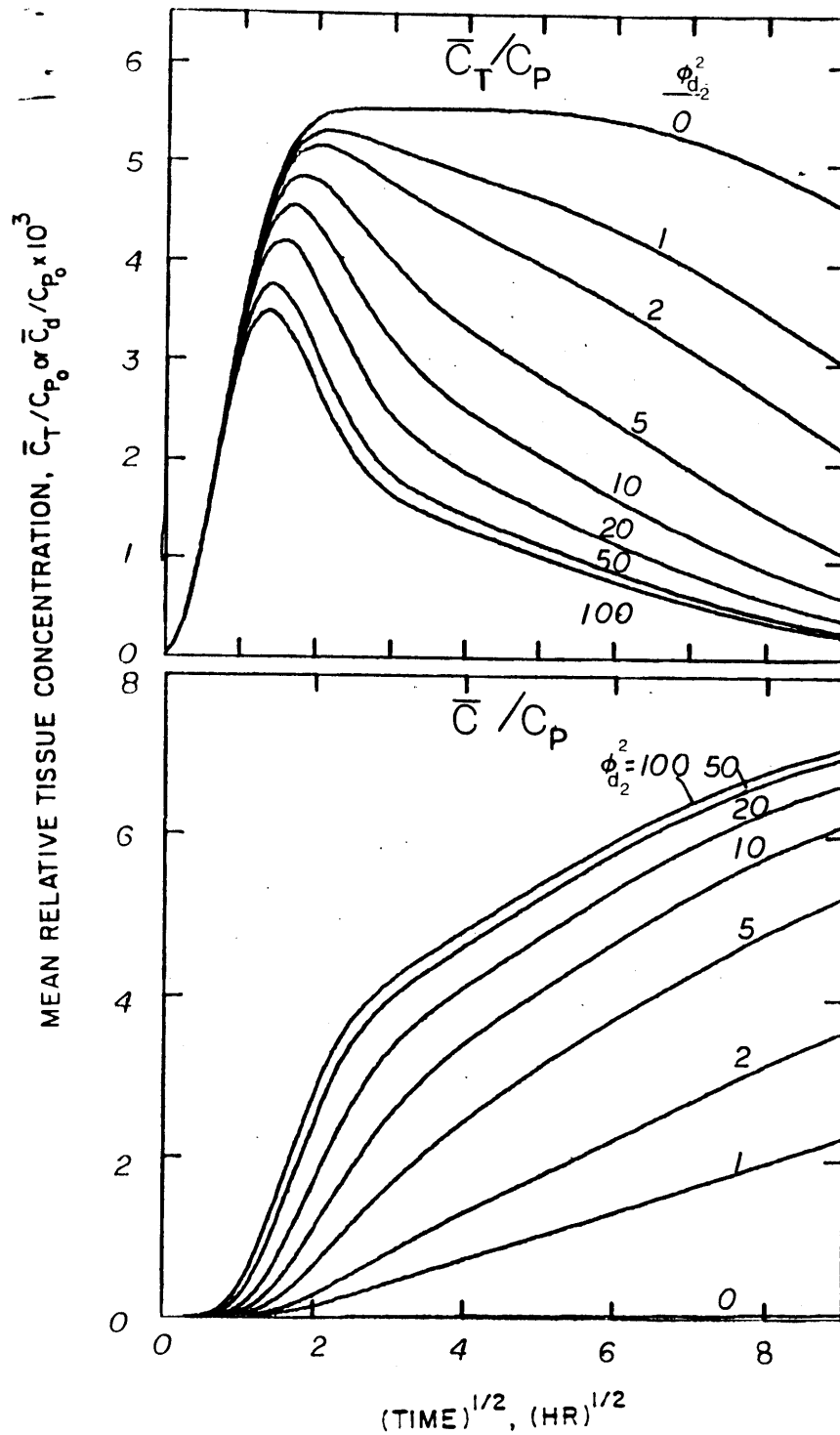


Figure 5-35: Effect of $\phi_{d_2}^2$ on mLDL mean relative tissue concentrations and cumulative degradation. All other parameters are listed in Table 5-VIII for case D from fits of data without aberrant profiles.

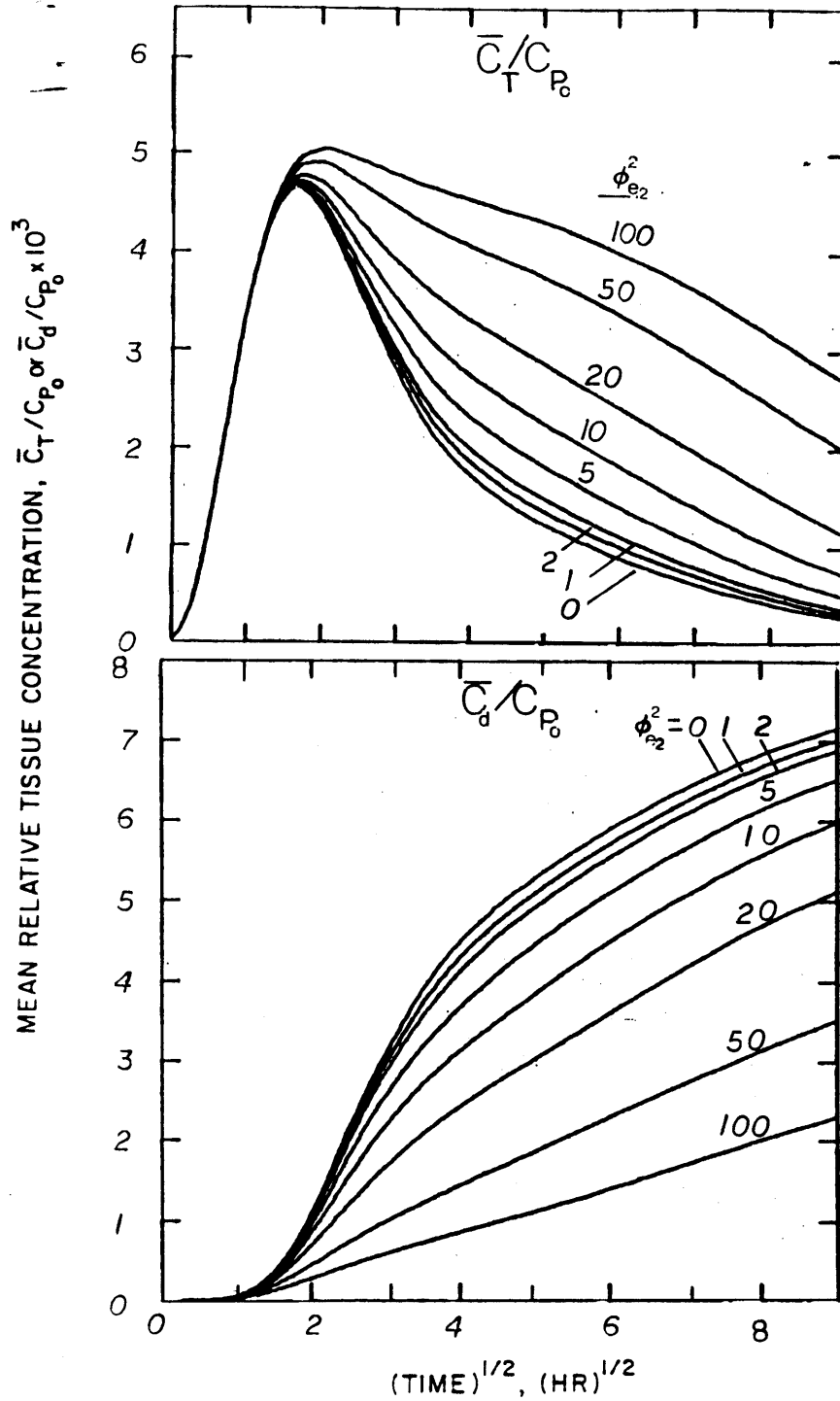


Figure 5-36: Effect of ϕ_{e2}^2 on mLDE mean relative concentrations and cumulative degradation. All other parameters are listed in Table 5-VIII for case D from fits of data without aberrant profiles.

unimportant. Fry [1985] has modeled albumin transport in vitro. Bratzler et al. [1977c] and Truskey et al. [1981] have utilized a less realistic model and examined a wide range of parameter estimates to obtain qualitative consistency between theoretical and experimental transmural profiles although estimates for cell metabolic rate constants and measurements of cumulative degradation were unavailable for comparison.

The model developed to describe LDL transport and metabolism in the arterial wall is a synthesis of previously developed transport models (Bratzler [1974], Ramirez [1979], Tompkins [1983]) together with kinetic models of receptor-mediated and receptor-independent metabolism by cultured cells. Estimates for the rate constants were obtained by fitting kinetic models to cell culture data for receptor-mediated and receptor-independent metabolism, transport parameters were obtained by fitting 0.5 hr transmural profiles to a simplified version of the model, and the functional form of the time-varying mass transfer coefficients was determined by fitting mean relative concentrations of ^{14}C -sucrose labeled LDL and mLDL (\bar{C}_{T+d}/C_{p_0}). This parameter set served as the basis for an investigation of model predictions for transmural profiles, mean relative tissue concentration, and cumulative degradation at longer circulation times. Using constant values of Bi and Bi_c , no single data set could be found which yielded reasonable agreement between model predictions and data for LDL and mLDL transmural profiles and mean relative concentrations. Introduction of time-varying Biot numbers according to the empirical form obtained in Chapter 4 permitted quantitative comparison of model results with data. The model was fit to transmural profiles by nonlinear regression and estimates of m , ϕ_b^2 , ϕ_r^2 and $\phi_{d_1}^2$ were obtained. These metabolic parameters were chosen because: 1) rate constants for binding to the matrix and the number of binding sites were unknown; 2) the model was relatively insensitive to β and $\phi_{e_1}^2$

(Figures 5-30 and 5-32); and 3) rate constants for receptor-independent metabolism gave reasonable fits of mLDL transmural profiles. Fits obtained with all grand average profiles yielded a range of estimates for the parameters, suggesting that this data set was not sensitive to these parameters. When aberrant profiles at 4 and 24 hr were omitted from the grand averages, a consistent parameter set was obtained.

It is somewhat surprising that rate constants estimated from data for LDL metabolism by cultured cells could be used to estimate tissue concentrations and cumulative degradation in vivo, in light of published studies concerning morphological and metabolic changes of cells in culture (Chamley et al. [1977], Fowler et al. [1977], Chamley-Campbell et al. [1979], Yau-Young et al. [1981]). In culture, smooth muscle cells exhibit an increased content of lysosomal enzymes and undergo a process of dedifferentiation, with the loss of spontaneous contractions and a decrease in myosin content. Campbell et al. [1983] found that LDL degradation by rabbit aortic smooth muscle cells decreased by 80% during the first 8 to 10 days following isolation by enzymatic digestion, and this decrease was associated with morphological dedifferentiation. Interestingly, receptor number did not change during this time, suggesting that rate constants for receptor-mediated internalization (k_2) or degradation (k_3) were altered. (Attempts by other investigators to duplicate these results have been unsuccessful (P.F. Davies, personal communication).) Theoretical studies using time-varying Biot numbers for the data set in which aberrant LDL transmural profiles were excluded, do not support the notion that rate constants for LDL metabolism in the arterial wall in vivo are substantially different from values measured in culture.

Model predictions were also compared with transmural profiles at steady state for a step change in plasma concentration estimated from linear systems theory (Figures 5-23, 5-24). For LDL, model predictions agreed reasonably well with

calculated profiles based upon fits of all transmural profiles although better agreement was obtained when aberrant profiles were removed from the analysis. Agreement with estimated mLDL profile at steady state was less satisfactory, possibly as a result of poor fits of transmural profiles.

Additional comparisons between the detailed model predictions and estimates from linear systems theory can be made by computing the mean relative tissue concentration ($\bar{\psi}_T(\infty)$) and steady state rate of degradation (R_d) in response to a step change in plasma concentration neglecting endothelial cell metabolism. $\bar{\psi}_T(\infty)$ was calculated by integration of equation (5-71) over the thickness of the tissue to yield the following expressions for LDL and mLDL:

LDL

$$\bar{\psi}_T(\infty) = \bar{\psi}_f(\infty) \left[1 + \frac{1}{m} + \frac{1}{K} + \frac{\beta\phi_r^2}{(\phi_{d_1}^2 + \phi_{e_1}^2)K} + \frac{\phi_i^2}{\phi_{d_2}^2 + \phi_{e_2}^2} \right] \quad (5-90)$$

mLDL

$$\bar{\psi}_T(\infty) = \bar{\psi}_f(\infty) \left[1 + \frac{1}{m} + \frac{\phi_i^2}{\phi_{d_2}^2 + \phi_{e_2}^2} \right] \quad (5-91)$$

For the cases considered in the model calculations, (i.e. $Pe = 0$, $R = 1$, and $K_2 = \epsilon_f K_1 = -Bi_c$) $\psi_f(\infty)$ is:

$$\begin{aligned} \psi_f(\infty) = (1-f)\epsilon_f \left\{ Bi_c \left[\frac{Bi_{c_o}}{\cosh(\alpha_o)} - [Bi_{c_o} + \alpha_o \tanh(\alpha_o)] \right] (\cosh(\alpha_o) - 1) \right. \\ \left. + \left[Bi_o [Bi_{c_o} \tanh(\alpha_o) + \alpha_o] + \frac{\alpha_o Bi_{c_o}}{\cosh(\alpha_o)} \right] \sinh(\alpha_o) \right\} / \\ \left[\alpha_o \left((Bi_o Bi_{c_o} + \alpha_o^2) \tanh(\alpha_o) + \alpha_o (Bi_{c_o} + Bi_o) \right) \right] \quad (5-92) \end{aligned}$$

The dimensionless rate of degradation for a step change in plasma concentration is

the sum of the respective rates for receptor-mediated and receptor-independent degradation (see equation (5-54)):

$$\frac{R_d L^2}{D_e} = \phi_{d_1}^2 \bar{\psi}_{L_{Ri}}(\infty) + \phi_{d_2}^2 \bar{\psi}_{L_i}(\infty) \quad (5-93)$$

where R_d is the steady state rate of degradation (hr^{-1}). Equation (5-92) can be expressed in terms of $\bar{\psi}_f(\infty)$ by substitution of equation (5-75) for $\bar{\psi}_{L_{Ri}}(\infty)$ and (5-76) for $\bar{\psi}_{L_i}(\infty)$ to yield:

$$\frac{R_d L^2}{D_e} = \left[\frac{\beta \phi_{d_1}^2 \phi_r^2}{K(\phi_{d_1}^2 + \phi_{e_1}^2)} + \frac{\phi_{d_2}^2 \phi_i^2}{\phi_{d_2}^2 + \phi_{e_2}^2} \right] \bar{\psi}_f(\infty) \quad (5-94)$$

The term in brackets is equal to α_o^2 (equation (5-72)) and equation (5-94) simplifies to:

$$\frac{R_d L^2}{D_e} = \alpha_o^2 \bar{\psi}_f(\infty) \quad (5-95)$$

$\bar{\psi}_T(\infty)$ and R_d were calculated from equations (5-90) to (5-95) and are listed in Table 5-IX. Parameters obtained with all profiles give higher estimates of $\bar{\psi}_T(\infty)$ and lower estimates of R_d than with parameters obtained from fits of profiles from which the aberrant profiles were excluded. $\bar{\psi}_T(\infty)$ for mLDL is 21% to 29% of the value obtained with LDL, whereas R_d is 10% to 12% of the value calculated for LDL. For comparison, estimates of $\bar{\psi}_T(\infty)$ and R_d obtained from linear systems theory are also presented in Table 5-IX. Estimates of $\bar{\psi}_T(\infty)$ from linear systems theory are larger than the values estimated from the transport model; the difference is largest for mLDL (210%) and smallest for LDL data without the aberrant profiles (1.8% to 26%). For LDL, values of R_d calculated from linear systems theory are

only 2% to 15% less than model predictions and are within the error calculated for linear systems analysis. R_d for mLDL is 2.5 times larger than the value calculated from the theoretical model.

The concentrations of $\bar{\psi}_T(\infty)$, $\bar{\psi}_f(\infty)$, $\bar{\psi}_b(\infty)$, $\bar{\psi}_{LR}(\infty)$, $\bar{\psi}_{L_{Ri}}(\infty)$, and $\bar{\psi}_{L_i}(\infty)$ are listed in Table 5-X. Freely diffusible LDL accounts for 21% - 30% of the total tissue concentration, and cell associated concentrations account for another 16% - 30%. Interestingly, model predictions indicate that 30% to 50% of the total concentration is bound to the extracellular matrix. Sensitivity analysis indicated that although binding can slow down the rate of degradation, cumulative degradation, and R_d , are unaffected by binding to the matrix (Figures 5-27 and 5-28). As a result of the possible effect of binding to the extracellular matrix on the tissue concentration, independent estimates of the rate constants for binding (k_a and k_d) and number of binding sites are needed.

Equation (5-94) permits direct evaluation of the relative contribution of receptor-mediated and receptor-independent pathways. The fractional contribution of the receptor-mediated pathway is simply the ratio of the rate of receptor-mediated degradation to the total rate of degradation:

$$\frac{(R_d)_{RM}}{R_d} = \frac{\beta\phi_{d_1}^2\phi_r^2/[K(\phi_{d_1}^2+\phi_{e_1}^2)]}{\beta\phi_{d_1}^2\phi_r^2/[K(\phi_{d_1}^2+\phi_{e_1}^2)] + \phi_{d_2}^2\phi_i^2/(\phi_{d_2}^2+\phi_{e_2}^2)} \quad (5-96)$$

where the numerator represents the steady state rate constant for receptor-mediated LDL degradation and the denominator is the sum of the rate constants for receptor-mediated and receptor-independent LDL metabolism and is equal to α_o^2 (equation (5-72)). The magnitudes of the values of the individual parameter groups in equation (5-96) are presented in Table 5-XI for parameter values listed in Table 5-VIII. For parameter estimates obtained by fitting all LDL grand average profiles

Table 5-IX: Comparison of Model Estimates of ψ_T and R_d with Estimates from Linear Systems Analysis

	Case	α_o	$\psi_T(\infty) \times 10^3$	$\theta(\infty) \times 10^3$	$R_d \times 10^4, \text{ hr}^{-1}$
Model Predictions					
LDL ¹	A	3.29	13.9	10.2	9.7
	B	2.40	14.8	9.2	8.6
	C	2.42	16.6	9.2	8.7
	D	2.37	15.5	9.1	8.8
LDL ²	A	3.24	12.4	10.2	9.3
	B	3.46	12.1	10.4	9.8
	C	3.24	12.5	10.2	9.6
	D	3.42	12.7	10.3	9.8
mLDL ³		2.00	3.54	9.9	1.1
Linear Systems Theory ⁴					
LDL ^{4a}			26 ± 20	8.1 ± 0.8	9.2 ± 1.6
LDL ^{4b}			16.3 ± 6.0	8.3 ± 0.8	9.2 ± 1.6
mLDL			7.3 ± 2.7	7.9 ± 0.9	2.8 ± 0.4

1. All LDL transmural profiles included in estimate. Parameter values are listed in Table 5-VIII.
2. LDL transmural profiles without aberrant profiles. Parameter values are listed in Table 5-VIII.
3. All mLDL profiles. Parameter values are listed in Table 5-VIII.
4. Results of linear systems theory from Table 4-VIII. 4a. all profiles
4b. without 4C6 and 24C1.

Table 5- X: Distribution of Tissue Concentrations at Steady State Following a Step Change in Plasma Concentration

Case	$\bar{\Psi}_T(\infty)$	$\bar{\Psi}_f(\infty)$	$\bar{\Psi}_b(\infty)$	$\bar{\Psi}_{LR}(\infty)$	$\bar{\Psi}_{L_{Ri}}(\infty)$	$\bar{\Psi}_{L_i}(\infty)$
LDL ¹ A	0.0139	0.0027 (19%)	0.0077 (56%)	0.0001 (0.7%)	0.0042 (30%)	0.0016 (11%)
B	0.0148	0.0045 (31%)	0.0068 (46%)	0.00004 (0.3%)	0.0008 (5%)	0.0027 (18%)
C	0.0166	0.0045 (27%)	0.0048 (29%)	0.00016 (0.9%)	0.0044 (27%)	0.0026 (16%)
D	0.0155	0.0047 (30%)	0.0058 (37%)	0.00008 (0.5%)	0.0022 (14%)	0.0028 (18%)
LDL ² A	0.0124	0.0027 (22%)	0.0063 (51%)	0.00009 (0.8%)	0.0018 (14%)	0.0013 (13%)
B	0.0121	0.0025 (20%)	0.0062 (51%)	0.00010 (0.8%)	0.0019 (16%)	0.0015 (12%)
C	0.0125	0.0028 (22%)	0.0061 (49%)	0.00010 (0.8%)	0.0019 (15%)	0.0016 (13%)
D	0.0127	0.0025 (20%)	0.0062 (49%)	0.00012 (0.9%)	0.0024 (19%)	0.0015 (12%)
mLDL ³	0.0035	0.0009 (24%)	0.0022 (62%)			0.0005 (14%)

1. Parameter values obtained from nonlinear regression of all LDL transmural profiles (Figure 5-17) and are listed in Table 5-VIII.
2. Parameter values obtained from nonlinear regression of all LDL transmural profiles without experiments 4C6 and 24C1 (Figure 5-19) and are listed in Table 5-VIII.
3. Parameter values obtained from nonlinear regression of all mLDL transmural profiles (Figure 5-21) and are listed in Table 5-VIII.

* Values in parentheses represent percent of total concentration

the contribution of the receptor-mediated pathway is variable, accounting for 27% (case D) to 63% (case A) of the steady state rate of degradation. When the aberrant profiles at 4 and 24 hr were excluded, the receptor-mediated contribution ranged from 62% to 66%. These results are consistent with calculations presented in Chapter 2 (equation (2-64)), based upon LDL receptor down-regulation in culture, which indicated that both receptor-mediated and receptor-independent mechanisms contribute to the removal of solute from the tissues.

It has frequently been assumed that the contribution of receptor-mediated metabolism can be quantitatively evaluated by subtracting the tissue concentration or rate of degradation of mLDL from the corresponding quantity for LDL (Pittman et al. [1982a,b], Carew et al. [1984]). For the steady state rate of degradation in response to a step change in plasma concentration, such an approach assumes that the fractional contribution of the receptor-mediated pathway, equation (5-95), can be rewritten in the same form as equation (4-15c):

$$\frac{(R_d)_{\text{RM}}}{R_d} = \frac{(R_d)_{\text{LDL}} - (R_d)_{\text{mLDL}}}{(R_d)_{\text{LDL}}} \quad (4-15c)$$

$(R_d)_{\text{LDL}} - (R_d)_{\text{mLDL}}$ can be determined by substituting equation (5-94) for R_d to yield:

$$\begin{aligned} (R_d)_{\text{LDL}} - (R_d)_{\text{mLDL}} = & \\ & \frac{\beta \phi_{d_1}^2 \phi_r^2}{K(\phi_{d_1}^2 + \phi_{e_1}^2)} (\bar{\psi}_f(\infty))_{\text{LDL}} - \frac{\phi_{d_2}^2 \phi_i^2}{\phi_{d_2}^2 + \phi_{e_2}^2} [(\bar{\psi}_f(\infty))_{\text{mLDL}} - (\bar{\psi}_f(\infty))_{\text{LDL}}] \quad (5-97) \end{aligned}$$

The tabulated concentrations in Table 5-X indicate that $\bar{\psi}_f(\infty)$ is different for LDL and mLDL, since the concentrations are influenced to different extents by

Table 5-XI: Importance of Receptor-Mediated and Receptor-Independent Degradation

		$\frac{\beta\phi_{d_1}^2\phi_r^2}{[K(\phi_{d_1}^2+\phi_{e_1}^2)]}$	$\frac{\phi_{d_2}^2\phi_i^2}{(\phi_{d_2}^2+\phi_{e_2}^2)}$
All Profiles ¹	A	6.82	4.00
	B	1.78	4.00
	C	1.87	4.00
	D	1.54	4.00
Without 4C6 ² and 24C1	A	6.82	4.18
	B	7.98	4.00
	C	6.51	4.00
	D	7.73	4.00
mLDL ³		4.00	

1. Parameter values obtained from nonlinear regression of all LDL transmural profiles (Figure 5-17) and are listed in Table 5-VIII.
2. Parameter values obtained from nonlinear regression of all LDL transmural profiles without experiments 4C6 and 24C1 (Figure 5-19) and are listed in Table 5-VIII.
3. Parameter values obtained from nonlinear regression of all mLDL transmural profiles (Figure 5-21) and are listed in Table 5-VIII.

degradation. Consequently, $(R_d)_{LDL} - (R_d)_{mLDL}$ is not equal to $\beta\phi_{d_1}^2\phi_r^2/[K(\phi_{d_1}^2+\phi_{e_1}^2)]$. Thus, equation (5-97) does not correctly yield the fractional contribution of receptor-mediated metabolism. This does not mean that modified LDL is of no use. On the contrary, modified forms of LDL are valuable probes for the study of receptor-independent metabolism. Differences in the steady state tissue concentrations and rates of degradation of LDL and mLDL reflect the

activity of receptor-mediated and receptor-independent pathways. The presence of diffusional limitations, which influence LDL and mLDL to different extents, prevents the direct comparison of the metabolism of these two lipoproteins.

It is instructive to examine model predictions for LDL and mLDL concentrations freely diffusible, bound to the extracellular matrix, and cell associated in order to examine the relative importance of cellular metabolism and binding to the extracellular matrix. Results are presented in Figures 5-37 and 5-38 for LDL based upon parameter values obtained with and without aberrant transmural profiles, and in Figure 5-39 for mLDL. Concentrations of total ($\bar{\theta}_T$), freely diffusible ($\bar{\theta}_f$), bound ($\bar{\theta}_b$), and total cellular ($\bar{\theta}_{LR} + \bar{\theta}_{L_{Ri}} + \bar{\theta}_{L_i}$) species, which for mLDL is simply $\bar{\theta}_{L_i}$, are presented in Figures 5-37A, 5-38A, and 5-39. $\bar{\theta}_f$, $\bar{\theta}_{LR}$, $\bar{\theta}_{L_{Ri}}$, and $\bar{\theta}_{L_i}$ are presented in Figures 5-37B and 5-38B.

The concentrations plotted in Figures 5-37 to 5-39 display similar trends. Freely diffusible solute is the major tissue concentration during the first hour and reaches a maximum at about one hr. Cell associated concentrations become appreciable after about one hr and reach a maximum value between 3 and 4 hr. For profiles calculated using parameters obtained from fits of transmural LDL profiles without aberrant profiles (Figure 5-38), total cell associated concentrations exceed freely diffusible concentrations, although $\bar{\theta}_{LR}$, $\bar{\theta}_{L_{Ri}}$, and $\bar{\theta}_{L_i}$ are all less than $\bar{\theta}_f$ (Figure 5-38B). Binding to the extracellular matrix is unimportant during the first few hours, reaching a maximum between 16 and 24 hr. Since dissociation is slower than association ($\phi_b^2 m < \phi_b^2$) and the Thiele moduli for receptor-mediated and receptor-independent metabolism, matrix-bound LDL becomes the predominant concentration at long circulation times.

The mean relative concentrations of $\bar{\theta}_{L_{Ri}}$ and $\bar{\theta}_{L_i}$ represent the relative contribution of receptor-mediated and receptor-independent pathways to cellular

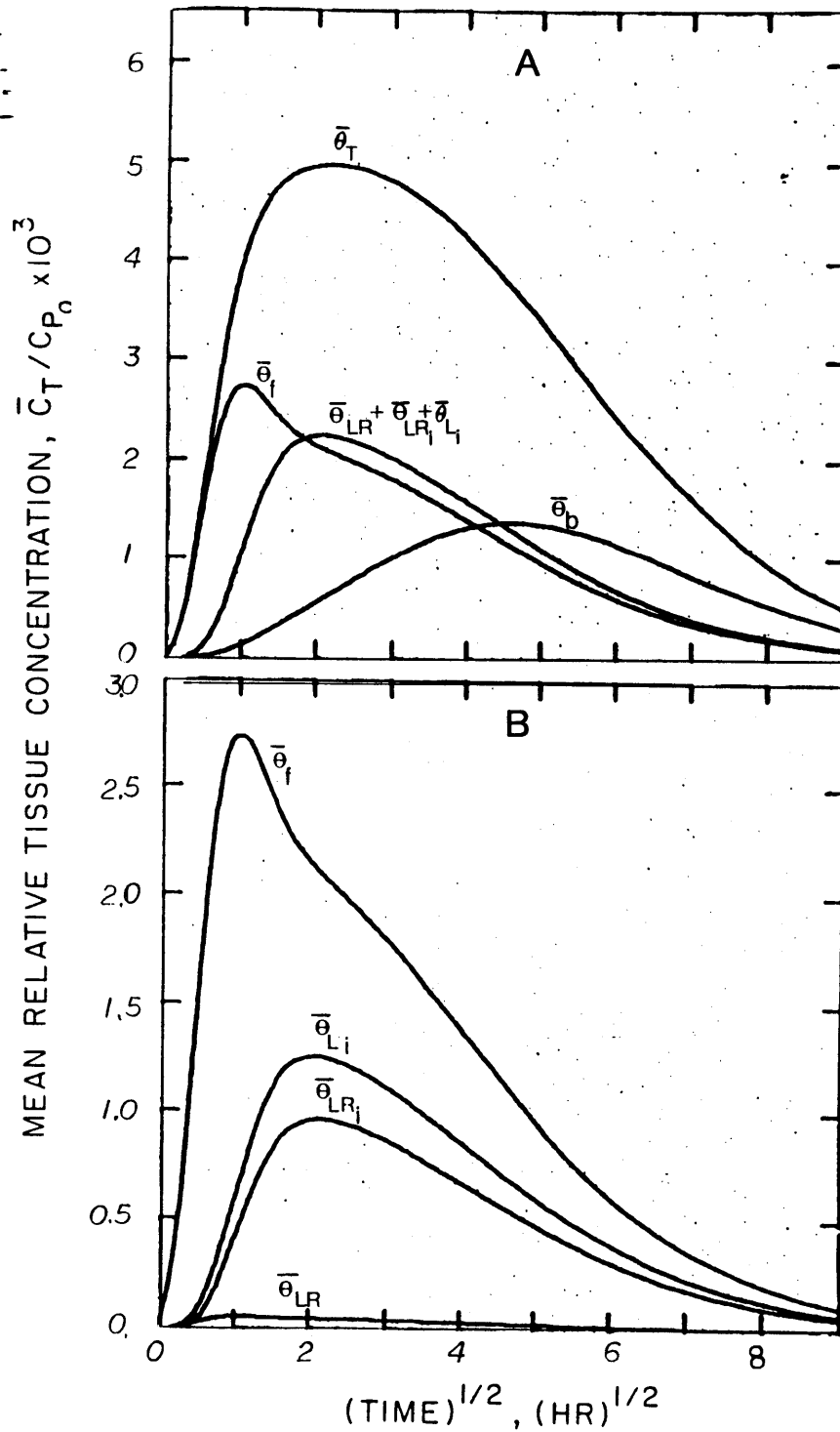


Figure 5-37: Predicted mean relative concentrations of (A) $\bar{\theta}_T, \bar{\theta}_f, \bar{\theta}_b$, and total cellular concentration $(\bar{\theta}_{LR} + \bar{\theta}_{LRi} + \bar{\theta}_{Li})$, and (B) $\bar{\theta}_f, \bar{\theta}_{LR}, \bar{\theta}_{LRi}$, and $\bar{\theta}_{Li}$. Parameters are those obtained from best of transmural LDL profiles (case D, Figure 5-17).

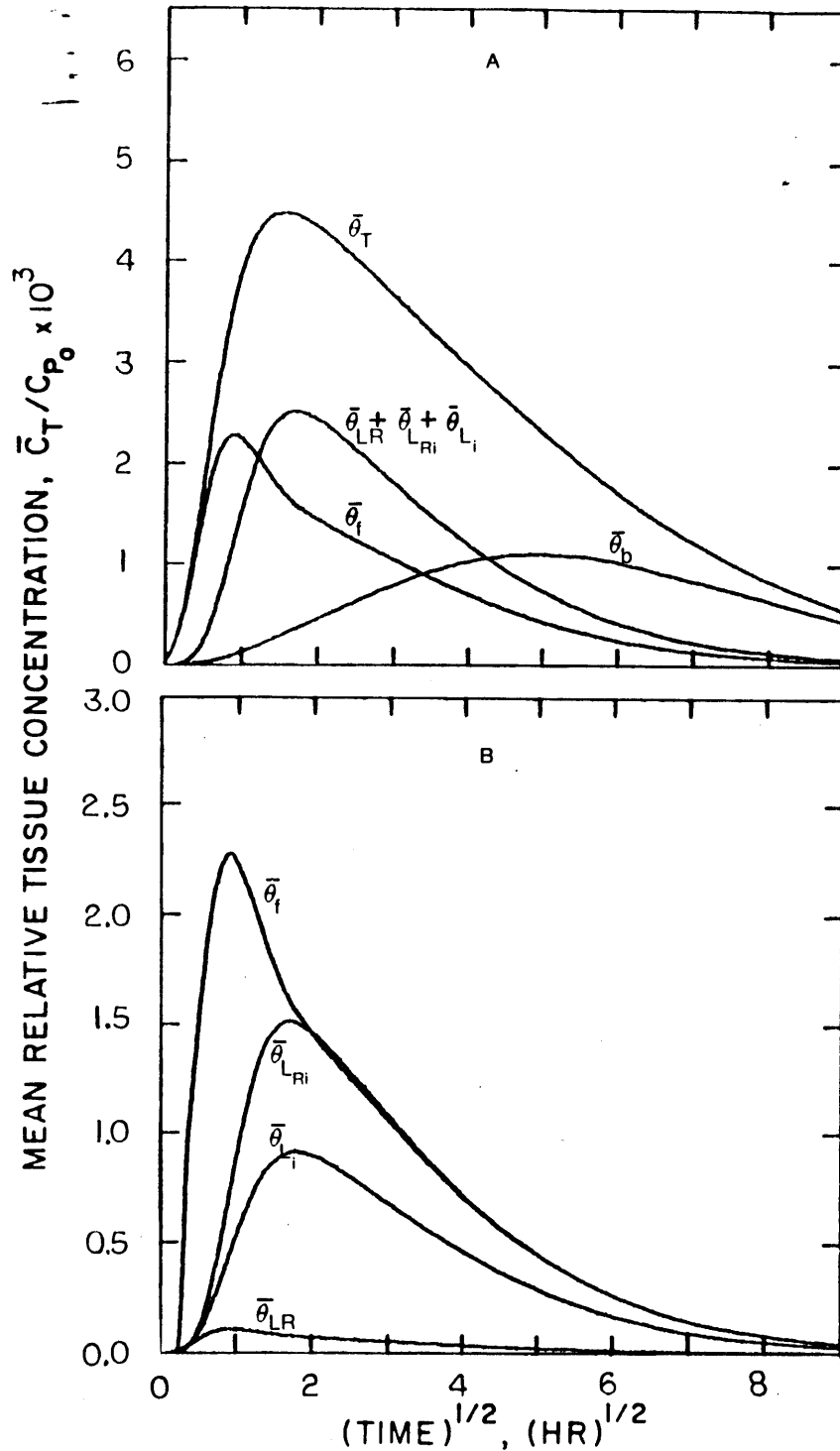


Figure 5-38: Predicted mean relative LDL concentrations of (A) $\bar{\theta}_T, \bar{\theta}_f, \bar{\theta}_b,$ and total cellular concentration $(\bar{\theta}_{LR} + \bar{\theta}_{LRi} + \bar{\theta}_{Li})$, and (B) $\bar{\theta}_f, \bar{\theta}_{LR}, \bar{\theta}_{LRi},$ and $\bar{\theta}_{Li}$. Parameters are those obtained from best fit of transmural LDL profiles excluding experiments 4C6 and 24C1 (case D, Figure 5-19).

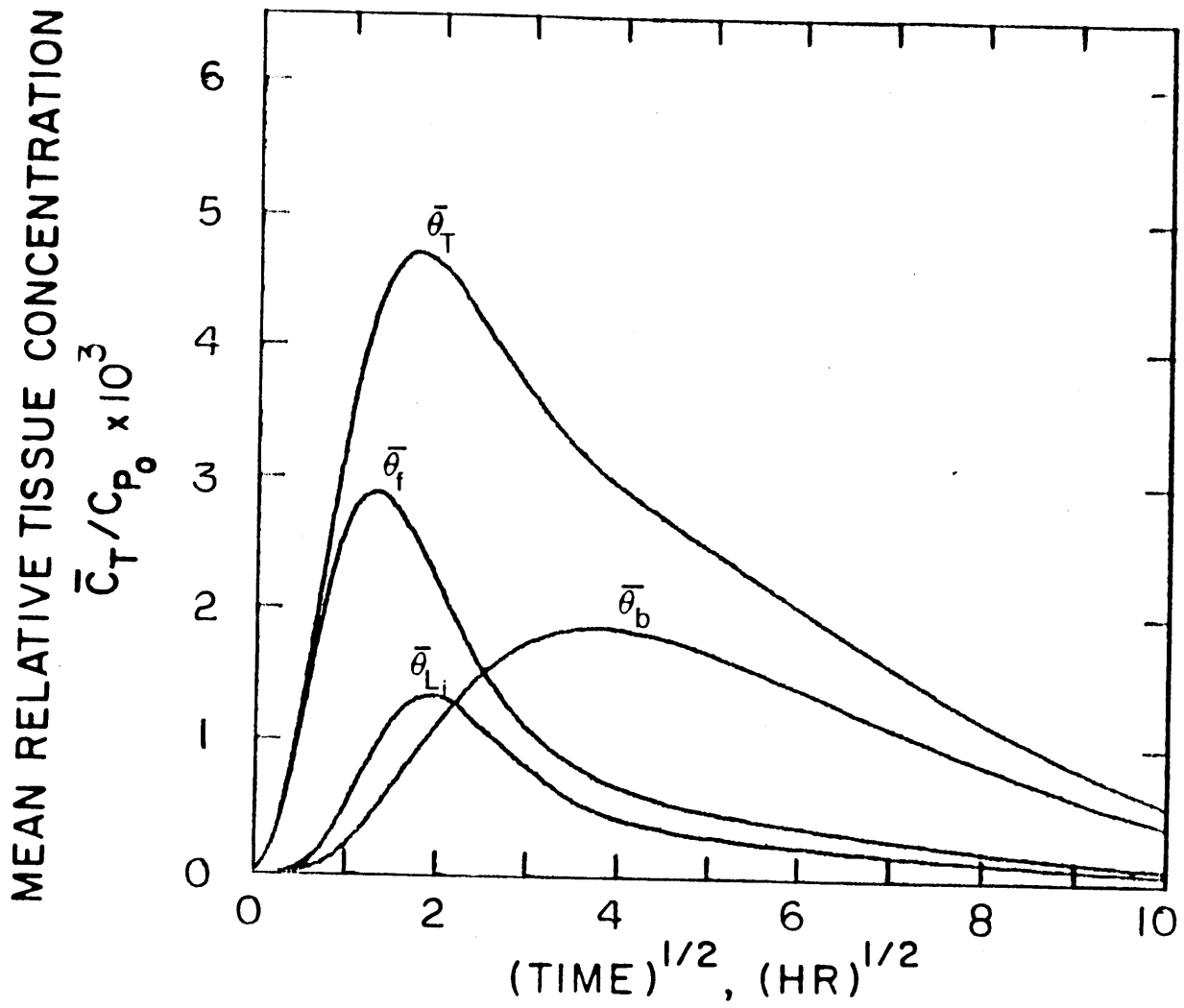


Figure 5-39: Predicted mean relative mLDL concentrations of $\bar{\theta}_T$, $\bar{\theta}_f$, $\bar{\theta}_b$, and $\bar{\theta}_{L_i}$. Parameters are those obtained from best fit of transmural mLDL profiles (Figure 5-21).

internalization. Using parameter values obtained from fits of all LDL transmural profiles (Figure 5-17), the receptor-independent pathway accounts for the bulk of intracellular LDL (Figure 5-37B). When model calculations are performed using the parameters obtained from fitting the LDL transmural profiles without experiments 4C6 and 24C1, the contribution of the receptor-mediated pathway is more important (Figure 5-38B). The value of ϕ_r^2 used to calculate the concentrations in Figure 5-38 is about three times larger than the value used in Figure 5-37. For both values of ϕ_r^2 , the concentration of receptor-bound LDL is low and is less than 10% of the free concentration at all times.

During the formulation of the mathematical model, it was assumed that the interstitial concentration of labeled LDL is sufficiently low that few receptors are occupied with radiolabeled LDL and binding could be modeled as a pseudo-first order reaction. The results plotted in Figures 5-37B and 5-38B indicate that θ_{LR} reaches a maximum concentration at about one hr. Evaluation of the fraction of receptors occupied at this time can be used to assess the maximum error in this assumption. The fraction of receptors occupied ($f_R = \frac{[LR]}{[R]}$ where [LR] and [R] are expressed in units of receptors/cell) is related to θ_{LR} :

$$\theta_{LR} = \frac{C_{LR}}{C_{p_0}} = \frac{[LR]M_w \epsilon_c}{C_{p_0} V_c N} = \frac{[R]f_R M_w \epsilon_c}{C_{p_0} V_c N} \quad (5-98)$$

where C_{p_0} is in units of g/ml, [LR] is in units of g LDL protein/mg cell protein, and V_c is in units of cm^3 . The average value of C_{p_0} from all experiments is 90 $\mu\text{g/ml}$. Transmural profiles of C_{LR} were obtained at one hr using parameters for LDL metabolism listed in Table 5-VII from which f_R was calculated by means of equation (5-98). The results are plotted in Figure 5-40. Results for the two different estimates of $[R]_T$ are similar. There is a gradient in the fraction of

receptors occupied reflecting the gradient in LDL concentration. At most 7% of the receptors are occupied indicating that LDL does behave as a tracer in the arterial wall. If, however, the arterial smooth muscle cells were exposed to the plasma concentration of LDL, a substantial fraction of receptors would be occupied and the linearization assumption is no longer valid.

Model predictions of cumulative LDL and mLDL degradation are in good agreement with the experimental measurements obtained by Navarro [1984]. Cumulative degradation is sensitive to the contribution provided by luminal endothelial cells (Figures 5-25 and 5-26). Reasonable results were obtained using a time-varying Thiele modulus for nonspecific internalization with $\phi_{ie_0}^2$ between 0.1 and 0.2. For these values of $\phi_{ie_0}^2$, the endothelium accounts for between 16% and 32% of $\Theta_d(\infty)$. Similar results were obtained using a constant value of ϕ_{ie}^2 about an order of magnitude less than $\phi_{ie_0}^2$. Further study of endothelial cell metabolism is needed.

Carew et al. [1984] have measured the separate contribution of the endothelium to cumulative LDL degradation in the rabbit aorta, and found that between 31% and 55% of aortic degradation was attributed to the intima. These investigators obtained transmural profiles of C_{T+d} at 24 hr by autoradiographic methods. There is a steep gradient in the number of grains for the initial 15% of the media.

Model predictions of transmural profiles of LDL degradation products at 24 hr are presented in Figure 5-41 using parameters obtained by fitting LDL profiles without aberrant profiles (case D, Table 5-VIII). Profiles were generated without (A) and with (B) endothelial cell metabolism. When endothelial cell metabolism is neglected, the profile is concave and the profiles reflect the transmural profile at that time. Including endothelial cell metabolism results in a steep intimal gradient.

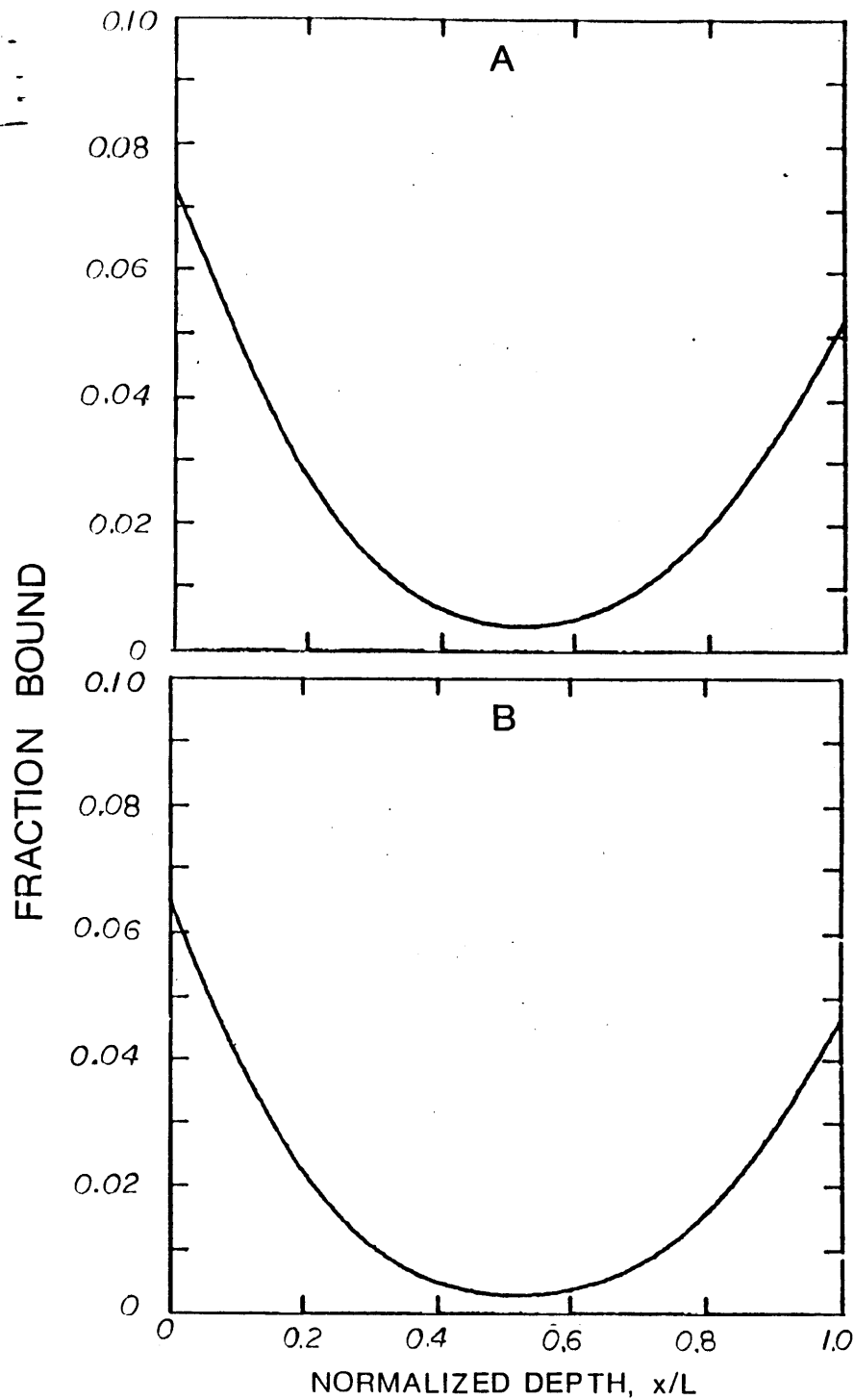


Figure 5-40: Transmurial profile of the fraction of receptors bound to LDL at 1 hr calculated using parameter values from best fit of (A) LDL transmurial profiles (case D, Figure 5-17); and (B) LDL transmurial profiles without experiments 4C6 and 24C1 (case D, Figure 5-19). Parameter values are listed in Table 5-VIII.

The gradient may actually be steeper than plotted since concentrations were calculated at intervals of x/L equal to 0.05. Nevertheless, the profile in Figure 5-41B qualitatively resembles the results obtained by Carew et al. [1984] and indicates the importance of endothelial cell metabolism.

The time varying Biot numbers have a significant effect upon tissue concentrations and cumulative degradation and results are sensitive to changes in the values of f and γ' . Decreasing either value leads to increased tissue concentrations and cumulative degradation. As noted in Chapter 4, time-varying permeabilities suggest an alteration of LDL, either in plasma as a result of aggregation or binding to other proteins, or on the endothelial cell surface. Whatever the nature of the alteration, it does not appear to influence the metabolism of LDL by smooth muscle cells since good agreement between data and theory was obtained using constant metabolic parameters.

Finally, it is interesting to note that the experimental and theoretical studies described in this thesis support many of the hypotheses put forth by Bratzler et al. [1977c] concerning the relative importance of diffusion, binding to the matrix, and cellular metabolism. Thiele moduli for internalization and degradation of LDL by smooth muscle cells listed in Table 5-VIII are large, indicating that internalization and degradation are rapid relative to diffusion and degradation serves as an internal sink for the removal of lipoproteins from tissue. Degradation does not influence mean relative concentrations for times less than four hr, although the shapes of the transmural profiles are affected. The receptor-mediated pathway contributes between 33% and 66% of total degradation. Degradation is the primary factor involved in removing LDL from tissue. The Thiele modulus for binding to the extracellular matrix is less than the values for receptor-mediated and receptor-independent metabolism and binding occurs more slowly. Dissociation from the

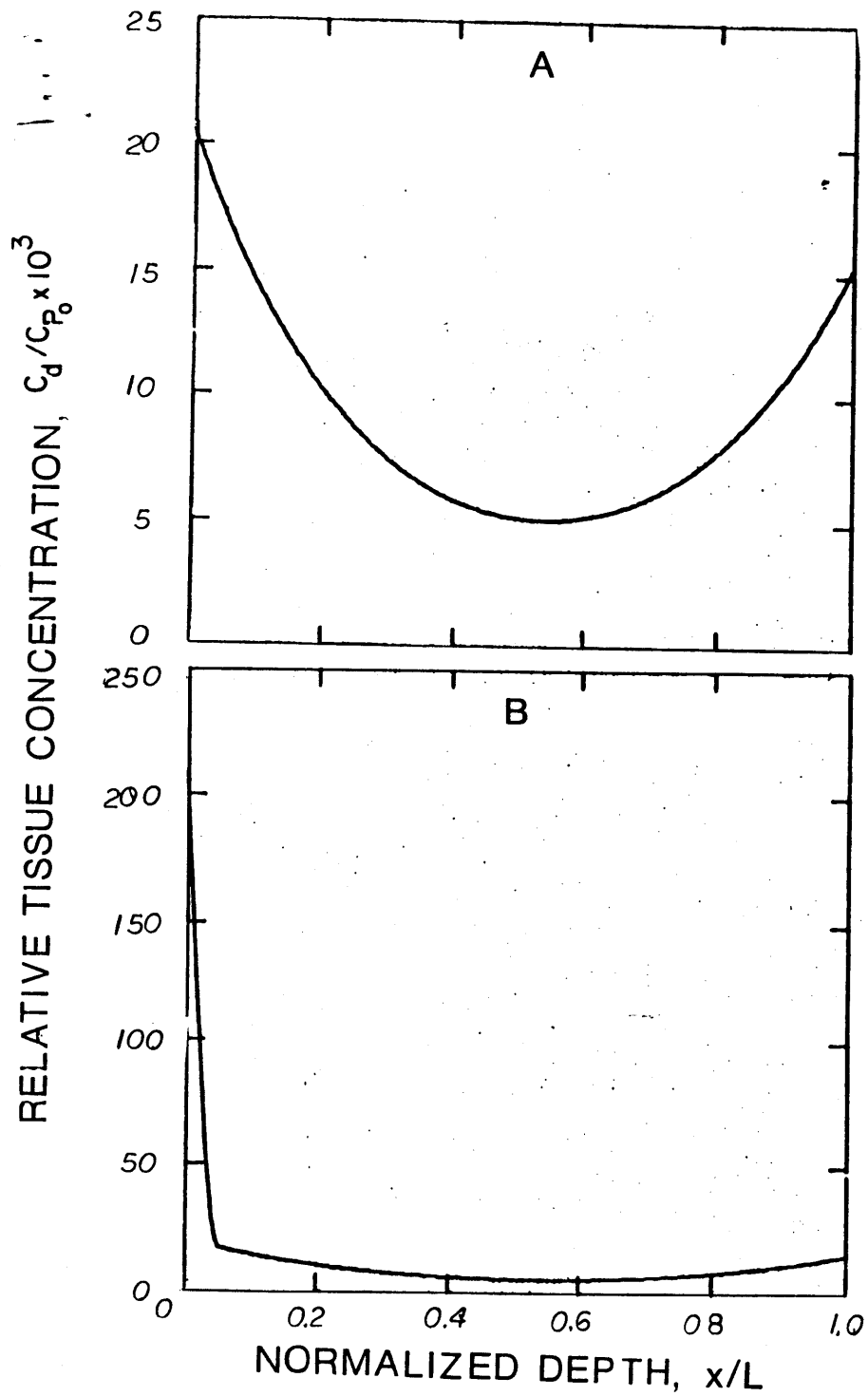


Figure 5-41: Transmurial profile of cumulative degradation products of LDL at 24 hr calculated using parameter values from best fit of LDL transmurial profiles without experiments 4C6 and 24C1 (Figure 5-19) without (A) and with (B) endothelial cell metabolism. Parameter values are listed in Table 5-VIII (case D).

matrix is half as fast as binding ($m \approx 0.5$) resulting in the accumulation of bound solute. At long times most of the LDL is bound to the matrix and matrix-bound LDL accounts for 50% of the total tissue concentration at steady state.

Chapter 6

Conclusions and Recommendations

6.1 Conclusions

1. Kinetic models of receptor-mediated and receptor-independent LDL metabolism have been used to determine rate constants for LDL metabolism by cultured aortic smooth muscle cells. The model most consistent with data consists of a single intracellular compartment from which degradation and exocytosis occur.
2. Following coculture of smooth muscle cells with endothelial cells, LDL binding, internalization, and degradation by smooth muscle cells are increased. Kinetic analysis revealed that the number of receptors and the rate constant for receptor-independent metabolism are increased.
3. Stimulation of smooth muscle cell LDL metabolism by endothelial cells appears to be mediated by endothelial cell derived growth factors as well as by low molecular weight nonmitogenic factors which require cell-cell interactions in order to be active.
4. In vivo, ^{125}I -labeled LDL and mLDL transmural profiles in the rabbit aorta are similar at all times studied. The arterial wall degrades LDL and mLDL.
5. Calculations of the steady state tissue concentration and rate of degradation in response to a step change in plasma concentration indicate that receptor-mediated metabolism is important in the rabbit arterial wall in vivo.
6. Mass transfer coefficients for LDL and mLDL are not constant with time, but decrease with increasing circulation time.
7. Agreement between mathematical predictions and data for transmural profiles and cumulative degradation was obtained using metabolic rate constant from cell culture studies, transport parameters from 0.5 hr experiments, and time-varying mass transfer coefficients.
8. Degradation is the major mechanism for the removal of LDL from the

vessel wall and the receptor-mediated pathway accounts for about 60% of cumulative degradation. Binding to the extracellular matrix is important at long circulation times.

6.2 Recommendations

1. Experiments should be performed to determine the cause of the time-varying mass transfer coefficients.
2. In vitro and in vivo experiments should be performed to measure rate constants for binding to the extracellular matrix and the number of binding sites.
3. Cell culture studies should be initiated to further explore interactions between LDL and endothelial cells.
4. The in vivo studies in Chapter 4 should be extended to examine LDL metabolism in regions of high permeability to LDL.
5. Quantitative autoradiography should be used to determine transmural profiles of LDL degradation products using ^{125}I -labeled tyramine-cellobiose as a marker of degradation.
6. The in vivo studies should also be extended to examine LDL metabolism in the arterial wall under pathological conditions, such as hypercholesterolemia.

Appendix A

Estimation of Rate Constants for Receptor-Mediated LDL Metabolism from Published Data

A.1 LDL Binding at 4°C

At 4 °C internalization and degradation do not occur and LDL metabolism consists solely of reversible binding of LDL to its receptor. A material balance on receptor-bound LDL yields:

$$\frac{d[LR]}{dt} = k_1[L_o][R] - k_{-1}[LR] \quad (A-1)$$

where $[L_o]$ represents the initial ligand concentration which is essentially constant throughout the experiment. The total number of receptors per cell is constant and is equal to the amounts of free and ligand bound receptor on the cell:

$$[R_T] = [R] + [LR] \quad (A-2)$$

The solution to equations (A-1) and (A-2) for an initial ligand-receptor complex concentration of zero is:

$$[LR] = \frac{[R_T][L_o]}{K_d + [L_o]}(1 - e^{-kt}) \quad (A-3)$$

where $K_d = k_{-1}/k_1$ and $k = k_1[L_o] + k_{-1}$.

Pitas et al. [1979] have measured the kinetics of LDL binding to its receptor at 4 °C in order to determine k_1 and k_2 . The half-time of ligand binding to its receptor has been determined at several concentrations. From equation (A-3), the half-time is equal to :

$$\frac{\ln 2}{t_{1/2}} = k_1[L_o] + k_{-1} \quad (A-4)$$

A plot of $\frac{\ln 2}{t_{1/2}}$ is linear with slope k_1 and intercept k_{-1} . The rate constants determined by Pitas et al. [1979] are listed in row 1 of Table A-I.

Pitas et al. [1979] have separately measured dissociation of LDL from its receptor at 4 °C. In this experiment ^{125}I -LDL was allowed to bind to the receptor at 4 °C for 2 hr, after which the cells were washed to remove unbound ^{125}I -LDL. Fresh medium containing unlabeled LDL was added, and the dissociation of LDL from its receptor was measured. k_{-1} was then determined by linear regression of the logarithm of the amount bound vs. time and is presented in row 2 of Table A-I. The two values of k_{-1} are slightly different which may simple be due to experimental variability.

Goldstein et al. [1976] have also measured LDL binding to fibroblasts at 4 °C and Basu et al. [1978] have measured LDL binding to isolated fibroblast membranes at 4 °C (Figures A-1 and A-2, respectively). Only a single ligand concentration was used in these studies (10 $\mu\text{g}/\text{ml}$ in Goldstein et al. [1976], and 12.5 $\mu\text{g}/\text{ml}$ in Basu et al. [1978]). These data were fit to equation (A-3) by nonlinear regression using the known values of K_d (see Table A-2). The results are plotted in Figures A-1 and A-2, and the rate constants are listed in Table A-I.

The value of k_1 obtained by Pitas et al. [1979] is three times larger than the values estimated from the data of Goldstein et al. [1976] and Basu et al. [1978]. Estimates of k_{-1} also vary by a factor of three. Since all three studies were performed with human fibroblasts, the different estimates may reflect variations among the population. These results indicate that at 4 °C, dissociation is quite slow with a half-time of 100 to 385 min.

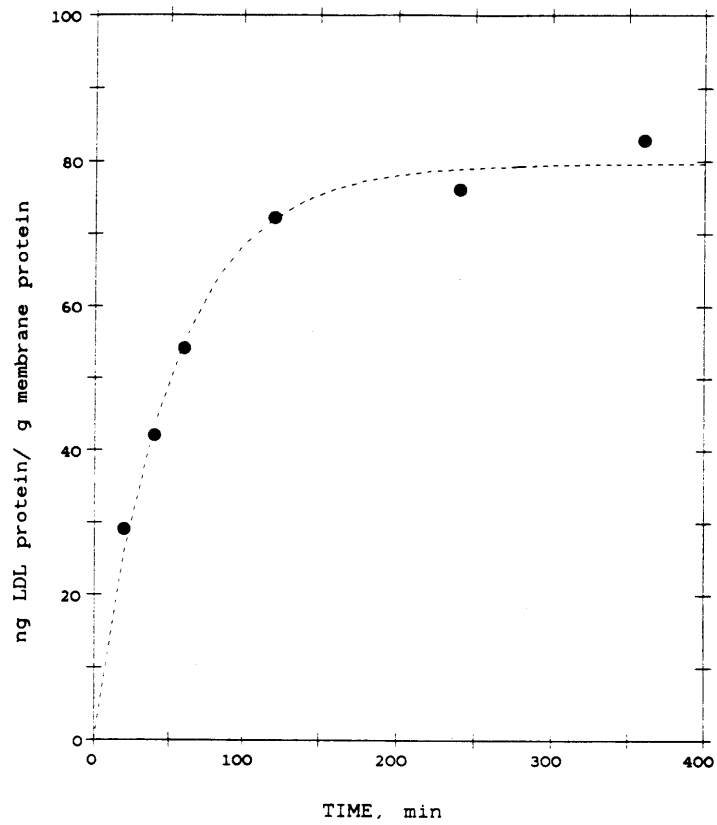


Figure A-1: Fitting data of Goldstein et al. [1976]

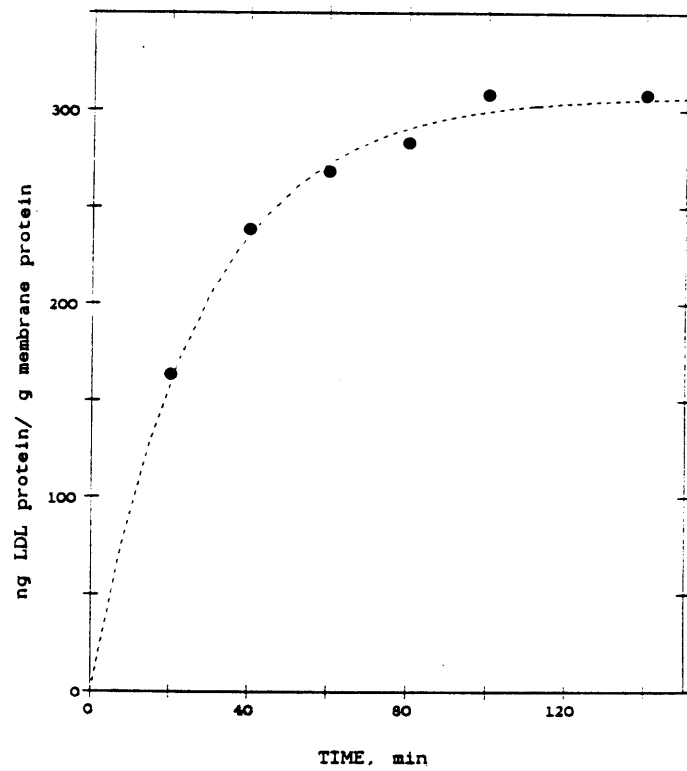


Figure A-2: Fitting data of Basu et al. [1978]

Table A-1: Rate Constants for LDL Binding to its Receptor at 4 °C

Lipoprotein	Cells	$k_1, M^{-1}min^{-1}$	k_{-1}, min^{-1}	Reference
human LDL	human fibroblasts	0.33×10^7	0.0038 0.0028	Pitas et al. [1979]
human LDL	human fibroblasts	0.09×10^7	0.0018	Goldstein et al. [1976]
human LDL	human fibroblast membranes	0.11×10^7	0.0069	Basu et al. [1978]

The equilibrium dissociation constant (K_d) at 4 °C measured by a variety of investigators has been compiled and is presented in Table A-2. Except for the value obtained by Aulinskas et al. [1981], estimates of the equilibrium constant for LDL-receptor binding on fibroblasts, smooth muscle cells, endothelial cells, and hepatocytes from human, rat, and rabbit are quite similar. Carcinoma cells, however, exhibit larger values of K_d , suggesting a reduced affinity for the receptor.

A.2 Receptor-Mediated LDL Metabolism at 37 °C

There are no published experimental studies concerned with the estimation of rate constants for LDL metabolism at 37 °C, although there is a considerable amount of data from which individual constants can be calculated. The available experiments are of three types: 1) binding, internalization, and degradation as a function of LDL concentration and time; 2) pulse-chase experiments in which cells are incubated with labeled LDL at 4 °C to allow LDL to bind to receptors (pulse), washed, incubated at 37 °C with unlabeled LDL, and the bound, internalized, and degraded are measured as a function of time (chase); and 3) pulse-chase experiments

Table A-II: Equilibrium Constants for LDL Binding at 4 °C

Lipoprotein	Cells	K_d , M x 10 ⁹	Reference
human LDL	human fibroblasts	2.8 ± 0.4	Pitas et al. [1979]
human LDL	human fibroblasts	2.0	Goldstein et al. [1976]
human LDL	human fibroblasts	6.0 ± 1.7	Basu et al. [1978]
human LDL	human fibroblasts	2.8	Innerarity et al. [1980]
human LDL	human fibroblasts	6.0	Lee et al. [1982]
human LDL	human fibroblasts	2.1	Witte et al. [1982]
human LDL	bovine embryonic SMC	32, 68	Aulinskas et al. [1981]
human LDL	human liver membranes	3.0	Kita et al. [1981]
human LDL	human endometrial carcinoma	40	Gal et al. [1982]
human LDL	human cervical carcinoma	72	Gal et al. [1982]
rat LDL	rat fibroblasts	2.9	Innerarity et al. [1980]
rat LDL	rat SMC	5.8	Innerarity et al. [1980]
rabbit LDL	rabbit aortic endothelial cells	2.0	Reckless et al. [1978]
rabbit LDL	rabbit liver membranes	2.8	Kita et al. [1981]

in which cells are incubated with labeled LDL at 37 °C (pulse), washed and incubated with heparin (to remove surface-bound LDL) at 4 °C, incubated at 37 °C with unlabeled LDL, and internalized and degraded LDL are measured (chase). The model represented by equations (2-21) to (2-23) was used to estimate rate constants for these various experiments.

Brown and Goldstein [1976] performed pulse-chase experiments (type 2 listed above) from which the rate constants for internalization (k_2) and degradation (k_3) were determined. In this experiment human fibroblasts were incubated with 10 $\mu\text{g/ml}$ ^{125}I -LDL for 2 hr at 4 °C to allow cells to bind to receptors. The cells were then washed to remove unbound ligand and incubated at 37 °C with medium containing 10 $\mu\text{g/ml}$ unlabeled LDL. Bound, internalized, and degraded LDL were measured at various times following warming to 37 °C (Figure 4 of Brown and Goldstein [1976]). Results are presented in Figure A-3. A material balance at each time indicates that negligible amounts of ^{125}I -LDL appear in the extracellular at 37°C. Thus, dissociation from the receptors and exocytosis are unimportant in this experiment. For this experiment equations (2-21) to (2-23) reduce to (k_{-1} and k_5 equal to zero):

$$\frac{d[LR]}{dt} = -k_2[LR] \quad (\text{A-5})$$

$$\frac{d[L_{Ri}]}{dt} = k_2[LR] - k_3[L_{Ri}] \quad (\text{A-6})$$

$$\frac{d[L_{Rd}]}{dt} = k_3[L_{Ri}] \quad (\text{A-7})$$

At the start of the chase period the surface bound ligand concentration was $[LR_0]$, some ligand was intracellular with concentration $[L_{Ri}]$ (3.6 ng/mg), and the amount degraded was zero. (The presence of intracellular LDL at 4 °C is perplexing. This

may be an artifact of the technique used to measure internalized LDL - dissolution of cells in 0.1 N NaOH. Nevertheless, this quantity of intracellular LDL was included in the model.) These equations are linear with the following solutions:

$$[LR] = [LR]_0 e^{-k_2 t} \quad (A-8)$$

$$[L_{Ri}] = [LR]_0 \frac{k_2}{k_2 - k_3} (e^{-k_3 t} - e^{-k_2 t}) + [L_{Ri}]_0 e^{-k_3 t} \quad (A-9)$$

$$[L_{Rd}] = [LR]_0 \frac{k_2 k_3}{k_2 - k_3} \left(\frac{1 - e^{-k_3 t}}{k_3} - \frac{1 - e^{-k_2 t}}{k_2} \right) + [L_{Ri}]_0 (1 - e^{-k_3 t}) \quad (A-10)$$

In order to fit equations (A-8)-(A-10) to the results of Brown and Goldstein [1976], internalization of receptor-bound LDL was assumed to be complete after 2 hr and any residual surface-bound ^{125}I -LDL represents nonspecific binding. ^{125}I -LDL bound at 2 hr (1.6 ng/mg) was subtracted from the amount bound at all other times.

Equations (A-8)-(A-10) were fit to the multiresponse data of Brown and Goldstein [1976] by minimization of the determinant of the \mathbf{F} matrix (equation (2-41)). Data and fits are presented in Figure A-3. k_2 is equal to $0.20 \pm 0.02 \text{ min}^{-1}$ and k_3 is equal to $0.015 \pm 0.002 \text{ min}^{-1}$. In a similar set of experiments reported in Goldstein et al. [1977] in which only surface-bound LDL was measured during the chase period, k_2 is $0.25 \pm 0.02 \text{ min}^{-1}$ for normal human fibroblasts; for fibroblasts from patients heterozygous with familial hypercholesterolemia, a substantial fraction of receptor-bound LDL remains on the cell surface and is not internalized, but for LDL which is internalized, k_2 is 0.19 min^{-1} for JLD's cells and 0.21 min^{-1} for AD's cells (Figure A-4) (Goldstein et al. [1977]).

Estimates of k_{-1} were obtained from pulse chase experiments of Brown and

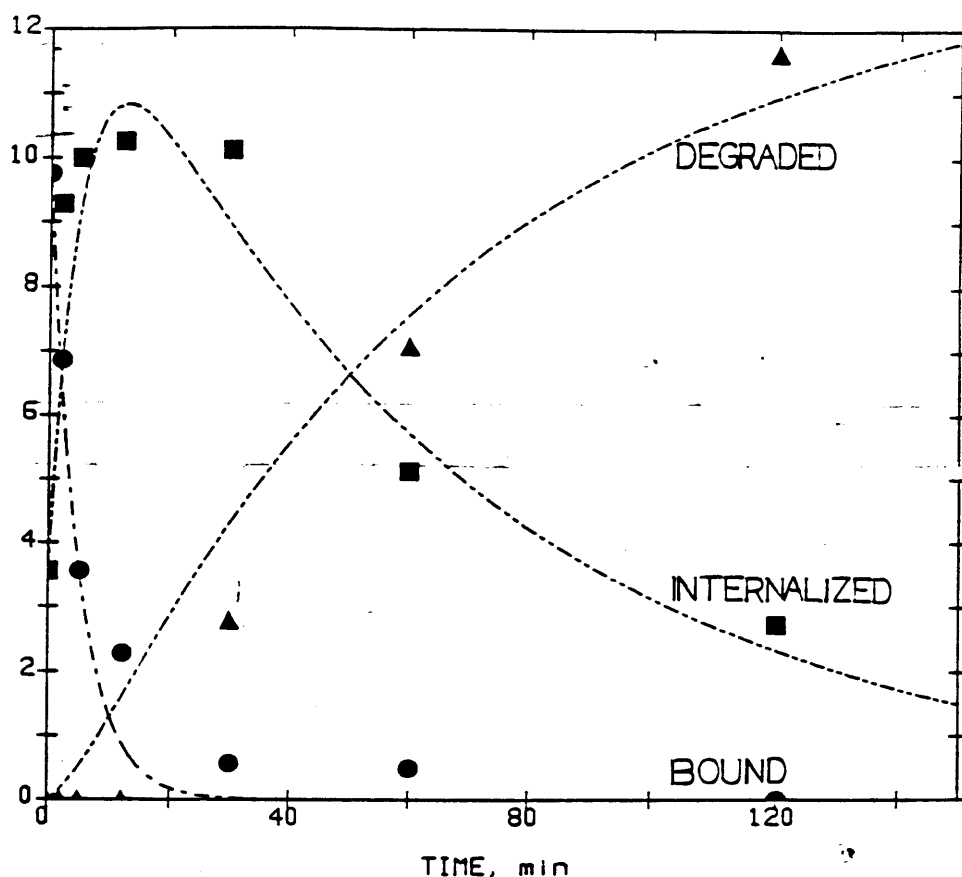


Figure A-3: Fitting Pulse-Chase Results of Brown and Goldstein [1976]

Goldstein [1976] and Goldstein et al. [1977] performed pulse-chase experiments with fibroblasts from a patient homozygous for familial hypercholesterolemia in which binding is normal, but internalization does not occur (patient JD). Semilogarithmic plots of the fraction of LDL bound during 37 °C chase period are presented in Figure A-5 and estimates of k_{-1} are $0.0076 \pm 0.0003 \text{ min}^{-1}$ for results of Brown and Goldstein [1976] and $0.0153 \pm 0.0006 \text{ min}^{-1}$ for results of Goldstein et al. [1977]. The variability in the estimates may simply reflect normal experimental variability or an effect of subculturing since cells are from the same patient.

Aulinskas et al. [1981] performed slightly different pulse-chase experiments than Brown and Goldstein [1976] in order to study exocytosis (type 3 listed above). Bovine smooth muscle cells were incubated with $40 \text{ } \mu\text{g/ml}$ ^{125}I -LDL for 4 hr at 37

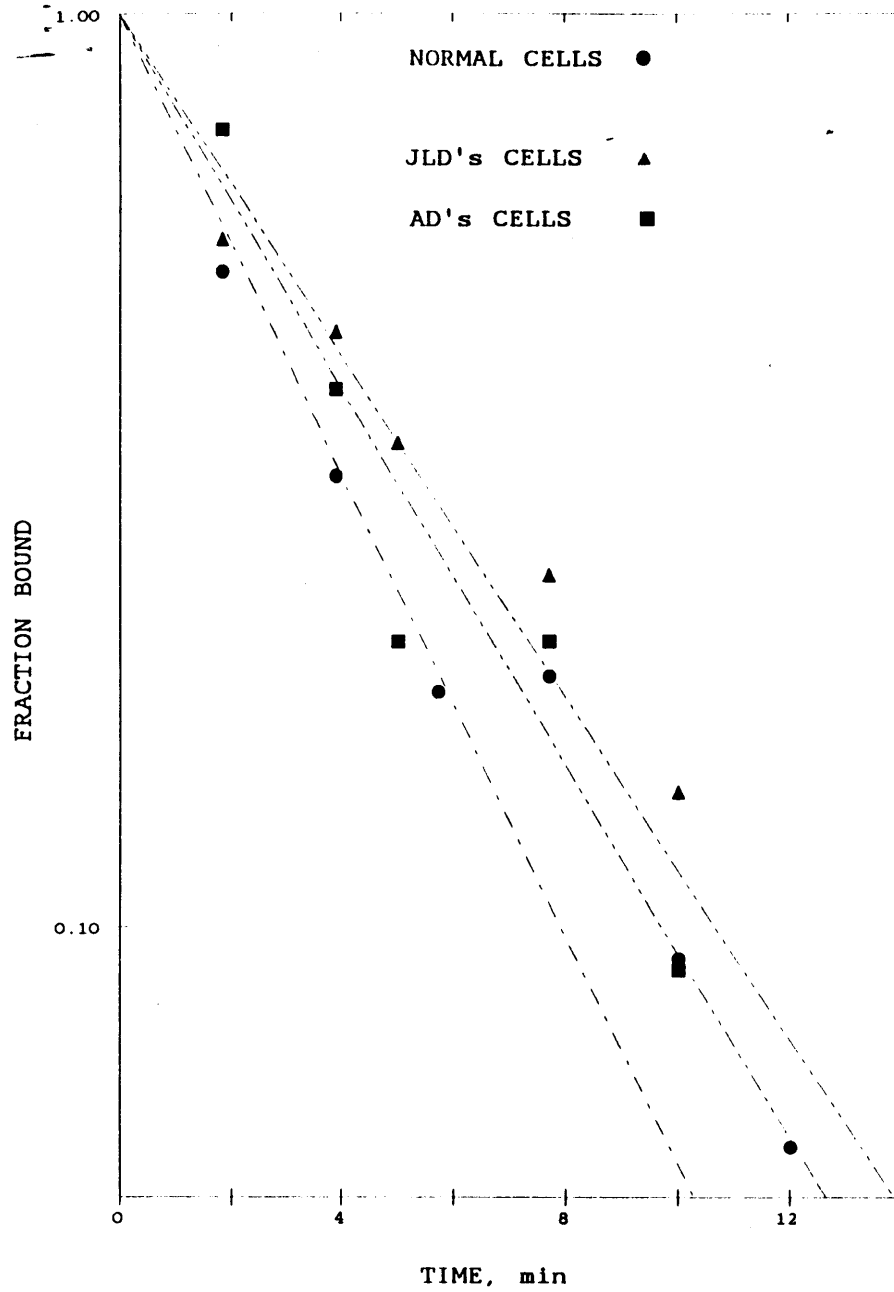


Figure A-4: LDL internalization in normal human fibroblasts and fibroblasts from patients heterozygous for familial hypercholesterolemia.

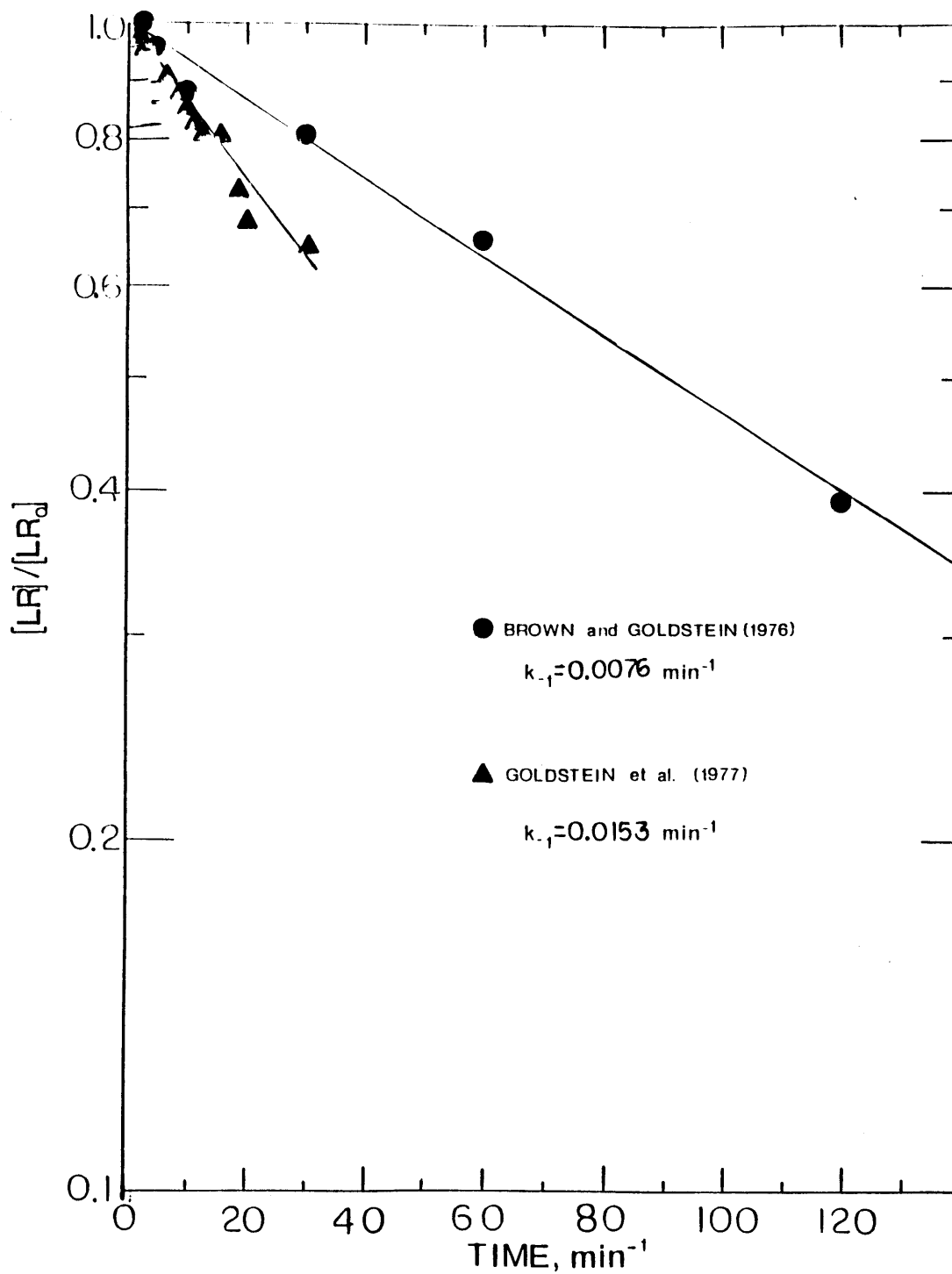


Figure A-5: Semilogarithmic plot of the decrease in the fraction of LDL bound to the cell surface of fibroblasts from patient JD, homozygous for familial hypercholesterolemia.

°C. The cells were then washed at 4 °C to remove nonspecifically bound LDL and were incubated with heparin to remove receptor-bound LDL on the cell surface. The cells, containing only intracellular ^{125}I -LDL, were then incubated at 37 °C. Cell associated, degraded, and medium LDL were measured at various times. This is the same type of experiment discussed in Section 2.5.4. This experiment differs from the experiment of Brown and Goldstein [1976] in two important respects: one, the pulse incubation is at 37 °C, and two, receptor-bound LDL is removed prior to the chase period.

For this type of experiment, the material balances reduce to:

$$\frac{d[L_{Ri}]}{dt} = -(k_3 + k_5)[L_{Ri}] \quad (\text{A-11})$$

$$\frac{d[L_{Rd}]}{dt} = k_3[L_{Ri}] \quad (\text{A-12})$$

Initially, the intracellular concentration is $[L_{Rio}]$ and all other concentrations are zero. The solutions are:

$$[L_{Ri}] = [L_{Rio}]e^{-(k_3 + k_5)t} \quad (\text{A-13})$$

$$[L_{Rd}] = \frac{[L_{Rio}]k_3}{k_3 + k_5} \left(1 - e^{-(k_3 + k_5)t}\right) \quad (\text{A-14})$$

Equations (A-13) and (A-14) were fit to the data of Aulinskas et al. [1981] by minimization of the determinant of the matrix \mathbf{F} (equation (2-41)) and the results are presented in Figure A-6. k_3 is equal to $0.007 \pm 0.001 \text{ min}^{-1}$ and k_5 is equal to $0.0022 \pm 0.0006 \text{ min}^{-1}$.

The association constant for LDL binding to human skin fibroblasts was estimated from the short-time kinetic data of Figure 6 of Goldstein et al. [1976]. Cells were incubated with $10 \mu\text{g/ml}$ ^{125}I -LDL for times ranging from 0.5 min to 30

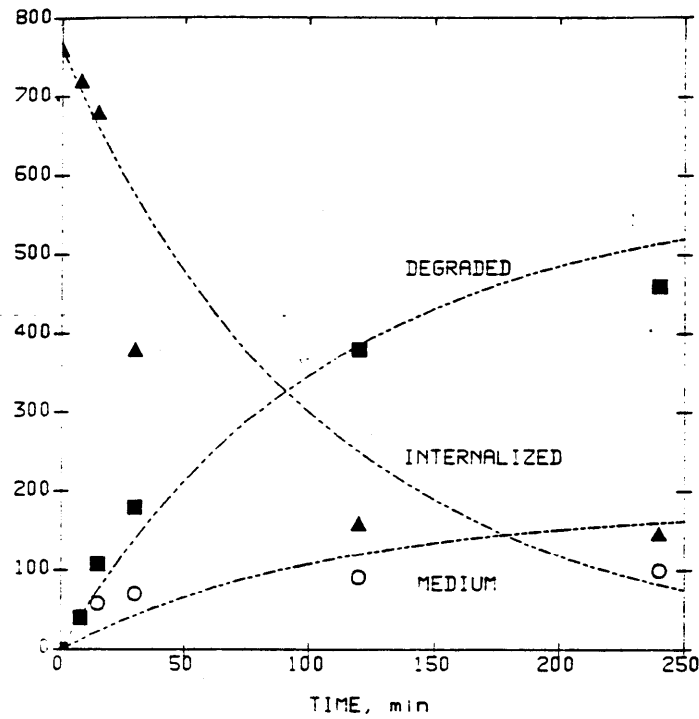


Figure A-6: Pulse-chase experiments of Aulinskas et al. [1981]. Smooth curves represent best fit of equations (A-13) and (A-14) to data.

min. During this time there is little degradation. Material balances for bound and internalized LDL yield:

$$\frac{d[LR]}{dt} = k_1[L_o][R_T] - k[LR] \quad (A-15)$$

$$\frac{d[L_{Ri}]}{dt} = k_2[LR] \quad (A-16)$$

where $k = k_1[L_o] + k_{-1} + k_2$.

The solutions to equations (A-15) and (A-16) are:

$$[LR] = \frac{[L_o][R_T]}{K_{int} + [L_o]}(1 - e^{-kt}) \quad (A-17)$$

$$[L_{Ri}] = \frac{k_2[L_o][R_T]}{K_{int} + [L_o]} t - \frac{1 - e^{-kt}}{k} \quad (A-18)$$

Table A-III: Rate Constants Estimated from Published Data

$k_1, M^{-1} \text{ min}^{-1} \times 10^{-7}$	$k_{-1}, \text{ min}^{-1}$	$k_2, \text{ min}^{-1}$	$k_3, \text{ min}^{-1}$	$k_5, \text{ min}^{-1}$	Cell Type	Growth State	LDL	Reference
0.50 ± 0.17		0.25 ± 0.07	0.0057 ± 0.0006	0.0082 ± 0.0047	Bovine Aortic Smooth Muscle	Quiescent, Subconfluent	Human	This Study
		0.20 ± 0.02	0.015 ± 0.002		Human Skin Fibroblasts	Growing, Subconfluent	Human	Brown and Goldstein [1976]
		0.015 ± 0.001			Human Skin Fibroblasts	Growing, Subconfluent	Human	Goldstein et al. [1977]
		0.008 ± 0.001			Human Skin Fibroblasts	Growing, Subconfluent	Human	Brown and Goldstein [1976]
			0.25 ± 0.02			Human Skin Fibroblasts	Growing, Subconfluent	Human
1.7 ± 0.5		0.20 ± 0.02			Human Skin Fibroblasts	Growing, Subconfluent	Human	Goldstein et al. [1976]
			0.007 ± 0.001	0.0020 ± 0.0006	Bovine Aortic Smooth Muscle	Confluent	Human	Aulinkas et al. [1981]
0.26 ± 0.04		0.10 ± 0.02	0.013 ± 0.001		Bovine Heart Endothelial Cells	Growing, Subconfluent	Human	Vlodavsky et al. [1978]
0.68 ± 0.09		0.25 (fixed)	0.011 ± 0.001	0.026 ± 0.003				
0.24 ± 0.05		0.02 ± 0.01	0.0022 ± 0.0005	0.0048 ± 0.0015	Rabbit Aortic Endothelial Cells	Growing, Subconfluent	Rabbit	Reckless et al. [1978]
0.40 ± 0.07		0.05 ± 0.01	0.0071 ± 0.0009		Monkey Aortic Smooth Muscle	Confluent	Monkey	Eisele et al. [1980]

Equations (A-17) and (A-18) were fit to data in Figure 6 of Goldstein et al. [1976] by minimization of the the determinant of the meatrix \mathbf{F} . The results are presented in Figure A-7 for $k_1 = 1.7 \pm 0.5 \times 10^7 \text{ M}^{-1} \text{ min}^{-1}$ and $k_2 = 0.20 \pm 0.02 \text{ min}^{-1}$.

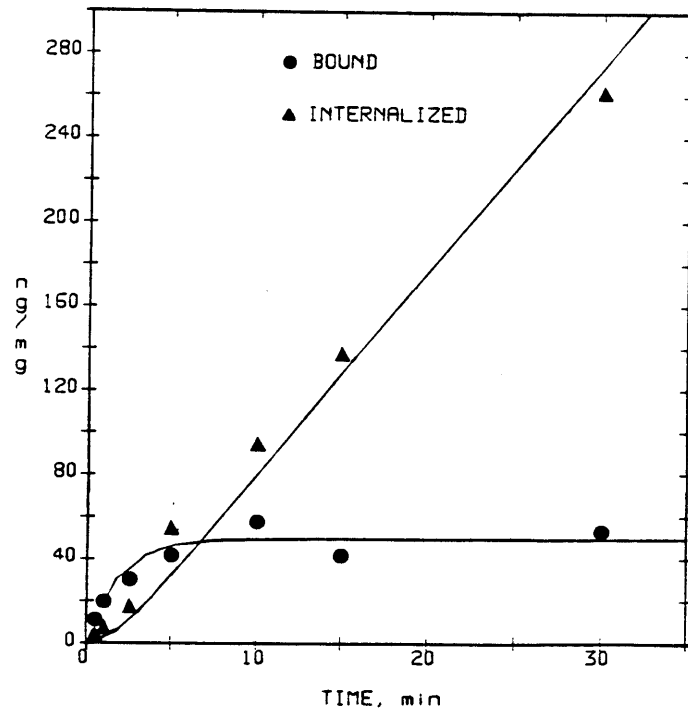


Figure A-7: Short-Time Kinetics of Binding and Internalization (from Goldstein et al. [1976]).

Published data are available for LDL metabolism as a function of concentration and time by rabbit aortic endothelial cells (Reckless et al. [1978]), bovine aortic endothelial cells (Vlodavsky et al. [1978]), and monkey aortic smooth muscle cells (Eisele et al. [1980]). k_1 , k_2 , k_3 , and k_5 were determined by fitting equations (2-24) to (2-26) by minimization of the determinant of the matrix \mathbf{F} . The fits are presented in Figures A-8 to A-10 and the rate constants are listed in Table A-III. Fits of the data of Reckless et al. [1978] (Figure A-9) and Eisele et al. [1980] (Figure A-10) are quite good, whereas the fits of binding and internalization as

functions of time for the data of Vlodavsky et al. [1978] show a systematic error between model fits and data. Including exocytosis (i.e. k_5) in the model did not improve the fit, and the resulting value of k_5 was not different from zero. The estimated value for receptor-mediated endocytosis is quite low ($k_2 = 0.10 \text{ min}^{-1}$). Fixing k_2 at the value obtained in this study (0.25 min^{-1}) improved the fit for internalization as a function of time, but had no effect upon binding (dashed curve in Figure A-9). For k_2 fixed at 0.25 min^{-1} , k_1 increases, k_3 decrease, and k_5 is nonzero ($0.026 \pm 0.003 \text{ min}^{-1}$).

Rate constants estimated from published data are presented in Table A-III. The range of values of k_1 and k_3 are similar to those which have been obtained with bovine smooth muscle cells (see Table 2-III). The internalization rate constant (k_2) in bovine and aortic endothelial cells and monkey smooth muscle cells are significantly less than those in human skin fibroblasts and bovine smooth muscle cells. These results suggest that internalization may be slower in endothelial cells and monkey smooth muscle cells than in other cell types. In the experiments of Brown and Goldstein [1976] (row 2), Vlodavsky et al. [1978] (row 8), and Eisele et al. [1980] (row 10) data could be fit without including exocytosis. Inclusion of exocytosis in the model generally led to poorer fits. From the results presented in Chapter 2, the value of k_5 is close to estimated values of k_3 , indicating that if exocytosis were occurring, then it would have a significant effect upon the temporal behavior of internalized and degraded LDL.

$K_{\text{int}} = (k_1 + k_2)/k_5$, the ratio of rate constants for internalization and dissociation receptor to receptor-ligand binding, can be determined from the binding isotherm at 37°C and is widely reported in the literature. Values of K_{int} from a number of studies are summarized in Table A-IV. K_{int} for human fibroblasts ranges from 12.4 to $46.4 \times 10^{-9} \text{ M}$. This range is similar to that obtained with bovine

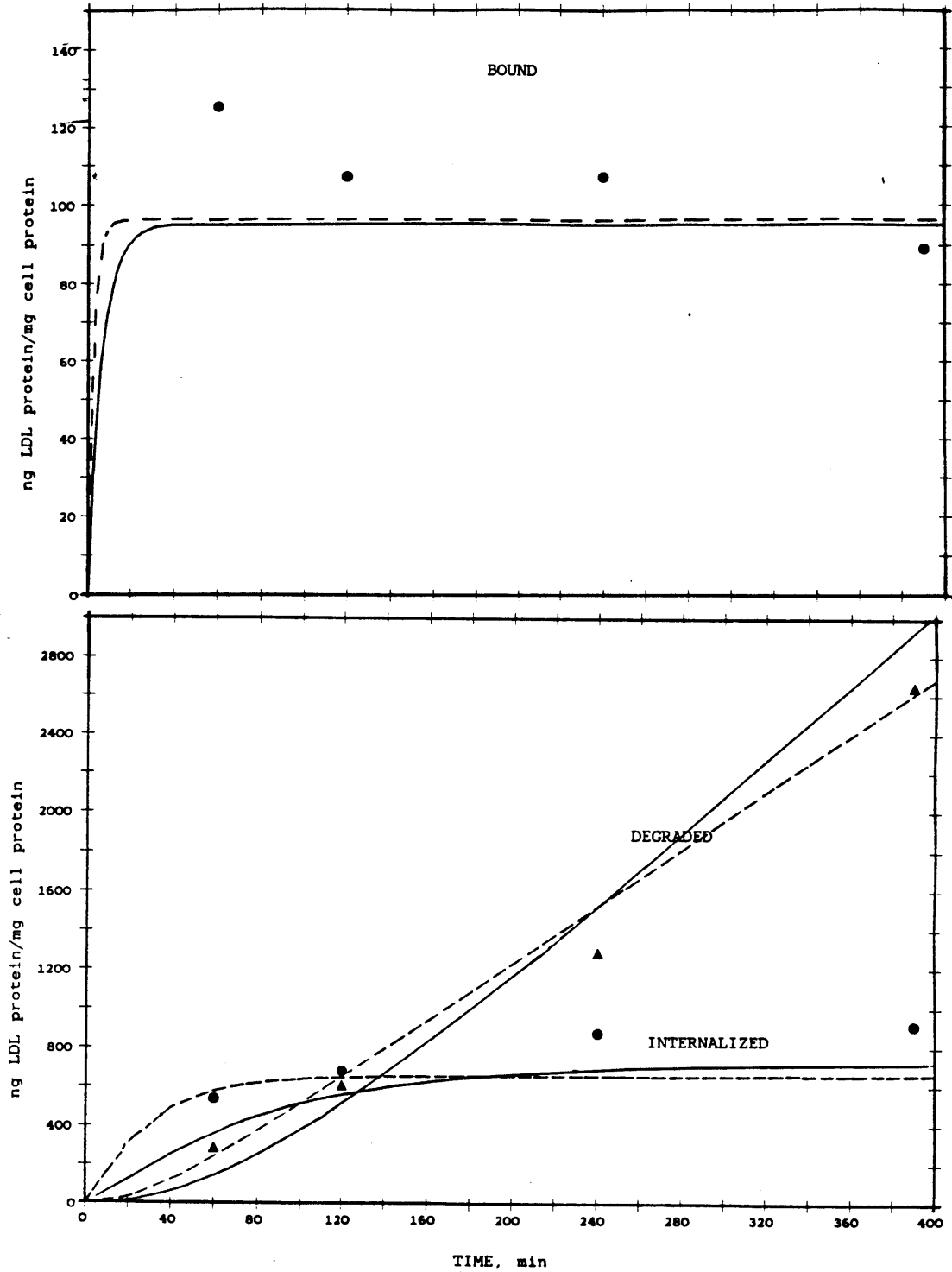


Figure A-8: Fitting Data of Vlodavsky et al. [1978]. Cells were incubated with $10 \mu\text{g/ml}$ ^{125}I -LDL. Solid curves represent best fits for $k_5 = 0$.

Dashed curves represent best fits for a fixed value of $k_2 = 0.25 \text{ min}^{-1}$.

Rate constants are listed in Table A-III.

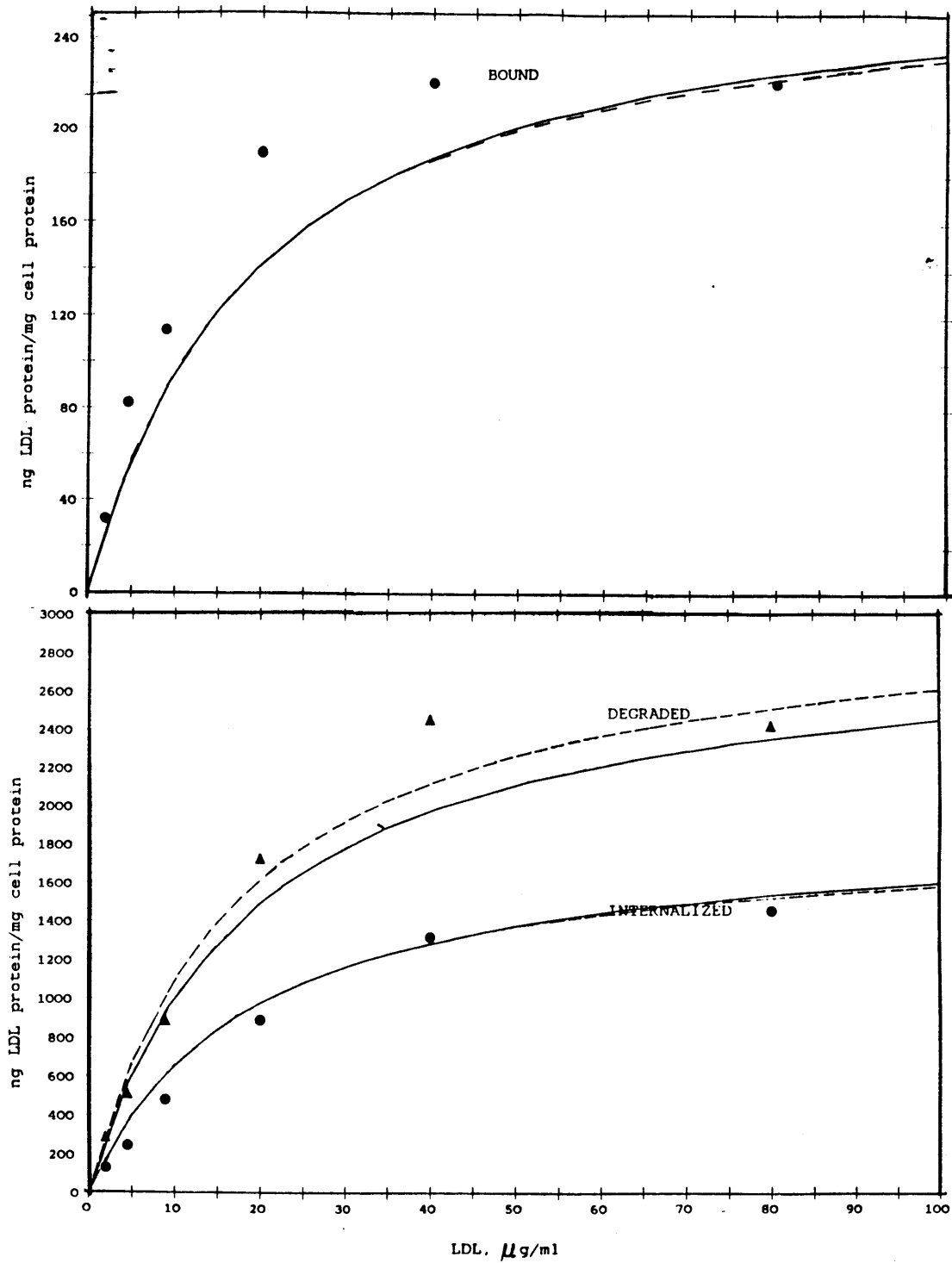


Figure A-8 (cont.) Fitting Data of Vlodavsky et al. [1978]. Binding, internalization, and degradation were measured after a 3 hr incubation.

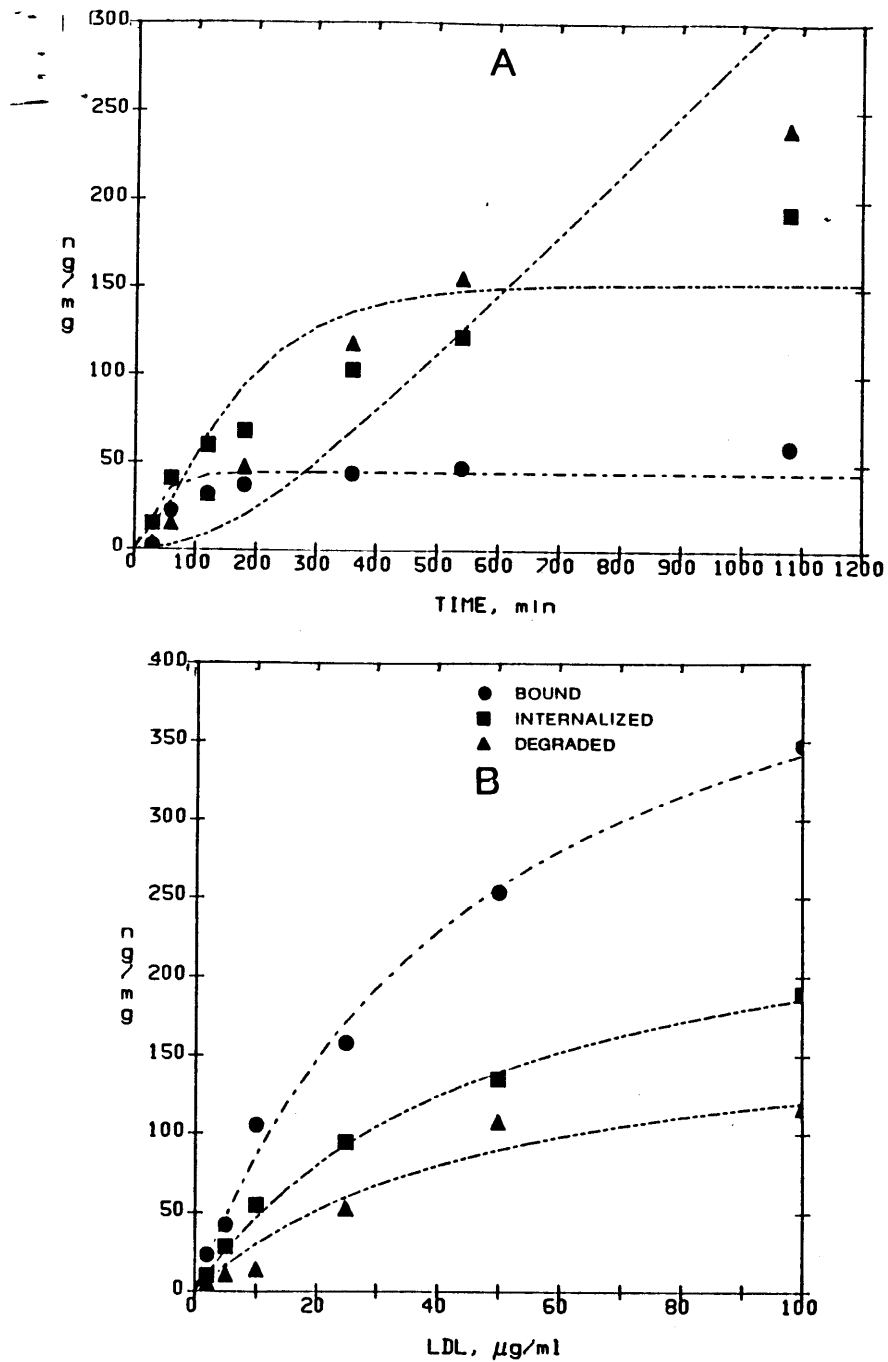


Figure A-9: Fitting Data of Reckless et al. [1978]. Binding, internalization, and degradation were measured as a function of time with 10 $\mu\text{g}/\text{ml}$ ^{125}I -LDL (A), and as a function of concentration at 3 hr (B).

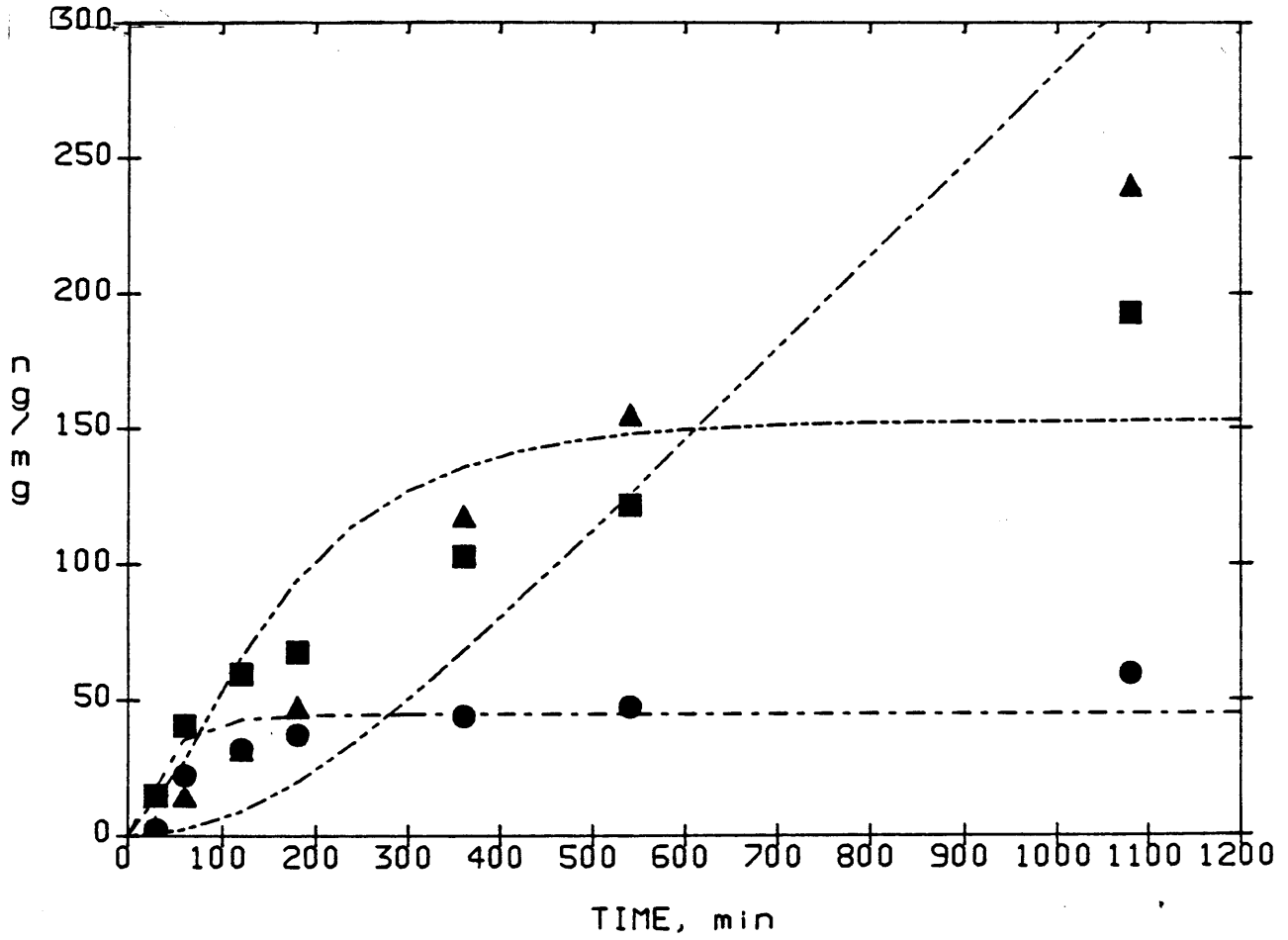


Figure A-10: Fitting Data of Eisele et al. [1980]. Binding, internalization, and degradation were measured following incubation with $10 \mu\text{g/ml}$ ^{125}I -LDL. K_{int} was measured separately (Table A-IV).

smooth muscle cells. Values of K_{int} for rabbit and monkey smooth muscle cells and bovine endothelial cells also fall within this range, whereas K_{int} for human and bovine endothelial cells fall outside this range.

Table A-IV: K_{int} at 37 °C

LDL	Cells	$K_{int}, M \times 10^9$	Reference
human	HSF*	22	Brown and Goldstein [1976]
human	HSF	12.4 ± 3.4	Goldstein et al. [1976] ¹
human	HSF	31.4 ± 9.9	Goldstein et al. [1976] ²
human	HSF	27	Lee et al. [1982]
human	HSF	14	Chait et al. [1979]
human	HSF	46.4	Drevon et al. [1981]
monkey	monkey SMC ⁺	13	Eisele et al. [1980]
human	human EC [#]	7.9 ± 0.9	van Hinsbergh et al. [1983]
rabbit	rabbit SMC	44 ± 4	Reckless et al. [1979]
rabbit	rabbit EC	99 ± 4	Reckless et al. [1978]
human	bovine EC	31 ± 13	Vlodavsky et al. [1978]
human	bovine SMC	50 ± 10	This Study

* HF: human fibroblasts

+ SMC: smooth muscle

EC: endothelial cells

¹ from equilibrium binding isotherm of Goldstein et al. [1976]

² from kinetic data (Figure A-6) of Goldstein and Brown [1976]

Appendix B

Minimization Criterion for Multiple Response Data

B.1 Derivation of Minimization Criterion

Parameter estimation of cell culture data requires simultaneous regression of responses for bound, internalized, and degraded ligand. Weighted least squares (equation (2-40)) is valid only when the variance-covariance matrix is known. Box and Draper [1965] have developed a generalized criterion (equation (2-41)). An expanded form of their derivation is presented below.

Let y_{ir} represent the i th observation ($i=1,\dots,m$) of the r th response ($r=1,\dots,n$). y_{ir} can be modeled as:

$$y_{ir} = f_r(\mathbf{b}, \mathbf{x}_i) + e_{ir} \quad (B-1)$$

where $f_r(\mathbf{b}, \mathbf{x}_i)$ is the model prediction for the r th response, \mathbf{x}_i is the vector of independent variables at the i th observation, \mathbf{b} is the parameter vector (elements β_k), and e_{ir} is the corresponding error or residual vector. The errors are normally distributed with mean of zero and covariance of σ_{st} , where s and t represent different responses. The variance-covariance matrix, \mathbf{S} of the n responses during the i th observation is:

$$\mathbf{S} = \begin{bmatrix} \sigma_{11} & \sigma_{12} \cdots & \sigma_{1n} \\ \sigma_{21} & \sigma_{22} \cdots & \sigma_{2n} \\ \sigma_{n1} & \sigma_{n2} \cdots & \sigma_{nn} \end{bmatrix} = \{\sigma_{st}\} \quad (B-2)$$

where the diagonal elements, σ_{ss} are the variances and the off-diagonal terms are

the covariances. The variance-covariance matrix is symmetric (i.e. $\sigma_{st} = \sigma_{ts}$). The elements of the inverse of the variance-covariance matrix, \mathbf{S}^{-1} , are represented as σ^{st} .

The distribution of the responses can be expressed as a probability density function, $p(\mathbf{Y}|\mathbf{b}, \sigma^{st})$, which represents the probability that the vector of responses assumes a certain value for known parameter vector and variance-covariance matrix. For the case in which the parameter vector and variance-covariance matrix are not known *a priori* and the response vector has been determined, one wishes to calculate $p(\mathbf{b}|\mathbf{Y})$ which is related to $p(\mathbf{Y}|\mathbf{b}, \sigma^{st})$ by Bayes' theorem.

Each response is multivariate normal and the joint probability density function of the vector of all responses, \mathbf{y} , is (Box and Draper [1965]):

$$p(\mathbf{y}|\mathbf{b}, \sigma^{st}) = (2\pi)^{-mn/2} \det(\mathbf{S}^{-1})^{m/2} \exp\left(-\frac{1}{2} \sum_{s=1}^n \sum_{t=1}^n \sigma^{st} \phi_{st}\right) \quad (B-3)$$

where

$$\phi_{st} = \sum_{i=1}^m (y_{is} - f_s(\mathbf{b}, x_{is}))(y_{it} - f_t(\mathbf{b}, x_{it})) = \sum_{i=1}^m e_{is} e_{it} \quad (B-4)$$

represents the sums of squares and sums of products of the errors. ϕ_{st} are elements of the matrix \mathbf{F} defined in equation (2-41).

The parameter vector \mathbf{b} is estimated for known values of the vector \mathbf{y} . If the variance-covariance matrix is known, then \mathbf{b} can be determined from equation (B-3) by the method of maximum likelihood (Himmelblau [1970], p. 146). Generally, this is not the case and \mathbf{S} is unknown. Box and Draper [1965] have applied Bayes' Theorem (Himmelblau [1970], pp. 397, 398) to obtain $p(\mathbf{b}|\mathbf{y})$, the posterior density function. From Bayes' theorem the posterior density function is:

$$\underline{p}(\mathbf{b}|\mathbf{y}) = \int_{\text{all } \sigma^{st}} p(\mathbf{y}|\mathbf{b}, \sigma^{st}) p(\mathbf{b}, \sigma^{st}) d\sigma^{st} \quad (B-5)$$

where $p(\mathbf{b}|\sigma^{st})$ is the prior density function and represents the expected behavior of the parameter vector and variance-covariance matrix. If observations for data sets i and j are made separately, and the observations in one data set do not depend upon observations in another data set, then the observations are considered to be independent. For independent observations (Box and Draper [1965]):

$$p(\mathbf{b}, \sigma^{st}) = p(\mathbf{b}) p(\sigma^{st}) \quad (B-6)$$

Box and Draper [1965] have determined that $p(\mathbf{b})$ is approximately constant and $p(\sigma^{st})$ is equal to $\mathbf{S}^{-1(n+1)/2}$. Thus, equation (B-5) becomes:

$$p(\mathbf{b}|\mathbf{y}) = C_1 \int_{\text{all } \sigma^{st}} (2\pi)^{mn/2} \det(\mathbf{S}^{-1})^{-(m-n-1)/2} \exp\left(-\frac{1}{2} \sum_{s=1}^n \sum_{t=1}^n \sigma^{st} \phi_{st}\right) d\sigma^{st} \quad (B-7)$$

where C_1 is equal to $p(\mathbf{b})$.

The integral in equation (B-7) is the same as that used to obtain the moments of the Wishart distribution, the multivariate generalization of the χ^2 distribution (Chatfield and Collins [1980]). $p(\mathbf{b}|\mathbf{Y})$ is calculated from the first moment of the Wishart distribution (Wilks [1962]):

$$p(\mathbf{b}|\mathbf{y}) = C_1 C_2 \det(\mathbf{F})^{-n/2} \quad (B-8)$$

where C_2 is a normalizing constant. Equation (B-8) states that the posterior density function ($p(\mathbf{b}|\mathbf{y})$) is maximized when the determinant of \mathbf{F} is minimized. Also, \mathbf{F} is the Bayesian estimate of \mathbf{S} .

B.2 Numerical Determination of the Parameter Estimates

Minimization of equation (2-41) is computationally difficult (Jutan [1976]). Jutan [1976] describes an iterative procedure in which the variance-covariance matrix is calculated for an initial value of the parameter vector, (\mathbf{b}_0), and the parameter vector is revised by calculating a correction vector using the estimated variance-covariance matrix. The variance-covariance matrix is estimated from equation (B-4) for \mathbf{b}_0 . The correction vector is determined from the minimum of the likelihood with respect to \mathbf{b} for a fixed variance-covariance matrix.

The likelihood function is the integrand in equation (B-5) for σ^{st} calculated from an estimate of \mathbf{b} , (\mathbf{b}_0):

$$L(\mathbf{b}, \sigma^{st} | \mathbf{y}) = p(\mathbf{y} | \mathbf{b}, \sigma^{st}) p(\mathbf{b}, \sigma^{st}) \quad (B-9)$$

$$L(\mathbf{b}, \sigma^{st} | \mathbf{y}) = (2\pi)^{-mn/2} \det(\mathbf{S}^{-1})^{(m-n-1)/2} \exp\left(-\frac{1}{2} \sum_{s=1}^n \sum_{t=1}^n \sigma^{st} \phi_{st}\right) \quad (B-10)$$

Both \mathbf{S} and σ^{st} depend on the prior estimate of \mathbf{b} , \mathbf{b}_0 (i.e. $\mathbf{S} = \mathbf{S}(\mathbf{b}_0)$ and $\sigma^{st} = \sigma^{st}(\mathbf{b}_0)$). Generally, it is more convenient to work with the logarithm of the likelihood function:

$$\ln[L(\mathbf{b}, \sigma^{st} | \mathbf{y})] = -\frac{mn}{2} \ln(2\pi) - \frac{m-n-1}{2} \ln \det(\mathbf{S}^{-1}) - \frac{1}{2} \sum_{s=1}^n \sum_{t=1}^n \sigma^{st} \phi_{st} \quad (B-11)$$

Taking the derivative of equation (B-11) with respect to the parameters (β_k) yields:

$$\frac{\partial \ln L}{\partial \beta_k} = -\frac{1}{2} \sum_{s=1}^n \sum_{t=1}^n \sigma^{st} \frac{\partial \phi_{st}}{\partial \beta_k} \quad (B-12)$$

From the definition of ϕ_{st} , equation (B-4), the derivative on the right hand side of equation (B-12) is:

$$\frac{\partial \phi_{st}}{\partial \beta_k} = \sum_{i=1}^m \frac{\partial f_s}{\partial \beta_k} [y_{it} - f_t(x_{it}, \beta_k)] - \sum_{i=1}^m \frac{\partial f_t}{\partial \beta_k} [y_{is} - f_s(x_{is}, \beta_k)] \quad (B-13)$$

Substituting equation (B-13) into equation (B-12) yields:

$$\begin{aligned} \frac{\partial \ln L}{\partial \beta_k} &= \frac{1}{2} \sum_{s=1}^n \sum_{t=1}^n \sum_{i=1}^m \sigma^{st} \frac{\partial f_s}{\partial \beta_k} [y_{it} - f_t(x_{it}, \beta_k)] \\ &+ \frac{1}{2} \sum_{s=1}^n \sum_{t=1}^n \sum_{i=1}^m \sigma^{st} \frac{\partial f_t}{\partial \beta_k} [y_{is} - f_s(x_{is}, \beta_k)] \end{aligned} \quad (B-14)$$

Since σ^{st} is symmetric, the two terms on the right hand side of (B-13) are identical. Adding them together and setting the derivative of the likelihood to zero, the minimum of the likelihood with respect to the β_k is:

$$\sum_{s=1}^n \sum_{t=1}^n \sum_{i=1}^m \sigma^{st} \frac{\partial f_s}{\partial \beta_k} [y_{it} - f_t(x_{it}, \beta_k)] = 0 \quad (B-15)$$

or, in terms of residuals:

$$\sum_{s=1}^n \sum_{t=1}^n \sum_{i=1}^m \sigma^{st} \frac{\partial e_{is}}{\partial \beta_k} e_{it} = 0 \quad (B-16)$$

Equation (B-16) is a generalization of the normal equations for least squares regression and minimizing equation (B-16) is equivalent to minimizing (Draper and Smith [1981], p. 461):

$$\sum_{s=1}^n \sum_{t=1}^n \sum_{i=1}^m \sigma^{st} (y_{is} - f_s(\mathbf{b}, x_{is}))(y_{it} - f_t(\mathbf{b}, x_{it})) = \sum_{i=1}^m e_{is} e_{it} \quad (B-17)$$

Equation (B-17) formally resembles the generalization of least squares developed by Aitken (Box and Draper [1965], Hunter [1966]), except that σ^{st} is updated with each additional guess.

B.3 Example

As an example of the advantages associated with simultaneous regression of multiple response data, consider the following sequential reaction (Box and Draper [1965]):



Material balances on species A, B, and C yield:

$$\frac{d[A]}{dt} = -k_1[A] \quad (B-19a)$$

$$\frac{d[B]}{dt} = k_1[A] - k_2[B] \quad (B-19b)$$

$$\frac{d[C]}{dt} = k_2[B] \quad (B-19c)$$

Initially, $[A] = 1$, and $[B] = [C] = 0$ for which equations (B-19a,b,c) have the following solutions:

$$[A] = e^{-k_1 t} \quad (B-20a)$$

$$[B] = \frac{k_1}{k_1 - k_2} (e^{-k_2 t} - e^{-k_1 t}) \quad (B-20b)$$

$$[C] = 1 - \frac{1}{k_1 - k_2} (k_1 e^{-k_2 t} - k_2 e^{-k_1 t}) \quad (B-20c)$$

In order to determine the two rate constants the following experiment was performed. Reactant A at a concentration of 1 (arbitrary units) was placed in 12 tubes which were sealed and heated to temperature T. At six different times two tubes were cooled and the concentrations of A, B, C were measured. The resulting measurements which were obtained are listed in Table B-I (data from Box and Draper [1965]). The rate constants k_1 and k_2 were determined by fitting all three responses and responses B and C by minimization of the determinant of the matrix

Table B-I: Data for Example

time, min	[A]	[B]	[C]
0.5	0.959	0.025	0.028
0.5	0.914	0.061	0.000
1.0	0.855	0.152	0.068
1.0	0.785	0.197	0.096
2.0	0.628	0.130	0.090
2.0	0.617	0.249	0.118
4.0	0.480	0.184	0.374
4.0	0.423	0.298	0.358
8.0	0.166	0.147	0.651
8.0	0.205	0.050	0.684
16.0	0.034	0.000	0.899
16.0	0.054	0.047	0.991

F as well as by fitting responses B and C alone by nonlinear regression using Marquardt's method. The results are listed in Table B-II along with the linearized estimate of the standard deviations. Parameter values are very similar for all four different estimates. The advantage of regression of multiple response data can be determined by examining the estimated standard deviations. Fitting all three responses results in the smallest standard deviations. Fitting B or C alone results in less accurate estimates of the rate constants.

The values in parentheses listed in Table B-II are those obtained by Box and Draper [1965]. They are almost identical to the values obtained using the minimization technique described above which serves to validate the method used in this study. Box and Draper [1965] calculated a Bayesian estimate of the 99.75% confidence interval in the following manner:

$$\det(\mathbf{F}(\mathbf{b})) - \det(\mathbf{F}(\mathbf{b}_f)) = \exp\left(-\frac{1}{2}\chi^2\right) \quad (B-21)$$

where \mathbf{b}_f is the best estimate of the parameter vector obtained from minimization of

Table B-II: Parameter Estimates for Example

	k_1, min^{-1}	k_2, min^{-1}
All Responses	0.208 ± 0.008 (0.208)	0.495 ± 0.048 (0.493)
B and C	0.205 ± 0.015 (0.205)	0.500 ± 0.051 (0.499)
B alone	0.211 ± 0.038 (0.210)	0.504 ± 0.090 (0.504)
C alone	0.197 ± 0.033 (0.198)	0.535 ± 0.175 (0.530)

the determinant of \mathbf{F} and χ^2 is the multivariate chi-squared distribution. Their calculated 99.75% confidence limits are plotted in Figure B-1. The natural logarithms of the rate constants are plotted rather than the parameters themselves. The confidence intervals are dramatically reduced when all three responses are used. Fitting C alone produces a large crescent-shaped contour indicating a significant correlation among the parameters. This is a result of the symmetry between k_1 and k_2 in equation (B-20c). Interchanging the values of k_1 and k_2 results in the same values of C. Equation (B-20b) is not symmetric in k_1 and k_2 which results in a reduced correlation among the parameters. When two or three responses are used more information is supplied concerning the behavior of the parameters which further reduces the confidence interval. The estimated standard deviations are consistent with the more exact results obtained from the 99.75% confidence intervals.

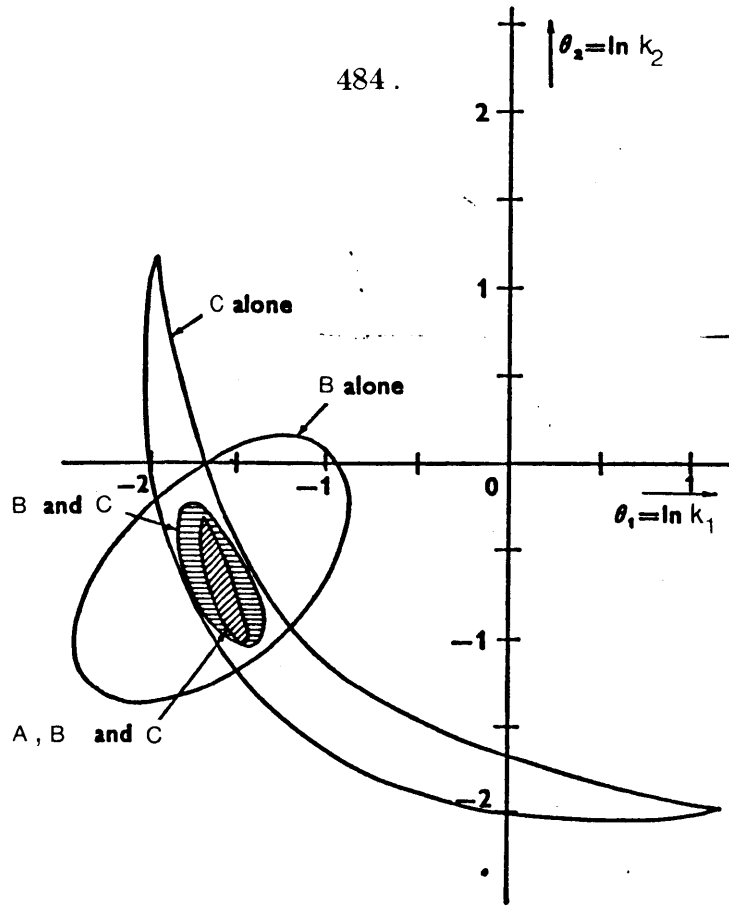


Figure B-1: Approximate 99.75% confidence contours (from Box and Draper [1965]).

Appendix C

Estimation of Steady-State Concentration and Rate of Degradation

The tissue concentration and amount of degradation of radiolabeled LDL and mLDL in the arterial wall are influenced by cellular metabolism within the vessel wall and the rate of removal from the plasma by other tissues. Because radiolabeled LDL and mLDL behave as tracers in the arterial wall, mathematical linearizations are possible. For a linear system, the tissue concentration, $\theta_T(t)$, in response to an arbitrarily decaying plasma concentration, $\theta_p(t)$, can be related to the response to a pulse input by means of the convolution integral (Himmelblau and Bischoff [1968], p. 108; Hildebrand [1976], pp. 63-64):

$$\theta_p(t) = \int_0^t H(\tau)\theta_p(t-\tau)d\tau \quad (C-1)$$

where $H(t)$ is the tissue concentration in response to a pulse input. $\theta_T(t)$ can be either the average concentration or the concentration at a single point. For LDL and mLDL, the plasma concentration can be described by a biexponentially decaying function (Berman [1979]).

In order to compare tissue concentrations of radiolabeled LDL and mLDL, in which the plasma decay curves are different, one would ideally like to determine either the pulse or step response. Numerical deconvolution to obtain the pulse response is difficult, requiring differentiation of data or a fitted function of data at $t=0$ (Gamel et al. [1973], veng Pedersen [1980a,b]). An alternative and simpler approach is to determine the steady-state tissue concentration in response to a step input (denoted $\psi_T(\infty)$).

In order to evaluate the steady-state response to a step input it is useful to note two properties of Laplace transforms:

1. Laplace transform of the integral of a function:

$$\mathcal{L} \left\{ \int_0^t f(\tau) d\tau \right\} = \frac{\bar{f}(s)}{s} \quad (C-2)$$

2. Final value theorem for Laplace transforms:

$$\lim_{s \rightarrow 0} s \bar{f}(s) = \lim_{t \rightarrow \infty} f(t) \quad (C-3)$$

Equation (C-3) is limited to functions which assume an unambiguous finite value in the limit as t approaches infinity (Hildebrand [1976], p. 84). Integration of $\theta_T(t)$ from 0 to t and application of the final value theorem yields:

$$\lim_{t \rightarrow \infty} \int_0^t \theta_T(\tau) d\tau = \lim_{s \rightarrow 0} s \frac{\bar{\theta}_T(s)}{s} = \bar{\theta}_T(s=0) \quad (C-4)$$

The Laplace transform of the convolution integral is (Hildebrand [1976]):

$$\bar{\theta}_T(s) = \bar{H}(s) \bar{\theta}_p(s) \quad (C-5)$$

Evaluating equation (C-5) at $s = 0$ and substituting into equation (C-4) yields:

$$\lim_{t \rightarrow \infty} \int_0^t \theta_T(\tau) d\tau = H(0) \bar{\theta}_p(0) \quad (C-6)$$

Equation (C-6) can be related to experimentally measurable quantities in order to obtain the steady-state response to a step input. The left hand side of equation (C-6) can be obtained by either numerical integration of $\theta_T(t)$ or by fitting $\theta_T(t)$ to a simple function and then integrating. $\bar{\theta}_p(s=0)$ can be evaluated if the functional form of the input is known. For a biexponential plasma decay:

$$\bar{\theta}_p(s) = \frac{C_1}{k_1 + s} + \frac{C_2}{k_2 + s} \quad (C-7a)$$

and

$$\bar{\theta}_p(0) = \frac{C_1}{k_1} + \frac{C_2}{k_2} \quad (C-7b)$$

Relation (C-7b) is identical to the reciprocal of the fractional catabolic rate (FCR) for a biexponential decay.

$\bar{H}(s=0)$ is simply the steady state value of the response to a step input, $\psi_T(\infty)$. To see this, note that for a step input ($\theta_p(t)=1$ for $t > 0$) the Laplace transform of $\theta_p(t)$ is $\bar{\theta}_p(s)=1/s$. Denoting the tissue concentration in response to a step input $\psi_T(t)$, equation (C-5) becomes:

$$\bar{\psi}_T(s) = \frac{\bar{H}(s)}{s} \quad (C-8a)$$

Applying the initial value theorem to equation (C-8a) yields:

$$\psi_T(\infty) = \lim_{s \rightarrow 0} s \frac{\bar{H}(s)}{s} = \lim_{s \rightarrow 0} \bar{H}(s) = \bar{H}(0) \quad (C-8b)$$

Inserting equations (C-7b) and (C-8b) into equation (C-6) and rearranging yields:

$$\psi_T(\infty) = FCR \int_0^{\infty} \theta_T(\tau) d\tau \quad (C-9)$$

Equation (C-9) can also be derived in the time domain by integration of equation (C-1) from 0 to ∞ :

$$\int_0^{\infty} \theta_T(t) dt = \int_0^{\infty} \int_0^t H(\tau) \theta_p(t-\tau) d\tau dt \quad (C-10)$$

Changing the order of integration:

$$\int_0^{\infty} \theta_T(t) dt = \int_0^t H(\tau) \int_0^{\infty} \theta_p(t-\tau) dt d\tau \quad (C-11)$$

$(t-\tau)$ can be replaced with a dummy variable, u , with limits of integration ranging from 0 to ∞ :

$$\int_0^{\infty} \theta_T(t) dt = \int_0^{\infty} H(\tau) d\tau \int_0^{\infty} \theta_p(u) du \quad (C-12)$$

The integral $\int_0^{\infty} H(\tau) d\tau$ is simply $\psi_T(\infty)$ (equation (C-8b)) and $\int_0^{\infty} \theta_p(u) du = C_1/k_1 + C_2/k_2 = 1/FCR$. Thus, by rearranging equation (C-12), equation (C-9) is obtained.

These results can be extended to determine the steady state rate of degradation in response to a step input. For a linear system the rate of degradation is proportional to the intracellular concentrations. Degradation is likely to occur by a combination of receptor-mediated and receptor-independent mechanisms and the total rate of degradation is equal to:

$$\frac{dC_d(t)}{dt} = k_{d_1} C_{i_1}(t) + k_{d_2} C_{i_2}(t) \quad (C-13)$$

where C_d is the concentration of ^{14}C -sucrose-labeled lipoprotein degraded in the vessel wall as defined in equation (4-15), C_{i_1} and C_{i_2} are the intracellular concentration of ^{14}C -sucrose-labeled protein internalized by receptor-mediated and receptor-independent mechanisms, respectively, and k_{d_1} and k_{d_2} are the corresponding degradation rate constants. In equation (4-15), C_d is made dimensionless by dividing by $(C_{p_0})_{^{14}\text{C}}$. Thus, equation (C-13) becomes:

$$\frac{d(C_d(t)/C_{p_o})_{^{14}\text{C}}}{dt} = k_{d_1} \left[\frac{C_{i_1}(t)}{C_{p_o}} \right]_{^{14}\text{C}} + k_{d_2} \left[\frac{C_{i_2}(t)}{C_{p_o}} \right]_{^{14}\text{C}} \quad (\text{C-14a})$$

For a tracer experiment, relative tissue concentrations of ^{14}C -sucrose-labeled proteins are equal to relative tissue concentrations of ^{125}I -labeled proteins (equation (4-6)). Let $\theta_d = C_d/C_{p_o}$, $\theta_{i_1} = C_{i_1}/C_{p_o}$ and $\theta_{i_2} = C_{i_2}/C_{p_o}$ where it is understood that θ_d represents the relative concentration of ^{14}C -sucrose-labeled proteins and θ_{i_1} and θ_{i_2} represent relative concentrations of either ^{125}I - or ^{14}C -sucrose-labeled proteins. Equation (C-14a) then becomes:

$$\frac{d\theta_d(t)}{dt} = k_{d_1} \theta_{i_1} + k_{d_2} \theta_{i_2} \quad (\text{C-14b})$$

Taking the Laplace transform of equation (C-14b) yields:

$$s\bar{\theta}_d(s) = k_{d_1} \bar{\theta}_{i_1}(s) + k_{d_2} \bar{\theta}_{i_2}(s) \quad (\text{C-15})$$

For a linear system $\bar{\theta}_{i_1}(s)$ and $\bar{\theta}_{i_2}(s)$ are related to $\bar{\theta}_T(s)$ by transfer functions, $\bar{G}_1(s)$ and $\bar{G}_2(s)$ (Wylie [1975], pp. 311, 312):

$$\bar{\theta}_{i_1}(s) = \bar{G}_1(s)\bar{\theta}_T(s) \quad \bar{\theta}_{i_2}(s) = \bar{G}_2(s)\bar{\theta}_T(s) \quad (\text{C-16})$$

A new transform can be defined such that $k_{d_1}\bar{G}_1(s) + k_{d_2}\bar{G}_2(s) = k_d\bar{G}(s)$. Thus, equation (C-15) becomes:

$$s\bar{\theta}_d(s) = k_d\bar{G}(s)\bar{\theta}_T(s) \quad (\text{C-17})$$

Inserting equation (C-5) into equation (C-17) and applying the final value theorem to calculate the cumulative amount of degradation at infinite time:

$$\theta_d(\infty) = \lim_{s \rightarrow 0} s \bar{\theta}_d(s) = \lim_{s \rightarrow 0} k_d \bar{G}(s) \bar{H}(s) \bar{\theta}_p(s) \quad (C-18a)$$

and

$$\theta_d(\infty) = k_d \bar{G}(0) \bar{H}(0) \bar{\theta}_p(0) \quad (C-18b)$$

Note that $\theta_d(\infty)$ is the cumulative degradation in response to a biexponentially decaying plasma concentration. Substituting equation (C-8) and (C-7b) into (C-18b) yields:

$$FCR\theta_d(\infty) = k_d \bar{G}(0) \psi_T(\infty) \quad (C-19)$$

The left hand side of equation (C-19) can be determined experimentally; $\theta_d(\infty)$ can be obtained by measuring degradation at long circulation times or by fitting $\theta_d(t)$ and extrapolating to infinity. The right hand side of (C-19) is related to the steady-state rate of degradation in response to a step input.

For a step input $\bar{\theta}_p(s) = 1/s$ and $\bar{\psi}_i(s)$, denoting the response to a step input, is obtained by substituting equation (C-5) into (C-16) to yield:

$$\bar{\psi}_{i_1}(s) = \frac{\bar{G}_1(s) \bar{H}(s)}{s} \quad \bar{\psi}_{i_2}(s) = \frac{\bar{G}_2(s) \bar{H}(s)}{s} \quad (C-20a)$$

The steady-state intracellular concentration in response to a step input can be determined by applying the final value theorem to equation (C-20a):

$$\bar{\psi}_{i_1}(\infty) = \lim_{s \rightarrow 0} s \bar{\psi}_{i_1}(s) = \lim_{s \rightarrow 0} \bar{G}_1(s) \bar{H}(s) = \bar{G}_1(0) \psi_T(\infty) \quad (C-20b)$$

$$\bar{\psi}_{i_2}(\infty) = \lim_{s \rightarrow 0} s \bar{\psi}_{i_2}(s) = \lim_{s \rightarrow 0} \bar{G}_2(s) \bar{H}(s) = \bar{G}_2(0) \psi_T(\infty) \quad (C-20c)$$

Substituting equations (C-20b) and (C-20c) into (C-19) and using the definition of $k_d \bar{G}(s)$ yields:

$$FCR\theta(\infty) = k_{d_1} \psi_{i_1}(\infty) + k_{d_2} \psi_{i_2}(\infty) \quad (C-21)$$

The right hand side of (C-21) is simply the normalized steady-state rate of

degradation in response to a step input. Thus,

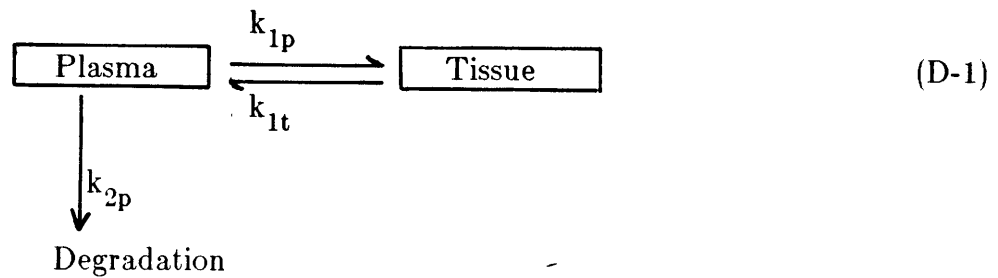
$$\underline{\dot{\theta}_i} = FCR\theta_d(\infty) \quad (C-22)$$

It is not possible to determine $\psi_i(\infty)$ without either measuring $\theta_i(t)$ or developing a detailed mathematical model in order to calculate the transfer function $\bar{G}(s)$.

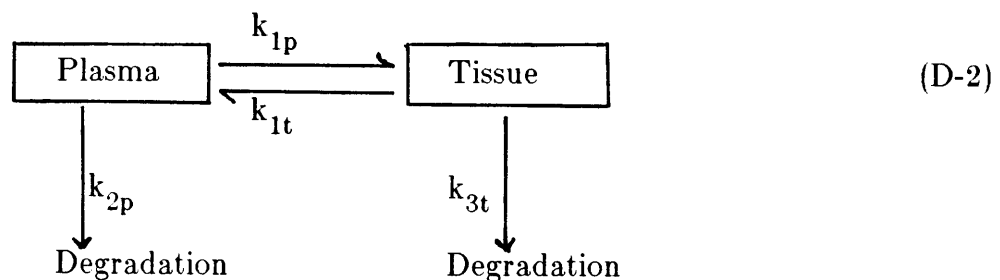
Appendix D

Pharmacokinetic Models of ^{125}I -LDL Plasma Decay Curves

The generally accepted model of ^{125}I -LDL plasma decay curves is the so-called two compartment mammillary model (Matthews [1966]). This model can be represented as:



All tissues are lumped into a single compartment and degradation is assumed to be from the plasma compartment. This model is a special case of a more general two compartment model (Berman [1979]):



This model is somewhat more realistic in that degradation of LDL by the tissues is considered. Two compartment models have been considered because, until recently, only plasma decay data have been available. Nevertheless, these models are gross oversimplifications of physiological processes and the rate constants do not have physiological correlates. LDL degradation occurs in many tissues, with the the

major sites of catabolism being the liver, adrenals, spleen, and kidneys (Steinberg [1983]). A distributed model with many metabolic sites is perhaps the most accurate pharmacokinetic model of LDL metabolism (Carew and Beltz [1982]).

For the model represented by equation (D-2), material balances on plasma and tissue concentrations of radiolabeled LDL are:

$$\frac{dC_p V_p}{dt} = -(k_{1p} + k_{2p})C_p V_p + k_{1t} C_t V_t \quad (D-3)$$

$$\frac{dC_t V_t}{dt} = k_{1p} C_p V_p - (k_{1t} + k_{3t})C_t V_t \quad (D-4)$$

where C_p and C_t are, respectively, tissue and plasma concentrations (cpm/ml), and V_p and V_t are plasma and tissue volumes, respectively. Initially C_p is C_{p_0} and C_t is 0.

The Laplace transforms of equations (D-3) and (D-4) are:

$$s\bar{C}_p - C_{p_0} = -(k_{1p} + k_{2p})\bar{C}_p + \frac{V_t}{V_p} k_{1t} \bar{C}_t \quad (D-5)$$

$$s\frac{V_t}{V_p} \bar{C}_t = k_{1p} \bar{C}_p - (k_{1t} + k_{3t})\frac{V_t}{V_p} \bar{C}_t \quad (D-6)$$

From equation (D-6), C_t can be expressed in terms of C_p . This expression is then inserted into equation (D-5), and, after rearrangement, yields:

$$\bar{C}_p = \frac{C_{p_0} (s + k_{1t} + k_{3t})}{(s + k_{1p} + k_{2p})(s + k_{1t} + k_{3t}) - k_{1p} k_{1t}} \quad (D-7)$$

The denominator can be rewritten as $(s + \lambda_1)(s + \lambda_2)$ where:

$$\lambda_1 + \lambda_2 = k_{1p} + k_{1t} + k_{2p} + k_{3t} \quad (D-8)$$

$$\lambda_1 \lambda_2 = (k_{1p} + k_{2p})(k_{1t} + k_{3t}) - k_{1p} k_{1t} \quad (D-9)$$

With this substitution, equation (D-7) becomes:

$$\bar{C}_p = \frac{C_{p_0} (s + k_{1t} + k_{3t})}{(s + \lambda_1)(s + \lambda_2)} \quad (D-10)$$

The solution to equation (D-10) can be obtained from a table of transforms (Arpaci [1966], pp. 344-346; transforms 13 and 19) and is:

$$\bar{C}_p = C_{p_0} \left[\frac{k_{1t} + k_{3t} - \lambda_2}{\lambda_1 - \lambda_2} e^{-\lambda_2 t} - \frac{k_{1t} + k_{3t} - \lambda_1}{\lambda_1 - \lambda_2} e^{-\lambda_1 t} \right] \quad (D-11)$$

Equation (D-11) predicts a biexponential decay which is consistent with experiment (equation (4-1)). Thus, the constants in equation (4-1) ($\frac{C_p}{C_{p_0}} = C_1 e^{-b_1 t} + C_2 e^{-b_2 t}$) are:

$$C_1 = - \frac{k_{1t} + k_{3t} - \lambda_1}{\lambda_1 - \lambda_1} \quad (D-12a)$$

$$C_2 = \frac{k_{1t} + k_{3t} - \lambda_2}{\lambda_1 - \lambda_2} \quad (D-12b)$$

$$b_1 = \lambda_1 \quad (D-12c)$$

$$b_2 = \lambda_2 \quad (D-12d)$$

C_1 and C_2 are not independent ($C_1 + C_2 = 1$), and it is not possible to determine all of the rate constants from the plasma decay curve.

Two useful quantities can be derived from the plasma decay curves, the mean residence time and the fractional catabolic rate (FCR). The mean residence time is

(Froment and Bischoff [1979], p. 594):

$$t = \frac{\int_0^\infty \tau C_p d\tau}{\int_0^\infty C_p dt} \tag{D-13}$$

The fractional catabolic rate has been defined by Berman [1979] as the reciprocal of the integral of the normalized plasma decay curve:

$$FCR = \frac{1}{\int_0^\infty (C_p/C_{p_0}) dt} \tag{D-14}$$

The mean residence time is a rather complicated expression in terms of the rate constants, whereas the fractional catabolic rate is simply related to the rate constants:

$$FCR = \frac{b_1 b_2}{C_1 b_2 + C_2 b_1} = k_2 + \frac{k_{1p} k_{3t}}{k_{1t} + k_{3t}} \tag{D-15}$$

A physical interpretation can be assigned to the fractional catabolic rate as follows. Consider the case in which the tissue rapidly equilibrates with the plasma. Equation (D-4) is at steady state:

$$C_t = \frac{k_{1p} C_p V_t/V_p}{k_{1t} + k_{3t}} \tag{D-16}$$

Inserting equation (D-16) into equation (D-3) yields:

$$\frac{dC_p}{dt} = - \left[k_{1p} + k_{2p} - \frac{k_{1p} k_{1t}}{k_{1t} + k_{3t}} \right] C_p \tag{D-17}$$

Rearranging equation (D-17) yields the desired result:

$$-\frac{dC_p}{dt} = - \left[k_{2p} + \frac{k_{1p}k_{3t}}{k_{1t} + k_{3t}} \right] C_p = -FCR C_p \quad (D-18)$$

Thus, the fractional catabolic rate represents the lumped first order rate constant when the tissue rapidly equilibrates with plasma.

Carew et al. [1984] have used a limiting case of the pharmacokinetic model presented in equation (D-2) to calculate the mass fraction degraded by the tissues, f_d . They assumed that all degradation occurred in the tissues (i.e. $k_{2p} = 0$). For this case, the tissue concentration can be obtained by inserting equation (D-11) into equation (D-4) and integrating:

$$\frac{C_t}{C_{p_0}} = \frac{V_p/V_T k_{1p} (e^{-\lambda_1 t} - e^{-\lambda_2 t})}{\lambda_2 - \lambda_1} \quad (D-19)$$

Since there is no degradation in the plasma, the rate of degradation is simply:

$$\frac{dV_t C_d / C_{p_0}}{dt} = k_{3t} V_t \frac{C_t}{C_{p_0}} \quad (D-20)$$

where C_d/C_{p_0} represents ^{14}C -sucrose labeled degradation products in the tissues.

Inserting equation (D-19) into (D-20) and integrating yields:

$$\frac{C_d}{C_{p_0}} = \frac{V_p k_{1p} k_{3t}}{V_t (\lambda_2 - \lambda_1)} \left[\frac{1 - e^{-\lambda_1 t}}{\lambda_1} - \frac{1 - e^{-\lambda_2 t}}{\lambda_2} \right] \quad (D-21)$$

For $k_{2p} = 0$, equation (D-9) reduces to:

$$\lambda_1 \lambda_2 = k_{1p} k_{3t} \quad (D-22)$$

Substituting equation (D-22) into equation (D-21) and rearranging yields an expression for the mass fraction degraded at time t , f_d :

$$f_d = \frac{V_t C_d}{V_p C_{p_0}} = \frac{\lambda_2(1 - e^{-\lambda_1 t})}{(\lambda_2 - \lambda_1)} - \frac{\lambda_1(1 - e^{-\lambda_2 t})}{(\lambda_2 - \lambda_1)} \quad (D-23)$$

Equation (D-23) is identical to equation (1) in Carew et al. [1982].

Appendix E

Solution of Transport Equations

The details of the method of solution of the partial differential equations which describe LDL transport and metabolism in the arterial media are covered in this Appendix. Problem formulation and nondimensionalization are discussed in the Chapter 5.

The dimensionless form of the conservation relations, boundary conditions, and initial conditions are summarized below:

Conservation Relations

$$\begin{aligned} \frac{\partial \theta_f}{\partial \tau} = & \frac{\partial \theta_f^2}{\partial \eta^2} - Pe \frac{\partial \theta_f}{\partial \eta} - \phi_b^2 (\theta_f - m\theta_b) - \phi_r^2 (\theta_f - (K-\beta)\theta_{LR}) \\ & - \phi_i^2 \theta_f + \phi_{e_1}^2 \theta_{LRi} + \phi_{e_2}^2 \theta_{Li} \end{aligned} \quad (E-1)$$

$$\frac{\partial \theta_b}{\partial \tau} = \phi_b^2 (\theta_f - m\theta_b) \quad (E-2)$$

$$\frac{\partial \theta_{LR}}{\partial \tau} = \phi_r^2 (\theta_f - K\theta_{LR}) \quad (E-3)$$

$$\frac{\partial \theta_{LRi}}{\partial \tau} = \phi_r^2 \beta \theta_{LR} - (\phi_{d_1}^2 + \phi_{e_1}^2) \theta_{LRi} \quad (E-4)$$

$$\frac{\partial \theta_{Li}}{\partial \tau} = \phi_i^2 \theta_f - (\phi_{d_2}^2 + \phi_{e_2}^2) \theta_{Li} \quad (E-5)$$

$$\frac{\partial \theta_d}{\partial \tau} = \phi_{d_1}^2 \theta_{LRi} + \phi_{d_2}^2 \theta_{Li} \quad (E-6)$$

Boundary Conditions

$$\eta = 0 \quad - \frac{Pe\theta_p}{\chi K_p}(1-R) + Bi(\theta_p - \frac{\theta_f}{\epsilon_f}) = \frac{1}{\epsilon_f}(-\frac{\partial\theta_f}{\partial\eta} + Pe\theta_f) \quad (E-7)$$

$$\eta = 1 \quad K_2\theta_p - K_1\theta_f = -\frac{\partial\theta_f}{\partial\eta} \quad (E-8a)$$

where

$$K_1 = Pe - Pe_l(1-R_l) - Pe_v(1-R_v) - Bi_l - Bi_c \quad (E-8b)$$

$$K_2 = -Pe_a(1-R_a)\epsilon_w - Bi_c\epsilon_f \quad (E-8c)$$

Initial Conditions

$$\tau < 0 \quad \theta_p = 0 \quad (E-9a)$$

$$\theta_f = \theta_b = \theta_{LR} = \theta_{L_{Ri}} = \theta_{L_i} = \theta_d = 0 \quad (E-9b)$$

$$\tau \geq 0 \quad \theta_p = \theta_p(\tau) \quad (E-9c)$$

The Laplace transform of the conservation relation for freely diffusible solute, equation (E-1), is:

$$s\bar{\theta}_f = \frac{d\bar{\theta}_f^2}{d\eta^2} - Pe \frac{d\bar{\theta}_f}{d\eta} - \phi_b^2(\bar{\theta}_f - m\bar{\theta}_b) - \phi_r^2(\bar{\theta}_f - (K-\beta)\bar{\theta}_{LR}) - \phi_i^2\bar{\theta}_f + \phi_{e_1}^2\bar{\theta}_{L_{Ri}} + \phi_{e_2}^2\bar{\theta}_i \quad (E-10)$$

Taking the Laplace transform of equations (E-2) to (E-5) and solving for θ_b , θ_{LR} , $\theta_{L_{Ri}}$, and θ_{L_i} in terms of θ_f yields:

$$\bar{\theta}_b = \frac{\phi_b^2\bar{\theta}_f}{s + m\phi_b^2} \quad (E-11)$$

$$\bar{\theta}_{LR} = \frac{\phi_r^2\bar{\theta}_f}{s + K\phi_r^2} \quad (E-12)$$

$$\bar{\theta}_{LRi} = \frac{\phi_r^2 \beta \bar{\theta}_{LR}}{s + \phi_{d_1}^2 + \phi_{e_1}^2} \quad (E-13)$$

$$\bar{\theta}_{LRi} = \frac{\phi_r^4 \beta \bar{\theta}_{LR}}{(s + \phi_{d_1}^2 + \phi_{e_1}^2)(s + K\phi_r^2)} \quad (E-14)$$

$$\bar{\theta}_i = \frac{\phi_i^2 \bar{\theta}_f}{s + \phi_{d_2}^2 + \phi_{e_2}^2} \quad (E-15)$$

Substituting equations (E-11) to (E-15) into equation (E-10) yields:

$$0 = \frac{d\bar{\theta}_f}{d\eta^2} - Pe \frac{d\bar{\theta}_f}{d\eta} - \bar{\theta}_f \left[s + \frac{s\phi_b^2}{s+m\phi_b^2} + \frac{\phi_r^2}{s+K\phi_r^2} \left(s + \beta\phi_r^2 - \frac{\phi_r^2\phi_{e_1}^2}{s+\phi_{d_1}^2+\phi_{e_1}^2} \right) + \phi_i^2 \left(1 - \frac{\phi_{e_2}^2}{s+\phi_{d_2}^2+\phi_{e_2}^2} \right) \right] \quad (E-16)$$

This ordinary differential equation has the following solution:

$$\bar{\theta}_f = \exp(Pe\eta/2) [C_1 \cosh(\alpha\eta) + C_2 \sinh(\alpha\eta)] \quad (E-17)$$

where

$$\alpha = \left[\frac{Pe^2}{4} + s + \frac{s\phi_b^2}{s+m\phi_b^2} + \frac{\phi_r^2}{s+K\phi_r^2} \left(s + \beta\phi_r^2 - \frac{\phi_r^2\phi_{e_1}^2}{s+\phi_{d_1}^2+\phi_{e_1}^2} \right) + \phi_i^2 \left(1 - \frac{\phi_{e_2}^2}{s+\phi_{d_2}^2+\phi_{e_2}^2} \right) \right]^{1/2} \quad (E-18a)$$

Note that α is a fifth order polynomial in s . For mLDL, ϕ_r^2 is zero and equation (E-18a) reduces to a third order polynomial in s .

$$\alpha = \left[\frac{Pe^2}{4} + s + \frac{s\phi_b^2}{s+m\phi_b^2} + \phi_i^2 \left(1 - \frac{\phi_{e_2}^2}{s+\phi_{d_2}^2+\phi_{e_2}^2} \right) \right]^{1/2} \quad (E-18b)$$

The integration constants C_1 and C_2 are evaluated from the Laplace transform of the boundary condition:

$$\eta = 0 \quad -\frac{d\bar{\theta}_f}{d\eta} + (Pe + Bi)\bar{\theta}_f = \frac{[Pe(1-R)/K_p\chi + Bi]\epsilon_f}{s} \quad (E-19)$$

$$\eta = 1 \quad -\frac{d\bar{\theta}_f}{d\eta} + K_1\bar{\theta}_f = \frac{K_2}{s} \quad (E-20)$$

The derivative of $\bar{\theta}_f$ with respect to η is:

$$\begin{aligned} \frac{d\bar{\theta}_f}{d\eta} = & \frac{Pe}{2} \exp(Pe\eta/2) [C_1 \cosh(\alpha\eta) + C_2 \sinh(\alpha\eta)] \\ & + \alpha \exp(Pe\eta/2) [C_1 \sinh(\alpha\eta) + \cosh(\alpha\eta)] \end{aligned} \quad (E-21)$$

By substituting equations (E-17) and (E-21) into equations (E-19) and (E-20) expressions for C_1 and C_2 are obtained:

$$C_1 = \frac{1}{s\Delta} \left\{ \epsilon_f \left[\frac{Pe(1-R)}{K_p\chi} + Bi \right] [(K_1 - Pe/2) \sinh(\alpha) - \alpha \cosh(\alpha)] + \alpha K_2 \exp(-Pe/2) \right\} \quad (E-22)$$

$$C_2 = \frac{1}{s\Delta} \left\{ (Pe/2 + Bi) K_2 \exp(-Pe/2) - \epsilon_f \left[\frac{Pe(1-R)}{K_p\chi} + Bi \right] [(K_1 - Pe/2) \cosh(\alpha) - \alpha \sinh(\alpha)] \right\} \quad (E-23)$$

where:

$$\Delta = [(Pe/2 + Bi)(K_1 - Pe/2) - \alpha^2] \sinh(\alpha) + \alpha(K_1 - Pe - Bi) \cosh(\alpha) \quad (E-24)$$

The resulting solution for freely diffusible protein concentration is:

$$\bar{\theta}_f = \frac{\exp(Pe[\eta-1]/2)}{s} \left\{ \epsilon_f \left[\frac{Pe(1-R)}{K_p\chi} + Bi \right] [(K_1 - Pe/2) \sinh(\alpha) - \alpha \cosh(\alpha)] \exp(Pe/2) \right.$$

$$\begin{aligned}
 & + \alpha K_2 \left[\cosh(\alpha \eta) + \left[(Pe/2 + Bi)K_2 \right. \right. \\
 & \left. \left. - \epsilon_f \left[\frac{Pe(1-R)}{K_p \chi} + Bi \right] \left[(K_1 - Pe/2) \cosh(\alpha) - \alpha \sinh(\alpha) \right] \exp(Pe/2) \right] \sinh(\alpha \eta) \right] \\
 & \left. \left[(Pe/2 + Bi)(K_1 - Pe/2) - \alpha^2 \right] \sinh(\alpha) + \alpha(K_1 - Pe - Bi) \cosh(\alpha) \right\} \quad (E-25)
 \end{aligned}$$

The inversion of equation (E-25) can be obtained by the method of residues. A simple pole exists at $s = 0$, and additional poles are located at those values of α which cause the denominator to vanish. These poles may exist for real values of α , i.e. $\alpha = \alpha_m$, or for imaginary values of α , i.e. $\alpha = i\lambda_m$. Although complex roots of the form $\alpha = a + ib$ may exist, analysis of the real and imaginary parts of the denominator of equation (E-25) for a number of limiting cases (large a , $a \ll b$, $b \ll a$) indicates that complex roots are not likely to occur (Ramirez [1979], p. 251).

For real values of α the denominator in equation (E-25) is zero when:

$$\tanh(\alpha_m) = \frac{-\alpha_m(K_1 - Pe - Bi)}{(Pe/2 + Bi)(K_1 - Pe/2) - \alpha_m^2} \quad (E-26)$$

where α_m are the real roots. For imaginary values of α , $\alpha = i\lambda_m$, the denominator of equation (E-25) is zero when:

$$\tan(\lambda_m) = \frac{-\lambda_m(K_1 - Pe - Bi)}{(Pe/2 + Bi)(K_1 - Pe/2) + \lambda_m^2} \quad (E-27)$$

Only two values of α_m (at most) satisfy equation (E-26), whereas an infinite number of values of λ_m satisfy equation (E-27). The values of the real roots depend upon the sign and magnitude of the groups $K_1 - Pe - Bi$ and $(Pe/2 + Bi)(K_1 - Pe/2)$. Examination of equations (E-8b) and (E-26) indicates that

$K_1 - Pe - Bi$ is negative. $K_1 - Pe/2$ may be positive or negative depending upon the relative sizes of K_1 and $Pe/2$. If $K_1 - Pe/2 < 0$ then, for positive values of α_m , $\tanh(\alpha_m)$ is positive, the right hand side of equation (E-26) is negative and there are no real roots. The same argument applies for negative values of α_m . If $K_1 - Pe/2 > 0$ then there is one real root. Two roots are possible when $K_1 - Pe - Bi$ and $K_1 - Pe > 0$, which implies significant convective transport from the lymphatics and venules into the tissue, a physically unrealistic situation. Typically, no real roots were observed.

Successive roots in equations (E-26) and (E-27) are evaluated by rewriting equations (E-26) and (E-27) in the form of $F(\alpha_m) = 0$. An initial guess of 0.01 is taken for α (or λ) and $F(\alpha)$ is evaluated. This continues until $F(\alpha)$ changes sign, at which point Newton's method is used to find the root in the interval between the change of signs (Finlayson [1980], p. 12). The next root is found in the same manner using an initial guess slightly larger than the root, α_m . (Usually 30 roots are sufficient to guarantee that the concentration is accurate to four decimal places.)

The residue at $s = 0$ was evaluated using equation (7-221) in Arpaci [1966]. It can be formulated as:

$$Residue(s=0) = \lim_{s \rightarrow 0} [s \bar{\Theta}_f(s) \exp(\tau s)] \quad (E-28)$$

The evaluation of this residue yields:

$$Residue(s=0) = \exp(Pe[\eta-1]/2) \left\{ \left[\epsilon_f \left[\frac{Pe(1-R)}{K_p \chi} + Bi[(K_1 - Pe/2) \sinh(\alpha_o) - \alpha_o \cosh(\alpha_o)] \exp(Pe/2) + \alpha_o K_2 \cosh(\alpha_o \eta) + \left[(Pe/2 + Bi) K_2 - \epsilon_f \left[\frac{Pe(1-R)}{K_p \chi} + Bi \right] [(K_1 - Pe/2) \cosh(\alpha_o) - \alpha_o \sinh(\alpha_o)] \exp(Pe/2) \right] \sinh(\alpha_o \eta) \right] \right\} /$$

$$\left\{ [(Pe/2 + Bi)(K_1 - Pe/2) - \alpha_o^2] \sinh(\alpha_o) + \alpha_o(K_1 - Pe - Bi) \cosh(\alpha_o) \right\} \quad (E-29)$$

where

$$\alpha_o = \alpha(s=0) = \left[\frac{Pe^2}{4} + \frac{\beta\phi_r^2}{K} \left(1 - \frac{\phi_{e_1}^2}{\phi_{d_1}^2 + \phi_{e_1}^2} \right) + \phi_i^2 \left(1 - \frac{\phi_{e_2}^2}{\phi_{d_2}^2 + \phi_{e_2}^2} \right) \right]^{1/2} \quad (E-30a)$$

For methylated LDL ϕ_r^2 is zero and equation (E-30a) reduces to:

$$\alpha_o = \alpha(s=0) = \left[\frac{Pe^2}{4} + \phi_i^2 \left(1 - \frac{\phi_{e_2}^2}{\phi_{d_2}^2 + \phi_{e_2}^2} \right) \right]^{1/2} \quad (E-30b)$$

Two quantities can be defined from the evaluation of the residue at $s = 0$:

$$A(\eta) = \exp(Pe(\eta - 1)/2) \quad (E-31)$$

and

$$B(\eta) = \frac{\text{Residue}(s=0)}{A(\eta)} \quad (E-32)$$

The residue at $s = 0$ can be represented as:

$$\text{Residue}(s=0) = A(\eta)B(\eta) \quad (E-33)$$

The simple pole at $s = 0$ represents the steady state concentration of freely diffusible solute in response to a step input, $\Psi_f(\eta, \infty)$. To see this, note that from the final value theorem of Laplace Transforms (Appendix C, equation (C-3))

$$\lim_{t \rightarrow \infty} \Psi_f(\tau) = \lim_{s \rightarrow 0} s \bar{\Psi}_f(s).$$

For imaginary values of α there are an infinite number of roots. To obtain the poles of s , equation (E-18a) is solved for each value of $\alpha = i\lambda_m$. Equation (E-18a) is a fifth order polynomial in s and can be expressed in terms of $\alpha^2 = -\lambda_m^2$; thus each

value of $i\lambda_m$ yields five values of s , which are represented as $s_{m,n}$ (where m goes from 1 to infinity and n is one of the five roots of equation (E-18a)). For large values of λ_m these roots approach the five characteristic time constants of the system, which are $-\lambda_m$, $-m\phi_b^2$, $-K\phi_r^2$, $-(\phi_{d_1}^2 + \phi_{e_1}^2)$, and $-(\phi_{d_2}^2 + \phi_{e_2}^2)$.

The roots of $s_{m,n}$ were evaluated iteratively using an algorithm described in Lapidus. Equations (E-18a,b) are rewritten as general polynomials of the form:

$$f(x) = x^n + a_1x^{n-1} + a_2x^{n-2} + \dots + a_{n-1}x + a_n \tag{E-34}$$

$f(x)$ is evaluated, beginning at $x=0.01$, at increasing multiples of Δx until the sign of $f(x)$ changes. Newton's method is then applied between the regions of the sign change to evaluate x_1 . Using this value of x , the order of the polynomial is reduced by synthetic division to:

$$g(x) = \frac{f(x)}{(x-x_1)} = (x^{n-1} + b_1x^{n-2} + \dots + b_{n-2}x + b_{n-1}) \tag{E-35}$$

By using a starting value of x just beyond x_1 , the process is repeated to find x_2 . This is continued until the polynomial is reduced to a quadratic at which point the quadratic formula is applied to find the two remaining roots. Once all of the roots are found, Newton's method is applied to the original polynomial, $f(x)$, in order to improve the accuracy of the estimates obtained with the lower order polynomials obtained by synthetic division.

The infinite sum of residues can be obtained by the use of equation (7-225) in Arpaci [1966]. If each pole, $s_{m,n}$, is simple, the infinite sum of residues can be formulated as follows:

$$\sum_{m=1}^{\infty} \sum_{n=1}^5 \text{Residues}(s=s_{m,n}) = \sum_{m=1}^{\infty} \sum_{n=1}^5 \frac{U(\alpha)exp(sr)}{sT(\alpha)_s} \Big|_{s_{m,n}} \tag{E-36a}$$

or

$$\sum_{m=1}^{\infty} \sum_{n=1}^5 Residues(s=s_{m,n}) = \sum_{m=1}^{\infty} \sum_{n=1}^5 \frac{U(\alpha)exp(s\tau)}{sT(\alpha)_\alpha \alpha(s)_s} \Big|_{s_{m,n}} \quad (E-36b)$$

where

$$U(\alpha) = exp(Pe[\eta-1]/2) \left\{ \epsilon_f \left[\frac{Pe(1-R)}{\chi} + Bi \right] [(K_1 - Pe/2)sinh(\alpha) - \alpha cosh(\alpha)] exp(Pe/2) \right. \\ \left. + \alpha K_2 \right\} cosh(\alpha\eta) + \left\{ (Pe/2 + Bi)K_2 - \epsilon_f \left[\frac{Pe(1-R)}{\chi} + Bi \right] [(K_1 - Pe/2)cosh(\alpha) \right. \\ \left. - \alpha sinh(\alpha)] exp(Pe/2) \right\} sinh(\alpha\eta) \quad (E-37)$$

and

$$T(\alpha) = [(Pe/2 + Bi)(K_1 - Pe/2) - \alpha^2]sinh(\alpha) + \alpha(K_1 - Pe - Bi)cosh(\alpha) \quad (E-38a)$$

The notation $T(\alpha)_s$, $T(\alpha)_\alpha$, and $\alpha(s)_s$ represent the derivatives of the function with respect to the subscripted variable which are evaluated analytically:

$$\frac{dT}{ds} = \frac{dT}{d\alpha} \frac{d\alpha}{ds} \quad (E-38b)$$

$$\frac{dT}{d\alpha} = [(Pe/2 + Bi)(K_1 - Pe/2) - \alpha^2 + K_1 - Pe - Bi]cosh(\alpha) \\ + \alpha(K_1 - Pe - Bi - 2)sinh(\alpha) \quad (E-38c)$$

$$\frac{d\alpha}{ds} = \frac{1}{2\alpha} \left[1 + \frac{m\phi_b^4}{(s+m\phi_b^2)^2} + \frac{(K-\beta)\phi_r^4}{(s+K\phi_r^2)^2} \right. \\ \left. + \frac{\phi_r^4 \phi_{e_1}^2 (2s + \phi_{d_1}^2 + \phi_{e_1}^2 + \phi_r^2 K)}{(s+K\phi_r^2)^2 (s + \phi_{d_1}^2 + \phi_{e_1}^2)^2} + \frac{\phi_i^2 \phi_{e_2}^2}{(s + \phi_{d_2}^2 + \phi_{e_2}^2)^2} \right] \quad (E-38d)$$

The double summation in equation (E-36b) becomes:

$$\sum_{m=1}^{\infty} \sum_{n=1}^5 Residues(s=s_{m,n}) = -2A(\eta) \sum_{m=1}^{\infty} \sum_{n=1}^5 \frac{Q(\eta)_m exp(s_{m,n}\tau)}{s_{m,n} Z_{m,n}} \quad (E-39)$$

where

$$Q(\eta)_m = \frac{-\alpha U(\alpha)}{A(\eta)T(\alpha)_\alpha} \Big|_{s_{m,n}} \quad (E-40)$$

and

$$Z_{m,n} = 2 \alpha \frac{d\alpha}{ds} \Big|_{s_{m,n}} \quad (E-41)$$

The concentration of mobile solute in the interstitial fluid for a step change in plasma concentration, $\Psi_f(\eta, \tau)$ is obtained by adding together all residues:

$$\Psi_f(\eta, \tau) = \text{Residue}(s=0) + \sum_{m=1}^{\infty} \sum_{n=1}^5 \text{Residue}(s=s_{m,n}) \quad (E-42)$$

Substituting equation (E-33) for the residue of s at 0 and equation (E-39) for the residues of $s=s_{m,n}$ into equation (E-42) yields:

$$\Psi_f(\eta, \tau) = A(\eta) \left\{ B(\eta) - 2 \sum_{m=1}^{\infty} \sum_{n=1}^5 \frac{Q_{m,n} \exp(s_{m,n} \tau)}{s_{m,n} Z_{m,n}} \right\} \quad (E-43)$$

Ψ_b can be obtained by integration of equation (E-2), a linear first differential equation in time:

$$\Psi_b = \phi_b^2 \exp(-m\phi_b^2 \tau) \int_0^\tau \exp(m\phi_b^2 \tau') \Psi_f(\eta, \tau') d\tau' \quad (E-44)$$

Substituting equation (E-43) into (E-44) and performing the integration yields:

$$\Psi_b(\eta, \tau) = \phi_b^2 A(\eta) \left\{ B(\eta) G - 2 \sum_{m=1}^{\infty} \sum_{n=1}^5 \frac{Q_{m,n} G_1}{s_{m,n} Z_{m,n}} \right\} \quad (E-45)$$

where

$$G = \frac{1 - \exp(-m\phi_b^2\tau)}{m\phi_b^2} \quad (E-46a)$$

$$G_1 = \frac{\exp(s_{m,n}\tau) - \exp(-m\phi_b^2\tau)}{(s_{m,n} + m\phi_b^2)} \quad (E-46b)$$

Ψ_{LR} is obtained in a similar fashion by substituting equation (E-43) for Ψ_f into equation (E-3) and integrating:

$$\Psi_{LR}(\eta, \tau) = \phi_r^2 A(\eta) \left\{ B(\eta)LR - 2 \sum_{m=1}^{\infty} \sum_{n=1}^5 \frac{Q_{m,n} LR_1}{s_{m,n} Z_{m,n}} \right\} \quad (E-47)$$

where

$$LR = \frac{1 - \exp(-K\phi_r^2\tau)}{K\phi_r^2} \quad (E-48a)$$

$$LR_1 = \frac{\exp(s_{m,n}\tau) - \exp(-K\phi_r^2\tau)}{s_{m,n} + K\phi_r^2} \quad (E-48b)$$

Substitution of equation (E-47) into equation (E-4) and integrating yields $\Psi_{L_{Ri}}$:

$$\Psi_{L_{Ri}}(\eta, \tau) = \phi_r^4 \beta A(\eta) \left\{ \frac{B(\eta)(LRI - LRI_2)}{K\phi_r^2} - 2 \sum_{m=1}^{\infty} \sum_{n=1}^5 \frac{Q_{m,n}(LRI_1 - LRI_2)}{s_{m,n} Z_{m,n} (s_{m,n} + K\phi_r^2)} \right\} \quad (E-49)$$

where

$$LRI = \frac{1 - \exp(-(\phi_{d_1}^2 + \phi_{e_1}^2)\tau)}{\phi_{d_1}^2 + \phi_{e_1}^2} \quad (E-50a)$$

$$LRI_1 = \frac{\exp(s_{m,n}\tau) - \exp(-(\phi_{d_1}^2 + \phi_{e_1}^2)\tau)}{s_{m,n} + \phi_{d_1}^2 + \phi_{e_1}^2} \quad (E-50b)$$

$$LRI_2 = \frac{\exp(-K\phi_r^2\tau) - \exp(-(\phi_{d_1}^2 + \phi_{e_1}^2)\tau)}{\phi_{d_1}^2 + \phi_{e_1}^2 - K\phi_r^2} \quad (E-50c)$$

In a similar fashion, substitution of equation (E-43) into equation (E-6) yields ψ_{L_i} :

$$\psi_{L_i}(\eta, \tau) = \phi_i^2 A(\eta) \left\{ B(\eta)LI - 2 \sum_{m=1}^{\infty} \sum_{n=1}^5 \frac{Q_{m,n} LI_1}{s_{m,n} Z_{m,n}} \right\} \quad (E-51)$$

where

$$LI = \frac{1 - \exp(-(\phi_{d_1}^2 + \phi_{e_2}^2)\tau)}{\phi_{d_2}^2 + \phi_{e_2}^2} \quad (E-52a)$$

$$LI_1 = \frac{\exp(s_{m,n}\tau) - \exp(-(\phi_{d_2}^2 + \phi_{e_2}^2)\tau)}{s_{m,n} + \phi_{d_2}^2 + \phi_{e_2}^2} \quad (E-52b)$$

ψ_d is obtained by substituting equations (E-49) for $\psi_{L_{Ri}}$ and (E-51) for ψ_{L_i} into equation (E-6) and integrating:

$$\psi_d(\eta, \tau) = \phi_{d_1}^2 \phi_r^4 \beta A(\eta) \left\{ \frac{B(\eta)}{K\phi_r^2} \left[\frac{\tau - LRI}{\phi_{d_1}^2 + \phi_{e_1}^2} - \frac{(LR - LRI)}{\phi_{d_1}^2 + \phi_{e_1}^2 - K\phi_r^2} \right] - 2 \sum_{m=1}^{\infty} \sum_{n=1}^5 \frac{Q_{m,n}}{s_{m,n} Z_{m,n} (s_{m,n} + K\phi_r^2)} \left[\frac{S_1 - LRI}{s_{m,n} + \phi_{d_1}^2 + \phi_{e_1}^2} - \frac{LR - LRI}{\phi_{d_1}^2 + \phi_{e_1}^2 - K\phi_r^2} \right] \right\}$$

$$+ \phi_{d_2}^2 \phi_i^2 A(\eta) \left\{ \frac{B(\eta)(\tau - LI)}{\phi_{d_2}^2 + \phi_{e_2}^2} - 2 \sum_{m=1}^{\infty} \sum_{n=1}^5 \frac{Q_{m,n}(S_1 - LI)}{s_{m,n} Z_{m,n} (s_{m,n} + \phi_{d_2}^2 + \phi_{e_2}^2)} \right\} \quad (E-53)$$

where

$$S_1 = \frac{\exp(s_{m,n}\tau) - 1}{s_{m,n}} \quad (E-54)$$

At steady state equation (E-43) and equations (E-45) to (E-49) become:

$$\psi_f = A(\eta)B(\eta) \quad (E-55a)$$

$$\psi_b = \frac{A(\eta)B(\eta)}{m} = \frac{\psi_f}{m} \quad (E-55b)$$

$$\psi_{LR} = \frac{A(\eta)B(\eta)}{K} = \frac{\psi_f}{K} \quad (E-55c)$$

$$\psi_{L_{Ri}} = \frac{\beta \phi_r^2 A(\eta)B(\eta)}{K(\phi_{d_1}^2 + \phi_{e_1}^2)} = \frac{\beta \phi_r^2 \psi_f}{K(\phi_{d_1}^2 + \phi_{e_1}^2)} \quad (E-55d)$$

$$\psi_{L_i} = \frac{\phi_i^2 A(\eta)B(\eta)}{\phi_{d_2}^2 + \phi_{e_2}^2} = \frac{\phi_i^2 \psi_f}{\phi_{d_2}^2 + \phi_{e_2}^2} \quad (E-55e)$$

$$\begin{aligned} \psi_d = & \frac{\phi_{d_1}^2 \beta \phi_r^2}{K(\phi_{d_1}^2 + \phi_{e_1}^2)} \left\{ \psi_f \left[\tau - \frac{1}{\phi_{d_1}^2 + \phi_{e_1}^2} \right] - \frac{1}{K \phi_r^2} + 2 \sum_{m=1}^{\infty} \sum_{n=1}^5 \frac{Q_{m,n} A(\eta)}{s_{m,n} Z_{m,n}} \right\} \\ & + \frac{\phi_{d_2}^2 \phi_i^2}{\phi_{d_2}^2 + \phi_{e_2}^2} \left\{ \psi_f \left[\tau - \frac{1}{\phi_{d_2}^2 + \phi_{e_2}^2} \right] + 2 \sum_{m=1}^{\infty} \sum_{n=1}^5 \frac{Q_{m,n} A(\eta)}{s_{m,n} Z_{m,n}} \right\} \quad (E-55f) \end{aligned}$$

The steady state rate of degradation is simply the derivative of equation (E-55f) with respect to the dimensionless time.

$$\frac{R_d L^2}{D_e} = \frac{d\bar{\psi}_d}{d\tau} = \left[\frac{\phi_{d_1}^2 \beta \phi_r^2}{K(\phi_{d_1}^2 + \phi_{e_1}^2)} + \frac{\phi_{d_2}^2 \phi_i^2}{\phi_{d_2}^2 + \phi_{e_2}^2} \right] \psi_f \quad (E-55g)$$

The bracketed terms on the right hand side of equation (E-55g) represent lumped rate constants for steady state first order degradation of LDL by receptor-mediated and receptor-independent mechanisms, respectively.

The total steady state tissue concentration is:

$$\psi_T = \psi_f + \psi_b + \psi_{LR} + \psi_{L_{Ri}} + \psi_{L_i} \quad (E-56)$$

Substitution of equations (E-55a) through (E-55e) into equation (E-56) yields:

$$\psi_T = \psi_f \left[1 + \frac{1}{m} + \frac{1}{K} + \frac{\beta \phi_r^2}{K(\phi_{d_1}^2 + \phi_{e_1}^2)} + \frac{\phi_i^2}{\phi_{d_2}^2 + \phi_{e_2}^2} \right] \quad (E-57)$$

The corresponding solution for a decaying plasma concentration with either a constant or time-varying mass transfer coefficients is obtained by application of Duhamel's superposition integral. For mobile solute the integral is:

$$\theta_f(\eta, \tau) = \psi_f(\eta, \tau) D(0) + \int_0^\tau \psi_f(\eta, \tau - \tau') \frac{dD(\tau')}{d\tau'} d\tau' \quad (E-58)$$

where $D(\tau')$ is the disturbance function. Two cases have been considered. The first is that of a decaying plasma concentration and constant Bi and Bi_c for which:

$$D(\tau) = \theta_p(\tau) = \sum_{i=1}^2 a_i e^{-b_i \tau} \quad (E-59a)$$

The second case is that of a decaying plasma concentration and time-varying mass transfer coefficients represented by equation (4-25) for which the disturbance

function is:-

$$D(\tau) = [1 - f(1 - e^{-\gamma' \tau})] \theta_p(\tau) = [1 - f(1 - e^{-\gamma' \tau})] \sum_{i=1}^2 a_i e^{-b_i \tau} \quad (E-59b)$$

where $\gamma' = \frac{\gamma D_e}{L^2}$ and γ is the time constant for the changing mass transfer coefficient defined in equation (4-25). For both disturbance functions, equations (E-59a) and (E-59b), $D(0)$ in equation (E-58) is 1. Note that equation (E-59a) is a limiting case of equation (E-59b) for $f=0$. The solution presented below is for a disturbance function represented by equation (E-59b).

The concentrations in response to time-varying permeabilities were calculated for the boundary condition at $\eta = 1$ represented by equation (E-8) and a rejection coefficient of one at the intimal surface. Bi and Bi_c are represented by the same decay function, although the initial values are assumed to be different. That is,

$$Bi(\tau) = Bi_o [1 - f(1 - e^{-\gamma' \tau})] \quad (E-60a)$$

$$Bi_c(\tau) = Bi_{c_o} [1 - f(1 - e^{-\gamma' \tau})] \quad (E-60b)$$

More general solutions can be obtained by assuming different values of f and γ' for Bi and Bi_c .

Substituting equations (E-60b) and (E-58) into equation (E-59) yields the mobile solute concentration in response to time-varying permeabilities and a decaying plasma concentration.

$$\theta_f(\eta, \tau) = A(\eta) \left\{ B(\eta) \sum_{i=1}^2 a_i [(1-f) \exp(-b_i \tau) + f \exp(-(\gamma' + b_i) \tau)] - 2 \sum_{m=1}^{\infty} \sum_{n=1}^5 \frac{Q_{m,n} [\exp(s_{m,n} \tau) + (1-f)FB + fFBG]}{s_{m,n} Z_{m,n}} \right\} \quad (E-61)$$

where

$$FB = \sum_{i=1}^2 \frac{a_i b_i (\exp(-b_i \tau) - \exp(s_{m,n} \tau))}{s_{m,n} + b_i} \quad (E-62a)$$

$$FBG = \sum_{i=1}^2 \frac{a_i (\gamma' + b_i) (\exp(-(\gamma' + b_i) \tau) - \exp(s_{m,n} \tau))}{s_{m,n} + b_i + \gamma'} \quad (E-62b)$$

Equations analogous to equation (E-61) can be obtained for θ_b , θ_{LR} , $\theta_{L_{Ri}}$, θ_{L_i} , and θ_d , by substitution of equation (E-61) into equations (E-2) to (E-6) and integrating. The solutions for these concentrations are:

$$\theta_b(\eta, \tau) = \phi_b^2 A(\eta) \left\{ B(\eta) \sum_{i=1}^2 [(1-f)BB_1 i + fBB_2 i] - 2 \sum_{m=1}^{\infty} \sum_{n=1}^5 \frac{Q_{m,n}}{s_{m,n} Z_{m,n}} \left[G_1 + \sum_{i=1}^2 \frac{(1-f)a_i b_i (BB_1 i - G_1)}{s_{m,n} + b_i} + \sum_{i=1}^2 \frac{f a_i (\gamma' + b_i) (BB_2 i - G_1)}{s_{m,n} + b_i + \gamma'} \right] \right\} \quad (E-63)$$

where

$$BB_1 i = \frac{[\exp(-b_i \tau) - \exp(-m\phi_b^2 \tau)]}{m\phi_b^2 - b_i} \quad (E-64a)$$

$$BB_2 i = \frac{\exp(-(b_i + \gamma') \tau) - \exp(-m\phi_b^2 \tau)}{m\phi_b^2 - (\gamma' + b_i)} \quad (E-64b)$$

$$\begin{aligned} \theta_{LR}(\eta, \tau) = \phi_r^2 A(\eta) & \left\{ B(\eta) \sum_{i=1}^2 a_i [(1-f)LRB_1 i + fLRB_2 i] - 2 \sum_{m=1}^{\infty} \sum_{n=1}^5 \frac{Q_{m,n}}{s_{m,n} Z_{m,n}} \left[LR_1 \right. \right. \\ & \left. \left. + \sum_{i=1}^2 \frac{(1-f)a_i b_i (LRB_1 i - LR_1)}{s_{m,n} + b_i} + \sum_{i=1}^2 \frac{f a_i (\gamma' + b_i) (LRB_2 i - LR_1)}{s_{m,n} + b_i + \gamma'} \right] \right\} \end{aligned} \quad (E-65)$$

where

$$LRB_1 i = \frac{e(-b_i \tau) - \exp(-K\phi_r^2 \tau)}{K\phi_r^2 - b_i} \quad (E-66a)$$

$$LRB_2 i = \frac{\exp(-(b_i + \gamma')\tau) - \exp(-K\phi_r^2 \tau)}{K\phi_r^2 - (\gamma' + b_i)} \quad (E-66b)$$

$$\begin{aligned} \theta_{L_{Ri}}(\eta, \tau) = \beta \phi_r^2 A(\eta) & \left\{ B(\eta) \left[\sum_{i=1}^2 \frac{a_i (1-f) [LRIB_1 i - LRI_2]}{K\phi_r^2 - b_i} + \sum_{i=1}^2 \frac{a_i f [LRIB_2 i - LRI_2]}{K\phi_r^2 - (\gamma' + b_i)} \right] \right. \\ & \left. - 2 \sum_{m=1}^{\infty} \sum_{n=1}^5 \frac{Q_{m,n}}{s_{m,n} Z_{m,n}} \left[\frac{LRI_1 - LRI_2}{K\phi_r^2 + s_{m,n}} - \sum_{i=1}^2 \frac{(1-f)a_i b_i}{s_{m,n} + b_i} \left(\frac{LRIB_1 i - LRI_2}{K\phi_r^2 - b_i} - \frac{LRI_1 - LRI_2}{K\phi_r^2 + s_{m,n}} \right) \right] \right\} \\ & + \sum_{i=1}^2 \frac{f a_i (\gamma' + b_i)}{s_{m,n} + b_i} \frac{LRIB_2 i - LRI_2}{K\phi_r^2 - (\gamma' + b_i)} - \frac{LRI_1 - LRI_2}{K\phi_r^2 + s_{m,n}} \end{aligned} \quad (E-67)$$

where

$$LRIB_1 i = \frac{\exp(-b_i \tau) - e(-(\phi_{d_1}^2 + \phi_{e_1}^2)\tau)}{\phi_{d_1}^2 + \phi_{e_1}^2 - b_i} \quad (E-68a)$$

$$LRIB_2 i = \frac{\exp(-(b_i + \gamma')\tau) - \exp(-(\phi_{d_1}^2 + \phi_{e_1}^2)\tau)}{\phi_{d_1}^2 + \phi_{e_1}^2 - (\gamma' + b_i)} \quad (E-68b)$$

$$\Theta_{L_i}(\eta, \tau) = \phi_i^2 A(\eta) \left\{ B(\eta) \sum_{i=1}^2 a_i [(1-f)LIB_1 i + fLIB_2 i] - 2 \sum_{m=1}^{\infty} \sum_{n=1}^5 \frac{Q_{m,n}}{s_{m,n} Z_{m,n}} \left[LI_1 \right. \right. \\ \left. \left. + \sum_{i=1}^2 \frac{(1-f)a_i b_i (LIB_1 i - LI_1)}{s_{m,n} + b_i} + \sum_{i=1}^2 \frac{f a_i (\gamma' + b_i) (LIB_2 i - LI_1)}{s_{m,n} + b_i + \gamma'} \right] \right\} \quad (E-69)$$

where

$$LIB_1 i = \frac{\exp(-b_i \tau) - \exp(-(\phi_{d_2}^2 + \phi_{e_2}^2) \tau)}{\phi_{d_2}^2 + \phi_{e_2}^2 - b_i} \quad (E-70a)$$

$$LIB_2 i = \frac{\exp(-(b_i + \gamma') \tau) - \exp(-(\phi_{d_2}^2 + \phi_{e_2}^2) \tau)}{\phi_{d_2}^2 + \phi_{e_2}^2 - (\gamma' + b_i)} \quad (E-70b)$$

$$\Theta_d = \phi_{d_1}^2 \phi_r^4 \beta A(\eta) \left\{ B(\eta) \sum_{i=1}^2 \left[\frac{a_i (1-f)}{K \phi_r^2 - b_i} \left(\frac{Bi - LRI}{\phi_{d_1}^2 + \phi_{e_1}^2 - b_i} - \frac{LR - LRI}{\phi_{d_1}^2 + \phi_{e_1}^2 - \phi_r^2 K} \right) \right. \right. \\ \left. \left. + \sum_{i=1}^2 \frac{a_i f}{K \phi_r^2 - (\gamma' + b_i)} \left(\frac{BG_i - LRI}{\phi_{d_1}^2 + \phi_{e_1}^2 - (b_i + \gamma')} - \frac{1LR - 1LRI}{\phi_{d_1}^2 + \phi_{e_1}^2 - \phi_r^2 K} \right) \right. \right. \\ \left. \left. - 2 \sum_{m=1}^{\infty} \sum_{n=1}^5 \frac{Q_{m,n}}{s_{m,n} Z_{m,n}} \left[\frac{1}{K \phi_r^2 + s_{m,n}} \left(\frac{S_1 - LRI}{s_{m,n} + \phi_{d_1}^2 + \phi_{e_1}^2} - \frac{LR - LRI}{\phi_{d_1}^2 + \phi_{e_1}^2 - \phi_r^2 K} \right) \right. \right. \right. \\ \left. \left. + \sum_{i=1}^2 \frac{(1-f)a_i b_i}{s_{m,n} + b_i} \left(\frac{1}{K \phi_r^2 - b_i} \left(\frac{Bi - LRI}{\phi_{d_1}^2 + \phi_{e_1}^2 - b_i} - \frac{LR - LRI}{\phi_{d_1}^2 + \phi_{e_1}^2 - \phi_r^2 K} \right) \right) \right. \right. \\ \left. \left. - \frac{1}{K \phi_r^2 + s_{m,n}} \left(\frac{S_1 - LRI}{\phi_{d_1}^2 + \phi_{e_1}^2 + s_{m,n}} - \frac{LR - LRI}{\phi_{d_1}^2 + \phi_{e_1}^2 - \phi_r^2 K} \right) \right] \right\}$$

$$\begin{aligned}
& + \sum_{i=1}^2 \frac{fa_i(\gamma' + b_i)}{s_{m,n} + b_i + \gamma'} \left(\frac{1}{K\phi_r^2 - (\gamma' + b_i)} \left(\frac{BGi - LRI}{\phi_{d_1}^2 + \phi_{e_1}^2 - (\gamma' + b_i)} - \frac{LR - LRI}{\phi_{d_1}^2 + \phi_{e_1}^2 - \phi_r^2 K} \right) \right. \\
& \left. - \frac{1}{K\phi_r^2 + s_{m,n}} \left(\frac{S - LRI}{\phi_{d_1}^2 + \phi_{e_1}^2 + s_{m,n}} - \frac{LR - LRI}{\phi_{d_1}^2 + \phi_{e_1}^2 + s_{m,n}} \right) \right) \Bigg\} \\
& + \phi_2^2 \phi_i^2 A(\eta) \left\{ B(\eta) \sum_{i=1}^2 a_i \left(\frac{(1-f)[1Bi - 1LI]}{\phi_{d_2}^2 + \phi_{e_2}^2 - b_i} + \frac{f[BGi - LI]}{\phi_{d_2}^2 + \phi_{e_2}^2 - (\gamma' + b_i)} \right) \right. \\
& - 2 \sum_{m=1}^{\infty} \sum_{n=1}^5 \frac{Q_{m,n}}{s_{m,n} Z_{m,n}} \left[\frac{S_1 - LI}{\phi_{d_2}^2 + \phi_{e_2}^2 + s_{m,n}} \right. \\
& + \sum_{l=1}^2 \frac{(1-f)a_l b_l}{s_{m,n} + b_l} \left(\frac{Bl - LI}{\phi_{d_2}^2 + \phi_{e_2}^2 - b_l} - \frac{S_1 - LI}{\phi_{d_2}^2 + \phi_{e_2}^2 + s_{m,n}} \right) \\
& \left. \left. + \sum_{l=1}^2 \frac{fa_l(\gamma' + b_l)}{s_{m,n} + \gamma' + b_l} \left(\frac{BG_l - LI}{\phi_{d_2}^2 + \phi_{e_2}^2 - (\gamma' + b_l)} - \frac{1S - 1LI}{\phi_{d_2}^2 + \phi_{e_2}^2 + s_{m,n}} \right) \right] \right\} \tag{E-71}
\end{aligned}$$

where

$$Bi = \frac{1 - \exp(-b_i \tau)}{b_i} \tag{E-72a}$$

$$BGi = \frac{1 - \exp(-(\gamma' + b_i) \tau)}{\gamma' + b_i} \tag{E-72b}$$

A limiting case of equation (E-60b) which is of interest is the tissue concentration for a step change in plasma concentration in which the Biot numbers are decaying with time according to equations (E-60a,b). For this case the time

constants for plasma decay (b_1 and b_2 in equations (E-61) to (E-72) are equal to 0 and $\theta_p = 1.0$) and the disturbance function, $D(\tau)$ in equation (E-59b) reduces to:

$$D(\tau) = 1 - f(1 - e^{-\gamma'\tau}) \quad (E-73)$$

Tissue concentrations and cumulative degradation can be calculated using Duhamel's superposition integral, equation (E-58), or by taking the limit as b_1 and b_2 go to zero in equations (E-61) to (E-73). The resulting concentrations are:

$$\psi_f(\eta, \tau) = A(\eta) \left\{ B(\eta) [(1-f)(1 - \exp(-\gamma'\tau))] - 2 \sum_{m=1}^{\infty} \sum_{n=1}^5 \frac{Q_{m,n}}{s_{m,n} Z_{m,n}} \left[\exp(s_{m,n}\tau) + fGS \right] \right\} \quad (E-74)$$

where

$$GS = \frac{\gamma' [\exp(-\gamma'\tau) - \exp(s_{m,n}\tau)]}{s_{m,n} + \gamma'} \quad (E-75)$$

$$\begin{aligned} \psi_b(\eta, \tau) = & \phi_b^2 A(\eta) \left\{ B(\eta) [(1-f)1B + fGB] \right. \\ & \left. - 2 \sum_{m=1}^{\infty} \sum_{n=1}^5 \frac{Q_{m,n}}{s_{m,n} Z_{m,n}} \left[G_1 + \frac{f\gamma'(GB - G_1)}{s_{m,n} + \gamma'} \right] \right\} \quad (E-76) \end{aligned}$$

where

$$GB = \frac{(\exp(-\gamma'\tau) - \exp(-m\phi_b^2\tau))}{m\phi_b^2 - \gamma'} \quad (E-77)$$

$$\begin{aligned} \Psi_{LR}(\bar{\eta}, \tau) = & \phi_r^2 A(\eta) \left\{ B(\eta) \left[(1-f)LR + fGLR \right] \right. \\ & \left. - 2 \sum_{m=1}^{\infty} \sum_{n=1}^5 \frac{Q_{m,n}}{s_{m,n} Z_{m,n}} \left[LR_1 + \frac{f\gamma'(GLR - LR_1)}{s_{m,n} + \gamma'} \right] \right\} \end{aligned} \quad (E-78)$$

where

$$GLR = \frac{(\exp(-\gamma'\tau) - \exp(-K\phi_r^2\tau))}{K\phi_r^2 - \gamma'} \quad (E-79)$$

$$\begin{aligned} \Psi_{L_{Ri}}(\eta, \tau) = & \beta\phi_r^2 A(\eta) \left\{ B(\eta) \left[\frac{(1-f)(LRI - LRI_2)}{K\phi_r^2} + \frac{f(GLRI - LRI_2)}{K\phi_r^2 - \gamma'} \right] \right. \\ & \left. - 2 \sum_{m=1}^{\infty} \sum_{n=1}^5 \frac{Q_{m,n}}{s_{m,n} Z_{m,n}} \left[\frac{LRI_1 - LRI_2}{K\phi_r^2 + s_{m,n}} + \frac{fa_i\gamma'(GLRI - LRI_2)}{s_{m,n}} \left(\frac{1}{K\phi_r^2 - \gamma'} - \frac{1}{K\phi_r^2 + s_{m,n}} \right) \right] \right\} \end{aligned} \quad (E-80)$$

where

$$GLRI = \frac{\exp(-\gamma'\tau) - \exp(-(\phi_{d_1}^2 + \phi_{e_1}^2)\tau)}{\phi_{d_1}^2 + \phi_{e_1}^2 - \gamma'} \quad (E81)$$

$$\begin{aligned} \Psi_{L_i}(\eta, \tau) = & \phi_i^2 A(\eta) \left\{ B(\eta) \left[(1-f)LI + fGLI \right] \right. \\ & \left. - 2 \sum_{m=1}^{\infty} \sum_{n=1}^5 \frac{Q_{m,n}}{s_{m,n} Z_{m,n}} \left[LI + \frac{f\gamma'(GLI - LI_1)}{s_{m,n} + \gamma'} \right] \right\} \end{aligned} \quad (E-82)$$

$$GLRI = \frac{(\exp(-\gamma'\tau) - e(-(\phi_{d_2}^2 + \phi_{e_2}^2)\tau))}{\phi_{d_2}^2 + \phi_{e_2}^2 - \gamma'} \quad (E-83)$$

$$\begin{aligned}
\psi_d = & \phi_{d_1}^{-2} \phi_r^4 \beta A(\eta) \left\{ B(\eta) \left[\frac{(1-f)}{K \phi_r^2} \left(\frac{\tau - LRI}{\phi_{d_1}^2 + \phi_{e_1}^2} - \frac{LR - LRI}{\phi_{d_1}^2 + \phi_{e_1}^2 - \phi_r^2 K} \right) \right. \right. \\
& + \left. \left. \frac{f}{K \phi_r^{2-\gamma'}} \left(\frac{L_1 - LR}{\phi_{d_1}^2 + \phi_{e_1}^2 - \gamma'} - \frac{LR - LRI}{\phi_{d_1}^2 + \phi_{e_1}^2 - \phi_r^2 K} \right) \right] \right. \\
& - 2 \sum_{m=1}^{\infty} \sum_{n=1}^5 \frac{Q_{m,n}}{s_{m,n} Z_{m,n}} \left[\frac{1}{K \phi_r^2 + s_{m,n}} \left(\frac{S_1 - LRI}{s_{m,n} + \phi_{d_1}^2 + \phi_{e_1}^2} - \frac{LR - LRI}{\phi_{d_1}^2 + \phi_{e_1}^2 - \phi_r^2 K} \right) \right. \\
& + \left. \frac{f a_i \gamma'}{s_{m,n} + \gamma'} \left[\frac{1}{K \phi_r^2 - \gamma'} \left(\frac{L_1 - LRI}{\phi_{d_1}^2 + \phi_{e_1}^2 - \gamma'} - \frac{LR - LRI}{\phi_{d_1}^2 + \phi_{e_1}^2 - \phi_r^2 K} \right) \right. \right. \\
& - \left. \left. \frac{1}{K \phi_r^2 + s_{m,n}} \left(\frac{S_1 - LRI}{\phi_{d_1}^2 + \phi_{e_1}^2 + s_{m,n}} - \frac{1LR - 1LRI}{\phi_{d_1}^2 + \phi_{e_1}^2 - \phi_r^2 K} \right) \right] \right] \left. \right\} \\
& + \phi_{d_2}^2 \phi_i^2 A(\eta) \left\{ B(\eta) \left[\frac{(1-f)[\tau - LI]}{\phi_{d_2}^2 + \phi_{e_2}^2} + \frac{f[L_1 - LI]}{\phi_{d_2}^2 + \phi_{e_2}^2 - \gamma'} \right] \right. \\
& - 2 \sum_{m=1}^{\infty} \sum_{n=1}^5 \frac{Q_{m,n}}{s_{m,n} Z_{m,n}} \left[\frac{S_1 - LI}{\phi_{d_2}^2 + \phi_{e_2}^2 + s_{m,n}} \right. \\
& + \left. \left. \frac{f \gamma'}{s_{m,n} + \gamma'} \left(\frac{L_1 - LI}{\phi_{d_2}^2 + \phi_{e_2}^2 - \gamma'} - \frac{S_1 - LI}{\phi_{d_2}^2 + \phi_{e_2}^2 + s_{m,n}} \right) \right] \right] \left. \right\} \tag{E-84}
\end{aligned}$$

where

$$L_1 = \frac{(1 - \exp(-\gamma' \tau))}{\gamma'} \tag{E-85}$$

Steady state equations can be derived in the same fashion as before by taking

the limit as τ becomes very large.

$$\psi_f = A(\eta)B(\eta) \quad (E-86a)$$

$$\psi_b = \frac{A(\eta)B(\eta)}{m} = \frac{(1-f)\psi_f}{m} \quad (E-86b)$$

$$\psi_{LR} = \frac{A(\eta)B(\eta)}{K} = \frac{\psi_f}{K} \quad (E-86c)$$

$$\psi_{LRi} = \frac{\beta\phi_r^2 A(\eta)B(\eta)}{K(\phi_{d_1}^2 + \phi_{e_1}^2)} = \frac{\beta\phi_r^2 \psi_f}{K(\phi_{d_1}^2 + \phi_{e_1}^2)} \quad (E-86d)$$

$$\psi_{Li} = \frac{\phi_i^2 A(\eta)B(\eta)}{\phi_{d_2}^2 + \phi_{e_2}^2} = \frac{\phi_i^2 \psi_f}{\phi_{d_2}^2 + \phi_{e_2}^2} \quad (E-86e)$$

$$\psi_d = \frac{\phi_{d_1}^2 \beta\phi_r^2 A(\eta)}{K(\phi_{d_1}^2 + \phi_{e_1}^2)} \left\{ B(\eta) \left[\tau - \frac{1}{\phi_{d_1}^2 + \phi_{e_1}^2} - \frac{1}{K\phi_r^2} \right] + 2 \sum_{m=1}^{\infty} \sum_{n=1}^5 \frac{Q_{m,n}}{s_{m,n}^2 Z_{m,n}} \right\} \\ + \frac{\phi_{d_2}^2 \phi_i^2 A(\eta)}{\phi_{d_2}^2 + \phi_{e_2}^2} \left\{ B(\eta) \left[\tau - \frac{1}{\phi_{d_2}^2 + \phi_{e_2}^2} \right] + 2 \sum_{m=1}^{\infty} \sum_{n=1}^5 \frac{Q_{m,n}}{s_{m,n}^2 Z_{m,n}} \right\} \quad (E-86f)$$

The steady state rate of degradation is simply the derivative of equation (E-86f) with respect to the dimensionless time.

$$\frac{R_d L^2}{D_e} = \frac{d\psi_d}{d\tau} = \left[\frac{\beta\phi_r^2 \phi_{d_1}^2}{K(\phi_{d_1}^2 + \phi_{e_1}^2)} + \frac{\phi_i^2 \phi_{d_2}^2}{\phi_{d_2}^2 + \phi_{e_2}^2} \right] \psi_f \quad (E-86g)$$

Appendix F Data from Cell Culture Experiments

This appendix contains selected data obtained from cell culture experiments presented in Chapters 2 and 3, the results of the trinitrobenzenesulfonic acid test to determine the extent of methylation, and the correlation between smooth muscle cell mass and cell number. The author maintains a copy of all data not presented in this Appendix.

Calculation of ^{125}I -LDL bound, internalized, and degraded Cells were grown on 35 mm plastic dishes and incubated with ^{125}I -LDL for various times after which bound, internalized, and degraded ^{125}I -LDL and the mg of cell protein were measured according to the procedures presented in the Material and Methods section of Chapter 2. Raw data were obtained as cpm/dish for tissue radioactivity and mg cell protein/dish for cell mass. In addition, the specific activity (SA), cpm/ng LDL protein, of ^{125}I -LDL was determined for each preparation after iodination and dialysis. The cell associated concentrations were reported as ng ^{125}I -LDL protein/mg cell protein which was calculated as:

$$\text{ng}^{125}\text{I-LDL/mg cell protein} = \frac{(\text{cpm/dish})/\text{SA}}{(\text{mg cell protein/dish})} \quad (\text{F-1})$$

1. Kinetic Studies: Receptor-Mediated Metabolism

BSMC6 mg cell protein	LDL, $\mu\text{g/ml}$	t, min	ng ^{125}I -LDL Bound	protein/mg Intern.	cell protein Degraded
0.222	10.13	15.0	8.2	31.3	0.0
0.269	10.13	15.0	8.1	38.9	2.3
0.282	10.13	15.0	6.1	38.7	6.5
0.260	10.13	30.0	3.8	61.5	0.0
0.239	10.13	30.0	4.2	61.1	0.0
0.233	10.13	30.0	2.0	61.0	2.4
0.269	10.13	60.0	10.6	98.4	27.8
0.284	10.13	60.0	7.2	99.1	35.1
0.307	10.13	60.0	5.0	79.5	31.2
0.269	10.13	120.0	9.0	133.2	119.0
0.277	10.13	120.0	9.0	133.0	121.3
0.246	10.13	120.0	8.1	104.8	109.6
0.282	10.13	240.0	9.4	153.2	299.4
0.294	10.13	240.0	9.1	153.7	318.4
0.282	10.13	240.0	9.0	163.4	352.1
0.284	10.13	360.0	5.7	119.7	354.3
0.275	10.13	360.0	6.2	133.0	425.9
0.275	10.13	360.0	7.2	138.6	484.8
0.277	1.00	240.0	1.5	15.8	35.6
0.271	1.00	240.0	1.2	16.1	39.9
0.265	1.00	240.0	1.25	15.7	35.4
0.294	5.35	240.0	4.0	70.6	165.4
0.271	5.35	240.0	4.7	73.0	196.1
0.299	5.35	240.0	3.6	63.4	189.5
0.290	10.13	240.0	10.1	164.5	262.8
0.303	10.13	240.0	8.5	155.8	312.5
0.286	10.13	240.0	9.0	149.8	290.5
0.250	22.82	240.0	9.1	139.1	215.0
0.288	22.82	240.0	11.5	202.0	299.2
0.297	22.82	240.0	12.1	178.6	320.3
0.243	60.90	240.0	14.1	256.2	356.7
0.256	60.90	240.0	15.8	250.2	425.2
0.254	60.90	240.0	19.9	205.4	402.3
0.267	108.6	240.0	9.7	211.2	290.8
0.265	108.6	240.0	16.9	201.5	352.0
0.267	108.6	240.0	20.2	242.8	418.1

BSMC10 mg cell protein	LDL, $\mu\text{g/ml}$	t, min	ng ^{125}I -LDL Bound	protein/mg Intern.	cell protein Degraded
0.254	10.42	5.00	5.50	12.10	0.00
0.250	10.42	5.00	4.87	14.70	0.00
0.226	10.42	5.00	4.61	12.84	0.00
0.177	10.42	10.0	3.36	13.09	0.00
0.174	10.42	10.0	8.08	8.82	0.39
0.168	10.42	10.0	6.37	6.21	1.03
0.282	10.42	15.0	4.00	12.8	0.19
0.239	10.42	15.0	4.32	16.5	1.16
0.267	10.42	15.0	4.76	18.1	4.36
0.295	10.42	20.0	2.76	17.4	0.00
0.234	10.42	20.0	2.98	20.2	3.50
0.247	10.42	20.0	3.57	17.6	3.50
0.217	10.42	30.0	3.77	26.2	0.00
0.305	10.42	30.0	3.55	32.1	1.90
0.295	10.42	30.0	4.24	32.0	4.10
0.269	10.42	60.0	4.80	58.1	0.00
0.215	10.42	60.0	5.80	61.0	11.1
0.273	10.42	60.0	3.72	39.6	8.40
0.187	10.42	120.	2.51	40.6	0.0
0.166	10.42	120.	2.84	40.0	19.1
0.190	10.42	120.	3.16	37.8	16.1
0.194	10.42	240.	3.50	55.4	3.00
0.173	10.42	240.	4.50	53.3	27.3
0.172	10.42	240.	3.66	61.4	31.6
0.253	1.010	240.	0.64	7.47	13.4
0.232	1.010	240.	1.32	6.68	5.80
0.247	1.010	240.	0.70	7.44	4.40
0.229	2.00	240.	2.71	15.9	15.5
0.295	2.00	240.	1.65	14.4	20.3
0.295	2.00	240.	1.32	14.1	17.4
0.190	5.070	240.	3.33	22.4	23.2
0.190	5.070	240.	2.84	19.7	30.6
0.219	5.070	240.	2.24	19.1	30.9
0.275	10.42	240.	3.56	54.8	72.1
0.308	10.42	240.	3.77	50.5	74.8
0.297	15.00	240.	10.36	98.2	121.2
0.287	15.00	240.	6.94	97.1	129.0
0.332	15.00	240.	6.11	86.7	111.8
0.330	20.67	240.	13.46	90.5	88.5

0.275	-- 20.67	240.	15.25	122.2	177.8
0.273	- 20.67	240.	17.91	133.3	191.3
0.351	- 30.91	240.	0.53	101.2	165.3
0.371	30.91	240.	4.90	122.5	147.5
0.312	30.91	240.	11.94	133.2	181.3
0.223	48.76	240.	19.46	126.4	72.0
0.217	48.76	240.	34.35	172.2	133.1
0.243	48.76	240.	22.25	138.7	103.1
0.232	100.5	240.	11.96	159.9	74.5
0.206	100.5	240.	19.92	166.1	170.1
0.208	100.5	240.	20.02	161.4	198.9

BSMC29 mg cell protein	LDL, $\mu\text{g/ml}$	t, min	ng ^{125}I -LDL Bound	protein/mg Intern.	cell protein Degraded
0.040	9.87	5.00	2.21	11.0	0.0
0.051	9.87	5.00	2.68	4.90	8.8
0.045	9.87	10.0	1.07	1.4	0.0
0.049	9.87	10.0	1.63	5.2	0.0
0.072	9.87	30.0	2.88	33.1	10.0
0.064	9.87	30.0	0.41	22.9	0.0
0.070	9.87	60.0	1.94	41.7	70.5
0.055	9.87	60.0	8.91	68.7	200.3
0.073	9.87	120.0	3.11	49.1	110.7
0.085	9.87	240.0	2.23	49.1	0.0
0.066	9.87	240.0	7.03	99.7	56.9
0.075	4.14	240.0	0.0	51.6	32.8
0.070	4.14	240	1.23	52.7	33.9
0.079	18.52	240.0	2.92	69.7	181.9
0.075	18.52	240.0	3.59	80.1	162.2
0.060	28.98	240.0	8.21	160.5	240.0
0.055	28.98	240.0	9.87	189.6	315.3
0.058	50.37	240.0	5.80	204.8	174.4
0.047	50.37	240.0	11.70	259.8	255.7

BSMC33 mg cell protein	LDL, $\mu\text{g/ml}$	t, min	ng ^{125}I -LDL Bound	protein/mg Intern.	cell protein Degraded
0.250	12	2	4.12	3.23	0.0
0.268	12	2	3.62	2.07	0.0
0.162	12	5	7.67	9.46	0.0
0.166	12	5	6.96	13.17	0.0
0.141	12	10	9.91	32.6	0.0
0.127	12	10	11.74	38.7	0.0
0.192	12	30	9.81	109.7	3.25
0.158	12	30	12.01	113.7	0.0
0.153	12	60	14.13	198.9	0.0
0.182	12	60	10.35	170.0	0.0
0.166	12	120	17.27	358.4	28.4
0.168	12	120	14.35	318.4	14.2
0.184	12	240	15.62	447.2	129.1
0.196	12	240	11.49	388.7	115.8
0.184	5.24	240	8.22	200.9	75.8
0.182	5.24	240	4.12	202.8	72.0
0.200	18.92	240	18.09	518.3	218.5
0.154	18.92	240	19.09	638.7	234.4
0.186	28.33	240	21.82	791.2	306.2
0.174	28.33	240	24.46	640.3	187.7
0.202	53.21	240	29.3	742.9	153.5
0.208	53.21	240	28.64	699.6	100.4

BSMC35 mg cell protein	LDL, $\mu\text{g/ml}$	t, min	ng ^{125}I -LDL Bound	protein/mg Intern.	cell protein Degraded
0.199	7.91	2.0	1.62	1.27	0.0
0.220	7.91	2.0	1.66	1.37	0.0
0.218	7.91	2.0	1.52	0.87	0.0
0.294	7.91	5.0	1.05	1.8	6.6
0.299	7.91	5.0	1.59	3.6	0.0
0.326	7.91	10.	1.53	0.9	0.0
0.319	7.91	10.	1.16	1.8	0.0
0.311	7.91	10.	1.40	4.4	0.0
0.284	7.91	30.	1.47	13.5	0.0
0.319	7.91	30.	1.04	13.9	0.0
0.155	7.91	30.	1.48	20.0	0.0
0.355	7.91	60.	1.64	48.8	8.2
0.193	7.91	60.	4.26	31.1	23.5
0.208	7.91	60.	4.98	39.7	23.5
0.343	7.91	120	1.79	30.6	24.0
0.347	7.91	120	1.71	34.4	22.1
0.254	7.91	120	1.76	34.7	14.4
0.315	7.91	240	2.39	43.0	38.0
0.324	7.91	240	1.85	32.9	26.4
0.353	7.91	240	1.42	35.2	29.4
0.376	4.00	240	0.65	19.2	1.4
0.343	4.00	240	0.57	13.9	9.8
0.292	4.00	240	0.70	19.0	11.9
0.290	19.6	240	5.09	120.4	74
0.332	19.6	240	5.29	62.8	42.1
0.269	33.2	240	3.72	112.1	95.4
0.305	33.2	240	6.78	85.3	71.7
0.317	33.2	240	3.91	102.1	62.9
0.239	56.3	240	7.97	167.5	173.6
0.345	56.3	240	10.5	139.9	177.5
0.199	56.3	240	7.81	233.4	287.5

BSMC40 mg cell protein	LDL, $\mu\text{g/ml}$	t, min	ng ^{125}I -LDL Bound	protein/mg Intern.	cell protein Degraded
0.282	10.82	2.00	0.85	1.14	0.0
0.214	10.82	2.00	1.38	0.83	0.0
0.242	10.82	2.00	1.02	0.92	0.0
0.232	10.82	5.00	1.28	3.36	0.0
0.227	10.82	5.00	1.38	3.69	0.0
0.228	10.82	5.00	1.49	2.82	0.0
0.206	10.82	10.0	1.31	8.18	15.72
0.219	10.82	10.0	2.01	8.30	7.90
0.199	10.82	10.0	1.73	9.75	6.14
0.229	10.82	30.0	1.91	25.62	5.76
0.236	10.82	30.0	1.71	23.66	1.34
0.210	10.82	30.0	2.38	26.51	5.30
0.242	10.82	60.0	2.42	28.66	22.88
0.219	10.82	60.0	2.50	32.78	17.46
0.238	10.82	60.0	2.38	30.65	13.04
0.236	10.82	120.	2.03	34.0	13.33
0.231	10.82	120.	2.37	33.18	19.93
0.229	10.82	120.	2.65	34.33	22.85
0.283	10.82	240.	2.54	52.5	22.30
0.282	10.82	240.	2.35	44.2	45.78
0.261	10.82	240.	2.78	52.3	54.96
0.266	3.950	240.	2.16	31.0	32.7
0.274	3.950	240.	1.64	32.3	39.2
0.263	3.950	240.	1.52	30.0	42.7
0.251	20.64	240.	5.42	102.8	83.4
0.242	20.64	240.	5.83	109.3	127.5
0.253	20.64	240.	5.00	99.1	95.7
0.289	56.73	240.	8.23	129.7	94.3
0.265	56.73	240.	8.63	135.1	119.1
0.272	56.73	240.	7.53	135.7	146.9

2. Kinetic Studies: Receptor-Independent metabolism

BSMC6 mg cell protein	t, min	LDL, $\mu\text{g/ml}$	ng ^{125}I -LDL Bound	protein/mg Intern.	cell protein Degraded
0.282	2.97	15	10.13	7.8	0.0
0.280	2.24	15	10.13	10.0	0.0
0.269	3.45	15	10.13	9.1	2.3
0.260	5.38	30	10.13	11.6	0.0
0.239	2.46	30	10.13	10.1	0.0
0.282	2.58	30	10.13	11.6	2.5
0.297	3.0	60	10.13	16.9	0.0
0.265	3.1	60	10.13	18.1	1.6
0.260	3.3	60	10.13	21.1	0.0
0.286	2.4	120	10.13	24.2	1.3
0.299	2.6	120	10.13	23.4	8.8
0.295	9.4	120	10.13	22.3	8.8
0.269	2.6	240	10.13	31.0	12.1
0.277	2.6	240	10.13	31.9	24.0
0.282	2.1	240	10.13	31.5	25.1
0.269	7.0	360	10.13	33.3	16.8
0.237	2.1	360	10.13	29.4	25.5
0.243	2.3	360	10.13	28.6	25.0
0.244	0.58	240	1.00	3.5	0.7
0.256	0.46	240	1.00	4.3	1.2
0.286	0.31	240	1.00	4.3	1.2
0.252	2.65	240	5.35	19.7	3.0
0.269	1.75	240	5.35	20.1	8.8
0.301	2.54	240	5.35	22.1	12.0
0.252	4.4	240	10.13	29.9	5.5
0.271	3.5	240	10.13	31.4	17.6
0.280	5.5	240	10.13	36.6	19.9
0.284	8.3	240	22.80	91.8	26.7
0.300	10.4	240	22.80	84.8	41.9
0.280	14.9	240	60.90	180.1	95.0
0.282	10.3	240	60.90	151.6	126.2
0.303	11.3	240	60.90	204.9	121.8
0.275	30.9	240	108.0	309.6	161.0
0.282	20.9	240	108.0	354.4	274.7
0.284	20.8	240	108.0	340.3	256.6

BSMC10 mg cell protein	t, min	LDL, $\mu\text{g/ml}$	ng ^{125}I -LDL Bound	protein/mg Intern.	cell protein Degraded
0.340	2.91	5	10.42	2.7	0.0
0.322	4.11	5	10.42	5.6	0.0
0.387	6.51	5	10.42	5.6	1.89
0.260	1.68	10	10.42	6.53	0.0
0.252	1.94	10	10.42	4.71	2.07
0.254	1.47	10	10.42	3.95	0.82
0.239	1.84	15	10.42	6.93	0.0
0.263	2.38	15	10.42	9.06	0.11
0.200	5.26	15	10.42	8.62	3.43
0.226	1.20	20	10.42	11.90	0.0
0.211	2.73	20	10.42	7.20	0.0
0.290	0.85	20	10.42	6.72	0.0
0.185	5.14	30	10.42	8.16	0.0
0.209	3.65	30	10.42	8.80	0.0
0.179	5.56	30	10.42	11.0	4.98
0.260	0.98	60	10.42	8.84	0.0
0.260	1.38	60	10.42	10.64	0.76
0.250	6.04	60	10.42	9.92	1.46
0.175	1.46	120	10.42	13.82	0.0
0.179	1.39	120	10.42	13.87	0.0
0.222	1.44	120	10.42	13.12	1.08
0.155	2.03	240	10.42	19.60	16.07
0.203	2.83	240	10.42	19.11	12.85
0.194	1.47	240	10.42	19.82	14.62
0.291	0.77	240	1.01	1.89	0.0
0.269	0.39	240	1.01	1.78	0.13
0.293	0.42	240	1.01	1.95	0.18
0.196	1.08	240	2.00	5.50	0.0
0.186	1.34	240	2.00	5.15	3.13
0.192	1.00	240	2.00	5.04	1.68
0.284	1.11	240	5.07	8.78	3.18
0.302	0.64	240	5.07	7.75	6.05
0.262	0.66	240	5.07	7.56	0.0
0.243	2.39	240	10.42	17.47	0.0
0.264	2.13	240	10.42	17.14	7.71
0.275	2.54	240	10.42	18.11	7.96
0.354	5.62	240	15.00	35.4	31.5
0.326	10.4	240	15.00	33.4	15.0
0.310	12.4	240	15.00	44.1	14.8

0.267	--19.6	240	20.67	70.3	42.6
0.226	22.9	240	20.67	61.4	27.1
0.210	32.3	240	20.67	75.6	25.5
0.219	9.01	240	30.91	74.0	5.0
0.245	13.9	240	30.91	87.4	18.3
0.232	17.3	240	30.91	75.0	14.3
0.302	17.3	240	48.76	96.9	0.0
0.286	20.1	240	48.76	110.9	56.6
0.301	22.6	240	48.76	104.1	51.0
0.310	21.5	240	100.45	210.7	0.0
0.334	71.8	240	100.45	175.9	100.9
0.302	32.5	240	100.45	199.2	100.4

BSMC29 mg cell protein	t, min	LDL, $\mu\text{g/ml}$	ng ^{125}I -LDL Bound	protein/mg Intern.	cell protein Degraded
0.047	1.75	5	10830	8.89	0.0
0.047	1.64	5	10830	12.06	0.0
0.045	1.94	10	10830	15.7	0.0
0.049	3.59	10	10830	15.6	0.0
0.072	2.84	30	10830	15.21	52.5
0.064	1.35	30	10830	15.1	0.0
0.070	0.44	60	10830	19.90	25
0.055	0.84	60	10830	30.5	109.4
0.077	2.18	120	10830	32.14	52.8
0.087	1.50	120	10830	39.6	38.2
0.081	3.73	240	10830	52.5	18.7
0.068	3.69	240	10830	67.8	37.4
0.085	1.35	240	4330	30.2	4.5
0.066	0.15	240	4330	32.6	21.5
0.066	1.34	240	18100	124.5	9.8
0.072	2.54	240	18100	114.8	0.0
0.057	4.93	240	28980	169.4	224.5
0.055	3.58	240	28980	194.4	164.4
0.049	14.8	240	50370	418.0	149.3
0.057	12.2	240	50370	400.4	29.8

BSMC33 mg cell protein	t, min	LDL, $\mu\text{g/ml}$	ng ^{125}I -LDL Bound	protein/mg Intern.	cell protein Degraded
0.237	0.87	2	12000	2.06	0.0
0.223	1.11	2	12000	1.32	0.0
0.290	0.95	5	12000	4.27	0.0
0.284	1.35	5	12000	7.00	0.0
0.248	2.77	10	12000	10.8	0.0
0.168	1.23	10	12000	6.8	0.0
0.193	1.59	30	12000	16.9	0.0
0.151	1.07	30	12000	20.0	0.0
0.252	2.38	60	12000	25.1	0.0
0.313	1.50	60	12000	29.0	0.0
0.301	1.14	120	12000	30.6	0.0
0.414	0.91	120	12000	28.9	0.0
0.143	2.32	240	12000	51.2	61.9
0.240	1.86	240	12000	62.0	28.6
0.2220	0.88	240	5240	27.3	13.6
0.290	0.90	240	5240	24.5	0.3

BSMC35 mg cell protein	t, min	LDL, $\mu\text{g/ml}$	ng ^{125}I -LDL Bound	protein/mg Intern.	cell protein Degraded
0.237	0.70		9720	2.5	0.0
0.223	0.63	2	9720	2.0	0.0
0.290	0.95	5	9720	2.4	2.8
0.284	0.36	5	9720	2.3	7.3
0.248	0.54	10	9720	8.4	19.1
0.168	0.42	10	9720	9.4	40.6
0.193	0.66	30	9720	8.1	27.0
0.151	0.93	30	9720	11.2	41.6
0.252	0.81	60	9720	10.5	0.0
0.313	0.35	60	9720	8.2	0.0
0.301	0.84	120	9720	10.5	0.0
0.414	0.19	120	9720	7.9	0.0
0.143	1.70	240	9720	32.8	30.8
0.240	1.06	240	9720	21.8	5.4
0.220	3.58	240	51200	83.8	210.6
0.290	11.9	240	51200	82.8	166.3

BSMC40 mg cell protein	t, min	LDL, $\mu\text{g/ml}$	ng ^{125}I -LDL Bound	protein/mg Intern.	cell protein Degraded
0.223	0.88	2	10820	1.45	0.0
0.201	1.13	2	10820	1.90	0.0
0.310	0.42	2	10820	1.66	0.0
0.225	0.69	5	10820	3.13	0.0
0.225	0.75	5	10820	3.25	0.0
0.227	0.66	5	10820	3.08	0.0
0.219	1.01	10	10820	5.13	16.64
0.223	1.01	10	10820	4.15	6.18
0.231	0.80	10	10820	4.80	7.36
0.238	0.95	30	10820	7.69	3.72
0.206	0.57	30	10820	8.14	3.84
0.219	0.84	30	10820	8.61	7.38
0.236	0.63	60	10820	12.66	6.32
0.231	0.76	60	10820	10.80	6.84
0.238	0.54	60	10820	11.96	4.66
0.231	0.98	120	10820	15.10	17.32
0.227	1.22	120	10820	15.05	26.08
0.238	1.64	120	10820	16.74	11.14
0.278	1.13	240	10820	19.89	8.36
0.273	0.90	240	10820	19.01	30.32
0.285	1.12	240	10820	19.26	32.08
0.274	0.56	240	3950	8.89	4.33
0.280	0.48	240	3950	9.45	3.51
0.293	0.51	240	3950	9.61	7.17
0.263	1.69	240	20690	39.9	36.32
0.280	1.51	240	20690	38.0	21.32
0.257	2.02	240	20690	42.8	29.52
0.259	2.64	240	56730	96.3	94.5
0.251	3.89	240	56730	91.8	150.9
0.297	3.67	240	56730	84.9	86.5

3. Pulse Chase Experiments

BSMC15

t, min	ng LDL/mg		ng LDL/mg	
	Total Intern.	Total Degraded	Nonsp. Intern.	Nonsp. Degraded
0.0	35.2	0.0	6.2	0.0
0.0	28.4	0.0	6.4	0.0
0.0	28.8	0.0	7.5	0.0
15	23.2	2.5	5.4	0.7
15	24.2	2.5	7.0	0.7
15	21.3	3.9	6.9	0.4
30	18.2	2.4	5.3	0.5
30	22.7	4.1	6.5	0.8
30	30.3	6.2	5.9	1.1
45	18.2	2.4	5.5	0.5
45	20.9	3.0	5.4	0.9
45	19.7	3.1	5.1	0.5
60	18.8	2.5	4.7	0.5
60	20.2	3.9	4.7	0.5
60	24.6	3.6	4.6	0.8
120	10.1	3.3	4.2	0.5
120	16.9	4.5	4.2	0.5
120	13.3	2.5	4.3	0.5

BSMC21	t, min	ng LDL/mg		ng LDL/mg	
		Total Intern.	Total Degraded	Nonsp. Intern.	Nonsp. Degraded
	0.0	93.8	0.0	27.5	0.0
	0.0	101	0.0	28.1	0.0
	5.0	94.7	0.73	22.1	0.0
	5.0	84.5	0.61	18.0	0.0
	10	87.8	2.17	17.2	0.0
	10	79.9	2.17	19.8	0.0
	15	56.1	3.23	18.2	0.0
	15	73.7	1.88	18.1	0.0
	30	65.3	1.84	14.5	0.0
	30	69.0	1.72	15.9	0.0
	45	54.0	2.61	19.0	0.0
	45	66.9	3.28	12.9	0.0
	60	54.7	1.89	12.9	0.0
	60	55.3	2.61	14.5	0.0
	120	58.3	2.97	18.8	0.0
	120	44.1	3.63	12.0	0.0

BSMC26

t, min	ng LDL/mg		ng LDL/mg	
	Total Intern.	Total Degraded	Nonsp. Intern.	Nonsp. Degraded
0.0	36.2	0.0	10.1	0.0
0.0	40.0	0.0	10.1	0.0
0.0	38.8	0.0	9.1	0.0
5.0	35.5	4.5	9.1	3.4
5.0	40.7	6.8	9.7	3.0
5.0			9.2	4.2
11	33.4	3.4	9.5	4.4
11	37.2	4.7	8.2	3.1
11	36.3	4.0	8.4	3.5
22	31.0	6.6	7.8	3.3
22	35.3	7.1	11.0	2.3
22	39.6	6.2	9.3	3.0
30	29.4	5.0	8.5	2.9
30	28.1	5.5	8.4	2.5
30	30.5	5.3	8.7	1.5
45	22.4	3.2	8.4	0.1
45	26.6	4.0	7.5	3.2
45	26.1	3.7	7.6	2.4
60	21.4	3.8	7.6	0.0
60	22.9	4.1	7.9	1.7
60	32.9	8.5	7.5	0.5
120	19.8	9.1	9.2	0.2
120	20.9	12.1	7.3	0.9
120	22.7	8.6	6.4	0.0

FB31

t, min	ng LDL/mg		ng LDL/mg	
	Total Intern.	Total Degraded	Nonsp. Intern.	Nonsp. Degraded
0.0	144.4	0.0	109.6	0.0
0.0	135.4	0.0	145.2	0.0
0.0	185.8	0.0	151.3	0.0
16	114.4	7.7	86.2	0.6
16	109.0	7.4	108.3	0.2
16	117.6	10.9	100.0	0.1
29	107.6	12.1	67.0	0.0
29	109.7	11.2	71.0	0.7
29	109.7	11.2	73.7	0.8
44	103.6	22.3	84.6	0.7
44	120.0	32.0	63.3	2.4
44	107.0	26.3	1.1	3.0
56	105.2	30.9	70.5	2.6
56	103.4	29.2	87.8	5.2
56	140.8	34.2	62.2	3.1
69	83.8	26.0	105.2	2.6
69	83.6	29.1	38.6	5.4
69	88.0	32.5	39.3	3.2

FB36

t, min	ng LDL/mg		ng LDL/mg	
	Total Intern.	Total Degraded	Nonsp. Intern.	Nonsp. Degraded
0.0	118.5	0.0	46.7	0.0
0.0	120.2	0.0	38.5	0.0
0.0	135.0	0.0	32.9	0.0
0.0	167.7	0.0	32.9	0.0
10	93.8	4.5	25.1	0.0
10	93.1	3.2	23.6	0.3
10	107.7	5.1	25.3	0.1
10	113.2	8.2	22.3	1.0
20	86.0	7.9	24.2	0.6
20	93.7	7.5	22.2	0.8
20	101.3	9.7	22.2	0.8
20	121.0	10.5	22.2	0.8
30	83.2	12.7	21.8	1.9
30	95.9	16.9	13.6	0.7
30	100.8	16.5	19.9	2.0
30	81.6	18.1	14.7	1.7
45	68.6	20.8	17.8	2.7
45	73.1	23.4	19.3	3.9
45	79.5	22.8	19.5	4.2
45	72.3	25.5	18.3	4.1
58	64.7	34.7	10.7	2.3
58	61.0	31.4	17.6	5.4
58	78.2	39.7	18.2	6.1
58	91.1	49.4	15.1	5.0
120	36.6	27.1	11.8	3.5
120	49.6	38.9	14.4	5.9
120	52.4	39.8	14.8	4.9
120	54.3	43.2	11.1	4.6

4. Results of Trinitrobenzenesulfonic Acid Test

Cell Culture Experiments: BSMC38

Δ Abs at 280 nm

Conc, mg protein/ml	LDL	mLDL
0.8	0.36	0.25

In Vivo Experiments

1. 4M3

Δ Abs at 280 nm

Conc, mg protein/ml	LDL	mLDL
1.0	0.55 0.58	0.35
0.8	0.41 0.36	0.31
0.6	0.32	0.27

2. 24m3

Δ Abs at 280 nm

Conc, mg protein/ml	LDL	mLDL
1.0	0.65	
0.8	0.67 0.66	0.51
0.6	0.49 0.52	0.37

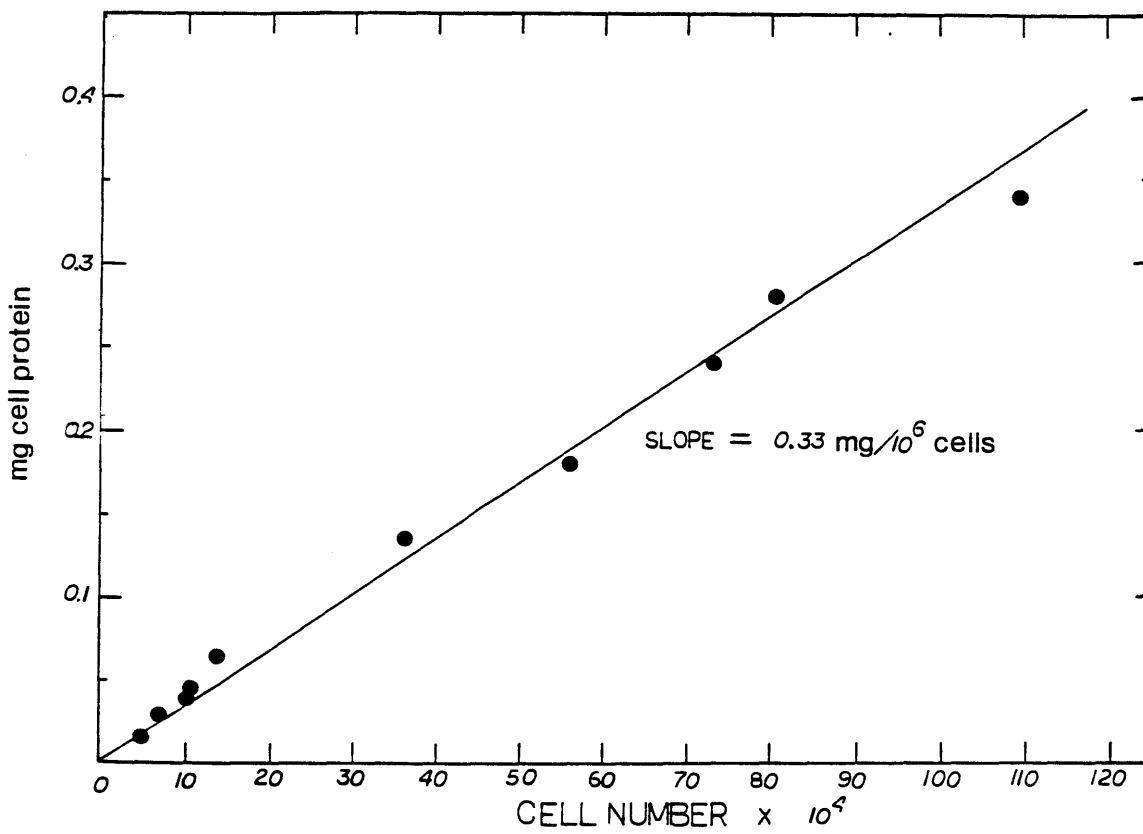


Figure F-1: Correlation between smooth muscle cell mass and cell number.

Appendix G

Data from In Vivo Experiments

This appendix contains all data obtained in in vivo experiments including plasma concentrations and transmural concentrations as well as the results of the calculations to determine the steady state profile in response to a step change in plasma concentration.

1. PLASMA DECAY CURVES OF ^{125}I -LDL

Expt. 30C1		Expt. 30C2		Expt. 30C3	
$C_{p_0} = 3.9 \times 10^7$ cpm/ml		$C_{p_0} = 3.4 \times 10^7$ cpm/ml		$C_{p_0} = 4.9 \times 10^7$ cpm/ml	
t, hr	C_p/C_{p_0}	t, hr	C_p/C_{p_0}	t, hr	C_p/C_{p_0}
0.10	0.95	0.09	0.87	0.09	0.95
0.26	0.91	0.27	0.75	0.26	0.87
0.43	0.82	0.43	0.55	0.42	0.80
Expt. 4C3		Expt. 4C4		Expt. 4C5	
$C_{p_0} = 3.3 \times 10^7$ cpm/ml		$C_{p_0} = 4.7 \times 10^7$ cpm/ml		$C_{p_0} = 5.1 \times 10^7$ [7] cpm/ml	
t, hr	C_p/C_{p_0}	t, hr	C_p/C_{p_0}	t, hr	C_p/C_{p_0}
0.09	1.00	0.10	1.00	0.09	1.03
0.50	0.89	0.49	0.90	0.50	0.85
1.02	0.81	1.51	0.80	1.49	0.58
1.98	0.63	2.51	0.68	2.49	0.43
2.87	0.54	3.58	0.57	3.50	0.35
3.46	0.49				
Expt. 4C6		Expt. 4C8			
$C_{p_0} = 4.37 \times 10^7$ cpm/ml		$C_{p_0} = 3.62 \times 10^7$ cpm/ml			
t, hr	C_p/C_{p_0}	t, hr	C_p/C_{p_0}		
0.14	0.94	0.08	1.02		
0.49	0.81	0.31	0.99		
1.52	0.51	1.49	0.68		
		2.70	0.63		
		3.81	0.55		

Expt. 24C1
 $C_{p_0} = 2.32 \times 10^7$ cpm/ml

t, hr	C_p/C_{p_0}
0.09	1.01
0.51	0.88
2.93	0.62
5.42	0.45
8.65	0.31
19.8	0.18
20.8	0.16
23.8	0.15

Expt. 24C2
 $C_{p_0} = 3.76 \times 10^7$

t, hr	C_p/C_{p_0}
0.08	0.98
0.50	0.92
2.00	0.74
3.75	0.62
7.22	0.51
22.0	0.24
23.7	0.23

Expt. 24C3
 $C_{p_0} = 5.65 \times 10^7$ cpm/ml

t, hr	C_p/C_{p_0}
0.08	0.98
0.52	0.91
2.03	0.69
4.3	0.57
8.4	0.40
21.0	0.21
22.5	0.20
24.0	0.19

Expt. 24C4
 $C_{p_0} = 3.04 \times 10^7$ cpm/ml

t, hr	C_p/C_{p_0}
0.08	0.98
0.36	0.84
2.35	0.51
4.13	0.37
17.9	0.14
23.9	0.09

Expt. 72C1
 3.21×10^7 cpm/ml

t, hr	C_p/C_{p_0}
0.08	0.98
0.51	0.86
2.33	0.54
7.00	0.24
24.5	0.094
47.6	0.034
72.0	0.016

Expt. 72C2
 3.26×10^7 cpm/ml

t, hr	C_p/C_{p_0}
0.10	0.98
0.46	0.81
2.68	0.57
20.7	0.13
26.2	0.074
41.3	0.016
48.7	0.010
71.9	0.005

Expt. 30M1

$$C_{p_0} = 3.57 \times 10^7 \text{ cpm/ml}$$

t, hr	C_p/C_{p_0}
0.08	0.98
0.25	0.94

Expt. 30M2

$$C_{p_0} = 2.16 \times 10^7 \text{ cpm/ml}$$

t, hr	C_p/C_{p_0}
0.08	0.95
0.14	0.91
0.21	0.87

Expt. 4M3

$$C_{p_0} = 4.79 \times 10^7 \text{ cpm/ml}$$

t, hr	C_p/C_{p_0}
0.09	1.03
0.52	0.91
1.50	0.84
2.53	0.75
3.53	0.73

Expt. 4M1 Expt 4M2

$$C_{p_0} = 1.55 \times 10^7 \text{ cpm/ml}$$

t, hr	C_p/C_{p_0}
0.13	1.01
0.25	1.00
0.51	0.95
0.96	0.93
1.51	0.91
2.48	0.86
2.99	0.82
3.83	0.81

Expt. 4M4

$$C_{p_0} = 1.71 \times 10^7 \text{ cpm/ml}$$

t, hr	C_p/C_{p_0}
0.08	1.00
0.25	0.96
1.05	0.82
1.48	0.81

$$C_{p_0} = 3.20 \times 10^7 \text{ cpm/ml}$$

t, hr	C_p/C_{p_0}
0.08	1.01
0.49	0.91
1.71	0.79
3.08	0.65
3.89	0.73

Expt. 24M1
 $C_{p_0} = 2.62 \times 10^7$ cpm/ml

t, hr	C_p/C_{p_0}
0.08	0.98
0.49	0.94
1.96	0.80
4.15	0.63
6.43	0.63
10.4	0.51
22.8	0.35
23.8	0.35

Expt. 24M2
 $C_{p_0} = 4.38 \times 10^7$ cpm/ml

t, hr	C_p/C_{p_0}
0.08	0.99
0.49	0.89
1.42	0.81
2.94	0.72
6.31	0.66
18.6	0.48
21.9	0.47
23.7	0.43

Expt. 24M3
 $C_{p_0} = 4.86 \times 10^7$ cpm/ml

t, hr	C_p/C_{p_0}
0.08	0.98
0.50	0.98
2.45	0.86
4.30	0.78
6.49	0.71
19.5	0.60
21.4	0.57
23.9	0.53

Expt. 24M4
 $C_{p_0} = 2.46 \times 10^7$ cpm/ml

t, hr	C_p/C_{p_0}
0.07	0.97
0.50	0.96
3.62	0.82
15.3	0.68
19.5	0.60
23.9	0.49

Expt. 72M1
 $C_{p_0} = 2.67 \times 10^7$ cpm/ml

t, hr	C_p/C_{p_0}
0.14	0.98
0.56	0.95
2.85	0.78
6.08	0.66
16.8	0.44
29.4	0.37
42.6	0.25
51.6	0.19
65.8	0.14
71.0	0.12

Expt. 72M2
 $C_{p_0} = 6.4 \times 10^7$ cpm/ml

t, hr	C_p/C_{p_0}
0.08	0.99
0.52	0.96
5.27	0.63
18.9	0.35
28.9	0.24
39.5	0.15
52.4	0.09
63.6	0.06
71.8	0.05

2. TRANSMURAL LDL PROFILES The radioactivity in each tissue slice was normalized with respect to the initial plasma concentration of radiolabeled lipoprotein as follows:

$$\frac{C_T}{C_{p_0}} = \frac{R/(A\Delta Lf)}{C_{p_0}} \quad (G-1)$$

where

R = net counting rate (counts/min)

A = area of tissue slice (cm²)

ΔL = thickness of tissue slice (cm)

C_{p₀} = net cpm/ml plasma at t = 0

f = area correction factor

The net counts per minute (R) for each sample was calculated by subtracting the background counting rate, R_b, from the observed sample counting rate, R_s:

$$R = R_s - R_b \quad (G-2)$$

The area in equation (G-1) was determined by weighing the outline of the tissue perimeter traced onto transparent plastic sheets. Knowing the weight of the sheet per cm², and the weight of the plastic tissue outline, the area of the tissue sample was calculated:

$$A = D \times W \quad (G-3)$$

where
D = weight of plastic sheet per cm²
W = weight of plastic sheet outline

The thickness (ΔL) of the tissue section was taken from the microtome setting.

In all studies the setting was 10 μm and two samples were counted in each tube.

Some slices represented some fraction, f , of the original area. This fraction was estimated visually as the tissue was being sliced.

Usually five to seven sections were taken from each aorta. These samples are coded beginning with the letters A through G. A represents samples above the first intercostal artery, B represents samples between the first and second intercostals, C represents samples between the second and third intercostals, D represents samples between the third and fourth intercostals, E represents samples between the fourth and fifth intercostals, F represents samples between the fifth and sixth intercostals, and G represents samples between the sixth and seventh intercostals.

Experiment 30C1: 0.5 hr

A30C1		B30C1		C30C1	
η	$\theta_T \times 10^3$	η	$\theta_T \times 10^3$	η	$\theta_T \times 10^3$
0.039	9.48	0.039	24.9	0.036	4.81
0.115	5.41	0.115	3.01	0.107	1.55
0.192	1.77	0.192	1.50	0.179	0.93
0.269	0.78	0.269	4.94	0.250	0.98
0.346	0.71	0.346	2.98	0.321	1.15
0.423	1.50	0.423	1.58	0.393	0.42
0.577	2.01	0.500	1.60	0.464	1.42
0.654	0.62	0.654	0.78	0.536	1.34
0.731	1.49	0.731	0.94	0.607	0.61
0.808	3.76	0.808	2.35	0.679	0.49
0.885	5.35			0.750	0.96
0.962	11.0			0.821	1.84

D30C1		E30C1		F30C1	
η	$\theta_T \times 10^3$	η	$\theta_T \times 10^3$	η	$\theta_T \times 10^3$
0.036	5.21	0.022	4.60	0.039	5.64
0.107	1.82	0.087	0.68	0.115	2.10
0.179	0.48	0.174	2.22	0.192	0.65
0.250	0.32	0.261	0.32	0.269	0.39
0.321	0.83	0.348	0.20	0.346	0.35
0.393	0.21	0.435	0.22	0.423	0.75
0.464	0.19	0.522	0.36	0.500	0.39
0.536	0.98	0.608	0.24	0.577	0.39
0.607	0.14	0.783	0.39	0.654	0.21
0.679	0.39	0.809	1.41	0.731	0.30
0.750	1.03			0.808	0.45
0.821	0.83			0.885	0.65
				0.962	2.57

η	G30C1 $\theta_T \times 10^3$
0.045	9.32
0.136	2.80
0.227	0.99
0.318	1.05
0.409	1.00
0.500	0.94
0.591	1.01
0.682	1.40

Experiment 30C2; 0.5 hr

A30C2		B30C2		C30C2	
η	$\theta_T \times 10^3$	η	$\theta_T \times 10^3$	η	$\theta_T \times 10^3$
0.039	11.5	0.022	5.50	0.023	6.98
0.115	2.76	0.174	2.14	0.091	6.25
0.192	1.15	0.261	1.22	0.182	1.62
0.269	0.75	0.348	0.60	0.273	0.46
0.346	0.80	0.435	0.77	0.364	0.17
0.423	1.40	0.522	0.62	0.455	0.23
0.500	0.54	0.609	0.33	0.546	0.26
0.577	0.52	0.696	1.56		
0.654	1.14	0.783	1.17		

D30C2		E30C2	
η	$\theta_T \times 10^3$	η	$\theta_T \times 10^3$
0.039	25.4	0.056	7.68
0.115	1.40	0.167	5.39
0.192	1.55	0.278	1.12
0.269	1.03	0.389	0.58
0.346	0.26	0.500	0.51
0.423	1.25	0.611	0.63
0.500	0.35		
0.577	0.09		

Experiment 30C3

A30C3		B30C3		C30C3	
η	$\theta_T \times 10^3$	η	$\theta_T \times 10^3$	η	$\theta_T \times 10^3$
0.042	6.58	0.046	6.34	0.023	10.7
0.125	6.06	0.136	3.57	0.091	4.24
0.208	2.61	0.227	2.21	0.182	4.09
0.295	1.63	0.318	1.68	0.273	2.99
0.375	1.19	0.409	1.36		
0.456	1.28	0.500	1.33		
0.542	1.12				
0.625	1.15				

D30C3		E30C3	
η	$\theta_T \times 10^3$	η	$\theta_T \times 10^3$
0.046	9.59	0.042	14.6
0.136	3.31	0.125	3.21
0.227	2.41	0.208	1.80
0.318	2.22	0.295	1.64
0.409	1.61	0.375	1.46
0.500	1.45	0.458	1.25
0.591	1.67	0.542	0.91
0.682	1.89	0.625	1.12
		0.708	1.44

Experiment 4C3; 4 hr

B4C3		C4C3		D4C3	
η	$\theta_T \times 10^3$	η	$\theta_T \times 10^3$	η	$\theta_T \times 10^3$
0.016	6.39	0.042	7.46	0.039	10.4
0.063	4.98	0.125	3.46	0.115	3.62
0.125	7.97	0.208	2.98	0.192	1.92
0.188	7.92	0.292	2.72	0.269	2.69
0.250	3.38	0.375	2.98	0.346	2.04
0.313	3.93	0.458	2.19	0.423	2.95
0.375	3.26	0.542	3.09	0.500	2.18
0.438	4.12	0.708	2.23	0.577	2.23
0.500	3.84	0.792	1.55		
0.563	3.04	0.875	2.71		
0.625	3.81	0.958	3.50		
0.688	2.98				
0.750	2.52				

E4C3		F4C3		G4C3	
η	$\theta_T \times 10^3$	η	$\theta_T \times 10^3$	η	$\theta_T \times 10^3$
0.042	8.05	0.136	16.6	0.046	21.2
0.125	3.60	0.227	7.89	0.136	6.85
0.208	2.14	0.318	4.11	0.227	2.34
0.292	2.24	0.409	3.63	0.318	4.18
0.375	1.25	0.500	4.37	0.409	3.18
0.458	1.65	0.591	3.53	0.500	2.59
0.542	2.23	0.682	6.26	0.591	5.10
0.625	1.97	0.773	6.33		
0.708	2.73	0.864	6.21		
0.792	2.09				
0.875	2.67				

Experiment 4C4: 4 hr

A4C4		B4C4		C4C4	
η	$\theta_T \times 10^3$	η	$\theta_T \times 10^3$	η	$\theta_T \times 10^3$
0.046	15.7	0.039	8.02	0.063	10.2
0.136	5.12	0.115	5.90	0.187	4.92
0.227	2.13	0.192	4.25	0.313	1.98
0.318	1.13	0.269	2.77	0.438	1.02
0.409	2.63	0.346	2.21	0.563	0.90
0.500	0.84	0.423	1.46	0.688	1.63
0.591	2.07	0.500	1.14		
0.082	1.47	0.577	2.24		

D4c4		E4C4		F4C4	
η	$\theta_T \times 10^3$	η	$\theta_T \times 10^3$	η	$\theta_T \times 10^3$
0.026	10.2	0.063	21.7	0.028	30.3
0.105	18.5	0.188	15.8	0.111	19.0
0.211	8.41	0.313	6.17	0.222	10.2
0.316	2.35			0.333	9.2
0.421	2.55			0.444	11.0
0.526	1.83				
0.632	1.69				

Experiment 4C5: 4 hr

A4C5		B4C5		C4C%	
η	$\theta_T \times 10^3$	η	$\theta_T \times 10^3$	η	$\theta_T \times 10^3$
0.042	9.42	0.022	11.2	0.036	7.28
0.125	5.49	0.087	7.31	0.107	3.84
0.208	4.27	0.174	5.86	0.179	4.69
0.292	4.10	0.261	3.31	0.250	3.77
0.375	3.59	0.348	4.28	0.321	3.39
0.458	3.34	0.440	3.37	0.393	4.47
0.542	2.67	0.522	2.55	0.404	5.51
0.625	4.22	0.608	2.85	0.536	3.20
		0.695	3.04	0.607	3.36
D4C5		E4C5		F4C5	
η	$\theta_T \times 10^3$	η	$\theta_T \times 10^3$	η	$\theta_T \times 10^3$
0.039	7.56	0.042	6.45	0.042	12.8
0.115	5.95	0.125	5.79	0.120	6.19
0.192	5.07	0.208	4.93	0.208	5.27
0.269	5.02	0.292	4.32	0.292	4.51
0.346	5.16	0.375	4.78	0.375	4.34
0.423	3.67	0.458	3.59	0.458	4.53
0.500	2.28	0.542	6.24	0.542	3.67
0.571	4.35	0.625	6.43	0.625	4.32
0.654	3.65	0.708	5.03		
0.731	3.14				

Experiment 4C6: 4 hr

A4C6		B4C6		C4C6	
η	$\theta_T \times 10^3$	η	$\theta_T \times 10^3$	η	$\theta_T \times 10^3$
0.046	13.9	0.042	11.6	0.039	22.2
0.136	14.0	0.125	12.1	0.115	14.4
0.227	8.22	0.208	10.9	0.192	9.77
0.318	12.7	0.292	8.53	0.269	17.8
0.409	10.7	0.375	8.22	0.346	20.5
0.500	7.50	0.458	4.92	0.423	7.25
		0.542	9.89	0.500	3.38
		0.625	10.94	0.654	7.31
				0.808	5.92
				0.885	5.77
				0.962	4.92

Experiment 4C8

B4C8		C4C8		D4C8	
η	$\theta_T \times 10^3$	η	$\theta_T \times 10^3$	η	$\theta_T \times 10^3$
0.024	3.01	0.050	8.39	0.028	7.20
0.095	1.79	0.150	2.19	0.091	1.37
0.191	1.16	0.250	0.84	0.182	0.69
0.286	0.57	0.350	0.66	0.272	0.58
0.381	0.66	0.450	0.54	0.304	0.69
0.476	0.48	0.550	0.63	0.455	0.83
0.571	0.78			0.546	0.86
0.668	0.65			0.636	1.52
				0.727	

E4C8		F4C8		G4C8	
η	$\theta_T \times 10^3$	η	$\theta_T \times 10^3$	η	$\theta_T \times 10^3$
0.056	6.95	0.028	5.08	0.028	5.82
0.167	2.30	0.111	3.66	0.108	2.84
0.278	1.06	0.222	0.97	0.167	0.85
0.389	0.52	0.333	0.40	0.278	0.64
0.500	0.48	0.444	0.78	0.389	0.55
0.611	0.65	0.556	0.62	0.500	0.53
0.722	0.66	0.667	1.31	0.611	0.56
0.833	0.88			0.722	3.94
0.944	3.28			0.833	10.4
				0.944	11.6

Experiment 24C1; 24 hr

η	A24C1 $\theta_T \times 10^3$	η	B24C2 $\theta_T \times 10^3$	η	C24C3 $\theta_T \times 10^3$
0.046	10.1	0.020	11.9	0.021	7.23
0.136	9.86	0.080	11.3	0.083	7.94
0.227	10.4	0.160	10.4	0.167	7.99
0.318	11.3	0.240	10.6	0.250	7.61
0.409	11.9	0.320	11.0	0.333	9.26
0.500	10.8	0.400	10.1	0.417	9.45
0.591	11.9	0.480	10.6	0.500	8.91
0.682	11.6	0.560	11.3	0.583	9.55
0.773	10.9	0.640	10.6	0.667	3.25
0.864	10.5	0.720	9.82	0.750	8.01
0.955	8.97			0.833	7.78

η	E24C1 $\theta_T \times 10^3$	η	G24C1 $\theta_T \times 10^3$
0.023	10.2	0.020	8.66
0.091	6.48	0.080	8.59
0.182	5.67	0.160	6.74
0.273	3.97	0.240	7.07
0.364	4/57	0.320	5.84
0.455	5.51	0.400	6.96
0.546	6.75	0.480	7.45
0.636	4.65	0.560	10.3
0.727	5.74	0.640	8.00
0.818	5.12		

Experiment 24C2: 24 hr

A24C2		B24C2		C24C2	
η	$\theta_T \times 10^3$	η	$\theta_T \times 10^3$	η	$\theta_T \times 10^3$
0.020	3.32	0.039	4.54	0.022	3.33
0.080	2.74	0.115	2.54	0.087	2.08
0.160	1.88	0.192	2.69	0.174	1.52
0.240	1.72	0.269	2.73	0.261	1.50
0.320	2.09	0.340	2.13	0.348	1.28
0.400	1.84	0.423	2.23	0.434	1.76
0.480	1.91	0.500	1.77	0.527	1.87
0.560	2.20	0.577	2.69	0.609	1.92
0.640	2.06	0.654	1.54	0.696	1.66
0.720	2.64	0.731	1.47		
0.800	3.23	0.808	2.08		
0.880	4.54				
0.960	3.85				

D24C2		E24C2		F24C2	
η	$\theta_T \times 10^3$	η	$\theta_T \times 10^3$	η	$\theta_T \times 10^3$
0.021	4.48	0.020	5.76	0.023	2.67
0.083	2.02	0.080	2.52	0.068	3.40
0.188	2.57	0.160	1.37	0.136	1.39
0.256	1.65	0.240	1.27	0.227	1.56
0.333	1.30	0.320	1.11	0.318	1.43
0.417	0.96	0.400	1.24	0.409	1.18
0.500	2.02	0.480	0.88	0.500	1.50
0.583	1.62	0.560	1.02	0.591	1.54
0.667	1.50	0.640	1.32	0.682	1.16
0.750	1.71				

G24C2	
η	$\theta_T \times 10^3$
0.023	3.75
0.095	1.96
0.191	0.82
0.286	0.80
0.381	0.74
0.476	0.63
0.571	0.73
0.667	0.77
0.762	1.02
0.857	1.75
0.952	4.11

Experiment 24C3: 24 hr

A24C3		B24C3		C24C3	
η	$\theta_T \times 10^3$	η	$\theta_T \times 10^3$	η	$\theta_T \times 10^3$
0.026	9.33	0.050	4.91	0.046	4.67
0.105	3.47	0.150	4.09	0.136	3.86
0.211	2.73	0.250	2.08	0.227	2.91
0.316	2.88	0.350	1.67	0.318	2.95
0.421	2.19	0.450	2.22	0.409	2.78
0.526	2.38	0.550	2.21	0.500	2.43
0.632	2.10	0.650	2.75	0.591	1.77
0.736	1.90	0.750	3.12	0.682	2.31
0.889	2.36	0.850	3.16		
0.947	2.35	0.950	4.31		

D24C3	
η	$\theta_T \times 10^3$
0.044	5.60
0.130	3.44
0.217	3.24
0.304	2.96
0.391	2.37
0.478	2.30
0.565	2.50
0.652	1.82
0.739	2.18

E24C3	
η	$\theta_T \times 10^3$
0.023	11.8
0.068	6.05
0.136	4.32
0.227	2.73
0.318	2.29

F24C3	
η	$\theta_T \times 10^3$
0.046	2.07
0.136	4.01
0.227	3.27
0.318	3.26
0.409	2.45
0.500	2.30
0.591	1.84

G24C3	
η	$\theta_T \times 10^3$
0.024	5.26
0.095	2.29
0.191	2.80
0.286	2.07
0.381	2.29
0.476	2.95
0.571	1.87
0.667	2.62
0.762	2.93

Experiment 24C4: 24 hr

A24C4		B24C4		D24C4	
η	$\theta_T \times 10^3$	η	$\theta_T \times 10^3$	η	$\theta_T \times 10^3$
0.02	3.14	0.021	2.86	0.019	2.11
0.06	2.83	0.063	1.99	0.058	2.04
0.10	1.93	0.104	1.78	0.096	1.92
0.14	1.87	0.146	1.51	0.135	1.97
0.18	1.55	0.208	8.21	0.173	3.49
0.24	1.44	0.292	2.20	0.212	7.49
0.34	1.37	0.375	1.81	0.269	1.79
0.40	1.75	0.458	1.76	0.346	1.43
0.48	1.63	0.542	1.80	0.423	2.26
0.56	1.96	0.625	2.17	0.500	2.28
0.64	1.22	0.708	2.27	0.577	1.43
0.72	1.78	0.792	2.07	0.654	2.24
0.80	1.81	0.875	2.98	0.731	1.93
0.88	2.39	0.958	2.65	0.808	2.01
0.96	2.84			0.885	1.96
				0.962	1.64

E24C4		F24C4		G24C4	
η	$\theta_T \times 10^3$	η	$\theta_T \times 10^3$	η	$\theta_T \times 10^3$
0.023	3.22	0.021	5.93	0.02	3.14
0.068	2.39	0.063	2.26	0.06	1.22
0.136	2.00	0.204	2.26	0.10	2.58
0.227	3.80	0.146	2.03	0.16	2.28
0.318	1.69	0.188	2.71	0.24	1.93
0.409	2.18	0.229	2.18	0.32	1.79
0.500	1.66	0.292	1.56	0.40	2.34
0.591	1.62	0.375	1.65	0.48	3.21
0.682	2.53	0.458	1.56	0.56	2.57
0.773	3.17	0.542	1.49	0.64	2.43
0.864	2.09	0.626	1.48	0.72	2.56
0.955	2.37	0.708	1.68	0.80	2.95
		0.792	2.30	0.88	3.12
		0.875	1.72	0.96	2.91
		0.958	1.74		

Experiment 72C1; 72 hr

A72C1		B72C1		C72C1	
η	$\theta_T \times 10^3$	η	$\theta_T \times 10^3$	η	$\theta_T \times 10^3$
0.046	1.25	0.024	2.09	0.05	1.30
0.136	2.31	0.095	0.77	0.15	0.85
0.217	0.60	0.191	0.77	0.25	0.86
0.318	1.68	0.286	0.47	0.35	0.36
0.409	1.75	0.364	0.47	0.45	1.03
0.500	1.40	0.476	0.69	0.55	0.68
0.591	0.98	0.571	0.65	0.65	0.67
0.682	1.70	0.607	0.82	0.75	1.20
0.773	1.11	0.762	1.41		
0.863	1.40	0.857	1.37		
		0.952	1.69		

D72C1		E72C1		F72C1	
η	$\theta_T \times 10^3$	η	$\theta_T \times 10^3$	η	$\theta_T \times 10^3$
0.023	0.65	0.025	0.98	0.05	0.71
0.091	0.48	0.10	0.78	0.15	0.62
0.182	0.56	0.20	0.44	0.25	0.38
0.273	0.50	0.30	0.43	0.35	0.65
0.364	0.65	0.40	0.41	0.45	0.47
0.455	0.59	0.475	0.33	0.55	0.49
0.546	0.53	0.55	0.38	0.65	0.64
0.636	0.58	0.65	0.61	0.75	0.48
0.727	0.66	0.75	1.10	0.85	0.91
		0.85	1.43	0.95	1.34
		0.95	1.98		

Experiment 72C2

B72C2		C72C2		D72C2	
η	$\theta_T \times 10^3$	η	$\theta_T \times 10^3$	η	$\theta_T \times 10^3$
0.046	0.23	0.022	0.53	0.05	1.29
0.136	0.21	0.087	0.36	0.15	0.38
0.227	0.12	0.174	0.21	0.25	0.37
0.318	0.17	0.261	0.22	0.35	0.65
0.409	0.24	0.347	0.19	0.45	0.35
0.500	0.33	0.435	0.13	0.55	0.38
0.591	0.52				
0.682	0.16				
0.773	0.25				

E72C2		F72C2		G72C2	
η	$\theta_T \times 10^3$	η	$\theta_T \times 10^3$	η	$\theta_T \times 10^3$
0.026	2.26	0.024	0.57	0.05	0.37
0.105	1.10	0.095	0.87	0.15	0.22
0.211	0.27	0.191	0.33	0.25	0.27
0.316	0.26	0.286	0.48	0.35	0.37
0.421	0.63	0.381	0.53	0.45	0.72
0.526	0.09	0.476	0.44	0.55	0.46
0.632	0.01	0.571	0.79	0.65	0.18
0.737	0.27	0.667	0.41	0.75	
0.842	0.37	0.762	0.23		
0.947	0.18	0.857	0.66		
		0.952	0.55		

Transmural mLDL Profiles

Experiment 30M1: 0.5 hr

A30M1		B30M1		C30M1	
η	$\theta_T \times 10^3$	η	$\theta_T \times 10^3$	η	$\theta_T \times 10^3$
0.125	5.12	0.042	7.99	0.05	13.5
0.208	3.44	0.125	2.61	0.15	5.85
0.292	0.29	0.208	0.34	0.25	3.18
0.375	0.31	0.292	0.47	0.35	0.53
0.458	0.41	0.376	0.31	0.45	0.92
0.542	0.38	0.458	0.42	0.55	0.82
0.625	0.61	0.542	0.47	0.75	0.86
0.708	0.63	0.625	0.28	0.85	1.33
0.792	0.69	0.708	0.31	0.95	1.83
0.875	1.39	0.792	0.42		
0.958	2.15	0.875	0.59		
		0.953	3.99		
D30M1		E30M1		F30M1	
η	$\theta_T \times 10^3$	η	$\theta_T \times 10^3$	η	$\theta_T \times 10^3$
0.118	11.0	0.167	11.5	0.056	6.24
0.205	1.23	0.278	4.49	0.167	4.65
0.353	1.20	0.389	3.22	0.278	3.49
0.471	0.71	0.500	1.32	0.389	2.03
0.488	1.32			0.500	1.298
0.706	0.81			0.611	0.66
0.824	0.89			0.722	2.44
				0.833	1.678
				0.944	2.93

Experiment 30M2: 0.5 hr

A30M2		C30M2		D30M2	
η	$\theta_T \times 10^3$	η	$\theta_T \times 10^3$	η	$\theta_T \times 10^3$
0.028	4.16	0.026	7.91	0.063	22.4
0.111	1.61	0.105	3.23	0.188	2.18
0.222	0.60	0.211	1.50	0.313	1.51
0.333	0.92	0.316	0.59	0.438	0.18
0.444	1.57	0.421	0.40	0.563	0.04
0.556	2.48	0.526	0.35	0.688	1.29
		0.632	1.07		

E30M2		F30M2		G30M2	
η	$\theta_T \times 10^3$	η	$\theta_T \times 10^3$	η	$\theta_T \times 10^3$
0.028	13.6	0.024	14.1	0.026	13.3
0.083	2.13	0.071	3.34	0.079	4.84
0.167	0.89	0.119	1.78	0.132	1.48
0.278	0.51	0.167	1.50	0.211	0.69
0.389	0.63	0.238	0.70	0.263	0.56
0.500	0.12	0.333	0.32	0.368	0.47
0.611	0.29	0.429	0.41	0.474	0.07
0.722	0.34	0.524	0.77	0.579	0.35
		0.548	1.49	0.684	0.77
				0.711	2.32
				0.763	3.66

Experiment 4M1: hr

A4M1		B4M1	C4M1		
η	$\theta_T \times 10^3$	η	$\theta_T \times 10^3$	η	$\theta_T \times 10^3$
0.039	4.34	0.032	7.39	0.069	7.88
0.115	1.48	0.097	6.01	0.138	2.85
0.192	1.33	0.161	2.60	0.207	1.88
0.269	0.85	0.226	2.94	0.276	1.16
0.235	0.76	0.290	1.69	0.345	1.47
0.423	0.77	0.355	1.27	0.414	1.14
0.500	0.72	0.419	2.02	0.483	1.66
0.577	1.48	0.484	4.54	0.552	0.62
0.654	2.25	0.548	7.85	0.621	1.34
0.731	5.15	0.613	8.02	0.690	3.59
0.808	7.43	0.677	9.01	0.759	9.36
0.885	10.2	0.742	13.3	0.828	15.57
		0.968	12.8		

D4M1		E4M1	F4M1		
η	$\theta_T \times 10^3$	η	$\theta_T \times 10^3$		
0.136	3.31	0.095	10.5	0.115	4.59
0.227	3.38	0.191	4.23	0.192	2.14
0.318	1.80	0.285	2.01	0.269	1.34
0.409	1.45	0.381	0.66	0.346	1.76
0.500	1.03	0.476	0.64	0.423	2.14
0.591	1.21	0.571	2.73	0.500	1.76
		0.667	5.69	0.577	3.70
				0.654	9.03

η	G4M1 $\theta_T \times 10^3$
0.107	9.47
0.179	3.97
0.250	3.88
0.321	1.55
0.393	2.15
0.464	2.33
0.536	3.41
0.607	2.18
0.679	3.03
0.750	7.18

Experiment 4M2: 4 hr

A4M2		B4M2		C4M2	
η	$\theta_T \times 10^3$	η	$\theta_T \times 10^3$	η	$\theta_T \times 10^3$
0.259	2.54	0.136	3.30	0.05	6.96
0.370	1.37	0.227	1.57	0.15	2.31
0.444	0.54	0.318	0.76	0.25	2.35
0.519	0.46	0.409	0.50	0.35	1.51
0.593	0.68	0.500	2.08	0.45	0.87
0.667	1.12	0.591	1.03	0.55	1.00
0.741	2.65	0.682	2.06	0.65	2.63
0.815	4.08	0.773	3.60		
0.889	6.11	0.864	4.28		
		0.955	5.23		

D4M2		E4M2		F4M2	
η	$\theta_T \times 10^3$	η	$\theta_T \times 10^3$	η	$\theta_T \times 10^3$
0.046	19.0	0.05	6.96	0.046	6.54
0.134	5.87	0.15	2.30	0.136	4.38
0.227	3.17	0.25	1.13	0.227	3.89
0.318	2.12	0.35	0.25	0.318	1.08
0.409	1.95	0.45	0.37	0.409	0.90
0.500	1.01	0.55	0.23	0.500	0.44
0.591	1.71	0.65	0.39	0.591	1.11
0.682	4.49	0.75	0.63	0.682	1.87
		0.85	1.70	0.773	2.63
		0.95	3.28	0.864	4.31
				0.955	8.72

Experiment 4M3; 4 hr

A4M3		B4M3		C4M3	
η	$\theta_T \times 10^3$	η	$\theta_T \times 10^3$	η	$\theta_T \times 10^3$
0.026	10.6	0.056	5.28	0.063	9.83
0.105	5.33	0.167	3.43	0.188	7.31
0.211	5.45	0.278	2.21	0.313	4.21
0.316	4.73	0.389	2.66		
0.421	3.92	0.500	2.58		
0.526	2.55	0.611	3.67		
0.632	2.85	0.722	2.68		
0.737	6.27				
0.842	10.30				
0.947	15.18				

D4M3		E4M3		F4M3	
η	$\theta_T \times 10^3$	η	$\theta_T \times 10^3$	η	$\theta_T \times 10^3$
0.071	7.76	0.045	3.73	0.022	13.7
0.143	5.50	0.136	2.33	0.087	4.23
0.238	4.26	0.227	2.03	0.174	4.76
0.333	5.21	0.318	2.04	0.261	1.11
0.429	2.31	0.409	1.89	0.348	1.48
0.524	2.41	0.500	2.01	0.435	2.69
0.619	2.39			0.522	2.21
				0.609	4.00

G4M3	
η	$\theta_T \times 10^3$
0.040	4.93
0.120	1.99
0.200	2.45
0.280	2.39
0.360	2.01
0.440	2.47
0.520	1.93

Experiment 4M4: 4 hr

A4M4		B4M4		C4M4	
η	$\theta_T \times 10^3$	η	$\theta_T \times 10^3$	η	$\theta_T \times 10^3$
0.019	10.4	0.028	18.7	0.02	14.9
0.056	7.22	0.063	5.56	0.06	6.19
0.093	3.23	0.125	2.05	0.12	2.98
0.130	4.13	0.208	1.27	0.20	2.85
0.167	3.45	0.292	1.60	0.28	1.10
0.204	3.60	0.375	1.43	0.36	0.91
0.241	2.12	0.458	1.41	0.44	0.54
0.296	1.67	0.542	2.72	0.52	0.69
0.370	1.18	0.625	1.94	0.60	1.32
0.444	1.73			0.68	1.63
0.519	1.28				
0.593	1.33				
0.667	2.55				
0.741	5.67				

D4M4		E4M4		F4M4	
η	$\theta_T \times 10^3$	η	$\theta_T \times 10^3$	η	$\theta_T \times 10^3$
0.021	9.61	0.02	10.0	0.026	13.7
0.063	9.65	0.06	5.46	0.105	2.60
0.125	2.46	0.10	2.99	0.211	2.07
0.208	1.11	0.16	1.25	0.316	1.90
0.292	0.38	0.24	2.44	0.421	1.53
0.375	1.34	0.32	1.38	0.526	1.54
0.458	0.19	0.40	1.81		
0.542	1.22	0.48	2.25		
0.625	0.78				

Experiment 24M1: 24 hr

A24M1		B24M1		D24M1	
η	$\theta_T \times 10^3$	η	$\theta_T \times 10^3$	η	$\theta_T \times 10^3$
0.024	9.96	0.042	4.49	0.046	5.04
0.095	4.81	0.125	3.50	0.136	4.17
0.190	3.61	0.208	3.73	0.227	4.36
0.286	4.85	0.292	3.98	0.318	3.40
0.381	3.17	0.375	3.80	0.409	2.52
0.476	3.45	0.458	3.15	0.500	2.42
0.571	3.30	0.542	3.03	0.591	2.19
0.667	2.90	0.625	2.61	0.682	2.06
0.762	3.11	0.708	3.43	0.773	2.04
0.857	5.24	0.792	4.70		
		0.875	6.41		
		0.958	5.02		

E24M1	
η	$\theta_T \times 10^3$
0.042	4.47
0.125	3.72
0.208	3.86
0.292	3.73
0.375	4.20
0.458	4.04
0.542	3.14
0.625	3.31
0.708	3.38

Experiment 24M2: 24 hr

η	A24M2 $\theta_T \times 10^3$	η	B24M2 $\theta_T \times 10^3$	η	E24M2 $\theta_T \times 10^3$
0.05	2.05	0.024	3.42	0.022	4.60
0.15	1.16	0.095	1.61	0.087	0.95
0.25	1.04	0.191	1.37	0.174	0.79
0.35	1.55	0.286	0.88	0.261	0.59
0.45	0.92	0.381	0.88	0.348	0.71
0.65	0.74	0.476	0.83	0.434	0.75
0.75	1.77	0.571	0.91	0.522	0.44
		0.667	0.70	0.609	0.49
		0.762	0.72	0.696	0.91
		0.833	1.41	0.783	0.60
		0.952	2.33	0.870	0.98

Experiment 24M3

A24M3		B24M3		C24M3	
η	$\theta_T \times 10^3$	η	$\theta_T \times 10^3$	η	$\theta_T \times 10^3$
0.046	11.0	0.04	6.52	0.022	5.82
0.136	7.43	0.08	3.31	0.087	2.92
0.227	6.06	0.16	2.67	0.174	2.81
0.318	4.66	0.24	2.01	0.261	2.30
0.409	3.00	0.32	2.12	0.348	1.81
0.500	2.82	0.40	1.49	0.435	1.62
0.591	2.18	0.48	1.08	0.522	1.07
0.682	1.89	0.56	0.85	0.609	1.20
0.773	1.66	0.64	0.60	0.696	1.18
0.864	2.82	0.72	0.73	0.783	2.25
		0.80	1.43	0.870	3.06
		0.88	3.81	0.957	5.09
		0.96	9.20		

D24M3		E24M3		F24M3	
η	$\theta_T \times 10^3$	η	$\theta_T \times 10^3$	η	$\theta_T \times 10^3$
0.022	6.96	0.022	5.96	0.024	6.52
0.087	3.03	0.087	3.45	0.095	3.57
0.174	2.45	0.174	2.44	0.191	2.63
0.261	2.26	0.261	2.05	0.286	2.37
0.348	2.23	0.348	1.79	0.381	1.87
0.435	1.64	0.435	1.54	0.476	1.32
0.522	1.71	0.522	1.28	0.571	1.74
0.609	1.17	0.609	1.35	0.667	1.44
0.696	1.29	0.694	1.00	0.762	1.83
0.783	1.35	0.783	1.67	0.857	3.16
		0.870	2.59	0.952	4.57
		0.957	4.31		

Experiment 24M4: 24 hr

H24M4		G24M4		F24M4	
η	$\theta_T \times 10^3$	η	$\theta_T \times 10^3$	η	$\theta_T \times 10^3$
0.026	7.02	0.025	2.97	0.024	3.72
0.077	2.67	0.075	0.74	0.071	2.97
0.132	1.74	0.150	1.18	0.119	1.18
0.211	0.91	0.250	0.90	0.191	0.71
0.312	1.58	0.350	0.65	0.286	0.59
0.421	3.17	0.450	0.75	0.381	0.29
0.526	0.45	0.550	0.94	0.476	0.24
0.632	1.80	0.650	1.02	0.571	0.98
0.736	5.48	0.750	8.02	0.667	2.04
		0.850	17.4	0.702	3.70
				0.857	5.93
				0.952	7.32

E24M3		D24M3		C24M3	
η	$\theta_T \times 10^3$	η	$\theta_T \times 10^3$	η	$\theta_T \times 10^3$
0.024	6.03	0.024	6.08	0.031	3.27
0.095	3.38	0.095	2.90	-0.094	1.16
0.191	0.81	0.191	0.77	0.188	1.24
0.286	0.91	0.286	0.40	0.313	1.12
0.381	0.61	0.380	0.72	0.458	1.02
0.476	0.66	0.500	0.34	0.563	1.06
0.571	1.19	0.571	0.62	0.688	1.10
0.667	1.96	0.667	1.91	0.813	1.19
0.762	4.60	0.762	4.23	0.938	3.92
0.857	7.05	0.857	4.64		
0.952	0.13	0.952	5.40		

η	A24M4 $\theta_T \times 10^3$
0.024	2.90
0.095	1.16
0.190	1.24
0.286	1.11
0.381	1.20
0.476	1.46
0.571	1.94

Experiment 72M1: 72 hr

G72M1		F72M1		E72M1	
η	$\theta_T \times 10^3$	η	$\theta_T \times 10^3$	η	$\theta_T \times 10^3$
0.046	1.64	0.046	1.67	0.05	1.70
0.136	0.34	0.136	0.47	0.15	0.37
0.227	0.25	0.227	0.53	0.25	0.35
0.318	0.49	0.318	0.73	0.35	0.41
0.409	0.14	0.409	0.49	0.45	0.52
0.500	0.25	0.500	0.68	0.55	0.49
0.591	0.29	0.591	0.26	0.65	0.69
0.682	0.44	0.682	0.76	0.75	0.72
		0.773	1.06		
		0.864	1.65		

D72M1		C72M1		B72M1	
η	$\theta_T \times 10^3$	η	$\theta_T \times 10^3$	η	$\theta_T \times 10^3$
0.04	2.26	0.042	1.22	0.046	1.45
0.12	1.43	0.125	0.31	0.136	0.53
0.20	0.97	0.208	0.25	0.227	0.36
0.28	0.50	0.292	0.22	0.318	0.27
0.36	0.52	0.375	0.28	0.409	0.23
0.44	0.63	0.458	0.38	0.500	0.29
0.52	0.50	0.542	0.24	0.591	0.39
		0.625	0.46	0.682	0.40
		0.708	0.63	0.773	0.45

η	$\theta_T \times 10^3$
0.042	1.67
0.125	0.40
0.208	0.56
0.292	0.44
0.375	0.28
0.458	0.45
0.542	0.44
0.625	0.52
0.708	0.49
0.792	0.72
0.876	1.37

Experiment 72M2: 72 hr

G72M2		F72M2		D72M3	
η	$\theta_T \times 10^3$	η	$\theta_T \times 10^3$	η	$\theta_T \times 10^3$
0.036	1.22	0.019	0.95	0.042	1.25
0.107	0.68	0.074	1.04	0.125	0.53
0.179	0.47	0.148	0.58	0.208	0.46
0.250	0.72	0.222	0.95	0.292	0.24
0.321	0.75	0.296	1.00	0.375	0.38
0.392	0.51	0.370	0.84	0.458	0.35
0.464	0.71	0.444	1.40	0.542	0.30
0.536	0.70	0.519	1.08	0.625	0.61
0.607	1.13	0.593	1.29	0.708	0.60
		0.667	1.39	0.792	0.62
				0.875	0.88
				0.958	1.07

C72M1		B72M1		A72M1	
η	$\theta_T \times 10^3$	η	$\theta_T \times 10^3$	η	$\theta_T \times 10^3$
0.042	1.01	0.042	0.61	0.039	1.46
0.125	0.63	0.125	0.50	0.115	1.04
0.208	0.14	0.208		90	0.192
0.292	0.62	0.292	0.46	0.269	0.94
0.375	0.65	0.375	0.09	0.346	0.83
0.458	0.50	0.458	0.08	0.423	0.59
0.542	0.43	0.542	0.64	0.500	0.37
0.625	0.78	0.625	0.35	0.577	0.79
0.708	0.91	0.708	0.76	0.654	0.51
0.792	0.63	0.792	0.31		
0.875	0.98	0.875	0.60		
0.958	0.86	0.958	1.15		

Best-Fit Empirical Curves of Transmural Profiles

$$\theta_T = \bar{\alpha}(e^{-\beta_1 t} - e^{-\beta_2 t})$$

LDL: all profiles

η	$\alpha \times 10^3$	β_1, hr^{-1}	β_2, hr^{-1}
0.032	12.6 ± 0.3	0.034 ± 0.002	3.40 ± 0.032
0.103	9.74 ± 0.70	0.041 ± 0.006	0.95 ± 0.17
0.194	6.87 ± 1.80	0.028 ± 0.011	0.61 ± 0.40
0.296	6.96 ± 1.73	0.034 ± 0.009	0.34 ± 0.12
0.397	8.05 ± 2.92	0.037 ± 0.013	0.21 ± 0.07
0.492	8.33 ± 3.00	0.037 ± 0.012	0.18 ± 0.08
0.591	10.4 ± 3.1	0.040 ± 0.008	0.14 ± 0.03
0.686	6.57 ± 1.86	0.032 ± 0.009	0.22 ± 0.07
0.785	5.12 ± 0.17	0.025 ± 0.001	0.66 ± 0.06
0.882	6.00 ± 0.26	0.028 ± 0.003	1.12 ± 0.13
0.957	5.85 ± 0.83	0.022 ± 0.018	1097 ± 0.0

LDL: without 4C6 and 24C1

0.032	12.8 ± 0.7	0.041 ± 0.005	3.31 ± 0.55
0.103	9.24 ± 1.18	0.049 ± 0.012	1.03 ± 0.30
0.194	5.33 ± 0.35	0.030 ± 0.004	0.95 ± 0.17
0.296	3.59 ± 0.06	0.026 ± 0.001	0.86 ± 0.04
0.397	3.34 ± 0.07	0.024 ± 0.001	0.71 ± 0.04
0.492	2.99 ± 0.04	0.021 ± 0.005	0.62 ± 0.24
0.591	3.21 ± 0.11	0.024 ± 0.001	0.55 ± 0.05
0.686	3.15 ± 0.21	0.021 ± 0.003	0.74 ± 0.14
.785	4.51 ± 0.29	0.026 ± 0.004	0.81 ± 0.15
.882	4.18 ± 0.01	0.021 ± 0.001	1.83 ± 0.01
0.957	6.79 ± 0.58	0.029 ± 0.008	846018 ± 0.01

mLDL η	$\alpha \times 10^3$	β_1, hr^{-1}	β_2, hr^{-1}
0.031	11.9 ± 0.2	0.031 ± 0.001	4.92 ± 0.37
0.104	5.72 ± 0.03	0.028 ± 0.001	4.14 ± 0.10
0.198	3.38 ± 0.37	0.021 ± 0.005	1.46 ± 0.44
0.292	2.42 ± 0.68	0.016 ± 0.010	0.86 ± 0.77
0.397	2.99 ± 1.84	0.024 ± 0.019	0.27 ± 0.23
0.500	2.78 ± 0.63	0.023 ± 0.007	0.39 ± 0.16
0.596	2.30 ± 0.10	0.018 ± 0.001	0.87 ± 0.01
0.675	5.96 ± 1.55	0.045 ± 0.013	0.51 ± 0.24
0.784	10.2 ± 4.0	0.058 ± 0.018	0.41 ± 0.21
0.870	10.9 ± 0.3	0.032 ± 0.001	0.36 ± 0.02
0.957	9.42 ± 1.11	0.025 ± 0.006	0.76 ± 0.26

Appendix H Computer Codes

This Appendix contains the computer codes used in Chapters 2 and 5. The program used to calculate the determinant of the matrix F consists of a main program, MRA, which calls all subroutines. The user supplies a model to be fit to the data which is contained in the subroutine MODEL. Two model programs have been supplied one used to fit receptor-mediated binding to a lumped model with exocytosis and the other to calculate the in vivo tissue concentrations at 0.5 hr. MRA calls the subroutine MVEST which, in turn, calls the subroutine MODEL in order to calculate the minimum to $\det(F)$. MVEST also calls three other subroutines, INVERT, PIVOT, and MDERIV.

```
C   THIS PROGRAM CALCULATES THE OBJECTIVE FUNCTION FOR THE ANALYSIS OF
C   MULTIRESPONSE DATA. THE OBJECTIVE FUNCTION USED IS THAT DERIVED BY
C   BOX AND DRAPER (BIOMETRIKA, 52; 355-365; 1965). THE MAIN PROGRAM
C   READS THE NUMBER OF DATA POINTS, N, THE DATA POINTS FOR THE RESPONSES
C   Y1,Y3,Y2 AS WELL AS PARAMETER ESTIMATES. THE SUBROUTINE MVEST IS CALLED
C   TO CALCULATE THE OBJECTIVE FUNCTION, THE VALUE OF WHICH IS RE-
C   TURNED TO THE MAIN PROGRAM AND PRINTED.
C
C
```

```
      IMPLICIT DOUBLE PRECISION(A-H,O-Z)
      DIMENSION BETA(3),Y(3,300),X(1,300),PW(3,300,3),A(3,300),
1A1(3,300)
      DIMENSION YSUM(3),YBAR(3),SSREG(3),SSQR(3),XMSREG(3),XMSRES(3),
1XF(3)
      COMMON/CC/NO,NI,YZ(3,100)
      OPEN(1,FILE='IN1')
      OPEN(2,FILE='IN2')
      OPEN(3,FILE='OUT')
      READ (1,*) NDATA,NO,NPAR,NI
      DO 10 I=1,NDATA
      READ (1,*) (X(L,I),L=1,NI),(Y(J,I),J=1,NO)
10  CONTINUE
      READ (2,*) (BETA(K),K=1,NPAR)
```

```
C
C   INITIALIZE
      DEL=1.0E-04
      NFIG=5
      RLAM=0.01
      FACT=10.0
      RLMAX=1.0D+06
      RLMIN=1.0D-06
      MAXITR=50
```

```
CALL MVEST(DEL,NFIG,NDATA,RLAM,FACT,RLMAX,RLMIN,MAXITR,  
1NI,NO,NPAR,BETA,Y,X,PW,A,A1)  
DO 20 I=1,3  
  YSUM(I)=0.0  
  YBAR(I)=0.0  
20 CONTINUE  
DO 22 I=1,3  
DO 21 J=1,NDATA  
21 YSUM(I)=YSUM(I)+Y(I,J)  
22 YBAR(I)=YSUM(I)/FLOAT(NDATA)  
DO 23 I=1,3  
23 PRINT*, 'YBAR(I)= ',YBAR(I)  
END
```



```

C      THIS SUBROUTINE CALCULATES PREDICTED VALUES OF THE FUNCTIONS
C      AND THE RESIDUALS USED IN THE ANALYSIS OF
C      MULTIRESPONSE DATA.
C
C      SUBROUTINE MODEL(Y,X,BETA,NPAR,NDATA,A)
C      IMPLICIT DOUBLE PRECISION(A-H,O-Z)
C      REAL K1,K11,K2,K3,K,KINT,KX,K3L,K3D
C      DIMENSION BETA(5),Y(3,50),X(2,50),A(3,50)
C
C      SPECIFY THE FUNCTIONS, CFI(X), WHICH ARE TO BE FITTED TO DATA.
C
C      CF1(X)=RO*LO/(LO+KINT)*(1.0-EXP(-K*X))
C      CF2(X)=K2*RO*LO/(KINT+LO)*((1.0-EXP(-KX*X))/KX
1+ (EXP(-KX*X)-EXP(-K*X))/(KX-K))
C      CF3(X)=K3*K2*RO*LO/(LO+KINT)*(X/KX+(EXP(-(KX)*X)-1.0)/(KX*KX)
1- ((1-EXP(-K*X))/K-(1-EXP(-KX*X))/KX)/(KX-K))
C      K1=BETA(1)*BETA(1)
C      K2=BETA(2)*BETA(2)
C      K3=BETA(3)*BETA(3)
C      KX=BETA(4)*BETA(4)
C      RO=BETA(5)
C      K11=0.0
C      KINT=(K11+K2)/K1
C
C      CALCULATE RESIDUALS
C
C      DO 20 I=1,NDATA
C      T=X(2,I)
C      LO=X(1,I)
C      K=(K1+LO+K11+K2)
C      A(1,I)=Y(1,I)-CF1(T)
C      A(2,I)=Y(2,I)-CF2(T)
C      A(3,I)=Y(3,I)-CF3(T)
20  CONTINUE
C      RETURN
C      END

```

SUBROUTINE MVEST(DEL,NFIG,NDATA,RLAM,FACT,RLMAX,RLMIN,MAXITR,NI,
1NO,NPAR,BETA,Y,U,PW,A,A1)

IMPLICIT DOUBLE PRECISION(A-H,O-Z)

C DIMENSION SET FOR 25 PARAMETERS (NPAR=25) AND 10 DIFFERENT
C RESPONSES.

DIMENSION BETA(25),SC(25),DELB(25),G(25)

COMMON/A/Z(25,25),D(10,10),RI(25,25)

COMMON/B/AAA(25,25)

C GENERAL DIMENSIONS TAKEN FROM CALLING PROGRAM

DIMENSION A(NO,NDATA),A1(NO,NDATA),PW(NO,NDATA,NPAR)

DIMENSION Y(NO,NDATA),U(NI,NDATA)

INTEGER T,TL,T1

C

C

C

C

C

C

C

C

C

C

C

C

C

C

C

C

C

C

C

C

C

C

C

C

C

C

C

C

C

C

C

C

INITIALIZE

SNGL(X)=X

NPRT=-1

T1=1

NY=NO

TL=NDATA

IFAIL=0

```

ITER=0
CRIT=5.0*10.0**(-NFIG)
NUM=TL-T1+1
RNUM=FLOAT(NUM)
NUMA=NUM-NO-1
RNUMA=FLOAT(NUMA)
PRINT*, 'SEARCH WILL HALT ITERATIONS EXCEED', MAXITR
PRINT*, 'OR IF RLAM EXCEEDS ', RLMAX
PRINT*, '    INITIAL VALUE OF RLAM', RLAM
PRINT*, '    USING DATA FOR T=1 TO T=', TL
PRINT*, '    INITIAL GUESS OF PARAMETERS'
WRITE(3,260)
260  FORMAT(/,10X, '    INITIAL GUESS OF PARAMETERS ',/)
DO 309 I=1,NPAR
WRITE(3,261) I, BETA(I)
261  FORMAT(1X, ' BETA(', I3, ') ', F14.6)
309  PRINT*, '    BETA(', I, ')=', BETA(I)
IF(NPRT.GE.0) GO TO 9
PRINT*, '    INPUTS U(J,T) J=1, ', NI
DO 7 T=1,TL
PRINT*, T, (U(J,T), J=1, NI)
7    CONTINUE
PRINT*, '    OUTPUTS Y(I,T) I=1, ', NO
DO 4 T=1,TL
PRINT*, T, (Y(I,T), I=1, NO)
4    CONTINUE
9    CONTINUE
C
C    START ITERATIVE MARQUARDT SEARCH
C
C
100  ITER=ITER +1
IFGRAD=0
PRINT*, '    ITERATION', ITER
IF(ITER.LE.MAXITR) GO TO 3789
PRINT*, 'ITERATION NUMBER EXCEEDING ', MAXITR
PRINT*, '    STOPPING'
IF(ITER.GT.1) GO TO 9375
C
C    CALCULATE AT=S
C
CALL MODEL(Y,U,BETA,NPAR,NDATA,A)
PRINT*, 'THANK GOD ITS FRYDAY'
DO 4397 I=1,NO
DO 4397 J=1,NO
SUM=0.0
DO 4398 T=T1,TL
4398  SUM=SUM+ (A(I,T)*A(J,T))
4397  D(I,J)=SUM/RNUMA
C    TYPE 'CONDITIONAL D MATRIX'
C    DO 4399 I=1,NO

```

```

C      TYPE I, (D(I, J), J=1, NO)
C4399  CONTINUE
      CALL INVERT(NO, DET, IER, 1)
      PRINT*, '      DETERMINANT OF CONDITIONAL MATRIX', DET
      PRINT*, '      RESIDUALS      I=1, ', NO
      DO 5675 I=1, TL
      PRINT*, T, (A(I, T), I=1, NO)
5675  CONTINUE
      RETURN
3789  CONTINUE
      IF(ITER.GT.1) GO TO 61
      IF(NPRI.GT.0) GO TO 61
C      TYPE '      INITIAL PARAMETER VECTOR'
C      DO 1008 K=1, NPAR
C1008  TYPE BETA(K)
61     CONTINUE
C
C      COMPUTE RESIDUALS AND DERIVATIVE OF RESIDUALS
C
      IF(ITER.EQ.1) GO TO 400
      CALL MDERIV(Y, U, BETA, NPAR, A, A1, PW, DEL, NO, NI, NDATA)
      GO TO 401
400   CALL MODEL(Y, U, BETA, NPAR, NDATA, A)
      PRINT*, 'HELLO'
      CALL MDERIV(Y, U, BETA, NPAR, A, A1, PW, DEL, NO, NI, NDATA)
401   CONTINUE
C
C      COMPUTE CONDITIONAL MINIMUM WITH RESPECT TO D AND INVERT
C
      PRINT*, 'GREETINGS'
      ICV=0
      IF(ITER.GT.1) GO TO 4620
86    DO 10 I=1, NO
      DO 10 J=1, NO
      SUM=0.0
      DO 11 T=T1, TL
11    SUM=SUM+A(I, T)*A(J, T)
10    D(I, J)=SUM/RNUMA
4620  CONTINUE
      IF(NPRI.GE.0) GO TO 3
C      TYPE '      CONDITIONAL D MATRIX'
C      DO 2 I=1, NO
C      DO 900 J=1, NO
C      TYPE D(I, J)
C900  CONTINUE
C2    CONTINUE
      IF(ICV.EQ.1) GO TO 85
3     CONTINUE
      IF(ITER.GT.1) GO TO 68
      CALL INVERT(NO, DET, IER, 1)
      DETSAV=DET

```

```

IF(NPRT.GT.0) GO TO 1013
PRINT*, '    DETERMINANT OF CONDITIONAL D MATRIX:', DET
1013 CONTINUE
C
C    CONSTRUCT Z MATRIX
C
68 CONTINUE
DO 15 K=1,NPAR
DO 15 L=K,NPAR
SUM=0.0
DO 16 T=T1,TL
DO 16 IV=1,NO
DO 16 IU=1,NO
16 SUM=SUM+(PW(IV,T,K))*RI(IV,IU)*(PW(IU,T,L))
Z(K,L)=SUM
15 CONTINUE
IF(NPAR.EQ.1)GO TO 9601
DO 9602 K=2,NPAR
LL=K-1
DO 9602 L=1,LL
9602 Z(K,L)=Z(L,K)
9601 CONTINUE
IF(NPRT.GE.0) GO TO 41
ICLK=0
98 CONTINUE
C    TYPE '    Z MATRIX AND RI MATRIX'
C    DO 42 I=1,NPAR
C    TYPE '    ROW ',I
C    DO 1015 L=1,NPAR
C    TYPE Z(I,L),RI(I,L)
C1015 CONTINUE
C42 CONTINUE
IF(ICLK.EQ.1) GO TO 97
41 CONTINUE
C
C    CONSTRUCT G VECTOR
C
DO 17 K=1,NPAR
SUM=0.0
DO 18 T=T1,TL
DO 18 IV=1,NO
DO 18 IU=1,NO
18 SUM=SUM+PW(IV,T,K)*RI(IV,IU)*A(IU,T)
G(K)=SUM
17 CONTINUE
IF(NPRT.GE.0) GO TO 43
97 CONTINUE
C    TYPE '    G VECTOR'
C    DO 1016 K=1,NPAR
C1016 TYPE G(K)
IF(ICLK.EQ.1) GO TO 96

```

```

43      CONTINUE
C
C      COMPUTE SCALING VECTOR
C
      DO 44 K=1,NPAR
44      SC(K)=SQRT(Z(K,K))
      IF(NPRI.GE.0) GO TO 45
      PRINT*, '      SCALING VECTOR'
      DO 1018 K=1,NPAR
      PRINT*, SC(K)
1018     CONTINUE
45      CONTINUE
C
C      COMPUTE SCALED LINEAR EQUATIONS AND INCLUDE
C      CONSTRAINT PARAMETER
C
      DO 46 K=1,NPAR
46      G(K)=G(K)/SC(K)
      DO 47 K=1,NPAR
      DO 47 L=K,NPAR
      Z(K,L)=Z(K,L)/(SC(K)*SC(L))
47      CONTINUE
      IF(NPAR.EQ.1) GO TO 9610
      DO 9611 K=2,NPAR
      LL=K-1
      DO 9611 L=1,LL
9611     Z(K,L)=Z(L,K)
9610     CONTINUE
      NOTRY=0
99      NOTRY=NOTRY+1
      IF(IFGRAD.EQ.1) GO TO 96
      DO 369 K=1,NPAR
369     Z(K,K)=Z(K,K)+RLAM
      QS=RLAM
      IF(NPRI.GE.0) GO TO 96
      PRINT*, '      SCALED LINEAR EQUATIONS  RLAM=',RLAM,NOTRY
      ICHK=1
      GO TO 98
96      CONTINUE
      IF(NPRI.LT.0) GO TO 9146
      PRINT*, ' RLAM= ',RLAM,NOTRY
9146     CONTINUE
C
C      SOLVE SCALED EQUATIONS AND COMPUTE NEW PARAMETER VECTOR BETA
C
      IF(RLAM.LE.1001) GO TO 2501
      DIST=1.0/RLAM
      IFGRAD=1
      IF(NPRI.GT.0) GO TO 2502
      PRINT*, 'USING GRADIENT SEARCH DISTANCE FACTOR= ',DIST
2502     CONTINUE

```

```

DO 2503 I=1,NPAR
DO 2503 J=1,NPAR
RI(I,J)=0.0
IF(I.NE.J) GO TO 500
RI(I,J)=DIST
500 CONTINUE
2503 CONTINUE
GO TO 2504
2501 CONTINUE
CALL INVERT(NPAR,Q,IER,2)
2504 CONTINUE
DO 51 K=1,NPAR
DELB(K)=0.0
DO 52 L=1,NPAR
52 DELB(K)=DELB(K)+RI(K,L)*G(L)
51 DELB(K)=-DELB(K)/SC(K)
IF(NPRT.GT.0) GO TO 48
PRINT*, 'PROPOSED CORRECTIONS FOR PARAMETER VECTOR TRIAL',NOTRY
DO 910 K=1,NPAR
PRINT*, DELB(K)
910 CONTINUE
48 CONTINUE
DO 252 K=1,NPAR
BETA(K)=BETA(K)+DELB(K)
252 CONTINUE
C
C TEST FOR CONVERGENCE
C
DO 53 K=1,NPAR
IF(ABS(DELB(K)/BETA(K)).GT.CRIT) GO TO 89
53 CONTINUE
GO TO 90
C
C IF CONVERGENCE NOT ACHIEVED SEE IF NEW PARAMETER VECTOR
C REDUCES D
C
89 ICV=1
IF(NPRT.GT.0) GO TO 87
PRINT*, 'PROPOSED NEW PARAMETER VECTOR'
DO 1007 K=1,NPAR
PRINT*, BETA(K)
1007 CONTINUE
87 CONTINUE
C
C CALCULATE AT=S
C
CALL MODEL(Y,U,BETA,NPAR,NDATA,A)
GO TO 86
85 CALL INVERT(NO,DET,IER,1)
IF(NPRT.GT.0) GO TO 1040
PRINT*, ' DETERMINANT OF PROPOSED CONDITIONAL D ', DET

```

```

1040  CONTINUE
      IF(DET-DETSAV) 71,72,72
C
C
C      IF D REDUCED, REDUCE RLAM AND START NEW ITERATION
C
C
71    IF(NPRT.GE.0) GO TO 73
      PRINT*, ' PROPOSED VECTOR REDUCES D'
73    RLAM=RLAM/FACT
      IF(RLAM.LT.RLMIN) RLAM=RLMIN
      DETSAV=DET
      GO TO 100
C
C      IF D NOT REDUCED INCREASE AND SOLVE LINEAR EQUATIONS
72    CONTINUE
      DO 364 K=1,NPAR
364   Z(K,K)=Z(K,K)-RLAM
      IF(RLAM.LT.RLMAX) GO TO 77
      PRINT*, ' RLAM HAS REACHED ', RLMAX, ' HALTING SEARCH'
9375  IFAIL=1
      MAXERR=1
      ERRMAX=ABS(DELB(1)/BETA(1))
      IF(NPAR.EQ.1) GO TO 826
      DO 827 K=2,NPAR
      IF(ABS(DELB(K)/BETA(K)).LE.ERRMAX) GO TO 827
      MAXERR=K
      ERRMAX=ABS(DELB(K)/BETA(K))
827   CONTINUE
826   CONTINUE
      PRINT*, 'CONVERGENCE TO',NFIG, ' SIGNIFICANT FIGURES NOT REACHED'
      PRINT*, ' MAXIMUM RELATIVE ERROR IN BETA: ',MAXERR
      PRINT*, ' MAXIMUM RELATIVE ERROR: ',ERRMAX
      PRINT*, ' ABSOLUTE ERROR: ',DELB(MAXERR)
      QS=0.0
      GO TO 829
77    CONTINUE
      DO 75 K=1,NPAR
75    BETA(K)=BETA(K)-DELB(K)
      RLAM=FACT*RLAM
      GO TO 99
C
C      IF CONVERGENCE ACHIEVED
C
C
90    CONTINUE
      PRINT*, ' CONVERGENCE TO ',NFIG, ' SIGNIFICANT FIGURES AT'
      WRITE(3,200) NFIG,ITER
200   FORMAT(/,1X, ' CONVERGENCE TO ',I3, ' SIGNIFICANT FIGURES AT '
1,/, ' ITERATION ', I3)
      PRINT*, ' ITERATION',ITER
      PRINT*, ' DETERMINANT: ',DET

```



```

DEBT=DET
WRITE(3,210) DET
210  FORMAT(/,1X,'    DETERMINANT: ', E14.6)
829  CONTINUE
      PRINT*, '    PARAMETER VECTOR'
      DO 1031 K=1,NPAR
1031  PRINT*, ' BETA(',K,')= ',BETA(K)
      PRINT*, '    COVARIANCE MATRIX OF RESIDUAL VECTOR'
      WRITE(3,270)
270  FORMAT(1X,/,1X,'    COVARIANCE MATRIX OF RESIDUAL VECTOR',/)
      DO 128 I=1,NO
      WRITE(3,201) I,(D(I,J),J=1,NO)
201  FORMAT(1X,I3,5X,10E14.6)
      PRINT*, I,(D(I,J),J=1,NO)
128  CONTINUE
      DO 7143 I=1,NO
7143  DELB(I)=SQRT(D(I,I))
      DO 7144 I=1,NO
      DO 7144 J=1,NO
7144  D(I,J)=D(I,J)/(DELB(I)*DELB(J))
      PRINT*, '    CORRELATION MATRIX OF RESIDUAL VECTOR'
      DO 7146 I=1,NO
      DO 7148 J=1,NO
      D(I,J)=D(I,J)/(DELB(I)*DELB(J))
7148  CONTINUE
7146  CONTINUE
C
C
C    CALCULATE ESTIMATED COVARIANCE MATRIX OF PARAMETERS
C
      DO 102 K=1,NPAR
      DO 102 L=1,NPAR
      IF(K.NE.L) Q=0.0
      IF(K.EQ.L) Q=QS
102  Z(K,L)=SC(K)*SC(L)*(Z(K,L)-Q)
      DO 6149 I=1,NPAR
6149  SC(I)=1.0/SQRT(Z(I,I))
      DO 6148 I=1,NPAR
      DO 6148 J=1,NPAR
6148  Z(I,J)=Z(I,J)*SC(I)*SC(J)
      CALL INVERT(NPAR,DET,IER,2)
      DO 6147 I=1,NPAR
      DO 6147 J=1,NPAR
6147  RI(I,J)=RI(I,J)*SC(I)*SC(J)
      PRINT*, ' ESTIMATES OF PARAMETER STATISTICS'
      PRINT*, ' PARAMETER ', '    ESTIMATE ', '    S.D.'
      WRITE(3,202)
202  FORMAT(/,1X,' PARAMETER ',5X,' ESTIMATE ',10X,' S.D. ',/)
      DO 4783 K=1,NPAR
      IF(RI(K,K).GT.0.0) GO TO 1638
      PRINT*, 'ELEMENT ',K, ', ', K, ' OF COVARIANCE MATRIX'

```

```

PRINT*, RI(K,K)
GO TO 1616
1638 CONTINUE
SC(K)=SQRT(RI(K,K))
WRITE(3,203) K,BETA(K),SC(K)
203 FORMAT(1X,' BETA(',I3,')= ',3X,F14.8,3X,F14.8)
PRINT*, ' BETA(',K,') ',BETA(K),' ',SC(K)
4783 CONTINUE
IF(NO.GT.1) GO TO 2312
SSQ=0.0
DO 2313 T=T1,TL
2313 SSQ=SSQ+A(1,T)**2
PRINT*, ' SUM OF SQUARED RESIDUALS: ',SSQ
WRITE(3,204) SSQ
204 FORMAT(/,1X,' SUM OF SQUARED RESIDUALS: ',E14.6)
2312 CONTINUE
DO 4685 I=1,NPAR
DO 4685 J=1,NPAR
4685 RI(I,J)=RI(I,J)/(SC(I)*SC(J))
PRINT*, ' ESTIMATED CORRELATION MATRIX OF PARAMETERS '
WRITE(3,205)
205 FORMAT(/,1X,' ESTIMATED CORRELATION MATRIX OF PARAMETERS',/)
DO 105 I=1,NPAR
PRINT*, RI(I,L)
WRITE(3,206) (RI(I,L),L=1,NPAR)
206 FORMAT(1X,25F14.6)
105 CONTINUE
1616 CONTINUE
IF(NPRI.GT.0) GO TO 499
PRINT*, 'RESIDUALS'
WRITE(3,207)
207 FORMAT(/,1X,' RESIDUALS ',/)
DO 503 T=T1,TL
PRINT*, (A(I,T),I=1,NO)
WRITE(3,208) (A(I,T), I=1,NO)
208 FORMAT(1X,10F14.6)
503 CONTINUE
DO 4401 I=1,NO
DO 4401 J=1,NO
SUM1=0.0
DO 4400 T=1,NDATA
4400 SUM1=SUM1+(AAA(I,T)*AAA(J,T))
4401 D(I,J)=SUM1
PRINT*, ' MATRIX '
DO 4402 I=1,NO
4402 PRINT*, (D(I,J), J=1,NO)
C CALL INVERT(NO,DT,IER,1)
C DT=DT/(NPAR-1)
C XFF=DT/DEBT
C PRINT*, ' DT ',DT
C PRINT*, ' F STATISTIC ', XFF

```

```
C      WRITE(3,209) XFF
C209   FORMAT(1X,'      F STATISTIC ',E14.6)
499    CONTINUE
      IF(<IFAIL.NE.1) GO TO 7650
      PRINT*, 'TERMINATION BECAUSE OF USER SPECIFIED CONDITIONS'
7650   CONTINUE
      RETURN
      END
```

```

SUBROUTINE INVERT(MA,DETA,IER,IWHICH)
IMPLICIT DOUBLE PRECISION(A-H,O-Z)
C DIMENSIONS SET FOR MAXIMUM NPAR=25, NO=10
COMMON/DUM/IR(25),IC(25)
COMMON/A/AA(25,25),D(10,10),A(25,25)
COMMON/B/AAA(25,25)
IF(IWHICH.EQ.2) GO TO 651
DO 652 I=1,MA
DO 652 J=1,MA
652 A(I,J)=D(I,J)
GO TO 653
651 CONTINUE
DO 654 I=1,MA
DO 654 J=1,MA
654 A(I,J)=AA(I,J)
653 CONTINUE
IER=0
DO 1 I=1,MA
IR(I)=0
1 IC(I)=0
DETA=1.0
DO 123 IJKL=1,MA
CALL PIVOT(MA,I,J)
PIV=A(I,J)
C MAXIMUM VALUE OF DETERMINANT= 1.0E+50
Z1=LOG10(ABS(PIV))
Z2=LOG10(ABS(DETA))
Z=Z1+Z2
IF(Z.GE.50.) GO TO 528
DETA=PIV*DETA
GO TO 529
528 DETA=1.0E+50
529 CONTINUE
IF(PIV.EQ.0.0) GO TO 17
IR(I)=J
IC(J)=I
PIV=1.0/PIV
DO 5 K=1,MA
5 A(I,K)=A(I,K)*PIV
A(I,J)=PIV
DO 9 K=1,MA
IF(K.EQ.I) GO TO 9
PIV1=A(K,J)
DO 8 L=1,MA
8 A(K,L)=A(K,L)-PIV1*A(I,L)
A(K,J)=PIV1
9 CONTINUE
PIV1=A(I,J)
DO 11 K=1,MA
11 A(K,J)=-PIV1*A(K,J)
A(I,J)=PIV1

```

```
123  CONTINUE
      DO 16 I=1,MA
      K=IC(I)
      M=IR(I)
      IF(K.EQ.I) GO TO 16
      DEIA=-DEIA
      DO 14 L=1,MA
      TEMP=A(K,L)
      A(K,L)=A(I,L)
14    A(I,L)=TEMP
      DO 15 L=1,MA
      TEMP=A(L,M)
      A(L,M)=A(L,I)
15    A(L,I)=TEMP
      IC(M)=K
      IR(K)=M
16    CONTINUE
      RETURN
17    IER=1
      PRINT*, 'ERROR IN SUBROUTINE INVERT'
      STOP
      END
```

```
SUBROUTINE PIVOT(MA, I, J)
IMPLICIT DOUBLE PRECISION(A-H, O-Z)
COMMON/A/AA(25,25),D(10,10),A(25,25)
COMMON/DUM/IR(25),IC(25)
COMMON/B/AAA(25,25)
NA=MA
I=0
J=0
TEST=0.0
DO 5 K=1,MA
IF(IR(K).NE.0) GO TO 5
DO 4 L=1,NA
IF(IC(L).NE.0) GO TO 4
X=ABS(A(K,L))
IF(X.LT.TEST) GO TO 4
I=K
J=L
TEST=X
4 CONTINUE
5 CONTINUE
RETURN
END
```

```
SUBROUTINE MDERIV(Y,U,THETA,NPAR,A,A1,PW,DEL,NO,NI,NDATA)
IMPLICIT DOUBLE PRECISION(A-H,O-Z)
C THIS SUBROUTINE CALCULATES THE DERIVATIVES OF THE RESIDUALS
C DIMENSION OF ETA(NPAR); OTHERS DIMENSIONED SAME AS IN MVEST
C SET FOR MAXIMUM NPAR=25, NO=10
DIMENSION ETA(25),THETA(25)
DIMENSION PW(NO,NDATA,NPAR)
DIMENSION Y(NO,NDATA),U(NI,NDATA),A(NO,NDATA),A1(NO,NDATA)
DO 10 K=1,NPAR
DO 11 L=1,NPAR
11 ETA(L)=THETA(L)
ETA(K)=THETA(K)*(1+DEL)
IF (THETA(K).NE.O.) GO TO 50
ETA(K)=DEL
50 CONTINUE
CALL MODEL(Y,U,ETA,NPAR,NDATA,A1)
X=THETA(K)
IF (X.NE.O.O) GO TO 51
X=1.0
51 CONTINUE
DO 10 J=1,NDATA
DO 10 I=1,NO
10 PW(I,J,K)=(A1(I,J)-A(I,J))/(DEL*X)
RETURN
END
```

Subroutine to calculate tissue concentrations for convection-diffusion model with no metabolism.

```

C      E1 IS THE POROSITY
C      L IS THE THICKNESS OF THE MEDIA IN CM
C      D IS THE EFFECTIVE DIFFUSIVITY, CM**2/SEC
C      P IS THE PECLET NUMBER FOR THE MEDIA, P=V*L/(E1*D)
C      BE IS THE BIOT NUMBER FOR THE ARTERIAL ENDOTHELIUM:
C      BE=KE*L/(E1*D), WHERE KE IS THE MASS TRANSFER COEFFICIENT FOR
C      VESICULAR TRANSPORT ACROSS THE ARTERIAL ENDOTHELIUM
C      K2 AND K3 ARE LUMPED PARAMETERS FOR THE BOUNDARY CONDITION
C      AT THE MEDIA-ADVENTITIA INTERFACE
C      R IS THE REJECTION COEFF AT THE LUMINAL SIDE OF THE MEDIA
C      TI IS TIME IN MINUTES
C      TAU IS THE FOURIER NUMBER, TAU=TI*D/L**2
C      ETA IS DIMENSIONLESS DISTANCE, X/L
C      AP AND BP ARE PLASMA ISOTOPE DECAY COEFFS
C      SUBROUTINE MODEL(Y,X,BETA,NPAR,NDATA,A)
C      IMPLICIT DOUBLE PRECISION(A-H,O-Z)
C      COMMON/BB/CT(270),AP(2),BPTIME1,BPTIME2,XL(100),YL,E1
C      DIMENSION BETA(NPAR),Y(1,NDATA),X(1,NDATA),A(1,NDATA)
C      DIMENSION BP(2),RXL(2),GL(301),F(300),GRL(301),FR(300)
C      DIMENSION QEXP(2),QEXPA(2)
C      COSH(X)=.5*(EXP(X)+EXP(-X))
C      BE=BETA(1)
C      NN=30
C      GRL(1)=0.100D-02
C      R=1.0
C      XK2=BETA(2)
C      XK3=BETA(3)
C      D=BETA(4)*BETA(4)
C      P=BETA(5)
C      P=0.1
C      XF=0.0
C      BETAP=0.0
C      XK3=E1*XK2
C      XK1=1.0
C      ZZ=(P*(1.-R)+BE)*E1*EXP(.5*P)
C      YY=XK2-.5*P*XK1
C      WW=.5*P+BE
C      VV=XK2-(P+BE)*XK1
C      TOL=0.0000001
C
C      POSSIBILITY OF ROOTS ON REAL AXIS (OTHER THAN S = ZERO)
C
C      IF(XK1.EQ.0.0) GO TO 200
C      BETA1=-VV/XK1
C      BETA2=YY*WW/XK1
C      BR=BETA1/BETA2
C      IF(BETA1) 110,200,100

```



```

100 IF(BETA2) 200,200,101
101 IF(BR-1.) 180,200,200
110 IF(BETA2) 120,200,130
120 IF(BR-1.) 125,160,160
125 BB=SQRT(-BETA2)
    FUN=0.5*BR*BB
    IF(FUN-TANH(BB)) 200,170,190
130 NREAL=1
    GRL(1)=SQRT(BETA2)+0.01
    XINCR=0.05
    BB=0.0
    GO TO 250
160 NREAL=1
    BB=SQRT(-BETA2)
    GRL(1)=BB
    XINCR=0.05
    GO TO 250
170 NREAL=1
    RXL(1)=BB
    GO TO 149
180 NREAL=1
    GRL(1)=0.01
    XINCR=0.05*SQRT(BETA2)
    BB=0.0
    GO TO 250
190 NREAL=2
    GRL(1)=0.01
    XINCR=0.05*BB
    GO TO 250
200 NREAL=0
    GO TO 149
250 CONTINUE
C
C   CALCULATE REAL POLES
C
    DO 600 K=1,NREAL
    DO 300 N=1,300
    FR(N)=(YY*WW-XK1*(GRL(N)*GRL(N)))*TANH(GRL(N))+GRL(N)*VV
    IF(ABS(FR(N)).LE.TOL) GO TO 599
    IF(N-1)146,146,140
146 GRL(N+1)=GRL(N)+5.0*XINCR
    GO TO 300
140 IF(FR(N)/FR(N-1))145,143,143
143 W=FLOAT(K)
    GRL(N+1)=GRL(N)+5.0*XINCR+(W-1)
300 CONTINUE
145 CONTINUE
C
C   NEWTON'S METHOD ALGORITHM
C
    GRLL=GRL(N)

```

```

DO-400 L=1,100
FRR=(YY*WW-(XK1*GRL*GRL))*TANH(GRL)+GRL*VV
IF(GRL.LE.100) GO TO 350
FRRP=VV-2.*XK1*GRL*TANH(GRL)
GO TO 351
350 CONTINUE
FRRP=VV-2.*XK1*GRL*TANH(GRL)+(YY*WW-XK1*(GRL*GRL))/
1(COSH(GRL)*COSH(GRL))
351 CONTINUE
GRL=GRL-FRR/FRRP
IF(ABS(FRR).LE.TOL) GO TO 150
400 CONTINUE
STOP 'NO CONVERGENCE IN REPOLES'
599 GRL=GRL(N)
150 RXL(K)=GRL
PRINT*, 'REAL ROOTS'
PRINT*, ' RXL ', RXL(K)
IF(NREAL.EQ.1) GO TO 600
IF(K.EQ.2) GO TO 600
GRL(1)=BB
600 CONTINUE
149 CONTINUE
C
C CALCULATE IMAGINARY POLES
C
C THIS SECTION CALCULATES THE ROOTS OF THE EQUATION F(XL(N))=0
C USING NEWTON'S ALGORITHM. AN INITIAL GUESS IS SUPPLIED AND
C F(GL(N)) IS CALCULATED. IF F(GL(N)) IS NOT A ROOT THEN GL(N+1)
C IS FOUND BY ADDING 0.3 TO GL(N), AND F(GL(N+1)) CALCULATED.
C IF THE SIGNS OF F(GL(N+1)) AND F(GL(N)) ARE DIFFERENT,
C NEWTON'S METHOD IS APPLIED ABOUT F(GL(N+1)). IF THE SIGNS DONT
C DIFFER THEN THE PROCEDURE IS REPEATED UNTIL THE SIGNS DIFFER,
C AND THEN NEWTON'S METHOD IS APPLIED TO THE LATTER TERM.
C
GL(1)=0.01
DO 1100 K=1,50
DO 800 N=1,50
C
C TEST TO DETERMINE IF GL(N) IS A ROOT
C
F(N)=(YY*WW+XK1*GL(N)*GL(N))*SIN(GL(N))+GL(N)*VV*COS(GL(N))
IF(ABS(F(N)).LE.TOL) GO TO 899
IF(N-1) 135,135,136
135 GL(N+1)=GL(N)+1.0
GO TO 800
136 IF(F(N)/F(N-1)) 138,137,137
137 GL(N+1)=GL(N)+0.5
800 CONTINUE
138 CONTINUE
C
C NEWTON'S METHOD ALGORITHM

```

```

C
  GLL=GL(N)
  DO 189 L=1,100
  FF=(YY*WW+(XK1*GLL*GLL))*SIN(GLL)+GLL*VV*COS(GLL)
  FP=(YY*WW+VV+(XK1*GLL*GLL))*COS(GLL)+(2.*XK1-VV)*GLL*SIN(GLL)
  GLL=GLL-FF/FP
  IF (ABS(FF).LE.TOL) GO TO 900
139  CONTINUE
  PRINT*, 'GLL= ',GLL, ' FF= ',FF
  PRINT*, ' YY= ',YY, ' WW= ',WW
  PRINT*, ' XK1= ',XK1, ' VV= ',VV
  STOP 'NO CONVERGENCE IN IMPOLES'
899  GLL=GL(N)
900  XL(K)=GLL
  GL(1)=XL(K)+0.05
1100 CONTINUE
C
C   PERFORM SUMMATIONS
C
  A0=SQRT(0.25*P**2)
  BC=ZZ*(YY*SINH(A0)-A0*XK1*COSH(A0))+A0*XK3
  BS=WW*XK3-ZZ*(YY*COSH(A0)-A0*XK1*SINH(A0))
  BD=(YY*WW-XK1*A0**2)*SINH(A0)+A0*VV*COSH(A0)
  BC1=BE*E1*EXP(0.5*P)*(YY*SINH(A0)-A0*XK1*COSH(A0))
  BS1=-BE*E1*EXP(0.5*P)*(YY*COSH(A0)-A0*XK1*SINH(A0))
C
  TI=30.0
  DO 1000 JETA=1,NDATA
  IF(P.GE.0.0) GO TO 7900
  P=0.0001
7900 CONTINUE
  ETA=X(1,JETA)
  TAU=TI*60*D/(YL*YL)
  BP(1)=BPTIME1*TI/TAU
  BP(2)=BPTIME2*TI/TAU
  F2A=0.0
  F2=0.
  B2=0.
  BB2=0.0
  DO 500 K=1,2
  QEXP(K)=EXP(-BP(K)*TAU)
  QEXPA(K)=EXP(-(BETAP+BP(K))*TAU)
  F2A=F2A+AP(K)*((1-XF)*QEXP(K)+XF*QEXPA(K))
500  F2=F2+AP(K)*EXP(-BP(K)*TAU)
  F1=0.
  F3=0.
  FR1=0.
  FR3=0.
  DO 211 M=1,NN
  S=-0.25*P*P-XL(M)**2
  F3K=0.

```

```

F3AK=0.0
QC=ZZ*(YY*SIN(XL(M))-XL(M)*XK1*COS(XL(M)))+XL(M)*XK3
QS=WW*XK3-ZZ*(YY*COS(XL(M))+XL(M)*XK1*SIN(XL(M)))
QD=(YY*WW+XK1*XL(M)**2+VV)*COS(XL(M))+XL(M)*(2.*XK1-VV)
1*SIN(XL(M))
Q=XL(M)*(QC*COS(XL(M)*ETA)+QS*SIN(XL(M)*ETA))/QD
IF((S*TAU).LT.-100.) GO TO 205
EXPST=EXP(S*TAU)
GO TO 210
205 EXPST=0.
210 CONTINUE
F1=F1+Q*EXPST/S
DO 418 K=1,2
F3AK=F3AK+XF*AP(K)*(BETAP+BP(K))/(S*(S+BETAP+BP(K)))*
1(QEXPA(K)-EXPST)
418 F3K=F3K+AP(K)*BP(K)*(QEXP(K)-EXPST)/(S*(S+BP(K)))
F3=F3+(1-XF)*Q*F3K+Q*F3AK
211 CONTINUE
FR1=0.0
FR3=0.0
C
IF(NREAL.EQ.0.) GO TO 693
DO 692 L=1,NREAL
FR3K=0.
FR3AK=0.0
SR=-0.25*P*P+RXL(L)**2
COSHQ=COSH(RXL(L))
SINHQ=SINH(RXL(L))
QRC=ZZ*(YY*SINHQ-RXL(L)*XK1*COSHQ)+RXL(L)*XK3
QRS=WW*XK3-ZZ*(YY*COSHQ-RXL(L)*XK1*SINHQ)
QRD=(YY*WW-XK1*RXL(L)**2+VV)*COSHQ-RXL(L)*(2.*XK1-VV)*SINHQ
QR=-RXL(L)*(QRC*COSH(RXL(L)*ETA)+QRS*SINH(RXL(L)*ETA))/QRD
IF(SR*TAU.GT.120) GO TO 750
REX=EXP(SR*TAU)
GO TO 751
750 REX=0.0
751 CONTINUE
FR1=FR1+QR*REX/S
DO 518 K=1,2
FR3AK=FR3AK+AP(K)*XF*(BETAP+BP(K))/(S*(SR+BETAP+BP(K)))*
1(QEXPA(K)-REXP)
518 FR3K=FR3K+AP(K)*BP(K)*(QEXP(K)-REX)/(S*(SR+BP(K)))
FR3=FR3+(1-XF)*QR*FR3K+QR*FR3AK
692 CONTINUE
693 CONTINUE
C
C CALCULATE CT(ETA)
C
AX=EXP(.5*P*(ETA-1.))
IF(P.NE.0.0) GO TO 699
B=(XK3+BE*E1*(XK2-1.0)+ETA*BE*(XK3-E1*XK2))/(BE*(XK2-1.0)+XK2)

```

```
      BA=(BE*E1*(XK2-1.0)+ETA*BE*(XK3-E1*XK2))/(BE*(XK2-1.0)+XK2)
      BBB=B-BA
      GO TO 700
699    B=(BC*COSH(A0*ETA)+BS*SINH(A0*ETA))/BD
      BBB=B-BA
700    CT(JETA)=AX*(-2*F1-2*F3+B*F2-2*FR1-2*FR1)
      A(1,JETA)=Y(1,JETA)-CT(JETA)
1000  CONTINUE
      RETURN
      END
```

The following two programs were used to calculate tissue concentrations and mean relative concentrations, respectively. Two subroutines are called, IMPOLES1 and ROOTS. IMPOLES1 calculates the imaginary roots and ROOTS finds the roots to a fifth order polynomial.

```

C      E1 IS THE POROSITY
C      L IS THE MEDIAL THICKNESS (CM)
C      D IS THE EFFECTIVE DIFFUSIVITY (CM**2/SEC)
C      P IS THE MEDIAL PECLET NUMBER
C      BE IS THE ENDOTHELIAL BIOT NUMBER
C      K2 AND K3 ARE LUMPED PARAMETERS FOR THE BOUNDARY CONDITION
C      AT ETA=1
C      R IS THE LUMINAL REJECTION COEFFICIENT
C      TI IS THE TIME (MINUTES)
C      TAU IS THE FOURIER NUMBER
C      ETA IS THE DIMENSIONLESS DISTANCE
C      AP AND BP ARE THE PLASMA ISOTOPE DECAY COEFFICIENTS. PHIB, PHIR,
C      PHII, PHIE1, AND PHIE2 ARE THE THIELE MODULI FOR BINDING
C      TO THE EXTRACELLULAR MATRIX, BINDING TO THE LDL RECEPTOR ON THE CELL
C      SURFACE, NONSPECIFIC INTERNALIZATION, AND RECEPTOR-MEDIATED AND
C      NONSPECIFIC EXOCYTOSIS, RESPECTIVELY.
C      XM IS THE INVERSE OF THE EQUILIBRIUM CONSTANT FOR EXTRACELLULAR
C      BINDING. XK IS THE RATIO OF RATE CONSTANTS FOR DISSOCIATION FROM
C      THE RECEPTORS AND INTERNALIZATION TO BINDING TO THE RECEPTORS.
C      GAM IS THE RATIO OF INTERNALIZATION TO BINDING. OM AND YK2 ARE
C      RATIOS OF DEGRADATION AND EXOCYTOSIS TO INTERNALIZATION BY
C      RECEPTOR-MEDIATED AND NONSPECIFIC PROCESSES, RESPECTIVELY.
      IMPLICIT DOUBLE PRECISION(A-H,O-Z)
C      REAL S,SZ,F1N,F3N,B1N,B3N,XI1N,XI3N,F3NK,B3NK,XI3NK,
C      1F1,F3,B1,B3,XI1,XI3,CEXPST,R1,R3,R1N,R3N,R3NK,RI1,RI3,RI3N,RI1N,RI3NK
      DIMENSION AP(2),BP(2),XL(200),XP(200),CF(200),CI(200),
      1CB(200),CD(200),CT(200),CR(200),CRI(200),CIT(200),F(50),G(51),
      2S(200,5),SZ(200,5),QEXP(2)
      DIMENSION QEXPA(2)
      OPEN(1,FILE='IN')
      OPEN(2,FILE='INFO')
      OPEN(3,FILE='OUTP')
      OPEN(4,FILE='DECAY')
      OPEN(7,FILE='ENTRIES')
      OPEN(8,FILE='FREE')
      OPEN(16,FILE='BOUND')
      OPEN(17,FILE='CELLULAR')
      OPEN(18,FILE='STEADY')
      OPEN(19,FILE='DEGRAD')
      READ(1,*) XKE2,P,XKE1,R,D,YL, TI, XM, PHIB, PHIR, XK, YK2, GAM, OM,
      1PHII, PHIE1, PHIE2, XF, BETA
      READ(4,*) AP(1), AP(2), BPTIME1, BPTIME2
      READ(7,*) E1, TOL, XK1, NN, NP
      XK2=XKE2*YL/(D*E1)
      BE=XKE1*YL/(D*E1)

```

```

      XK3=E1*XK2
      WRITE(2,26) AP(1),AP(2),BPTIME1,BPTIME2
      WRITE(2,27)XK2,XK3,P,BE,R,D,YL,TI,XM,PHIB,PHIR,XK,YK2,GAM,OM,PHII,
1PHIE1,PHIE2,XF,BETA
26  FORMAT( ' PLASMA DECAY COEFFICIENTS: ',4F10.6,/,/)
27  FORMAT( ' INPUT PARAMETERS: ' ,/, ' K2= ',F6.3,11X,' K3= ',F6.3,
1/, ' P= ',F6.2,11X,' BE=',F6.3,/, ' R= ',F6.2,11X,' D= ',E11.3,/,
2' L= ',F8.4,9X,' TI=' ,F5.0,/, ' XM=',F6.3,9X,' PHIB= ',F6.3,
3/, 'PHIR='F6.3,10X,'K=',F6.3,/, ' K2= ',F6.3,10X,' GAMMA= ',F6.3,
4/, 'OMEGA= ',F6.3,10X,' PHII= ',F6.3,/, ' PHIE1= ',F6.3,10X,
5' PHIE2= ',F6.3,/, ' XF= ',F6.3,10X,' BETA= ',F6.3)
      TAU=TI*60.*D/YL**2
      PRINT*, ' TAU= ', TAU
      BP(1)=BPTIME1*TI/TAU
      BP(2)=BPTIME2*TI/TAU
      ZZ=(P*(1.-R)+BE)*E1*EXP(0.5*P)
      ZZA=BE*E1*EXP(0.5*P)
      YY=XK2-0.5*P*XK1
      WW=0.5*P+BE
      VV=XK2-(P+BE)*XK1
C
C  POSSIBILITY OF POLES ON THE REAL AXIS
C
      BETA1=-VV/XK1
      BETA2=YY*WW/XK1
      BR=BETA1/BETA2
      IF(BETA1) 110,200,100
100  IF(BETA2) 200,200,101
101  IF(BR-1.) 140,200,200
110  IF(BETA2) 120,200,140
120  IF(BR-1.) 125,140,140
125  BB=DSQRT(-BETA2)
      FUN=.5*BR*BB
      IF(FUN-TANH(BB)) 200,140,190
140  NREAL=1
      GO TO 195
190  NREAL=2
195  CONTINUE
      PRINT*, 'WARNING: THIS PROGRAM DOES NOT ACCOUNT FOR POLES
1ON THE REAL AXIS'
      WRITE(10,196) NREAL
196  FORMAT('NUMBER OF POLES ON THE REAL AXIS (OTHER THAN S=0): ', I3)
200  CONTINUE
C
C  CALL SUBROUTINES
C
C  WRITE(2,88)
C88  FORMAT( /,/, ' POLES ON THE IMAGINARY AXIS: ',/)
      PRINT*, ' ITS A WONDERFUL WORLD WE LIVE IN, MR. ROGERS'
      CALL IMPOLES1(ZZ,YY,WW,VV,XK1,TOL,NN,XL,IER)
      PRINT*, ' BACK FROM IMPOLES1'

```

```

IF(IER.EQ.2) GO TO 7700
IF(XM.NE.0.0000) GO TO 780
ALPHO=DSQRT(0.25*P**2+PHIB+GAM/XK*(PHIR-PHIE1/OM)+
1PHII-PHIE2/YK2)
GO TO 781
780 CONTINUE
IF(PHIR.EQ.0.0) GO TO 779
ALPHO=DSQRT(0.25*P**2+(GAM/XK)*(PHIR-PHIE1/OM)+
1PHII-PHIE2/YK2)
GO TO 778
779 CONTINUE
IF(PHII.NE.0.0) GO TO 726
ALPHO=DSQRT(0.25*P**2)
GO TO 778
726 CONTINUE
ALPHO=DSQRT(0.25*P**2+PHII-PHIE2/YK2)
778 CONTINUE
PRINT*, ' ALPHO= ',ALPHO
781 BC=ZZ*(YY*SINH(ALPHO)-ALPHO*XK1*COSH(ALPHO))+ALPHO*XK3
BS=WW*XK3-ZZ*(YY*COSH(ALPHO)-ALPHO*XK1*SINH(ALPHO))
BD=(YY*WW-XK1*ALPHO**2)*SINH(ALPHO)+ALPHO*VV*COSH(ALPHO)
BCA=ZZA*(YY*SINH(ALPHO)-ALPHO*XK1*COSH(ALPHO))
BSA=-ZZA*(YY*COSH(ALPHO)-ALPHO*XK1*SINH(ALPHO))
C
C NOTE: IT IS ASSUMED THAT IF PHIR IS EQUAL TO ZERO, THEN RECEPTOR-
C MEDIATED METABOLISM TERMS ARE EQUAL TO ZERO
C
CALL SZFIND(XL,P,XM,PHIB,PHIR,XK,YK2,GAM,OM,PHII,PHIE1,PHIE2,
1NN,NUMN,S,SZ)
PRINT*, ' NUMN ',NUMN
C
C PERFORM SUMMATIONS
C
F2=0.
F2A=0.0
B2=0.
B2A=0.0
X12=0.
X12A=0.0
R2=0.0
R2A=0.0
RI2=0.0
D12=0.0
D22=0.0
RI2A=0.0
D12A=0.0
D22A=0.0
DO 500 K=1,2
QEXP(K)=EXP(-BP(K)*TAU)
QEXPA(K)=EXP(-(BETA+BP(K))*TAU)
F2=F2+AP(K)*QEXP(K)

```



```

F2A=F2A+AP(K)*((1-XF)*QEXP(K)+XF*QEXPA(K))
IF(XM*PHIB*TAU.GT.120.)GO TO 603
BEXP=EXP(-XM*PHIB*TAU)
GO TO 604
603 BEXP=0.0
604 CONTINUE
B2=B2+AP(K)/(XM*PHIB-BP(K))*(QEXP(K)-BEXP)
B2A=B2A+AP(K)*(1-XF)/(XM*PHIB-BP(K))*(QEXP(K)-BEXP)+
1AP(K)*XF/(XM*PHIB-(BP(K)+BETA))*(QEXPA(K)-BEXP)
IF(PHII*YK2*TAU.GT.120)GO TO 615
PEXP=EXP(-PHII*YK2*TAU)
GO TO 606
615 PEXP=0.0
606 CONTINUE
XI2=XI2+AP(K)/(PHII*YK2-BP(K))*(QEXP(K)-PEXP)
XI2A=XI2A+AP(K)*(1-XF)/(YK2*PHII-BP(K))*(QEXP(K)-PEXP)+
1AP(K)*XF/(YK2*PHII-(BP(K)+BETA))*(QEXPA(K)-PEXP)
IF(XK*PHIR*TAU.GT.120)GO TO 616
REXP=EXP(-XK*PHIR*TAU)
GO TO 607
616 REXP=0.0
607 CONTINUE
R2=R2+AP(K)/(XK*PHIR-BP(K))*(QEXP(K)-REXP)
R2A=R2A+AP(K)*(1-XF)/(XK*PHIR-BP(K))*(QEXP(K)-REXP)+
1AP(K)*XF/(XK*PHIR-(BETA+BP(K)))*(QEXPA(K)-REXP)
IF(PHIR*OM*TAU.GT.120)GO TO 617
RIEXP=EXP(-PHIR*OM*TAU)
GO TO 608
617 RIEXP=0.0
608 CONTINUE
IF(PHIR.EQ.0.0)GO TO 744
RI2=RI2+AP(K)/(XK*PHIR-BP(K))*((QEXP(K)-RIEXP)/(PHIR*OM-BP(K))
1-(REXP-RIEXP)/(PHIR*(OM-XK)))
RI2A=RI2A+AP(K)*(1-XF)/(XK*PHIR-BP(K))*((QEXP(K)-RIEXP)/(PHIR*OM-BP(K))
1-(REXP-RIEXP)/(PHIR*(OM-XK)))+AP(K)*XF/(XK*PHIR-(BETA+BP(K)))*
2((QEXPA(K)-RIEXP)/(PHIR*OM-(BETA+BP(K)))-(REXP-RIEXP)/(PHIR*(OM-XK)))
D12=D12+AP(K)/(XK*PHIR-BP(K))*(((1-QEXP(K))/BP(K)-(1-RIEXP)/
1(PHIR*OM))/(PHIR*OM-BP(K))-((1-REXP)/(XK*PHIR)-(1-RIEXP)/(PHIR*OM))/
2(PHIR*(OM-XK)))
D12A=D12A+AP(K)*(1-XF)/(XK*PHIR-BP(K))*(((1-QEXP(K))/BP(K)-(1-RIEXP)/
1(PHIR*OM))/(PHIR*OM-BP(K))-((1-REXP)/(PHIR*OM)-(1-RIEXP)/(PHIR*OM))/(PHIR*
2(OM-XK)))+AP(K)*XF/(XK*PHIR-(BETA+BP(K)))*(((1-QEXPA(K))/(BETA+BP(K))-
3(1-RIEXP)/(PHIR*OM))/(PHIR*OM-(BETA+BP(K)))-((1-REXP)/(XK*PHIR)-
4(1-RIEXP)/(PHIR*OM))/(PHIR*(OM-XK)))
744 CONTINUE
IF(PHII.EQ.0.0)GO TO 747
D22=D22+AP(K)/(YK2*PHII-BP(K))*((1-QEXP(K))/BP(K)-(1-PEXP)/
1(PHII*YK2))
D22A=D22A+AP(K)*(1-XF)/(YK2*PHII-BP(K))*((1-QEXP(K))/BP(K)-
1(1-PEXP)/(YK2*PHII))+AP(K)*XF/(YK2*PHII-(BETA+BP(K)))*((1-QEXPA(K))/
2(BETA+BP(K))-(1-PEXP)/(PHII*YK2))

```

```
GO TO 748
747 D22=0.0
    D22A=0.0
748 CONTINUE
500 CONTINUE
    PRINT*, 'D22 ', D22, ' D22A ', D22A
    PRINT*, 'D12 ', D12, ' D12A ', D12A
    DO 1000 JETA=0, NP
    XNP=FLOAT(NP)
    ETA=JETA/XNP
    F1=0.
    F3A=0.0
    F3B=0.0
    F3=0.
    B1=0.
    B3=0.
    XI1=0.
    XI3=0.
    R1=0.
    R3=0.
    RI1=0.
    RI3=0.
    D11=0.
    D21=0.
    D13=0.
    D23=0.
    DO 650 M=1, NN
    F1N=0.
    F3AN=0.0
    B3AN=0.0
    R3AN=0.0
    RI3AN=0.0
    XI3AN=0.0
    D23AN=0.0
    D13AN=0.0
    F3N=0.
    B1N=0.
    B3N=0.
    R1N=0.
    RI1N=0.
    XI1N=0.
    XI3N=0.
    R3N=0.
    RI3N=0.
    D11N=0.
    D13N=0.
    D21N=0.
    D23N=0.
    DO 630 N= 1, NUMN
    F3NK=0.
    B3NK=0.
```

```

XI3NK=0.
R3NK=0.
RI3NK=0.
D13NK=0.
D23NK=0.
F3ANK=0.0
B3ANK=0.0
XI3ANK=0.0
R3ANK=0.0
RI3ANK=0.0
D13ANK=0.0
D23ANK=0.0
IF(S(M,N)+TAU.LT.-120.) GO TO 605
CEXPST=EXP(S(M,N)+TAU)
GO TO 609
605 CEXPST=0.
609 CONTINUE
DO 610 K=1,2
IF(BP(1).NE.0.000) GO TO 56
F3NK=0.
B3NK=0.
XI3NK=0.
R3NK=0.
RI3NK=0.
D13NK=0.
D23NK=0.
F3ANK=0.0
B3ANK=0.0
XI3ANK=0.0
R3ANK=0.0
RI3ANK=0.0
D13ANK=0.0
D23ANK=0.0
GO TO 57
56 F3NK=F3NK+AP(K)*BP(K)*(QEXP(K)-CEXPST)/
1(SZ(M,N)*(S(M,N)+BP(K)))
F3ANK=F3ANK+AP(K)*XF*(BETA+BP(K))/(SZ(M,N)*(S(M,N)+BP(K)+BETA))*
1(QEXPA(K)-CEXPST)
B3NK=B3NK+AP(K)*BP(K)/(SZ(M,N)*(S(M,N)+BP(K)))*((QEXP(K)-
1BEXP)/(PHIB*XM-BP(K))-(CEXPST-BEXP)/(S(M,N)+PHIB*XM))
B3ANK=B3ANK+AP(K)*XF*(BETA+BP(K))/(SZ(M,N)*(S(M,N)+BETA+BP(K)))*
1((QEXPA(K)-BEXP)/(XM*PHIB-(BETA+BP(K)))-(CEXPST-BEXP)/(S(M,N)+XM*PHIB))
XI3NK=XI3NK+AP(K)*BP(K)/(SZ(M,N)*(S(M,N)+BP(K)))*((QEXP(K)-
1PEXP)/(YK2*PHII-BP(K))-(CEXPST-PEXP)/(S(M,N)+PHII*YK2))
XI3ANK=XI3ANK+AP(K)*XF*(BETA+BP(K))/(SZ(M,N)*(S(M,N)+BETA+BP(K)))*
1((QEXPA(K)-PEXP)/(PHII*YK2-(BETA+BP(K)))-(CEXPST-PEXP)/(YK2*PHII+S(M,N)))
IF(PHIR.EQ.0.0) GO TO 745
R3NK=R3NK+AP(K)*BP(K)/(SZ(M,N)*(S(M,N)+BP(K)))*((QEXP(K)-REXP)/
1(XK*PHIR-BP(K))-(CEXPST-REXP)/(S(M,N)+XK*PHIR))
R3ANK=R3ANK+AP(K)*XF*(BETA+BP(K))/(SZ(M,N)*(S(M,N)+BETA+BP(K)))*
1((QEXPA(K)-REXP)/(XK*PHIR-(BETA+BP(K)))-(CEXPST-REXP)/(XK*PHIR+S(M,N)))

```

```

      RI3NK=RI3NK+AP(K)*BP(K)/(SZ(M,N)*(S(M,N)+BP(K)))*(1./(XK*PHIR-BP(K))
1*((QEXP(K)-RIEXP)/(PHIR*OM-BP(K))-(REXP-RIEXP)/(PHIR*(OM-XK)))
2-1./(S(M,N)+XK*PHIR)*((CEXPST-RIEXP)/(PHIR*OM+S(M,N))-(REXP-
3RIEXP)/(PHIR*(OM-XK)))
      RI3ANK=RI3ANK+AP(K)*XF*(BETA+BP(K))/(SZ(M,N)*(S(M,N)+BETA+BP(K)))*
1(((QEXPA(K)-RIEXP)/(PHIR*OM-(BETA+BP(K)))-(REXP-RIEXP)/(PHIR*(OM-XK)))/
2(XK*PHIR-(BETA+BP(K)))-((CEXPST-RIEXP)/(PHIR*OM+S(M,N))-(REXP-RIEXP)
3/(PHIR*(OM-XK)))/(XK*PHIR+S(M,N)))
      D13NK=D13NK+AP(K)*BP(K)/(SZ(M,N)*(S(M,N)+BP(K)))*(((1-QEXP(K))/BP(K)-
1(1-RIEXP)/(PHIR*OM))/(PHIR*OM-BP(K))-((1-REXP)/(PHIR*XK)-(1-RIEXP)/
2(PHIR*OM))/(PHIR*(OM-XK)))/(XK*PHIR-BP(K))-(((CEXPST-1)/S(M,N)-
3(1-RIEXP)/(PHIR*OM))/(S(M,N)+PHIR*OM)-((1-REXP)/(PHIR*XK)-(1-RIEXP)/
4(PHIR*OM))/(PHIR*(OM-XK)))/(S(M,N)+XK*PHIR))
      D13ANK=D13ANK+AP(K)*XF*(BETA+BP(K))/(SZ(M,N)*(S(M,N)+BETA+BP(K)))*
1(((1-QEXPA(K))/(BETA+BP(K))-(1-RIEXP)/(PHIR*OM))/(PHIR*OM-(BETA+BP(K)))-
2((1-REXP)/(XK*PHIR)-(1-RIEXP)/(PHIR*OM))/(PHIR*(OM-XK)))/(XK*PHIR-(BETA+
3BP(K)))-(((CEXPST-1)/S(M,N)-(1-RIEXP)/(PHIR*OM))/(PHIR*OM+S(M,N))-
4((1-REXP)/(XK*PHIR)-(1-RIEXP)/(PHIR*OM))/(PHIR*(OM-XK)))/(XK*PHIR+S(M,N)))
745  CONTINUE
      IF(PHII.EQ.0.0) GO TO 749
      D23NK=D23NK+AP(K)*BP(K)/(SZ(M,N)*(S(M,N)+BP(K)))*(((1-QEXP(K))/BP(K)
1-(1-PEXP)/(PHII*YK2))/(YK2*PHII-BP(K))-((CEXPST-1)/S(M,N)-(1-PEXP)/
2(YK2*PHII))/(S(M,N)+YK2*PHII))
      D23ANK=D23ANK+AP(K)*XF*(BETA+BP(K))/(SZ(M,N)*(S(M,N)+BETA+BP(K)))*(((1-
1QEXPA(K))/(BETA+BP(K))-(1-PEXP)/(YK2*PHII))/(YK2*PHII-(BETA+BP(K)))-
2((CEXPST-1)/S(M,N)-(1-PEXP)/(PHII*YK2))/(YK2*PHII+S(M,N)))
      GO TO 750
749  D23NK=0.0
      D23ANK=0.0
750  CONTINUE
610  CONTINUE
57   CONTINUE
      F1N=F1N+CEXPST/SZ(M,N)
      F3N=F3N+F3NK
      F3AN=F3AN+F3ANK
      B1N=B1N+(CEXPST-BEXP)/(SZ(M,N)*(PHIB*XM+S(M,N)))
      B3N=B3N+B3NK
      B3AN=B3AN+B3ANK
      XI1N=XI1N+(CEXPST-PEXP)/(SZ(M,N)*(YK2*PHII+S(M,N)))
      XI3N=XI3N+XI3NK
      XI3AN=XI3AN+XI3ANK
      IF(PHIR.EQ.0.0) GO TO 746
      R1N=R1N+(CEXPST-REXP)/(SZ(M,N)*(S(M,N)+XK*PHIR))
      R3N=R3N+R3NK
      R3AN=R3AN+R3ANK
      RI1N=RI1N+1./(SZ(M,N)*(S(M,N)+XK*PHIR))*((CEXPST-RIEXP)/
1(PHIR*OM+S(M,N))-(REXP-RIEXP)/(PHIR*(OM-XK)))
      RI3N=RI3N+RI3NK
      RI3AN=RI3AN+RI3ANK
      D11N=D11N+1./SZ(M,N)*(((CEXPST-1)/S(M,N)-(1-RIEXP)/(PHIR*OM))/
1(S(M,N)+PHIR*OM)-((1-REXP)/(XK*PHIR)-(1-RIEXP)/(PHIR*OM))/(PHIR*(OM

```

```

2-XK)))/(S(M,N)+XK*PHIR))
746  CONTINUE
      D13N=D13N+D13NK
      D13AN=D13AN+D13ANK
      IF(PHII.EQ.0.0) GO TO 751
      D21N=D21N+1./(SZ(M,N)*(S(M,N)+YK2*PHII))*((CEXPST-1)/S(M,N)-
1(1-PEXP)/(YK2*PHII))
      GO TO 752
751  D21N=0.0
752  CONTINUE
      D23N=D23N+D23NK
      D23AN=D23AN+D23ANK
630  CONTINUE
      QC=ZZ*(YY*SIN(XL(M))-XL(M)*XK1*COS(XL(M)))+XL(M)*XK3
      QS=WW*XK3-ZZ*(YY*COS(XL(M))+XL(M)*XK1*SIN(XL(M)))
      QD=(YY*WW+XK1*XL(M)**2+VV)*COS(XL(M))+XL(M)*(2.*XK1-VV)*SIN(XL(M))
      Q=XL(M)*(QC*COS(XL(M)*ETA)+QS*SIN(XL(M)*ETA))/QD
      QCA=ZZA*(YY*SIN(XL(M))-XL(M)*XK1*COS(XL(M)))
      QSA=-ZZA*(YY*COS(XL(M))+XL(M)*XK1*SIN(XL(M)))
      QA=XL(M)*(QCA*COS(XL(M)*ETA)+QSA*SIN(XL(M)*ETA))/QD
      QB=Q-QA
      F1=F1+Q*F1N
      F3=F3+(1-XF)*Q*F3N+Q*F3AN
      B1=B1+Q*B1N
      B3=B3+(1-XF)*Q*B3N+Q*B3AN
      XI1=XI1+Q*XI1N
      XI3=XI3+(1-XF)*Q*XI3N+Q*XI3AN
      R1=R1+Q*R1N
      R3=R3+(1-XF)*Q*R3N+Q*R3AN
      RI1=RI1+Q*RI1N
      RI3=RI3+(1-XF)*Q*RI3N+Q*RI3AN
      D11=D11+Q*D11N
      D13=D13+(1-XF)*Q*D13N+Q*D13AN
      D21=D21+Q*D21N
      D23=D23+(1-XF)*Q*D23N+Q*D23AN
650  CONTINUE
      C  PRINT*, 'F1 ', F1
      C
      C  CALCULATE CONCENTRATIONS
      C
      A=EXP(.5*P*(ETA-1.))
      B=(BC*COSH(ALPHO*ETA)+BS*SINH(ALPHO*ETA))/BD
      BA=(BCA*COSH(ALPHO*ETA)+BSA*SINH(ALPHO*ETA))/BD
      BBB=B-BA
      C  PRINT*, 'B ', B, ' BA ', BA
      IF(PHIR.EQ.0.0) GO TO 1014
      SS=A*B*(1+1/XM+1/XK+GAM/(OM*XK)+1/YK2)
      SS1=A*((1-XF)*B)*(1+1/XM+1/XK+GAM/(OM*XK)+1/YK2)
      GO TO 1015
1014 SS=A*B*(1+1/XM+1/YK2)
      SS1=A*((1-XF)*B)*(1+1/XM+1/YK2)

```

```

1015  CONTINUE
      WRITE(18,911) ETA,SS1
911   FORMAT(1X,F10.3,' ',',',E11.4)
      CF(JETA)=A*(B*F2A-2.*F1-2.*F3)
      WRITE(8,910) ETA,CF(JETA)
910   FORMAT(1X,F10.3,' ',',',E11.4)
      CB(JETA)=A*PHIB*(-2.*B1+B*B2A-2.*B3)
      WRITE(16,920) ETA,CB(JETA)
920   FORMAT(1X,F10.3,' ',',',E11.4)
      CI(JETA)=A*PHII*(-2.*XI1+B*XI2A-2.*XI3)
      CR(JETA)=PHIR*A*(B*R2A-2*R1-2*R3)
      CRI(JETA)=PHIR*PHIR*GAM*A*(B*RI2A-2*RI1-2*RI3)
      CIT(JETA)=CI(JETA)+CR(JETA)+CRI(JETA)
C     PRINT*, ' CI ',CI(JETA), ' CR ',CR(JETA), ' CRI ',CRI(JETA)
      WRITE(17,930) ETA,CR(JETA)
930   FORMAT(1X,F10.3,' ',',',E11.4)
      CT(JETA)=CF(JETA)+CB(JETA)+CIT(JETA)
      WRITE(3,990) ETA, CT(JETA)
990   FORMAT(1X,F10.3,' ',',',E11.4)
      CD(JETA)=(PHIR*OM-PHIE1)*GAM*PHIR*PHIR*A*(-2*D11+B*D12A-2*D13)+
2(PHII*YK2-PHIE2)*PHII*A*(-2*D21+B*D22A-2*D23)
      WRITE(19,995) ETA,CD(JETA)
995   FORMAT(1X,F10.3,' ',',',E11.4)
C
C     CALCULATE FLUX AT ETA=0.0
C
      CP=0.0
      DO 800 K=1,2
800   CP=CP+AP(K)*QEXP(K)
1000  CONTINUE
      XFLUX=P*(1.-R)*CP+BE*(CP+E1-CF(1))
      PRINT*, 'FLUX AT ETA=0.0: ',XFLUX
      GO TO 7701
7700  PRINT*, 'NO CONVERGENCE IN IMPOLES SUBROUTINE'
7701  CONTINUE
      END

```

```

C
C
C   THIS SUBROUTINE CALCULATES THE ROOTS TO THE EQUATION F(XL(N))=0
C   USING NEWTON'S METHOD. AN INITIAL GUESS, GL(N), IS SUPPLIED AND
C   F(GL(N)) IS CALCULATED. IF F(GL(N)) IS NOT A ROOT THEN GL(N+1) IS
C   CALCULATED BY ADDING 0.3 TO GL(N), AND F(GL(N+1)) IS CALCULATED.
C   IF THE SIGN OF F(GL(N+1)) IS DIFFERENT THAN THE SIGN OF F(GL(N)),
C   NEWTON'S METHOD IS APPLIED ABOUT F(GL(N+1)). IF THE SIGNS DO NOT
C   DIFFER THEN THE PROCEDURE IS REPEATED UNTIL THE SIGNS DIFFER, AND
C   AND NEWTON'S METHOD IS APPLIED TO THE LATTER TERM.
C
C
C   SUBROUTINE IMPOLES1(ZZ,YY,WW,VV,XK1,TOL,NN,XL,IER)
C   IMPLICIT DOUBLE PRECISION(A-H,O-Z)
C   DIMENSION XL(100),F(101),GL(101)
C   GL(1)=0.01
C   DO 1000 K=1,NN
C   DO 800 N=1,25
C
C   TEST TO DETERMINE IF GL(N) IS A ROOT
C
C   F(N)=(YY*WW+XK1*(GL(N)*GL(N)))*SIN(GL(N))+GL(N)*VV*COS(GL(N))
C   IF(ABS(F(N)).LE.TOL) GO TO 899
C   IF(N-1) 135,135,140
135  CONTINUE
C   GL(N+1)=GL(N)+1.0
C   GO TO 800
140  IF(F(N)/F(N-1)) 145,143,143
143  GL(N+1)=GL(N)+0.5
800  CONTINUE
145  CONTINUE
C
C   NEWTON'S METHOD ALGORITM
C
C   GLL=GL(N)
C   DO 600 L=1,25
C   FF=(YY*WW+(XK1*GLL*GLL))*SIN(GLL)+GLL*VV*COS(GLL)
C   FP=(YY*WW+VV*(XK1*GLL*GLL))*COS(GLL)+(2.*XK1-VV)*GLL*SIN(GLL)
C   GLL=GLL-FF/FP
C   IF(ABS(FF).LE.TOL) GO TO 900
600  CONTINUE
C   PRINT*, ' NO CONVERGENCE'
C   IER=2
C   GO TO 901
899  GLL=GL(N)
900  XL(K)=GLL
C   MM=K+N
C   WRITE(2,101) K,XL(K)
101  FORMAT(1X,I3,1X,F14.6)
C   GL(1)=XL(K)+.05
1000 CONTINUE

```

901 CONTINUE
IER=1
RETURN
END


```

C      THIS SUBROUTINE CALCULATES THE REAL, NEGATIVE ROOTS OF AN NTH
C      ORDER POLYNOMIAL (F(X)=0) BY NEWTON'S METHOD.  THE PROGRAM
C      BEGINS AT X=0.0 AND EVALUATES F(X) AT INTERVALS OF -0.1.
C      THIS CONTINUES UNTIL F(X) CHANGES SIGN.  NEWTON'S METHOD IS
C      THEN APPLIED TO DETERMINE THE ROOT.  THE POLYNOMIAL IS THEN
C      DIVIDED BY X-X0, WHERE X0 IS THE ROOT, TO YIELD AN NTH-1 ORDER
C      POLYNOMIAL.  THE SECOND ROOT IS THEN DETERMINED AS ABOVE.  THIS
C      CONTINUES UNTIL A SECOND ORDER POLYNOMIAL IS PRODUCED WHICH IS THEN
C      SOLVED BY APPLICATION OF THE QUADRATIC FORMULA.
C      SUBROUTINE SZFIND(XL,P,XM,PHIB,PHIR,XK,YK2,GAM,OM,PHII,PHIE1,PHIE2,
1NN,NUMN,S,SZ)
      IMPLICIT DOUBLE PRECISION(A-H,O-Z)
      DIMENSION A(5),B(5),FX(50),S(200,5),XL(200),SZ(200,5),XP(200),AA(5)

C      INITIALIZE
C
C      DO 51 I=1,4
51      B(I)=0.0
      DO 52 I=1,50
52      FX(I)=0.0
      X=0.0
      EPS=1E-08
      DO 14 M=1,NN
14      XP(M)=XL(M)**2+0.25*P**2
      IF(PHIE1.EQ.0.0.AND.PHIB.EQ.0.0.AND.PHII.EQ.0.0) GO TO 1400
      IF(PHIR.EQ.0.0.AND.PHIB.EQ.0.0.AND.PHII.EQ.0.0) GO TO 1410
      IF(PHIR.EQ.0.) GO TO 1000
      IF(PHIB.EQ.0.) GO TO 1100
      NMAX=5
      NUMN=5
      KNOT=1
      GO TO 1200
1400     CONTINUE
      NMAX=2
      NUMN=2
      DO 1401 M=1,NN
      BB=PHIR*(XK+1)+XP(M)
      C=PHIR*(PHIR+GAM+XP(M)*XK)
      S(M,1)=- (BB+SQRT(BB*BB-4*C))/2
      S(M,2)=C/S(M,1)
1401     CONTINUE
      DO 1402 M=1,NN
      DO 1402 J=1,2
1402     SZ(M,J)=S(M,J)*(1+(XK-GAM)*(PHIR/(S(M,J)+XK*PHIR))**2)
      GO TO 16
1410     NUMN=1
      NMAX=1
      DO 1411 M=1,NN
      S(M,1)=-XP(M)
      SZ(M,1)=S(M,1)
      PRINT*, 'S(M,1) ', S(M,1)

```

```

1411  CONTINUE
      GO TO 16
1100  NMAX=4
      NUMN=4
      KNOT=1
      GO TO 1200
1000  CONTINUE
      IF (PHIB.EQ.0.0) GO TO 1001
      NMAX=3
      NUMN=3
      GO TO 1200
1001  NUMN=2
      NMAX=2
      DO 1403 M=1, NN
      BBB=XP(M)+PHII*(YK2+1)
      CCC=PHII*(YK2*(XP(M)+PHII)-PHIE2)
      S(M,1)=- (BBB+SQRT(BBB*BBB-4*CCC))/2
      S(M,2)=CCC/S(M,1)
C     PRINT*, 'S(M,1) ', S(M,1), ' S(M,2) ', S(M,2)
1403  CONTINUE
      DO 1404 M=1, NN
      DO 1404 J=1, 2
      SZ(M, J)=S(M, J)*(1+PHII*PHIE2/((S(M, J)+PHII*YK2)**2))
1404  CONTINUE
      GO TO 16
1200  CONTINUE
      DO 200 M=1, NN
      IF (M.EQ.1) GO TO 1201
      X=S(M-1, 1)
1201  CONTINUE
      NMAX=NUMN
      IF (NMAX.EQ.3) GO TO 1050
      A(1)=PHIR*(XK+OM+1)+PHIB*(XM+1)+PHII*(YK2+1)+XP(M)
      A(2)=PHIR*(PHII*YK2*(XK+OM+1)+PHIR*(OM*(XK+1)+GAM)+XM*PHIB)+
1PHIB*(XM+1)*(PHIR*(XK+OM)+PHII*YK2)+(XP(M)+PHII)*(PHIR*(XK+OM)+
2XM*PHIB)+PHII*((XP(M)+PHII)*YK2-PHIE2)
      A(3)=PHIR*PHIR*(XK*OM+PHII*YK2+(GAM+OM)*(XM*PHIB+PHII*YK2)
1+GAM*(OM*PHIR
2-PHIE1))+PHIR*PHIB*(XM+1)*(PHII*YK2*(XK+OM)+PHIR*XK*OM)+
3PHIR*(XP(M)+PHII)*(PHIR*OM*XK+XM*PHIB*(XK+OM))+PHIR*XM*PHIB*PHII*YK2
4+PHII*(PHIR*(XK+OM)+XM*PHIB)*((XP(M)+PHII)*YK2-PHIE2)
      A(4)=PHIR*PHIR*(PHIB*PHII*YK2*((XM+1)*XK*OM+XM*(GAM+OM))+
1GAM*(OM*PHIR-PHIE1)*(XM*PHIB+PHII*YK2))+PHIR*((XP(M)+PHII)*
2PHIR*OM*XK+XM*PHIB+PHII*((XP(M)+PHII)*YK2-PHIE2)*(PHIR*OM*XK+
3XM*PHIB*(XK+OM)))
      A(5)=PHIR*PHIR*XM*PHIB*PHII*(YK2+GAM*(OM*PHIR-PHIE1)+
10M*XK*((XP(M)+PHII)*YK2-PHIE2))
      GO TO 1051
1050  A(1)=XP(M)+PHIB*(XM+1)+PHII*(YK2+1)
      A(2)=PHIB*PHII*YK2*(XM+1)+XP(M)*(XM*PHIB+PHII*YK2)+PHII*(PHII*YK2+
1XM*PHIB-PHIE2)

```

```

A(3)=XM*PHIB*PHII*(YK2*(XP(M)+PHII)-PHIE2)
1051 CONTINUE
DO 17 II=1,NUMN
17 AA(II)=A(II)
DO 20 J=1,5
KK=K
IF(M.GT.1) GO TO 13
DO 10 K=2,500
FX(1)=A(NMAX)
IF(K.LI.25) GO TO 777
X=X-1
GO TO 778
777 CONTINUE
X=X-0.1
778 CONTINUE
FX(K)=X
DO 11 L=1,NMAX-1
FX(K)=(A(L)+FX(K))*X
11 CONTINUE
FX(K)=FX(K)+A(NMAX)
C
C TEST FOR A CHANGE OF SIGN
C
IF(FX(K)/FX(K-1).LE.0.0) GO TO 15
10 CONTINUE
PRINT*, ' NO SIGN CHANGE AFTER 200 ITERATIONS '
GO TO 16
15 CONTINUE
IF(KK.GT.25) GO TO 19
X=X+0.1
GO TO 18
19 X=X/1.5
18 CONTINUE
C
C NEWTON'S METHOD ALGORITHM
C
13 CONTINUE
IF(M.EQ.1) GO TO 707
X=S(M-1,J)
707 CONTINUE
DO 40 K=1,40
F=X
U=FLOAT(NMAX)
FP=U*X
DO 12 MM=1,NMAX-1
V=FLOAT(NMAX-MM)
F=(A(MM)+F)*X
IF(MM.EQ.(NMAX-1)) GO TO 901
FP=(V*A(MM)+FP)*X
901 CONTINUE
12 CONTINUE

```

```

F=F+A(NMAX)
FP=FP+A(NMAX-1)
XX=X
X=X-F/FP
W=(X-XX)/X
IF(ABS(W).LE.EPS) GO TO 30
40 CONTINUE
PRINT*, ' NO CONVERGENCE '
GO TO 16
30 S(M,J)=X
C
C SYNTHETIC DIVISION TO REDUCE ORDER OF POLYNOMIAL
C
NMAX=NMAX-1
B(1)=A(1)+S(M,J)
A(1)=B(1)
C IF(NMAX.EQ.1) GO TO 76
DO 60 L=2,NMAX
B(L)=A(L)+B(L-1)*S(M,J)
A(L)=B(L)
60 CONTINUE
IF(NMAX.EQ.2) GO TO 70
20 CONTINUE
70 CONTINUE
C PRINT*, 'A(1) ',A(1), ' A(2) ',A(2)
IF(A(1)*A(1).LT.4*A(2)) GO TO 701
S(M,J+1)=(-A(1)+SQRT(A(1)*A(1)-4*A(2)))/2.
GO TO 702
701 S(M,J+1)=-PHIR*XK*0.98
702 CONTINUE
S(M,J+2)=A(2)/S(M,J+1)
C76 S(M,J+1)=A(2)/S(M,J)
C
C IMPROVEMENT OF S(M,N) ESTIMATES BY NEWTON'S METHOD
C
DO 500 N=1,NUMN
X=S(M,N)
DO 499 LK=1,40
F=X
U=FLOAT(NUMN)
FP=U*X
DO 501 MM=1,NUMN-1
V=FLOAT(NUMN-MM)
F=(AA(MM)+F)*X
IF(MM.EQ.(NUMN-1)) GO TO 502
FP=(C*AA(MM)+FP)*X
502 CONTINUE
501 CONTINUE
F=F+AA(NUMN)
FP=FP+AA(NUMN-1)
XX=X

```

```

X=X-F/FP
W=(X-XX)/X
IF(ABS(W).LE.EPS) GO TO 503
499 CONTINUE
PRINT*, ' NO CONVERGENCE IN ROOTS CORRECTION LOOP '
PRINT*, ' W ', W, ' EPS ', ' X ',X
GO TO 16
503 S(M,N)=X
C PRINT*, ' N ',N,' S(M,N) ',S(M,N)
500 CONTINUE
200 CONTINUE
WRITE(2,71)
71 FORMAT(1X,' ROOTS OF S(M,N) ')
DO 99 M=1,NN
WRITE(2,72) (S(M,N),N=1,5)
72 FORMAT(1X,5F14.6)
99 CONTINUE
DO 5000 M=1,NN
DO 5000 N=1,NUMN
IF(NMAX.EQ.3) GO TO 4000
SZ(M,N)=S(M,N)*(1+XM*(PHIB/(S(M,N)+XM*PHIB))**2+((PHIR/((S(M,N)+
1XK*PHIR)*(S(M,N)+PHIR*OM))**2)*((XK-GAM)*((S(M,N)+PHIR*OM)**2)+
2GAM*PHIE1*(2*S(M,N)+PHIR*(OM+XK))+PHII*PHIE2/((S(M,N)+PHII*YK2)
3**2))
GO TO 4001
4000 SZ(M,N)=S(M,N)*(1+XM*(PHIB/(S(M,N)+XM*PHIB))**2+PHII*PHIE2/((S(M,N)+
1PHII*YK2)**2))
4001 CONTINUE
5000 CONTINUE
16 CONTINUE
RETURN
END

```

```

      IMPLICIT DOUBLE PRECISION(A-H,O-Z)
      DIMENSION AP(2),BP(2),XL(200),XP(200),QEXP(2),F(50),G(51),S(200,5),
1SZ(200,5),QEXPA(2)
      OPEN(1,FILE='INIT')
      OPEN(2,FILE='INFO')
      OPEN(3,FILE='OUTP')
      OPEN(4,FILE='DECAY')
      OPEN(7,FILE='ENTRIES')
      OPEN(8,FILE='FREE')
      OPEN(16,FILE='BOUND')
      OPEN(17,FILE='CELLULAR')
      OPEN(18,FILE='DEGRAD')
      OPEN(19,FILE='INF01')
      OPEN(20,FILE='DEG1')
      OPEN(21,FILE='DEG2')
      OPEN(22,FILE='CR')
      OPEN(23,FILE='CRI')
      OPEN(14,FILE='CIX')
      READ(1,*) XKE2,P,XKE1,R,D,YL,XM,PHIB,PHIR,XK,YK2,GAM,OM,PHII,
1PHIE1,PHIE2,XF,BETA,PHIE
      READ(4,*) AP(1),AP(2),BPTIME1,BPTIME2
      READ(7,*) E1,TOL,XK1,NN,NP
      XK2=XKE2*YL/(D*E1)
      BE=XKE1*YL/(D*E1)
      XK3=E1*XK2
      WRITE(2,26) AP(1),AP(2),BPTIME1,BPTIME2
      WRITE(2,27)XK2,XK3,P,BE,R,D,YL,XM,PHIB,PHIR,XK,YK2,GAM,OM,PHII,
1PHIE1,PHIE2,XF,BETA,PHIE
26  FORMAT( ' PLASMA DECAY COEFFICIENTS: ',4F10.6,/,/)
27  FORMAT( ' INPUT PARAMETERS: ',/, ' K2= ',F8.3,9X, ' K3= ',F6.3,
1/, ' P= ',F6.2,11X, ' BE= ',F6.3,/, ' R= ',F6.2,11X, ' D= ',E11.3,/,
2' L= ',F8.4,9X,/, ' XM=',F6.3,9X, ' PHIB= ',F6.3,
3/, ' PHIR= ',F6.3,10X, ' XK=',F6.3,/, ' K2= ',F6.3,/, ' GAMMA=',F6.3,10X,
4' OMEGA=',F6.3,/, ' PHII=',F6.3,10X, ' PHIE1=',F6.3,/, ' PHIE2=',F6.3,/,
5' XF= ',F6.3,10X, ' BETA= ',F6.3,/, ' PHIE= ',F6.3,/)
      ZZ=(P*(1.-R)+BE)*E1*EXP(0.5*P)
      ZZA=BE*E1*EXP(0.5*P)
      ZZB=E1*P*(1-R)*EXP(0.5*P)
      YY=XK2-0.5*P*XK1
      WW=0.5*P+BE
      VV=XK2-(P+BE)*XK1

C
C  POSSIBILITY OF POLES ON THE REAL AXIS
C
      BETA1=-VV/XK1
      BETA2=YY*WW/XK1
      BR=BETA1/BETA2
      IF(BETA1) 110,200,100
100 IF(BETA2) 200,200,101
101 IF(BR-1.) 140,200,200
110 IF(BETA2) 120,200,140

```

```

120 IF(BR=1.) 125,140,140
125 BB=DSQRT(-BETA2)
      FUN=.5*BR*BB
      IF(FUN-TANH(BB)) 200,140,190
140 NREAL=1
      GO TO 195
190 NREAL=2
195 CONTINUE
      PRINT*, 'WARNING: THIS PROGRAM DOES NOT ACCOUNT FOR POLES
10N THE REAL AXIS'
      WRITE(10,196) NREAL
196 FORMAT( ' NUMBER OF POLES ON THE REAL AXIS (OTHER THAN S=0): ', I3)
200 CONTINUE
C
C
C CALL SUBROUTINES
C
      CALL IMPOLES1(ZZ,YY,WW,VV,XK1,TOL,NN,XL,IER)
      IF(IER.EQ.2) GO TO 7700
      IF(XM.NE.0.0000) GO TO 780
      ALPHO=DSQRT(0.25*P**2+PHIB+GAM/XK*(PHIR-PHIE1/OM)+PHII-PHIE2/YK2)
      SHA=SINH(ALPHO)
      CHA=COSH(ALPHO)
      GO TO 782
780 CONTINUE
      IF(PHIR.EQ.0.0) GO TO 1011
      ALPHO=DSQRT(.25*P**2+(GAM/XK)*(PHIR-PHIE1/OM)+PHII-PHIE2/YK2)
      GO TO 1012
1011 ALPHO=DSQRT(0.25*P**2+PHII-PHIE2/YK2)
1012 CONTINUE
      SHA=SINH(ALPHO)
      CHA=COSH(ALPHO)
782 CONTINUE
      IF(ALPHO-P/2.GT.1E-10) GO TO 781
      BN1=(ZZ*(YY*SHA-ALPHO*CHA)+ALPHO*XK3)*EXP(-P/2)*
1(EXP(P)-1+P)
      BN2=(WW*XK3-ZZ*(YY*CHA-ALPHO*SHA))*EXP(-P/2)*
1(EXP(P)-1-P)
      BD=(YY*WW-XK1*ALPHO**2)*SHA+ALPHO*VV*CHA
      B=(BN1+BN2)/(2*P*BD)
      BA=(ZZA*(YY*SHA-ALPHO*CHA)*EXP(-P/2)*(EXP(P)-1+P)-ZZA*(YY*CHA-ALPHO*
1SHA)*EXP(-P/2)*(EXP(P)-1-P))/(2*P*BD)
      BBB=B-BA
      GO TO 783
781 BN1=ZZ*((P/2.-YY)*(1-EXP(-P/2.))*CHA)+(P*YY/(2.*ALPHO)-ALPHO)*EXP(-P/2.)
1*SHA)
      BN2=XK3*((WW-P/2.)*(-EXP(-P/2.))+CHA)-(P*WW/(2.*ALPHO)-ALPHO)*SHA)
      BQ=4.*ALPHO/(4.*ALPHO**2-P*P)
      BD=(YY*WW-XK1*ALPHO**2)*SHA+ALPHO*VV*CHA
      B=BQ*(BN1+BN2)/BD
      BA=BQ/BD*ZZA*((P/2-YY)*(1-EXP(-P/2))*CHA)+(P*YY/(2*ALPHO)-ALPHO)*

```

```

1EXP(-P/2)*SHA)
  BBB=B-BA
783  CONTINUE
      PRINT*, 'ALPHO=', ALPHO
      IF(PHIR.EQ.0.0) GO TO 1014
      SSD1=0.0
      SSD2=0.0
      SS=B*(1+1/XM+1/XK+GAM/(OM*XK)+1/YK2)
      SS1=B*(1-XF)*(1+1/XM+1/XK+GAM/(OM*XK)+1/YK2)
C    SS1=(BBB+BA*(1-XF))*(1+1/XM+1/XK+GAM/(OM*XK)+1/YK2)
      GO TO 1015
1014 SS=B*(1+1/XM+1/YK2)
      SS1=B*(1-XF)*(1+1/XM+1/YK2)
C    SS1=(BBB+BA*(1-XF))*(1+1/XM+1/YK2)
1015 CONTINUE
      D22SS=0.0
      BP(1)=BPTIME1*YL*YL/(60*D)
      BP(2)=BPTIME2*YL*YL/(60*D)
      D12SS=0.0
      IF(PHIR.EQ.0.0) GO TO 1111
      D12SS=1/(PHIR*OM*PHIR*XK)*(AP(1)/BP(1)+AP(2)/BP(2))
      DO 1112 K=1,2
1112 SSD1=SSD1+1/(PHIR*OM*PHIR*XK)*B*AP(K)*XF/(BETA+BP(K))
1111 CONTINUE
      D22SS=1/(PHII*YK2)*(AP(1)/BP(1)+AP(2)/BP(2))
      DO 1113 K=1,2
1113 SSD2=SSD2+1/(PHII*YK2)*B*XF*AP(K)/(BETA+BP(K))
      CUM=(PHIR*OM-PHIE1)*GAM*PHIR*PHIR*D12SS*B+(PHII*YK2-PHIE2)*PHII*
1D22SS*B
      CUM1=(PHIR*OM-PHIE1)*GAM*PHIR*PHIR*(D12SS*(1-XF)*B+SSD1)+
1(PHII*YK2-PHIE2)*PHII*(D22SS*(1-XF)*B+SSD2)
      XR=(PHII*YK2-PHIE2)/(YK2*PHII)
      CUME=XR*PHIE*(AP(1)/BP(1)+AP(2)/BP(2))
      CUME1=XR*PHIE*((1-XF)*(AP(1)/BP(1)+AP(2)/BP(2))+
1XF*(AP(1)/(BP(1)+BETA)+AP(2)/(BP(2)+BETA)))
C
C
C
C    SS IS THE STEADY STATE TISSUE CONCENTRATION FOR CONSTANT KE
C    SS1 IS THE STEADY STATE TISSUE CONCENTRATION FOR DECREASING KE
C    CUM IS THE CUMULATIVE AMOUNT DEGRADED PER UNIT VOLUME OF TISSUE
C    FOR CONSTANT KE
C    CUM1 IS THE CUMULATIVE AMOUNT DEGRADED PER UNIT VOLUME OF TISSUE
C    FOR DECREASING KE
C    CUME IS THE CUMULATIVE AMOUNT DEGRADED BY THE ENDOTHELIAL CELLS
C    PER UNIT VOLUME OF TISSUE FOR CONSTANT KE
C    CUME1 IS THE CUMULATIVE AMOUNT DEGRADED BY THE ENDOTHELIAL CELLS
C    PER UNIT VOLUME OF TISSUE FOR DECREASING KE
C
C
      PRINT*, 'ALPHO ', ALPHO
      PRINT*, ' SS ', SS, ' SS1 ', SS1

```



```

PRINT*, ' CUM ', CUM, ' CUM1 ', CUM1
PRINT*, ' CUME ', CUME, ' CUME1 ', CUME1
WRITE(2, 29) ALPHO, SS, SS1, CUM, CUM1, CUME, CUME1
29  FORMAT(1X, 'ALPHA= ', F14.6, '/', 1X, 'STEADY STATE TOTAL= ', F14.6, '/', 1X,
1'DECAYING KE: STEADY STATE TOTAL=', F14.6, '/', 1X,
2'CUMULATIVE AMOUNT DEGRADED= ', F14.6, '/', 1X,
3'DECAYING KE: CUMULATIVE AMOUNT DEGRADED= ', F14.6, '/',
4'EC DEGRADATION = ', F14.6, '/',
5'DECAYING KE: EC DEGRADATION= ', F14.6)
CALL SZFIND(XL, P, XM, PHIB, PHIR, XK, YK2, GAM, OM, PHII, PHIE1, PHIE2,
1NN, NUMN, S, SZ)
PRINT*, 'NUMN=', NUMN
WRITE(2, 28)
28  FORMAT(1X, 'TIME, hr', 2X, 'TOTAL', 5X, 'FREE', 6X, 'BOUND', 5X,
1'CELLULAR', 3X, 'DEGRADED', 2X, 'EC DEGRADED', ./.)
WRITE(19, 280)
280  FORMAT(1X, 'TIME, hr', 2X, 'CR', 5X, 'CRI', 5X, 'CI', 5X, 'CD1', 5X, 'CD2')

```

C
C
C

PERFORM SUMMATIONS

```

F2=0.
B2=0.
X12=0.
R2=0.0
RI2=0.0
D12SS=0.0
D22SS=0.0
D12=0.0
D22=0.0
TI=5.0
DO 1000 KK=1, 19
TAU=TI*D*60/(YL*YL)
BP(1)=BPTIME1*TI/TAU
BP(2)=BPTIME2*TI/TAU
F2=0.
F2A=0.0
B2=0.
B2A=0.0
X12=0.
X12A=0.0
R2=0.0
R2A=0.0
RI2=0.0
RI2A=0.0
D12SS=0.0
D12SSA=0.0
D22SS=0.0
D22SSA=0.0
D12=0.0
D12A=0.0

```

```

D22=0.0
D22A=0.0
CDE=0.0
DO 500 K=1,2
QEXP(K)=EXP(-BP(K)*TAU)
QEXPA(K)=EXP(-(BETA+BP(K))*TAU)
F2=F2+AP(K)*QEXP(K)
F2A=F2A+AP(K)*((1-XF)*QEXP(K)+XF*QEXPA(K))
IF(XM*PHIB*TAU.GT.120.)GO TO 603
BEXP=EXP(-PHIB*XM*TAU)
GO TO 604
603 BEXP=0.0
604 CONTINUE
B2=B2+AP(K)/(XM*PHIB-BP(K))*(QEXP(K)-BEXP)
B2A=B2A+AP(K)*(1-XF)/(XM*PHIB-BP(K))*(QEXP(K)-BEXP)+
1AP(K)*XF/(XM*PHIB-(BETA+BP(K)))*(QEXPA(K)-BEXP)
IF(((PHII*YK2)*TAU).GT.120.)GO TO 615
PEXP=EXP(-(PHII*YK2)*TAU)
GO TO 606
615 PEXP=0.0
606 CONTINUE
XI2=XI2+AP(K)/(PHII*YK2-BP(K))*(QEXP(K)-PEXP)
XI2A=XI2A+AP(K)*(1-XF)/(YK2*PHII-BP(K))*(QEXP(K)-PEXP)+
1AP(K)*XF/(YK2*PHII-(BETA+BP(K)))*(QEXPA(K)-PEXP)
CDE=CDE+AP(K)*(1-XF)/(PHII*YK2-BP(K))*((1-QEXP(K))/BP(K)-
1(1-PEXP)/(PHII*YK2))+XF*AP(K)/(PHII*YK2-BETA-BP(K))*
2((1-EXP(-(BP(K)+BETA)*TAU))/(BP(K)+BETA)-(1-PEXP)/(PHII*YK2))
IF(XK*PHIR*TAU.GT.120)GO TO 616
REXP=EXP(-XK*PHIR*TAU)
GO TO 607
616 REXP=0.0
607 CONTINUE
R2=R2+AP(K)/(XK*PHIR-BP(K))*(QEXP(K)-REXP)
R2A=R2A+AP(K)*(1-XF)/(XK*PHIR-BP(K))*(QEXP(K)-REXP)+
1AP(K)*XF/(XK*PHIR-(BETA+BP(K)))*(QEXPA(K)-REXP)
IF(PHIR*OM*TAU.GT.120)GO TO 617
RIEXP=EXP(-PHIR*OM*TAU)
GO TO 608
617 RIEXP=0.0
608 CONTINUE
IF(PHIR.EQ.0.0)GO TO 1019
RI2=RI2+AP(K)/(XK*PHIR-BP(K))*((QEXP(K)-RIEXP)/(PHIR*OM-BP(K))
1-(REXP-RIEXP)/(PHIR*(OM-XK)))
RI2A=RI2A+AP(K)*(1-XF)/(XK*PHIR-BP(K))*((QEXP(K)-RIEXP)/(PHIR*OM-BP(K))
1-(REXP-RIEXP)/(PHIR*(OM-XK)))+AP(K)*XF/(XK*PHIR-(BETA+BP(K)))*
1((QEXPA(K)-RIEXP)/(PHIR*OM-(BETA+BP(K)))-(REXP-RIEXP)/(PHIR*(OM-XK)))
D12=D12+AP(K)/(XK*PHIR-BP(K))*(((1-QEXP(K))/BP(K)-(1-RIEXP)/
1(PHIR*OM))/(PHIR*OM-BP(K))-((1-REXP)/(XK*PHIR)-(1-RIEXP)/(PHIR*OM))/
2(PHIR*(OM-XK)))
D12A=D12A+AP(K)*(1-XF)/(XK*PHIR-BP(K))*(((1-QEXP(K))/BP(K)-(1-RIEXP)/
1(PHIR*OM))/(PHIR*OM-BP(K))-((1-REXP)/(PHIR*OM)-(1-RIEXP)/(PHIR*OM)))/(PHIR*

```

```

2(OM-XK)))+AP(K)*XF/(XK*PHIR-(BETA+BP(K)))*(((1-QEXPA(K))/(BETA+BP(K))-
3(1-RIEXP)/(PHIR*OM))/(PHIR*OM-(BETA+BP(K)))-((1-REXP)/(XK*PHIR)-
4(1-RIEXP)/(PHIR*OM))/(PHIR*(OM-XK)))
D1ZSS=D12SS+AP(K)/(BP(K)*PHIR*OM*PHIR*XK)
1019 CONTINUE
D22=D22+AP(K)/(YK2*PHII-BP(K))*((1-QEXP(K))/BP(K)-(1-PEXP)/
1(PHII*YK2))
D22A=D22A+AP(K)*(1-XF)/(YK2*PHII-BP(K))*((1-QEXP(K))/BP(K)-
1(1-PEXP)/(YK2*PHII))+AP(K)*XF/(YK2*PHII-(BETA+BP(K)))*((1-QEXPA(K))/
2(BETA+BP(K))-(1-PEXP)/(PHII*YK2))
D22SS=D22SS+AP(K)/(BP(K)*PHII*YK2)
500 CONTINUE
PRINT*, 'F2 ', F2, ' F2A ', F2A
PRINT*, 'D12 ', D12, ' D12A ', D12A
PRINT*, 'BBB ', BBB, ' BA ', BA
F1=0.0
F3B=0.0
F3C=0.0
F3=0.0
B1=0.0
B3=0.0
XI1=0.0
XI3=0.0
R1=0.0
R3=0.0
RI1=0.0
RI3=0.0
D11=0.0
D21=0.0
D13=0.0
D23=0.0
DO 650 M=1, NN
F1N=0.0
F3N=0.0
F3AN=0.0
B1N=0.0
B3N=0.0
B3AN=0.0
XI1N=0.0
XI3N=0.0
XI3AN=0.0
R3N=0.0
R3AN=0.0
R1N=0.0
RI1N=0.0
RI3N=0.0
RI3AN=0.0
D11N=0.0
D13N=0.0
D13AN=0.0
D21N=0.0

```

```

D23N=0.0
D23AN=0.0
DO 680 N= 1, NUMN
F3NK=0.0
B3NK=0.0
XI3NK=0.0
R3NK=0.0
RI3NK=0.0
D13NK=0.0
D23NK=0.0
F3ANK=0.0
B3ANK=0.0
XI3ANK=0.0
R3ANK=0.0
RI3ANK=0.0
D13ANK=0.0
D23ANK=0.0
IF((REAL(S(M,N)*TAU)).LT.-120.) GO TO 605
CEXPST=EXP(S(M,N)*TAU)
GO TO 609
605 CEXPST=0.0
609 CONTINUE
DO 610 K=1,2
IF(BP(1).EQ.0.000) GO TO 57
F3NK=F3NK+AP(K)*BP(K)*(QEXP(K)-CEXPST)/
1(SZ(M,N)*(S(M,N)+BP(K)))
F3ANK=F3ANK+XF*AP(K)*(BETA+BP(K))/(SZ(M,N)*(S(M,N)+BETA+BP(K)))*
1(QEXPA(K)-CEXPST)
B3NK=B3NK+AP(K)*BP(K)/(SZ(M,N)*(S(M,N)+BP(K)))*((QEXP(K)-
1BEXP)/(XM*PHIB-BP(K))-(CEXPST-BEXP)/(S(M,N)+XM*PHIB))
B3ANK=B3ANK+XF*AP(K)*(BETA+BP(K))/(SZ(M,N)*(S(M,N)+BETA+BP(K)))*
1((QEXPA(K)-BEXP)/(XM*PHIB-(BETA+BP(K)))-(CEXPST-BEXP)/(S(M,N)+XM*PHIB))
XI3NK=XI3NK+AP(K)*BP(K)/(SZ(M,N)*(S(M,N)+BP(K)))*((QEXP(K)-
1PEXP)/(PHII*YK2-BP(K))-(CEXPST-PEXP)/(S(M,N)+PHII*YK2))
XI3ANK=XI3ANK+XF*AP(K)*(BETA+BP(K))/(SZ(M,N)*(S(M,N)+BETA+BP(K)))*
1((QEXPA(K)-PEXP)/(PHII*YK2-(BETA+BP(K)))-(CEXPST-PEXP)/(YK2*PHII+S(M,N)))
IF(PHIR.EQ.0.0) GO TO 1023
R3NK=R3NK+AP(K)*BP(K)/(SZ(M,N)*(S(M,N)+BP(K)))*((QEXP(K)-REXP)/
1(XK*PHIR-BP(K))-(CEXPST-REXP)/(S(M,N)+XK*PHIR))
R3ANK=R3ANK+XF*AP(K)*(BP(K)+BETA)/(SZ(M,N)*(S(M,N)+BETA+BP(K)))*
1((QEXPA(K)-REXP)/(XK*PHIR-(BETA+BP(K)))-(CEXPST-REXP)/(XK*PHIR+S(M,N)))
RI3NK=RI3NK+AP(K)*BP(K)/(SZ(M,N)*(S(M,N)+BP(K)))*(1./(XK*PHIR-BP(K))
1*((QEXP(K)-RIEXP)/(PHIR*OM-BP(K))-(REXP-RIEXP)/(PHIR*(OM-XK)))
2-1./(S(M,N)+XK*PHIR)*((CEXPST-RIEXP)/(PHIR*OM+S(M,N))-(REXP-
3RIEXP)/(PHIR*(OM-XK))))
RI3ANK=RI3ANK+AP(K)*XF*(BETA+BP(K))/(SZ(M,N)*(S(M,N)+BETA+BP(K)))*
1(((QEXPA(K)
2-RIEXP)/(PHIR*OM-(BETA+BP(K)))-(REXP-RIEXP)/(PHIR*(OM-XK)))/(XK*PHIR-
3(BETA+BP(K)))-((CEXPST-RIEXP)/(PHIR*OM+S(M,N))-(REXP-RIEXP)
4/(PHIR*(OM-XK)))/(XK*PHIR+S(M,N)))
D13NK=D13NK+AP(K)*BP(K)/(SZ(M,N)*(S(M,N)+BP(K)))*(((1-QEXP(K))/BP(K)-

```

```

1(1-RIEXP)/(PHIR*OM)/(PHIR*OM-BP(K))-((1-REXP)/(PHIR*XK)-(1-RIEXP)/
2(PHIR*OM))/(PHIR*(OM-XK))/(XK*PHIR-BP(K))-(((CEXPST-1)/S(M,N)-
3(1-RIEXP)/(PHIR*OM))/(S(M,N)+PHIR*OM)-((1-REXP)/(PHIR*XK)-(1-RIEXP)/
4(PHIR*OM))/(PHIR*(OM-XK)))/(S(M,N)+XK*PHIR))
D13ANK=D13ANK+XF*AP(K)*(BETA+BP(K))/(SZ(M,N)*(S(M,N)+BETA+BP(K)))*
1(((1-QEXPA(K))/(BETA+BP(K))-(1-RIEXP)/(PHIR*OM))/(PHIR*OM-(BETA+BP(K)))-
2((1-REXP)/(XK*PHIR)-(1-RIEXP)/(PHIR*OM))/(PHIR*(OM-XK)))/(XK*PHIR-(BETA+
3BP(K)))-(((CEXPST-1)/S(M,N)-(1-RIEXP)/(PHIR*OM))/(PHIR*OM+S(M,N))-
4((1-REXP)/(XK*PHIR)-(1-RIEXP)/(PHIR*OM))/(PHIR*(OM-XK)))/(XK*PHIR+S(M,N)))
1023 CONTINUE
D23NK=D23NK+AP(K)*BP(K)/(SZ(M,N)*(S(M,N)+BP(K)))*(((1-QEXP(K))/BP(K)
1-(1-PEXP)/(PHII*YK2))/(YK2*PHII-BP(K))-(((CEXPST-1)/S(M,N)-(1-PEXP)/
2(YK2*PHII)))/(S(M,N)+YK2*PHII))
D23ANK=D23ANK+AP(K)*XF*(BETA+BP(K))/(SZ(M,N)*(S(M,N)+BETA+BP(K)))*(((1-
1QEXPA(K))/(BETA+BP(K))-(1-PEXP)/(YK2*PHII))/(YK2*PHII-(BETA+BP(K)))-
2(((CEXPST-1)/S(M,N)-(1-PEXP)/(PHII*YK2))/(YK2*PHII+S(M,N))))
610 CONTINUE
57 F1N=F1N+CEXPST/SZ(M,N)
F3N=F3N+F3NK
F3AN=F3AN+F3ANK
B1N=B1N+(CEXPST-BEXP)/(SZ(M,N)*(PHIB*XM+S(M,N)))
B3N=B3N+B3NK
B3AN=B3AN+B3ANK
XI1N=XI1N+(CEXPST-PEXP)/(SZ(M,N)*(YK2*PHII+S(M,N)))
XI3N=XI3N+XI3NK
XI3AN=XI3AN+XI3ANK
IF(PHIR.EQ.0.0) GO TO 1021
R1N=R1N+(CEXPST-REXP)/(SZ(M,N)*(S(M,N)+XK*PHIR))
R3N=R3N+R3NK
R3AN=R3AN+R3ANK
RI1N=RI1N+1./SZ(M,N)*(S(M,N)+XK*PHIR))*((CEXPST-RIEXP)/
1(PHIR*OM+S(M,N))-(REXP-RIEXP)/(PHIR*(OM-XK)))
RI3N=RI3N+RI3NK
RI3AN=RI3AN+RI3ANK
D11N=D11N+1./SZ(M,N)*(((CEXPST-1)/S(M,N)-(1-RIEXP)/(PHIR*OM))/
1(S(M,N)+PHIR*OM)-((1-REXP)/(XK*PHIR)-(1-RIEXP)/(PHIR*OM))/(PHIR*(OM
2-XK)))/(S(M,N)+XK*PHIR))
1021 CONTINUE
D13N=D13N+D13NK
D13AN=D13AN+D13ANK
D21N=D21N+1./SZ(M,N)*(S(M,N)+YK2*PHII))*((CEXPST-1)/S(M,N)-
1(1-PEXP)/(YK2*PHII))
D23N=D23N+D23NK
D23AN=D23AN+D23ANK
630 CONTINUE
QN1=(ZZ*(YY*SIN(XL(M))-XL(M)*COS(XL(M)))+XL(M)*XK3)*
1(SIN(XL(M))+P/(2.*XL(M))*COS(XL(M))-P/(2.*XL(M))*EXP(-P/2.))
QN2=(WW*XK3-ZZ*(YY*COS(XL(M))+XL(M)*SIN(XL(M))))*(EXP(-P/2)+
1(P/(2.*XL(M))*SIN(XL(M))-COS(XL(M))))
QD=(YY*WW+XK1*XL(M)**2+VV)*COS(XL(M))+XL(M)*(2.*XK1-VV)*SIN(XL(M))
Q=4*XL(M)*XL(M)*(QN1+QN2)/(QD*(4.*XL(M)*XL(M)+P*P))

```

```

QA=4*XL(M)*XL(M)*ZZA*((YY*SIN(XL(M))-XL(M)*COS(XL(M)))*(SIN(XL(M))+
1P/(2*XL(M))*COS(XL(M))-P/(2*XL(M))*EXP(-P/2))-(YY*COS(XL(M))+XL(M)*
2SIN(XL(M)))*(EXP(-P/2)+(P/2*XL(M))*SIN(XL(M))-COS(XL(M))))/(QD*
3(4*XL(M)*XL(M)+P*P))
QB=Q-QA
F1=F1+Q*F1N
F3=F3+(1-XF)*Q*F3N+Q*F3AN
C F3=F3+(QB+(1-XF)*QA)*F3N+QA*F3AN
B1=B1+Q*B1N
B3=B3+(1-XF)*Q*B3N+Q*B3AN
C B3=B3+(QB+(1-XF)*QA)*B3N+QA*B3AN
XI1=XI1+Q*XI1N
XI3=XI3+(1-XF)*Q*XI3N+Q*XI3AN
C XI3=XI3+(QB+(1-XF)*QA)*XI3N+QA*XI3AN
R1=R1+Q*R1N
R3=R3+(1-XF)*Q*R3N+Q*R3AN
C R3=R3+(QB+(1-XF)*QA)*R3N+QA*R3AN
RI1=RI1+Q*RI1N
RI3=RI3+(1-XF)*Q*RI3N+Q*RI3AN
C RI3=RI3+RI3N*(QB+(1-XF)*QA)+QA*RI3AN
D11=D11+Q*D11N
D13=D13+(1-XF)*Q*D13N+Q*D13AN
C D13=D13+(QB+(1-XF)*QA)*D13N+QA*D13AN
D21=D21+Q*D21N
D23=D23+(1-XF)*Q*D23N+Q*D23AN
C D23=D23+(QB+(1-XF)*QA)*D23N+QA*D23AN
650 CONTINUE
C
C CALCULATE CONCENTRATIONS
C
PRINT*, 'D13 ', D13, ' D23 ', D23
CF=(-2.*F1+B*F2A-2.*F3)
SXTI=SQRT(TI/60)
WRITE(8,910) SXTI,CF
910 FORMAT(1X,F10.3,' ',E11.4)
CB=PHIB*(-2.*B1+B*B2A-2.*B3)
WRITE(16,920) SXTI,CB
920 FORMAT(1X,F10.3,' ',E11.4)
CI=PHII*(-2.*XI1+B*XI2A-2.*XI3)
CR=PHIR*(B*R2A-2*R1-2*R3)
CRI=PHIR*PHIR*GAM*(B*RI2A-2*RI1-2*RI3)
CIT=CI+CR+CRI
SXTI=SQRT(TI/60)
WRITE(22,34) SXTI,CR
34 FORMAT(1X,F10.3,' ',E11.4)
WRITE(23,35) SXTI,CRI
35 FORMAT(1X,F10.3,' ',E11.4)
WRITE(14,36) SXTI,CI
36 FORMAT(1X,F10.3,E11.4)
WRITE(17,930) SXTI,CIT
930 FORMAT(1X,F10.3,' ',E11.4)

```

```

CT=CF+CB+CIT
WRITE(3,990) SXTI, CT
990  FORMAT(1X,F10.3,' ',',',E11.4)
      CD=(PHIR*OM-PHIE1)*GAM*PHIR*PHIR*(-2*D11+B*D12A-2*D13)+
1(PHII*YK2-PHIE2)*PHII*(-2*D21+B*D22A-2*D23)+PHIE*XR*PHII*YK2*CDE
      CD1=(PHIR*OM-PHIE1)*GAM*PHIR*PHIR*(-2*D11+B*D12A-2*D13)
      CD2=(PHII*YK2-PHIE2)*PHII*(-2*D21+B*D22A-2*D23)
      CDE1=XR*PHIE*PHII*YK2*CDE
      PRINT*, 'CDE1 ',CDE1
      WRITE(18,995)SXTI,CD
995  FORMAT(1X,F10.3,' ',',',E11.4)
      WRITE(20,32)SXTI,CD1
32   FORMAT(1X,F10.3,' ',',',E11.4)
      WRITE(21,33)SXTI,CD2
33   FORMAT(1X,F10.3,' ',',',E11.4)
      XTI=TI/60
      WRITE(2,30)XTI,CT,CF,CB,CIT,CD,CDE1
30   FORMAT(1X,F7.3,3X,E8.3,3X,E8.3,3X,E8.3,3X,E8.3,3X,E8.3,3X,E8.3)
      WRITE(19,31)XTI,CR,CRI,CI,CD1,CD2
31   FORMAT(1X,F7.3,3X,E8.3,3X,E8.3,3X,E8.3,3X,E8.3,3X,E8.3)
      TI=TI*1.5
1000 CONTINUE
      GO TO 7701
7700 PRINT*, 'NO CONVERGENCE IN IMPOLES SUBROUTINE'
7701 CONTINUE
      END

```

REFERENCES

- Adams, C.J., Maury, K.M., and Storrie, B. 1982. Exocytosis of pinocytotic contents by chinese hamster ovary cells. J. Cell. Biol. **93**: 632-637.
- Adams, C.W.M., Virag, S., Morgan, R.S., and Orton, C.C. 1968. Dissociation of ³H-cholesterol and ¹²⁵I-labelled plasma protein influx in normal and atheromatous rabbit aorta. J. Atherosclerosis. Res. **8**: 679-696.
- Adams, C.W.M., Morgan, R.S., and Bayliss, O.B. 1970. The differential entry of ¹²⁵I-albumin into mildly and severely atheromatous rabbit aorta. Nature **210**: 175-176.
- Adams, C.W.M., and Bayliss, O.B. 1977. Permeability of inner and outer layers of rat and rabbit aortic wall. Atherosclerosis **26**: 419-426.
- Alberts, B., Bray, D., Lewis, J., Roff, M., Roberts, K., and Watson, J.D. 1983. Molecular Biology of the Cell. Garland Publishing, Inc., NY.
- Altstiel, L. and Branton, D. 1983. Fusion of coated vesicles with lysosomes: measurement with a fluorescence assay. Cell **32**: 921-929.
- Amenta, J.S. and Waters, L.L. 1960. The precipitation of serum lipoproteins by mucopolysaccharides extracted from aortic tissue. Yale J. Biol. Med. **33**: 112-121.
- Anderson, J.L., and Quinn, J.A. 1974. Restricted transport in small pores. Biophys. J. **14**: 130-150.
- Anderson, R.G.W., Goldstein, J.L., and Brown, M.S. 1976. Localization of low density lipoprotein receptors on plasma membrane of normal human fibroblasts and their absence in cells from a familial hypercholesterolemia homozygote. Proc. Natl. Acad. Sci. USA **73**: 2434-2438.
- Anderson, R.G.W., Brown, M.S., and Goldstein, J.L. 1977a. Role of the coated endocytic vesicle in the uptake of receptor bound low density lipoprotein in human fibroblasts. Cell **10**: 351-364.
- Anderson, R.G.W., Goldstein, J.L., and Brown, M.S. 1977b. A mutation that impairs the ability of lipoprotein receptors to localise in coated pits on the cell surface of human fibroblasts. Nature **270**: 695-699.
- Anderson, R.G.W., Brown, M.S., Beisiegel, U., and Goldstein, J.L. 1982. Surface

distribution and recycling of the low density lipoprotein receptor as visualized with antireceptor antibodies. J. Cell Biol. 93: 523-531.

Arminski, L., Weinbaum, S., and Pfeffer, R. 1980. Time dependent theory for vesicular transport across vascular endothelium. J. Theor. Biol. 85: 13-43.

Arpaci, V.S. 1966. Conduction Heat transfer. Addison-Wesley Publishing Co., Reading, MA.

Attie, A.D., Pittman, R.C., Watanabe, Y., and Steinberg, D. 1981. Low density lipoprotein receptor deficiency in cultured hepatocytes of the WHHL rabbit. J. Biol. Chem. 256: 9709-9792.

Aulinskas, T.H., van der Westhuyzen, D.R., Bierman, E.L., Gevers, W., and Coetzee, G.A. 1981. Retroendocytosis of low density lipoprotein by cultured bovine aortic smooth muscle cells. Biochim. Biophys. Acta. 664: 255-265.

Aulinskas, T.H., van der Westhuyzen, D.R., and Coetzee, G.A. 1983. Ascorbate increases the number of low density lipoprotein receptors in cultured arterial smooth muscle cells. Atherosclerosis 47: 159-171.

Aulinskas, T.H., Oram, J.F., Bierman, E.L., Coetzee, G.A., Gevers, W., and van der Westhuyzen, D.R. 1985. Retro-endocytosis of low density lipoprotein by cultured human skin fibroblasts. Arteriosclerosis 5: 45-54.

Baetscher, M., and Brune, K. 1983. An in vitro system for measuring endothelial permeability under hydrostatic pressure. Exp. Cell Res. 148: 541-547.

Barak, L.S., and Webb, W.W. 1982. Diffusion of low density lipoprotein-receptor complex on human fibroblasts. J. Cell. Biol. 95: 846-852.

Barrett, T.E., Gadjusek, C.M., Schwartz, S.M., McDougall, J.K., and Benditt, E.P. 1984. Expression of the *sis* gene by endothelial cells in culture and *in vivo*. Proc. Natl. Acad. Sci. USA 81: 6772-6774.

Basu, S.K., Goldstein, J.L., Anderson, R.G.W., and Brown, M.S. 1976. Degradation of cationized low density lipoprotein and regulation of cholesterol metabolism in homozygous familial hypercholesterolemia fibroblasts. Proc. Natl. Acad. Sci. USA 73: 3178-3182.

Basu, S.K., Goldstein, J.L., and Brown, M.S. 1978. Characterization of the low density lipoprotein receptor in membranes prepared from human fibroblasts.

J. Biol. Chem. 253: 3852-3856.

Basu, S.K., Goldstein, J.L., Anderson, R.G.W., and Brown, M.S. 1981. Monensin interrupts the recycling of low density lipoprotein receptors in human fibroblasts. Cell 24: 493-502.

Bell, F.P., Adamson, I.L., and Schwartz, C.J. 1974a. Aortic endothelial permeability to albumin: focal and regional patterns of uptake and transmural distribution of ^{131}I -albumin in the young pig. Exp. Mol. Pathol. 20: 57-68.

Bell, F.P., Gallus, A.S., and Schwartz, C.J. 1974b. Focal and regional patterns of uptake and transmural distribution of ^{131}I -fibrinogen in the pig aorta in vivo. Exp. Mol. Pathol. 20: 281-292.

Berman, M. 1979. Kinetic analysis of turnover data. Prog. Biochem. Pharmacol. 15: 67-108.

Besterman, J.M., Airhart, J.A., Woodworth, R.C., and Low, R.B. 1981. Exocytosis of pinocytosed fluid in cultured cells: kinetic evidence for rapid turnover and compartmentation. J. Cell. Biol. 91: 716-727.

Bierman, E.L., Stein, O., and Stein, Y. 1974. Lipoprotein uptake by cultured human arterial smooth muscle cells. Circ. Res. 35: 136-150.

Bihari-Varga, M., and Vegh, M. 1967. Quantitative studies on the complexes formed between aortic mucopolysaccharides and serum lipoproteins. Biochim. Biophys. Acta. 144: 202-210.

Bilheimer, D.W., Eisenberg, S., and Levy, R.J. 1972. The metabolism of very low density lipoprotein proteins. I. Preliminary in vitro and in vivo observations. Biochim. Biophys. Acta. 260: 212-221.

Bilheimer, D.W., Watanabe, Y., Kita, T. 1982. Impaired receptor-mediated catabolism of low density lipoprotein in the WHHL rabbit, an animal model of familial hypercholesterolemia. Proc. Natl. Acad. Sci. USA 79: 3305-3309.

Bowen-Pope, D.F., and Ross, R. 1982. Platelet-derived growth factor. II. Specific binding to cultured cells. J. Biol. Chem. 257:5161-5171.

Box, G.E.P., and Draper, N.R. 1965. The Bayesian estimation of common parameters from several responses. Biometrika 52: 355-365.

Bradby, G.H.V., Walton, K.W., and Watts, R., 1979. The binding of total low density lipoproteins in human arterial intima affected and unaffected by atherosclerosis. Atherosclerosis 32: 403-422.

Bratzler, R.L. 1974. The Transport Properties of Arterial Tissue. Doctoral Thesis. Massachusetts Institute of Technology, Cambridge, MA

Bratzler, R.L., Chisolm, G.M., Colton, C.K., Smith, K.A., Zilversmit, D.B., and Lees, R.S. 1977a. The distribution of labeled albumin across the rabbit thoracic aorta in vivo. Circ. Res. 40: 182-190.

Bratzler, R.L., Chisolm, G.M., Colton, C.K., Smith, K.A., and Lees, R.S. 1977b. The distribution of labeled low-density lipoproteins across the rabbit thoracic aorta in vivo. Atherosclerosis 28: 289-307.

Bratzler, R.L., Colton, C.K., and Smith, K.A. 1977c. Theoretical Models for transport of LDL in the arterial wall. in Atherosclerosis. G.W. Manning and M. Daria-Haust, editors, Plenum Publishing Corp., NY: 943-951.

Bratzler, R.L., and Schwarz, E.A. 1977. Convective and diffusive transport of labelled albumin through rabbit aortic tissue. Proc. 30th Ann. Conf. Eng. Med. Biol.: 318.

Brenner, H., and Gaydos, L.J. 1977. The constrained Brownian motion of spherical particles in cylindrical pores of comparable radius. J. Coll. Int. Sci. 58: 312-356.

Bretscher, M.S. 1984. Endocytosis: relation to capping and cell locomotion. Science 224: 681-686.

Bridges, K., Harford, J., Ashwell, G., and Klausner, R.D. 1982. Fate of receptor and ligand during endocytosis of asialoglycoproteins by isolated hepatocytes. Proc. Natl. Acad. Sci. USA 79: 350-354.

Brown, M.S., and Goldstein, J.L. 1974. Familial hypercholesterolemia: defective binding of lipoproteins to cultured fibroblasts associated with impaired regulation of 3-Hydroxy-3-methylglutaryl coenzyme A reductase activity. Proc. Nat'l. Acad. Sci. USA 71: 788-792.

Brown, M.S., Dana, S.E., and Goldstein, J.L. 1974. Regulation of 3-hydroxy-3-methylglutaryl coenzyme A reductase activity in cultured human fibroblasts. J. Biol. Chem. 249: 789-796.

- Brown, M.S., and Goldstein, J.L. 1975. Regulation of the activity of the low density lipoprotein receptor in human fibroblasts. Cell 6: 307-316.
- Brown, M.S., and Goldstein, J.L. 1976. Analysis of a mutant strain of human fibroblasts with a defect in the internalization of receptor-bound low density lipoprotein. Cell 9: 663-674.
- Brown, M.S., Ho, Y.K., and Goldstein, J.L. 1976. The low density lipoprotein pathway in human fibroblasts: relation between cell surface receptor binding and endocytosis of low density lipoprotein. Ann. N.Y. Acad. Sci. 275: 244-257.
- Brown, M.S., Kovanen, P.T., and Goldstein, J.L. 1980. Evolution of the LDL receptor concept- from cultured cells to intact animals. Ann. NY Acad. Sci. 348: 48-65.
- Brown, M.S., Anderson, R.G.W., and Goldstein, J.L. 1983. Recycling receptors: The round-trip itinerary of migrant membrane proteins. Cell 32: 663-667.
- Brown, M.S., and Goldstein, J.L. 1983. Lipoprotein metabolism in the macrophage: Implications for cholesterol deposition in atherosclerosis. Ann. Rev. Biochem. 52: 223-261.
- Bucher, B., Travo, P., Laurent, P., and Stoclet, J.C. 1982. Vascular smooth muscle cell hypertrophy during maturation in rat thoracic aorta. Volumetric and morphometric studies. Cell Biol. Intl. Rep. 6: 883-892.
- Buck, R.C. 1958. The fine structure of endothelium of large arteries. Biophys. and Biochem. Cytol. 4: 187-190.
- Buja, L.M., Kita, T., Goldstein, J.L., Watanabe, Y., and Brown, M.S. 1983. Cellular pathology of progressive atherosclerosis in the WHHL rabbit. Atherosclerosis 3: 87-101.
- Burke, J.M., and Ross, R. 1979. Synthesis of connective tissue macromolecules by smooth muscle. Intl. Rev. Conn. Tiss. Res. 8: 119-157.
- Burstein, M., Scholnick, and Morfin, R. 1970. Rapid method for the isolation of lipoproteins from human serum by precipitation with polyanions. J. Lipid Res. 11: 583-595.
- Butler, M., Imamura, T., Thomas, J., and Thilly, W.G. 1983. High yields from microcarrier cultures by medium perfusion. J. Cell Sci. 61: 351-363.

- Calvert, G.D., Scott, P.J., and Sharpe, D.N. 1975. The plasma and tissue turnover and distribution of two radio-iodine-labelled pig plasma low density lipoproteins. Atherosclerosis 22: 601-628.
- Camejo, G., Lalaguna, F., Lopez, F., and Starosta, R. 1980. Characterization and properties of a lipoprotein-complexing proteoglycan from human aorta. Atherosclerosis 35: 307-320.
- Camejo, G. 1982. The interaction of lipids and lipoproteins with the extracellular matrix of arterial tissue: its possible role in atherogenesis. Adv. in Lipid Res. 19: 1-53.
- Campbell, G.R., Chamley-Campbell, J.H., and Burnstock, G. 1981. Differentiation and phenotypic modulation of arterial smooth muscle cells. in Structure and Function of the Circulation. Vol. 3, C.J. Schwartz, N.T. Werthessen, and S. Wolf, editors, Plenum Press, NY: 357-400.
- Campbell, J.H., Popadyneec, L., Nestel, P.J., and Campbell, G.R. 1983. Lipid accumulation in arterial smooth muscle cells. Influence of phenotype. Atherosclerosis 47: 279-295.
- Carberry, J.J. 1976. Chemical and Catalytic Reaction Engineering. New York: McGraw-Hill Book Co: 194-243.
- Carew, T.E., and Beltz, W.F. 1982. Kinetics of low density lipoproteins labeled with ^{14}C -sucrose: Theoretical basis of a method for tracing the sites of apoprotein degradation in vivo. in Lipoprotein Kinetics and Modeling. M. Berman, S.M. Grundy, and B.V. Howard, editors. Academic Press, NY:169-179.
- Carew, T.E., Pittman, R.C., and Steinberg, D. 1982. Tissue sites of degradation of native and reductively methylated ^{14}C -sucrose-labeled low density lipoprotein in rats. J. Biol. Chem. 257: 8001-8008.
- Carew, T.E., Pittman, R.C., Marchand, E.R., and Steinberg, D. 1984. Measurement in vivo of irreversible degradation of low density lipoprotein in the rabbit aorta. Arteriosclerosis 4: 214-224.
- Caro, C.G., Fitzgerald, J.M., Schroter, R.C. 1971. Atheroma and arterial wall shear: observation, correlation and proposal of a shear dependent mass transfer mechanism for atherogenesis. Proc. Roy. Soc. Lond. Ser. B 177: 109-159.

- Caro, C.G.-1973. Transport of materials between blood and wall in arteries. in Atherogenesis: Initiating Factors. Ciba Foundation Symposium, 12 (new series): 187-205.
- Caro, C.G., and Nerem, R.M. 1973. Transport of ^{14}C -4-cholesterol between serum and wall in the perfused dog common carotid artery. Circ. Res. 32: 187-205.
- Caro, C.G. 1974. Transport of ^{14}C -4-cholesterol between perfusing serum and dog common carotid artery: a shear dependent process. Cardiovasc. Res. 8: 194-203.
- Caro, C.G., Lever, M.J., Laver-Rudich, Z., Meyer, F., Liron, N., Ebel, W., Parker, K.H., and Winlove, C.P. 1980. Net albumin transport across the wall of the rabbit common carotid artery perfused in situ. Atherosclerosis 37: 497-511.
- Caro, C.G., Lever, M.J., and Tedgui, A. 1981. The distribution volume of albumin and sucrose in arteries subjected to normal mechanical stresses. J. Physiol. (Lond.) 320: 38p-39p.
- Carpenter, G., and Cohen, S. 1975. ^{125}I -labeled human epidermal growth factor. J. Cell Biol. 71: 159-171.
- Casley-Smith, J.R., and Chin, J.C. 1971. The passage of cytoplasmic vesicles across endothelial and mesothelial cells. J. Microscop. 93: 167-184.
- Castellot, J.J., Addonizio, M., Rosenberg, R., and Karnovsky, M.J. 1981. Cultured endothelial cells produce a heparin-like inhibitor of smooth muscle cell growth. J. Cell. Biol. 90: 372-379.
- Chait, A., Bierman, E.L., and Albers, J.J. 1979. Low density lipoprotein receptor activity in fibroblasts cultured from diabetic donors. Diabetes 28: 914-918.
- Chait, A., Ross, R., Albers, J.J., and Bierman, E.L. 1980. Platelet-derived growth factor stimulates activity of LDL receptors. Proc. Natl. Acad. Sci. USA 77: 4084-4088.
- Chamley, J.H., Campbell, G.R., McConnell, J.D., and Groschel-Stewart, U. 1977. Comparison of vascular smooth muscle cells from adult human, monkey, and rabbit in primary culture and in subculture. Cell Tiss. Res. 177: 503-522.

Chamley-Campbell, J., Campbell, G.R., and Ross, R. 1979. The smooth muscle cell in culture. Physiol Rev. 59: 1-61.

Chamley-Campbell, J.H., Campbell, G.R., and Ross, R. 1981. Phenotype-dependent response of cultured aortic smooth muscle to serum mitogens. J. Cell Biol. 89: 379-383.

Chamley-Campbell, J.H., and Campbell, G.R. 1981. What controls smooth muscle phenotype? Atherosclerosis 40: 347-357.

Chatfield, C., and Collins, A.J. 1980. Introduction to Multivariate Analysis. Chapman and Hall, London: 104-107.

Chien, S. 1978. Transport across arterial endothelium. in Progress in Hemostasis and Thrombosis. Vol. 4, T. Spaet, editor, Grune and Stratton, NY: 1-36.

Chien, S., Lee, M.L., Laufer, L.S., and Handley, D.A., Weinbaum, S., Caro, C.G., and Usami, S. 1981. Effects of oscillatory mechanical disturbances on macromolecular uptake. Arteriosclerosis 1: 326-336.

Chien, S., Laufer, L., and Handley, D.A. 1982. Vesicle distribution in the arterial endothelium determined with ruthenium red as an extracellular marker. J. Ultrastructural Res. 79: 198-206.

Ciechanover, A., Schwartz, A.L., Dautry-Varsat, A., and Lodish, H.F. 1983a. Kinetics of internalization and recycling of transferrin and the transferrin receptor in a human hepatoma cell line. J. Biol. Chem. 258: 9681-9689.

Ciechanover, A., Schwartz, A.L., and Lodish, H.F. 1983b. The asialoglycoprotein receptor internalizes and recycles independently of the transferrin and insulin receptors. Cell 32: 267-275.

Cliff, W.J. 1971. The ultrastructure of aortic elastic tissue as revealed by prolonged treatment with OsO₄. Exp. Mol. Pathol. 15: 220-229.

Coetzee, G.A., Stein, O., and Stein, Y. 1979. Uptake and degradation of low density lipoproteins (LDL) by confluent, contact-inhibited bovine and human endothelial cells exposed to physiological concentrations of LDL. Atherosclerosis 33: 425-431.

Coltoff-Schiller, B., Goldfischer, S., Adamany, A.M., and Wolinsky, H. 1976. Endocytosis by vascular smooth muscle cells in vivo and in vitro. Am. J.

Pathol 83:45-60.

Colton, C.K., Smith, K.A., Merrill, E.W., and Farrell, P.C. 1971. Permeability studies with cellulosic membranes. J. Biomed. Mater. Res. 5: 459-488.

Colton, C.K., Friedman, S., Wilson, D.E., and Lees, R.S. 1972. Ultrafiltration of lipoproteins through a synthetic membrane: implications for the filtration theory of atherogenesis. J. Clin. Invest. 51: 2472-2481.

Comper, W.D., and Laurent, T.C. 1978. Physiological function of connective tissue polysaccharides. Physiol. Rev. 58: 255-315.

Cornicelli, J.A., Witte, L.D., and Goodman, D.S. 1983. Inhibition of LDL degradation in cultured human fibroblasts induced by endothelial cell-conditioned medium. Arteriosclerosis 3: 560-567.

Cornhill, J.F., Levesque, M.J., Herderick, E.E., Nerem, R.M., Kilman, J.W., and Vasko, J.S. 1980. Quantitative study of rabbit aortic endothelium using vascular casts. Atherosclerosis 35: 321-337.

Cornwall, D.G., and Kruger, F.A. 1961. Molecular complexes in the isolation and characterization of plasma lipoproteins. J. Lipid Res. 2: 110-130.

Crossley, J.M., Spraggs, S.P., Creeth, J.M., Noble, N., and Slack, J. 1981. Anomalous temperature dependence of frictional coefficients: diffusion and sedimentation of low-density lipoproteins, albumin, and polystyrene latex. Biopolymers 21: 233-245.

Danon, D., and Skutelsky, E. 1976. Endothelial surface charge and its possible relationship to thrombogenesis. Ann. NY Acad. Sci. 275: 47-63.

Dautry-Varsat, A., Ciechanover, A., and Lodish, H.F. 1983. pH and the recycling of transferrin during receptor-mediated endocytosis. Proc. Natl. Acad. Sci. USA 80: 2258-2262.

Davies, P.F., and Ross, R. 1978. Mediation of pinocytosis in cultured arterial smooth muscle and endothelial cells by platelet-derived growth factor. J. Cell Biol. 79: 663-671.

Davies, P.F., and Ross, R. 1980. Growth-mediated, density dependent inhibition of endocytosis in cultured arterial smooth muscle cells. Exp. Cell Res. 129: 329-336.

Davies, P.F., Shelden, S.C. III, Schwartz, S.M. 1980. Enhanced rates of fluid pinocytosis during exponential growth and monolayer regeneration by cultured arterial endothelial cells. J. Cell Physiol. 102: 119-127.

Davies, P.F. 1981. Microcarrier culture of vascular endothelium. Exp. Cell Res. 134: 365-374.

Davies, P.F., and Kuczera, L. 1981. Endocytic vesicles and surface invaginations in cultured vascular endothelium: a morphometric comparison. J. Ultrastruct. Res. 79: 198-206.

Davies, P.F., Rennke, H.G., and Cotran, R.S. 1981. Influence of molecular charge upon the endocytosis and intracellular fate of peroxidase activity in cultured arterial endothelium. J. Cell Sci. 49: 69-86.

Davies, P.F. 1982. Microcarrier cultures in vascular endothelial research. Dev. Biol. Stand. 50: 125-137.

Davies, P.F., and Kerr, C. 1982a. Modification of LDL metabolism by growth factors in cultured vascular cells and human skin fibroblasts. Dependence on duration of exposure. Biochim. Biophys. Acta. 712: 26-32.

Davies, P.F., and Kerr, C. 1982b. Cocultivation of vascular endothelium and smooth muscle cells using microcarrier techniques. Exp. Cell Res. 141: 455-457.

Davies, P.F., Kerr, C., and Eisenhaure, B. 1983. The microcarrier coculture system: interactions between endothelial and smooth muscle cells in vitro. in Atherosclerosis VI. G. Schettler, editor, Springer, Berlin:

Davies, P.F. 1984. Quantitative aspects of endocytosis in cultured endothelial cells. in Biology of Endothelial Cells, E.A. Jaffe, editor, Martinus Nijhoff Publishers, The Hague: 365-376.

Davies, P.F., Dewey, C.F., Jr., Bussolari, S.R., Gordon, E.J., and Gimbrone, M.J., Jr. 1984. Influence of hemodynamic forces on vascular endothelial function: in vitro studies of shear stress and pinocytosis in bovine aortic cells. J. Clin. Invest. 73: 1121-1129.

Davies, P.F., Truskey, G.A., Warren, H.B., O'Connor, S.E., and Eisenhaure, B. 1985. Metabolic cooperation between vascular endothelial cells and smooth muscle cells in coculture: Changes in low density lipoprotein metabolism. J. Cell. Biol. (In Press).

Dayton, S., and Hashimoto, S. 1970. Recent advances in molecular pathology: A review. Exp. Mol. Pathol. 13: 253-268.

DiCorleto, P.E. 1984. Cultured endothelial cells produce multiple growth factors for connective tissue cells. Exp. Cell Res. 153: 167-172.

DiCorleto, P.E., and Bowen-Pope, D.F. 1983. Cultured endothelial cells produce a platelet-derived growth factor-like protein. Proc. Natl. Acad. Sci. USA 80: 1919-1923.

DiCorleto, P.E., Gadjusek, C.M., Schwartz, S.M., and Ross, R. 1983. Biochemical properties of the endothelium-derived growth factor: comparison to other growth factors. J. Cell. Physiol. 114: 339-345.

Donovan, J.M. 1980. The metabolism and transport of low density lipoproteins in the arterial wall of rabbits. MS Thesis. Massachusetts Institute of Technology, Cambridge, MA.

Draper, N.R., and Smith, H. 1981. Applied Regression Analysis. John Wiley and Sons, Inc. NY:458-516.

Drevon, C.A., Attie, A.D., Pangburn, S.H., and Steinberg, D. 1981. Metabolism of homologous and heterologous lipoproteins by cultured rat and human skin fibroblasts. J. Lipid Res. 22: 37-46.

Duncan, L.E., Cornfield, J., and Buck, K. 1958. Circulation of iodinated albumin through aortic and other connective tissues of the rabbit. Circ. Res. 6: 244-255.

Duncan, L.E., Cornfield, J., and Buck, K. 1959. Circulation of labeled albumin through the aortic wall of the rabbit. Circ. Res. 7: 390-397.

Duncan, L.E., and Buck, K. 1961. Passage of labeled albumin into canine aortic wall in vivo and in vitro. Am. J. Physiol. 200: 622-624.

Duncan, L.E., Cornfield, J., and Buck, K. 1962. The effect of blood pressure on the passage of labeled plasma albumin into the canine aortic wall. J. Clin. Invest. 41: 1537-1545.

Duncan, L.E., Jr., Buck, K., and Lynch, A. 1963. Lipoprotein movement through canine aortic wall. Science 142: 972-973.

Duncan, L.E., Buck, K., and Lynch, A. 1965. The effect of presue and stretching

on the passage of labeled albumin into canine aortic wall. J. Atherosclerosis Res. 5: 69-79.

Eisele, B., Bates, S.R., and Wissler, R.W. 1980. Interaction of low density lipoproteins from normal and hyperlipemic rhesus monkeys with arterial smooth muscle cells in culture. Atherosclerosis 36: 9-24.

Ericson, C., Dahlen, G., and Berg, K. 1977. Interaction of isolated Lp(α) lipoprotein with calcium ions and glycosaminoglycans in vitro. Clin. Genet. 11: 433-440.

Eskin, S.G., Ives, C.L., McIntire, L.V., and Navarro, L.T. 1984. Response of cultured endothelial cells to steady flow. Microvasc. Res. 28: 87-94.

Feldman, S.A., and Glagov, S. 1971. Transmedial collagen and elastin gradients in human aortas: Reversal with age. Atherosclerosis 13: 385-394.

Fielding, P.E., Vlodaysky, I., Gospodarowicz, D., and Fielding, C.J. 1979. Effect of contact inhibition on the regulation of cholesterol metabolism in cultured vascular endothelial cells. J. Biol. Chem. 254: 749-755.

Fisher, W.R., Granade, M.E., and Mauldin, J.I. 1971. Hydrodynamic studies of human low density lipoprotein. Evaluation of the diffusion coefficient and the preferential hydration. Biochemistry 10: 1622-1629.

Fisher, W.R., Hammond, M.G., and Warmke, G.L. 1972. Measurement of the molecular weight weight variability of plasma low density lipoproteins among normals and subjects with hyper-B-lipoproteinemia. Demonstration of macromolecular heterogeneity. Biochemistry 11: 519-525.

Florey, L., and Sheppard, B.L. 1970. The permeability of arterial endothelium to horseradish peroxidase. Proc. Roy. Soc. Lond. B 174: 435-553.

Fogelman, A.M., Schechter, I., Seager, J., Hokom, M., Child, J.S., and Edwards, P.A. 1980. Malondialdehyde alteration of low density lipoproteins leads to cholesteryl ester accumulation in human monocyte-macrophages. Proc. Natl. Acad. Sci. USA 77: 2214-2218.

Folch, J.M., Lees, R.S., Sloan-Stanley, G.H. 1957. A simple method for the isolation and purification of total lipids from animal tissue. J. Biol. Chem. 226: 497-509.

Fowler, S., Shio, H., and Wolinsky, H. 1977. Subcellular fractionation and

morphology of calf aortic smooth muscle cells. J. Cell Biol. 75: 166-184.

Fox, P.L., and DiCorleto, P.E. 1984. Regulation of production of a platelet-derived growth factor-like protein by cultured bovine aortic endothelial cells. J. Cell. Physiol. 121: 298-308.

Froment, G.F., and Bischoff, K.B. 1979. Chemical Reactor Design and Analysis. John Wiley and Sons, NY.

Fry, D.L. 1973. Response of the arterial wall to certain physical factors. in Atherogenesis: Initiating Factors, Ciba Foundation Symp., 12 (new series): 93-124.

Fry, D.L. 1976. Hemodynamics forces in atherogenesis. in Cerebrovascular Diseases. P. Scheinberg, editor, Raven Press, NY: 77-95.

Fry, D.L., Mahley, R.W., Oh, S.Y., Lewis, S.J., Plowman, F., and Swyt, C.R. 1980. Quantitative microautoradiography of arteries: comparison of radioactivity to silver. Am. J. Physiol. 239: H289-H295.

Fry, D.L., Mahley, R.W., Oh, S.Y., and Swyt, C.R. 1981a. Aortic transmural serum protein transport: effect of concentration, time, and location. Am. J. Physiol. 240: H54-H61.

Fry, D.L., Mahley, R.W., and Oh, S.Y. 1981b. Effect of arterial stretch on transmural albumin and Evan's blue dye transport. Am. J. Physiol. 240: H645-H649.

Fry, D.L. 1983. Effect of pressure and stirring on in vitro aortic transmural ¹²⁵I-albumin transport. Am. J. Physiol. 245: H977-H991.

Fry, D.L. 1985. Mathematical model of arterial transmural transport. Am. J. Physiol. H240-H263.

Furie, M.B., Cramer, E.B., Naprstek, B.L., and Silverstein, S.C. 1984. Cultured endothelial cell monolayers that restrict the transendothelial passage of macromolecules and electrical current. J. Cell Biol. 98: 1033-1041.

Gadjusek, C., DiCorleto, P., Ross, R., and Schwartz, S.M. 1980. An endothelial cell-derived growth factor. J. Cell Biol. 85: 467-472.

Gal, D., Simpson, E.R., Porter, J.C., and Snyder, J.M. 1982. Defective internalization of low density lipoprotein in epidermoid cervical cancer

cells. J. Cell Biol. 92: 597-603.

Gamble, W., Vaughen, M., Kruth, H.S., and Avigan, J. 1978. Procedure for determination of free and total cholesterol in micro- and nanogram amounts suitable for studies with cultured cells. J. Lipid Res. 19: 1068-1070.

Gamel J, Rousseau WF, Katholi CR, Mesel E. Pitfalls in digital computation of the impulse response of vascular beds from indicator dilution curves. Circ Res 1973; 32: 516-523.

Gardell, S., Baker, J., Caterson, B., Heinegard, D., and Roden, L. 1980. Link protein and a hyaluronic acid binding region as components of aorta proteoglycan. Biochem. Biophys. Res. Comm. 95: 1823-1831.

Gero, S., Gergely, J., Devenyi, T., Jakab, L., Szekely, J., and Virag, S. 1961. Role of intimal mucoid substances in the pathogenesis of atherosclerosis. I. Complex formation in vitro between mucopolysaccharides from atherosclerotic aortic intimas and plasma β -lipoprotein and fibrinogen. J. Atherosclerosis Res. 1: 67-74.

Gerrity, R.G., and Cliff, W.J. 1975. The aortic tunica media in the developing rat. I. Quantitative stereological and biochemical analysis. Lab. Invest. 32: 585-600.

Ghosh, S., Finkelstein, J.N., Moss, D.B., and Schweppe, J.S. 1976. Evaluation of the permeability parameters (influx, efflux and volume of distribution) of arterial wall for LDL and other proteins. in Atherosclerosis: Drug Discovery. C.E. Day, editor. Plenum Publishing Corp., NY: 196-204.

Giddings, J.C., Kucera, E., Russell, C.P., and Myers, M.N. 1968. Statistical theory for the equilibrium distribution of rigid molecules in inert porous networks. J. Phys. Chem. 72: 4397-4408.

Gimbrone, M.A. 1976. Culture of vascular endothelium. in Progress in Hemostasis and Thrombosis. T.H. Spaet, editor, Grune and Stratton, NY: 1-28.

Glacken, M.W., and Sinskey, A.J. 1985. Ammonia production and glutamine metabolism of cultured mammalian cells. Biotech. Bioeng.: (submitted)

Glatz, C.E., and Vislocky, J.M. 1979. The kinetics of binding of serum low lipoproteins by immobilized heparin. Biochim. Biophys. Acta. 573: 382-393.

Goldstein, B., Wolfsky, C., and Bell, G. 1981. Interactions of low density

lipoprotein-receptors with coated pits on human fibroblasts: Estimate of the forward rate constant and comparison with diffusion limit. Proc. Natl. Acad. Sci. USA 78: 5695-5698.

Goldstein, B., Griego, R., and Wolfsky, C. 1984. Diffusion-limited forward rate constants in two dimensions. Application to the trapping of cell surface receptors by coated pits. Biophys. J. 46: 573-586.

Goldstein, J.L., and Brown, M.S. 1974. Binding and degradation of low density lipoproteins by cultured human fibroblasts. J. Biol. Chem. 249: 5153-5162.

Goldstein, J.L., Dana, S.E., and Brown, M.S. 1974. Esterification of low density lipoprotein cholesterol in human fibroblasts and its absence in homozygous familial hypercholesterolemia. Proc. Natl. Acad. Sci. USA 71: 4288-4292.

Goldstein, J.L., and Brown, M.S. 1976. The LDL pathway in human fibroblasts; a receptor-mediated mechanism for the regulation of cholesterol metabolism. in Current Topics in Cellular Regulation, Vol. 11, B.C. Horecker and E.R. Stadtman, editors, Academic Press, NY: 147-181.

Goldstein, J.L., Basu, S.K., Brunschede, G.Y., and Brown, M.S. 1976. Release of low density lipoprotein from its cell surface receptor by sulfated glycosaminoglycans. Cell 7: 85-95.

Goldstein, J.L., and Brown, M.S. 1977a. Atherosclerosis: the low density lipoprotein receptor hypothesis. Metabolism 26: 1257-1275.

Goldstein, J.L., and Brown, M.S. 1977b. The low density lipoprotein pathway and its relation to atherosclerosis. Ann. Rev. Biochem. 46: 897-930.

Goldstein, J.L., Brown, M.S., and Stone, N.J. 1977. Genetics of the LDL receptor: evidence that the mutations affecting binding and internalization are allelic. Cell 12: 629-641.

Goldstein, J.L., and Brown, M.S. 1977. The low density lipoprotein pathway and its relation to atherosclerosis. Ann. Rev. Biochem. 46: 897-930.

Goldstein, J.L., Basu, S.K., and Brown, M.S. 1983a. Receptor-mediated endocytosis of low density lipoproteins in cultured cells. Meth. Enzymol. 98: 241-260.

Goldstein, J.L. and Brown, M.S. 1983b. Familial hypercholesterolemia In

The Metabolic Basis of Inherited Disease. J.R. Stanbury, J.B. Wyngaarden, D.S. Frederickson, J.L. Goldstein and M.S. Brown, eds. 5th ed. McGraw-Hill, NY.

Goldstein, J.L., Kita, T., and Brown, M.S. 1983b. Defective lipoprotein receptors and atherosclerosis. N. Engl. J. Med. 304: 288-296.

Gosline, J.M. 1976. The physical properties of elastic tissue. in International Review of Connective Tissue Research, Vol. 7, D. Hall and D.S. Jackson, editors, Academic Press, NY: 211-249.

Gotto, A.M., Levy, R.I., Rosenthal, A.S., Birnbaumer, M.E., and Fredrickson, D.S. 1968. The structure and properties of human beta-lipoprotein and beta-apoprotein. Biochem. Biophys. Res. Comm. 31: 699-705.

Greenspan, P., and St. Clair, R.W. 1984. Retroendocytosis of low density lipoprotein. J. Biol. Chem. 259: 1703-1713.

Guyton, A.C. 1976. Textbook of Medical Physiology. Fifth Edition. W.B. Saunders, Philadelphia.

Habeeb, A.F.S.A. 1966. Determination of free amino groups in proteins by trinitrobenzene sulfonic acid. Anal. Biochem. 14: 328-336.

Harrison, R.G., and Massaro, T.A. 1976. Extracellular space of swine aorta measured with ¹⁴Csucrose. Am. J. Physiol. 231: 1806-1810.

Hascall, V.C., and Hascall, G.K. 1981. Proteoglycans. in Cell Biology of the Extracellular Matrix, E.D. Hay, editor, Plenum Press, NY: 39-63.

Hatch, F.T., and Lees, R.S. 1968. Practical methods for plasma lipoprotein analysis. Adv. Lipid Res. 6: 1-68.

Havel, R.J., Eder, H.A., and Brayden. 1955. The distribution and chemical composition of ultracentrifugally separated lipoproteins in human serum. J. Clin. Invest. 34: 1345-1353.

Heider, J.G. and Boyett, R.L. 1978. The picomole determination of free and total cholesterol in cells in culture. J. Lipid Res. 19: 514-518.

Heldin, C-H., Wasteson, A., and Westermark, B. 1982. Interaction of platelet-derived growth factor with its fibroblast receptor. J. Biol. Chem. 257: 4216-4221.

Henriksen, T., Mahoney, E.M., and Steinberg, D. 1981. Enhanced macrophage degradation of low density lipoprotein previously incubated with cultured endothelial cells: recognition by receptors for acetylated low density lipoproteins. Proc. Natl. Acad. Sci. USA 78: 6499-6503.

Henriksen, T., Mahoney, E.M., and Steinberg, D. 1982. Interactions of plasma lipoproteins with endothelial cells. Ann. NY Acad. Sci. 401: 102-116.

Henriksen, T., Mahoney, E.M., and Steinberg, D. 1983. Enhanced macrophage degradation of biologically modified low density lipoproteins. Arteriosclerosis 3: 149-159.

Herman, B., and Albertini, D.F. 1984. A time-lapse video intensification analysis of cytoplasmic organelle movements during endosome translocation. J. Cell Biol. 98: 565-576.

Hessler, J.R., Morel, D.W., Lewis, L.J., and Chisolm, G.M. 1983. Lipoprotein oxidation and lipoprotein induced cytotoxicity. Arteriosclerosis 3: 215-222.

Heuser, J. 1980. Three dimensional visualization of coated vesicle formation in fibroblasts. J. Cell. Biol. 84: 560-583.

Hildebrand, F.B. 1976. Advanced Calculus for Applications. Second Edition. Prentice-Hall, Inc., Englewood Cliffs, NJ.

Himmelblau, D.M. 1970. Process Analysis by Statistical Methods. New York: John Wiley and Sons, Inc: 298.

Himmelblau, D.M., Bischoff, K.B. 1968. Process Analysis and Simulation. New York: John Wiley and Sons.

Hillman, G.M., and Schlesinger, J. 1982. Lateral Diffusion of epidermal growth factor complexed to its surface receptors does not account for the thermal sensitivity of patch formation and endocytosis. Biochemistry 21: 1667-1672.

Hoff, H.F., and Gaubatz, J.W. 1975. Ultrastructural localization of plasma lipoproteins in human intracranial arteries. Virchows Arch. Path. Anat. Histol. 369: 111-121.

Hoff, H.F., Heideman, C.L., Jackson, R.L., Bayardo, R.J., Kim, H., and Gotto, A.M. 1975. Localization patterns of plasma apolipoproteins in human atherosclerotic lesions. Circ. Res. 37: 72-79.

Hoff, H.F., Jackson, R.L., and Gotto, A.M., Jr. 1976. Apo-lipoprotein localization in human atherosclerotic arteries in Atherosclerosis Drug Discovery, C.E. Day, editor, Plenum Publishing Corp., NY: 109-120.

Hoff, H.F., and Gaubatz, J.W. 1977. Ultrastructural localization of apolipoprotein B in human aortic and coronary atherosclerotic plaques. Exp. Mol. Pathol. 26: 214-227.

Hoff, H.F., Heideman, C.L., Gaubatz, J.W., Gotto, A.M., Erickson, E.E., and Jackson, R.L. 1977. Quantification of apolipoprotein B in grossly normal human aorta. Circ. Res. 40: 56-64.

Hoff, H.F., Heideman, C.J., Gaubatz, J.W., Scott, D.W., Titus, J.L., and Gotto, A.M., Jr. 1978. Correlation of apolipoprotein B retention with the structure of atherosclerotic plaques from human aortas. Lab. Invest. 38: 560-567.

Hoff, H.F., Bradley, W.A., Heideman, C.L., Gaubatz, J.L., Karagos, M.D., and Gotto, A.M., Jr. 1979. Characterization of low density lipoprotein-like particle in the human aorta from grossly normal and atherosclerotic regions. Biochim. Biophys. Acta. 573: 361-374.

Hoff, H.F., and Gaubatz, J.W. 1982. Isolation, purification, and characterization of a lipoprotein containing Apo B from human aorta. Atherosclerosis 42: 273-297.

Hollander, W. 1976. Unified concept on the role of acid mucopolysaccharides and connective tissue proteins in the accumulation of lipids, lipoproteins and calcium in the atherosclerotic plaque. Exp. Mol. Pathol. 25: 106-120.

Hunter, W.G. 1967. Estimation of unknown constants from multiresponse data. Ind. Eng. Chem. Fund. 6: 461-463.

Huttner, I., Boudet, M., and More, R.H. 1973a. Studies on protein passage through arterial endothelium: I. Structural correlates of permeability in rat arterial endothelium. Lab. Invest. 28: 672-677.

Huttner, I., Boudet, M., and More, R.H. 1973b. Studies on protein passage through arterial endothelium: II. Regional differences in permeability to fine structural protein tracers in arterial endothelium of normotensive rats. Lab. invest. 28: 678-685.

Iacopetta, B.J., and Morgan, E.H. 1983. The kinetics of transferrin endocytosis

and iron uptake from transferrin in rabbit reticulocytes. J. Biol. Chem. **258**: 9108-9115.

Innerarity, T.L., Pitas, R.E., and Mahley, R.W. 1980. Receptor binding of cholesterol-induced high-density lipoproteins containing predominantly apoprotein E to cultured fibroblasts with mutations at the low density lipoprotein receptor locus. Biochemistry **19**: 4359-4365.

Iverius, P.H. 1972. The interaction between human plasma lipoproteins and connective tissue glycosaminoglycans. J. Biol. Chem. **267**: 2607-2613.

Jan, K.M. 1984. Distribution of plasmalemmal vesicles on arterial endothelial surface as determined by freeze cleavage. Anat. Rec. **210**: 11-15.

Jutan, A. 1976. A parameter estimation program for multiresponse data using a Bayesian approach. McMaster University Technical Publication No. SOC-117.

Kaplan, J. 1981. Polypeptide-binding membrane receptors: analysis and classification. Science **212**: 14-20.

Kenagy, R., Bierman, E.L., and Schwartz, S. 1983. Regulation of low-density lipoprotein metabolism by cell density and proliferative state. J. Cell. Physiol. **116**: 404-408.

Kenagy, R., Bierman, E.L., Schwartz, S., and Albers, J.J. 1984. Metabolism of low density lipoprotein by bovine endothelial cells as a function of cell density. Arteriosclerosis **4**: 365-371.

Kezdy, F.J. 1977. Physical properties, chemical composition and structure of circulating lipoproteins. in The Lipoprotein Molecule, H. Peters, editor, Plenum Press, NY: 83-90.

Kita, T., Brown, M.S., Watanabe, Y., and Goldstein, J.L. 1981. Deficiency of low density lipoprotein receptors in liver and adrenal gland of the WHHL rabbit, an animal model of familial hypercholesterolemia. Proc. Natl. Acad. Sci. USA **78**: 2268-2272.

Kramsch, D.M., and Hollander, W.M. 1973. The interaction of serum and arterial apoproteins with elastin and its role in the lipid accumulation in atherosclerotic plaques. J. Clin. Invest. **52**: 236-247.

Lapidus, L. 1962. Digital Computation for Chemical Engineers. McGraw-Hill Book Co., NY.

- Latimer, H.B., and Sawin, P.B. 1957. Morphological studies of the rabbit. Anat. Rec. **129**: 457-472.
- Leake, D.S., and Bowyer, D.E. 1981. Quantitative studies of pinocytosis by arterial endothelial and smooth muscle cells in culture. Exp. Mol. Pathol. **35**: 84-97.
- Leake, D.S., Muir, E.M., and Bowyer, D.E. 1982. Modification of the rate of pinocytosis in arterial smooth muscle cells in culture. Exp. Mol. Pathol. **36**: 262-275.
- Lee, D.M. 1976. Isolation and characterization of low density lipoproteins. in Low Density Lipoproteins, C.E. Day and R.S. Levy, editors, Plenum press, NY: 3-47.
- Lee, H-C, Paz, M.A., and Gallop, P.M. 1982. Low density lipoprotein receptor binding in aging human diploid fibroblasts in culture. J. Biol. Chem. **257**: 8912-8918.
- Lehninger, A.L. 1975. Biochemistry. Second Edition, Worth Publishers, Inc., NY.
- Linsenmayer, T.F. 1981. Collagen. in Cell Biology of the Extracellular Matrix, E.D. Hay, editor, Plenum Press, NY: 1-38.
- Lowry, D.H., Rosebrough, N.J., Farr, A.I., and Randall, R.J. 1951. Protein measurement with Folin-phenol reagent. J. Biol. Chem. **193**: 265-275.
- Mahley, R.W., Innerarity, T.L., Pitas, R.E., Weisgraber, K.H., Brown, J.H., and Gross, E. 1977. Inhibition of lipoprotein binding to cell surface receptors of fibroblasts following selective modification of arginyl residues in arginine-rich and B lipoproteins. J. Biol. Chem. **252**: 7279-7287.
- Mahley, R.W., Innerarity, T.L., Weisgraber, K.h., and Oh, S.Y. 1979a. Altered metabolism (in vivo and in vitro) of plasma lipoproteins after selective chemical modification of lysine residues of the apoproteins. J. Clin. Invest. **64**: 743-750.
- Mahley, R.W., Weisgraber, K.H., and Innerarity, T.L. 1979b. Interaction of plasma lipoproteins containing apolipoproteins B and E with heparin and cell surface receptors. Biochim. Biophys. Acta. **575**: 81-91.
- Mahley, R.W., Weisgraber, K.H., Innerarity, T.L., and Windmueller, H.G. 1979c.

Accelerated clearance of low-density and high-density lipoproteins and retarded clearance of E apoprotein-containing lipoproteins from the plasma of rats after modification of lysine residues. Proc. Nat'l. Acad. Sci. 76: 1746-1750.

Mahley, R.W., Weisgraber, K.H., Melchior, G.W., Innerarity, T.L., Holcombe, K.S. 1980. Inhibition of receptor-mediated clearance of lysine and arginine modified lipoproteins from the plasma of rats and monkeys. Proc. Natl. Acad. Sci. USA 77: 225-229.

Mahoney, E.M., Hamill, A.L., Scott, W.A., and Cohn, Z.A. 1977. Response of endocytosis to altered fatty acyl composition of macrophage phospholipids. Proc. Natl. Acad. Sci. USA 74: 4895-4899.

Margolis, S. 1967. Separation and size determination of human serum lipoproteins by agarose gel filtration. J. Lipid Res. 8: 501-507.

Marquardt, D.W. 1963. An algorithm for least-squares estimation of nonlinear parameters. J. Soc. Ind. Appl. Math. 11: 431-441.

Marshall, S., and Olefsky, J.M. 1980. The endocytotic-internalization pathway of insulin metabolism: relationship to insulin degradation and activation of glucose transport. Endocrinology 107: 1937-1945.

Massaro, T.E., Glatz, C.E., Peppas, N.A., Chisolm, G.M., and Colton, C.K. 1979. Distribution of glycosaminoglycans in connective tissue layers of the rabbit aorta. Artery 5: 1-13.

Mathews, M.B. 1975. Connective Tissue. in Macromolecular Structure and Evolution, Springer Verlag, NY:

Matthews, C.M.E. 1960. The theory of tracer experiments with ¹³¹I-labeled plasma proteins. Phys. in Med. and Biol. 33: 36-.

McFarlane, A.S. 1958. Efficient trace labeling of proteins with iodine. Nature (London) 182: 53.

McMurtrey, J., Radhakrishnamurthy, B., Dalferes, E.R., Jr., Berenson, G.S., and Gregory, J.D. 1979. Isolation of proteoglycan-hyaluronate complexes from bovine aorta. J. Biol. Chem. 254: 1621-1626.

Means, G.E., and Feeney, R.E. 1968. Reductive alkylation of amino groups in proteins. Biochemistry 7: 2192-2201.

- Merion M., and Sly, W.S. 1983. The role of intermediate vesicles in the adsorptive endocytosis of ligand to lysosomes by human fibroblasts. J. Cell Biol. 96: 644-650.
- Miller, N.E., Weinstein, D.B., and Steinberg, D. 1977. Binding, internalization, and degradation of high density lipoprotein by cultured normal human fibroblasts. J. Lipid. Res. 18: 438-450.
- Miller, N.E., Weinstein, D.B., and Steinberg, D. 1978. Uptake and degradation of high density lipoprotein: comparison of fibroblasts from normal subjects and from hypercholesterolemic subjects. J. Lipid Res. 19: 644-653.
- Mitterer, A., Eigner, W.D., Schirz, J., Jurgens, G., and Holasek, A. 1982. Physicochemical characterization of soluble complexes of human serum low density lipoprotein with heparin. Intl. J. Biol. Macromol. 4: 227-232.
- Morel, D.W., Hessler, J.R., and Chisolm, G.M. 1983. Low density lipoprotein cytotoxicity induced by free radical peroxidation of lipid. J. Lipid Res. 24: 1070-1076.
- Morrel, E.M. 1983. Transport of ^{125}I -LDL through punctate regions of enhanced permeability in rabbit aorta, in vivo. MS Thesis, Massachusetts Institute of Technology, Cambridge, MA.
- Morris, C.J., Bradby, G.H.V., and Walter, K.W. 1978. Fibrous long spacing collagen in human atherosclerosis. Atherosclerosis 31: 345-354.
- Mourao, P.A.S., and Bracamonte, C.A. 1984. The binding of human aortic glycosaminoglycans and proteoglycans to plasma low density lipoproteins. Atherosclerosis 50: 133-146.
- Muir, E.M., and Bowyer, D.E. 1984. Inhibition of pinocytosis and induction of release of lysosomal contents by lysosomal overload of arterial smooth muscle cells in vitro. Atherosclerosis 50: 85-92.
- Muller, K., Laggner, P., Glatter, O., Kostner, G. 1978. The structure of human plasma low-density lipoprotein B. Eur. J. Biochem. 82: 73-90.
- Navarro, MC. 1984. Metabolism of Low Density Lipoprotein in Rabbit Arterial Wall SM Thesis, Cambridge, Massachusetts: Massachusetts Institute of Technology.
- Nerem, R.M., Mosberg, A.T., and Schwerin, W.D. 1976. Transendothelial transport of ^{131}I -albumin. Biorheology 13: 71-77.

- Nerem, R.M., Levesque, M.J., and Cornhill, J.F. 1981. Vascular endothelial morphology-as an indicator of the pattern of blood flow. J. Biomech. Eng. 103: 172-176.
- Nilsson, J., Ksiazek, T., and Thyberg, J. 1983. Endocytosis of cationic and anionic proteins in cultivated arterial smooth muscle cells. Exp. Cell Res. 143: 359-365.
- Noma, A., Takahashi, T., and Wada, T. 1981. Elastin-lipid interaction in the arterial wall. Part 2. In vitro binding of lipoprotein-lipids to arterial elastin and inhibitory effect of high density lipoproteins on the process. Atherosclerosis 38: 373-382.
- Noma, A., Hirayama, T., and Yachi, A. 1983. Studies on the binding of plasma low density lipoproteins to arterial elastin. Conn. Tiss. Res. 11: 123-133.
- Okishio, T. 1961. Studies on the transfer of ^{131}I -labeled serum lipoproteins into the aorta of rabbits with experimental atherosclerosis. Med. J. Osaka Univ. 11: 367-391.
- Oegema, T.R., Hascall, V.C., and Eisenstein, R. 1979. Characterization of bovine aorta proteoglycan extracted with guanidine hydrochloride in the presence of protease inhibitors. J. Biol. Chem. 254: 1312-1318.
- Ogston, A.G. 1958. The spaces in a uniform random suspension of fibers. Trans. Faraday Soc. 54: 1754-1757.
- Oram, J.F., Albers, J.J., and Bierman, J.J. 1980. Rapid regulation of the activity of the low density lipoprotein receptor of cultured human fibroblasts. J. Biol. Chem. 255: 475-485.
- Orci, L., Carpenter, J.L., Perrelet, A., Anderson, R.G.W., Goldstein, J.L., and Brown, M.S. 1978. Occurrences of low density lipoprotein receptors within large pits on the surface of human fibroblasts as demonstrated by freeze etching. Exp. Cell Res. 13: 1-13.
- Packard CJ, Slater HR, and Shepherd CJ. The reticulo-endothelial system and low density lipoprotein metabolism in the rabbit. Biochim Biophys Acta 1982; 712: 412-419.
- Pan, Y.T., Kruski, A.W., and Elbein, A.D. 1978. Binding of [^3H]Heparin to human plasma low density lipoproteins. Arch. Biochem. Biophys. 189: 231-240.

- Pastan, I.H., and Willingham, M.C. 1981. Receptor-mediated endocytosis of hormones in cultured cells. Ann. Rev. Physiol. 43: 239-250.
- Pastan, I.H., and Willingham, M.C. 1983. Receptor-mediated endocytosis: coated pits, receptosomes and the Golgi. Top. in Biol. Sci. 8: 250-254.
- Pearse, D.C., and Paule, W.J. 1960. Electron microscopy of elastic arteries; the thoracic aorta of the rat. J. Ultrastruct. Res. 3: 469-483.
- Pearse, B.M.F., and Bretscher, M.S. 1981. Membrane recycling by coated vesicles. Ann. Rev. Biochem. 50: 85-101.
- Pelikan, P., Gimbrone, M.A., Jr., and Cotran, R.S. 1979. Distribution and movement of anionic cell surface sites in cultured human vascular endothelial cells. Atherosclerosis 32: 69-80.
- Peters, T.J., Muller, M., and DeDuve. 1972. Lysosomes of the arterial wall. I. Isolation and subcellular fractionation of cells from normal rabbit aorta. J. Exp. Med. 136: 1117-1139.
- Pitas, R.E., Innerarity, T.L., Arnold, K.S., and Mahley, R.W. 1979. Rate and equilibrium constants for binding of apo-E HDL_c (a cholesterol-induced lipoprotein) and low density lipoproteins to human fibroblasts: Evidence for multiple receptor binding of apo-E HDL_c.
- Pitas, R.E., Boyles, J., Mahley, R.W., and Bissell, D.M. 1985. Uptake of chemically modified low density lipoproteins in vivo as mediated by specific endothelial cells. J. Cell Biol. 100: 103-117.
- Pittman, R.C., and Steinberg, D. 1978. A new approach for assessing cumulative lysosomal degradation of proteins or other macromolecules. Biochem. Biophys. Res. Comm. 81: 1254-1259.
- Pittman, R.C., Green, S.R., Attie, A.D., and Steinberg, D. 1979a. Radiolabeled sucrose covalently linked to protein. J. Biol. Chem. 254: 6876-6879.
- Pittman, R.C., Attie, A.D., Carew, T.E., and Steinberg, D. 1979b. Tissue sites of degradation of low density lipoprotein: application of a method for determining the fate of plasma proteins. Proc. Natl. Acad. Sci. USA 76: 5345-5349.
- Pittman, R.C., Attie, A.D., Carew, T.E., and Steinberg, D. 1982a. Tissue sites of catabolism of rat and human low density lipoproteins in rats. Biochim. Biophys. Acta. 710: 7-14.

Pittman, R.C., Carew, T.E., Attie, A.D., Witzum, J.L., Watanabe, Y., and Steinberg D. 1982b. Receptor-dependent and receptor independent degradation of low density lipoprotein in normal rabbits and in receptor-deficient mutant rabbits. J. Biol. Chem. 257: 7994-8000.

Pittman, R.C., Carew, T.E., Glass, C.K., Green, S.R., Taylor, C.A., Jr., and Attie, A.D. 1983. A radioiodinated, intracellularly trapped ligand for determining the sites of plasma protein degradation in vivo. Biochem. J. 212: 791-800.

Poole, B., and Ohkuma, S. 1981. Effect of weak bases on the intralysosomal pH in mouse peritoneal macrophages. J. Cell Biol. 90: 665-669.

Pratten, M.K., Duncan, R., and Lloyd, J.B. 1980. Adsorptive and passive pinocytotic uptake in Coated Vesicles, C.D. Ockleford and A. Whyte, editors, Cambridge University Press, Cambridge: 179-218.

Ramirez, C.A. 1979. Transport of ^{125}I -albumin across the normal and injured rabbit thoracic aorta in vivo. Doctoral Thesis. Massachusetts Institute of Technology, Cambridge, MA.

Ramirez, C.A., Colton, C.K., Smith, K.A., Stemerman, M.B., and Lees, R.S. 1984. Transport of ^{125}I -albumin across normal and deendothelialized rabbit thoracic aorta in vivo. Arteriosclerosis 4: 283-291.

Reckless, J.P.D., Weinstein, D.B., and Steinberg, S. 1978. Lipoprotein and cholesterol metabolism in rabbit arterial endothelial cells in culture. Biochim. Biophys. Acta. 529: 475-487.

Reckless, J.P.D., Weinstein, D.B., and Steinberg, D.B. 1979. The metabolism of low and high density lipoproteins and the control of sterol synthesis in cultured smooth muscle cells from multiple arterial sites in a single rabbit. (Unpublished Manuscript).

Reichl, D., Simons, L.A., Myant, N.B., Pflug, J.J., and Mills, G.L. 1975. The lipids and lipoproteins of human peripheral lymph, with observations on the transport of cholesterol from plasma and tissue in lymph. Clin. Sci. Mol. Med. 45: 313-329.

Reidy, M.A., and Bowyer, D.E. 1977. Scanning electron microscopy of arteries: The morphology of aortic endothelium in haemodynamically stressed areas associated with branches. Atherosclerosis 26: 181-194.

Rhodin, J.A.G. 1977. Architecture of the vessel wall. in Handbook of Physiology. Section 2, The Cardiovascular System. Vol. II, Vascular Smooth Muscle, American Physiological Society, Bethesda: 1-31.

Rodriguez, F. 1982. Principles of Polymer Systems. Second Edition, McGraw-Hill Book Co., NY.

Ross, R. 1971. The smooth muscle cell. II. Growth of smooth muscle in culture and formation of elastic fibers. J. Cell Biol. 50: 172-186.

Ross, R., and Glomset, J.A. 1976. The pathogenesis of atherosclerosis. New Engl. J. Med. 295: 369-376.

Rubenstein, B., and Steiner, G. 1976. Fractionation of human low density lipoprotein by column chromatography. Can. J. Biochem. 22: 1023-1028.

Rubin, B.T. 1977. A theoretical model of the pinocytotic vesicular transport process in endothelial cells. J. Theor. Biol. 64: 619-647.

Rucker, R.B., and Tinker, D. 1977. Structure and metabolism of arterial elastin. in International Review of Experimental Pathology. Vol. 17, G.W. Richter and M.A. Epstein, editors, Academic Press, NY: 1-47.

Saffman, P.G., and Delbruck, M. 1975. Brownian motion in biological membranes. Proc. Natl. Acad. Sci. USA 72: 3111-3113.

Salisbury, B.G.J., and Wagner, W.D. 1981. Isolation and preliminary characterization of proteoglycans dissociatively extracted from human aorta. J. Biol. Chem. 256: 8050-8057.

Sasaki, J., and Cottam, G.L. 1982. Glycosylation of LDL decreases its ability to interact with high-affinity receptors of human fibroblasts in vitro and decreases its clearance from rabbit plasma in vivo. Biochim. Biophys. Acta. 713: 199-207.

Satterfield, C.N., Colton, C.K., Pitcher, W.H., Jr. 1973. Restricted diffusion in liquids within fine pores. AIChE J. 19: 628-635.

Schechter, I., Fogelman, A.M., Haberland, M.E., Seager, J., Holsome, M., and Edwards, P.A. 1981. The metabolism of native and malondialdehyde-altered low density lipoproteins by human monocyte-macrophages. J. Lipid Res. 22: 63-71.

Schleicher, E., Deufel, T., and Wieland, O.H. 1981. Non-enzymatic glycosylation of human serum lipoproteins. FEBS Lett. **129**: 1-4.

Schneiderman, G., Pritchard, W.F., Ramirez, C.A., Colton, C.K., Smith, K.A., and Stemerman, M.B. 1983. Rabbit aortic medial thickness under relaxed and specified simulated in vivo conditions. Am. J. Physiol. **245**: H623-H627.

Schnitzer, J.J. 1983. Transport of ^{125}I -low density lipoprotein across the rabbit aortic wall: a quantitative autoradiographic study. Doctoral Thesis. Massachusetts Institute of Technology, Cambridge, MA.

Schumaker, V.N. 1973. Hydrodynamic analysis of human low density lipoproteins. Acc. Chem. Res. **6**: 398-403.

Schwartz, A.L., Fridovich, S.E., and Lodish, H.F. 1982. Kinetics of internalization and recycling of the asialoglycoprotein receptor in a hepatoma cell line. J. Biol. Chem. **257**: 4230-4237.

Schwartz, S.M., and Benditt, E.P. 1972. Studies on aortic intima. I. Structure and permeability of rat thoracic aortic intima. Am. J. Pathol. **66**: 241-254.

Scott, J.E. 1984. In vitro protein uptake and distribution in the rabbit aortic wall. Massachusetts Institute of Technology, Cambridge, MA.

Shepherd, J., Bicker, S., Lorimer, A.R., and Packard, C.J. 1979. Receptor-mediated low density lipoprotein catabolism in man. J. Lipid Res. **20**: 999-1006.

Shepherd, J., Slater, H.R., Packard, C.J. 1982. Low density lipoprotein receptor activity in man, in Lipoprotein Kinetics and Modeling. M. Berman, S.M. Grundy, and B.V. Howard, editors. Academic Press NY: 157-168.

Shiraham, T., and Cohen, A.S. 1972. The role of mucopolysaccharides in vesicle architecture and endothelial transport. J. Cell. Biol. **52**: 198-206.

Shore, B., and Shore, V. 1975. Rabbits as a model for the study of hyperlipoproteinemia and atherosclerosis. in Atherosclerosis Drug Discovery. C.E. Day, editor, Plenum Publishing Corp. NY: 123-142.

Siflinger, A., Parker, K., and Caro, C.G. 1975. Uptake of ^{125}I -albumin by the endothelial surface of the isolated dog common carotid artery: effect of certain physical factors and metabolic inhibitors. Card. Res. **9**: 478-489.

Simionescu, N., Siomionescu, M., and Palade, G. 1976. Recent studies on vascular endothelium. Ann. NY Acad. Sci. 275: 64-75.

Singh, J.P., Chaikin, M.A., Pledges, W.J., Scher, C.D., and Stiles, C.D. 1983. Persistence of mitogenic response to platelet-derived growth factor (competence) does not reflect a long-term interaction between growth factor and target cell. J. Cell Biol. 96: 1497-1502.

Skutelsky, E., and Danon, D. 1976. Redistribution of surface anionic sites on the luminal front of blood vessel endothelium after interaction with poly cationic ligands. J. Cell. Biol. 71: 232-241.

Slater, H.R., Packard, C.J., Bicker, S., and Shepherd, J. 1980. Effects of cholestyramine on receptor-mediated plasma clearance and tissue uptake of human low density lipoproteins in the rabbit. J. Biol. Chem. 255: 10210-10213.

Slater, H.R., Packard, C.J., Shepherd, J. 1982a. Receptor-independent catabolism of low density lipoprotein. J. Biol. Chem. 257: 307-310.

Slater, H.R., Packard, C.J., Shepherd, J. 1982b. Measurement of receptor-independent lipoprotein catabolism using 1,2-cyclohexanedione-modified low density lipoprotein. J. Lipid Res. 23: 92-96.

Slater, H.R., Shepherd, J., Packard, C.J. 1982c. Receptor-mediated catabolism and tissue uptake of human low density lipoprotein in the cholesterol-fed, atherosclerotic rabbit. Biochim. Biophys. Acta. 713: 435-445.

Smith, E.B., and Slater, R. 1970. The chemical and immunological assay of low density lipoproteins extracted from the human thoracic intima. Atherosclerosis 13: 293-304.

Smith, E.B., Massie, I.B., and Alexander, K.M. 1976. The release of an immobilized lipoprotein fraction from atherosclerotic lesions by incubation with plasmin. Atherosclerosis 25: 71-84.

Smith, E.B., and Staples, E.M. 1980. Distribution of plasma proteins across the human aortic wall. Atherosclerosis 37: 579-590.

Sniderman, A.D., Carew, T.E., and Steinberg, D. 1975. Turnover and tissue distribution of ¹²⁵I-labeled low density lipoprotein in swine and dogs. J. Lipid Res. 16: 293-299.

- Somer, J.B., and Schwartz, C.J. 1971. Focal ^3H -cholesterol uptake in the pig aorta. Atherosclerosis 13: 293-304.
- Spector, W.S. 1956. Handbook of Biological Data. W.B. Saunders, Philadelphia.
- Sprague, E.A., Kelley, J.L., and Schwartz, C.J. 1982. Growth, structure and function of baboon aortic smooth muscle cells in culture. Exp. Mol. Pathol. 37: 48-66.
- Srinivasan, S.R., Dolan, P., Radhakrishnamurthy, R., Pargaonkar, P.S., and Berenson, G.S. 1975a. Lipoprotein-acid mucopolysaccharide complexes of human atherosclerotic lesions. Biochim. Biophys. Acta. 388: 58-70.
- Srinivasan, S.R., Radhakrishnamurthy, B., and Berenson, G.S. 1975b. Studies on the interaction of heparin with serum lipoproteins in the presence of Ca^{++} , Mg^{++} , and Mn^{++} . Arch. Biochem. Biophys. 170: 334-340.
- Srinivasan, S.R., Radhakrishnamurthy, B., Dalferes, E.R., Jr., and Berenson, G.S. 1978. Interactions of lipoproteins and connective tissue components in human atherosclerotic plaques. in Intl. Conf. on Atherosclerosis, L.A. Carlson et al., editors, Raven Press, NY: 585-588.
- Srinivasan, S.R., Yost, K., Radhakrishnamurthy, B., Dalferes, E.R., Jr., and Berenson, G.S. 1980. Lipoprotein-hyaluronate associations in human aorta fibrous plaque lesions. Atherosclerosis 36: 25-37.
- Steile, J.C.H., and Reynolds, J.A. 1979. Molecular weight and hydrodynamic properties of apolipoprotein B in guanidine hydrochloride and sodium dodecyl sulfate solutions. J. Biol. Chem. 254: 1639-1643.
- Stein, Y., and Stein, O. 1973. Lipid synthesis and degradation and lipoprotein transport in mammalian aorta. in Atherogenesis: Initiating Factors . Ciba Found. Symp. 12 (new series): 165-184.
- Stein, O., Stein, Y., and Eisenberg, S. 1973. A radioautographic study of the transport of ^{125}I -labeled serum lipoproteins in rat aorta. Z. Zellforsch 138: 223-237.
- Stein, O., and Stein, Y. 1975. Comparative uptake of rat and human serum low-density lipoproteins by rat aortic smooth muscle cells in culture. Circ. Res. 36: 436-443.
- Stein, O., Weinstein, D.B., Stein, Y., and Steinberg, D. 1976. Binding,

internalization, and degradation of low density lipoprotein by normal human fibroblasts and by fibroblasts from a case of homozygous familial hypercholesterolemia. Proc. Natl. Acad. Sci. **73**: 14-18.

Stein, O., and Stein, Y. 1980. Bovine aortic endothelial cells display macrophage-like properties towards acetylated ¹²⁵I-labelled low density lipoprotein. Biochim. Biophys. Acta. **620**: 631-635.

Steinbrecher, U.P., Witzum, J.L., Kesaniemi, and Elam, R.L.: 1983. Comparison of glycosylated low density lipoprotein with methylated or cyclohexanedione-treated low density lipoprotein in the measurement of receptor-independent low density lipoprotein catabolism. J. Clin. Invest. **71**: 960-964.

Steinbrecher, U.P., Parthasarathy, S., Leake, D.S., Witzum, J.L., and Steinberg, D. 1984. Modification of low density lipoprotein by endothelial cells involves lipid peroxidation and degradation of low density lipoprotein phospholipids. Proc. Natl. Acad. Sci. USA **81**: 3883-3887.

Steinman, R.M., and Cohn, Z.A. 1972. The interaction of soluble horseradish peroxidase with mouse peritoneal macrophages in vitro. J. Cell Biol. **55**: 186-194.

Steinman, R.M., Silver, J.M., and Cohn, Z.A. 1974. Pinocytosis in fibroblasts. J. Cell Biol. **63**: 949-969.

Steinman, R.M., Brodie, S.E., and Cohn, Z.A. 1976. Membrane flow during pinocytosis. J. Cell. Biol. **68**: 665-687.

Steinman, R.M., Mellman, I.S., Muller, W.A., and Cohn, Z.A. 1983. Endocytosis and the recycling of plasma membrane. J. Cell. Biol. **96**: 1-27.

Stemerman, M.B. 1981. Effects of moderate hypercholesterolemia on rabbit endothelium. Arteriosclerosis **1**: 25-32.

Stemerman, M.B., Colton, C.K., and Morrel, E.M. 1984. Perturbations of the endothelium. in Prog. Hemostasis and Thromb. T.H. Spaet, editor, Grune and Stratton, NY: 289-324.

Stiles, C.D. 1983. The molecular biology of platelet-derived growth factor. Cell **33**: 653-655.

Tanzawa, K., Shimada, Y., Kuroda, M., Toujita, Y., Arai, M., and Watanabe, H. 1980. WHHL-rabbit: a low density lipoprotein receptor-deficient animal for

familial hypercholesterolemia. FEBS Lett. 118: 81-84.

Taylor, R.F., Price, T.H., Schwartz, S.M., and Dale, D.C. 1981. Neutrophil-endothelial cell interactions on endothelial monolayers grown on micropore filters. J. Clin. Invest. 67: 584-587.

Tedgui, A., and Lever, M.J. 1985. The interaction of convection and diffusion in the transport within the media of the rabbit thoracic aorta. Submitted to the Am. J. Physiol.

Territo, M., Berliner, J.A., and Fogelman, A.M. 1984. Effect of monocyte migration on low density lipoprotein transport across endothelial cell monolayers. J. Clin. Invest. 74: 2279-2284.

Todd, M.E., Lage, C.G., and Osborne, D.N. 1983. The dimensional characteristics of smooth muscle in rat blood vessels. Circ. Res. 53: 319-331.

Tokita, K., Kanno, K., and Ikeda, K. 1977. Elastin subfraction as a binding site for lipids. Atherosclerosis 28: 111-119.

Tolleshaug, H., Hobgood, K.K., Brown, M.S., and Goldstein, J.L. 1983. The LDL receptor locus in familial hypercholesterolemia: multiple mutations disrupt transport and processing of a membrane receptor. Cell 32: 941-951.

Tompkins, R.G. 1983. In vivo transport of low-density lipoproteins in the arterial wall of squirrel monkeys. Doctoral Thesis, Massachusetts Institute of Technology, Cambridge, MA.

Truskey, G.A., Colton, C.K., and Smith, K.A. 1981. Quantitative analysis of protein transport in the arterial wall. in Structure and Function of the Circulation. C.J. Schwartz, N.T. Werthessen, and S. Wolf, editors, Plenum Publishing Corp., NY: 287-355.

Truskey, G.A., and Davies, P.F. 1985. Effects of ammonium ion derived from bovine endothelial cells upon low density lipoprotein degradation in cultured vascular smooth muscle cells. Cell Biol. Intl. Rep. 9: 323-330.

Tycko, B., and Maxfield, F.R. 1982. Rapid acidification of endocytic vesicles containing α_2 -macroglobulin. Cell 28: 643-651.

van Hinsbergh, V.W.M., Havekes, L., Emeis, J.J., van Corven, E., and Scheffer, M. 1983. Low density lipoprotein metabolism by endothelial cells from human umbilical cord arteries and veins. Arteriosclerosis 3: 547-559.

- van Hinsbergh, V.W.M. 1984. LDL cytotoxicity. Atherosclerosis 53: 113-118.
- Vasile, E., Simionescu, M., and Simionescu, N. 1983. Visualization of the binding, endocytosis, and transcytosis of low-density lipoprotein in the arterial endothelium in situ. J. Cell Biol. 96: 1677-1689.
- veng Pedersen, P. 1980a. Model-independent method of analyzing input in linear pharmacokinetic systems having polyexponential impulse response. I: Theoretical analysis. J. Pharm. Sci. 69: 298-305.
- veng Pedersen, P. 1980b. Model-independent method of analyzing input in linear pharmacokinetic systems having polyexponential impulse response. II: Numerical evaluation. J. Pharm. Sci. 69: 305-311.
- Vermeer, B.J., Havekes, L., Wijsam, M.C., and Emeis, J.J. 1980. Immunoelectronmicroscopical investigations on the adsorptive endocytosis of low density lipoprotein by human fibroblasts. Exp. Cell. Res. 129: 201-210.
- Vijayagopul, P., Srinivasan, S.R., Radhakrishnamurthy, B., and Berenson, G.S. 1981. Interaction of serum lipoproteins and a proteoglycan from bovine aorta. J. Biol. Chem. 256: 8234-8241.
- Vlodavsky, I. Fielding, P.E., Fielding, C.J., and Gospodarowicz, D. 1978. Role of contact inhibition in the regulation of receptor-mediated uptake of low density lipoprotein in cultured vascular endothelial cells. Proc. Natl. Acad. Sci. USA 75: 356-360.
- Vogel, A., Raines, E., Kariya, B., Rivest, M-J., and Ross, R. 1978. Coordinate control of 3T3 cell proliferation by platelet-derived growth factor and plasma components. Proc. Natl. Acad. Sci. USA 75: 2810-2814.
- Wall, D.A., Wilson, G., and Hubbard, A.L. 1980. The galactose specific recognition system of mammalian liver: the route of ligand internalization in rat hepatocytes. Cell 21: 79-93.
- Watanabe, Y. 1980. Serial inbreeding of rabbits with hereditary hyperlipidemia (WHHL-rabbits). Atherosclerosis 36: 261-268.
- Webb, W.W., Barak, L.S., Tank, D.W., and Wu, E.S. 1982. Molecular mobility on the cell surface. Biochem. Soc. Symp. 46: 191-205.
- Weinstein, D.B., Carew, T.E., and Steinberg, D. 1976. Uptake and degradation of

LDL by swine arterial smooth muscle cells with inhibition of cholesterol biosynthesis. Biochim. Biophys. Acta. 424: 404-421.

Weigel, P.H., and Oka, J.A. 1982. Endocytosis and degradation mediated by the asialoglycoprotein receptor in isolated rat hepatocytes. J. Biol. Chem. 257: 1201-1207.

Weinbaum, S., Arminski, L., Pfeffer, R., and Chien, S. 1980, Theoretical models for endothelial junction formation and vesicular transport. in Hemodynamics and the Arterial Wall, Proceedings from a Specialists Meeting. R.M. Nerem and J.R. Guyton, editors, University of Houston, Houston: 42-46.

Weisgraber, K.H., Innerarity, T.L., and Mahley, R.W. 1978. Role of the lysine residues of plasma lipoproteins on high affinity binding to cell surface receptors on human fibroblasts. J. Biol. Chem. 253: 9053-9062.

Westermarck, B., Heldin, C.H., Ek, B., Johnsson, A., Mellstrom, K., Nister, M., and Wasteson, A. 1983. Biochemistry and biology of platelet-derived growth factor. in Growth and Maturation Factors, Vol. 1, G. Guroff, editor, John Wiley and Sons, NY: 73-115.

Whitaker, S. 1969. Fluid motion in porous media. Ind. Eng. Chem. Fund. 61: 14-28.

White, A., Handler, P., Smith, E.L., Hill, R.H., and Lehman, R. 1978. Principles of Biochemistry. McGraw-Hill Book Co., NY: 697.

Wight, T.N., and Ross, R. 1975. Proteoglycans in primate arteries. I. Ultrastructural localization and distribution in the intima. J. Cell Biol. 67: 660-674.

Wight, T.N. 1980. Vessel proteoglycans and thrombogenesis. in Progress in Hemostasis and Thrombosis. Vol. 5, T.H. Spaet, editor, Grune and Stratton, NY: 1-39.

Wiklund, O., Carew, T.E., and Steinberg, D. 1985. Role of the low density lipoprotein receptor in penetration of low density lipoprotein into rabbit aortic wall. Arteriosclerosis 5: 135-141.

Wiley, H.S., and Cunningham, D.D. 1981. A steady state model for analyzing the cellular binding, internalization and degradation of polypeptide ligands. Cell 25: 433-440.

- Wiley, H.S., and Cunningham, D.D. 1982. The endocytotic rate constant. J. Biol. Chem.-257: 4222-4229.
- Wilks, S.S. 1962. *Mathematical Statistics*. John Wiley and Sons, Inc., NY.
- Williams, K.E. 1981. Endocytosis and exocytosis in *Biochemistry of Cellular Regulation, Vol IV, The Cell Surface*, M.J. Clemens, editor. CRC Press, Boca Raton, FL: 189-214.
- Willingham, M.C., and Pastan, I. 1980. The receptosome: an intermediate organelle of receptor-mediated endocytosis in cultured fibroblasts. Cell 21: 67-77.
- Winlove, C.P., Davis, J., Baldwin, A., and Chabanel, A. 1982. Effects of particle size and perfusate composition on the uptake of colloidal gold by the rabbit thoracic aorta perfused in situ. Atherosclerosis 44: 99-111.
- Witte, L.D., and Cornicelli, J.A. 1980. Platelet-derived growth factor stimulates low density lipoprotein receptor activity in cultured human fibroblasts. Proc. Natl. Acad. Sci. USA 77: 5962-5966.
- Witte, L.D., Cornicelli, J.A., Miller, R.W., and Goodwin, D.S. 1982. Effects of platelet-derived and endothelial-derived growth factors on the low density lipoprotein receptor pathway in cultured human fibroblasts. J. Biol. Chem. 257: 5392-5401.
- Wolfsky, C., and Goldstein, B. 1984. Coated pits and low density lipoprotein receptor recycling. in *Cell Surface Dynamics*. A.S. Perelson, C. DeLisi, and F.W. Weigel, editors, Marcel Dekker, NY: 405-456.
- Wolinsky, H., and Glagov, S. 1967. Nature of species differences in the medial distribution of aortic vasa vasorum in mammals. Circ. Res. 20: 409-421.
- Wolinsky, H., Capron, L., and Fowler, S. 1979. Risk factors, lysosomes, and vascular disease. in *Atherosclerosis Reviews, Vol. 5*, R Paoletti and A.M. Gotto, Jr., editors, Raven press, NY: 125-147.
- Wylie, CR. *Advanced Engineering Mathematics*. 4th edition. New York: McGraw-Hill Book Co, 1975: 313-316.
- Yau-Young, A.O., Shio, H., and Fowler, S. 1981. Growth, biochemistry, and morphology of isolated rabbit aortic smooth muscle cells maintained in the presence or absence of serum. J. Cell. Physiol. 108: 461-473.

Zar, J.H. 1984. Biostatistical Analysis. Second Edition, Prentice Hall, Englewood Cliffs, NJ.

Zigmond, S.H., Sullivan, S.J., and Lauffenburger, D.A. 1982. Kinetic analysis of chemotactic peptide receptor modulation. J. Cell Biol. 92: 34-43.

Zilversmit, D.B. 1968. Cholesterol flux in the atherosclerotic plaque. Ann. NY Acad. Sci. 149: 710-724.